Increasing structural diversity of natural products by enzymatic or nonenzymatic reactions

Erhöhung der strukturellen Vielfalt von Naturstoffen durch enzymatische oder nichtenzymatische Reaktionen

Dissertation
zur Erlangung des Doktorgrades
der Naturwissenschaften
(Dr. rer. nat.)

dem Fachbereich Pharmazie
der Philipps-Universität Marburg

vorgelegt von

Ge Liao
aus Changsha, China

Marburg an der Lahn, 2020

Erstgutachter: **Prof. Dr. Shu-Ming Li**

Zweitgutachter: **Prof. Dr. Michael Keusgen**

Eingereicht am 01. Juli 2020

Tag der mündlichen Prüfung: 18. August 2020

Hochschulkennziffer: 1180

Dedicated to my family

Table of contents

List of publications

1. **Ge Liao***, Peter Mai*, Jie Fan, Georg Zocher, Thilo Stehle, and Shu-Ming Li (2018). Complete decoration of the indolyl residue in *cyclo*-L-Trp-L-Trp with geranyl moieties by using engineered dimethylallyl transferases. *Organic Letters*, 20 (22), 7201–7205, DOI: 10.1021/acs.orglett.8b03124. (*equal contribution)

2. **Ge Liao***, Jie Fan*, Lena Ludwig-Radtke, Katja Backhaus, and Shu-Ming Li (2020). Increasing structural diversity of natural products by Michael addition with *ortho*-quinone methide as the acceptor. *Journal of Organic Chemistry*, 85 (2), 1298–1307, DOI:10.1021/acs.joc.9b02971 (*equal contribution)

3. Jie Fan*, **Ge Liao***, Florian Kindinger, Lena Ludwig-Radtke, Wen-Bing Yin, and Shu-Ming Li (2019). Peniphenone and penilactone formation in *Penicillium crustosum* via 1,4-Michael additions of *ortho*-quinone methide from hydroxyclavatol to γ-butyrolactones from crustosic acid. *Journal of the American Chemical Society*, 141 (10), 4225–4229, DOI: 10.1021/jacs.9b00110. (*equal contribution)

4. Jie Fan*, **Ge Liao***, Lena Ludwig-Radtke, Wen-Bing Yin, and Shu-Ming Li (2020). Formation of terrestric acid in *Penicillium crustosum* requires redox-assisted decarboxylation and stereoisomerization. *Organic Letters*, 22 (1), 88–92, DOI: 10.1021/acs.orglett.9b04002. (*equal contribution)

Erklärung zum Eigenanteil

Titel der Publikation und Journal incl. Jahr, Heft, Seitzahl + doi **O: Originalarbeit** **Ü: Übersichtartikel/Review**	**Autoren**	**geschätzter Eigenanteil in %**	**Bitte angeben: angenommen/eingereicht**
Complete decoration of the indolyl residue in *cyclo*-L-Trp-L-Trp with geranyl moieties by using engineered dimethylallyl transferases. *Organic Letters*, 2018, 20 (22), 7201–7205 DOI: 10.1021/acs.orglett.8b03124. Originalarbeit	**Ge Liao***, Peter Mai*, Jie Fan, Georg Zocher, Thilo Stehle and Shu-Ming Li	30	angenommen
Increasing structural diversity of natural products by Michael addition with *ortho*-quinone methide as the acceptor. *Journal of Organic Chemistry*, 2020, 85 (2), 1298–1307 DOI: 10.1021/acs.joc.9b02971 Originalarbeit	**Ge Liao***, Jie Fan*, Lena Ludwig-Radtke, Katja Backhaus and Shu-Ming Li	40	angenommen
Peniphenone and penilactone formation in *Penicillium crustosum* via 1,4-Michael additions of *ortho*-quinone methide from hydroxyclavatol to γ-butyrolactones from crustosic acid. *Journal of the American Chemical Society*, 2019, 141 (10), 4225–4229 DOI: 10.1021/jacs.9b00110. Originalarbeit	Jie Fan*, **Ge Liao***, Florian Kindinger, Lena Ludwig-Radtke, Wen-Bing Yin and Shu-Ming Li	35	angenommen
Formation of terrestric acid in *Penicillium crustosum* requires redox-assisted decarboxylation and stereoisomerization. *Organic Letters*, 2020, 22 (1), 88–92 DOI: 10.1021/acs.orglett.9b04002. Originalarbeit	Jie Fan*, **Ge Liao***, Lena Ludwig-Radtke, Wen-Bing Yin and Shu-Ming Li	40	angenommen

*: These authors contributed equally to this work.

---------- ----------

Kandidat(in) **Unterschrift Betreuer(in)**

Abbreviations

The international system of units and units derived thereof have been used.

$[M+H]^+$	molecular ion plus proton
$[M-H]^-$	molecular ion minus proton
× *g*	gravitational acceleration
2-OG	2-oxoglutarate
6-MSA	6-methylsalicylic acid
aa	amino acid
A domain	adenylation domain
ACP domain	acyl carrier protein domain
AT domain	acyltransferase domain
bp	base pair
C domain	condensation domain
CD_3OD	deuterated methanol
$CDCl_3$	deuterated chloroform
CDP	cyclic dipeptide
cDNA	copy deoxyribonucleic acid
CLC	Claisen-like-cyclase
Cla	clavatol
CoA	coenzyme A
COSY	correlation spectroscopy
cyclo-L-Trp-L-Trp	*cyclo*-L-tryptophan-L-tryptophan
cyclo-L-Trp-L-Pro	*cyclo*-L-tryptophan-L-proline
cyclo-L-Trp-D-Pro	*cyclo*-L-tryptophan-D-proline
cyclo-D-Trp-L-Pro	*cyclo*-D-tryptophan-L-proline
cyclo-D-Trp-D-Pro	*cyclo*-D-tryptophan-D-proline
cyclo-L-Trp-L-Ala	*cyclo*-L-tryptophan-L-alanine
cyclo-L-Trp-D-Ala	*cyclo*-L-tryptophan-D-alanine
cyclo-D-Trp-L-Ala	*cyclo*-D-tryptophan-L-alanine
cyclo-D-Trp-D-Ala	*cyclo*-D-tryptophan-D-alanine
cyclo-L-Trp-L-Leu	*cyclo*-L-tryptophan-L-leucine

cyclo-L-Trp-L-Tyr	*cyclo*-L-tryptophan-L-tyrosine
cyclo-L-Trp-L-Phe	*cyclo*-L-tryptophan-L-phenylalanine
cyclo-L-Trp-Gly	*cyclo*-L-tryptophan-glycine
cyclo-L-Tyr-L-Tyr	*cyclo*-L-tyrosine-L-tyrosine
cyclo-L-Ser-L-Tyr	*cyclo*-L-serine-L-tyrosine
d	doublet
D_2O	deuterium oxide
Da	dalton
dd	double doublet
ddd	double double doublet
DH domain	dehydratase domain
DMA	dimethylallyl
DMAPP	dimethylallyl diphosphate
DMATS	dimethylallyltryptophan synthase
DMSO-d_6	deuterated dimethyl sulfoxide
DNA	deoxyribonucleic acid
dq	double quartet
dt	double triplet
DTT	dithiothreitol
E domain	epimerization domain
e.g.	exempli gratia
EIC	extracted ion chromatogram
ER domain	enoyl reductase domain
ESI	electrospray ionization
ETP	epipolythiodioxopiperazine
FPP	farnesyl diphosphate
gDNA	genomic deoxyribonucleic acid
GMM	glucose minimal medium
GPP	geranyl diphosphate
GGPP	geranylgeranyl diphosphate
HC	hydroxyclavatol
His_6	hexahistidine

HDA	hetero-Diels–Alder
HMBC	heteronuclear multiple bond correlation
HPLC	high performance liquid chromatography
HR-MS	high resolution-mass spectrometry
HR-PKS	highly reducing-polyketide synthase
HSQC	heteronuclear single quantum coherence
Hz	hertz
i.e.	id est
IMDA	intramolecular Diels–Alder
IPP	isopentenyl diphosphate
IPNS	isopenicillin N synthase
J	coupling constant
kbp	kilo base pairs
kcat	turnover number
kDa	kilodalton
K_M	Michaelis-Menten constant
KR domain	ketoreductase domain
KS domain	ketosynthase domain
LC-MS	liquid chromatography-mass spectrometry
Ile	isoleucine
m	multiplet
m/z	mass-to-charge ratio
mAU	milliabsorbance unit
Mb	mega base pairs
MHz	mega hertz
mRNA	messenger ribonucleic acid
Met	methionine
MeT domain	methyltransferase domain
multi	multiplicity
NADH	nicotinamide adenine dinucleotide (reduced form)
NADPH	nicotinamide adenine dinucleotide phosphate (reduced form)
NMR	nuclear magnetic resonance

NR-PKS	nonreducing-polyketide synthase
NRPS	nonribosomal peptide synthetase
P450	cytochrome P450
PCP domain	peptidyl carrier protein domain
PCR	polymerase chain reaction
PD	potato dextrose
PDB	potato dextrose broth
PEG	polyethylene glycol
Phe	phenylalanine
PKS	polyketide synthase
PKS-NRPS	polyketide synthase-nonribosomal peptide synthetase
PPi	inorganic pyrophosphate
ppm	parts per million
PR-PKS	partially reducing-polyketide synthase
PT	prenyltransferase
PT domain	product template domain
q	quartet
QM	quinone methide
RNA	ribonucleic acid
rpm	revolutions per minute
s	singlet
SAM	S-adenosyl-L-methionine
SAT domain	starter unit acyltransferase domain
SDS-PAGE	sodium dodecyl sulfate polyacrylamide gel electrophoresis
SM	secondary metabolite
t	triplet
TC	terpene cyclase
Thr	threonine
Tra	terrestric acid
T domain	thiolation domain
TB	terrific broth
td	triple doublet

TE domain	thioesterase domain
Tris	tris(hydroxymethyl)aminomethane
UV	ultraviolet
v/v	volume per volume
w/v	weight per volume
WT	wild-type
δ_C	chemical shift of ^{13}C
δ_H	chemical shift of ^{1}H

Summary

Secondary metabolites are generally low-molecule-mass compounds, also known as natural products. So far, millions of natural products with remarkably structural diversity have been found in nature. These include, but are not limited to, polyketides, nonribosomal peptides, alkaloids, and terpenoids. The structural divergence of natural products begins with the formation of basic skeletons by different backbone enzymes using fundamental building blocks derived from primary metabolism. Following modifications of the pre-matured scaffolds are catalyzed by tailoring enzymes such as oxidoreductases and transferases, thus completing the biosynthesis of end products with vast diversity and complexity. Enzymes from natural product biosynthetic pathways are versatile biocatalysts due to the merits of high efficiency and specificity. Harnessing biocatalytic potential of enzymes through chemoenzymatic synthesis has proven to be a useful tool for enriching chemical libraries. In addition to enzymatic catalysis, the occurrence of nonenzymatic events has also been found during the post-biosynthetic processing of natural products. These nonenzymatic reactions often occur with the involvement of reactive biosynthetic intermediates. Full exploitation of these intermediates for chemical synthesis can be used as an updated strategy to expand the chemical variety of natural products.

In a cooperation project with Dr. Peter Mai, five prenyltransferases (PTs) of the dimethylallyltryptophan synthase (DMATS) family, *i.e.* FtmPT1, BrePT, CdpC2PT, CdpNPT, and CdpC3PT, were selected for protein engineering. These PTs catalyze a regular or reverse transfer of the dimethylallyl residue (C_5) from dimethylallyl diphosphate (DMAPP) to the C-2 or C-3 position of indolyl residues in cyclic dipeptides (CDPs). To switch their prenyl donor specificity from DMAPP to geranyl diphosphate (GPP), protein sequence alignments of the five PTs with those of AtaPT and FgaPT2 led to the identification of the gatekeeping residues at Met364 in FtmPT1, Ile337 in BrePT, Thr351 in CdpC2PT, Met349 in CdpNPT, and Phe335 in CdpC3PT. Replacing the respective key amino acids by glycine resulted in the construction of FtmPT1_M364G, BrePT_I337G, CdpC2PT_T351G, CdpNPT_M349G, and CdpC3PT_F335G. These mutants showed clearly improved activity toward GPP but reduced activity toward DMAPP. As a result, 42 geranylated derivatives were obtained from the incubation mixtures of the generated mutants with 15 tested CDPs in the presence of GPP and their structures were elucidated by NMR and MS analyses. When using *cyclo*-L-Trp-L-Trp as the acceptor and GPP as the donor, the transfer of geranyl moieties to all seven possible positions of the indole nucleus can be achieved by the engineered enzymes. Prior to our study, only limited numbers of geranylated indole derivatives have been reported. This study significantly increased the structural diversity of geranylated products by structure-based protein engineering of available dimethylallyl transferases.

In a cooperation study with Dr. Jie Fan, the biosynthesis of peniphenone and penilactones in *Penicillium crustosum* PRB-2 was elucidated, which revealed occurrence of both enzymatic and nonenzymatic reactions during their formation. The hybrid PKS-NRPS TraA from the terrestric acid

pathway is involved in the formation of crustosic acid, which undergoes decarboxylation by the nonheme Fe^{II}/2-OG-dependent oxygenase TraH and subsequent reduction by the flavin-containing oxidoreductase TraD to afford terrestric acid. Both acids are precursors of the γ-butyrolactones. The nonreducing PKS ClaF from the clavatol pathway is responsible for the formation of clavatol, which is then oxidized to hydroxyclavatol by the nonheme Fe^{II}/2-OG-dependent oxygenase ClaD. Alongside with spontaneous dehydration of hydroxyclavatol to the reactive intermediate *ortho*-quinone methide (QM), nonenzymatic 1,4-Michael additions were initiated by the nucleophilic attack from the γ-butyrolactones to the *ortho*-QMs, leading to the sequential formation of peniphenone D and penilactone A as well as penilactones D and B.

In addition to utilizing enzymes from the natural biosynthetic machinery, an alternative strategy was used for structural diversification by taking advantage of reactive intermediates from the biosynthetic pathway of natural products. As mentioned above, the *ortho*-QM involved in the formation of peniphenone and penilactones was proven to be highly reactive and capable of reacting with γ-butyrolactones spontaneously under very mild conditions. As a following work, the reactivity of the *ortho*-QM derived from hydroxyclavatol was tested with 101 natural products or natural product-like compounds. These include flavonoids, hydroxynaphthalenes, coumarins, xanthones, anthraquinones, phloroglucinols, phenolic acids, indole derivatives, tyrosine analogues, and quinolines. LC-MS analysis revealed product formation in the incubation mixtures of 85 tested reactants. 32 clavatol-containing products were isolated from 23 selected incubations and identified by NMR and MS analyses. The cross-coupling between the tested nucleophiles and the *ortho*-QM from hydroxyclavatol occurs preferentially *via* C-C bonds at the *ortho*- or *para*-position of phenolic hydroxyl groups and the C-2 position of the indole ring. The obtained products were also tested for their biological activities. This study proved the *ortho*-QM as an excellent Michael acceptor for a variety of substances, suggesting the utilization of the reactive biosynthetic intermediate for accessing chemical diversity of natural products.

Zusammenfassung

Sekundärmetabolite sind im Allgemeinen niedermolekulare Verbindungen, die auch als Naturstoffe bezeichnet werden. Bisher wurden in der Natur Millionen von Naturstoffen mit bemerkenswerter struktureller Vielfalt gefunden. Dazu zählen unter anderem, aber nicht ausschließlich, Polyketide, nichtribosomale Peptide, Alkaloide und Terpenoide. Die strukturelle Divergenz von Naturstoffen beginnt mit der Bildung von Grundgerüsten durch verschiedene Rückgratenzyme unter Verwendung grundlegender Bausteine aus dem Primärstoffwechsel. Die Weiterverarbeitungen der Grundstrukturen werden durch modifizierende Enzyme wie Oxidoreduktasen und Transferasen katalysiert, wodurch die Biosynthese von Endprodukten mit großer Vielfalt und Komplexität abgeschlossen wird. Enzyme aus Naturstoffbiosynthesewegen sind aufgrund ihrer hohen Effizienz und Spezifität vielseitige Biokatalysatoren. Die Nutzung des biokatalytischen Potenzials von Enzymen durch chemoenzymatische Synthese hat sich als nützliches Mittel zur Erweiterung chemischer Bibliotheken erwiesen. Neben der enzymatischen Katalyse wurde auch das Auftreten nichtenzymatischer Reaktionen während des postbiosynthetischen Prozesses von Naturstoffen festgestellt. Solche Reaktionen treten häufig unter Beteiligung reaktiver Biosynthesezwischenprodukte auf. Die vollständige Nutzung dieser Zwischenprodukte für die chemische Synthese kann als neuartige Strategie zur Erweiterung der Variabilität von Naturstoffen dienen.

In einem Kooperationsprojekt mit Dr. Peter Mai wurden fünf Prenyltransferasen (PTs) der Dimethylallyltryptophan-Synthase (DMATS)-Familie, FtmPT1, BrePT, CdpC2PT, CdpNPT und CdpC3PT, für das Protein-Engineering ausgewählt. Diese PTs katalysieren eine Übertragung regulärer oder reverser Prenylreste (C_5) von Dimethylallyldiphosphat (DMAPP) auf die C-2- oder C-3-Position am Indolylring der cyclischen Dipeptide (CDPs). Um ihre Prenyldonorspezifität von DMAPP auf Geranyldiphosphat (GPP) umzustellen, wurden Gatekeeping-Reste durch Sequenzvergleich der fünf PTs mit denen von AtaPT und FgaPT2 identifiziert, nämlich Met364 in FtmPT1, Ile337 in BrePT, Thr351 in CdpC2PT, Met349 in CdpNPT und Phe335 in CdpC3PT. Das Ersetzen dieser Schlüsselaminosäuren durch Glycin führte zur Erstellung von FtmPT1_M364G, BrePT_I337G, CdpC2PT_T351G, CdpNPT_M349G und CdpC3PT_F335G Mutanten. Diese Mutanten zeigten eine deutlich verbesserte Aktivität gegenüber GPP, aber eine verringerte Aktivität mit DMAPP. Daraufhin wurden 42 geranylierte Derivate aus den Inkubationen der erzeugten Mutanten mit 15 getesteten CDPs in Gegenwart von GPP erhalten und deren Strukturen wurden mittels NMR- und MS aufgeklärt. Bei Verwendung von *cyclo*-L-Trp-L-Trp als Akzeptor und GPP als Donor kann der Transfer von Geranylresten auf alle sieben möglichen Positionen des Indolrings durch die modifizierten Enzyme erreicht werden. Vor unserer Studie wurde nur über eine geringe Anzahl geranylierter Indolderivate berichtet. Diese Studie erhöhte signifikant die strukturelle Vielfalt geranylierter Produkte durch strukturbasiertes Protein-Engineering verfügbarer Dimethylallyltransferasen.

In einer Kooperation mit Dr. Jie Fan wurde die Biosynthese von Peniphenon und Penilactonen in *Penicillium crustosum* PRB-2 aufgeklärt, wobei das Auftreten sowohl enzymatischer als auch nichtenzymatischer Reaktionen während ihrer Bildung festgestellt wurde. Der PKS-NRPS-Hybrid TraA aus dem Terrestric acid-Gencluster ist an der Bildung von Crustosic acid beteiligt, die durch die nicht-Häm-Fe^{II}/α-KG-abhängige Oxygenase TraH decarboxyliert und anschließend durch die flavinhaltige Oxidoreduktase TraD zu Terrestric acid reduziert wird. Beide Säuren sind Vorstufen der γ-Butyrolactone. Die nicht-reduzierende PKS ClaF aus dem Clavatolcluster ist für die Bildung von Clavatol verantwortlich, das dann durch die nicht-Häm-Fe^{II}/ α-KG-abhängige Oxygenase ClaD zu Hydroxyclavatol oxidiert wird. Nach spontaner Wasserabspaltung wird Hydroxyclavatol zum reaktiven Intermediat *ortho*-Chinonmethid (QM) überführt, das durch den nukleophilen Angriff der γ-Butyrolactone nichtenzymatische 1,4-Michael-Additionen initiiert. Dies führte zur aufeinanderfolgenden Bildung von Peniphenon D und Penilacton A sowie Penilacton D und B.

Zusätzlich zur Verwendung von Enzymen aus natürlichen Biosynthesewegen wurde eine alternative Strategie zur strukturellen Diversifizierung verwendet, indem reaktive Zwischenprodukte aus dem Biosyntheseweg von Naturstoffen genutzt wurden. Wie oben erwähnt, erwies sich das an der Bildung von Peniphenonen und Penilactonen beteiligte *ortho*-QM als hochreaktiv und ist in der Lage, unter sehr milden Bedingungen spontan mit γ-Butyrolactonen zu reagieren. In der folgenden Arbeit wurde die Reaktivität des von Hydroxyclavatol abgeleiteten *ortho*-QM mit 101 Naturstoffen oder naturstoffähnlichen Verbindungen getestet. Dazu gehören Flavonoide, Hydroxynaphthaline, Cumarine, Xanthone, Anthrachinone, Phloroglucine, Phenolsäuren, Indolderivate, Tyrosinanaloga und Chinoline. Die LC-MS-Analyse ergab eine Produktbildung in den Inkubationen mit 85 getesteten Verbindungen. 32 Clavatol-haltige Produkte wurden aus 23 ausgewählten Inkubationen isoliert und mittels NMR- und MS-Analyse identifiziert. Die Verknüpfungen zwischen den getesteten Nukleophilen und dem *ortho*-QM aus Hydroxyclavatol erfolgt bevorzugt über C-C-Bindungen an der *ortho*- oder *para*-Position von phenolischen Hydroxylgruppen und der C-2-Positionen des Indolrings. Die erhaltenen Produkte wurden auch auf ihre biologischen Aktivitäten getestet. Diese Studie beweist, dass das *ortho*-QM ein ausgezeichneter Michael-Akzeptor für eine Vielzahl von Substanzen ist, was die Verwendung des reaktiven Biosynthesezwischenprodukts für den Zugriff zur chemischen Vielfalt von Naturstoffen nahelegt.

1 Introduction

1.1 Natural products from filamentous fungi

The definition of natural products could be broadly used to describe compounds derived from a natural source. However, it is more specific to define natural products as low-molecule-mass compounds from secondary metabolite pathways.[1] From this point of view, natural products can also be termed as secondary metabolites (SMs). These compounds are not essential for the growth, development, and reproduction of the producing organism,[2, 3] but play important roles, for example, as chemical signals for communication,[4, 5] in defending the habitat or inhibiting the growth of competitors.[6-9]

Plants and microorganisms including prokaryotic actinobacteria and eukaryotic ascomycetes are the most frequent producers of biologically active natural products.[10-12] Among them, filamentous fungi serve as a representative and valuable source of fungal natural products. *Aspergillus*, *Penicillium*, *Fusarium*, and *Claviceps* are prominent genera of filamentous fungi growing in a polar fashion (extending in one direction) by elongation at the apex of the hypha, the so-called mycelium.[13] The filamentous fungi reproduce themselves either by the formation of conidia which are borne on specialized stalks called conidiophores, or by the formation of ascospores which are produced in specialized tube- or sac-like cells termed asci.[14, 15]

Driven by the discovery of penicillin and its development into an antibiotic, great progress has been achieved for the isolation and chemical characterization of a multitude of natural products from microorganisms in the last decades.[16-18] Up to the year 2017, over 230,000 natural products were listed in the *Dictionary of Natural Products*.[19, 20] Microbial metabolites are one of the most important constitution of reported natural products. Among them, approximately 45 % of microbial metabolites are produced by various fungi, especially filamentous fungi, underlying their importance as natural product sources.[10]

The classical strategy for the discovery of fungal natural products is mostly based on the adjustment of the cultivation condition, such as different medium with various nutrition or additives, different incubation time or temperature, different pH values, and so on. The following work flow to explore SMs from fungi includes extraction of the cultures by using solvents of different polarity, fractionation of the crude extracts by using column chromatography, as well as structural elucidation of purified compounds by spectral analysis (**Figure 1A**). However, rapid developments in sequencing technologies and bioinformatic analysis have revealed that a large amount of fungal biosynthetic gene clusters are not expressed or only lowly expressed under laboratory culture conditions, suggesting a plethora of fungal natural products awaiting to be discovered and exploited.[3, 21, 22] Therefore, new methods as shown in **Figure 1B** have been developed for the discovery of the hidden fungal natural products. These methods include epigenetic regulation,[23-25] global regulator[26-29] or pathway-specific regulator activation,[30-33] and heterologous expression in other hosts.[34-37]

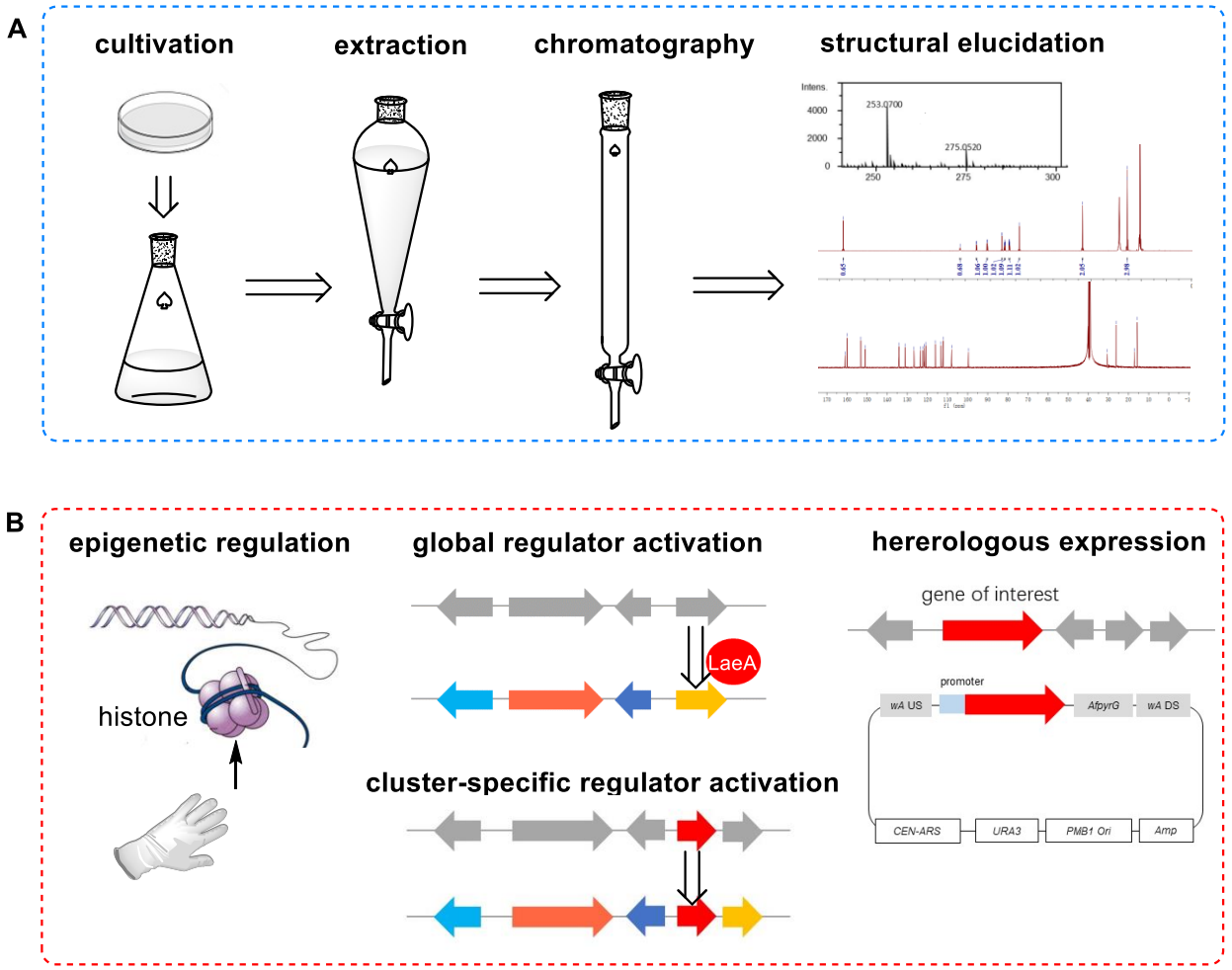

Figure 1. Work flow for isolation and identification of fungal natural products (A). Molecular strategies for activating silent biosynthetic gene clusters (B).

The majority of so far discovered fungal natural products can be roughly classified into four categories: polyketides, nonribosomal peptides, terpenoids, and alkaloids. Furthermore, hybrid products of two or more main classes have also been found in fungi, such as hybrid polyketide-nonribosomal peptides and hybrid polyketide-terpenes (**Figure 2**).[38]

Polyketides are a large group of structurally diverse and therapeutically important natural products. These compounds are usually biosynthesized by successive Claisen condensations between a malonate derivative and an acyl starter.[39] Representatives of polyketide are shown in **Figure 2**. Among them, patulin is a well-studied mycotoxin produced by a variety of molds and induces immunological, neurological, and gastrointestinal effects.[40, 41] The biosynthetic precursor of patulin is 6-methylsalicylic acid (6-MSA), one of the oldest known polyketides mainly found in *Penicillium* species.[42] Orsellinic acid is also an acetate-derived tetraketide similar to 6-MSA but it harbors an additional hydroxyl group. It was proven that orsellinic acid is the biosynthetic precursor of the cathepsin K inhibitors F9775 A and B.[43] Aflatoxin B_1, with its name derived from *Aspergillus flavus* toxin, is synthesized from its

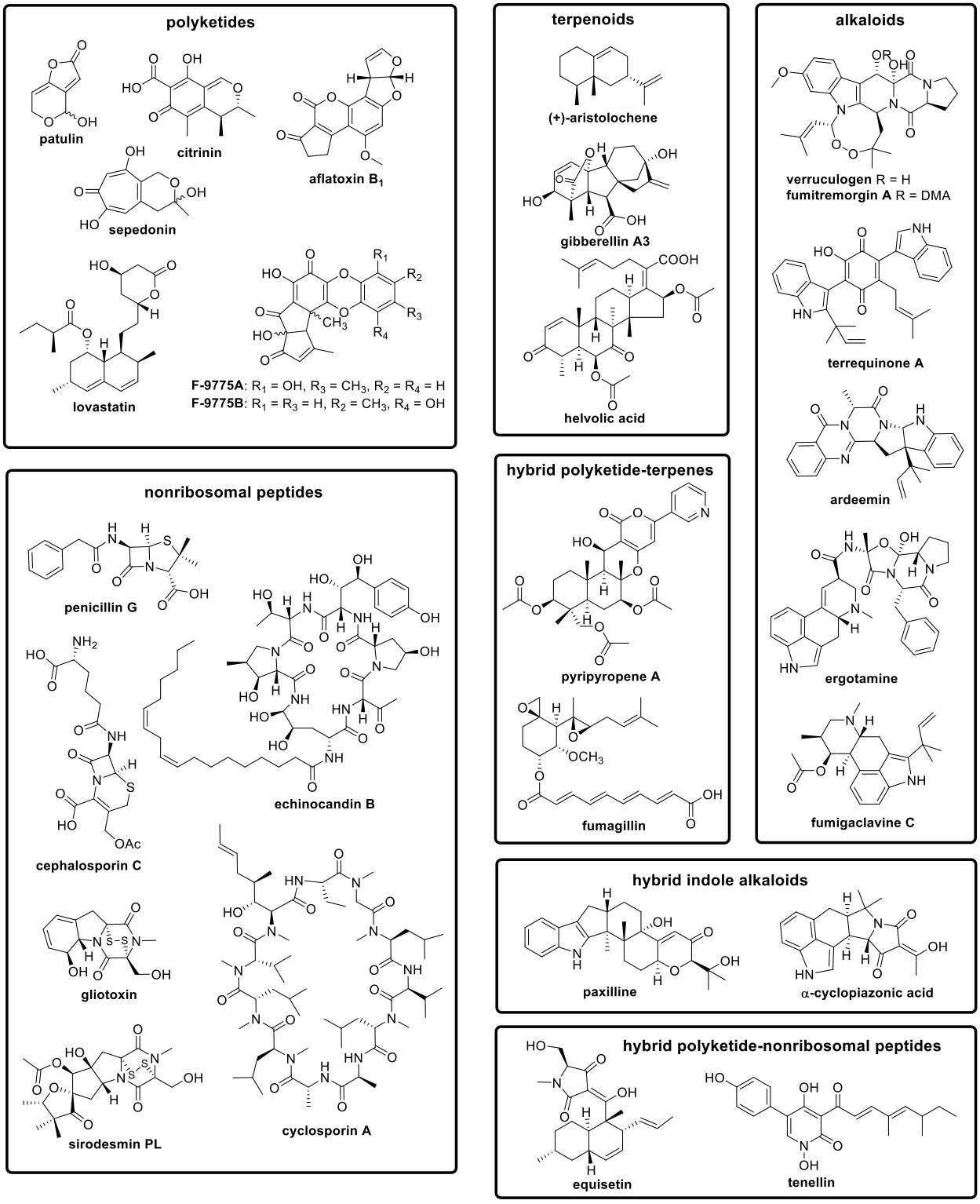

Figure 2. Representatives of fungal natural products

polyketide precursor norsolorinic acid *via* sterigmatocystin (the penultimate intermediate of aflatoxin) as a metabolic intermediate.[44-46] Citrinin is a potent mycotoxin with nephrotoxic activities and was firstly isolated from a culture of *Penicillium citrinum*.[47, 48] It is interesting that citrinin and sepedonin share similar biosynthetic precursors, but afterwards distinct modifications lead to the obvious differences in their structures.[49] Lovastatin, also known as mevinolin, was isolated from *Aspergillus terreus* in 1978 and developed into a clinically used drug to treat hypercholesterolemia.[50, 51] The structure of lovastatin is featured by the fused ring of the decalin system, which is formed by the Diels-Alder cycloaddition of a hexaketide.[52]

The second group of fungal natural products is nonribosomal peptides with large structural and functional diversities (**Figure 2**). The biosynthesis of nonribosomal peptides is similar to polyketides to some extent, but differs in the elongation step by C-N rather than C-C bond formation and by utilizing amino acids instead of acyl-CoA as building blocks.[53] β-Lactams are one of the most famous structural types among the so far identified nonribosomal peptides. Penicillin G from *Penicillium* fungi was a representative β-lactam antibiotic which has been applied to the treatment of bacterial infections and set a start of the golden age of researches on antibiotics.[54, 55] Cephalosporin C from *Cephalosporium acremonium* is another β-lactam antibiotic discovered after penicillin.[56] Gliotoxin from *Aspergillus fumigatus* contains a characteristic internal sulfur bridge, which is the structural motif of all epipolythiodioxopiperazines (ETPs).[57, 58] Sirodesmin PL from *Leptosphaeria maculans* also harbors such a unique sulfur bridge.[59] Furthermore, head-to-tail-cyclized peptides with large ring sizes include echinocandin B from *Aspergillus nidulans* with a linoleoyl side chain[60] and the immunosuppressant cyclosporin A from *Tolypocladium inflatum*.[61] The structure of cyclosporin A is featured by containing one D-configured alanine and two nonproteinogenic residues: L-aminobutyric acid and butenyl-methyl-L-threonine.

The third major group of fungal metabolites is undoubtedly terpenoids which can be typically classified as monoterpenes (C_{10}), sesquiterpenes (C_{15}), diterpenes (C_{20}), and triterpenes (C_{30}) (**Figure 2**). Despite the structural diversity, fungal terpenoids are biosynthetically originated from the C_5 units: dimethylallyl diphosphate (DMAPP) and isopentenyl diphosphate (IPP).[62] Head-to-tail condensation of DMAPP with two or three IPP moieties give farnesyl diphosphate (FPP) as the precursor of sesquiterpenoids and geranylgeranyl diphosphate (GGPP) as the precursor of diterpenoids. (+)-Aristolochene from *Penicillium roqueforti*[63] is a representative sesquiterpenoid that provides a biosynthetic scaffold for several mycotoxins including the sporogen-AO1,[64] PR-toxin,[65] and phomenone.[66] Gibberellin A3 as a typical example of diterpenoids is one of the longest-known classes of plant growth hormone.[67] Condensation of two FPP units in a head-to-head mode yields squalene as the precursor of triterpenoids. Helvolic acid isolated from *Cephalosporium caerulens* and *Aspergillus fumigatus* is an example of fungal triterpenoids exhibiting potent activity against gram-positive bacteria.[68, 69]

Moreover, alkaloids represent one of the largest classes of nitrogen-containing secondary metabolites in fungi (**Figure 2**). A major subgroup is dipeptidyl or tripeptidyl indole alkaloids.[70] Cyclic dipeptides (CDPs) with a characteristic diketopiperazines core structure are formed by condensation of two amino acids.[71] Verruculogen and its isoprenyl derivative fumitremorgin A are typical examples of

diketopiperazine that biosynthetically originated from brevianamide F by condensation of L-tryptophan and L-proline.[72, 73] Unlike diketopiperazines, terrequinone A from *Aspergillus nidulans* is biosynthetically derived from indole pyruvic acid instead of L-tryptophan, leading to a non-peptidic, homocyclic quinone core.[28, 74] Tripeptidyl indole alkaloids exemplified by ardeemin from *Aspergillus fischeri* was biosynthesized with the incorporation of anthranilic acid, L-alanine, and L-tryptophan.[75] In addition to the peptidyl indole alkaloids, ergot alkaloids featured by a tetracyclic ergoline ring system are also an important group of fungal alkaloids.[76, 77] Typical examples include lysergic acid derivatives like fumigaclavine C from *Aspergillus fumigatus*[78] and ergotamine produced by *Claviceps purpurea*,[79] which is structurally assembled from D-lysergic acid with L-alanine, L-phenylalanine, and L-proline.

Furthermore, hybrid products constructed by moieties of mixed origins have also been found in fungi (**Figure 2**). Examples of hybrid indole alkaloids include α-cyclopiazonic acid as an indole-polyketide hybrid which is biosynthesized *via* a *cyclo*-acetoacetyl-L-tryptophan intermediate in *Aspergillus flavus*,[80] as well as indole-diterpenoid hybrids comprising an indole ring and a GGPP-derived terpenoid moiety as exampled by paxilline from *Penicillium paxilli*.[81] Examples of polyketide-nonribosomal peptide hybrid compounds include tenellin from *Beauveria bassiana*[82] consisting of tyrosine and a polyketide-derived C_{12} unit and equisetin from *Fusarium heterosporum*[83] harboring a polyketide-derived decalin ring and an amino acid-derived tetramic acid ring. Further examples of polyketide-terpene hybrid compounds (meroterpenes) include pyripyropene A from *Aspergillus fumigatus* which used nicotinic acid, malonyl-CoA, and FPP as building blocks,[84, 85] as well as fumagillin from *Aspergillus fumigatus* containing an unsaturated chain as the polyketide portion and an modified terpenoid moiety originated from FPP.[86]

Although hundreds of thousands of compounds have been isolated and identified from fungi so far, what we have exploited is still just the tip of the iceberg of the treasure of natural products. Continuing efforts made by researches of different disciplines provide greater possibilities to, i) discover new compounds from either new identified species or existed known species; ii) expand our knowledge of chemical logic and enzymatic machinery of natural product biosynthesis; iii) broaden the applications of natural products in pharmaceutical industry and therefore benefits human being in every aspects.

1.2 Backbone enzymes responsible for the fundamental formation of natural products

The biosynthetic genes in fungi for the formation of a given natural product are typically located together on the genome. Such clusters usually consist of one or more backbone gene(s) as well as several genes for modifications.[87, 88] The backbone enzymes involved in the biosynthesis of fungal natural products generally include polyketide synthases (PKSs), nonribosomal peptide synthetases (NRPSs), terpene cyclases (TCs), and hybrid polyketide synthase-nonribosomal peptides synthetases (hybrid PKS-NRPSs). These enzymes usually catalyze the first step of biosynthesis to form a scaffold, which is afterwards modified by cluster-specific modifying enzymes in multiple biosynthetic steps to produce the final product.

1.2.1 Polyketide synthases

The biosynthesis of polyketides is catalyzed by PKSs in a manner reminiscent of fatty acid synthesis, building a network between primary and secondary metabolic pathways.[89] PKSs can be classified into three types according to their domain composition. Type I PKSs are large multifunctional proteins that can be further divided into iterative type I PKSs and modular type I PKSs.[89, 90] In modular type I PKSs, domains are organized into several modules with each module catalyzing one step of condensation. While in iterative type I PKSs, domains are clustered in a single module which used repeatedly for polyketide formation (**Figure 3**).[91] Iterative type I PKSs can be further divided into nonreducing PKSs (NR-PKSs), partially reducing PKSs (PR-PKSs), and highly reducing PKSs (HR-PKSs) based on the existence of domains that can catalyze the reduction and dehydration steps. Type II PKSs are dissociable multi-enzyme complexes that have sets of iteratively used individual proteins and typically produce polycyclic aromatic compounds (**Figure 3**).[92] Different from type I and type II PKS relatives, PKSs of type III are simple homodimer ketosynthases (KS) that mainly catalyze the formation of pyrone- and resorcinol-type aromatic polyketides (**Figure 3**).[93, 94]

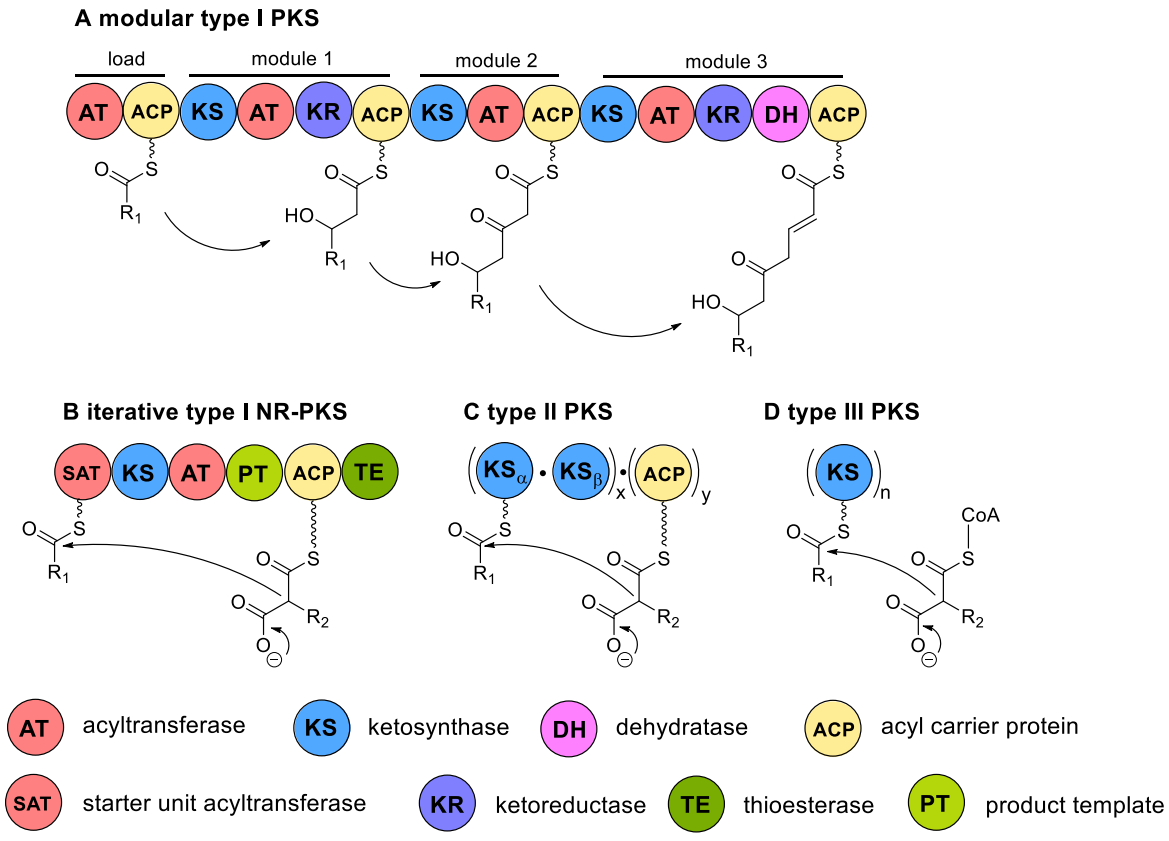

Figure 3. Domain structures of modular type I PKS (A), iterative type I NR-PKS (B), type II PKS (C), and type III PKS (D).

Fungal polyketides are, in most cases, products of iterative type I PKSs. The formation of polyketides catalyzed by PKSs commences with starter unit loading, followed by chain elongation and reduction, finalizing through polyketide cyclization and release. The basic domains required for polyketide

elongation include KS for catalyzing the decarboxylative Claisen condensation to extend the polyketide chain, acyltransferase (AT) for selection and recognition of the starter unit and extender unit, and acyl carrier protein (ACP) which shuttle growing polyketides between the active sites of the PKS. In addition to the minimal domain architecture of KS, AT, and ACP domains, further accessory domains for polyketide chain modification include ketoreductase (KR) domain for optional reduction of the β-keto to a hydroxyl group, dehydratase (DH) domain that catalyzes dehydration to generate an α,β-unsaturated thioester, and enoylreductase (ER) domain that further reduces the double bond to a saturated moiety.[90, 95]

The vast diversity and complexity of polyketides can be ascribed to the following strategies that are utilized by PKSs during the assembly process. Firstly, utilization of different starter and extender units by PKSs leads to the variation of polyketide skeletons. Examples of starter units are acetyl-CoA, propionyl-CoA, malonyl-CoA, benzoyl-CoA, and 4-coumaroyl-CoA. Extender units include malonyl-CoA, (2*S*)-methylmalonyl-CoA, (2*S*)-ethylmalonyl-CoA and chloroethylmalonyl-CoA.[95, 96] Secondly, PKSs employ different reduction domains to form polyketide chains with different unsaturation degree.[97] For example, a KR domain is required to reduce the β-keto group to β-hydroxyl group, an additional DH domain can transform the β-hydroxyl group to a double bond, and KR-DH-ER tridomain can catalyze a further reduction step to form a single bond. Thirdly, different cyclization mechanisms contribute to the polyketide variety, *e.g.* cyclization regioselectivity of the polyketide backbone controlled by product template (PT) domain or C-terminus thioesterase/Claisen-like-cyclase (TE/CLC) in fungal NR-PKSs.[98] In recent years, combinatorial biosynthesis was used as a new approach to generate large libraries of new compounds.[99] Such strategies include engineering modular PKSs by swapping and replacing PKS single domain or entire modules. For example, insertion of AT domains with altered specificity to incorporate a different starter or extender unit is proved to be an effective way to alter the structure of polyketides.[100, 101]

1.2.2 Nonribosomal peptide synthetases

The enzymatic machinery of NRPSs uses parallel chemical logic as PKSs to produce a wide range of nonribosomal peptides.[1] The NRPS action can occur in linear, iterative, and nonlinear modes.[53, 102] The domains of linear NRPSs are organized into modules and each module is used only once during the biosynthetic cycle. Therefore, the number of modules in linear NRPSs decides the number of amino acids incorporated in the released products. The modular architecture of linear system is typical for NRPSs, while iterative and nonlinear modes have been relatively rare reported. Iterative NRPSs repeatedly use the entire assembly line or certain modules until the biosynthetic process is finished. As a further variation of the iterative mode, domain composition of nonlinear NRPSs does not have a straightforward correlation with the sequence of catalytic steps, it reuses a certain domain instead of an entire module during the nonribosomal peptide biosynthesis.[102] Domain structures of apicidin synthetase APS1[103] as a linear NRPS, beauvericin synthetase BbBEAS[104] as an iterative NRPS, and vibriobactin synthetase VibF[105] as a nonlinear NPRS are shown in **Figure 4A**.

The minimal catalytic domains for peptide extension include adenylation (A), condensation (C), and thiolation (T) domain, which also known as peptidyl carrier protein (PCP). The A domain selects the

amino acid, activates it as the aminoacyl-AMP, and loads it onto the adjacent PCP domain.[106] The C domain catalyzes peptide bond formation between PCP-bound substrates. The amine of the incoming downstream aminoacyl-PCP attacks the thioester carbonyl of the elongating peptidyl chain to form a new peptide bond (**Figure 4B**).[107] During the elongation process, the PCP domain plays an important role in chain transfer from upstream to downstream and shuttling the aminoacyl-thioester intermediates between the A and C domains.[108] In addition to the minimal A-T-C domain architecture, extra domains required for the biosynthesis of nonribosomal peptides include the heterocyclization (Cy) as a variant of the C domain that catalyzes the cyclization/dehydration to form a thiazoline or oxazoline structure, the epimerization (E) domain to epimerize the L-configured amino acids into their D-form, and the thioesterase (TE) domain that releases the completed nonribosomal peptide from the assembly line.[109] TE domains exist commonly in bacterial NRPS, while not necessarily in fungal NRPS, which can alternatively use the terminal C domain to perform the cyclization.[110]

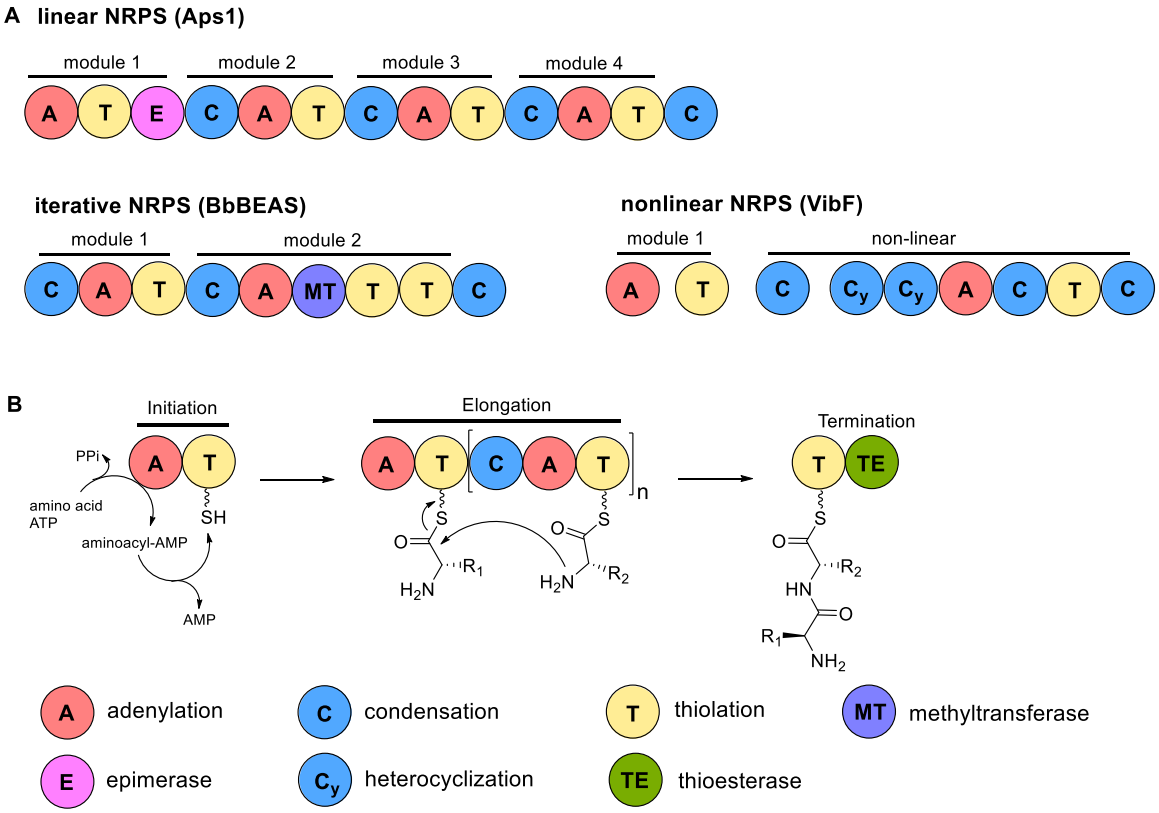

Figure 4. Domain structures of linear, iterative, and nonlinear NRPS (A). General reaction mechanism of NRPSs (B).

The structural abundance of NRPs in nature is partly due to the relaxed substrate specificity of NRPSs towards not only hundreds of nonproteinogenic amino acids but also fatty acids, β-amino acids and α-hydroxy acids.[111] Besides, on-assembly or post-assembly line modifications including epimerization, N-methylation, formylation, glycosylation and oxidation,[102] as well as different chain release actions such as hydrolysis, macrocyclization, and the C-terminal reduction release, also contribute to the diversity of nonribosomal peptides. Furthermore, redesigning an NRPS machinery is also a promising

option for the construction of new nonribosomal peptides. One representative example is engineering of the NRPS in the daptomycin biosynthetic pathway by exchanging single and multiple modules to produce a library of new daptomycin analogues.[112]

1.2.3 Polyketide synthase-nonribosomal peptide synthetases

One smart strategy that nature employed to diversify natural products is the creation of hybrid structures by PKS–NRPS or NRPS-PKS hybrid assembly lines. As aforementioned, PKSs construct polyketides *via* C-C bond formation by using acetic acid-type acyl building blocks, while NRPSs catalyze the production of peptides by C-N bond formation between amino acids. Both PKSs and NRPSs use carrier proteins to tether the growing chain, *i.e.* ACP for PKSs and PCP for NRPSs, which facilitate the transfer of distinct biosynthetic intermediates between heterologous subunits.[113]

In PKS-NRPS assembly lines, the ACP domain of PKS and the C domain of NRPS are critical for PKS-NRPS modular interaction. The NRPS C domain catalyzes the amide formation between the elongated polyketide chain attached at the upstream PKS ACP domain and the aminoacyl group tethered to the PCP domain of the same NRPS module.[113] Representative examples of fungal PKS-NRPS hybrid enzymes are aspyridone A synthetase ApdA incorporating L-tyrosine with the polyketide chain (**Figure 5A**)[114] and α-cyclopiazonic acid synthetase CpaS incorporating L-tryptophan with a polyketide moiety (**Figure 5A**),[115] as well as CheA and CcsA for the formation of the cytochalasan-type compounds chaetoglobosin A[116] and cytochalasin E,[117] respectively. Other examples include fusarin C synthetase FUSS,[118] equisetin synthetase EqiS,[83] tenellin synthetase TenS,[119] pseurotin A synthetase PsoA,[120] xyrrolin synthetase Pks3,[121] and desmethylbassianin synthetase DMBS.[122] Carlosic acid synthetase CaaA differs from the above-mentioned hybrid enzymes by accepting L-malic acid instead of an amino acid as substrate.[30] Sequence alignments revealed that the conserved aspartic acid (D235 in PheA), which is reported to stabilize the α-amino group in amino acid-utilizing PKS-NRPS enzymes,[106, 123] is replaced by an asparagine residue in CaaA.[30]

In NRPS-PKS assembly lines, the PCP domain of NRPS and the KS domain of PKS play an important role in the interaction of NRPS and PKS module. In this case, after receiving the aminoacyl chain from the PCP domain of the upstream NRPS module, the KS domain of PKS module catalyzes the C-C bond formation between the aminoacyl chain and the malonyl-type extender unit attached to the ACP domain of the same PKS module.[113] In contrast to PKS-NRPS hybrid enzymes, NRPS-PKS hybrid enzymes have been commonly reported in bacteria, but are relatively rare in fungi. TAS1 is the first hybrid NRPS-PKS reported from fungi catalyzing the formation of tenuazonic acid (**Figure 5B**).[124] It consists of a NRPS module and a sole KS domain at C-terminus. The TAS1 KS domain was proposed to be responsible for the product release, which is an atypical function of a KS domain.[124] Another newly identified NRPS-PKS enzyme is AnATPKS involved in the biosynthesis of the α-pyrone-containing compound pyrophen (**Figure 5B**).[125] Different from TAS1, the NRPS part of AnATPKS is composed of A domain and PCP domain for the recognition and activation of L-phenylalanine, and the PKS part consists of KS-AT-ACP as minimal domain to perform two rounds of chain elongation.[125]

In recent years, recombination of dissociated PKS and NRPS modules is a new fashion to create novel polyketide-nonribosomal peptide hybrid products. For example, both ApdA and CpaS are PKS-NRPS

hybrid enzymes as mentioned above. Coexpression of the PKS module of ApdA and the NRPS module of CpaS together with the enoylreductase ApdC in *Saccharomyces cerevisiae* led to the production of a preaspyridone analog with L-Trp instead of L-Tyr incorporation (**Figure 5C**).[126] This study presented a successful example of functional recombination of heterologous PKS and NRPS modules. Therefore, the application of recombinant gene fragments on hybrid assembly lines provides more possibilities to produce hybrid scaffolds with increased diversity and complexity.

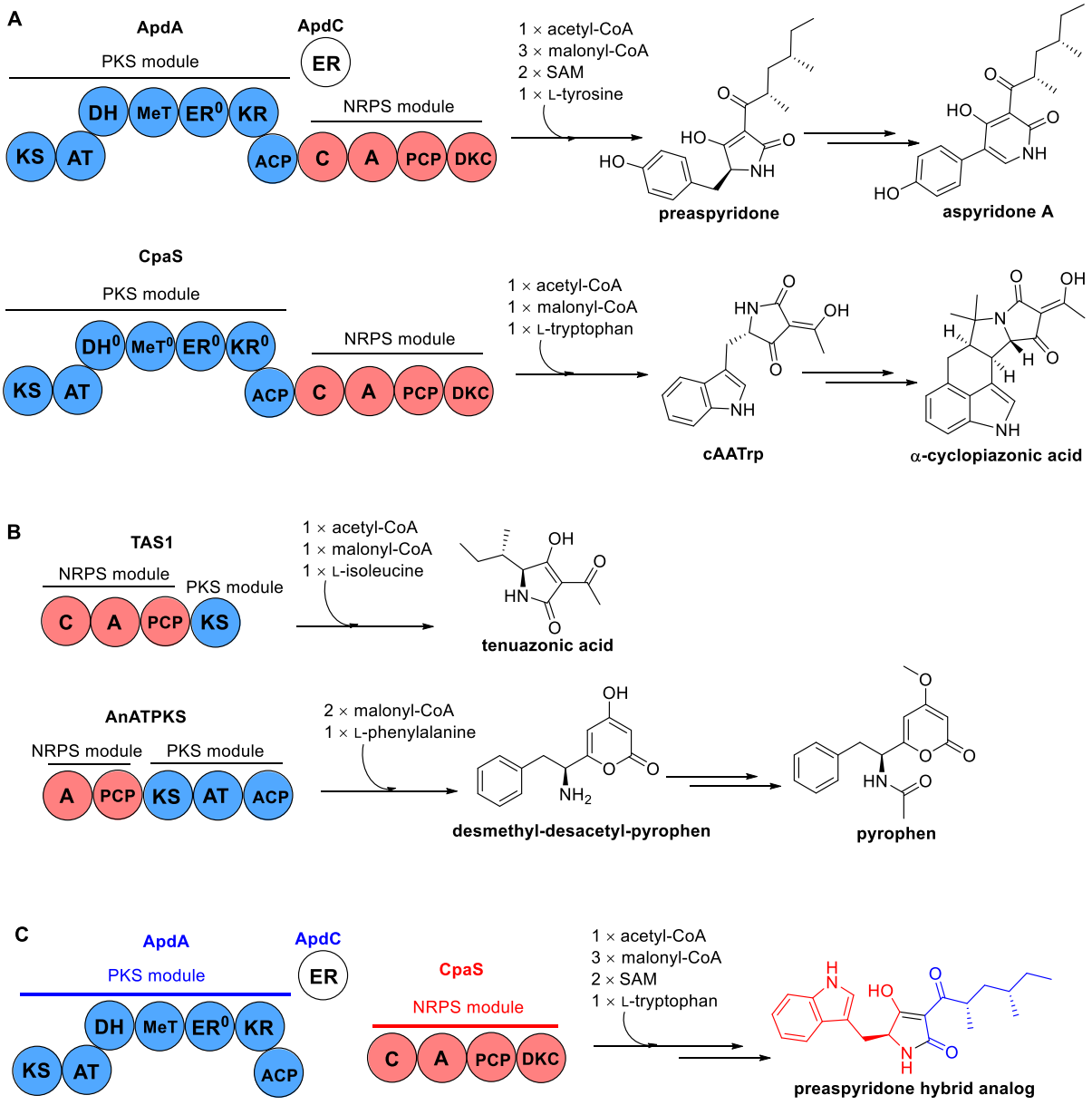

Figure 5. Representatives of fungal hybrid PKS-NRPS (A) and NRPS-PKS (B). Recombination of ApdA PKS module with CpaS NRPS module as an example for new hybrid product formation (C).

1.3 Post-assembly line modifications in natural product biosynthesis

In fungal biosynthetic gene clusters, the backbone genes are usually surrounded by several genes coding for modification enzymes including prenyltransferases (PTs), nonheme Fe^{II}/2-oxoglutarate (Fe^{II}/2-OG)-dependent oxygenases, flavin-containing oxidoreductases, cytochrome P450 monooxygenases. Therefore, once the scaffold is synthesized by a backbone enzyme, it can be further diversified by subsequent oxidation, reduction, rearrangement, and transfer reactions.

1.3.1 Prenyltransferases

Prenylation reactions occur commonly in nature, leading to a wide range of prenylated natural products with various biological activities.[127] PTs are responsible for the catalyzation of prenyl transfer reaction from different prenyl moieties (n × C_5) to various acceptors including nucleic acids and proteins, as well as aliphatic and aromatic molecules of low-molecular-weight.[128] Prenylation of small aromatic compounds is catalyzed by PTs generally belonging to UbiA-type, CloQ/NphB-type, and dimethylallyltryptophan synthase (DMATS)-type.[129]

UbiA-type PTs are membrane-bound enzymes and involved in the biosynthesis of both primary metabolites such as ubiquinones and menaquinones and secondary metabolites such as bitter acids and aurachins.[130] Members of this family are named after UbiA from *Escherichia coli* and possess a conserved (N/D)DXXD motif.[131, 132] They require metal ions such as Mg^{2+} for their catalytic activity.[133] PTs of CloQ/NphB-type and DMATS-type are soluble proteins with a characteristic $\alpha\beta\beta\alpha$ folds, termed PT-barrel, and most of them can function ion-independently.[134] The eponym for CloQ/NphB group is due to the first identified enzyme CloQ[135] involved in the biosynthesis of clorobiocin and later NphB[136] involved in the biosynthesis of the naphterpin derivatives.

PTs belonging to the DMATS superfamily have been intensively investigated in biochemistry, molecular biology, and structural biology during the past decades.[134] They catalyze the prenylation of aromatic substrates, mainly of indole derivatives, at either the first pathway-specific step or the later tailoring steps.[134, 137] One of the characteristics of DMATS enzyme is their substrate flexibility towards a broad spectrum of aromatic compounds. Conversion of indole derivatives, cyclic dipeptides, tyrosine derivatives, flavonoids, xanthones and hydroxynaphthalenes, to their prenylated derivatives are catalyzed by PTs of the DMATS type.[138] The first member of the DMATS superfamily is DmaW (4-DMATS) identified in the ergot alkaloid gene cluster in *Claviceps fusiformis*.[139] Later, FgaPT2 was identified from *Aspergillus fumigatus* as a ortholog of DmaW.[140] It catalyzes regular transfer of the dimethylallyl (DMA) moiety from DMAPP to the C-4 position of L-tryptophan, which is the first biosynthetic step of fumigaclavine C.[140] Systematic investigation on FgaPT2 has been carried out after its discovery. One of the most important achievement is the identification of the crystal structure of FgaPT2, which provided a theoretical basis for structure-based protein engineering.[141] After that, several other DMATS enzymes catalyzing prenylation of L-tryptophan have been identified from fungi. These include DmaW-Cs,[142] MaPT,[143] 5-DMATS,[144] 6-$DMATS_{Mo}$,[145] 7-DMATS,[146] and 7-$DMATS^{Neo}$ (**Table 1**).[147] In addition to these tryptophan PTs, SirD[148] from *Leptosphaeria maculans* and TyrPT[149] from *Aspergillus niger* are examples of known tyrosine *O*-prenyltransferases (**Table 1**). Another group of PTs of the DMATS superfamily accept tryptophan-containing CDPs as substrates. The first

identified PT of this group was FtmPT1 from *Aspergillus fumigatus*, which catalyzes C2-prenylation of brevianamide F (*cyclo*-L-Trp-L-Pro) as an early step for the biosynthesis of verruculogen/fumitremorgins.[150] Later, more CDP PTs have been found from fungi, such as NotF,[151] BrePT,[152] and CdpC2PT[153] for C2-prenylation; CdpNPT,[154] AnaPT,[155] and CdpC3PT[156] for C3-prenylation; CdpC7PT for C7-prenylation,[157] CTrpPT for both N1- and C7-prenylation (**Table 1**).[158] Furthermore, there are also some members of the DMATS group that transfer prenyl moieties onto other structural skeletons. Examples given in **Table 1** include TdiB,[159] PaxD,[160] XptB,[161] and NscD.[33]

Table 1 Overview of PTs of the DMATS superfamily and their producing organism.

enzyme	organism	product	involved biosynthetic pathway	reference
tryptophan prenyltransferases				
DmaW	*Claviceps fusiformis*	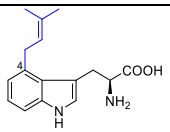	ergot alkaloids	139
FgaPT2	*Aspergillus fumigatus*		fumigaclavine C	140
DmaW-Cs	*Periglandula* sp.		ergot alkaloids	142, 162
MaPT	*Malbranchea aurantiaca*		unknown	143
5-DMATS	*Aspergillus clavatus*	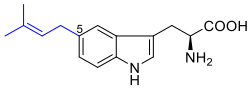	unknown	144
6-DMATS$_{MO}$	*Malbranchea olivasterospora*	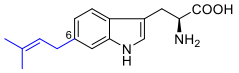	unknown	145
7-DMATS	*Aspergillus fumigatus*	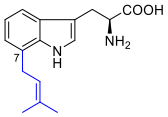	astechrome	146
7-DMATS^{Neo}	*Neosartorya* sp.		unknown	147
tyrosine prenyltransferases				
SirD	*Leptosphaeria maculans*	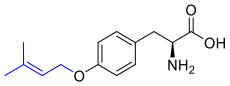	sirodesmin PL	148
TyrPT	*Aspergillus niger*		unknown	149
cyclic dipeptide prenyltransferases				
FtmPT1	*Aspergillus fumigatus*	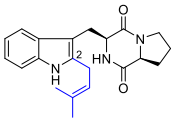	verruculogen/ fumitremorgin	150
NotF	*Aspergillus* sp.	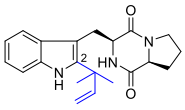	notoamide	151
BrePT	*Aspergillus versicolor*		brevianamide	152
CdpC2PT	*Neosartorya fischeri*	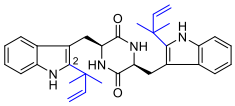	fellutanine	153
CdpNPT	*Aspergillus fumigatus*	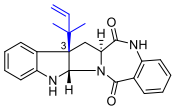	unknown	154
AnaPT	*Neosartorya fischeri*	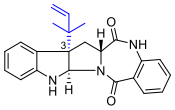	acetylaszonalenin	155

CdpC3PT	*Neosartorya fischeri*	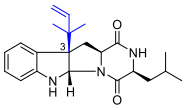	unknown	156
CdpC7PT	*Aspergillus terreus*	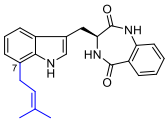	unknown	157
CTrpPT	*Aspergillus oryzae*	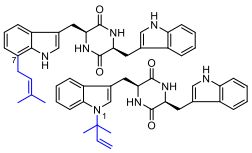	unknown	158
DMATSs of diverse substrates				
TdiB	*Aspergillus nidulans*	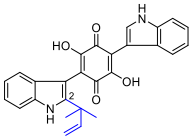	terrequinone A	159
PaxD	*Penicillium paxilli*	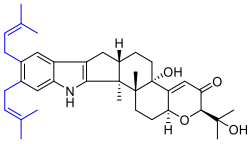	diprenylated paxillin, paspalitrem A	160
XptB	*Aspergillus nidulans*	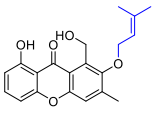	shamixanthone/ epishamixanthone	161
NscD	*Neosartorya fischeri*	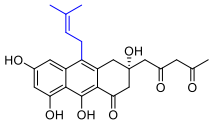	neosartoricin	33

Despite the extremely high abundance of prenylated products in nature, their diversity can be further expanded by using engineered PTs for chemoenzymatic synthesis. Since the crystal structure data of more and more aromatic PTs are available, it is becoming easier to recognize the gatekeeping residues related to the catalytic activities. For example, mutation of the Lys174 residue in FgaPT2 to alanine resulted in reverse C3-prenylation of L-tryptophan instead of regular C4-prenylation by the wild-type (**Scheme 1**).[163] And compared to the weak activity of the wild-type and almost no activity of FgaPT2_K174A towards CDPs, Arg244 mutants of FgaPT2 had increased acceptance of CDPs for regular C4-prenylation (**Scheme 1**).[164] Further combinational mutation on Lys174 and Arg244 yields FgaPT2_K174F_R244X (X = L, N, Q, Y) mutants leading to not only CDPs acceptance but also reverse C3-prenylation on the indole ring (**Scheme 1**).[165] Besides, site-saturation mutagenesis of Met328 in FgaPT2 switched the prenyl donor preference of the mutants from DMAPP to geranyl diphosphate (GPP) (**Scheme 1**).[166] Therefore, these successful engineering on FgaPT2 set examples for achieving extensive acceptance of aromatic substrates and shifted specificity towards prenyl donors, as well as alternative prenylation positions. This confirms structure-based protein engineering as a promising approach for producing new prenylated compounds.

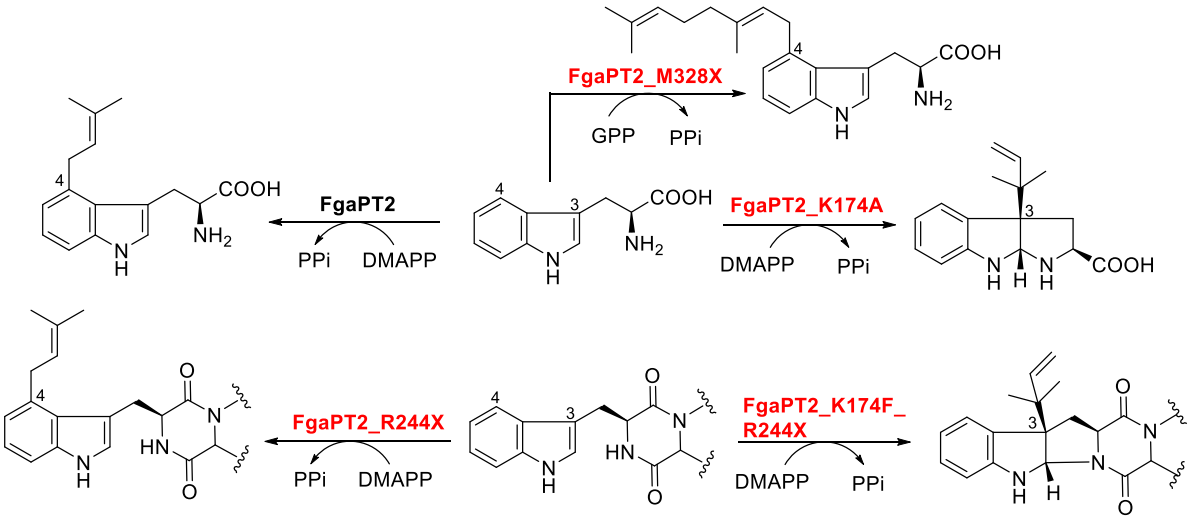

Scheme 1. Prenylation of L-tryptophan by FgaPT2 and the shifted catalytic activities of the mutants

1.3.2 Nonheme Fe^{II}/2-oxoglutarate-dependent oxygenases

Nonheme Fe^{II}/2-OG-dependent oxygenases are tailoring enzymes that decorate the carbon skeletons in the late stage of a given biosynthetic pathway to attain the final framework with an array of functional groups.[167, 168] They possess a conserved double-stranded β-helix fold with a 2-His-1-carboxylate facial triad that coordinates to an iron atom.[169] Three of the six ligands to the iron are occupied by two histidines and an Asp/Glu side chain carboxylate. The fourth and fifth ligands to the iron are mostly provided by the keto group and one of the carboxylate oxygens of 2-oxoglutarate (2-OG), the cosubstrate required for the catalytic activity of this enzyme family.[170] The oxidation step further requires activation of molecular oxygen for incorporation into substrate molecules. This is achieved by displacing one molecule of water (the sixth ligand) to vacate a site for binding with the O_2 molecule. During the catalytic cycle, oxidative decarboxylation of 2-OG releases a high energy Fe^{IV}=O (ferryl) intermediate as a strongly oxidizing agent, which is capable of performing homolysis of unactivated C–H bonds (**Figure 6A**).[168] This in return makes nonheme Fe^{II}/2OG-dependent oxygenases as multifunctional factories to catalyze a vast diversity of oxidative transformations.[168, 170] Examples as shown in **Figure 6B** include hydroxylation by AIP4H involved in the formation of *trans*-4-hydroxy-L-proline,[171] halogenation by AmbO5 for the formation of ambiguine A,[172] oxidative decarboxylation by *P*.IsnB involved in the biosynthesis of rhabduscin,[173] desaturation and spirocyclization by AusE for the construction of preaustinoid A3,[174, 175] epimerization and desaturation by CarC for the formation of (5*R*)-carbapenem,[176, 177] desaturation and epoxidation by AsqJ for the formation of cyclopepnin.[178]

Since the first discovery of nonheme Fe^{II}/2OG-dependent oxygenases in the 1960s, enzymes of this family have grown rapidly in number and variety of chemical reactions, as well as our understanding of catalytic mechanisms. In fungi, the first reported enzymes of this family were those involved in the biosynthesis of β-lactams.[179] Isopenicillin N-synthase (IPNS) represented the first crystal structure for the nonheme iron enzyme family.[180, 181] It is an atypical case that does not require 2-OG as cosubstrate.

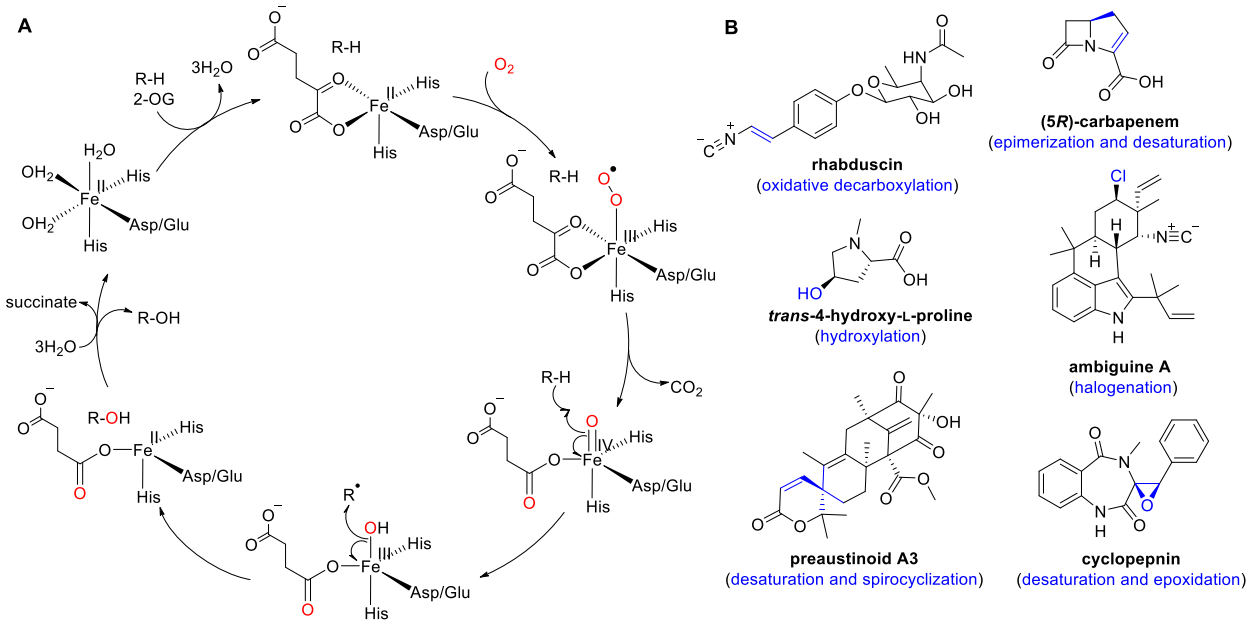

Figure 6. Catalytic mechanism of hydroxylation by nonheme Fe^{II}/2-OG-dependent oxygenases (A), and representative structures that formed with the involvement of nonheme Fe^{II}/2-OG-dependent oxygenases (B).

As shown in **Figure 7A**, an extra glutamine residue chelates the Fe^{II} center in addition to the common 2-His-1-carboxylate facial triad. The mechanism of IPNS was proposed to first proceed through the nucleophilic attack from the deprotonated amide nitrogen to the thioaldehyde to form the four-membered β-lactam ring, followed by attacking of the valinyl radical to the coordinated sulfur atom to form the five-membered thiazolidine ring, thus yielding the unique 4/5 fused ring system.[182] FtmOX1 involved in the biosynthesis of verruculogen is another nonheme Fe^{II}/2OG-dependent enzyme that is worth mentioning. Although biosynthesis of verruculogen was long believed to be formed from endoperoxidation of fumitremorgin B, the mechanism of the endoperoxide formation was not clear until characterization of FtmOX1 in 2009.[183] With the reported crystal structure, the catalytic mechanism of the endoperoxidation was proposed in a way that FtmOX1 probably uses the ferryl-oxo intermediate to first abstract the phenolic hydrogen of the tyrosine residue (Tyr224), then the generated tyrosyl radical abstracts a hydrogen atom from the substrate.[184] However, recent reinvestigation on FtmOX1 revealed that hydrogen donation not abstraction by another tyrosine residue (Tyr68) is involved in the endoperoxide installation.[185] The ferryl complex directly abstracts a hydrogen-atom from C21 of the substrate to generate the substrate radical. After the incorporation of one molecule of O_2, addition of the peroxyl radical to the olefin of another prenyl moiety completes the endoperoxide moiety installation. Following hydrogen-atom transfer from Tyr68 to C26 results in the accumulation of Tyr radicals, which is then quenched by inclusion of the reductant such as ascorbate (**Figure 7B**).[185] It is not surprising that with improved techniques, our knowledge on catalytic mechanisms of known Fe^{II}/2-OG enzymes is undergoing a updating process, and more Fe^{II}/2-OG enzymes with novel functions will be continuously discovered.

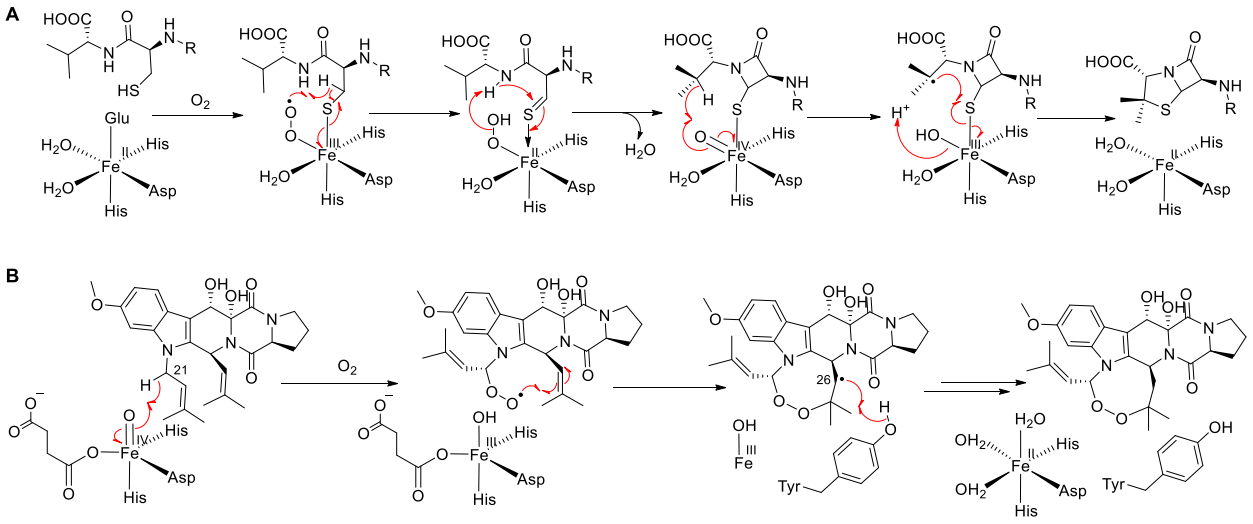

Figure 7. Mechanism of the fused β-lactam and thiazolidine ring formation catalyzed by IPNS (A), and mechanism of the endoperoxide formation by FtmOx1 (B).

By virtue of the ability to directly functionalize unactivated C–H bonds at the cost of 2-OG and O_2, nonheme Fe^{II}/2OG-dependent oxygenases can be used as a versatile platform to synthesize plenty of intricate natural products.[186] For example, total synthesis of tropolones is particularly challenging for chemists because of difficult construction of the non-benzannulated, highly substituted tropolone ring. However, one-pot dearomatization of 3-methylorcinaldehyde by flavin-dependent monooxygenase (FMO) TropB and following hydroxylation/ring-expansion by Fe^{II}/2-OG hydroxylase TropC led to efficient production of stipitatic aldehyde in 31 % isolated yield (54 % conversion).[187] This two-step approach set an example for leveraging the diversity of biosynthetic catalysts and synthetic chemistry communities. Therefore, with broad substrate scope and reaction repertoire, nonheme Fe^{II}/2OG-dependent oxygenases hold great potential as useful biocatalysts for chemoenzymatic synthesis of bioactive natural products.

1.3.3 Nonenzymatic events occurred in late stage of natural product biosynthesis

Compared to the tremendous variety of chemical reactions in synthetic organic chemistry, the occurrence of reactions within a living organism is usually restricted to rather mild conditions that the living system can tolerate. Still, nature created its own efficient way to expand the chemical processes in life science to the current level of diversity.[188, 189] One such strategy is the occurrence of nonenzymatic events during the post-biosynthesis of natural products. They often happen in cascade reactions with enzymatic reactions, because enzymatic products are, in some cases, chemically unstable intermediates. These intermediates can be highly reactive to undergo, *e.g.* condensation, dimerization, and lactonization, or possess electron-rich/deficient moieties that can easily be attacked by nucleophiles/electrophiles, thus triggering interesting chemical modifications of the pre-matured scaffolds.[190-201]

One major group of nonenzymatic reactions is occurred *via* quinone methides (QMs) as highly reactive intermediates. Although QMs have long been used as versatile reactants in chemical synthesis,[202, 203]

they have also been increasingly found in natural product biosynthetic pathways. The biosynthesis of fluostatin-type dimeric polyketides sets an excellent example for a nonenzymatic strategy used in the formation of C–C and C–N coupled homo-/hetero-dimers.[190] First spontaneous deacyloxylation of fluostatin D leads to a transient *para*-QM intermediate which is attacked by the electron-rich carbon of another fluostatin D to afford the dimeric products (**Figure 8A**).[190] Nonenzymatic dimerization *via ortho*-QMs was also suggested for the biosynthesis of sporormielones.[191] In addition to dimerization, the biosynthesis of elansolids in *Chitinophaga sancti* provides another example of macrolactonization *via* a *para*-QM intermediate. In this case, the nonenzymatic nucleophilic addition of the carboxylate onto a *para*-QM moiety of elansolid A3 yields elansolids A1/A2 (a pair of separable atropisomers) (**Figure 8B**).[192] There is also a situation where enzymatic and nonenzymatic reactions occur in parallel at a given biosynthetic step. Taking the biosynthesis of leporin as example, the first dehydration leads to an *E*-configured *ortho*-QM intermediate. Following hetero-Diels–Alder (HDA) reaction occurred both spontaneously and enzymatically. Interestingly, S-adenosyl-L-methionine (SAM)-dependent enzyme LepI does not repress the spontaneous intramolecular Diels–Alder (IMDA) reaction for the byproduct formation, but catalyzes an additional retro-Claisen rearrangement of the byproduct to the end product, thus completing a “byproduct cycle” process (**Figure 8C**).[193]

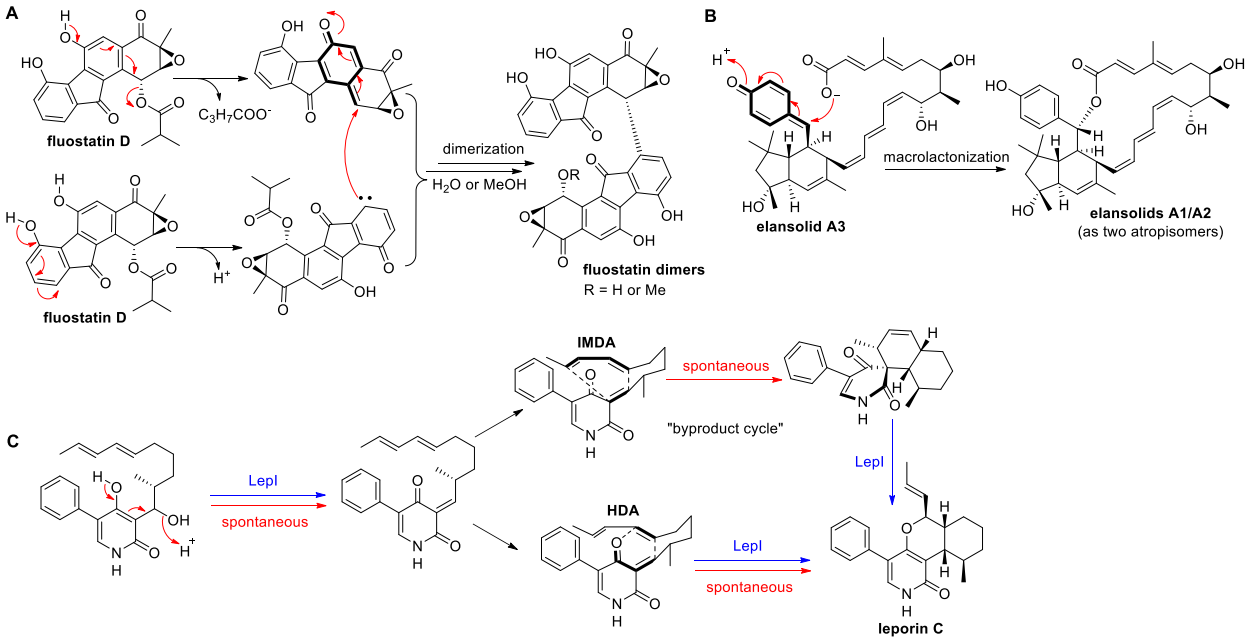

Figure 8. QMs as key biosynthetic intermediates involved in the formation of natural products

In addition to QM-initiated nonenzymatic reactions, amines are also found to be multipotent for the nonenzymatic initiation. In the biosynthesis of the pyridine-containing rubrolones, capture of ammonia or anthranilic acid by an amine acceptor, the 1,5-dione intermediate, leads to the nonenzymatic condensation process to afford the pyridine ring in rubrolone A or the pyridine inner salt moiety in rubrolone B (**Figure 9A**).[195] Similar nonenzymatic condensations between amines and carbonyl groups are also found in other well-studied cases. For example, discoipyrrole A is formed through a nonenzymatic multicomponent reaction of anthranilic acid, 4-hydroxybenzaldehyde, and 4-hydroxysattabacin (**Figure 9B**).[196] Another example is the construction of the jadomycin skeletons by

the nonenzymatic cascade reactions which starts with condensation between the amine of L-isoleucine/L-ornithine and the carbonyl group of an intermediate from oxepinone (**Figure 9C**).[197, 198]

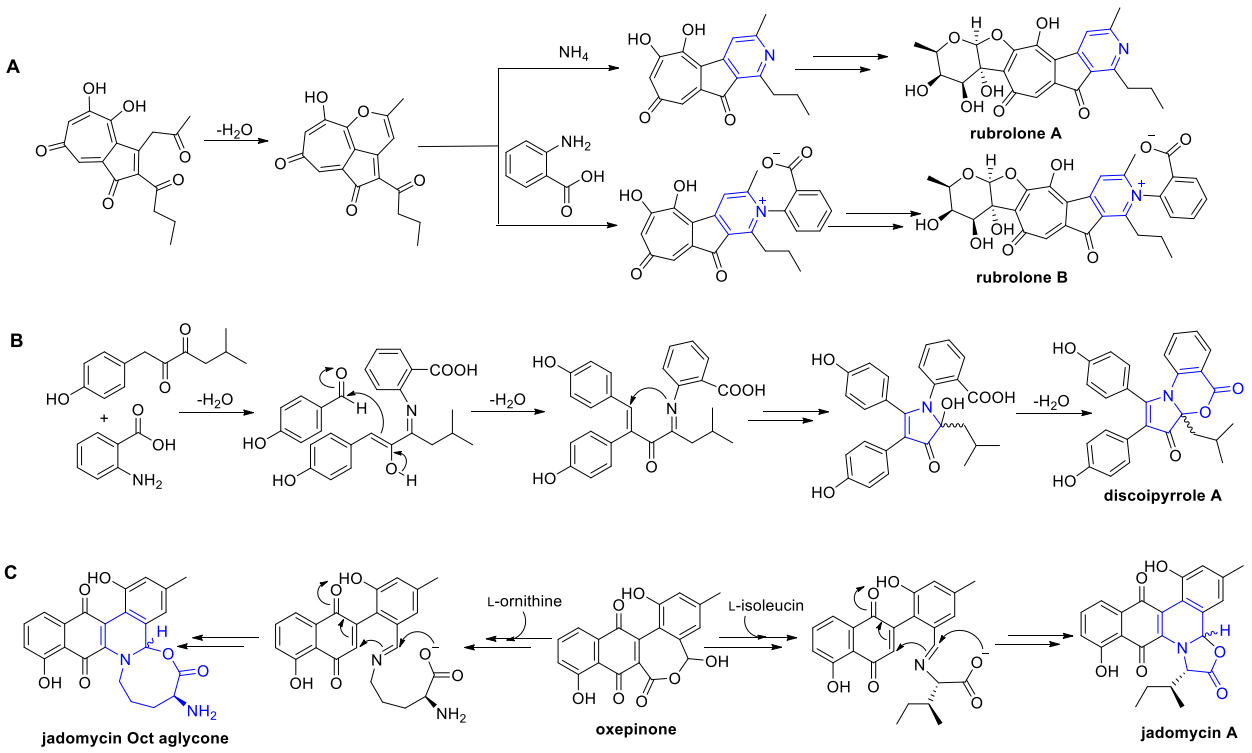

Figure 9. Examples of nonenzymatic condensations between amines and carbonyl groups

Except QMs and amines/imines as nonenzymatic initiation factors, formaldehyde is also reported to be involved in the nonenzymatic Baylis–Hillman reaction during the formation of bohemamine dimers. The intermediate A from bohemamine acts as the nucleophile to react with formaldehyde, leading to the formation of the primary alcohol intermediate B. This intermediate serves as the substrate for the following nucleophilic substitution of a second molecule of intermediate A to give dibohemamine A (**Figure 10A**).[199] Besides, nonenzymatic involvement of benzoquinone as the Michael acceptor is also reported in the biosynthesis of urdamycins. Urdamycin E is a sulphur-containing angucycline that formed by nucleophilic attack from the methylmercaptan, which derives from enzymatic cleavage of methionine, onto the 5,6-double bond of the urdamycin A (**Figure 10B**).[200] Shortly later, nonenzymatic condensations of urdamycin A with 4-hydroxyphenylpyruvic acid and indole-3-pyruvic acid were also found as the late steps in the biosynthesis of angucycline antibiotic urdamycins C and D, respectively.[201]

With the availability of highly reactive biosynthetic intermediates as starting points, natural product-like compounds can be easily diversified by feeding alternative precursors into the fermentation media. For example, 21 new elansolid derivatives were obtained by precursor-directed fermentation (**Figure 11A**).[204] Another impressive strategy is the combination of chemical synthesis and biosynthetic methods to diversify pseudo-natural products (**Figure 11B**). The multipotency of the biosynthetic

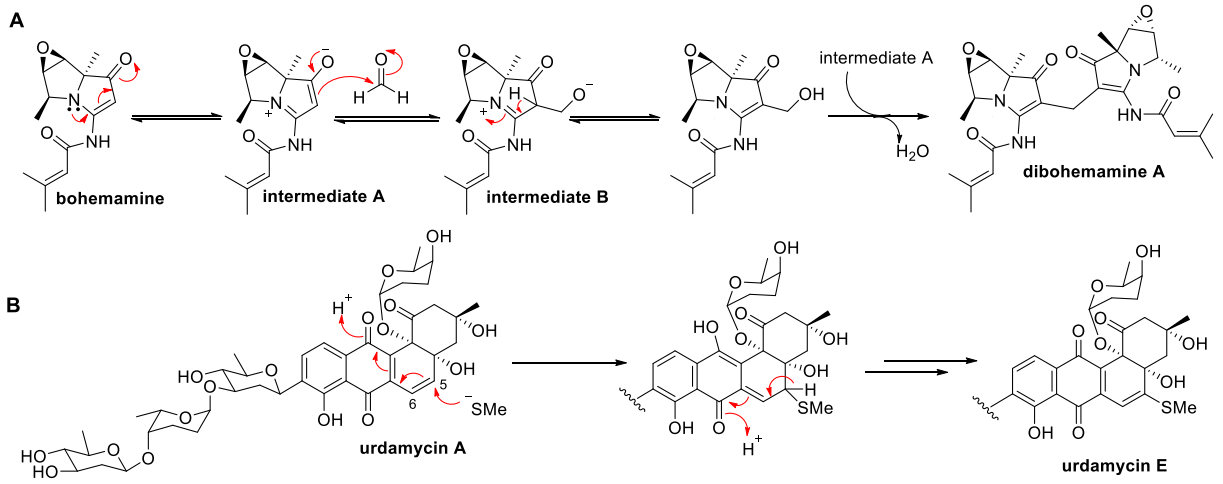

Figure 10. Examples of nonenzymatic reaction with the involvement of formaldehyde (A) or benzoquinone (B)

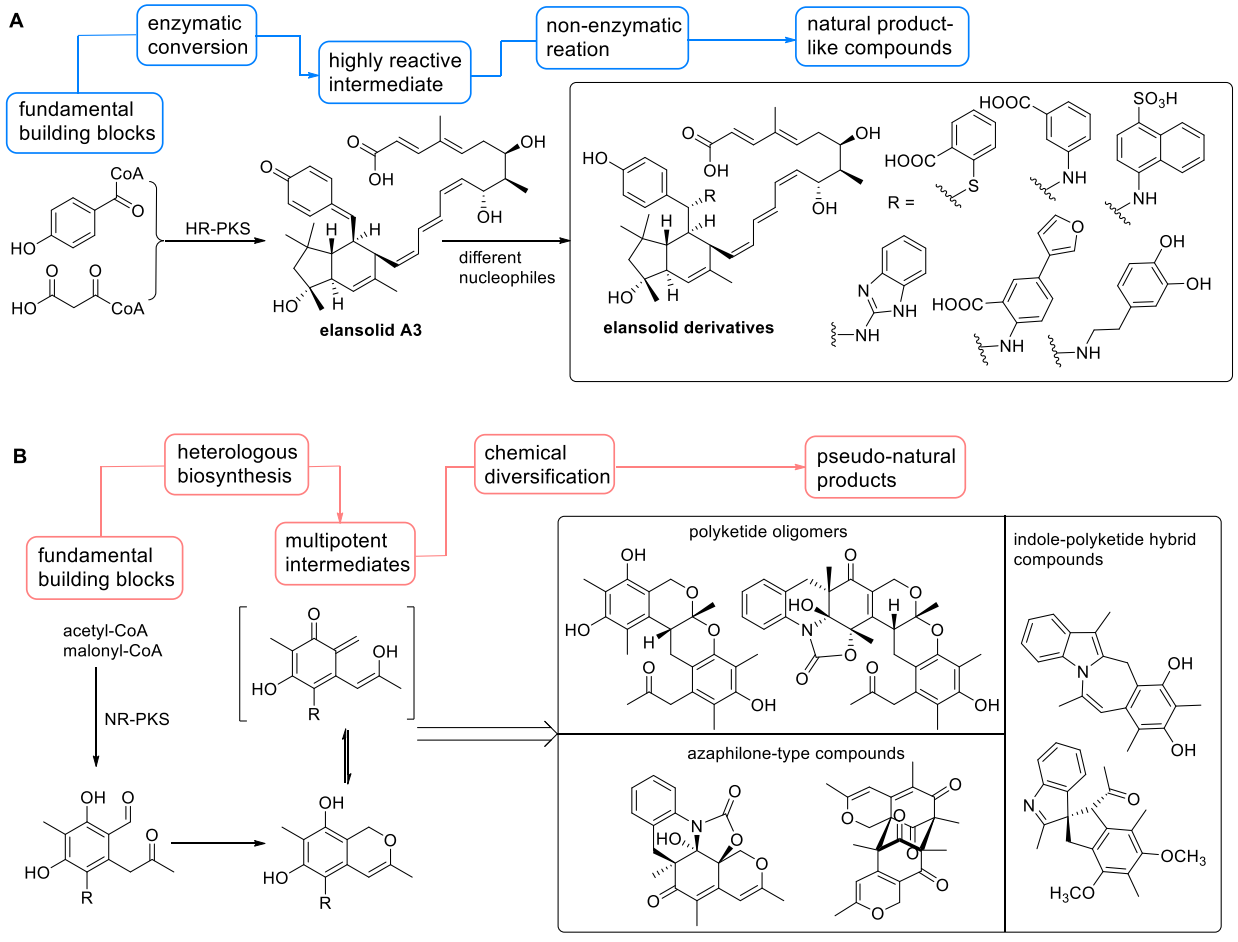

Figure 11. Two strategies of diversity-oriented synthesis. Generation of elansolid derivatives by precursor-feeding fermentation (A), creation of pseudo-natural products with different skeletons by combination of heterologous expression and chemical diversification methods (B).

intermediate produced by a fungal NR-PKS was exploited by heterologous expression and following chemical diversification.[205] The merit of such diversity-oriented semi-synthetic method is the nonlimiting expansion of polyketide frameworks. In this case, 41 pseudo-natural products with different carbon skeletons were rapidly and effectively generated. These include polyketide oligomers, azaphilone-type molecules, isoquinoline alkaloid-like compounds and indole–polyketide hybrids.[205]

Since an increasing number of natural products was found to involve one or more nonenzymatic steps during their biosynthesis, the line between natural products and non-natural products is becoming unclear. Non-natural products are often workup artifacts that formed during extraction or isolation process due to the external stimuli such as pH or temperature changes, exposure to light or oxygen, and organic solvents or chromatography media.[206] For example, methanol adducts are often found during isolation procedure as exemplified by agglomerin F[30] and pestapyrone C.[207] While formation of natural products is the results of using divergent pathways that begin with the formation of chemical scaffolds by backbone enzymes, and followed by multi-step enzymatic and nonenzymatic modifications. Further development of protein engineering, genetic manipulation, and chemoenzymatic synthesis provides more possibilities to enrich structural libraries for the discovery of novel drugs.

2 Aims of this thesis

In this thesis, the following issues have been addressed:

Geranylation of the indolyl residue in cyclic dipeptides by using engineered dimethylallyl transferases

PTs of the DMATS-type are known to exhibit substrate promiscuity. However, compared to the broad acceptance towards aromatic compounds, they have a narrowed tolerance towards prenyl donors. Transfer of C_5 units occurs frequently for fungal natural products, while transfer of longer prenyl donors, *i.e.* GPP (C_{10}), FPP (C_{15}), and GGPP (C_{20}), is relatively rare reported. So far, there are only limited numbers of PTs of the DMATS family were characterized for catalyzing the geranylation, which limited the diversification of geranylated natural products. In this study, manipulation of available PTs was carried out to switch their prenyl donor specificity from DMAPP to GPP. The following experiments were carried out in cooperation with Dr. Peter Mai:

- Sequence alignments of FtmPT1, BrePT, CdpC2PT, CdpNPT, and CdpC3PT with FgaPT2 and AtaPT to identify the gatekeeping residue for prenyl donor selectivity
- Construction of FtmPT1_M364G, BrePT_I337G, CdpC2PT_T351G, CdpNPT_M349G, CdpC3PT_F335G, and FgaPT2_M328G_R244Q by site-directed mutagenesis
- Overproduction and purification of the recombinant histidine-tagged mutants and their corresponding wild-type proteins
- Enzyme assays of the obtained mutants with 15 cyclic dipeptides in the presence of DMAPP and GPP in comparison to the enzymatic activity of the wild-type PTs
- LC-MS analysis of the incubation mixtures
- Isolation and structural elucidation of enzyme products by ^{1}H NMR and HR-ESI-MS analyses

Biosynthesis of peniphenone and penilactones in *Penicillium crustosum* requires the involvement of clavatol and terrestric acid from two independent pathways

Penilactones A and B are novel natural products consisting of two clavatol moieties and one γ-butyrolactone. Previous studies suggested that penilactones A and B were formed by Michael addition of an *ortho*-QM with (*R*)-5-methyltetronic acid or (*S*)-5-carboxylmethyltetronic acid, respectively. However, limited studies on penilactones A and B raise the question about, i) the biosynthetic origin of clavatol and tetronic acids, ii) the biosynthetic relationship between clavatol and the *ortho*-QM, and iii) the responsible enzyme for Michael additions. Besides, it is also interesting to investigate the mechanism for the conversion of the β-carboxylmethyl group to the α-methyl group at the C-5 position in the tetronate ring. To answer these questions, the following experiments were carried out in cooperation with Dr. Jie Fan:

- Sequencing the genome of *Penicillium crustosum* PRB-2 and analysis of the clavatol and terrestric acid biosynthetic gene clusters
- Deletion of the genes in clavatol (*claA*-*J*) and terrestric acid clusters (*traA*-*H*) by using the split marker strategy
- Heterologous expression of the NR-PKS gene *claF*, PKS-NRPS hybrid gene *traA*, and *traA* together with the enoyl reductase gene *traG* in *Aspergillus nidulans* LO8030
- Large-scaled fermentation of the wild-type strain, deletion mutants, and heterologous expression mutants for isolation and structure elucidation of the secondary metabolites
- Chemical synthesis of (5*R*)-methyltetronic acid and (5*S*)-carboxylmethyltetronic acid by Lena Ludwig-Radtke
- Feeding biosynthetic precursors in Δ*claD*, Δ*claF*, Δ*traA*, and Δ*traG* mutants
- *in vitro* biochemical investigation of the nonheme Fe^{II}/2OG-dependent oxygenases ClaD and TraH as well as the flavin-containing oxidoreductase TraD
- Incubation of hydroxyclavatol in ^{18}O-enriched water to prove the existence of *ortho*-QM
- Incubating hydroxyclavatol with (5*R*)-methyltetronic acid or (5*S*)-carboxylmethyltetronic acid in H_2O at room temperature to prove the nonenzymatic formation of penilactones A and B

Expanding structural diversity of natural products by Michael addition with *ortho*-quinone methide as the acceptor

In addition to penilactones A and B, there are numerous natural products found in fungi that also contain clavatol moieties in their structures. Our previous study revealed that penilactones A and B are formed by nonenzymatic 1,4-Michael additions *via* the *ortho*-QM derived from hydroxyclavatol. However, it is not clear whether other clavatol-containing compounds are also formed nonenzymatically in a similar way to penilactones A and B. To investigate the involvement of the *ortho*-QM derived from hydroxyclavatol in their formation and to expand the structural diversity of clavatol-containing compounds, the following experiments were carried out in cooperation with Dr. Jie Fan:

- Chemical synthesis of hydroxyclavatol by Lena Ludwig-Radtke
- Testing the reactivity of hydroxyclavatol with 102 different reactants and subsequent LC-MS analysis of the incubation mixtures
- Optimization of the incubation conditions for upscaled incubations
- Isolation of the reaction products by semi-preparative HPLC and structure elucidation by NMR and HR-ESI-MS analyses
- Screening and evaluating the antibacterial activity, acetylcholinesterase, and α-glucosidase inhibition activities for the isolated products

3 Results and discussion

3.1 Geranylation of the indolyl residue in cyclic dipeptides by using engineered dimethylallyl transferases

The frequent occurrence of prenylated compounds in nature makes PTs become one of the most important tailoring enzyme groups. PTs belonging to the DMATS superfamily catalyze the transfer reactions of prenyl (n x C_5) moieties from different prenyl donors onto various aromatic substrates, especially indole derivatives.[134] However, most of so far reported PTs are known for dimethylallyl (C_5) transfer reactions and only very few of them are capable of catalyzing geranyl (C_{10}) transfer.[208-212] In a previous study, a single point mutation at the site of Met328 in FgaPT2 changed its prenyl donor preference from DMAPP to GPP.[166] Following this work, we selected five CDP PTs, *i.e.* FtmPT1,[150] CdpC2PT,[153] BrePT,[152] CdpNPT[154], and CdpC3PT[156] for protein engineering. These enzymes catalyze regular or reverse prenylations at C-2 or C-3 position of the indole ring (**Scheme 2**).

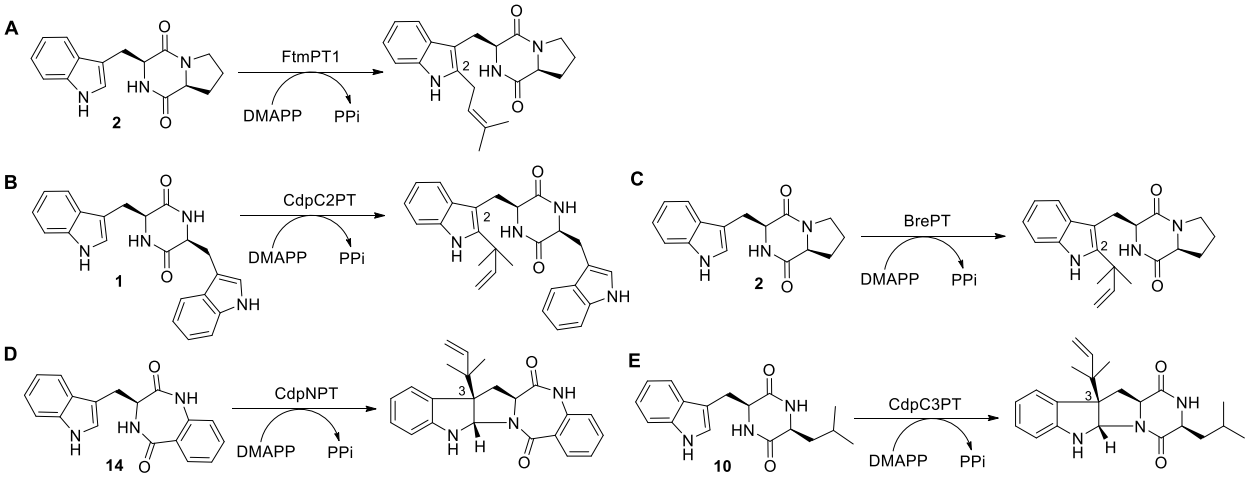

Scheme 2. The prenyl transfer reactions catalyzed by five CDP PTs with their natural or best accepted substrates

Enzyme assays of the above PTs in the presence of DMAPP were carried out to confirm the activity of the proteins. The following 15 tryptophan-containing CDPs were used as prenyl acceptors: *cyclo*-L-Trp-L-Trp (**1**), *cyclo*-L-Trp-L-Pro (**2**), *cyclo*-L-Trp-D-Pro (**3**), *cyclo*-D-Trp-L-Pro (**4**), *cyclo*-D-Trp-D-Pro (**5**), *cyclo*-L-Trp-L-Ala (**6**), *cyclo*-L-Trp-D-Ala (**7**), *cyclo*-D-Trp-L-Ala (**8**), *cyclo*-D-Trp-D-Ala (**9**), *cyclo*-L-Trp-L-Leu (**10**), *cyclo*-L-Trp-L-Tyr (**11**), *cyclo*-L-Trp-L-Phe (**12**), *cyclo*-L-Trp-Gly (**13**), (*S*)-benzodiazepinedione (**14**), and (*R*)-benzodiazepinedione (**15**). Incubation mixtures of the five PTs with GPP as the prenyl donor were analyzed by LC-MS to evaluate their activity towards GPP. The results showed that only CdpC2PT exhibited clear activities toward **1**, **2**, **14**, and **15** in the presence of GPP. CdpC3PT showed very low GPP acceptance toward **1**, **2**, **5**, and **14**. CdpNPT, FtmPT1, and BrePT had no activity when GPP was used as the prenyl donor.

It was reported that Gly326 in AtaPT was responsible for the enlarged pocket for prenyl donor binding.[209] Met328 in FgaPT2 was the gatekeeping residue for the prenyl donor selectivity.[166] Protein sequence alignments of the five aforementioned PTs with those of AtaPT and FgaPT2 showed corresponding residues at Met364 in FtmPT1, Ile337 in BrePT, Thr351 in CdpC2PT, Met349 in CdpNPT and Phe335 in CdpC3PT. Replacing the bulky amino acids by glycine led to the construction of the mutants FtmPT1_M364G, BrePT_I337G, CdpC2PT_T351G, CdpNPT_M349G, and CdpC3PT_F335G, respectively. Site-directed mutagenesis, overproduction of the recombinant proteins, and enzyme assays of the wild-type enzymes with DMAPP and GPP were performed by Dr. Peter Mai.

This PhD candidate used the generated mutants for enzyme assays to test their activity toward GPP. LC-MS analysis of the incubation mixtures demonstrated improved GPP acceptance but generally reduced activity towards DMAPP by the mutants. In comparison to no activity of CdpNPT, FtmPT1, and BrePT toward GPP, CdpNPT_M349G accepted all the tested CDPs (**1** − **15**) with total product yields ranging from 13.7 % to 95.8 %. The CDPs were converted by FtmPT1_M364G with total product yields ranging from 9.6 % to 75.4 % except the two benzodiazepinediones (**14** and **15**). In addition, strongly increased activity of BrePT_I337G toward GPP was observed for its natural substrate **2** from less than 0.5 % by the wild-type to 79.8 % by I337G. For CdpC3PT_F335G, conversion of **10** in the presence of GPP was significantly increased in contrast to the weak activity of CdpC3PT, while only slight improvement was observed for other CDPs. As for CdpC2PT_T351G, comparing with wild-type CdpC2PT, it showed distinct product formation or different ratios of the same product toward **1** − **15** in the presence of GPP.

Subsequent isolation of the enzyme products on HPLC and structural elucidation by interpretation of their ^{1}H NMR spectra were also carried out by this PhD candidate. Our results revealed the relaxed regiospecific geranylation of the enzyme products in either reverse or regular manner (**Scheme 3**). FtmPT1_M364G catalyzes the formation of both regularly C2- and C3-prenylated, and even regularly N1-prenylated products. BrePT_I337G still catalyzes solely or predominantly reverse geranylation at the C-2 position of **2** − **4**. Both CdpC2PT and its mutant CdpC2PT_T351G can catalyze geranyl transfer reaction, but with a distinct regioselectivity. The wild-type CdpC2PT catalyzes reverse C2-, regular C5- and C7-geranylation of **1**, while CdpC2PT_T351G catalyzes both reverse mono- and digeranylation at C-2 of **1**. Furthermore, reversely C3-geranylated and regularly C6-geranylated products were obtained from the incubation mixtures of CdpNPT_M349G with the selected substrates **1**, **5**, and **14**. Remarkably relaxed regioselectivity was observed for CdpC3PT_F335G in the presence of **10** and the structures of four products were determined as regularly N1- and C7-, reversely N1- and C3-geranylated compounds.

In summary, our results proved the site-directed mutation of the gatekeeping residues as an effective way to turn on or improve the GPP acceptance of five PTs. Alongside with the increased activity

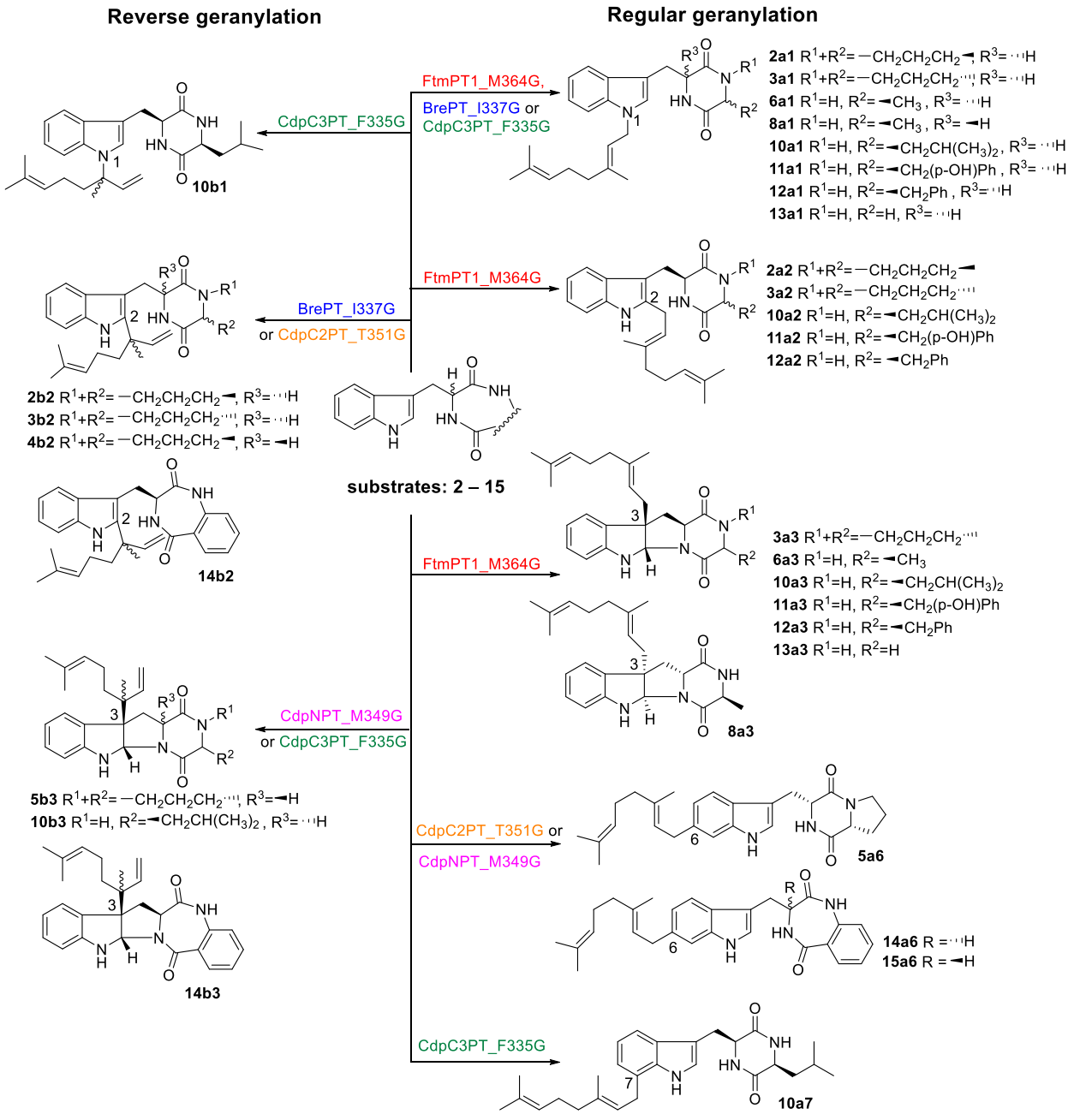

Scheme 3. Structures of enzyme products with different prenylation patterns

towards GPP, the mutants also showed reduced regiospecificity, leading to multiple prenylated product formation in one incubation. This requires more efforts for product isolation, however benefits in creation of diverse geranylated CDPs. Taking advantage of relaxed regioselective geranylation by the mutants, complete decoration of N-1 and the six nonbridgehead carbons of the indole ring was achieved when using **1** as the acceptor and GPP as the donor. The vacancy at C4-position of **1** was filled by the generation of a double mutant FgaPT2_M328G_R244Q. Thus, nine products with geranyl moieties at all possible positions of the indole ring of **1** can be obtained by one-step chemoenzymatic

reactions (**Scheme 4**). Prior to our study, geranylated indole derivatives were relatively rare reported from nature.[208-212] Our findings enrich the structural library of geranylated CDPs by providing 42 compounds of this group. Furthermore, it is possible to create more geranylated CDPs by mutation of additional available dimethylallyl transferases in a similar way.

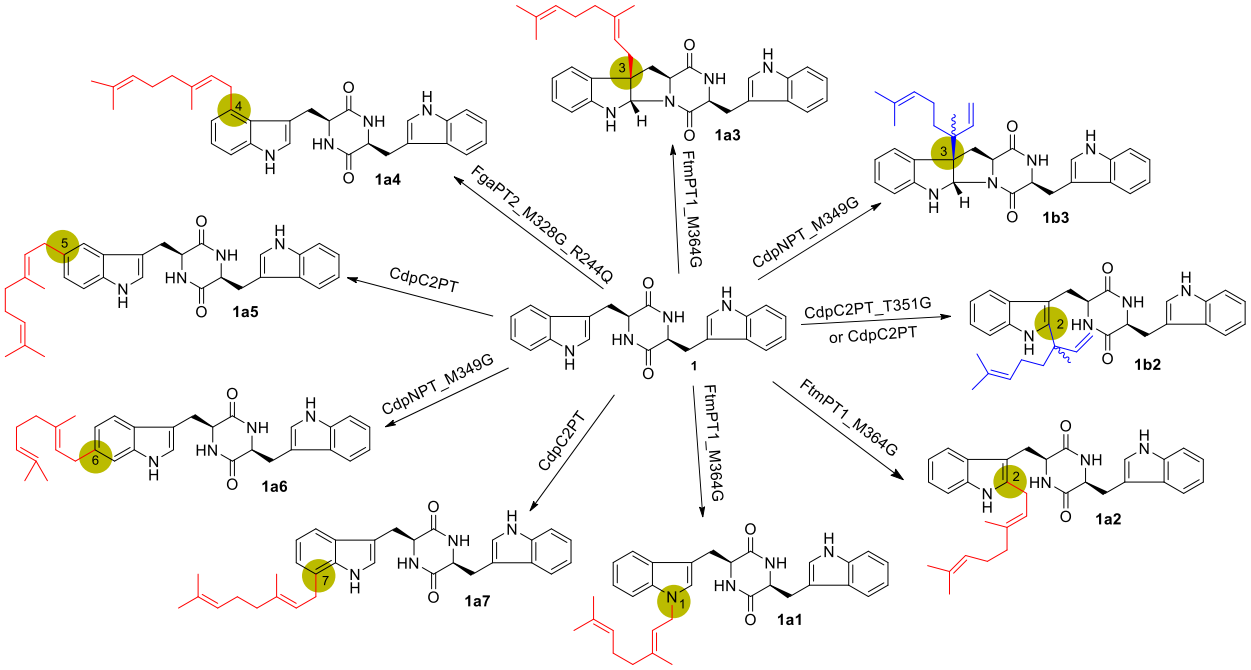

Scheme 4. Attachment of the geranyl moieties to different positions of **1** *via* one-step chemoenzymatic reactions

For details on this work, please see the publication (section 4.1)

Ge Liao*, Peter Mai*, Jie Fan, Georg Zocher, Thilo Stehle and Shu-Ming Li (2018). Complete decoration of the indolyl residue in *cyclo*-L-Trp-L-Trp with geranyl moieties by using engineered dimethylallyl transferases. *Organic Letters*, 20 (22), 7201–7205, DOI: 10.1021/acs.orglett.8b03124. (*equal contribution)

3.2 Biosynthesis of peniphenone and penilactones in *Penicillium crustosum* requires the involvement of clavatol and terrestric acid from two independent pathways

Penilactones A (**16**) and B (**17**) from *Penicillium crustosum* PRB-2 are rare natural products with novel structural skeletons (**Figure 12**).[213] It was proposed that penilactones A and B as well as their putative precursors peniphenone D (**18**) and penilactone D (**19**) were formed by Michael addition of the *ortho*-QM (**20**) with (5*R*)-methyltetronic acid (**21**) or (5*S*)-carboxylmethyltetronic acid (**22**), respectively.[213, 214] Although later biomimetic synthesis supported this hypothesis,[215] no genetic data is available for the biosynthesis of **16** and **17**. In this study, we proved the formation of **16** and **17** by two-step nonenzymatic Michael addition and the involvement of two pathways for the formation of the reaction substrates.

Peniphenone and penilactones (**16** – **19**) were isolated from a 30 days-old rice culture, thus confirming their production in *Penicillium crustosum* PRB-2. The stereochemistry of **16** – **19** was determined by comparison of CD spectra with the published data[213] or the chemically synthesized **21** and **22**. Other related secondary metabolites were isolated from a 7 days-old PD culture. These include clavatol (**23**), a new derivative of clavatol named hydroxyclavatol (**24**), and two derivatives of **24**, *i.e.* hydroxyclavatol methyl (**25**) and ethyl ether (**26**). The production of terrestric acid (**27**) as the predominant product in PRB-2 was also confirmed by isolation and structure elucidation. Meanwhile, a new compound termed crustosic acid (**28**) was identified as a carboxylated derivative of **27**. The stereochemistry of **27** and **28** were determined by comparison of the optical rotation with the published data of tetronic acids.[216, 217] The structures of these isolates are shown in **Figure 12**.

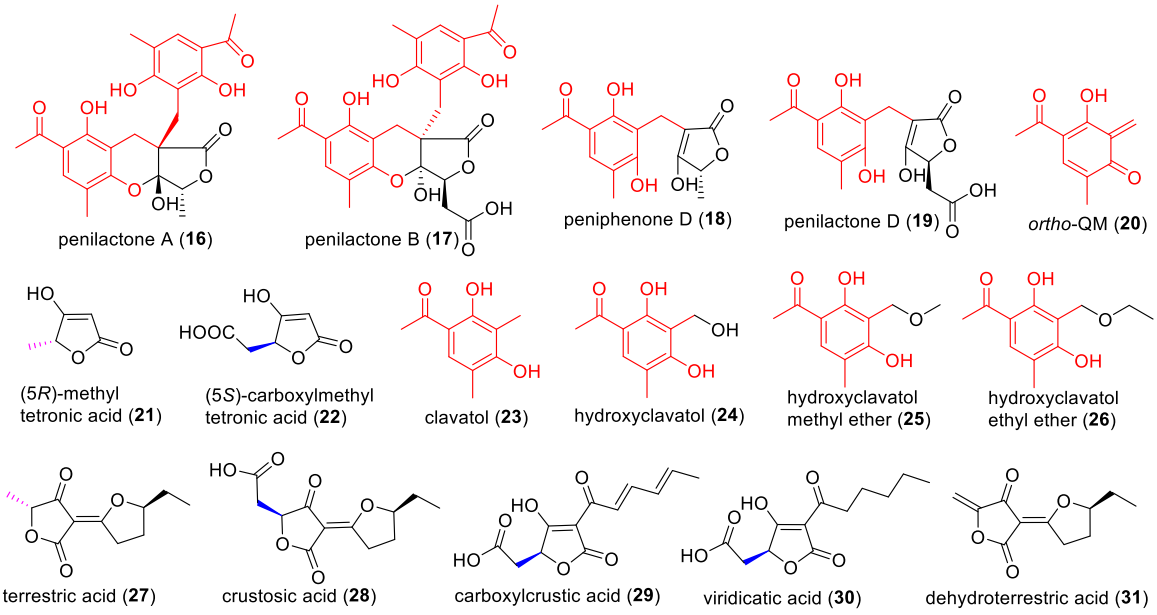

Figure 12. Structures of compounds isolated from *Penicillium crustosum* PRB-2 (**16 – 19** and **23 – 28**), heterologous expression mutants (**29** and **30**), and enzyme assay incubations (**31**).

The genome of *Penicillium crustosum* PRB-2 was then sequenced and 58 putative gene clusters were predicted by using AntiSMASH.[218] Two building blocks, *i.e.* clavatol moieties and the γ-butyrolactones, are required for structural construction of penilactones A and B. Therefore, we focused on two gene clusters for detailed investigation. One of the selected gene cluster contains a NR-PKS gene (*pcr3094*) termed *claF*. ClaF shares 57.7 % sequence identity with CitS.[48] Deletion of *claF* completely abolished the production of **16** – **19**, **23**, and **24**, while a large amount of **27** and **28** were accumulated. Feeding **23** to the Δ*claF* mutant restored the production of **16** – **19** and **24**. Heterologous expression of *claF* in *Aspergillus nidulans* LO8030[219] led to the accumulation of **23**. These results proved the involvement of ClaF in the biosynthesis of **16** – **19** by functioning as clavatol synthase. The gene deletion, heterologous expression, and biochemical investigation in this project were performed by Dr. Jie Fan. This PhD candidate is responsible for precursor feeding, isolation and structural elucidation of the secondary metabolites.

Another selected gene cluster contains a hybrid PKS-NRPS gene (*pcr11009*) termed *traA*. TraA shares a sequence identity of 69.6 % with CaaA in the biosynthetic pathway of carlosic acid,[30] which also possess a γ-butyrolactone core. Inactivation of *traA* led to the abolishment of **16** – **19**, **27**, and **28**, but remained the production of **23** and **24**. Feeding (5*R*)-methyltetronic acid (**21**) in Δ*traA* mutant restored the production of **16** and **18**, while **17** and **19** were restored when fed with (5*S*)-carboxylmethyltetronic acid (**22**). Further feeding experiments revealed that **16** and **18** were detected after feeding with **27**, while production of not only **16** – **19**, but also **27** were restored after feeding with **28**. It can be concluded that TraA is involved in the biosynthesis of tetronic acids **21**, **22**, **27**, and **28**, and these tetronic acids are involved in the formation of peniphenone and penilactones (**16** – **19**). Furthermore, to identify the function of TraA, the *traA* sequence was introduced into *Aspergillus nidulans* LO8030. The product yielded by the *traA* expression mutant was identified to be a carboxylmethyltetronic acid derivative with an unsaturated acyl chain, termed carboxylcrustic acid (**29**). Subsequent coexpression of *traA* with the putative enoyl reductase gene *traG* led to the production of another metabolite, viridicatic acid (**30**). These results proved the function of TraA for synthesizing **29** and TraG for the side chain reduction of **29** to **30**. However, the responsible enzyme for the conversion of **30** to **28** has not been identified yet.

After identification of the backbone genes, we proceed to investigate the metabolism of clavatol (**23**). Isolation of hydroxyclavatol (**24**) gave us a clue for searching oxidase genes in the clavatol cluster. The nonheme Fe^{II}/2-OG-dependent oxygenase ClaD and the cytochrome P450 ClaJ were considered as candidate enzymes for the hydroxylation step. Deletion of *claD* abolished the production of **16** – **19** and **24**. Feeding **24** in the Δ*claD* mutant restored the production of **16** – **19**. Further *in vitro* biochemical investigation of ClaD with **23** in the presence of ascorbic acid, $Fe[(NH_4)_2(SO_4)_2]$, and 2-OG led to clear detection of **24** by HPLC analysis. Thus, ClaD was identified as the responsible enzyme for the hydroxylation of **23** to **24**.

Alongside with the isolation of **24**, two ether derivatives (**25** and **26**) were also obtained. The conversion of **24** to **25** was observed during the isolation process when dissolving **24** in methanol. Incubation of **24** in methanol or ethanol at 25 °C for 16 h resulted in the formation of hydroxyclavatol methyl (**25**) and ethyl ether (**26**), respectively (**Scheme 5**). The ethers (**25** and **26**) can convert back to **24** in aqueous solution. These results suggested that the spontaneous formation of the ethers is highly possible *via* the *ortho*-QM (**20**). To prove the existence of **20**, compound **24** was incubated at 25 °C for 16 h in H_2O and $H_2{}^{18}O$, respectively. Subsequent MS analysis of the incubation mixtures proved the incorporation of ^{18}O into **24**, proving the equilibration between **24** and **20** in aqueous system (**Scheme 5**).

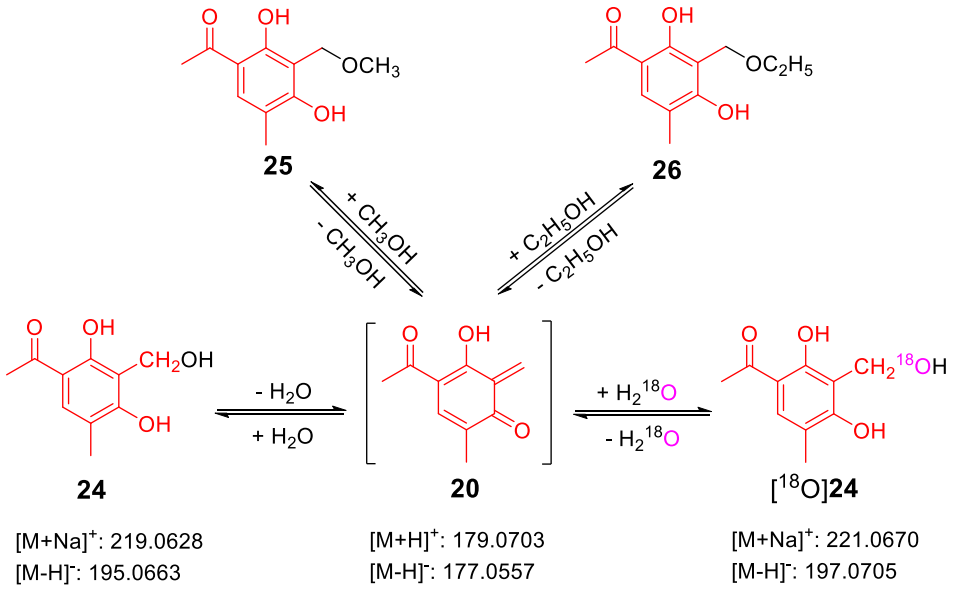

Scheme 5. The equilibration between hydroxyclavatol (**24**) and *ortho*-QM (**20**) in aqueous solution and the conversion between **20** and the ethers (**25** and **26**) in different alcohols.

Having proven the function of ClaD and the existence of the *ortho*-QM, we speculated that the P450 ClaJ could be responsible for catalyzing Michael addition of the two building blocks. Indeed, no production of **16** – **19** was detected in the *claJ* deletion mutant. However, when feeding the substrates to the *claJ* expression mutant, we unexpectedly observed the detection of **16** – **19** in the negative control. Hydroxyclavatol (**24**) was then incubated with the two tetronic acids **21** or **22** in water at 25 °C for 16 h. LC-MS analysis revealed that incubation of **24** with **21** carrying a 5α-methyl group led to the formation of **16** and **18**. Similarly, incubation of **24** with **22** carrying a 5β-carboxylmethyl group resulted in the formation of **17** and **19**. Further incubation of **24** with **18** or **19** led to the detection of **16** or **17**. Therefore, although the function of ClaJ is not clear, it was confirmed that the formation of **16** – **19** is nonenzymatic events. First dehydration of **24** yielded the highly reactive intermediate **20**, which served as the Michael acceptor attacked by the nucleophiles **21** or **22** to give **18** or **19**. Subsequent addition of a second molecule of **20** to **18** or **19** yielded the final product **16** or **17** (**Scheme 6**).

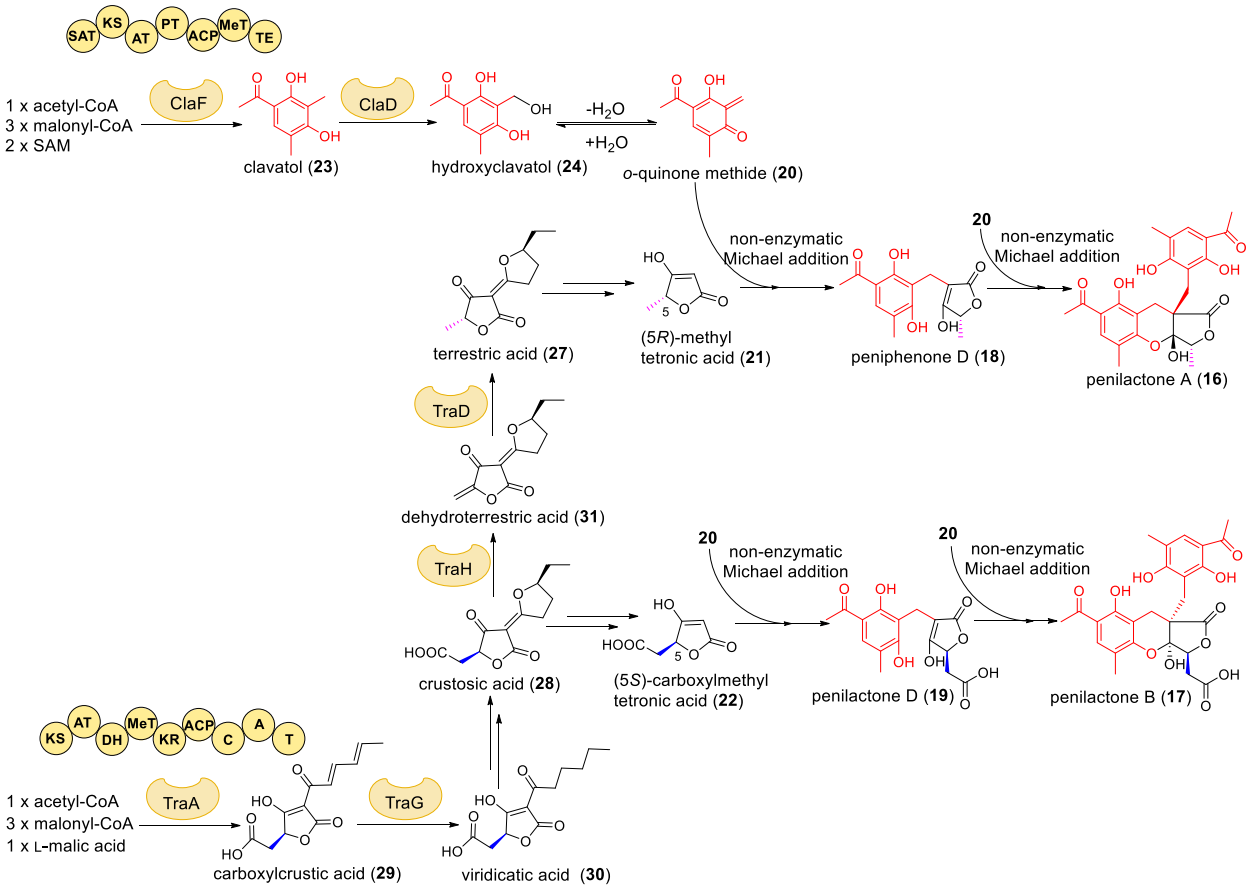

Scheme 6. Proposed biosynthesis of peniphenone and penilactones in *Penicillium crustosum* PRB-2 with the involvement of metabolites from clavatol and terrestric acid pathways

In addition to the formation mechanism of peniphenone and penilactones, we are also interested in the conversion of crustosic acid (**28**) to terrestric acid (**27**). **28** carries a 5β-carboxylmethyl group at the tetronate ring, differing from the 5α-methyl group in **27**. Similar situations are also found in other fungal tetronates. Examples are carlic acid and carlosic acid as 5 β-carboxylmethyl-containing tetronates, carolic acid and carolinic acid as 5 α-methyl-containing tetronates.[30, 217, 220] As aforementioned, feeding **28** in the *traA* deletion mutant led to the formation of **27**, implying **28** undergoes decarboxylation and isomerization to **27**. We took the Fe^{II}-2OG-dependent oxygenase TraH as the candidate enzyme for this transformation. Disruption of *traH* abolished **27** production, suggesting the role of TraH in the conversion of **28** to **27**. To further verify the function of TraH, the purified recombinant TraH was used for the enzyme assay with **28** in the presence of ascorbic acid, $Fe[(NH_4)_2(SO_4)_2]$, 2-OG, and dithiothreitol (DTT). Surprisingly, LC-MS analysis revealed an unexpected product peak with the molecular formula of $C_{11}H_{13}O_4$, instead of $C_{11}H_{15}O_4$ for **27**. Subsequent isolation led to the identification of the enzyme product as dehydroterrestric acid (**31**), which possesses an exocyclic double bond at the C-5 position (**Figure 12**). This result proved the role of TraH in catalyzing an oxidative decarboxylation of **28** to **31**. Therefore, another enzyme is required

for the reduction of the double bond to complete the conversion of **31** to **27**. For this purpose, we took detailed investigation on the flavin-containing oxidoreductase TraD. After overexpression of the gene in *Escherichia coli* and purification to near homogeneity, TraD was incubated with **31** in the presence of NADPH. LC-MS analysis of the reaction mixtures as well as isolation and structural elucidation confirmed the stereospecific reduction of **31** by TraD to **27**. Further coincubation of **28** with TraH and TraD showed sequential formation of the intermediate **31** and final product **27**. To sum up, these results proved that the transformation of **28** to **27** required first oxidative decarboxylation by TraH to afford an intermediate **31**, then stereospecific reduction of the double bond in **31** by TraD to install the α-methyl group in **27** (**Scheme 6**).

In conclusion, the biosynthesis of peniphenone and penilactones (**16** – **19**) was elucidated in this study as a combination of enzymatic and nonenzymatic reactions (**Scheme 6**). It contains enzymes originating from two sperate pathways to provide two building blocks for penilactone construction. The NR-PKS ClaF together with the nonheme Fe^{II}/2-OG-dependent oxygenase ClaD from the clavatol pathway are responsible for the formation of hydroxyclavatol (**24**). Spontaneous dehydration of **24** to the active intermediate *ortho*-QM (**20**) initiates the nonenzymatic Michael addition with tetronic acids **21** or **22** to form firstly **18** or **19**, then **16** or **17**. Compounds **21** and **22** are metabolites of terrestric acid (**27**) and crustosic acid (**28**) from the terrestric acid pathway. **28** is formed *via* carboxylcrustic (**29**) and viridicatic acid (**30**) as biosynthetic precursors. Decarboxylation and isomerization of **28** to **27** was catalyzed by the nonheme Fe^{II}/2-OG-dependent oxygenase TraH and the flavin-containing oxidoreductase TraD. This study sets an example for the formation of natural products with the involvement of enzymes from two independent pathways and nonenzymatic reactions *via ortho*-QM as the biosynthetic intermediate.

For details on this work, please see the publications (sections 4.2 and 4.3)

Jie Fan*, **Ge Liao***, Florian Kindinger, Lena Ludwig-Radtke, Wen-Bing Yin, and Shu-Ming Li (2019). Peniphenone and penilactone formation in *Penicillium crustosum* via 1,4-Michael additions of *ortho*-quinone methide from hydroxyclavatol to γ-butyrolactones from crustosic acid. *Journal of the American Chemical Society*, 141 (10), 4225–4229, DOI: 10.1021/jacs.9b00110. (*equal contribution)

Jie Fan*, **Ge Liao***, Lena Ludwig-Radtke, Wen-Bing Yin, and Shu-Ming Li (2020). Formation of terrestric acid in *Penicillium crustosum* requires redox-assisted decarboxylation and stereoisomerization. *Organic Letters*, 22 (1), 88–92, DOI: 10.1021/acs.orglett.9b04002. (*equal contribution)

3.3 Expanding structural diversity of natural products by Michael addition with *ortho*-quinone methide as the acceptor

Ortho-QMs are highly reactive intermediates that have long been used in chemical synthesis.[203, 221] Moreover, the involvement of *ortho*-QMs in the biosynthesis of natural products has also been reported. As introduced in section 1.3.3, the formation of fluostatin dimers,[190] elansolids,[192] and leporins[193] was proven to require nonenzymatic reactions *via* QMs as the key reaction steps. Our studies on the biosynthesis of penilactones A and B provide another example for the *ortho*-QM involving nonenzymatic formation.[222] In addition to penilactones A and B, there are several fungal natural products as coupling results of clavatol with α-pyrone, indole, quinone, lactones, and phenols. Examples include erabulenol B from *Penicillium* sp. FO-5637[223], peniphenones A – C from *Penicillium dipodomyicola* HN4-3A,[224] communols A – C[225] and penicophenones A and B[226] from *Penicillium commune*.

To investigate whether these clavatol-containing compounds are formed in a similar way as penilactones A and B, we chemically synthesized hydroxyclavatol and tested the reactivity of the *ortho*-QM derived from hydroxyclavatol with 102 reactants of different structural skeletons (**Table 2**). These include flavonoids, hydroxynaphthalenes, coumarins, xanthones, anthraquinones, phloroglucinols, phenolic acids, indole derivatives, tyrosine analogues, and quinolines. Both hydroxyclavatol and the reactants at a final concentration of 0.4 mM in 50 μL H_2O were incubated at 25 °C for 16 h without pH adjustment. After adding 50 μL acetonitrile and centrifuging at 13,000 rpm for 30 min, 5 μL of supernatant were subsequently subjected to LC-MS analysis. The tests of hydroxyclavatol with a wide array of reactants as well as analyzing the LC-MS data of the incubation mixtures were performed by Dr. Jie Fan. This PhD candidate took the isolation and structural elucidation of the coupling products. Accordingly, coupling products with $[M+H]^+$/$[M-H]^-$ ions being 178 Da larger than the corresponding reactants were detected in 86 out of 102 cases. Product formation with 10 % to 55 % conversion was detected for 49 reactants, product formation with 1 % to 10 % conversion was observed in 18 cases, and product formation in 19 incubations was only detectable by EIC of $[M+H]^+$/$[M-H]^-$ ions. Only 16 tested reactants showed no product formation in their incubation mixtures.

Among the tested reactants, phloroglucinol derivatives were found to be the most favorable Michael donors for the *ortho*-QM. All eight tested phloroglucinols were converted to the coupling products with product yields ranging from 10 % to 55 %. Besides, flavonoids, hydroxynaphthalenes, and quinolines are also suitable reactants for coupling with the *ortho*-QM. Products were detected in incubation mixtures of hydroxyclavatol with 15 of 16 tested flavonoids and 9 of 11 tested hydroxynaphthalenes. Incubations of hydroxyclavatol with 5 of 9 tested quinolines showed UV detectable product formation. However, incubation mixtures of hydroxyclavatol with coumarins, xanthones, anthraquinones, and phenolic acids showed either very low product yields or no product formation. Further investigation on the reaction activity of hydroxyclavatol with indole derivatives including L-tryptophan revealed up to

49 % conversion. In contrast, L-tyrosine and its analogues were generally poorly converted to their clavatol adducts. Coincubation of hydroxyclavatol with eight tryptophan-containing CDPs showed product formation with 9 % to 29 % yields, while no product was detected from coincubation of hydroxyclavatol with two tyrosine-containing CDPs. Also 2-aminobenzyl alcohol and even tris(hydroxymethyl)aminomethane (Tris) prepared as Tris-HCl buffer (pH 7.5) were tested with hydroxyclavatol leading to a clearly coupling product detection.

Table 2. Overview of different reactants tested with hydroxyclavatol and distribution of the reactant numbers for each structural group.

reactants	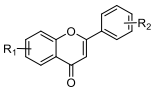	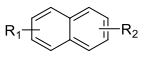	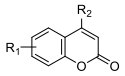	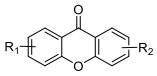	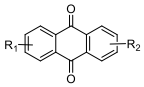	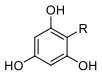
UV detectable (10%−55%)	7	5	1	0	0	8
UV detectable (1%−10%)	5	4	0	5	0	0
only detectable by EIC	3	0	2	0	2	1
no detectable product	1	2	2	1	2	0
total tested numbers	16	11	5	6	4	9
reactants	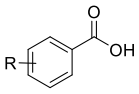	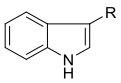	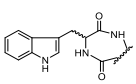	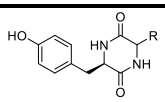	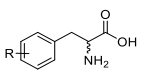	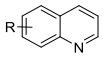
UV detectable (10%−55%)	3	9	7	0	3	4
UV detectable (1%−10%)	1	1	1	0	0	1
detected only by EIC	0	2	0	0	5	4
no detectable product	6	0	0	2	0	0
total tested numbers	10	12	8	2	8	9
Other tested reactants						
2-aminobenzyl alcohol	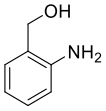	28 % conversion	tris(hydroxymethyl) aminomethane (Tris)	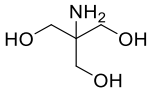	35 % conversion	

To improve the product yields for subsequent isolation and structural elucidation, the reaction condition was optimized from 25 °C for 16 h to 95 °C for 30 min for all incubations. LC-MS results generally revealed two to ten-fold higher conversion of the coupling products in most of the incubations at 95 °C. Product formation with 30 % to 99 % yields was achieved for 58 reactants, while a few incubations had no significant change under the increased temperature. Consequently, upscaled reactions were carried out at either 25 °C or 95 °C, which led to the isolation of 32 coupling products from incubations

of hydroxyclavatol with 23 selected reactants. For structural elucidation, ^{1}H NMR spectra were taken for 32 isolated products. In addition, ^{13}C NMR and HMBC spectra were also measured for 19 compounds. Biological activities, *e.g.* antibacterial, acetylcholinesterase and α-glucosidase inhibition activities were tested by Dr. Jie Fan.

The structures of coupling products originating from phenolic reactants are featured by the attachment of the clavatol unit to the *ortho*- or *para*-position of the hydroxyl group at the benzene ring. It was proposed that the *ortho*-QM generated from the spontaneous dehydration of hydroxyclavatol served as the acceptor for the nucleophilic carbon of phenols, which is due to *ortho*- or *para*-conjugation with the hydroxyl group (**Figure 13A**). As a result, a number of clavatol-phenol adducts were generated in this study (**Figure 13B**). These include clavatol-flavonoid adducts (**32** – **36**), clavatol-phloroglucinol

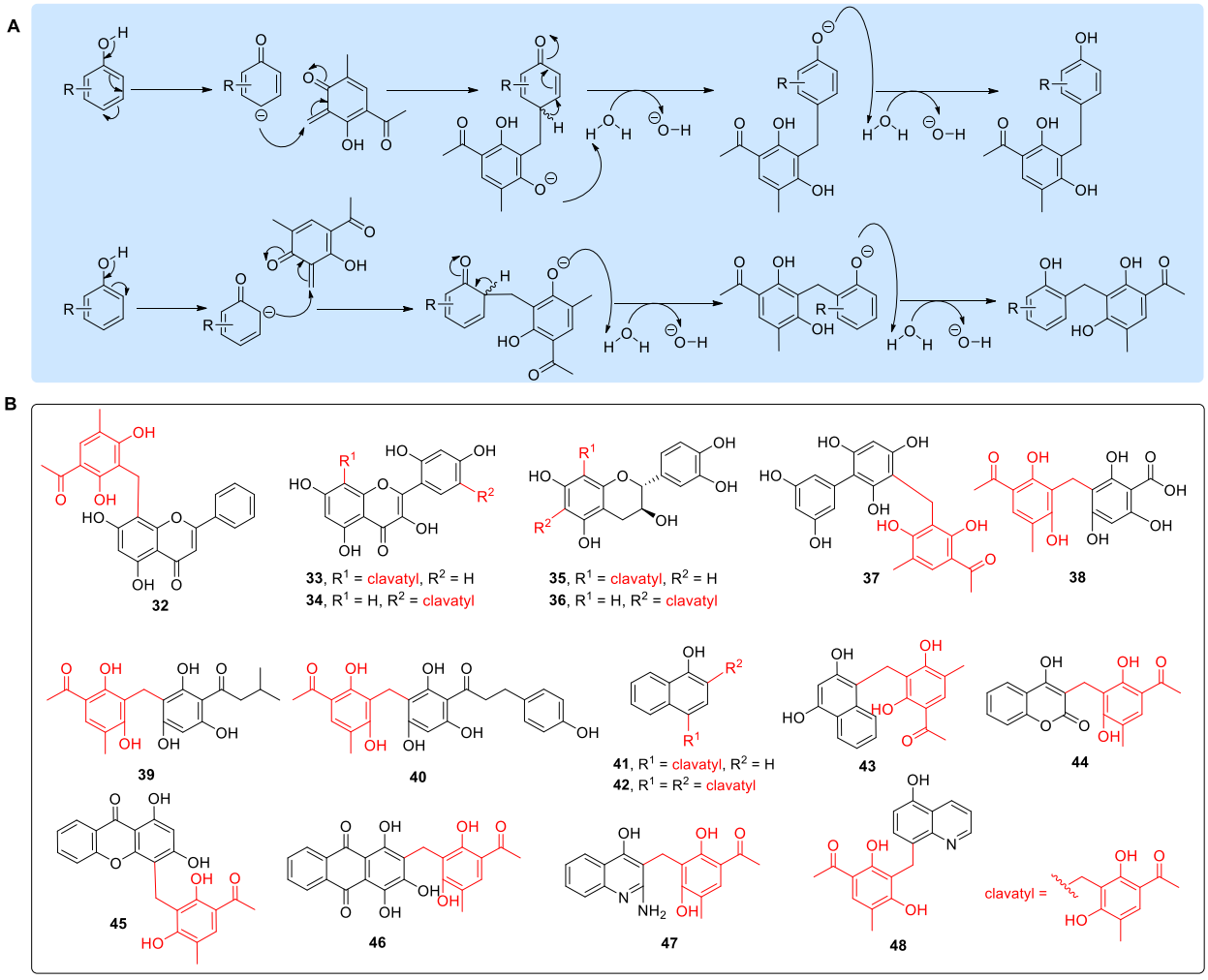

Figure 13. Reaction mechanisms of nucleophilic addition from the phenolic reactants to the *ortho*-QM intermediate (A) and structures of clavatol-phenol adducts (B).

adducts (**37** – **40**), and coupling products of clavatol with 1-naphthol (**41** and **42**), 1,3-dihydroxynaphthalene (**43**), 4-hydroxycoumarin (**44**), 1,3-dihydroxyxanthone (**45**), purpurin (**46**), 4-hydroxy-2-amino-quinoline (**47**), and 5-hydroxyquinoline (**48**).

Coupling products of indole derivatives are featured by carrying clavatol moieties at the C-2 or C-3 position. In these cases, the electron transfer within the indole ring enabled the Michael addition from the electron charged carbon to the electron deficient methylene group of the *ortho*-QM (**Figure 14A**). Accordingly, clavatol adducts with different indole derivatives (**49** – **52**) including tryptophan-containing CDPs (**53** – **59**) were obtained as representative structures (**Figure 14B**). Besides the above-mentioned C-C linked adducts, coupling compounds *via* C-N bond were also obtained as exampled by **61** – **63** (**Figure 14B**).

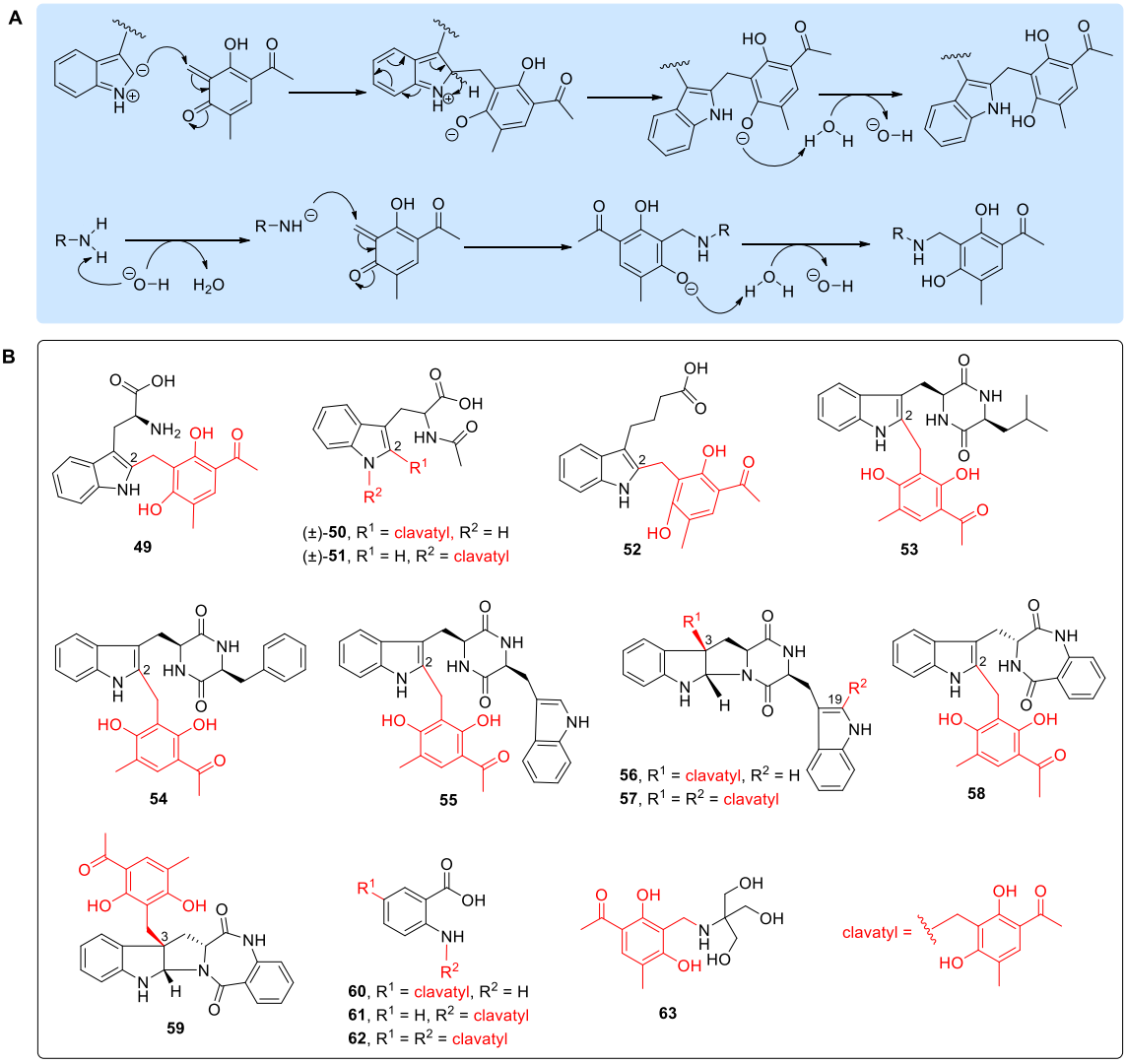

Figure 14. Reaction mechanisms of nucleophilic additions from the indole or amines to the *ortho*-QM intermediate (A). Structures of clavatol-indole adducts and C-N linked clavatol adducts (B).

Taken together, this study as an extended work of our previous research aimed at the application of the *ortho*-QM derived from hydroxyclavatol. It was proven that the *ortho*-QM can be served as an excellent Michael acceptor for a variety of natural or natural-like products, ranging from different phenolic compounds to indole derivatives. 32 clavatol-containing products were isolated and identified from selected incubations. These structures were either formed by incorporation of a clavatol unit onto the *ortho*- or *para*-position of phenolic hydroxyl groups or onto the C-2 position of indole skeletons. In a few cases, C-N linked clavatol adducts were also obtained. In analogy, it is possible that the clavatol-coupling natural products found from *Penicillium* species could also be formed by nonenzymatic Michael addition *via* the *ortho*-QM intermediate. Considering the high reactivity of the *ortho*-QM, more clavatol-containing compounds can be expected to be easily created artificially or naturally.

For details on this work, please see the publication (section 4.4)

Ge Liao*, Jie Fan*, Lena Ludwig-Radtke, Katja Backhaus, and Shu-Ming Li (2020). Increasing structural diversity of natural products by Michael addition with *ortho*-quinone methide as the acceptor. *Journal of Organic Chemistry*, 85 (2), 1298–1307, DOI:10.1021/acs.joc.9b02971 (*equal contribution)

4 Publications

4.1 Complete decoration of the indolyl residue in *cyclo*-L-Trp-L-Trp with geranyl moieties by using engineered dimethylallyl transferases

Organic LETTERS

Letter

Cite This: Org. Lett. 2018, 20, 7201−7205

pubs.acs.org/OrgLett

Complete Decoration of the Indolyl Residue in *cyclo*-L-Trp-L-Trp with Geranyl Moieties by Using Engineered Dimethylallyl Transferases

Ge Liao,[†,§] Peter Mai,[†,§] Jie Fan,[†] Georg Zocher,[‡] Thilo Stehle,[‡] and Shu-Ming Li*[,†]

[†]Institut für Pharmazeutische Biologie und Biotechnologie, Philipps-Universität Marburg, Robert-Koch Strasse 4, Marburg 35037, Germany

[‡]Interfakultäres Institut für Biochemie, Eberhard Karls Universität Tübingen, Tübingen 72076, Germany

Supporting Information

ABSTRACT: Mutation of the gatekeeping residues for prenyl donor selectivity in six dimethylallyl transferases significantly increased their activities toward geranyl diphosphate. Forty-two geranylated derivatives were obtained from 15 cyclic dipeptides by using the engineered enzymes. Taking *cyclo*-L-Trp-L-Trp as an example, the geranyl moiety can be attached to all seven possible positions of the indole nucleus. This study demonstrates a convenient way to increase the structural diversity of geranylated products by structure-based engineering of the available dimethylallyl transferases.

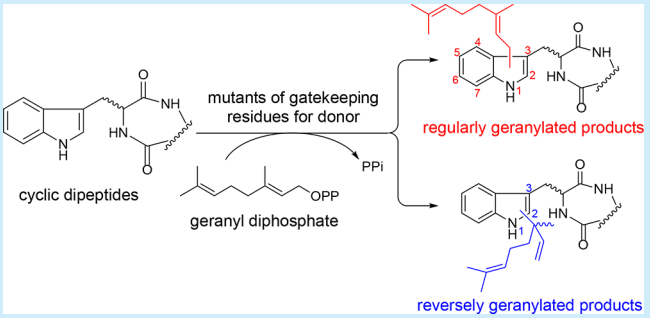

Prenylated natural products are hybrid structures containing prenyl moieties ($n \times C_5$) or derivatives thereof and are widely distributed in plants and microorganisms.[1−3] Among them, prenylated indole alkaloids including prenylated tryptophan-containing cyclic dipeptides (CDPs) usually exhibit a wide range of biological and pharmacological activities and, therefore, are important sources for drug discovery and development.[2,4,5] Representative structures such as notoamides,[6,7] roquefortines,[8] fumitremorgins,[9] and fellutanines[10−12] are commonly derived from CDPs and often decorated with one or more dimethylallyl (C_5) moieties (Figure 1).

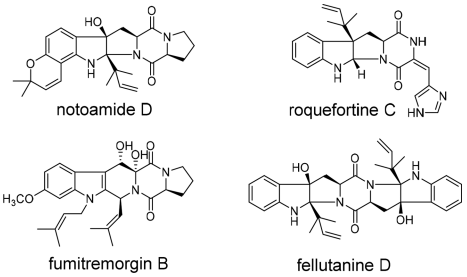

Figure 1. Representative examples of prenylated indole alkaloids derived from cyclic dipeptides.

The key reactions in the biosynthesis of the prenylated natural products are connections of the prenyl moiety with its acceptor catalyzed by prenyltransferases (PTs). PTs belonging to the dimethylallyltryptophan synthase (DMATS) superfamily catalyze the regiospecific Friedel−Crafts alkylation of aromatic substrates, mainly of indole derivatives.[13,14] The attachment of the C_5 unit to *N1* and the six nonbridgehead carbons at the indole ring can be achieved by the available indole PTs.[13−15] However, the transfer of the C_{10} unit (geranyl) onto the indole nucleus was rarely reported. Taking CDPs as examples, AnaPT from *Neosartorya fischeri* catalyzes in the presence of dimethylallyl diphosphate (DMAPP) reverse *C3*-prenylation and also uses geranyl diphosphate (GPP) for their *C6*- and *C7*-geranylation, as exemplified by cWW (**1**; for simplicity, one letter codes are used for proteinogenic amino acids) in Scheme 1.[16,17] AtaPT from *Aspergillus terreus* was reported to catalyze the *C4*-geranylation of **1**.[18] Our recent reinvestigation on this

Scheme 1. Reverse Dimethylallyl *C3*-PT AnaPT from *N. fischeri* Can Also Use GPP for *C6*- and *C7*-Geranylation[a]

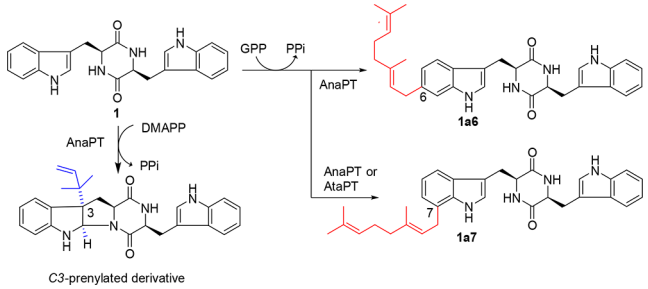

[a]AtaPT from *A. terreus* attaches a geranyl moiety to *C7* of **1**. To facilitate the reading flow, geranylated products are named by using substrate number, prenylation pattern (**a** for regular or normal and **b** for reverse prenylation), and prenylation position at the indole ring (**1** to **7** for *N1*- to *C7*-alkylated products), e.g., **1a6** for *C6*-regularly geranylated cWW.

Received: October 1, 2018
Published: October 31, 2018

DOI: 10.1021/acs.orglett.8b03124
Org. Lett. 2018, 20, 7201−7205

reaction revealed a *C7*- instead of a *C4*-geranylation (data not shown). Other CDPs with geranyl residues have not yet been reported. Furthermore, only a few members of PTs are able to accept GPP as a prenyl donor and act as geranyl transferases, *e.g.* TleC,[19] VrtC,[20] and AmbP1.[21] Therefore, it is necessary to find new geranyl transferases or to manipulate available dimethylallyl transferases for GPP acceptance to enrich the biocatalysis toolboxes.

Inspired by the activities of AtaPT and AnaPT toward GPP for prenylation of CDPs, we first evaluated the GPP acceptance of five dimethylallyl transferases, FtmPT1,[22] CdpNPT,[23] BrePT,[24] CdpC2PT,[25] and CdpC3PT,[26] in the presence of CDPs as acceptors. These enzymes catalyze regular (normal) or reverse prenylations at C-2 or C-3 of the indole ring. The tested CDPs include **1**, cWP (**2**) and its stereoisomers (**3**−**5**), cWA (**6**) and its stereoisomers (**7**−**9**), cWL (**10**), cWY (**11**), cWF (**12**), cWG (**13**), (*S*)-(**14**), and (*R*)-benzodiazepinedinone (**15**). HPLC analysis of the incubation mixtures showed that the five PTs well accepted their natural or best aromatic substrates in the presence of DMAPP (Figure S1 in the Supporting Information (SI)), confirming the presence of active proteins. In the presence of GPP, CdpC2PT showed clear activity toward **1**, **2**, **14**, and **15** (Figure S2). The other four enzymes exhibited very low (CdpC3PT toward **1**, **2**, **5**, and **14**, Figure 2, Figure S3) or no activity (CdpNPT, FtmPT1, and BrePT) (Figure 2, Figures S4−S6), when GPP was used as a prenyl donor.

AtaPT was previously reported to have broad tolerance for prenyl donors. The residue Gly326 was proven to contribute to the enlarged pocket for donor binding.[18] Mutation of Gly326 to methionine dramatically reduced the activity of G326M toward GPP and FPP, but substantially enhanced the catalytic activity with DMAPP. This proved that the size of the residue at 326 controls the prenyl donor selectivity in AtaPT. Mutation of Met328 in the tryptophan prenyltransferase FgaPT2 to small amino acids such as cysteine, threonine, serine, glycine, or alanine significantly increased the acceptance of GPP.[27] Encouraged by these findings, structure-based protein sequence alignments of AtaPT and FgaPT2 with the five PTs mentioned above led to the identification of the corresponding residues Met364 in FtmPT1, IIe337 in BrePT, Thr351 in CdpC2PT, Met349 in CdpNPT, and Phe335 in CdpC3PT (Figure 3, Figure S7).

Molecular modeling with the ternary crystal structures of FtmPT1 and CdpNPT[23,28] also uncovered Met364 in FtmPT1 and Met349 in CdpNPT as key residues for DMAPP selectivity (Figure S8). The side chain of this residue seals the active site to form a pocket for DMAPP. In the active site of both enzymes, GPP would clash with the side chain of the gatekeeping residue methionine. Therefore, reducing the steric pressure in the DMAPP binding site by replacement of this bulky residue with a small amino acid like glycine would increase the enzymatic activity toward GPP.

To switch the prenyl donor specificity from DMAPP to GPP for FtmPT1, BrePT, CdpNPT, and CdpC3PT and to expand the GPP acceptance of CdpC2PT, we replaced the mentioned amino acids of the five dimethylallyl transferases by glycine, resulting in the mutants FtmPT1_M364G, BrePT_I337G, CdpNPT_M349G, CdpC2PT_T351G, and CdpC3PT_F335G, respectively (see Table S1 for constructs and SI for description). As expected, replacing bulky amino acids by glycine significantly improved in most cases the CDP consumption in the presence of GPP (Figure 2, Figures S2−S6, S9). In comparison, the acceptance of DMAPP by the mutants was reduced to different levels (Figure S1). In sharp contrast to no activity in the presence of GPP by wild type CdpNPT, FtmPT1, and BrePT, all the tested CDPs (**1**−**15**) were accepted by CdpNPT_M349G with total product yields from 13.7% to 95.8% (Figure 2, Figures S4 and S9). **1**−**13** with a diketopiperazine ring were consumed by FtmPT1_M349G with total product yields from 9.6% to 75.4%. The two benzodiazepinediones **14** and **15** were not accepted (Figure 2, Figures S5 and S9).

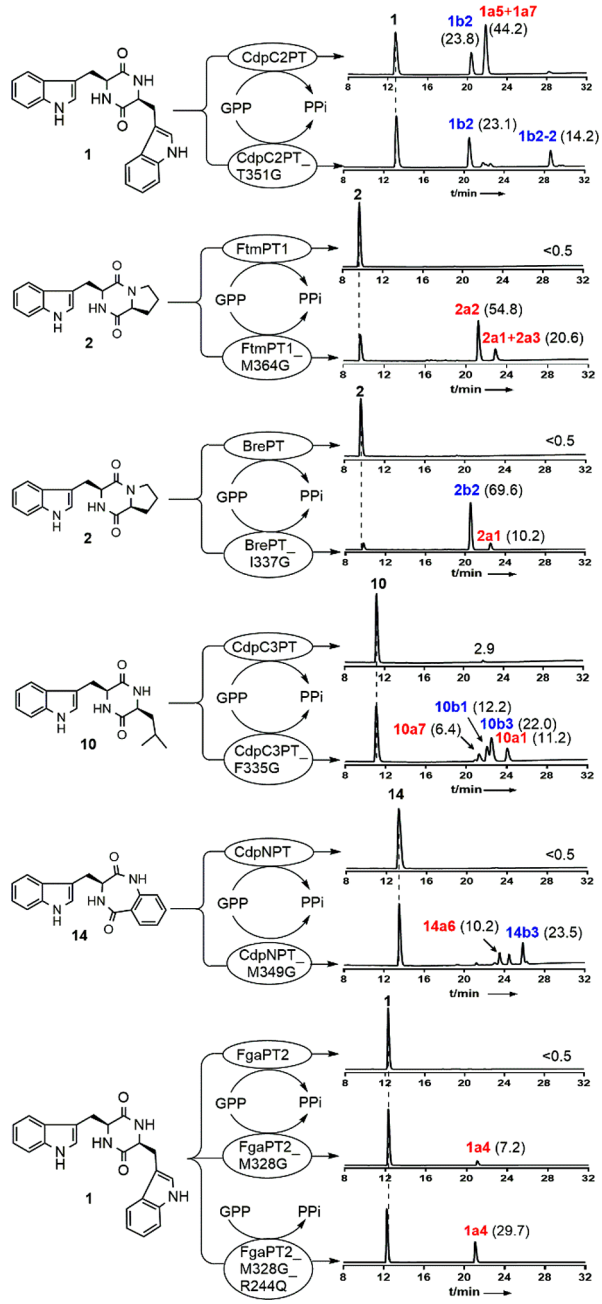

Figure 2. HPLC chromatograms of the incubation mixtures of six dimethylallyl transferases and their corresponding mutants with their natural or best accepted substrates in the presence of GPP. Regular geranylated products are labeled in red, and reverse, in blue. The product yields are given in parentheses after the product number. See please Figure S1 for their behavior toward DMAPP.

DOI: 10.1021/acs.orglett.8b03124
Org. Lett. 2018, 20, 7201−7205

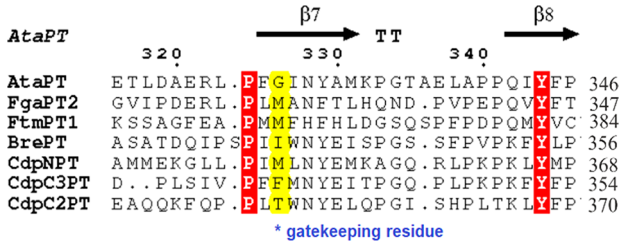

Figure 3. Selected region of structure-based alignments of PTs used in this study with AtaPT and FgaPT2. See Figure S7 for complete alignments.

The activity of BrePT toward GPP can be strongly increased by mutation at the gatekeeping residue Ile337, at least for its natural substrate **2** (79.8%) and the two stereoisomers **3** (71.4%) and **4** (28.4%) (Figure 2, Figure S6). In the case of CdpC3PT_F335G, conversion of almost all substrates was significantly increased, especially for **10**. Its conversion was improved from 2.9% by the wild type enzyme to 51.8% by this mutant (Figure 2, Figure S3). CdpC2PT_T351G exhibited different behaviors toward **1**−**15** from CdpC2PT, with distinct products or different ratios of the same products (Figure 2, Figures S2 and S9). Detailed inspection of the HPLC chromatograms of **1**−**15** with FtmPT1_M364G, BrePT_I337G, CdpNPT_M349G, CdpC2PT_T351G, and CdpC3PT_F335G (Figures S2−S6, S9) revealed the presence of one to four product peaks with different ratios. Most reactions have two or three products. This shows the relaxed regiospecific geranylation by the mutants in comparison to the wild type enzymes in the presence of DMAPP.

For structure elucidation, 41 representative products of selected substrates were isolated by preparative HPLC from different incubation mixtures (Table S2) and subjected to HR-ESI-MS and ^{1}H NMR analyses (Tables S2−S18, Figures S10−S54). Structure elucidation (see the SI) confirmed reverse or regular geranylation at different positions of the indole ring (Scheme 2).

Three of the tested PTs catalyze regular (FtmPT1) or reverse (BrePT and CdpC2PT) *C2*-prenylations of CDPs in the presence of DMAPP.[22,24,25] Structure elucidation proved that BrePT_I337G catalyzes solely or predominantly still reverse *C2*-geranylation of **2**− **4**. In the reaction mixtures of FtmPT1_M364G with six substrates, regularly *C2*-prenylated derivatives were obtained as major products, i.e. **1a2**, **2a2**, **3a2**, **10a2**, **11a2**, and **12a2**. Regularly *C3*-prenylated derivatives such as **1a3**, **3a3**, **6a3**, **8a3**, **10a3**, **11a3**, **12a3**, and **13a3** were identified in at least eight incubation mixtures. This is not surprising, because regularly *C3*-prenylated CDPs were also reported for FtmPT1 in the presence of DMAPP.[29] In that study, however, regularly *C2*-prenylated derivatives have been identified as the major products. Interestingly, in the assays of FtmPT1_M364G with GPP and **6**, **8**, and **13**, no *C2*-, but regularly *N1*- and *C3*-geranylated derivatives were obtained (Scheme 2, Figure S5). The behavior of CdpC2PT_T351G toward GPP also differs significantly from that of the wild type enzyme. For example, **1** was converted by CdpC2PT to **1b2**, **1a5**, and **1a7**, while CdpC2PT_T351G mainly catalyzes *C2*-geranylation, resulting in the formation of mono- (**1b2**) and digeranylated (**1b2-2**) derivatives (Figure 2, Figure S9). CdpC3PT and CdpNPT both catalyze reverse *C3*-prenylation of CDPs in the presence of DMAPP.[23,26] Reverse *C3*-geranylation was also detected for CdpNPT_M349G with

Scheme 2. Structures of Enzyme Products with Different Prenylation Patterns and Positions (Products of 1 Are Presented in Scheme 3)

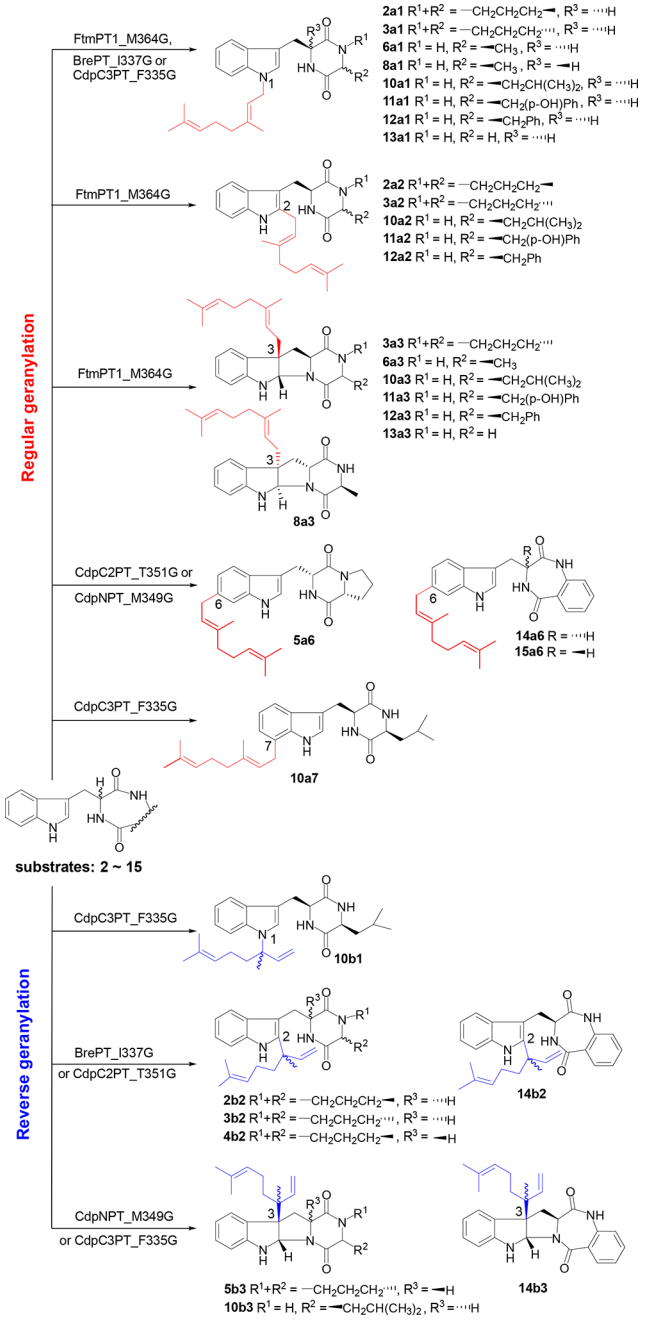

the selected substrates **1**, **5**, and **14**. In addition, regularly *C6*-geranylated products **1a6**, **5a6**, and **14a6** were also identified. In the incubation mixture of CdpNPT_M349G with **15**, the product **15a6** was even the predominant peak (Figure S4). CdpC3PT_F335G converted **10** to a mixture of at least four products **10a1**, **10b1**, **10b3**, and **10a7** with **10b3** as the major one (Figure S3). These results indicate the trends of *C6*- and *C7*-geranylation of CDPs by dimethylallyl transferases, which catalyze *C3*-prenylation in the presence of DMAPP, as observed for AnaPT (Scheme 1).[16,17]

In summary, our results presented in this study showed that replacing the gatekeeping residue not only changes the tolerance of PTs toward prenyl donor with longer chain but

DOI: 10.1021/acs.orglett.8b03124
Org. Lett. 2018, 20, 7201−7205

also breaks their regiospecificity, leading to several prenylated products in one incubation. To some extent, this change broadens their application in creation of structure diversity of geranylated indole derivatives. The possible reason for the relaxed regioselective prenylation by the mutants could be that the enlarged pocket allows the binding of aromatic substrates in different orientations. However, the reduced regioselectivity requires more efforts for product isolation. Therefore, further mutagenesis experiments are necessary in the future to increase the desired regio- and stereoselectivity. This would require more structural information, *e.g.* of the available single mutants of the gatekeeping residues. Nevertheless, the single mutants constructed in this study clearly showed different preferences toward the 15 tested CDPs and converted them to geranylated derivatives at various positions. As shown in Scheme 2, products obtained in this study also carry the geranyl moiety at the *N1*-, *C2*-, and *C3*-position of the pyrrole ring in a regular or reverse manner.

To the best of our knowledge, known geranylations of diverse substrates usually occur at the benzene ring of the indole nucleus, *e.g.* *C7*-geranylation of indolactam V by TleC, *C6*-geranylation of tryptophan derivatives by 6-DMATS$_{Sa}$, and *C6*- and *C7*-geranylation of CDPs by AnaPT.[16,19,30] As mentioned above, the reported *C4*-geranylation of **1** by AtaPT[18] should be at C-7. Attachment of the geranyl moiety has been reported at neither C-4 or C-5 nor at N-1, C-2, or C-3 prior to this study.

The achieved relaxed regioselective geranylation by the mutants encouraged us to decorate all nucleophilic reactive positions (N-1 and the six nonbridgehead carbons) at the indole ring of one CDP with the geranyl moiety. For this purpose, **1** has been selected as the favorable CDP. HPLC analysis of the incubation mixture of **1** and GPP with FtmPT1_M364G, CdpNPT_M349G, CdpC2PT, and CdpC2PT_T351G revealed the presence of two to four product peaks each with product yields between 37.4 and 68.0% (Figure S9). Isolation and structure elucidation confirmed geranylations at N-1 (**1a1**), C-2 (**1a2** and **1b2**), C-3 (**1a3** and **1b3**), C-5 (**1a5**), C-6 (**1a6**), and C-7 (**1a7**) of the indole ring (Scheme 3). To get the remaining *C4*-position filled by geranylation, we applied the mutant FgaPT2_M328G, which uses GPP for *C4*-geranylation of tryptophan.[27] HPLC analysis of the incubation mixture of **1** and GPP with FgaPT2_M328G indicated product formation with a low yield (7.2%, Figure 2). In another previous study, we demonstrated that mutation on Arg244 of FgaPT2 significantly increased the catalytic activity toward CDPs in the presence of DMAPP.[31] To enhance the geranylation of **1**, we combined mutations at Met328 and Arg244 and created the double mutant FgaPT2_M328G_R244Q. As shown in Figure 2, one peak with a product yield of 29.7% was detected. Structure elucidation confirmed the desired geranylated product **1a4** (Scheme 3). In this way, nine products with a geranyl moiety at all nucleophilic reactive positions of the indole ring can be obtained from **1** by one-step chemoenzymatic reactions (Scheme 3, Figure S9).

With the tremendously increasing availability of protein structures, structure-based enzyme engineering becomes more important for modification of drug-like molecules. Indolactam geranyl transferase (TleC) can be changed to dimethylallyl transferase by small-to-large mutation.[19] MpnD and PagF were changed from selective dimethylallyl to geranyl transferases by large-to-small substitution.[19,32] In analogy, our study provides

Scheme 3. Attachment of Geranyl Moiety to Different Positions of 1 via One-Step Chemoenzymatic Reactions

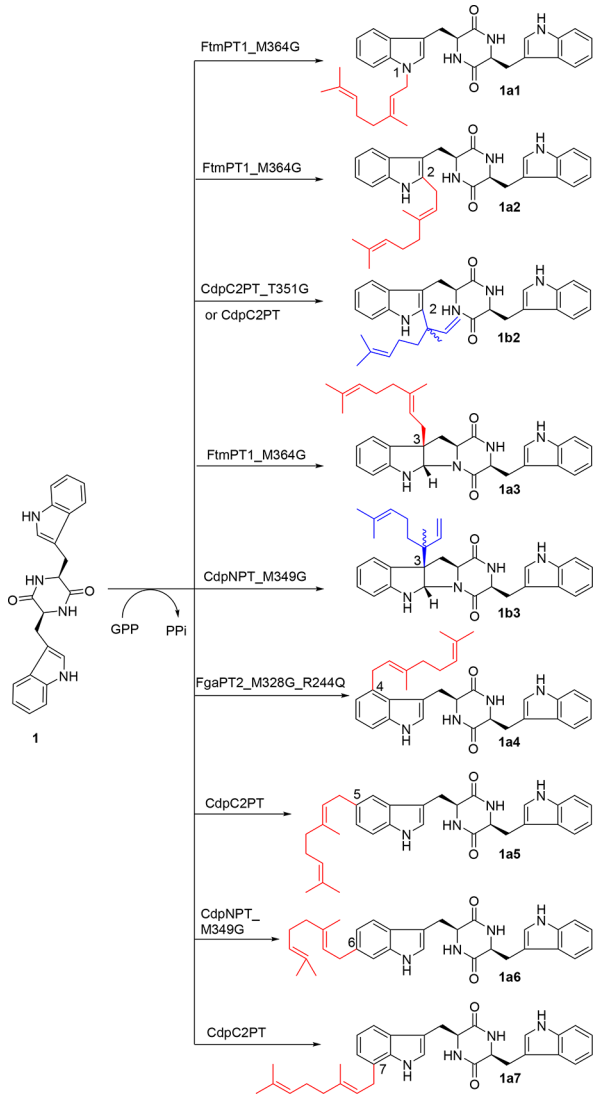

an excellent example for rational engineering of desirable enzymes. Mutation of the gatekeeping residues in six PTs turned on or improved the acceptance of GPP for geranylation of diverse CDPs. Forty-two geranylated products were obtained from *in vitro* enzymatic reactions of CDPs and GPP. Using **1** as an acceptor and GPP as a donor, N-1 and the six nonbridgehead carbons of the indole ring were decorated with geranyl moieties. Derivatives of other CDPs could also be obtained by the mutants described in this study or by mutation of additional available dimethylallyl transferase at the corresponding positions.

■ ASSOCIATED CONTENT

Supporting Information

The Supporting Information is available free of charge on the ACS Publications website at DOI: 10.1021/acs.orglett.8b03124.

Experimental procedures, structural elucidation, and NMR spectra of geranylated products (PDF)

DOI: 10.1021/acs.orglett.8b03124
Org. Lett. 2018, 20, 7201−7205

AUTHOR INFORMATION

Corresponding Author

*E-mail: shuming.li@staff.uni-marburg.de.

ORCID

Shu-Ming Li: 0000-0003-4583-2655

Author Contributions

§G.L. and P.M. contributed equally.

Notes

The authors declare no competing financial interest.

ACKNOWLEDGMENTS

We thank Rixa Kraut, Stefan Newel (University of Marburg) for synthesis of prenyl donors, taking MS and NMR spectra, respectively. S.M.L. acknowledges the DFG for funding the Bruker microTOF QIII mass spectrometer (INST 160/620-1). Ge Liao (201607565014) and Jie Fan (201507565006) are scholarship recipients from the China Scholarship Council.

REFERENCES

(1) Heide, L. *Curr. Opin. Chem. Biol.* **2009**, *13*, 171.
(2) Li, S. M. *Nat. Prod. Rep.* **2010**, *27*, 57.
(3) Fan, A.; Winkelblech, J.; Li, S.-M. *Appl. Microbiol. Biotechnol.* **2015**, *99*, 7399.
(4) Borthwick, A. D. *Chem. Rev.* **2012**, *112*, 3641.
(5) Wollinsky, B.; Ludwig, L.; Hamacher, A.; Yu, X.; Kassack, M. U.; Li, S. M. *Bioorg. Med. Chem. Lett.* **2012**, *22*, 3866.
(6) Kato, H.; Yoshida, T.; Tokue, T.; Nojiri, Y.; Hirota, H.; Ohta, T.; Williams, R. M.; Tsukamoto, S. *Angew. Chem., Int. Ed.* **2007**, *46*, 2254.
(7) Tsukamoto, S.; Kato, H.; Samizo, M.; Nojiri, Y.; Onuki, H.; Hirota, H.; Ohta, T. *J. Nat. Prod.* **2008**, *71*, 2064.
(8) García-Estrada, C.; Ullán, R. V.; Álbillos, S. M.; Fernández-Bodega, M. A.; Durek, P.; von Döhren, D. H.; Martín, J. F. *Chem. Biol.* **2011**, *18*, 1499.
(9) Li, S.-M. *J. Antibiot.* **2011**, *64*, 45.
(10) Nuber, B.; Hansske, F.; Shinohara, C.; Miura, S.; Hasumi, K.; Endo, A. *J. Antibiot.* **1994**, *47*, 168.
(11) Kozlovsky, A. G.; Vinokurova, N. G.; Adanin, V. M.; Burkhardt, G.; Dahse, H. M.; Gräfe, U. *J. Nat. Prod.* **2000**, *63*, 698.
(12) Kozlovsky, A. G.; Vinokurova, N. G.; Adanin, V. M.; Burkhardt, G.; Dahse, H.-M.; Gräfe, U. *J. Nat. Prod.* **2001**, *64*, 553.
(13) Winkelblech, J.; Fan, A.; Li, S.-M. *Appl. Microbiol. Biotechnol.* **2015**, *99*, 7379.
(14) Tanner, M. E. *Nat. Prod. Rep.* **2015**, *32*, 88.
(15) Yu, X.; Liu, Y.; Xie, X.; Zheng, X.-D.; Li, S.-M. *J. Biol. Chem.* **2012**, *287*, 1371.
(16) Pockrandt, D.; Li, S.-M. *ChemBioChem* **2013**, *14*, 2023.
(17) Yin, W.-B.; Xie, X.-L.; Matuschek, M.; Li, S.-M. *Org. Biomol. Chem.* **2010**, *8*, 1133.
(18) Chen, R.; Gao, B.; Liu, X.; Ruan, F.; Zhang, Y.; Lou, J.; Feng, K.; Wunsch, C.; Li, S.-M.; Dai, J.; Sun, F. *Nat. Chem. Biol.* **2017**, *13*, 226.
(19) Mori, T.; Zhang, L.; Awakawa, T.; Hoshino, S.; Okada, M.; Morita, H.; Abe, I. *Nat. Commun.* **2016**, *7*, 10849.
(20) Chooi, Y. H.; Wang, P.; Fang, J.; Li, Y.; Wu, K.; Wang, P.; Tang, Y. *J. Am. Chem. Soc.* **2012**, *134*, 9428.
(21) Liu, X.; Hillwig, M. L.; Koharudin, L. M.; Gronenborn, A. M. *Chem. Commun. (Cambridge, U. K.)* **2016**, *52*, 1737.
(22) Grundmann, A.; Li, S.-M. *Microbiology* **2005**, *151*, 2199.
(23) Schuller, J. M.; Zocher, G.; Liebhold, M.; Xie, X.; Stahl, M.; Li, S.-M.; Stehle, T. *J. Mol. Biol.* **2012**, *422*, 87.
(24) Yin, S.; Yu, X.; Wang, Q.; Liu, X. Q.; Li, S.-M. *Appl. Microbiol. Biotechnol.* **2013**, *97*, 1649.
(25) Mundt, K.; Li, S.-M. *Microbiology* **2013**, *159*, 2169.
(26) Yin, W.-B.; Yu, X.; Xie, X.-L.; Li, S.-M. *Org. Biomol. Chem.* **2010**, *8*, 2430.
(27) Mai, P.; Zocher, G.; Stehle, T.; Li, S.-M. *Org. Biomol. Chem.* **2018**, *16*, 7461.
(28) Jost, M.; Zocher, G.; Tarcz, S.; Matuschek, M.; Xie, X.; Li, S.-M.; Stehle, T. *J. Am. Chem. Soc.* **2010**, *132*, 17849.
(29) Wollinsky, B.; Ludwig, L.; Xie, X.; Li, S.-M. *Org. Biomol. Chem.* **2012**, *10*, 9262.
(30) Winkelblech, J.; Li, S.-M. *ChemBioChem* **2014**, *15*, 1030.
(31) Fan, A.; Li, S.-M. *Appl. Microbiol. Biotechnol.* **2016**, *100*, 5389.
(32) Estrada, P.; Morita, M.; Hao, Y.; Schmidt, E. W.; Nair, S. K. *J. Am. Chem. Soc.* **2018**, *140*, 8124.

DOI: 10.1021/acs.orglett.8b03124
Org. Lett. 2018, 20, 7201−7205

Supporting Information

Complete decoration of the indolyl residue in *cyclo*-L-Trp-L-Trp with geranyl moieties by using engineered dimethylallyl transferases

Ge Liao,[†,§] Peter Mai,[†,§] Jie Fan,[†] Georg Zocher,[‡] Thilo Stehle,[‡] and Shu-Ming Li[*,†]

[†] Institut für Pharmazeutische Biologie und Biotechnologie, Philipps-Universität Marburg, Robert-Koch Strasse 4, Marburg 35037, Germany

[‡] Interfakultäres Institut für Biochemie, Eberhard Karls Universität Tübingen,Tübingen 72076, Germany

[§]These authors contributed equally to this work.

SUPPORTING INFORMATION

Table of content

Experimental Procedures

Chemicals. Dimethylallyl diphosphate (DMAPP) and geranyl diphosphate (GPP) were chemically prepared according to the literature.[1] *Cyclo*-Trp-Pro isomers (**2** − **5**) and *cyclo*-Trp-Ala isomers (**6** − **9**) were synthesized according to the method published previously.[2,3] *Cyclo*-L-Trp-L-Pro and *cyclo*-L-Trp-D-Pro were synthesized from H-L-Trp-OMe·HCl and N-Boc-L-Pro-OH, *cyclo*-D-Trp-L-Pro and *cyclo*-D-Trp-D-Pro from H-D-Trp-OMe·HCl and N-Boc-D-Pro-OH. In analogy, the two pairs H-L-Trp-OMe·HCl and N-Boc-L-Ala-OH as well as H-D-Trp-OMe·HCl and N-Boc-D-Ala-OH were used for the preparation of the four stereoisomers of *cyclo*-Trp-Ala (**6** − **9**). (*R*)-benzodiazepinedione (**14**) and (*S*)-benzodiazepinedione (**15**) were synthesized by condensation of D- or L-tryptophan with isatoic anhydride in the presence of triethylamine according to the method described by Barrow and Sun.[4] Other cyclic dipeptides (**1**, **10** − **13**) were obtained from Bachem (Bubendorf, Switzerland).

Strains. *E. coli* strains M15 [pREP4] (Qiagen, Hilden, Germany), BL21(DE3) pLysS (Invitrogen, Karlsruhe, Germany), and XL1-Blue MRF´ (Stratagene, Amsterdam, the Netherlands) were used for the overproduction of recombinant proteins. Luria-Bertani (LB) medium supplemented with 50 µg/mL carbenicillin or 50 µg/mL kanamycin was used for cultivation of recombinant *E. coli* strains.

Site-directed mutagenesis. Plasmids harboring genes encoding recombinant PTs were used as DNA template for mutagenesis by PCR. To obtain specific mutations at desired gene position, (degenerated) primers were designed as described in the optimized site-directed mutagenesis protocols and synthesized by Eurofins Genomics GmbH (Ebersberg, Germany) or Seqlab GmbH (Göttingen, Germany) (Table S1).[5,6] Expand Long Template PCR System (Roche Diagnostics GmbH, Mannheim) was applied for PCR amplification. PCR reaction mixtures and thermal profiles were set as recommended by the manufacturer instructions. An annealing temperature of 62°C and elongation time of 8 min for *brePT*and *fgaPT2,* and 4 min for *ftmPT1*, *cdpNPT*, *cdpC2PT* and *cdpC3PT* were adjusted to the thermal profile. The obtained plasmids were subjected to sequencing to confirm the desired mutations in the respective constructs.

Protein overproduction and purification as well as enzyme assays. The recombinant histidine-tagged PTs, His_8-FgaPT2, His_5-BrePT, FtmPT1-His_6, CdpNPT-His_6, CdpC2PT-His_6, and His_6-CdpC3PT as well as the corresponding engineered mutants were overproduced in *E.coli* and purified by Ni-NTA affinity chromatography (Qiagen, Hilden) according to the published procedures.[7-11] The enzymatic reaction mixtures (50 µL) of FgaPT2, FtmPT1, and BrePT contained 50 mM Tris-HCl (pH 7.5), 10 mM $CaCl_2$, 1 mM cyclic dipeptide, 2 mM DMAPP or GPP, 0.7%–6% (v/v) glycerol, up to 5% (v/v) DMSO, and 10 µg of purified protein. For determination of the relative activities of CdpC2PT, CdpC3PT, and CdpNPT with different cyclic dipeptides, each reaction mixture (50 µL) contained 50 mM Tris-HCl (pH 7.5), 2 mM DTT, 1 mM aromatic substrate, 2 mM DMAPP or GPP, 0.7%–6% (v/v) glycerol, up to 5% (v/v) DMSO, and 50 µg purified protein for CdpC2PT and CdpC3PT and 30 µg for CdpNPT. The reaction mixtures were incubated at 37 °C for 2 h (FgaPT2, FtmPT1, and BrePT) or 16 h (CdpC2PT, CdpC3PT, and CdpNPT). The reaction mixtures were terminated by addition of one volume methanol. Before injecting to HPLC, the proteins were removed by centrifugation at 13,000 rpm for 20 min. The enzyme reactions of the mutated proteins were performed as for the wildtype enzymes. Product yields of the enzyme reactions were calculated from peak areas of prenylated products and substrates as analyzed on HPLC. Repeated enzyme assays were performed independently.

HPLC conditions for analysis and isolation of enzyme products. Analysis of reaction mixtures were performed on an Agilent series 1200 HPLC (Agilent Technologies, Böblingen, Germany) with an Agilent Eclipse XDB-C18 column (150 × 4.6 mm, 5 µm). Water (A) and acetonitrile (B) were used as solvents at flow rate of 0.5 mL/min. The substances were eluted with a linear gradient from 20–45 % B in 10 min, followed by 45–75% B in 5 min and 75–100% B in another 10 min. The column was then washed with 100 % (v/v) solvent B for 5 min and equilibrated with 5 % (v/v) solvent B for 5 min. Detection was carried out on a photodiode array detector and illustrated for aborptions at 296 nm. For isolation, the same HPLC equipment with a semipreparative Agilent ZORBAX Eclipse XDB C18 HPLC column (250 ×9.4 mm, 5 µm) at a fow rate of 2.5 mL/min was used. Water and acetonitrile were also used as solvents. Isocratic elution was performed with 75%, 80% or 85% acetonitrile/water for product isolation.

LC-MS analysis of enzyme reactions. LC-MS analysis was performed on a microTOF-Q III spectrometer (Bruker, Bremen, Germany) with an Agilent 1260 HPLC system (Agilent Technologies, Böblingen, Germany) by using the same column and elution condition. Electrospray positive ionization mode was selected for determination the accuracy masses. Sodium formate was used in each run for mass calibration. The masses were scanned in the range of m/z 100 − 1500. The capillary voltage was set to 4.5 kV and a collision energy of 8.0 eV. Data were evaluated with the Compass DataAnalysis 4.2 software (Bruker Daltonik, Bremen, Germany).

Preparation and identification of the reaction products. To prepare the enzyme products for structural elucidation, assays were carried out in large scales (10 − 20 mL) containing 2 mM GPP, 1 mM cyclic dipeptide, 10 mM $CaCl_2$ or 2 mM DTT, 50 mM Tris-HCl (pH 7.5), up to 5% (v/v) DMSO, and 2 − 10 mg purified recombinant protein per 10 mL mixtures. After incubation for 16 h at 37 °C, the reaction mixtures were extracted subsequently with double volume of ethyl acetate for three times. The organic phases were combined and concentrated under vacuum. The resulted residues were dissolved in MeOH and centrifuged at 13,000 rpm for 20 min. The enzyme products were then purified on a semi-preparative HPLC. ^{1}H NMR spectra were recorded on a JOEL ECA-500 MHz spectrometer (JEOL, Tokyo, Japan). All spectra were processed with MestReNova 6.1.0 (Metrelab). Chemical shifts are referenced to those of the solvent signals.

Structure-based protein sequence alignments. Protein sequence alignments were carried out by using the sequence alignment function of MEGA 5.2 and visualized with ESPript 3.0 (http://espript.ibcp.fr/ESPript/ESPript/). For the secondary structure prediction, AtaPT (accession number 5KCG, www.rcsb.org) was taken as a reference.

Molecular modeling and docking. The conformations of the mutants were calculated in silico using foldx.[12,13] Substrate docking was done manually for GPP using COOT[14] and DMAPP of FtmPT1 (pdb-code: 3I4X) and CdpNPT (pdb-code: 3O2K) as templates. The conformation of the prenyl donors were energetically optimized. Figure S8 was generated with pymol (The PyMOL Molecular Graphics System, Version 1.8 Schrödinger, LLC.).

Structural elucidation

In total, 42 enzyme products were obtained in this study. LC-HR-ESI-MS data (Table S2) showed that $[M+H]^+$ ions of 41 compounds are 136 Da larger than those of the respective substrates, proving the presence of a geranyl moiety each in their structures. In the case of **1b2-2**, the $[M+H]^+$ ion at m/z 645.4209 indicates a digeranylation. Inspection of the ^{1}H NMR spectra revealed that 31 products exhibited signals of regular geranyl moieties and 11 products are reversely geranylated products.

The different chemical shifts of the methylene group and of olefinic protons can be conveniently used to differentiate reversely or regularly prenylated derivatives, as exampled in Tables S3 and S4. The reverse geranyl moieties can be easily recognized by the presence of typical signals for three olefinic protons as two doublets around 5.0 and 5.2 ppm and one double doublets at 5.7 ppm with coupling constants of 17 and 10 Hz (Table S3). The chemical shifts of H-1' of regular geranyl moieties change dependently upon the attached position (Table S4). If the geranyl residue attached to an aromatic carbon like C-2, C-4, C-5, C-6 or C7, H-1' appears in the range of 3.3 − 3.7 ppm ($CDCl_3$). When it connected to C-3 of the indole ring, H-1' signal shifted upfield to 2.2 − 2.5 ppm ($CDCl_3$, Tables S3 and S4). In the case of attachment of a geranyl residue to nitrogen, the signal of H-1' will be shifted downfield to 4.6 − 4.8 ppm ($CDCl_3$).

According to the prenylation positions, the obtained products can be classified into 4 groups, i.e. *N1*-, *C2*-, and *C3*-geranylated products as well as those with geranyl moieties at C- 4 to C-7. These four groups can be easily distinguished by the signals of the protons H-2 and H-1' in their ^{1}H NMR as described above (Table S4). In total, 10 products were characterized as *N1*-geranylated derivatives including one reversely geranylated product (**10b1**). Although structures of *N1*-geranylated cyclic dipeptides have not been reported, signals in the aromatic region of the geranylated derivatives are nearly identical to those carrying a dimethylallyl moiety. Therefore, **1a1**, **2a1**, **3a1**, and **11a1** were identified by comparison with the reported NMR data of *N1*-prenylated compounds of the respective cyclic dipeptides.[10,15] Other five *N1*-geranylated products (**10a1**, **6a1**, **8a1**, **12a1**, and **13a1**) were characterized in comparison with their non-substituted substrates and tryptophan part of identified *N1*-geranylated products. **10b1** was identified as *cyclo*-N1-tert-geranyl-L-Trp-L-Leu based on the presence of typical signals for reverse geranyl moiety and *N1*-substitution pattern, as well as by comparison of the NMR data with those of cyclomarazine B.[16]

Differing from signals for *N1*-substitution pattern, regularly *C2*-geranylated products exhibited chemical shifts for H-1' at approx. 3.4 ppm ($CDCl_3$). **1a2**, **2a2**, and **10a2** were characterized by comparing with the reported NMR data of regularly *C2*-prenylated compounds. The characterization of reversely *C2*-geranylated products **1b2**, **1b2-2**, **2b2**, **3b2**, **4b2**, and **14b2** was carried out by comparison of their NMR data with those of the reported reversely *C2*-prenylated compounds of the respective cyclic dipeptides.[8,9,11] ^{1}H NMR spectra of **3a2**, **11a2**, and **12a2** exhibited similar signals for their geranyl moieties and indole skeleton, which also matched with the *C2*-substitution pattern. Therefore, six regularly and six reversely *C2*-geranylated indole derivatives were identified in this study.

C3-substitution pattern can be easily recognized in their ^{1}H NMR spectra. Ring closure between H-2 and H-12 resulted in upfield shifting of signal for H-2 from 6.4 − 7.2 ppm to 5.3 − 5.5 ppm and disappearance of the signal for H-12. **6a3**, **8a3**, **11a3**, and **13a3** were identified as regularly *C3*-geranylated cyclic dipeptides by comparing their NMR data with those of reported regularly *C3*-prenylated compounds of the respective cyclic dipeptides.[17] **1b3**, **5b3**, **10b3**, and **14b3** were characterized as reversely *C3*-geranylated products by comparison of their NMR data with those reported for reversely *C3*-prenylated derivatives.[15,17-19] Typical signals for regular *C3*-geranyaltion are easily observed not only for the aforementioned H-2 and H-12 protons, but also for H-1' of the C_{10} unit. Differing from the *N1*- or *C2*-susbstitution, signals of H-1' of *C3*-susbtitution shifted to approx. 2.4 ppm. Thus, **1a3**, **3a3**, **10a3**, and **12a3** were accordingly identified as regular *C3*-geranylated products. The relative configuration of geranyl and H-2 were determined according to ^{1}H-^{1}H vicinal coupling patterns of H-11 and chemical shifts of H-10syn of known *anti-cis* and *syn-cis* configured prenylated pyrroloindoline diketopiperazines that summarized in a previous paper.[15] With the exception for **5b3**, all *C3*-geranylated products obtained in this study have a *syn-cis* configuration.

In addition to the products with geranyl moieties at position 1 to 3 of the pyrrole ring, seven products with geranyl substitution at the benzene ring were also identified. A set of characteristic signals for three protons at the benzene ring was observed in their ^{1}H NMR spectra, which differs clearly from the coupling pattern consisting of four protons in the case of pyrrole ring substitution. The signals of the three coupling protons on the *C4*- and *C7*-geranylated benzene ring are found as doublet, triplet and doublet with coupling constants of approximate 7 − 8 Hz. In comparison, the signals of the three protons on the *C5*- and *C6*-geranylated benzene ring appear as two doublets with a coupling constant of approximate 8 Hz and one (broad) singlet. The difference between *C5*- and *C6*- as well as between *C4*- and *C7*-substitution in ^{1}H NMR spectra can be distinguished by the order of the signals of the three protons, as listed in Table S5. One *C4*-geranylated product **1a4**, four *C6*-geranylated derivatives **1a6**, **5a6**, **14a6**, and **15a6**, and two *C7*-geranylated compounds **1a7** and **10a7** were identified by comparing with the reported data of known geranylated compounds of the respective cyclic dipeptides.[20-22] **1a5** was identified as a *C5*-geranylated compound by the presence of nearly identical signals on the indole ring as those of *C5*-prenylated tryptophan derivatives.[23,24]

Table S1. List of primers and constructed plasmids used in this study.

Mutant	Plasmid	Template	Primer	Sequence (5`→3`)	Protein yield (mg/L culture)
BrePT_I337G	pPM81	pSY1[9]	I337G_f I337G_r	CCATC**GGG**TGGAACTACGAGATCAGTCCTGGG GTTCCA**CCC**GATGGGCGATGGGATCTGGTC	1.5
FtmPT1_M364G	pPM83	pAG012[8]	M364G_f M364G_r	TATG**GGG**TTCCACTTCCACCTGGACGGGAGTC GAAGTGGAA**CCC**CATAGGCGCCTCGAACCC	4.3
CdpNPT_M349G	pPM85	pHL5[10]	M349G_f M349G_r	CATT**GGG**CTGAACTATGAGATGAAGGCCGGCCAGC TCATAGTTCAG**CCC**AATGGGCAAGAGCCCTTTCTCC	1.6
CdpC2PT_T351G	pPM82	pKM16[11]	T351G_f T351G_r	TTTA**GGG**TGGAATTACGAGCTGCAACCTGGCATTTCCCATCC GCTCGTAATTCCA**CCC**TAAAGGGGGTTGAAATTTCTGCTGTGC	1.5
CdpC3PT_F335G	pPM86	pWY25[7]	F335G_f F335G_r	GTTC**GGG**ATGAACTACGAGATAACCCCGGGGCAGC CGTAGTTCAT**CCC**GAACGGCACAATGCTCAGAGGG	2.3
FgaPT2_M328G_R244Q	pPM46	pPM28[25]	R244Q_f R244Q_r	CAGTCCC**CAA**CTAGTGTCCTGTGATCTGACCAGTCCTGC GACACTAG**TTG**GGGACTGGCAGTGCTCTTGGAACCGC	2.5

Table S2. LC-HR-ESI-MS data of enzyme products.

Compund	Chemical formula	Isolated from	LC-HR-ESI-MS data $[M+H]^+$		Deviation [ppm]	Phisical description	approx. amount (mg)
			Calculated	Measured			
1a1	$C_{32}H_{36}N_4O_2$	**1** with FtmPT1_M364G	509.2911	509.2912	-0.3	colorless oil	1.1
2a1	$C_{26}H_{33}N_3O_2$	**2** with BrePT_I337G	420.2646	420.2660	-3.5	colorless oil	0.4
3a1	$C_{26}H_{33}N_3O_2$	**3** with FtmPT1_M364G	420.2646	420.2641	1.1	white powder	0.8
6a1	$C_{24}H_{31}N_3O_2$	**6** with FtmPT1_M364G	394.2489	394.2505	-4.0	colorless oil	0.8
8a1	$C_{24}H_{31}N_3O_2$	**8** with FtmPT1_M364G	394.2489	394.2488	0.4	colorless oil	1.0
10a1	$C_{27}H_{37}N_3O_2$	**10** with FtmPT1_M364G or CdpC3PT_F335G	436.2959	436.2963	-1.0	white powder	0.5
11a1	$C_{30}H_{35}N_3O_3$	**11** with FtmPT1_M364G	486.2751	486.2760	-1.8	white powder	0.6
12a1	$C_{30}H_{35}N_3O_2$	**12** with FtmPT1_M364G	470.2802	470.2823	-4.4	white powder	0.4
13a1	$C_{23}H_{29}N_3O_2$	**13** with FtmPT1_M364G	380.2333	380.2320	3.2	colorless oil	1.1
10b1	$C_{27}H_{37}N_3O_2$	**10** with CdpC3PT_F335G	436.2959	436.2963	-1.1	white powder	1.0
1a2	$C_{32}H_{36}N_4O_2$	**1** with FtmPT1_M364G	509.2911	509.2912	-0.2	colorless oil	1.0
2a2	$C_{26}H_{33}N_3O_2$	**2** with FtmPT1_M364G	420.2646	420.2655	-2.3	colorless oil	1.5
3a2	$C_{26}H_{33}N_3O_2$	**3** with FtmPT1_M364G	420.2646	420.2647	-0.3	white powder	1.1
10a2	$C_{27}H_{37}N_3O_2$	**10** with FtmPT1_M364G	436.2959	436.2961	-0.6	white powder	1.0
11a2	$C_{30}H_{35}N_3O_3$	**11** with FtmPT1_M364G	486.2751	486.2763	-2.5	colorless oil	1.0
12a2	$C_{30}H_{35}N_3O_2$	**12** with FtmPT1_M364G	470.2802	470.2797	1.1	white powder	0.1
1b2	$C_{32}H_{36}N_4O_2$	**1** with CdpC2PT or CdpC2PT_T351G	509.2911	509.2923	-2.4	white powder	1.3
1b2-2	$C_{42}H_{52}N_4O_2$	**1** with CdpC2PT_T351G	645.4163	645.4209	-7.1	colorless oil	0.8
2b2	$C_{26}H_{33}N_3O_2$	**2** with BrePT_I337G or CdpC2PT_T351G	420.2646	420.2655	-2.2	white powder	2.0
3b2	$C_{26}H_{33}N_3O_2$	**3** with BrePT_I337G	420.2646	420.2651	-1.4	colorless oil	1.3
4b2	$C_{26}H_{33}N_3O_2$	**4** with BrePT_I337G	420.2646	420.2649	-0.8	colorless oil	1.1
14b2	$C_{28}H_{31}N_3O_2$	**14** with CdpC2PT_T351G	442.2489	442.2487	0.5	colorless oil	1.1
1a3	$C_{32}H_{36}N_4O_2$	**1** with FtmPT1_M364G	509.2911	509.2901	2.1	colorless oil	0.9
3a3	$C_{26}H_{33}N_3O_2$	**3** with FtmPT1_M364G	420.2646	420.2654	-2.0	white powder	0.6
6a3	$C_{24}H_{31}N_3O_2$	**6** with FtmPT1_M364G	394.2489	394.2495	-1.5	colorless oil	0.7
8a3	$C_{24}H_{31}N_3O_2$	**8** with FtmPT1_M364G	394.2489	394.2508	-4.9	colorless oil	0.7
10a3	$C_{27}H_{37}N_3O_2$	**10** with FtmPT1_M364G	436.2959	436.2946	2.8	colorless oil	1.1
11a3	$C_{30}H_{35}N_3O_3$	**11** with FtmPT1_M364G	486.2751	486.2780	-6.0	white powder	0.5
12a3	$C_{30}H_{35}N_3O_2$	**12** with FtmPT1_M364G	470.2802	470.2820	-3.7	white powder	0.2
13a3	$C_{23}H_{29}N_3O_2$	**13** with FtmPT1_M364G	380.2333	380.2342	-2.5	colorless oil	0.4
1b3	$C_{32}H_{36}N_4O_2$	**1** with CdpNPT_M349G	509.2911	509.2931	-4.0	colorless oil	0.9
5b3	$C_{26}H_{33}N_3O_2$	**5** with CdpNPT_M349G	420.2646	420.2647	-0.3	colorless oil	0.8
10b3	$C_{27}H_{37}N_3O_2$	**10** with CdpC3PT_F335G	436.2959	436.2968	-2.2	white powder	0.5
14b3	$C_{28}H_{31}N_3O_2$	**14** with CdpNPT_M349G	442.2489	442.2487	0.5	colorless oil	1.1
1a6	$C_{32}H_{36}N_4O_2$	**1** with CdpNPT_M349G	509.2911	509.2925	-2.8	colorless oil	1.4
5a6	$C_{26}H_{33}N_3O_2$	**5** with CdpNPT_M349G	420.2646	420.2650	-1.0	colorless oil	1.6
14a6	$C_{28}H_{31}N_3O_2$	**14** with CdpNPT_M349G or CdpC2PT_T351G	442.2489	442.2482	1.5	colorless oil	0.5
15a6	$C_{28}H_{31}N_3O_2$	**15** with CdpNPT_M349G or CdpC2PT_T351G	442.2489	442.2493	-0.9	colorless oil	1.1
1a4	$C_{32}H_{36}N_4O_2$	**1** with FgaPT2_M328G_R244Q	509.2911	509.2917	-1.1	colorless oil	1.7
1a5	$C_{32}H_{36}N_4O_2$	**1** with CdpC2PT	509.2911	509.2891	4.0	white powder	1.2
1a7	$C_{32}H_{36}N_4O_2$	**1** with CdpC2PT	509.2911	509.2894	3.3	white powder	1.2
10a7	$C_{27}H_{37}N_3O_2$	**10** with CdpC3PT_F335G	436.2959	436.2968	-2.1	colorless oil	0.3

Table S3. Chemical shifts (ppm) of protons on regularly and reversely *C3*-substituted geranyl moiety of *cyclo*-L-Trp-L-Leu ($CDCl_3$).

	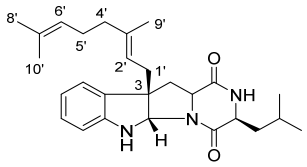 *C3*-regular	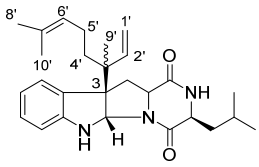 *C3*-reverse
H-1’	2.40, dd, 14.3, 7.4, 1H	5.26, d, 10.8, 1H
	2.44, dd, 14.3, 7.9, 1H	5.07, d, 17.4, 1H
H-2’	5.17, br t, 7.6, 1H	5.77, dd, 17.4, 10.8, 1H
H-4’	2.04, m, 2H	1.76, dd, 16.0, 7.7, 2H
H-5’	1.99, m, 2H	1.58, m, 1H*
	-	1.22, ddd, 17.5, 11.5, 5.6, 1H
H-6’	5.06, br t, 6.6, 1H	4.98, br t, 7.3, 1H
H-8’	1.68, s, 3H	1.63, s, 3H
H-9’	1.60, s, 3H	1.10, s, 3H
H-10’	1.52, s, 3H	1.51, s, 3H

[*] signal is overlapping with water.

Table S4. Typical proton signals of *N1*-, *C2*-, *C3*-, or benzene ring-geranylated derivatives.

	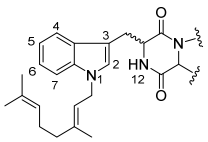	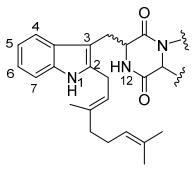	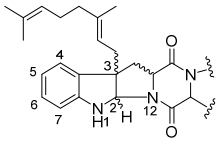	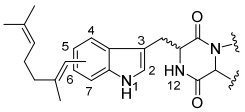
	N1-substitution[b]	*C2*-substitution[b]	*C3*-substitution[c]	benzene ring-substitution[b]
H-1’ [a]	4.6 − 4.8 ppm	3.3 − 3.5 ppm	2.2 − 2.5 ppm	3.4 − 3.7 ppm
H-1	-	7.8 − 8.0 ppm	-	7.9 − 8.2 ppm
H-2	6.4 − 7.2 ppm	-	5.3 − 5.5 ppm	6.5 − 7.2 ppm
H-12	5.6 − 5.8 ppm	5.6 − 5.8 ppm	-	5.6 − 6.0 ppm
benzene ring	AA’BB’ system	AA’BB’ system	AA’BB’ system	ABX system

[a] Here only referred to H-1’ of regular geranylated products. [b] chemical shifts in $CDCl_3$. [c] chemical shifts in CD_3OD.

Table S5. Signal of protons on the substituted benzene ring of *cyclo*-L-Trp-L-Trp (CD_3COCD_3).

	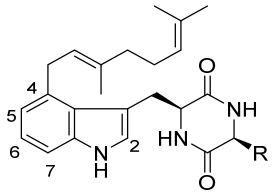	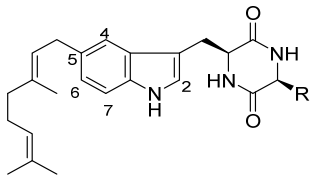	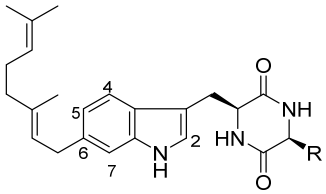	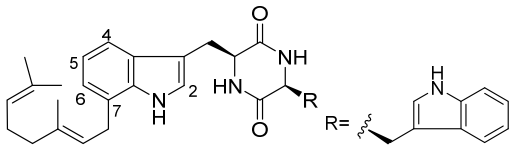
	C4-substitution	*C5*-substitution	*C6*-substitution	*C7*-substitution
H-2	7.10, d, 2.5	6.76, d, 2.4	6.70, d, 2.4	6.63, d, 2.5
H-4	-	7.34, d, 1.6	7.37, d, 8.1	7.33, d, 7.0
H-5	6.76, d, 7.3	-	6.88, dd, 8.1, 1.5	6.96, dd, 7.5, 7.0
H-6	6.94, dd, 8.0, 7.3	6.94, dd, 8.3, 1.6	-	6.93, d, 7.5
H-7	7.14, d, 8.0	7.24, d, 8.3	7.15, d, 1.5	-
	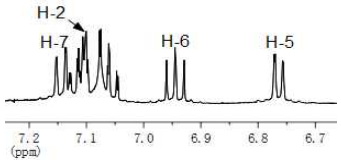	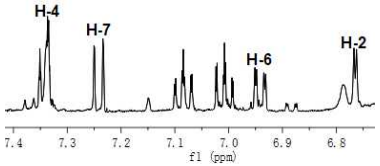	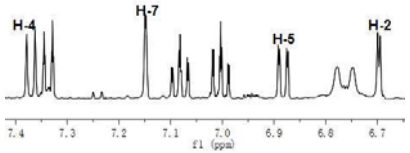	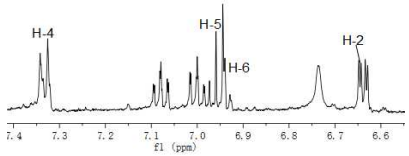

Table S6. ^{1}H NMR data of N1-geranylated derivatives (**1a1**, **2a1**, and **3a1)**.

Compound	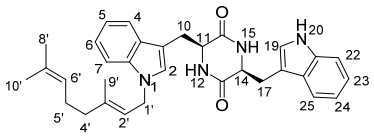 **1a1** ($CDCl_3$)	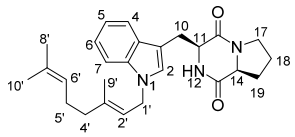 **2a1** (CD_3OD)	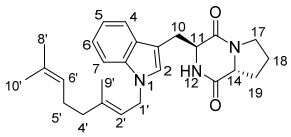 **3a1** ($CDCl_3$)
Position.	δ_H, multi., *J* in Hz	δ_H, multi., *J* in Hz	δ_H, multi., *J* in Hz
2	6.42, s, 1H	7.05, s, 1H	6.96, s, 1H
4	7.58, d, 7.9, 1H	7.58, d, 8.0, 1H	7.60, d, 8.0, 1H
5	7.15, dd, 8.0, 7.0, 1H[a]	7.03, dd, 8.0, 7.1, 1H	7.12, dd, 8.0, 7.0, 1H
6	7.22, dd, 8.0, 7.0, 1H[b]	7.13, dd, 8.0, 7.1, 1H	7.20, dd, 8.0, 7.0, 1H
7	7.28, d, 8.0, 1H	7.30, d, 8.3, 1H	7.30, d, 8.0, 1H
10	3.23, dd, 14.4, 3.5, 1H[c]	3.44, m, 1H	3.33, dd, 14.6, 6.8, 1H
	2.50, dd, 14.4, 8.4, 1H[d]	3.24, m, 1H	3.21, dd, 14.6, 3.4, 1H[†]
11	4.18, m, 1H	3.98, ddd, 11.0, 6.3, 1.7, 1H	4.22, ddd, 6.8, 3.8, 3.4, 1H
12	5.70, s, 1H	-	5.80, d, 3.8, 1H
14	4.18, m, 1H	4.41, br t, 5.0, 1H	3.57, ddd, 12.0, 8.7, 8.5, 1H
15	5.72, s, 1H	-	-
17	3.24, dd, 14.4, 3.7, 1H[c]	3.37, m, 2H[§]	3.23, m, 1H[†]
	2.40, dd, 14,4, 8.6, 1H[d]	-	2.97, dd, 11.0, 6.3, 1H
18	-	1.67, m, 1H	1.87, m, 1H[e]
	-	0.88, m, 1H	1.49, m, 1H[e]
19	6,57, s, 1H	1.95, m, 1H	2.12, dtd, 12.0, 7.0, 1.6, 1H
	-	1.32, m, 1H	1.74, dtd, 12.0, 11.5, 8.1, 1H[e]
20	8.07, s, 1H	-	-
22	7.36, d, 8.0, 1H	-	-
23	7.21, dd, 8.0, 7.0, 1H[b]	-	-
24	7.12, dd, 8.0, 7.0, 1H[a]	-	-
25	7.52, d, 8.0, 1H	-	-
1’	4.59, dd, 15.6, 6.8, 1H	4.73, d, 6.6, 2H	4.67, d, 6.8, 2H
	4.64, dd, 15.6, 6.6, 1H	-	-
2’	5.30, br t, 6.8, 1H	5.33, br t, 6.8, 1H	5.31, br t, 6.7, 1H
4’	2.08, m, 2H	2.06, m, 2H	2.09, m, 2H
5’	2.04, m, 2H	2.12, m, 2H	2.04, m, 2H
6’	5.04, br t, 6.6, 1H	5.06, br t, 6.9, 1H	5.05, br t, 6.6, 1H
8’	1.82, s, 3H	1.85, s, 3H	1.81, s, 3H
9’	1.65, s, 3H	1.62, s, 3H	1.66, s, 3H
10’	1.56, s, 3H	1.57, s, 3H	1.58, s, 3H

Chemical shifts (δ) are given in ppm and coupling constants in Hz. [a~e] assignments of signals with the same letter are interchangeable. [†] signals are overlapping with each other. [§] signals are overlapping with those of solvent.

Table S7. ^{1}H NMR data of *N1*-geranylated derivatives (**6a1**, **8a1**, **10a1**, and **10b1)**.

Compound	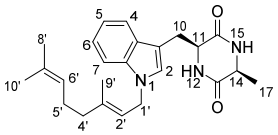 **6a1** (CD_3OD)	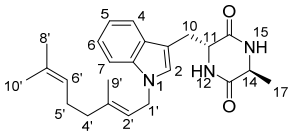 **8a1** (CD_3OD)	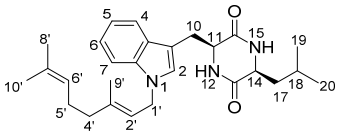 **10a1** ($CDCl_3$)	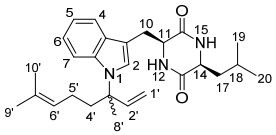 **10b1** ($CDCl_3$)
Position	δ_H, multi., *J* in Hz	δ_H, multi., *J* in Hz	δ_H, multi., *J* in Hz	δ_H, multi., *J* in Hz
2	6.99, s, 1H	6.97, s, 1H	7.00, s, 1H	7.17, s, 1H
4	7.56, d, 8.0, 1H	7.55, d, 8.0, 1H	7.61, d, 8.2, 1H	7.59, d, 7.2, 1H
5	6.99, dd, 8.0, 7.0, 1H	6.98, t, 8.0, 1H	7.13, dd, 8.2, 6.9, 1H	7.10, dd, 8.4, 7.2, 1H
6	7.08, dd, 8.0, 7.0, 1H	7.08, t, 8.0, 1H	7.22, dd, 8.2, 6.9, 1H	7.13, dd, 8.4, 7.2, 1H
7	7.26, d, 8.0, 1H	7.26, d, 8.0, 1H	7.31, d, 8.2, 1H	7.53, d, 7.2, 1H
10	3.41, dd, 14.6, 3.7, 1H	3.40, dd, 14.5, 3.9, 1H	3.50, dd, 14.7, 3.6, 1H	3.55, dd, 14.8, 3.8, 1H
	3.08, dd, 14.6, 4.5, 1H	3.06, dd, 14.5, 4.6, 1H	3.14, dd, 14.7, 8.8, 1H	3.09, dd, 14.8, 9.3, 1H
11	4.23, ddd, 4.5, 3.7, 1.5, 1H	4.15, ddd, 4.6, 3.9, 1.5, 1H	4.30, br d, 8.8, 1H	4.30, br d, 9.3, 1H
12	-	-	5.80, s, 1H	5.79, s, 1H
14	3.66, qd, 7.0, 1.2, 1H	3.29, m, 1H[§]	3.90, br d, 10.2, 1H	3.93, br d, 10.1, 1H
15	-	-	5.85, s, 1H	5.88, s, 1H
17	0.29, d, 7.0, 3H	1.04, d, 7.0, 3H	1.62, ddd, 13.8, 10.2, 3.8, 1H	1.68, ddd, 13.7, 10.1, 3.7, 1H
	-	-	1.03, ddd, 13.8, 10.2, 4.6, 1H	1.20, ddd, 13.7, 10.1, 4.5, 1H
18	-	-	1.50, m, 1H	1.59, m, 1H[*]
19	-	-	0.85, d, 6.6, 3H[a]	0.88, d, 6.5, 3H[b]
20	-	-	0.83, d, 6.6, 3H[a]	0.87, d, 6.5, 3H[b]
1’	4.69, d, 6.9, 2H	4.66, dd 15.0, 7.2, 1H	4.66, dd, 14.3, 6.5, 1H	5.29, d, 10.8, 1H
	-	4.71, dd, 15.0, 7.1, 1H	4.70, dd, 14.3, 7.0, 1H	5.18, d, 17.6, 1H
2’	5.29, br t, 7.2, 1H	5.25, br t, 7.2, 1H	5.35, br t, 7.0, 1H	6.15, dd, 17.6, 10.8, 1H
4’	2.08, m, 2H	2.07, m, 2H	2.11, m, 2H	2.27, ddd, 14.9, 12.9, 5.8, 1H
	-	-	-	1.97, ddd, 12.9, 11.4, 3.8, 1H
5’	2.02, m, 2H	2.01, m, 2H	2.06, m, 2H	1.91, m, 1H
	-	-	-	1.50, m, 1H[*]
6’	5.02, br t, 6.9, 1H	5.01, br t, 7.2, 1H	5.06, br t, 6.7, 1H	4.99, br t, 7.2, 1H
8’	1.81, s, 3H	1.80, s, 3H	1.82, s, 3H	1.42, s, 3H
9’	1.59, s, 3H	1.57, s, 3H	1.67, s, 3H	1.61, s, 3H
10’	1.54, s, 3H	1.53, s, 3H	1.59, s, 3H	1.73, s, 3H

Chemical shifts (δ) are given in ppm and coupling constants in Hz. [$^{a-b}$] assignments of signals with the same letter are interchangeable. [*] signals are overlapping with those of water. [§] signals are overlapping with those of solvent.

Table S8. ^{1}H NMR data of *N1*-geranylated derivatives (**11a1**, **12a1**, and **13a1**).

Compound	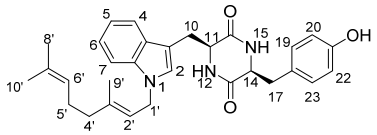 **11a1** (CD_3OD)	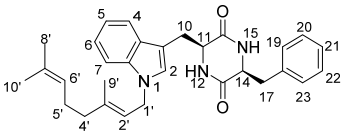 **12a1** (CD_3OD)	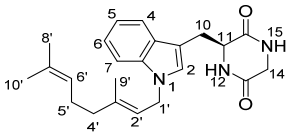 **13a1** ($CDCl_3$)
Position	δ_H, multi., *J* in Hz	δ_H, multi., *J* in Hz	δ_H, multi., *J* in Hz
2	7.02, s, 1H	6.98, s, 1H	7.01, s, 1H
4	7.61, d, 8.0, 1H	7.58, d, 7.5, 1H	7.62, d, 8.0, 1H
5	7.10, dd, 8.0, 7.0, 1H	7.06, dd, 8.0, 7.0, 1H	7.13, dd, 8.0, 7.0, 1H
6	7.19, dd, 8.0, 7.0, 1H	7.15, dd, 8.0, 7.0, 1H	7.23, dd, 8.0, 7.0, 1H
7	7.32, d, 8.0, 1H	7.28, d, 7.5, 1H	7.32, d, 8.0, 1H
10	3.02, dd, 14.6, 4.0, 1H	2.97, dd, 14.7, 4.4, 1H	3.48, dd, 14.6, 3.7, 1H
	2.90, dd, 14.6, 5.4, 1H	2.90, dd, 14.7, 5.1, 1H	3.18, dd, 14.6, 8.6, 1H
11	4.18, ddd, 5.4, 4.0, 1.0, 1H	4.15, dd, 5.1, 4.4, 1H	4.28, br d, 8.6, 1H
12	-	-	5.67, s, 1H
14	3.82, ddd, 9.0, 3.7, 1.1, 1H	3.83, ddd, 8.9, 3.6, 1.0, 1H	3.81, ddd, 17.3, 2.3, 1.0, 1H
	-	-	3.49, ddd, 17.3, 2.8, 1.9, 1H
15	-	-	5.87, s, 1H
17	2.57, dd, 13.6, 3.7, 1H	2.58, dd, 13.5, 3.6, 1H	-
	1.32, dd, 13.6, 9.0, 1H	1.26, dd, 13.5, 8.9, 1H	-
19	6.34, d, 8.6, 1H	6.44, dd, 7.2, 2.0, 1H	-
20	6.58, d, 8.6, 1H	7.10, m, 1H[†]	-
21	-	7.10, m, 1H[†]	-
22	6.58, d, 8.6, 1H	7.10, m, 1H[†]	-
23	6.34, d, 8.6, 1H	6.44, dd, 7.2, 2.0, 1H	-
1’	4.69, dd, 15.2, 6.8, 1H	4.68, dd, 15.2, 6.8, 1H	4.66, dd, 15.5, 7.0, 1H
	4.73, dd, 15.2, 6.5, 1H	4.72, dd, 15.2, 6.5, 1H	4.70, dd, 15.5, 6.6, 1H
2’	5.31, br t, 6.8, 1H	5.27, br t, 6.8, 1H	5.34, br t, 7.0, 1H
4’	2.03, m, 2H	1.98, m, 2H	2.10, m, 2H
5’	1.99, m, 2H	1.93, m, 2H	2.05, m, 2H
6’	5.01, br t, 6.9, 1H	4.95, br t, 6.9, 1H	5.06, br t, 6.9, 1H
8’	1.84, s, 3H	1.79, s, 3H	1.82, s, 3H
9’	1.61, s, 3H	1.56, s, 3H	1.66, s, 3H
10’	1.53, s, 3H	1.47, s, 3H	1.59, s, 3H

Chemical shifts (δ) are given in ppm and coupling constants in Hz. [†] signals are overlapping with each other.

Table S9. ^{1}H NMR data of *C2*-geranylated derivatives (**1a2**, **2a2**, and **3a2**).

Comound	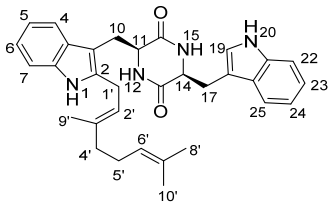 **1a2** ($CDCl_3$)	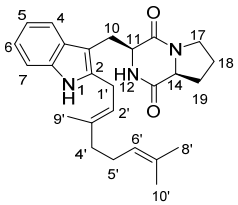 **2a2** ($CDCl_3$)	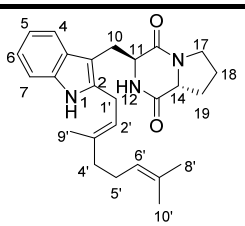 **3a2** ($CDCl_3$)
Position	δ_H, multi., *J* in Hz	δ_H, multi., *J* in Hz	δ_H, multi., *J* in Hz
1	7.99, s, 1H[a]	7.93, s, 1H	7.89, s, 1H
4	7.50, d, 8.0, 1H	7.47, d, 7.8, 1H	7.51, d, 7.2, 1H
5	7.10, dd, 8.0, 7.0, 1H[b]	7.09, dd, 7.8, 7.1, 1H	7.08, dd, 8.5, 7.2, 1H
6	7.11, dd, 8.0, 7.0, 1H[c]	7.15, dd, 8.1, 7.1, 1H	7.11, dd, 8.5, 7.2, 1H
7	7.28, d, 8.0, 1H[d]	7.30, d, 8.1, 1H	7.25, m, 1H[§]
10	3.22, dd, 14.7, 3.8, 1H	3.67, dd, 15.1, 3.8, 1H[†]	3.40, dd, 14.8, 5.7, 1H
	3.02, dd, 14.7, 7.3, 1H	2.96, dd, 15.1, 11.5, 1H	3.15, dd, 14.8, 4.3, 1H
11	4.27, m, 1H	4.37, ddd, 11.5, 3.8, 1.3, 1H	4.25, dd, 5.7, 4.3, 1H
12	5.63, s, 1H	5.61, br s, 1H	5.79, br s, 1H
14	4.13, br d, 10.0, 1H	4.06, ddd, 8.4, 7.0, 1.3, 1H	3.53, ddd, 11.8, 8.8, 8.2, 1H
15	5.76, s, 1H	-	-
17	3.29, dd, 14.2, 3.2, 1H	3.71, m, 1H[†]	3.17, m, 1H
	2.01, dd, 14.2, 10.0, 1H	3.59, ddd, 11.7, 8.8, 3.9, 1H	2.72, dd, 11.0, 6.4, 1H
18	-	2.02, m, 1H[††]	1.82, m, 1H
	-	1.91, m, 1H	1.38, m, 1H
19	6.25, s, 1H	2.33, m, 1H	2.05, dtd, 13.0, 6.7, 1.5, 1H
	-	2.02, m, 1H[††]	1.68, m, 1H
20	7.94, s, 1H[a]	-	-
22	7.32, d, 8.0, 1H[d]	-	-
23	7.18, dd, 8.0, 7.0, 1H[c]	-	-
24	7.15, dd, 8.0, 7.0, 1H[b]	-	-
25	7.50, d, 8.0, 1H	-	-
1’	3.34, dd, 16.1, 6.3, 1H	3.46, dd, 14.4, 5.4, 1H	3.43, dd, 16.5, 7.0, 1H
	3.38, dd, 16.1, 6.9, 1H	3.51, dd, 14.4, 5.6, 1H	3.47, dd, 16.5, 7.3, 1H
2’	5.31, br t, 6.9, 1H	5.32, br t, 7.3, 1H	5.31, br t, 7.3, 1H
4’	2.15, m, 2H[‡]	2.12, m, 2H[‡‡]	2.15, m, 2H
5’	2.15, m, 2H[‡]	2.12, m, 2H[‡‡]	2.13, m, 2H
6’	5.12, br t, 6.8, 1H	5.10, br t, 6.7, 1H	5.10, br t, 6.4, 1H
8’	1.75, s, 3H	1.73, s, 3H	1.73, s, 3H
9’	1.72, s, 3H	1.72, s, 3H	1.73, s, 3H
10’	1.64, s, 3H	1.62, s, 3H	1.63, s, 3H

Chemical shifts (δ) are given in ppm and coupling constants in Hz. [†,‡] signals are overlapping with each other. [§] signals are overlapping with those of solvent. [a-d] assignments of signals with the same letter are interchangeable. [*] signals are overlapping with those of water.

Table S10. ^{1}H NMR data of *C2*-geranylated derivatives (**10a2**, **11a2**, and **12a2**).

Comound	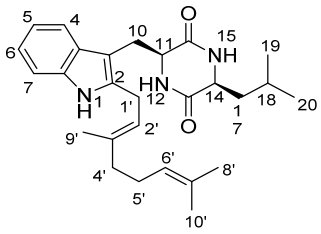 **10a2** ($CDCl_3$)	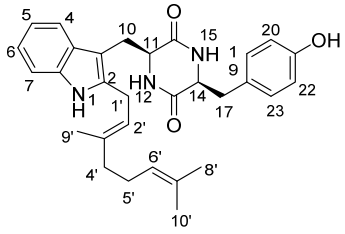 **11a2** (DMSO-d_6)	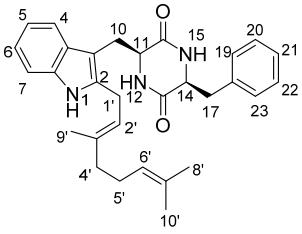 **12a2** (DMSO-d_6)
Position	δ_H, multi., *J* in Hz	δ_H, multi., *J* in Hz	δ_H, multi., *J* in Hz
1	7.93, s, 1H	10.61, s , 1H	10.62, s, 1H
4	7.53, d, 8.0, 1H	7.45, d, 8.0, 1H	7.45,d, 8.0, 1H
5	7.10, dd, 8.0, 7.0, 1H	6.93, dd, 8.0, 7.0, 1H	6.94, dd, 8.0, 7.0, 1H
6	7.14, dd, 8.0, 7.0, 1H	7.00, dd, 8.0, 7.0, 1H	7.00, dd, 8.0, 7.0, 1H
7	7.28, d, 8.0, 1H	7.23, d, 8.0, 1H	7.23, d, 8.0, 1H
10	3.43, dd, 14.7, 3.9, 1H	3.44, dd, 16.3, 7.0, 1H	3.43, dd, 16.0, 7.6, 1H
	3.19, dd, 14.7, 8.4, 1H	3.37, dd, 16.3, 7.3, 1H	3.37, dd, 16.4, 7.2, 1H
11	4.30, br d, 8.4, 1H	3.94, m, 1H	3.96, m, 1H
12	5.76, s, 1H	7.44, d, 3.0, 1H	7.57, d, 3.0, 1H
14	3.89, br d, 10.1, 1H	3.64, dt, 8.0, 4.0, 1H	3.73, dt, 8.2, 4.5, 1H
15	5.95, s, 1H	7.88, d, 2.7, 1H	7.94, d, 2.5, 1H
17	1.59, ddd, 13.5, 10.0, 3.7, 1H[*]	2.35, dd, 13.0, 4.0, 1H	2.40, dd, 13.2, 4.5, 1H
	1.00, ddd, 13.5, 10.0, 4.5, 1H	1.40, dd, 13.0, 8.0, 1H	1.50, dd, 13.6, 8.2, 1H
18	1.50, m, 1H	-	-
19	0.84, d, 6.5, 3H[a]	6.33, d, 8.5, 1H	6.54, dd, 7.0, 2.7, 1H
20	0.82, d, 6.5, 3H[a]	6.50, d, 8.5, 1H	7.11, m, 1H[‡]
21	-	-	7.11, m, 1H[‡]
22	-	6.50, d, 8.5, 1H	7.11, m, 1H[‡]
23	-	6.33, d, 8.5, 1H	6.54, dd, 7.0, 2.7, 1H
24	-	-	-
25	-	-	-
1’	3.49, d, 7.0, 2H	2.82, dd, 14.5, 6.5, 1H	2.81, dd, 14.8, 6.5, 1H
	-	2.86, dd, 14.5, 5.5, 1H	2.85, dd, 14.8, 6.0, 1H
2’	5.33, br t, 7.0, 1H	5.34, br t, 6.5, 1H	5.33, br t, 6.5, 1H
4’	2.14, m, 2H[†]	2.09, m, 2H	2.09, m, 2H
5’	2.14, m, 2H[†]	2.01, m, 2H	2.01, m, 2H
6’	5.11, br t, 6.7, 1H	5.10, br t, 6.0, 1H	5.10, br t, 6.8, 1H
8’	1.74, s, 3H[††]	1.74, s, 3H	1.74, s, 3H
9’	1.74, s, 3H[††]	1.62, s, 3H	1.62, s, 3H
10’	1.63, s, 3H	1.56, s, 3H	1.56, s, 3H
-OH	-	9.06, s, 1H	-

Chemical shifts (δ) are given in ppm and coupling constants in Hz. [a] assignments of signals with the same letter are interchangeable. [†, ‡] signals are overlapping with each other.

Table S11. ^{1}H NMR data of *C2*-geranylated derivatives (**1b2**, **1b2-2**, and **2b2**).

Compound	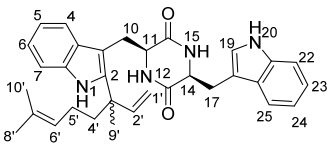 **1b2** ($CDCl_3$)	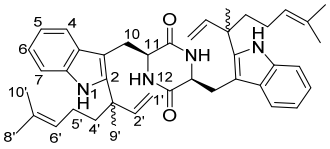 **1b2-2** ($CDCl_3$)	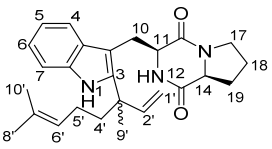 **2b2** (CD_3OD)
Position	δ_H, multi., *J* in Hz	δ_H, multi., *J* in Hz	δ_H, multi., *J* in Hz
1	8.03, s, 1H	8.07, s, 1H	-
4	7.40, d, 8.0, 1H	7.53, d, 8.0, 1H	7.47, d, 8.0, 1H
5	7.05, dd, 8.0, 7.1, 1H	7.13, dd, 8.0, 7.1, 1H	7.03, dd, 8.0, 7.1, 1H
6	7.15, dd, 8.0, 7.1, 1H	7.19, dd, 8.0, 7.1, 1H	7.10, dd, 8.0, 7.1, 1H
7	7.18, d, 8.0, 1H	7.33, d, 8.0, 1H	7.37, d, 8.0, 1H
10	3.58, dd, 14.6, 3.3, 1H	3.74, dd, 14.6, 3.5, 1H	3.66, dd, 15.1, 4.4, 1H
	3.05, dd, 14.6, 9.6, 1H	3.26, dd, 14.6, 11.8, 1H	3.14, dd, 15.1, 11.2, 1H
11	4.29, br d, 9.6, 1H	4.39, br d, 11.8, 1H	4.49, ddd, 11.2, 4.4, 1.4, 1H
12	5.69, s, 1H	5.72, s, 1H	-
14	4.29, br d, 9.6, 1H	-	4.22, ddd, 8.3, 6.4, 1.8, 1H
15	5.85, s, 1H	-	-
16	-	-	-
17	3.62, dd, 14.6, 3.3, 1H	-	3.61, m, 1H
	2.88, dd, 14.6, 11.3, 1H	-	3.55, ddd, 11.7, 8.6, 3.0, 1H
18	-	-	2.02, m, 1H
	-	-	1.94, m, 1H
19	7.10, d, 2.3, 1H	-	2.27, m, 1H
	-	-	1.94, m, 1H
20	8.16, s, 1H	-	-
21	-	-	-
22	7.30, d, 8.0, 1H	-	-
23	7.24, dd, 8.0, 7.0, 1H	-	-
24	7.20, dd, 8.0, 7.0, 1H	-	-
25	7.67, d, 8.0, 1H	-	-
1’	5.24, d, 10.7, 1H	5.31, d, 10.7, 1H	5.18, d, 10.3, 1H
	5.16, d, 17.5, 1H	5.24, d, 17.5, 1H	5.15, d, 17.5, 1H
2’	6.11, dd, 17.5, 10.7, 1H	6.20, dd, 17.5, 10.7, 1H	6.30, dd, 17.5, 10.7, 1H
4’	1.81, m, 2H	1.86, m, 2H	1.84, m, 2H
5’	1.91, m, 2H	1.95, m, 2H	1.94, m, 2H
6’	5.06, m, 1H	5.09, m, 1H	5.11, m, 1H
8’	1.64, s, 3H	1.64, s 3H	1.62, m, 3H
9’	1.50, s, 3H	1.53, s 3H	1.50, m, 3H
10’	1.51, s, 3H	1.57, s 3H	1.55, m, 3H

Chemical shifts (δ) are given in ppm and coupling constants in Hz.

Table S12. ^{1}H NMR data of *C2*-geranylated derivatives (**3b2**, **4b2**, and 1**4b2**).

Compound	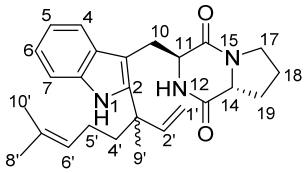	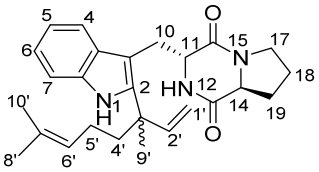	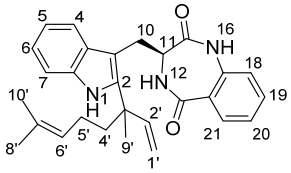
	3b2 (CD_3OD)	**4b2** (CD_3OD)	**14b2** ($CDCl_3$)
Position	δ_H, multi.,*J* in Hz	δ_H, multi., *J* in Hz	δ_H, multi., *J* in Hz
1	-	-	8.04, s, 1H
4	7.46, d, 8.0, 1H	7.46, d, 8.0, 1H	7.43, d, 8.0, 1H
5	6.98, dd, 8.0, 7.0, 1H	6.97, dd, 8.0, 7.0, 1H	7.07, dd, 8.0, 7.4, 1H
6	7.04, dd, 8.0, 7.0, 1H	7.04, dd, 8.0, 7.0, 1H	7.15, dd, 8.0, 7.4, 1H
7	7.30, d, 8.0, 1H	7.30, d, 8.0, 1H	7.31, d, 8.0, 1H
10	3.45, dd, 14.8, 5.3, 1H	3.45, dd, 14.8, 5.3, 1H	3.49, dd, 15.7, 10.0, 1H
	3.38, dd, 14.8, 6.5, 1H	3.38, dd, 14.8, 6.5, 1H	3.40, dd, 15.7, 4.8, 1H
11	4.18, dd, 6.5, 5.3, 1H	4.18, dd, 6.5, 5.3, 1H	4.22, td, 10.0, 4.8, 1H
12	-	-	6.04, d, 4.8, 1H
14	3.46, m, 1H	3.46, m, 1H	-
16	-	-	7.60, s, 1H
17	3.34, m, 2H[§]	3.34, m, 2H[§]	-
18	1.89, m, 1H	1.90, m, 1H	6.97, d, 8.0, 1H
	1.56, m, 1H	1.55, m, 1H	-
19	2.10, dtd, 12.3, 5.9, 1.0, 1H	2.10, dtd, 12.5, 6.5, 1.2, 1H	7.50, dd, 8.0, 7.4, 1H
	1.74, dtd, 12.3, 10.7, 7.0, 1H	1.74, dtd, 12.5, 11.0, 7.0, 1H	-
20	-	-	7.25, dd, 8.0, 7.4, 1H
21	-	-	7.84, dd, 8.0, 1H
1’	5.22, d, 10.6, 1H	5.22, d, 10.8, 1H	5.18, d, 10.7, 1H
	5.19, d, 17.5, 1H	5.19, d, 17.5, 1H	5.14, d, 17.6, 1H
2’	6.30, dd, 17.5, 10.6, 1H	6.30, dd, 17.5, 10.8, 1H	6.12, dd, 17.6, 10.7, 1H
4’	1.83, m, 2H	1.83, m, 2H	1.81, m, 2H
5’	1.86, m, 2H	1.87, m, 2H	1.90, m, 1H
6’	5.09, m, 1H	5.09, m, 1H	5.03, m, 1H
8’	1.53, s, 3H	1.53, s, 3H	1.56, s 3H
9’	1.49, s, 3H	1.49, s, 3H	1.51, s 3H
10’	1.61, s, 3H	1.61, s, 3H	1.64, s 3H

Chemical shifts (δ) ate given in ppm and coupling constants in Hz. [§] signals are overlapping with those of solvent.

Table S13. ^{1}H NMR data of *C3*-geranylated derivatives (**1a3**, **3a3**, **6a3**, and **8a3**).

Compound	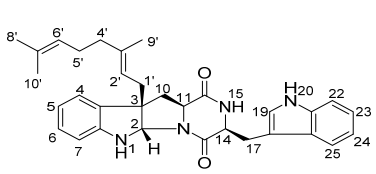 **1a3** ($CDCl_3$)	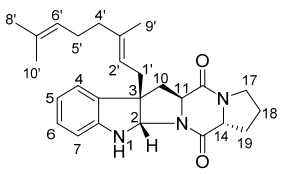 **3a3** ($CDCl_3$)	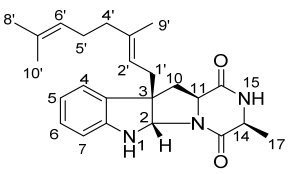 **6a3** (CD_3OD)	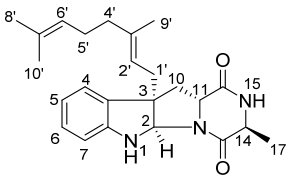 **8a3** (CD_3OD)
Position	δ_H, multi., *J* in Hz	δ_H, multi., *J* in Hz	δ_H, multi., *J* in Hz	δ_H, multi., *J* in Hz
2	5.67, s, 1H	5.54, s, 1H	5.28, s, 1H	5.35, s, 1H
4	7.08, d, 7.5, 1H	7.10, d, 7.4, 1H	7.11, d, 7.4, 1H	7.10, d, 7.4, 1H
5	6.77, t, 7.5, 1H	6.76, t, 7.4, 1H	6.69, t, 7.4, 1H	6.69, t, 7.4, 1H
6	7.10, m, 1H[†]	7.07, t, 7.4, 1H	7.00, t, 7.4, 1H	7.01, t, 7.4, 1H
7	6.66, br s, 1H	6.58, d, 7.4, 1H	6.57, d, 7.4, 1H	6.58, d, 7.4, 1H
10_{syn}	2.61, dd, 12.6, 6.0, 1H	2.64, dd, 12.0, 5.0, 1H	2.57, dd, 12.6, 6.2, 1H	2.58, dd, 12.5, 5.9, 1H
10_{anti}	2.22, dd, 12.6, 11,3, 1H	2.13, t, 12.0, 1H	2.22, dd, 12.6, 11.3, 1H	2.19, dd, 12.5, 11.5, 1H
11	3.98, ddd, 11.3, 6.0, 1.2, 1H	4.04, m, 1H[††]	4.02, dd, 11.3, 6.2, 1H	4.00, dd, 11.5, 5.9, 1H
14	4.33, br d, 11.0, 1H	4.04, m, 1H[††]	4.10, qd, 6.8, 2.0, 1H	3.87, qd, 7.1, 0.7, 1H
15	5.35, s, 1H	-	-	-
17	3.73, dd, 15.0, 3.7, 1H	3.92,ddd, 12.4, 7.3, 3.3, 1H	1.34, d, 6.8, 3H	1.34, d, 7.1, 3H
	2.97, dd, 15.0, 11.0, 1H	3.28,ddd, 12.4, 10.1, 4.1, 1H	-	-
18	-	1.98, m, 1H[‡]	-	-
	-	1.89, m, 1H	-	-
19	7.10, s, 1H[†]	2.41, m, 1H	-	-
	-	1.76, dtd, 12.0, 11.2, 9.1, 1H	-	-
20	8.14, s, 1H	-	-	-
22	7.39, d, 8.0, 1H	-	-	-
23	7.22, d, 8.0, 7.0, 1H	-	-	-
24	7.12, d, 8.0, 7.0, 1H	-	-	-
25	7.55, d, 8.0, 1H	-	-	-
1’	2.38, dd, 14.3, 7.3, 1H	2.45, dd, 14.0, 7.1, 1H	2.41, d, 7.8, 2H	2.42, d, 7.8, 2H
	2.42, dd, 14.3, 7.7, 1H	2.49, dd, 14.0, 7.8, 1H	-	-
2’	5.16, br t, 7.7, 1H	5.11, br t, 7.8, 1H	5.15, br t, 7.8, 1H	5.13, br t, 7.8, 1H
4’	1.99, m, 2H	2.02, m, 2H	2.02, m, 2H	2.00, m, 2H
5’	2.05, m, 2H	1.98, m, 2H[‡]	1.96, m, 2H	1.95, m, 2H
6’	5.06, br t, 6.6, 1H	5.04, br t, 6.6, 1H	5.03, br t, 6.8, 1H	5.02, br t, 6.7, 1H
8’	1.69, s, 3H	1.68, s, 3H	1.63, s, 3H	1.63, s, 3H
9’	1.60, s, 3H	1.59, s, 3H	1.56, s, 3H	1.55, s, 3H
10’	1.52, s, 3H	1.55, s, 3H	1.51, s, 3H	1.50, s, 3H

Chemical shifts (δ) are given in ppm and coupling constants in Hz. [a, b] assignments of signals with the same letter are interchangeable. [†, ‡] signals are overlapping with each other. H-10syn has a *cis*- and H-10anti a *trans*-configuration to H-11.

Table S14. ^{1}H NMR data of *C3*-geranylated derivatives (**10a3**, **11a3**, **12a3**, and **13a3**).

Compound	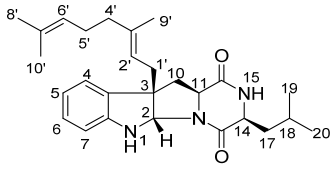 **10a3** ($CDCl_3$)	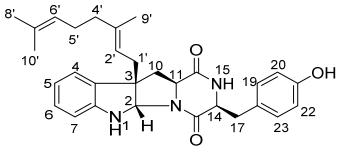 **11a3** (CD_3OD)	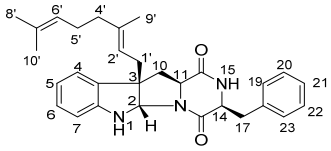 **12a3** (CD_3OD)	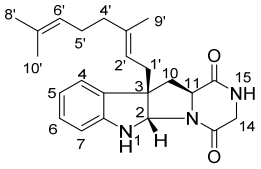 **13a3** (CD_3OD)
Position	δ_H, multi., *J* in Hz	δ_H, multi., *J* in Hz	δ_H, multi., *J* in Hz	δ_H, multi., *J* in Hz
2	5.29, s, 1H	5.15, s, 1H	5.15, s, 1H	5.32, s, 1H
4	7.10, d, 7.6, 1H	6.98, d, 7.4, 1H	6.97, d, 7.4, 1H[†]	7.10, d, 7.5, 1H
5	6.77, t, 7.6, 1H	6.62, t, 7.4, 1H	6.62, t, 7.4, 1H	6.69, t, 7.5, 1H
6	7.09, t, 7.6, 1H	6.95, t, 7.4, 1H	6.96, t, 7.4, 1H[†]	7.00, t, 7.5, 1H
7	6.61, d, 7.6, 1H	6.51, d, 7.4, 1H	6.51, d, 7.4, 1H	6.57, d, 7.5, 1H
10_{syn}	2.65, dd, 12.8, 6.1, 1H	2.23, dd, 12.0, 5.3, 1H	2.23, dd, 12.0, 5.4, 1H[††]	2.57, dd, 12.5, 5.9, 1H
10_{anti}	2.32, dd, 12.8, 11.2, 1H	1.11, t, 12.0, 1H	1.10, t, 12.0, 1H	2.21, dd, 12.5, 11.4, 1H
11	4.02, dd, 11.2, 6.1, 1H	3.76, ddd, 12.0, 5.3, 1.9, 1H	3.77, ddd, 12.0, 5.4, 2.0, 1H	4.00, dd, 11.4, 5.9, 1H
14	3.96, dd, 10.5, 3.2, 1H	4.32, td, 4.4, 2.0, 1H	4.39, td, 4.4, 2.0, 1H	4.05, dd, 16.6, 2.3, 1H
	-	-	-	3.70, d, 16.6, 1H
15	5.64, s, 1H	-	-	-
17	2.00, m, 1H[†]	3.15, dd, 13.9, 4.4, 1H	3.28, m, 1H[§]	-
	1.55, m, 1H	2.90, dd, 13.9, 4,4, 1H	3.02, dd, 13.8, 4.4, 1H	-
18	1.67, m, 1H	-	-	-
19	0.99, d, 6.6, 3H[a]	7.00, d, 8.7, 1H	7.19, dd, 8.0, 1.4, 1H	-
20	0.92, d, 6.6, 3H[a]	6.71, d, 8.7, 1H	7.29, m, 1H[‡]	-
21	-	-	7.25, m, 1H[‡]	-
22	-	6.71, d, 8.7, 1H	7.29, m, 1H[‡]	-
23	-	7.00, d, 8.7, 1H	7.19, dd, 8.0, 1.4, 1H	-
1’	2.40, dd, 14.3, 7.4, 1H	2.18, dd, 14.2, 8.0, 1H	2.14, dd, 14.0, 8.4, 1H	2.42, d, 7.6, 2H
	2.44, dd, 14.3, 7.9, 1H	2.27, dd, 14.2, 6.6, 1H	2.21, dd, 14.0, 6.0, 1H[††]	-
2’	5.17, br t, 7.6, 1H	4.91, br t, 8.0, 1H	4.99, br t, 8.4, 1H	5.15, br t, 7.6, 1H
4’	2.04, m, 2H	1.91, m, 2H	1.97, m, 2H[※]	2.01, m, 2H
5’	1.99, m, 2H[†]	1.97, m, 2H	1.90, m, 2H	1.95, m, 2H
6’	5.06, br t, 6.6, 1H	5.00, br t, 6.7, 1H	4.90, m, 1H[*]	5.03, br t, 6.4, 1H
8’	1.68, s, 3H	1.63, s, 3H	1.63, s, 3H	1.63, s, 3H
9’	1.60, s, 3H	1.54, s, 3H	1.54, s, 3H	1.56, s, 3H
10’	1.52, s, 3H	1.49, s, 3H	1.48, s, 3H	1.51, s, 3H

Chemical shifts (δ) are given in ppm and coupling constants in Hz. [§] signals are overlapping with those of solvent. [*] signals are overlapping with those of water. [†, ‡] signals are overlapping with each other. [a] assignments of signals with the same letter are interchangeable. [※] signals are overlapping with impurities. H-10syn has a *cis*- and H-10anti a *trans*-configuration to H-11.

Table S15. ^{1}H NMR data of *C3*-geranylated derivatives (**1b3**, **5b3**, **10b3**, and **14b3**).

Compund	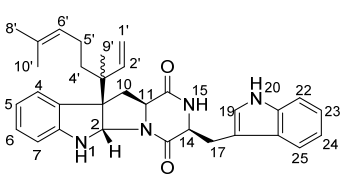 **1b3** ($CDCl_3$)	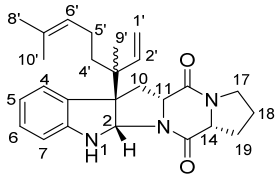 **5b3** ($CDCl_3$)	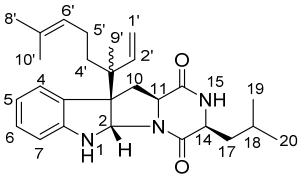 **10b3** ($CDCl_3$)	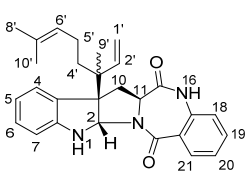 **14b3** ($CDCl_3$)
Position	δ_H, multi., *J* in Hz	δ_H, multi., *J* in Hz	δ_H, multi., *J* in Hz	δ_H, multi., *J* in Hz
2	5.63, s, 1H	5.49, s, 1H	5.57, s, 1H	5.64, s, 1H
4	7.13, d, 7.5, 1H[a]	7.16, d, 7.5, 1H	7.15, d, 7.5, 1H	7.14, d, 7.5, 1H
5	6.75, t, 7.5, 1H	6.72, t, 7.5, 1H	6.75, t, 7.5, 1H	6.71, t, 7.5, 1H
6	7.10, t, 7.5, 1H[a]	7.06, t, 7.5, 1H	7.10, t, 7.5, 1H	7.07, t, 7.5, 1H
7	6.61, d, 7.5, 1H	6.53, d, 7.5, 1H	6.58, d, 7.5, 1H	6.61, d, 7.5, 1H
10_{syn}	2.50, dd, 12.6, 6.4, 1H	2.80, dd, 13.8, 9.0, 1H	2.53, dd, 11.8, 6.0, 1H	3.48, dd, 13.8, 8.0, 1H
10_{anti}	2.45, dd, 12.6, 11.0, 1H	2.52, dd, 13.8, 8.9, 1H	2.49, dd, 11.8, 10.0, 1H	2.41, dd, 13.8, 8.7, 1H
11	3.90, ddd, 11.0, 6.4, 1.5, 1H	4.14, t, 8.9, 1H	3.95, m, 1H[†]	3.96, dd, 8.7, 8.0, 1H
14	4.31, ddd, 11.0, 3.5, 1.8, 1H	4.09, t, 8.0, 1H	3.95, m, 1H[†]	-
15	5.65, s, 1H	-	5.64, s, 1H	-
16	-	-	-	7.66, s, 1H
17	3.75, dd, 15.0, 3.6, 1H	3.45, m, 1H	2.02, ddd, 13.7, 10.0, 3.6, 1H	-
	2.97, dd, 15.0, 11.1, 1H	3.41, m, 1H	1.58, m, 1H[*]	-
18	-	2.04, m, 1H	1.68, m, 1H	6.88, d, 8.0, 1H
	-	1.87, m, 1H	-	-
19	7.10, d,1.2, 1H	2.32, dtd, 9.0, 6.6, 2.3, 1H	0.99, d, 6.6, 1H[b]	7.43, dd, 8.0,7.5, 1H
	-	1.97, ddd, 10.6, 6.3, 3.1, 1H	-	
20	8.13, s, 1H	-	0.91, d, 6.6, 1H[b]	7.21, dd, 7.9, 7.5, 1H[§]
21	-	-	-	7.83, d, 7.9, 1H
22	7.39, d, 8.0, 1H	-	-	-
23	7.23, dd, 8.0, 7.1, 1H	-	-	-
24	7.13, dd, 8.0, 7.1, 1H[a]	-	-	-
25	7.55, d, 8.0, 1H	-	-	-
1’	5.27, dd, 10.8, 1H	5.28, d, 10.9, 1H	5.26, d, 10.8, 1H	5.29, dd, 10.8, 1.0, 1H
	5.07, dd, 17.4, 1H	5.12, d, 17.6, 1H	5.07, d, 17.4, 1H	5.10, dd, 17.4, 1,0, 1H
2’	5.76, dd, 17.4, 10.8, 1H	5.78, dd, 17.6, 10.9, 1H	5.77, dd, 17.4, 10.8, 1H	5.82, dd, 17.4, 10.8 , 1H
4’	1.77, dd, 16.0, 8.0, 2H	1.76, m, 2H	1.76, dd, 16.0, 7.7, 2H	1.72, m, 1H
5’	1.59, ddd, 17.6, 12.7, 5.9, 1H[*]	1.56, m, 1H [*]	1.58, m, 1H[*]	1.78, m, 2H
	1.24, ddd, 17.6, 12.3, 7.6, 1H	1.20, m, 1H	1.22, ddd, 17.5, 11.5, 5.6, 1H	1.25, m, 1H
6’	5.00, br t, 7.1, 1H	4.99, br t, 7.0, 1H	4.98, br t, 7.3, 1H	5.01, br t, 6.8, 1H
8’	1.64, s, 3H	1.63, s, 3H	1.63, s, 3H	1.64, s, 3H
9’	1.09, s, 3H	1.13, s, 3H	1.10, s, 3H	1.12, s, 3H
10’	1.53, s, 3H	1.52, s, 3H	1.51, s, 3H	1.53, s, 3H

Chemical shifts (δ) are given in ppm and coupling constants in Hz. [†] signals are overlapping with each other. [§] signals are overlapping with those of solvent. [a, b] assignments of signals with the same letter are interchangeable. [*] signals are overlapping with those of water. H-10syn has a *cis*- and H-10anti a *trans*-configuration to H-11.

Table S16. ^{1}H NMR data of **1a4** and **1a5**.

Compound	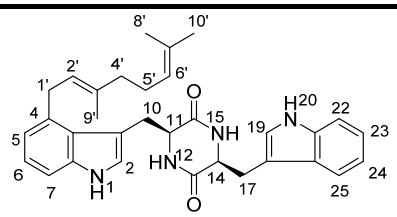 **1a4**	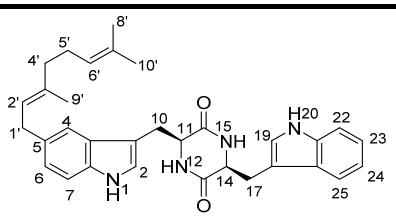 **1a5**
Position	δ_H, multi., *J* in Hz ($CDCl_3$)	δ_H, multi., *J* in Hz (CD_3COCD_3)	δ_H, multi., *J* in Hz (CD_3COCD_3)
1	8.18, s, 1H	9.98, s, 1H[a]	9.94, s, 1H[c]
2	7.05, d, 2.3, 1H	7.10, d, 2.5, 1H	6.76, d, 2.4, 1H[d]
4	-	-	7.34, d, 1.6, 1H[†]
5	6.90, d, 7.2, 1H	6.76, d, 7.3, 1H	-
6	7.09, dd, 8.2, 7.2, 1H	6.94, dd, 8.0, 7.3, 1H	6.94, dd, 8.3, 1.6, 1H
7	7.17, d, 8.2, 1H	7.14, d, 8.0, 1H	7.24, d, 8.3, 1H
10	3.54, dd, 14.8, 2.9, 1H	3.24, dd, 14.4, 3.0, 1H	3.00, dd, 14.5, 3.8, 1H
	1.84, dd, 14.8, 11.0, 1H	2.08, m, 1H[§]	2.17, dd, 14.5, 7.5, 1H
11	4.03, br d, 11.0, 1H	3.91, ddd, 4.9, 3.0, 2.7, 1H	4.03, ddd, 7.5, 3.8, 0.9, 1H
12	5.87, s, 1H	7.08, br s, 1H[b]	6.71, s, 1H[e]
14	4.32, m, 1H	4.23, ddd, 4.7, 2.5, 0.7, 1H	4.08, ddd, 7.0, 4.1, 1.2, 1H
15	5.63, s, 1H	6.49, s, 1H[b]	6.79, s, 1H[e]
17	3.31, dd, 14.7, 4.3, 1H	3.17, dd, 14.1, 4.8, 1H	3.05, dd, 14.2, 3.8, 1H
	3.26, dd, 14.7, 6.8, 1H	3.14, dd, 14.1, 4.5, 1H	2.45, dd, 14.2, 7.0, 1H
19	6.06, d, 2.2, 1H	6.00, d, 2.3, 1H	6.55, d, 2.4, 1H[d]
20	7.99, s, 1H	10.20, s, 1H[a]	10.10, s, 1H[c]
22	7.39, d, 8.0, 1H	7.37, d, 8.0, 1H	7.34, d, 8.0, 1H[†]
23	7.20, dd, 8.0, 7.0, 1H	7.06, dd, 8.0, 7.0, 1H	7.08, dd, 8.0, 7.0, 1H
24	7.25, dd, 8.0, 7.0, 1H	7.11, dd, 8.0, 7.0, 1H	7.01, dd, 8.0, 7.0, 1H
25	7.70, d, 8.0, 1H	7.65, d, 8.0, 1H	7.49, d, 8.0, 1H
1’	3.72, dd, 16.0, 6.7, 1H	3.69, d, 6.8, 2H	3.45, dd, 15.7, 6.7, 1H
	3.66, dd, 16.0, 6.7, 1H	-	3.41, dd, 15.7, 7.2, 1H
2’	5.29, br t, 6.6, 1H	5.30, br t, 6.8, 1H	5.41, br t, 7.2, 1H
4’	2.10, m, 2H	2.10, m, 2H	2.11, m, 2H
5’	2.04, m, 2H	2.02, m, 2H[§]	2.07, m, 2H[§]
6’	5.10, br t, 6.8	5.12, br t, 7.0, 1H	5.12, br t, 6.9, 1H
8’	1.71, s, 3H	1.72, s, 3H	1.76, s, 3H
9’	1.67, s, 3H	1.65, s, 3H	1.63, s, 3H
10’	1.58, s, 3H	1.58, s, 3H	1.57, s, 3H

Chemical shifts (δ) are given in ppm and coupling constants in Hz. [†] signals are overlapping with each other. [§] signals are overlapping with those of solvent. [a~e] assignments of signals with the same letter are interchangeable.

Table S17. ^{1}H NMR data of **5a6**, **14a6**, and **15a6**, **10a7**.

Compound	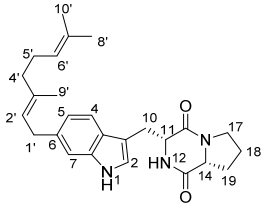 **5a6** ($CDCl_3$)	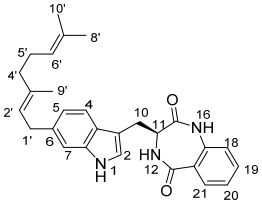 **14a6** ($CDCl_3$)	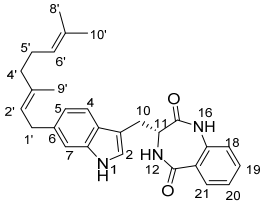 **15a6** ($CDCl_3$)	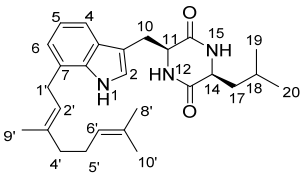 **10a7** ($CDCl_3$)
Position	δ_H, multi., *J* in Hz	δ_H, multi., *J* in Hz	δ_H, multi., *J* in Hz	δ_H, multi., *J* in Hz
1	8.00, s, 1H, 1H	7.98, s, 1H	7.99, s, 1H	8.15, s, 1H
2	7.20, s, 1H	7.12, d, 2.3, 1H	7.12, d, 2.3, 1H	7.08, d, 2.6, 1H
4	7.48, d, 8.1, 1H	7.42, d, 8.1, 1H	7.42, d, 8.1, 1H	7.49, d, 8.0, 1H
5	7.00, dd, 8.1, 1.5, 1H	6.95, dd, 8.1, 1.0, 1H	6.95, dd, 8.1, 1.1, 1H[††]	7.09, dd, 8.0, 7.3, 1H
6	-	-	-	7.04, d, 7.3, 1H
7	7.06, d, 1.5, 1H	7.17, d, 1.0, 1H	7.17, d, 1.1, 1H	-
10	3.75, dd, 15.0, 3.7, 1H	3.50, dd, 15.1, 5.7, 1H	3.50, dd, 15.2, 5.6, 1H	3.51, dd, 15.0, 3.8, 1H
	2.92, dd, 15.0, 11.1, 1H	3.20, dd, 15.1, 8.4, 1H	3.20, dd, 15.2, 8.1, 1H	3.16, dd, 15.0, 8.9, 1H
11	4.36, dd, 11.1, 3.7, 1H	4.13, ddd, 8.4, 5.6, 4.9, 1H	4.13, ddd, 8.4, 5.6, 4.9, 1H	4.31, br d, 9.0, 1H
12	5.71, s, 1H	6.02, d, 4.9, 1H	6.05, d, 4.7, 1H	5.85, s, 1H[a]
14	4.07, t, 8.1, 1H	-	-	3.90, br d, 10.4, 1H
15	-	-	-	5.79, s, 1H[a]
16	-	7.63, s, 1H	7.67, s, 1H	-
17	3.66, ddd, 11.5, 7.4, 7.4, 1H	-	-	1.58, m, 1H[*]
	3.59, ddd, 11.5, 8.7, 3.1, 1H	-	-	1.04, ddd, 14.6, 10.2, 4.4, 1H
18	2.01, m, 1H[†]	6.95, d, 8.0, 1H	6.96, d, 8.0, 1H[††]	1.51, m, 1H
	1.91, m, 1H	-	-	-
19	2.33, m, 1H	7.50, dd, 8.0, 7.4, 1H	7.50, dd, 8.0,7.4, 1H	0.85, d, 6.5, 3H[b]
	2.01, m, 1H[†]	-	-	-
20	-	7.26, dd, 7.9, 7.4, 1H[§]	7.26, dd, 7.9, 7.4, 1H[§]	0.84, d, 6.5, 3H[b]
21	-	7.91, d, 7.9, 1H	7.91, d, 7.9, 1H	-
1’	3.41, d, 7.2, 1H	3.44, d, 7.3, 2H	3.44, d, 7.4, 2H	3.57, d, 7.7, 2H
2’	5.39, br t, 7.4, 1H	5.37, br t, 7.3, 1H	5.37, br t, 8.0, 1H	5.42, br t, 7.5, 1H
4’	2.12, m, 2H	2.11, dd, 15.1, 7.3, 2H	2.12, dd, 14.7, 7.6, 2H	2.15, m, 2H
5’	2.06, m, 2H	2.04, m, 2H	2.04, m, 2H	2.11, m, 2H
6’	5.12, br t, 6.9, 1H	5.10, br t, 6.9, 1H	5.10, br t, 6.9, 1H	5.10, br t, 6.9, 1H
8’	1.74, s, 3H	1.72, s, 3H	1.72, s, 3H	1.81, s, 3H
9’	1.69, s, 3H	1.67, s, 3H	1.67, s, 3H	1.69, s, 3H
10’	1.60, s, 3H	1.59, s, 3H	1.59, s, 3H	1.61, s, 3H

Chemical shifts (δ) are given in ppm and coupling constants in Hz. [†] signals are overlapping with each other. [§] signals are overlapping with those of solvent. [a, b] assignments of signals with the same letter are interchangeable. [*] signals are overlapping with those of water.

Table S18. ^{1}H NMR data of **1a6**, and **1a7**.

Compound	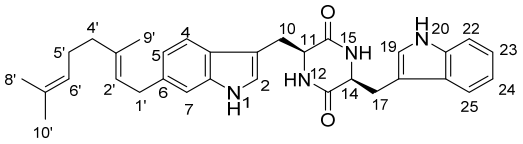 **1a6**		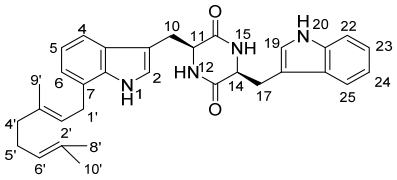 **1a7**	
Position	δ_H, multi., *J* in Hz ($CDCl_3$)	δ_H, multi., *J* in Hz (CD_3COCD_3)	δ_H, multi., *J* in Hz ($CDCl_3$)	δ_H, multi., *J* in Hz (CD_3COCD_3)
1	8.05, s, 1H	9.93, s, 1H	8.06, s, 1H	9.93, s, 1H
2	6.51, d, 2.3, 1H[a]	6.70, d, 2.4, 1H[b]	6.54, d, 2.3, 1H[d]	6.63, d, 2.5, 1H[f]
4	7.56, d, 8.0, 1H	7.37, d, 8.1, 1H	7.41, d, 7.5, 1H	7.33, d, 7.0, 1H
5	7.00, dd, 8.0, 1.3, 1H	6.88, dd, 8.1, 1.5, 1H	7.08, dd, 7.5, 7.2, 1H	6.96, dd, 7.5, 7.0, 1H
6	-	-	7.03, d, 7.2, 1H	6.93, d, 7.5, 1H
7	7.15, d, 1.3, 1H	7.15, d, 1.5, 1H	-	-
10	3.22, dd, 14.5, 3.5, 1H	2.99, dd, 14.3, 3.9, 1H	3.24, br d, 14.4, 1H	3.02, ddd, 14.0, 4.0, 3.5, 1H
	2.44, dd, 14.5, 8.5, 1H	2.26, dd, 14.3, 7.5, 1H	2.39, dd, 14.4, 8.8, 1H	2.19, ddd, 14.0, 7.0, 4.0, 1H
11	4.17, m, 1H	4.04, m, 1H	4.19, br t, 10.4, 1H	4.05, m, 1H
12	5.69, s, 1H	6.75, s, 1H[c]	5.73, s, 1H[e]	6.74, s, 1H
14	4.18, m, 1H	4.04, m, 1H	4.19, br t, 10.4, 1H	4.05, m, 1H
15	5.69, s, 1H	6.78, s, 1H[c]	5.70, s, 1H[e]	6.74, s, 1H
17	3.24, dd, 14.5, 3.5, 1H	3.03, dd, 14.4, 4.0, 1H	3.24, br d, 14.4, 1H	3.02, ddd, 14.0, 4.0, 3.5, 1H
	2.47, dd, 14.5, 8.5, 1H	2.34, dd, 14.3, 7.4, 1H	2.51, dd, 14,4, 8.3, 1H	2.19, ddd, 14.0, 7.0, 4.0, 1H
19	6.55, d, 2.2, 1H[a]	6.59, d, 2.4, 1H[b]	6.59, d, 2.3, 1H[d]	6.65, d, 2,2, 1H[f]
20	7.94, s, 1H	10.09, s, 1H	8.08, s, 1H	10.07, s, 1H
22	7.35, d, 8.0, 1H	7.34, d, 8.1, 1H	7.36, d, 8.0, 1H	7.33, d, 8.0, 1H
23	7.22, dd, 8.0, 7.0, 1H	7.08, dd, 8.1, 7.0, 1H	7.22, d, 8.0, 7.0, 1H	7.08, dd, 8.0, 7.0, 1H
24	7.14, dd, 8.0, 7.0, 1H	7.00, dd, 8.1, 7.0, 1H	7.15, d, 8.0, 7.0, 1H	7.00, dd, 8.0, 7.0, 1H
25	7.46, d, 8.0, 1H	7.46, d, 8.1, 1H	7.57, d, 8.0, 1H	7.46, d, 8.0, 1H
1’	3.45, d, 7.2, 2H	3.43, d, 7.3, 2H	3.50, d, 7.3, 2H	3.54, d, 7.0, 2H
2’	5.38, br t, 7.4, 1H	5.39, br t, 7.8, 1H	5.33, br t, 6.9, 1H	5.38, br t, 7.2, 1H
4’	2.13, m, 1H	2.10, m, 2H	2.07, m, 2H	2.07, m, 2H[§]
5’	2.06, m, 1H	2.03, m, 2H[§]	2.02, m, 2H	1.96, m, 2H
6’	5.11, br t, 7.0, 1H	5.11, br t, 6.9, 1H	5.05, br t, 6.6, 1H	5.04, br t, 6.9, 1H
8’	1.73, s, 3H	1.73, s, 3H	1.76, s, 3H	1.69, s, 3H
9’	1.68, s, 3H	1.63, s, 3H	1.68, s, 3H	1.63, s, 3H
10’	1.59, s, 3H	1.57, s, 3H	1.58, s, 3H	1.53, s, 3H

Chemical shifts (δ) are given in ppm and coupling constants in Hz. [§] signals are overlapping with those of solvent. [a–j] assignments of signals with the same letter are interchangeable. [*] signals are overlapping with those of water.

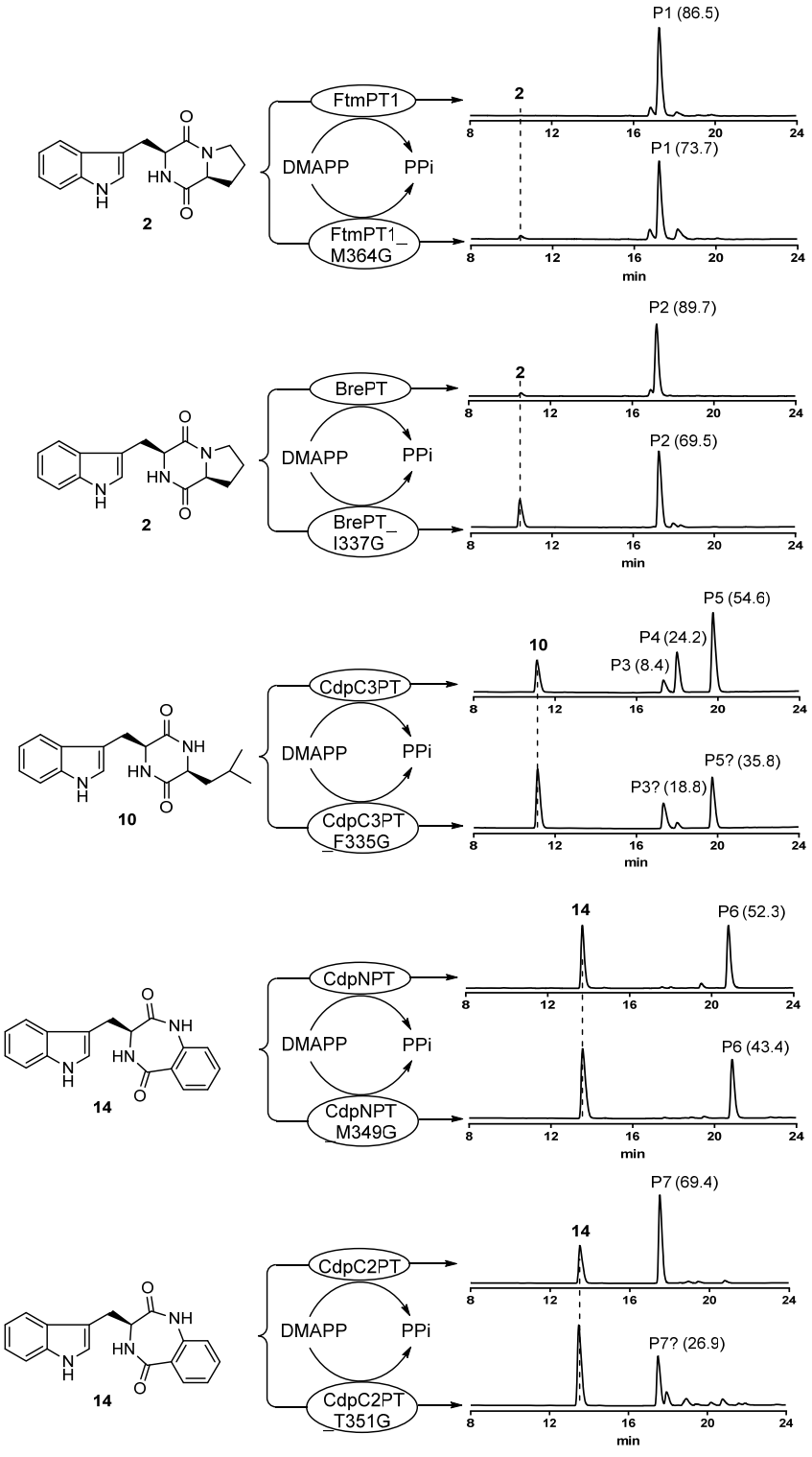

Figure S1 HPLC chromatograms of the incubation mixtures of cyclic dieptide PTs and their corresponding mutants with their natural or best substrates in the presence of DMAPP. The assays (50 µL) contained 50 mM Tris-HCl (pH 7.5), 10 mM $CaCl_2$, 1 mM cyclic dipeptide, 2 mM DMAPP, 0.7–6% (v/v) glycerol, up to 5% (v/v) DMSO, and 10 µg purified protein for FtmPT1 and BrePT, or 20 µg for CdpNPT, CdpC2PT, and CdpC3PT. The reaction mixtures were incubated at 37 °C for 2 h for FtmPT1 and BrePT, and 4h for CdpNPT, CdpC2PT and CdpC3PT. Detection was carried out with a photodiode array detector and illustrated for absorption at 296 nm. According to previous results,[7-9,11,18] P1 should be tryprostatin B, P2 deoxybrevianamide E, P5 *cyclo*-3*β*-prenyl-L-Trp-L-Leu, P6 (2*S*, 3*R*, 11*S*)-aszonalenin, and P7 (*S*)-2-tert-prenyl-benzodiazepinedione. The structures of P1, P2, and P6 have also been confirmed by NMR after isolation friom the incubation mixtures with the mutants.

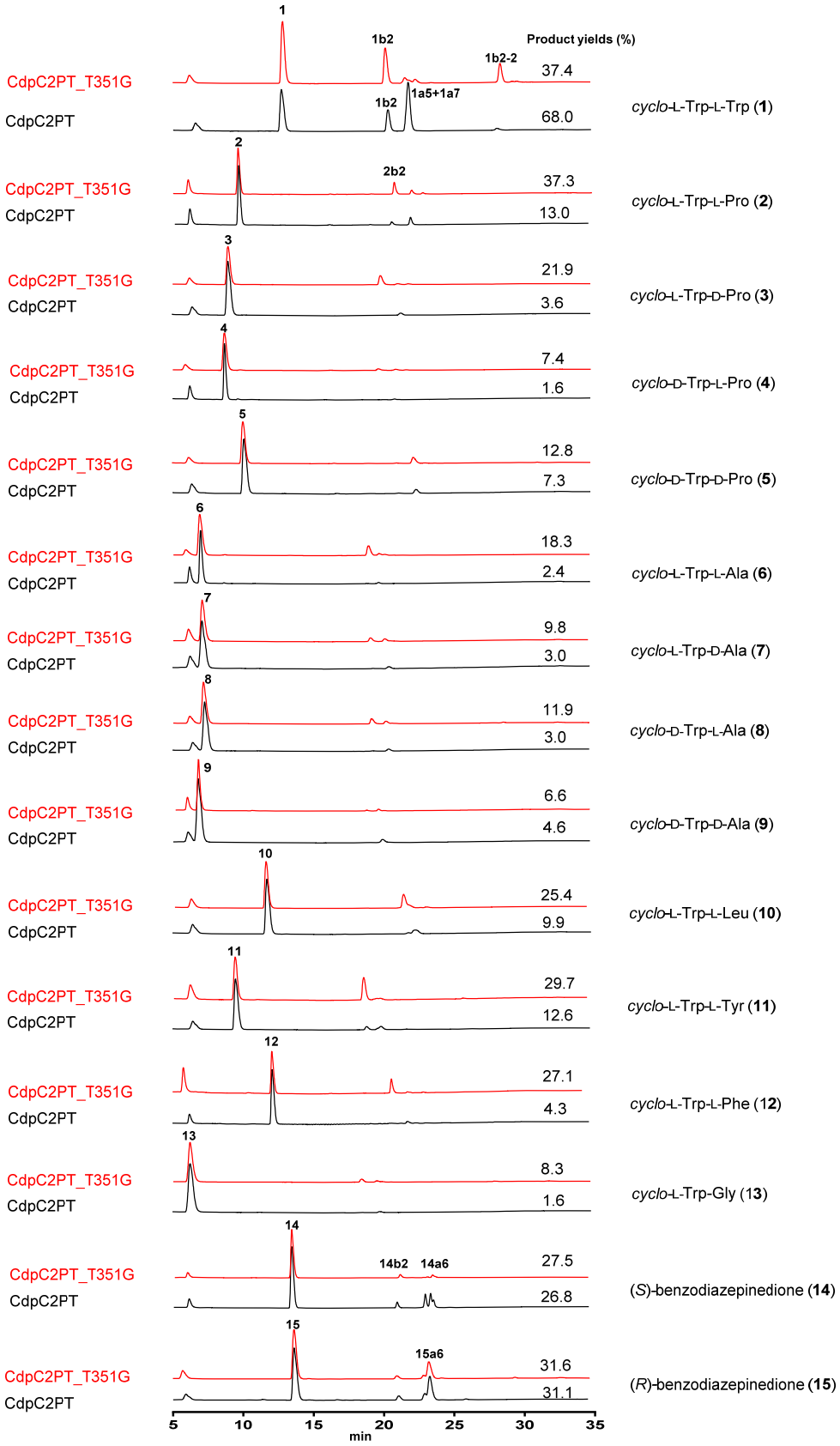

Figure S2 HPLC chromatograms of the incubation mixtures of CdpC2PT and CdpC2PT _T351G with 15 cyclic dipeptides in the presence of GPP. The assays (50 µL) contained 50 mM Tris-HCl (pH 7.5), 2 mM DTT, 1 mM cyclic dipeptide, 2 mM GPP, 5% (v/v) glycerol, up to 5% (v/v) DMSO, and 50 µg purified protein. The reaction mixtures were incubated at 37 °C for 16 h. Detection were carried out with a photodiode array detector and illustrated for absorption at 296 nm. The product yields (%) are given in average of two replicate.

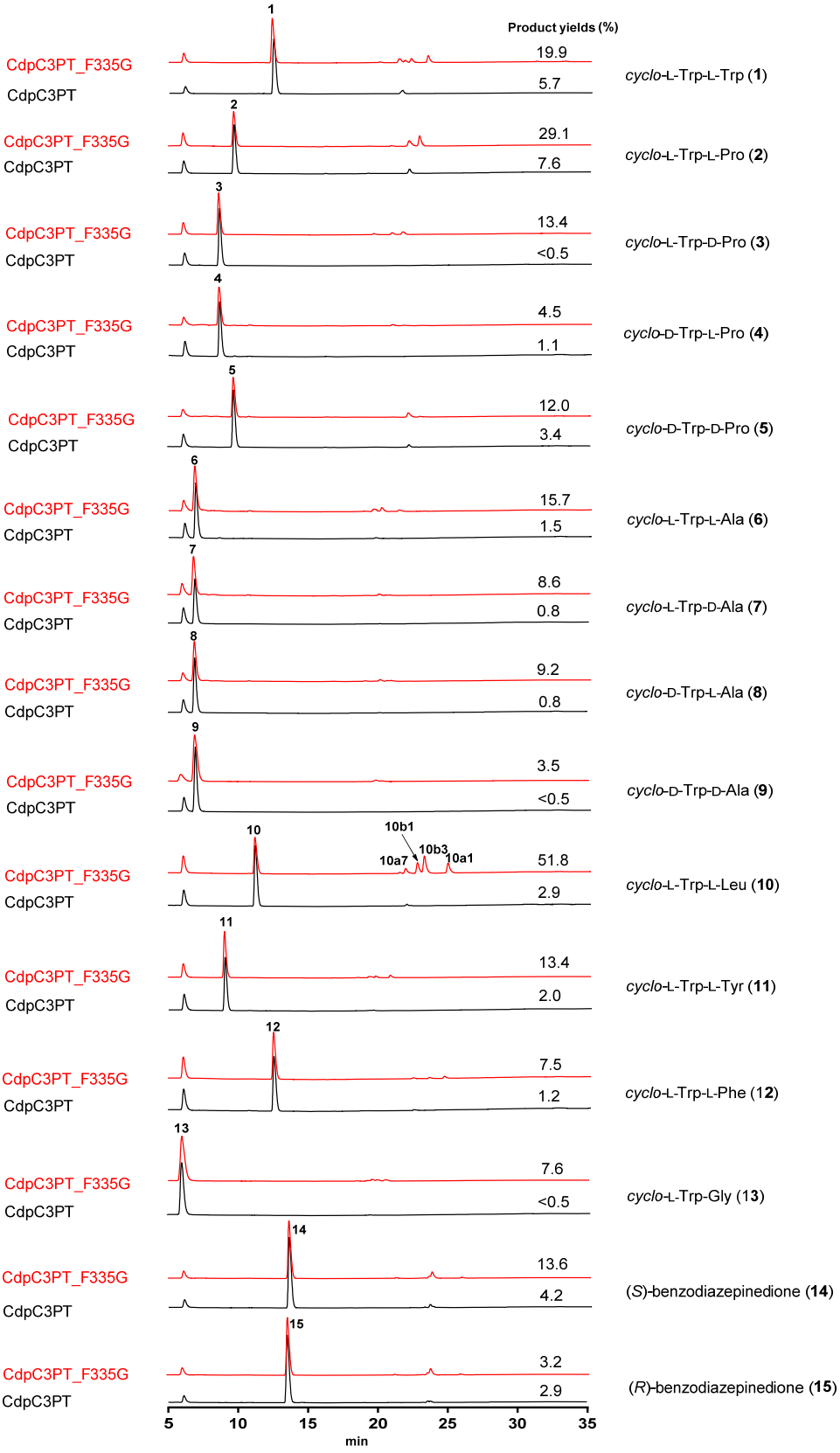

Figure S3 HPLC chromatograms of the incubation mixtures of CdpC3PT and CdpC3PT _F335G with 15 cyclic dipeptides in the presence of GPP. The assays (50 µL) contained 50 mM Tris-HCl (pH 7.5), 2 mM DTT, 1 mM cyclic dipeptide, 2 mM GPP, 3.3% (v/v) glycerol, up to 5% (v/v) DMSO, and 50 µg purified protein. The reaction mixtures were incubated at 37 °C for 16 h. Detection were carried out with a photodiode array detector and illustrated for absorption at 296 nm. The product yields (%) are given in average of two replicate.

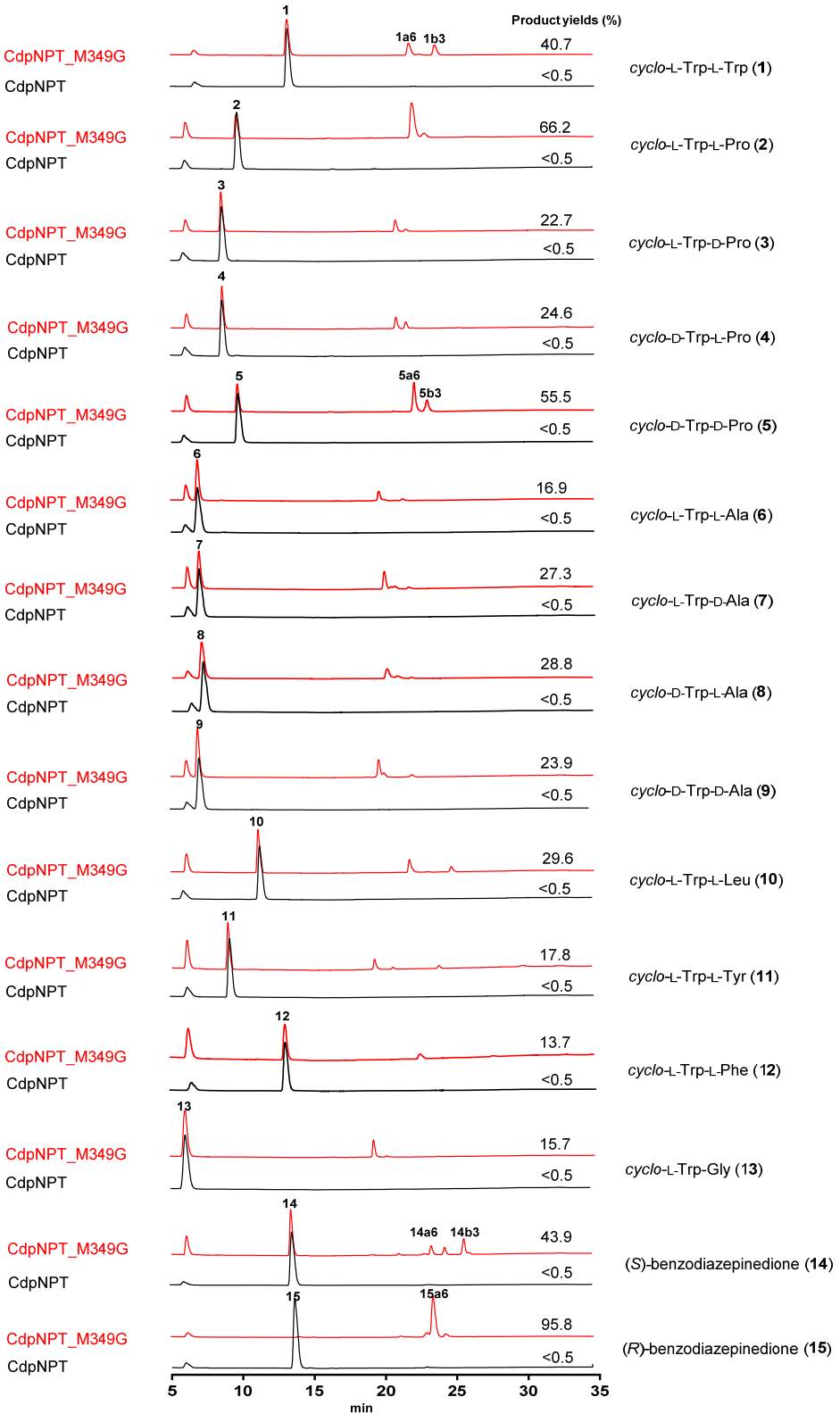

Figure S4 HPLC chromatograms of the incubation mixtures of CdpNPT and CdpNPT _M349G with 15 cyclic dipeptides in the presence of GPP. The assays (50 µL) contained 50 mM Tris-HCl (pH 7.5), 2 mM DTT, 1 mM cyclic dipeptide, 2 mM GPP, 5% (v/v) glycerol, up to 5% (v/v) DMSO, and 30 µg purified protein. The reaction mixtures were incubated at 37 °C for 16 h. Detection were carried out with a photodiode array detector and illustrated for absorption at 296 nm. The product yields (%) are given in average of two replicate.

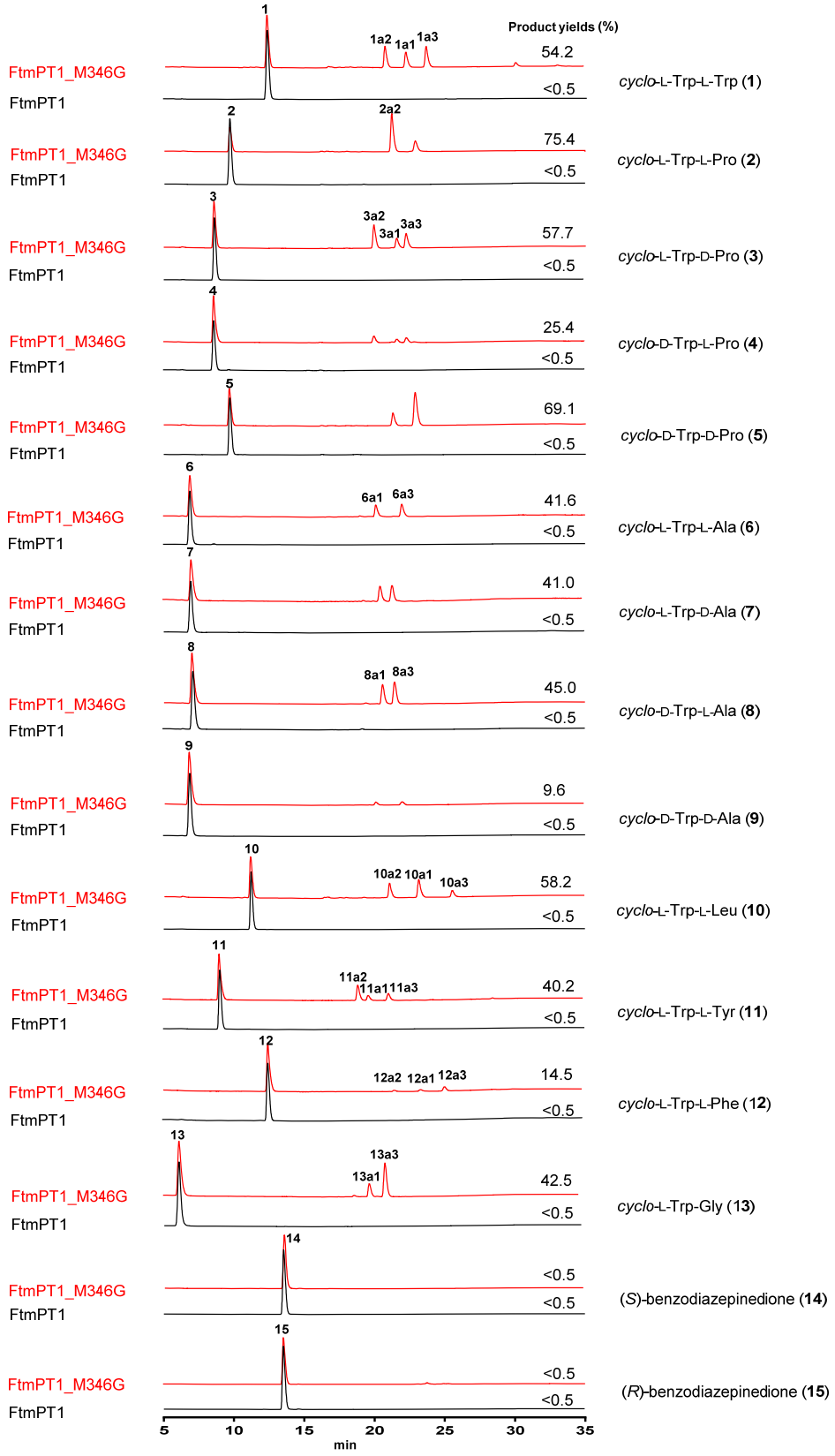

Figure S5 HPLC chromatograms of the incubation mixtures of FtmPT1 and FtmPT1_M364G with 15 cyclic dipeptides in the presence of GPP. The assays (50 µL) contained 50 mM Tris-HCl (pH 7.5), 10 mM $CaCl_2$, 1 mM cyclic dipeptide, 2 mM GPP, 0.7 % (v/v) glycerol, up to 5% (v/v) DMSO, and 10 µg purified protein. The reaction mixtures were incubated at 37 °C for 2 h. Detection were carried out with a photodiode array detector and illustrated for absorption at 296 nm. The product yields (%) are given in average of two replicate.

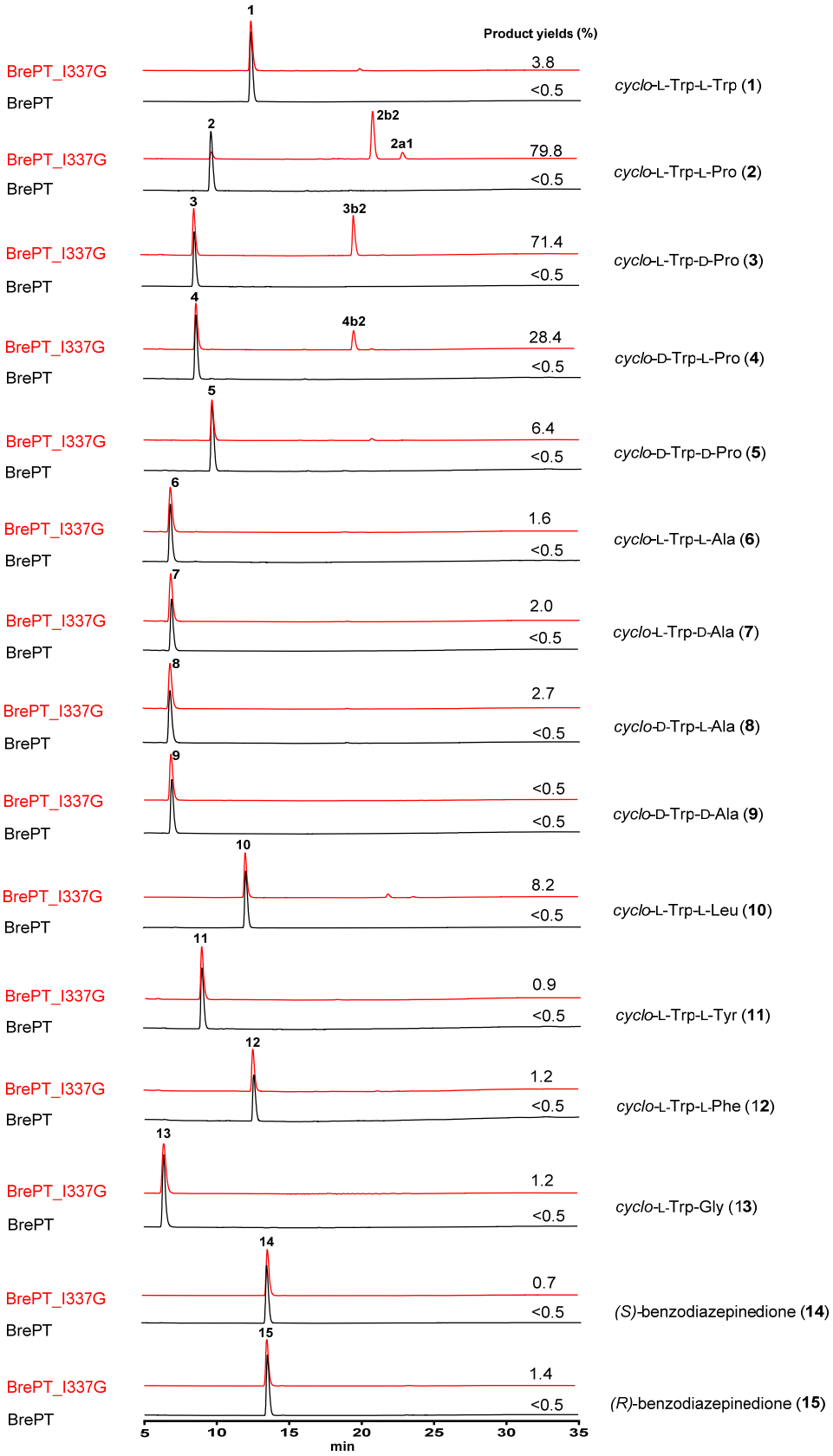

Figure S6 HPLC chromatograms of the incubation mixtures of BrePT and BrePT_I337G with 15 cyclic dipeptides in the presence of GPP. The assays (50 µL) contained 50 mM Tris-HCl (pH 7.5), 10 mM $CaCl_2$, 1 mM cyclic dipeptide, 2 mM GPP, 2% (v/v) glycerol, up to 5% (v/v) DMSO, and 10 µg purified protein. The reaction mixtures were incubated at 37 °C for 2 h. Detection were carried out with a photodiode array detector and illustrated for absorption at 296 nm. The product yields (%) are given in average of two replicate.

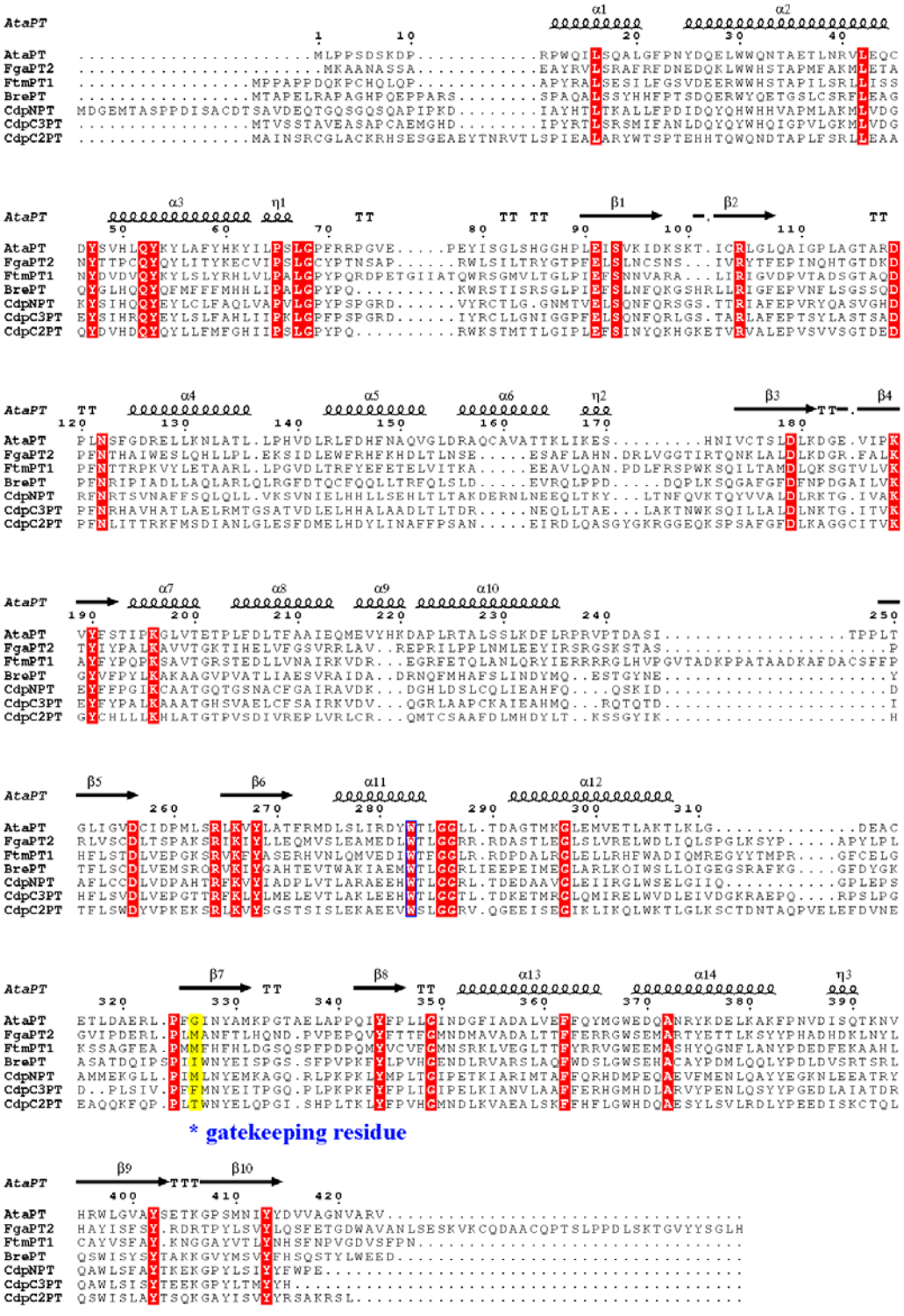

Figure S7 Protein alignments of AtaPT with PTs used in this study. AtaPT (PDB code: 5KCG), FgaPT2 (PDB code: 3I4Z), FtmPT1 (PDB code: 3O24), BrePT (GenBank: I4AY86.1), CdpC2PT (GenBank: AGR03830.1), CdpC3PT (GenBank: EAW17508.1), and CdpNPT (PDB code: 4E0T).

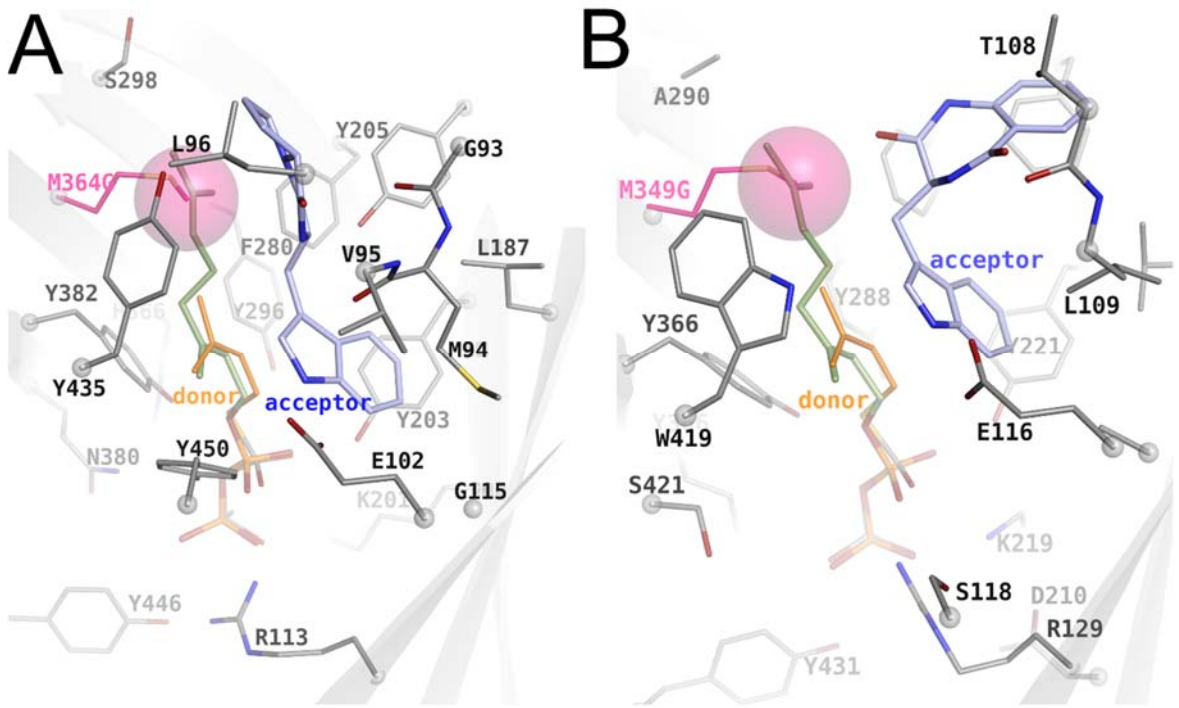

Figure S8: Models of catalysis for PTs. DMAPP (orange) and GPP (green) were modelled into the crystal structures of FtmPT1 (A) (pdb-code: 3I4X) with **2** (blue) and of CdpNPT (B) (pdb-code: 3O2K) with **14** (blue) as acceptor. The GPP molecule was modelled into the active site on the basis of the DMAPP binding of both enzymes. The pyrophosphate of the prenyl donor was kept as fixed anchor and the geranyl entity was placed into the DMAPP binding pocket by avoiding clashes with the active site residues of the enzyme variant where the gatekeeper residue was *in silico* mutated to glycine. In the native state, the gatekeeper residue (pink) would clash with the GPP molecule. This clash is emphasized by transparent spheres (pink).

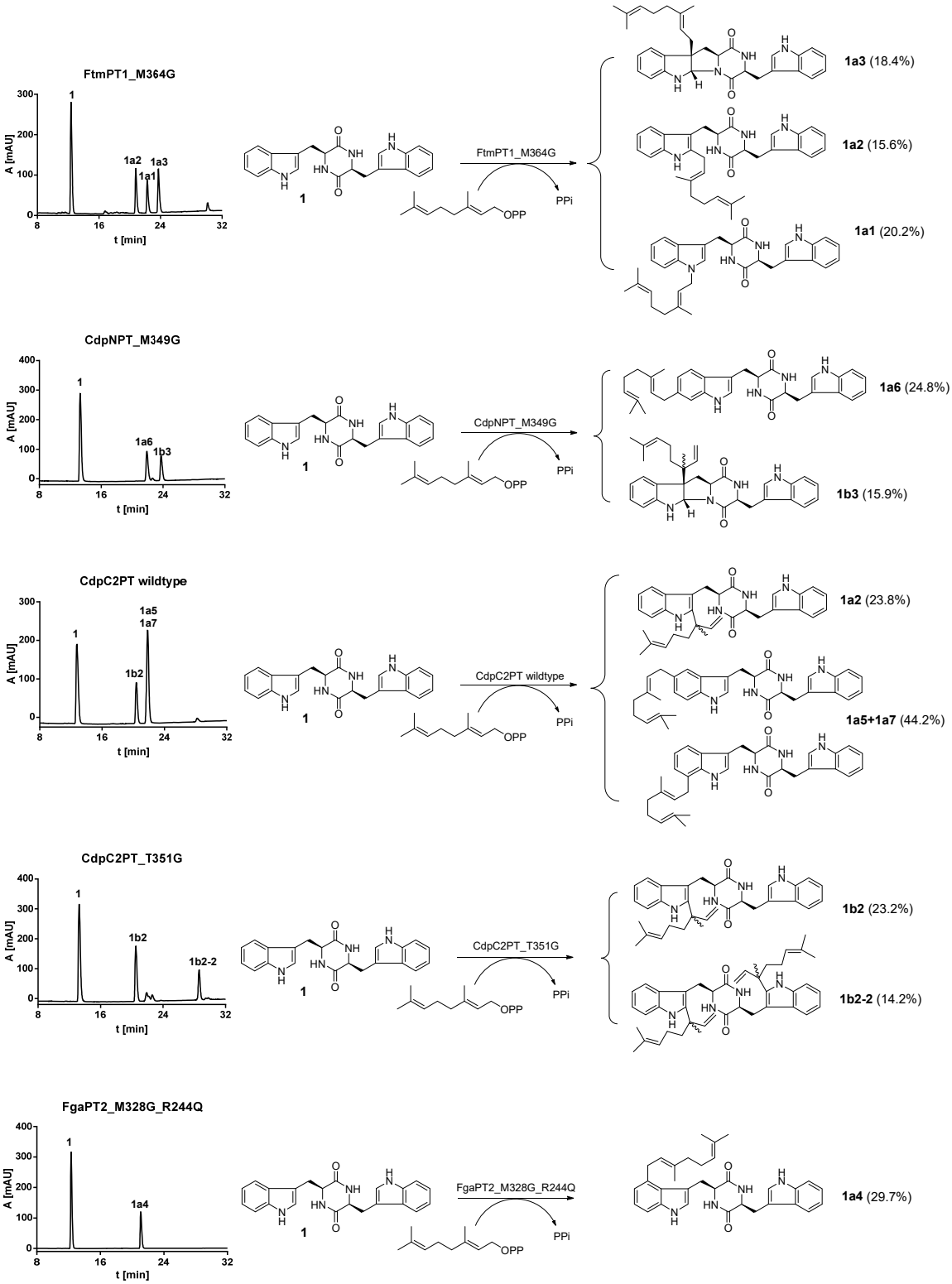

Figure S9 HPLC analysis of enzyme assays of FtmPT1_M364G, CdpNPT_M349G, CdpC2PT, and CdpC2PT_T351G with GPP and *cyclo*-L-Trp-L-Trp (**1**). The assay (50 µL) for FtmPT1_M364G contained 50 mM Tris-HCl (pH 7.5), 10 mM $CaCl_2$, 1 mM *cyclo*-L-Trp-L-Trp, 2 mM GPP, 0.7% (v/v) glycerol, 5% (v/v) DMSO, and 10 µg purified protein. The assay (50 µL) for CdpNPT_M349G contained 50 mM Tris-HCl (pH 7.5), 2 mM DTT, 1 mM *cyclo*-L-Trp-L-Trp, 2 mM GPP, 5% (v/v) glycerol, 5% (v/v) DMSO, and 30 µg purified protein. The assays for CdpC2PT and CdpC2PT_T351G contained 50 mM Tris-HCl (pH 7.5), 2 mM DTT, 1 mM *cyclo*-L-Trp-L-Trp, 2 mM GPP, 0.7-6% (v/v) glycerol, 5% (v/v) DMSO, and 50 µg purified protein. The reaction mixtures were incubated at 37 °C for 2 h for FtmPT1, and 16 h for CdpNPT_M349G, CdpC2PT and CdpC2PT_T351G. Detection were carried out with a photodiode array detector and illustrated for absorption at 296 nm. Product yields are given in parenthesis after compound numbers.

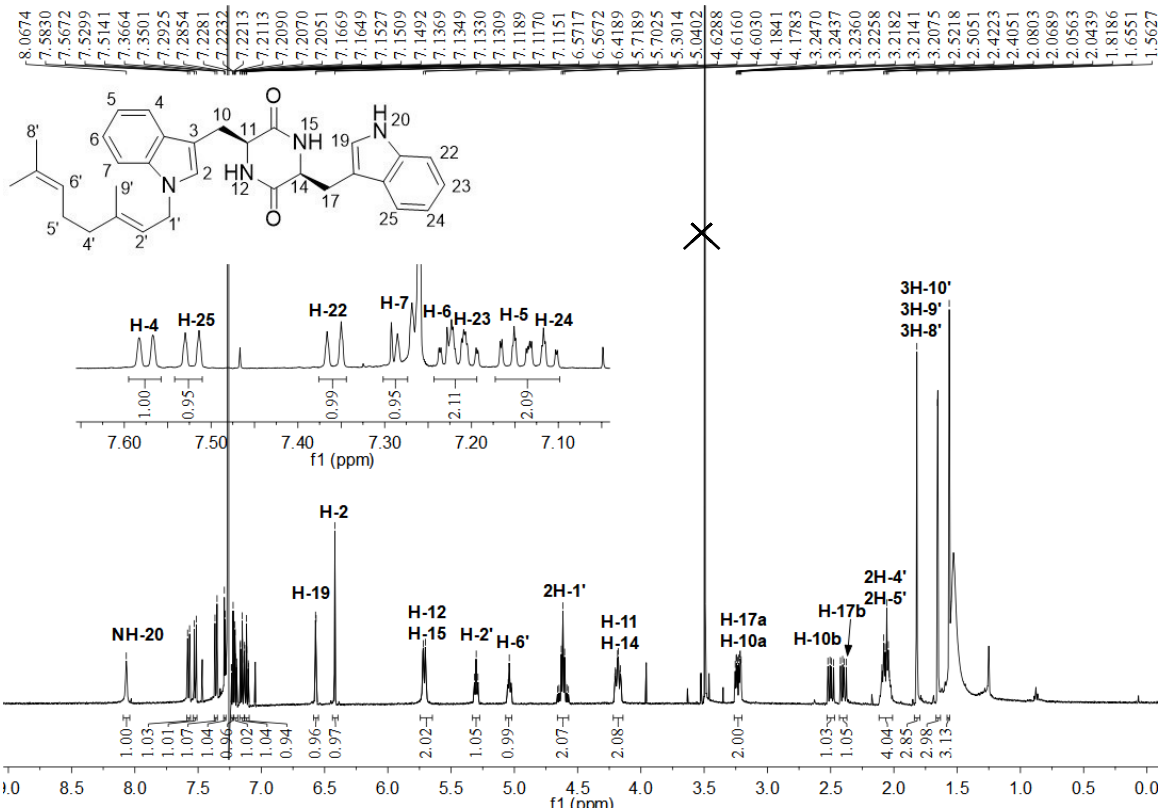

Figure S10 ^{1}H NMR spectrum of **1a1** in $CDCl_3$ (500MHz).

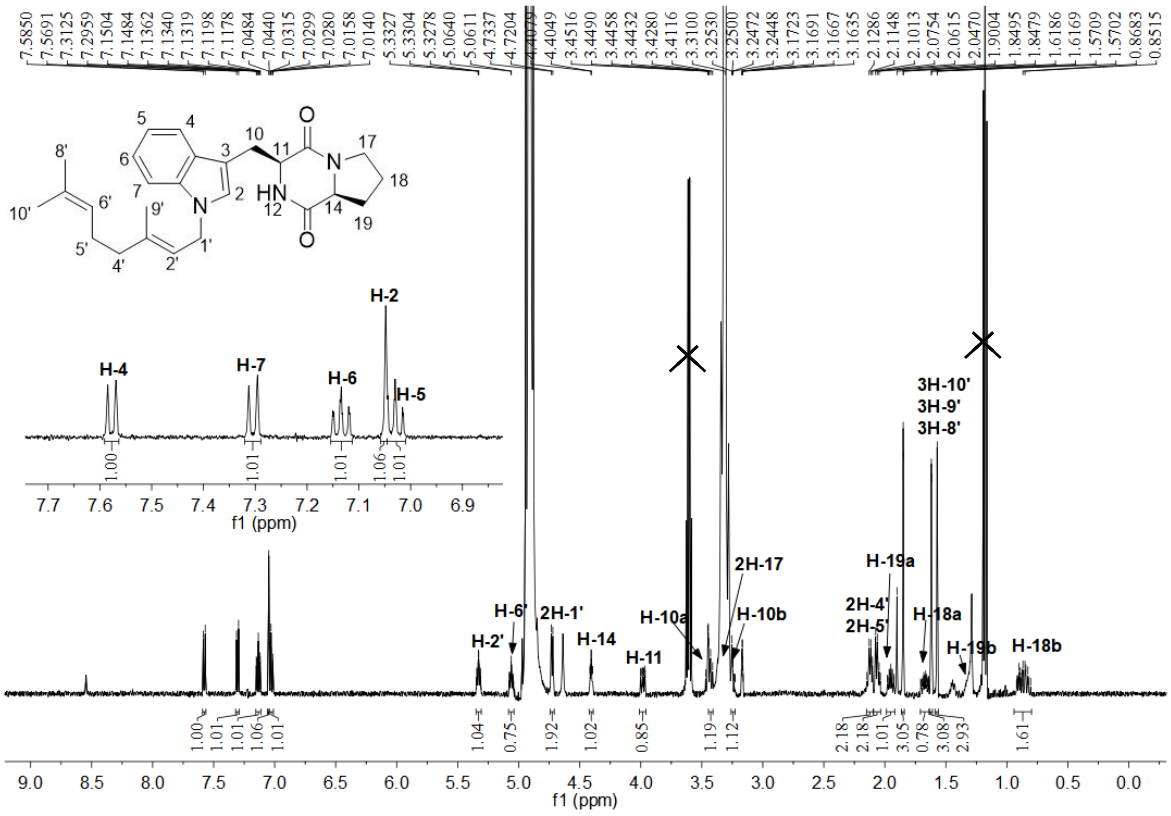

Figure S11 ^{1}H NMR spectrum of **2a1** in CD_3OD (500MHz).

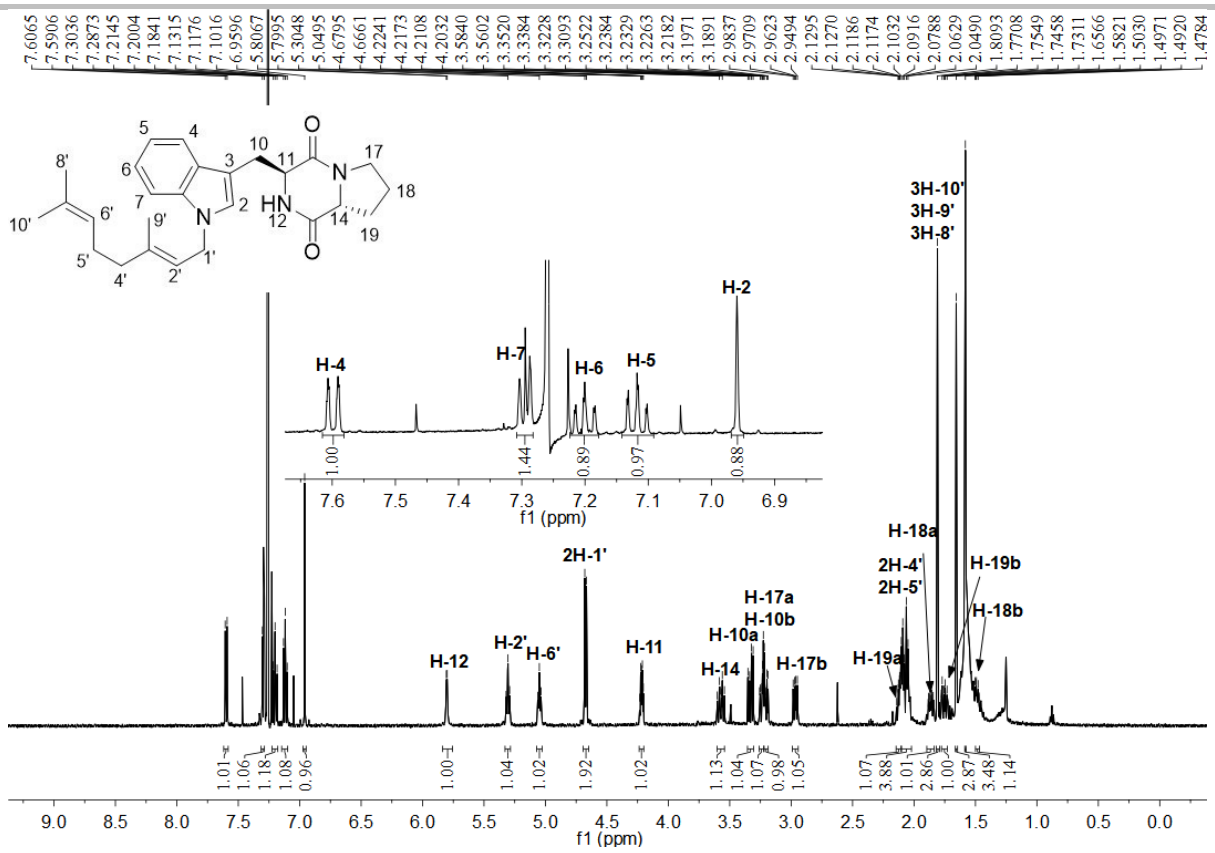

Figure S12 ^{1}H NMR spectrum of **3a1** in $CDCl_3$ (500MHz).

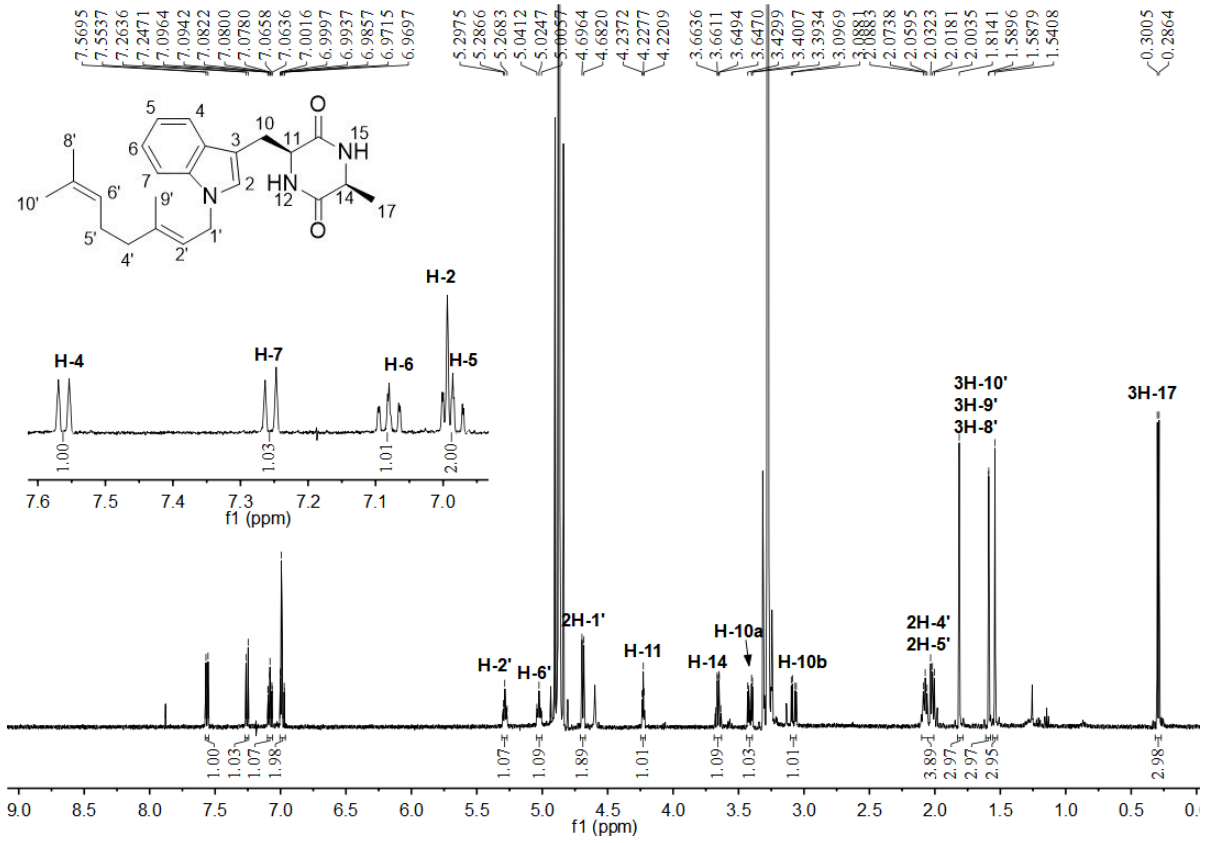

Figure S13 ^{1}H NMR spectrum of **6a1** in CD_3OD (500MHz).

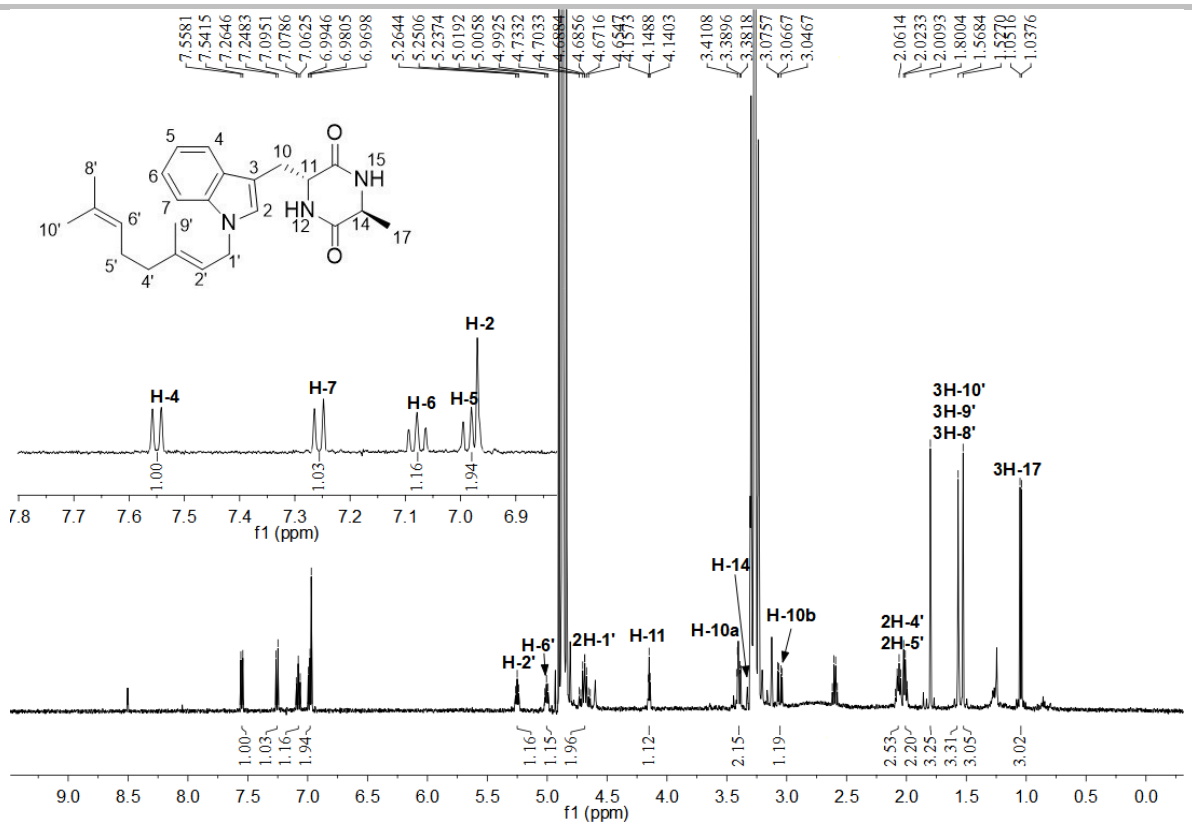

Figure S14 ^{1}H NMR spectrum of **8a1** in CD_3OD (500MHz).

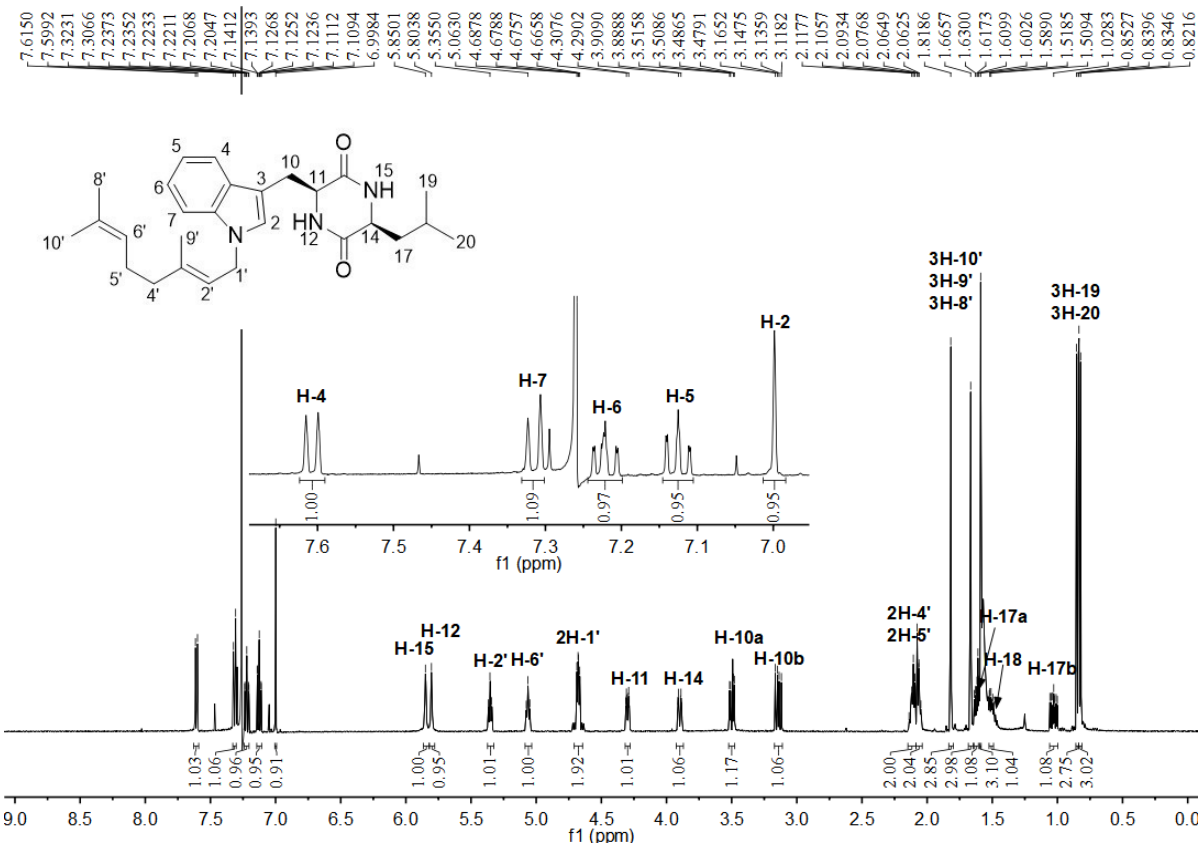

Figure S15 ^{1}H NMR spectrum of **10a1** in $CDCl_3$ (500MHz).

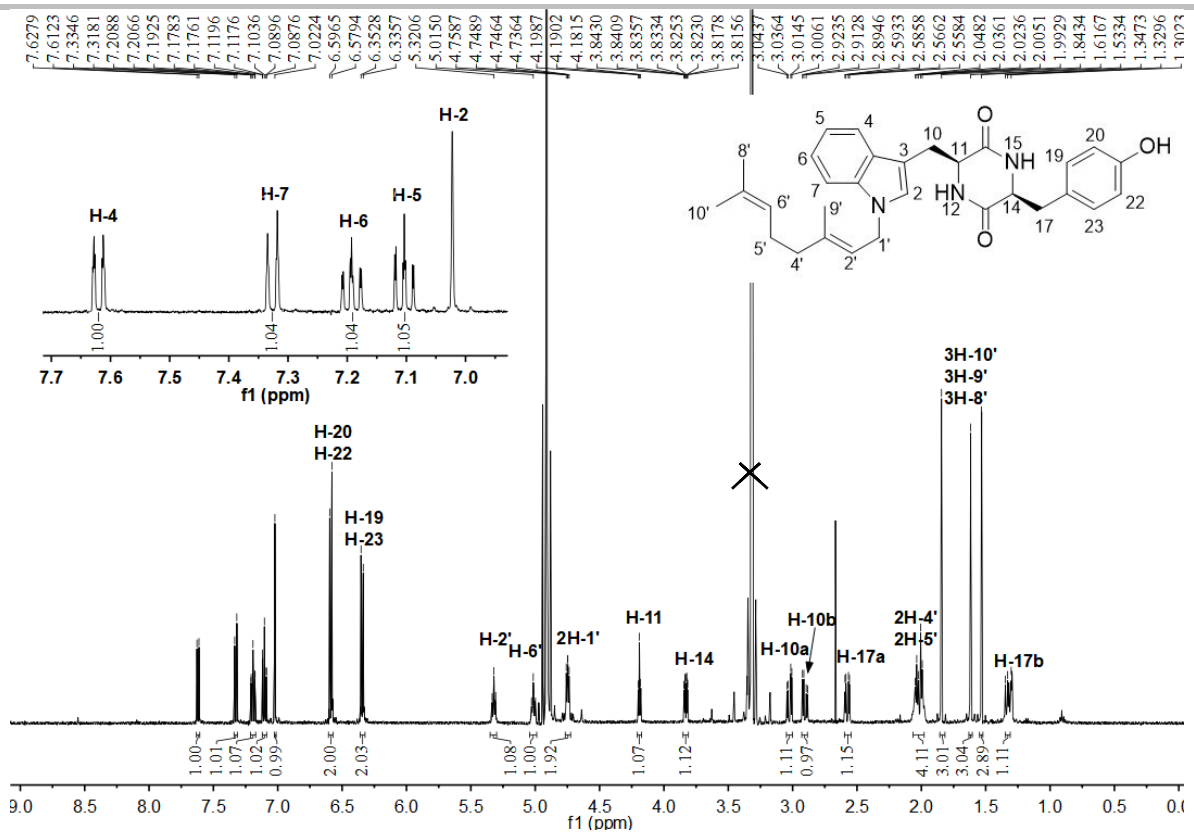

Figure S16 ^{1}H NMR spectrum of **11a1** in CD_3OD (500MHz).

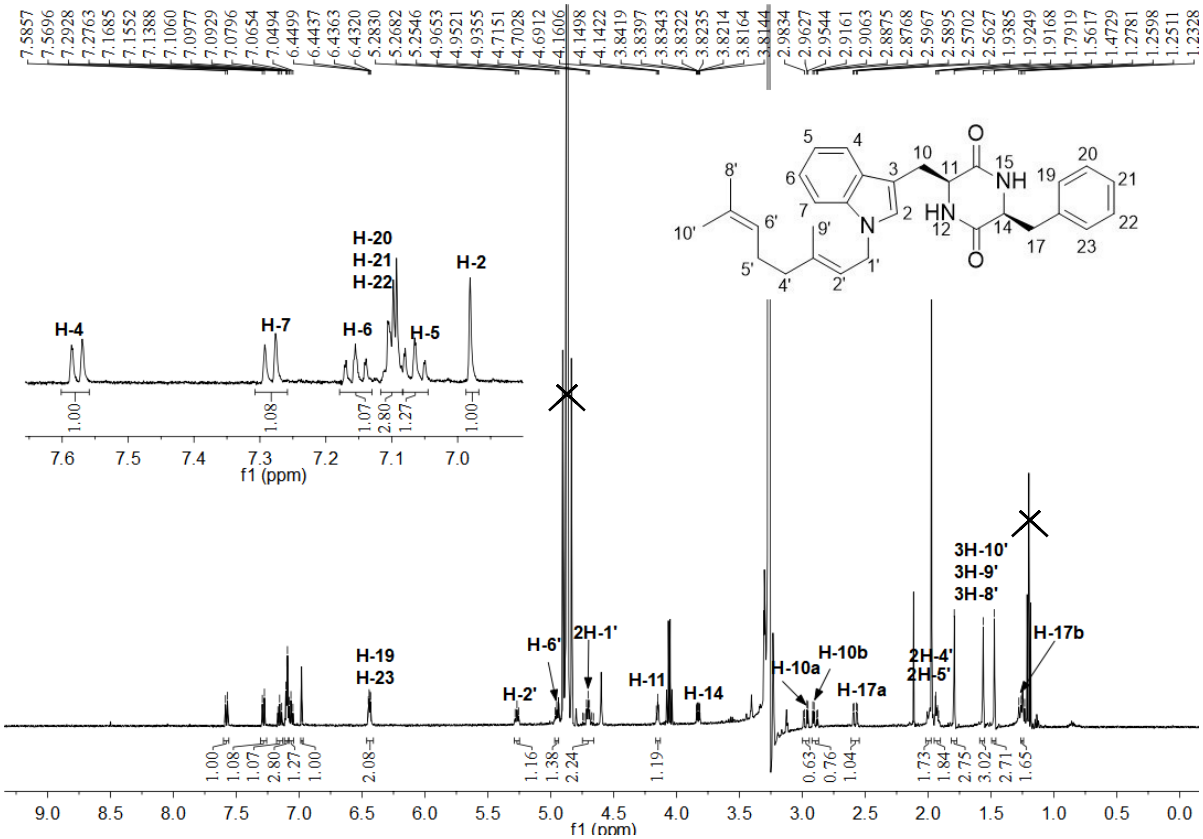

Figure S17 ^{1}H NMR spectrum of **12a1** in CD_3OD (500MHz).

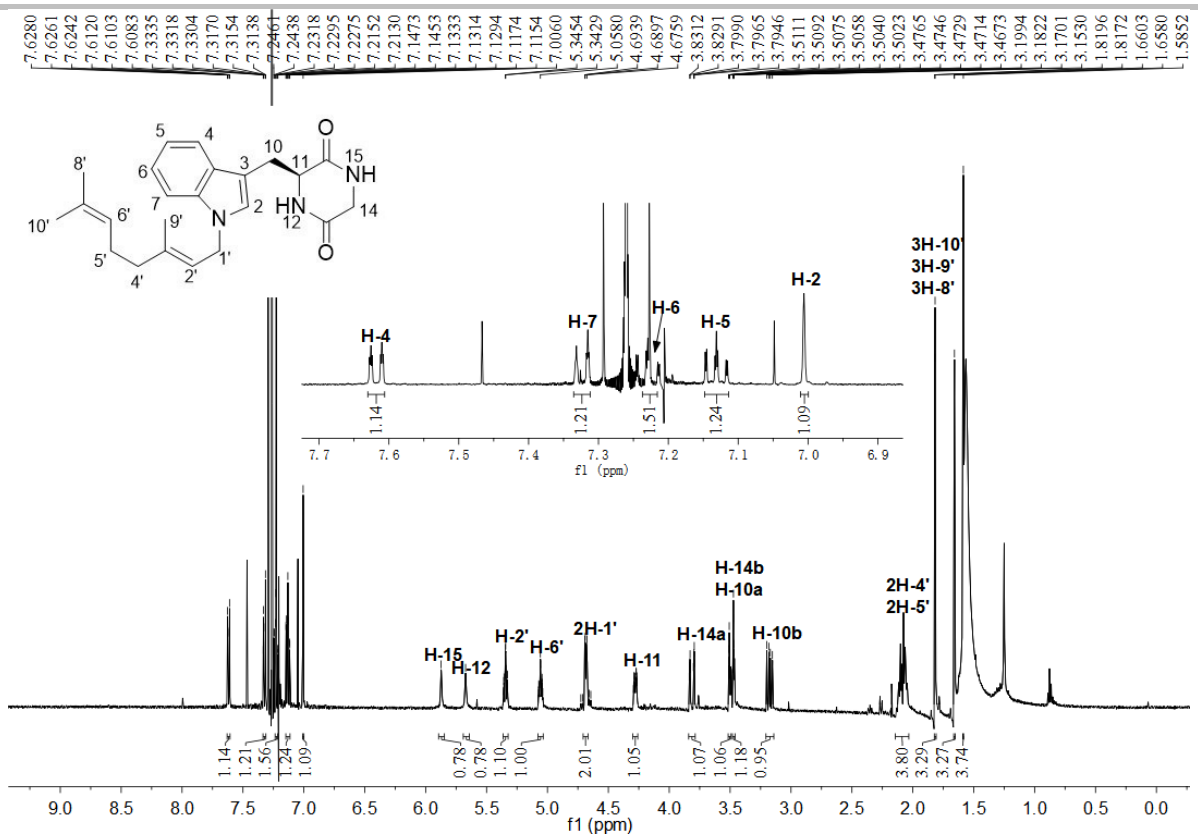

Figure S18 ^{1}H NMR spectrum of **13a1** in $CDCl_3$ (500MHz).

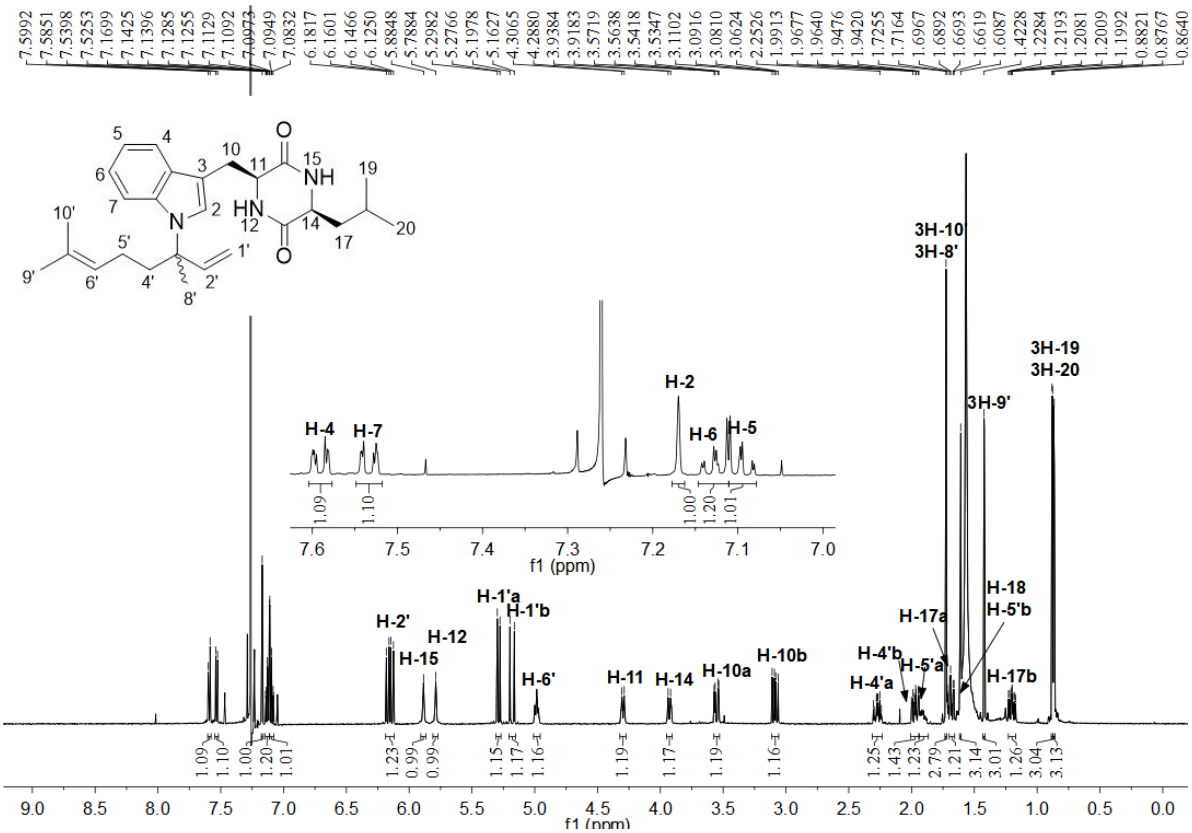

Figure S19 ^{1}H NMR spectrum of **10b1** in $CDCl_3$ (500MHz).

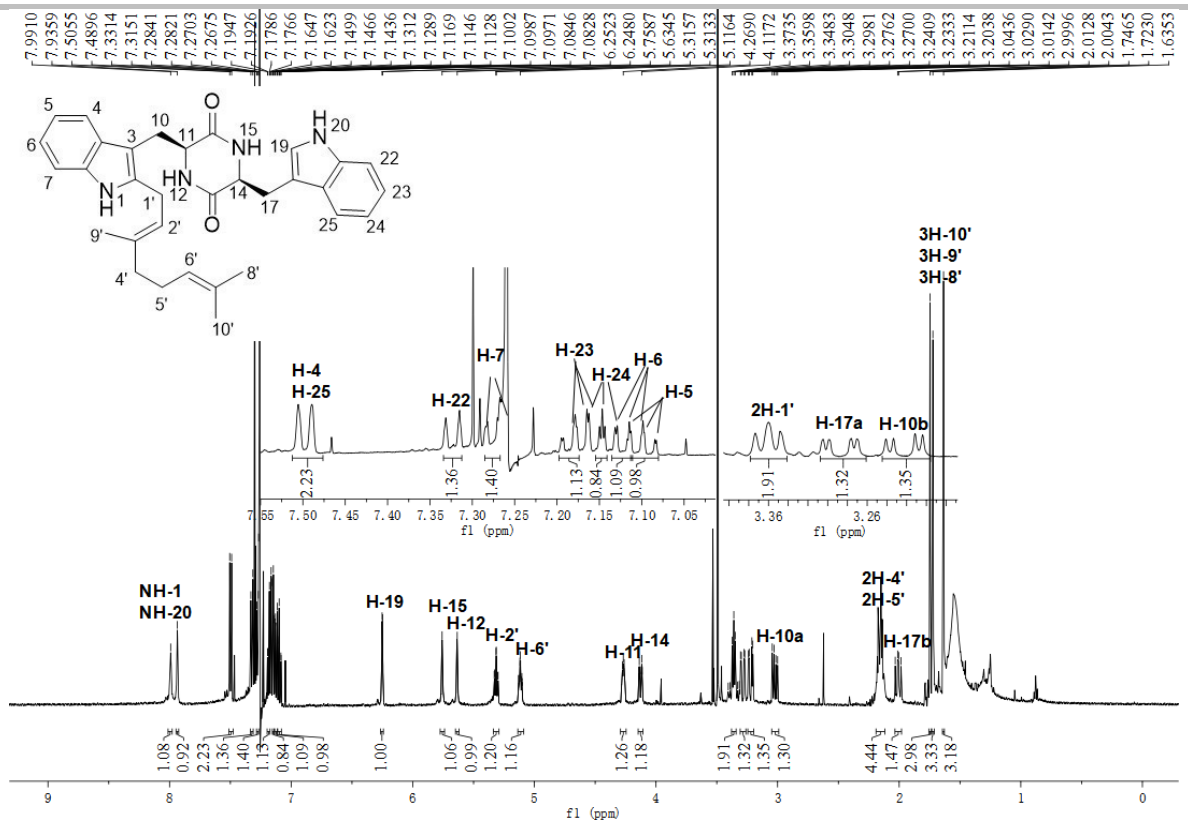

Figure S20 ^{1}H NMR spectrum of **1a2** in $CDCl_3$ (500MHz).

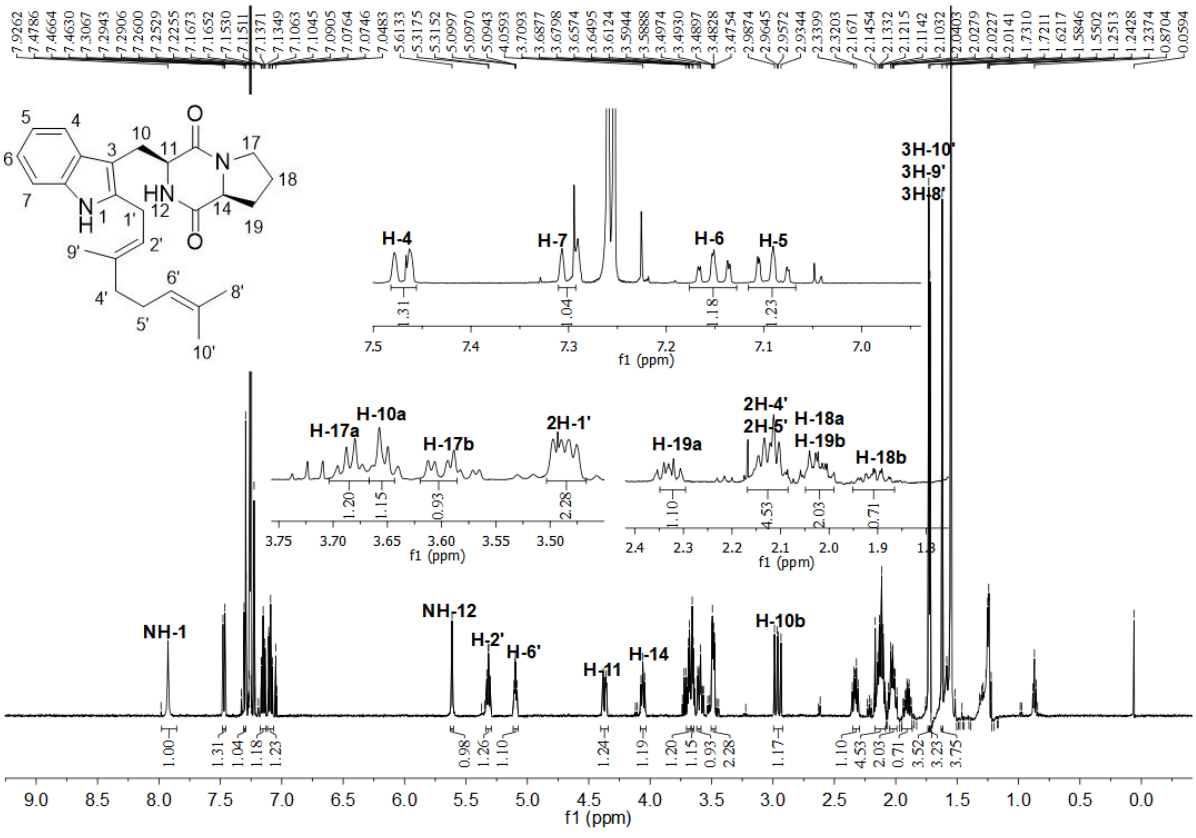

Figure S21 ^{1}H NMR spectrum of **2a2** in $CDCl_3$ (500MHz).

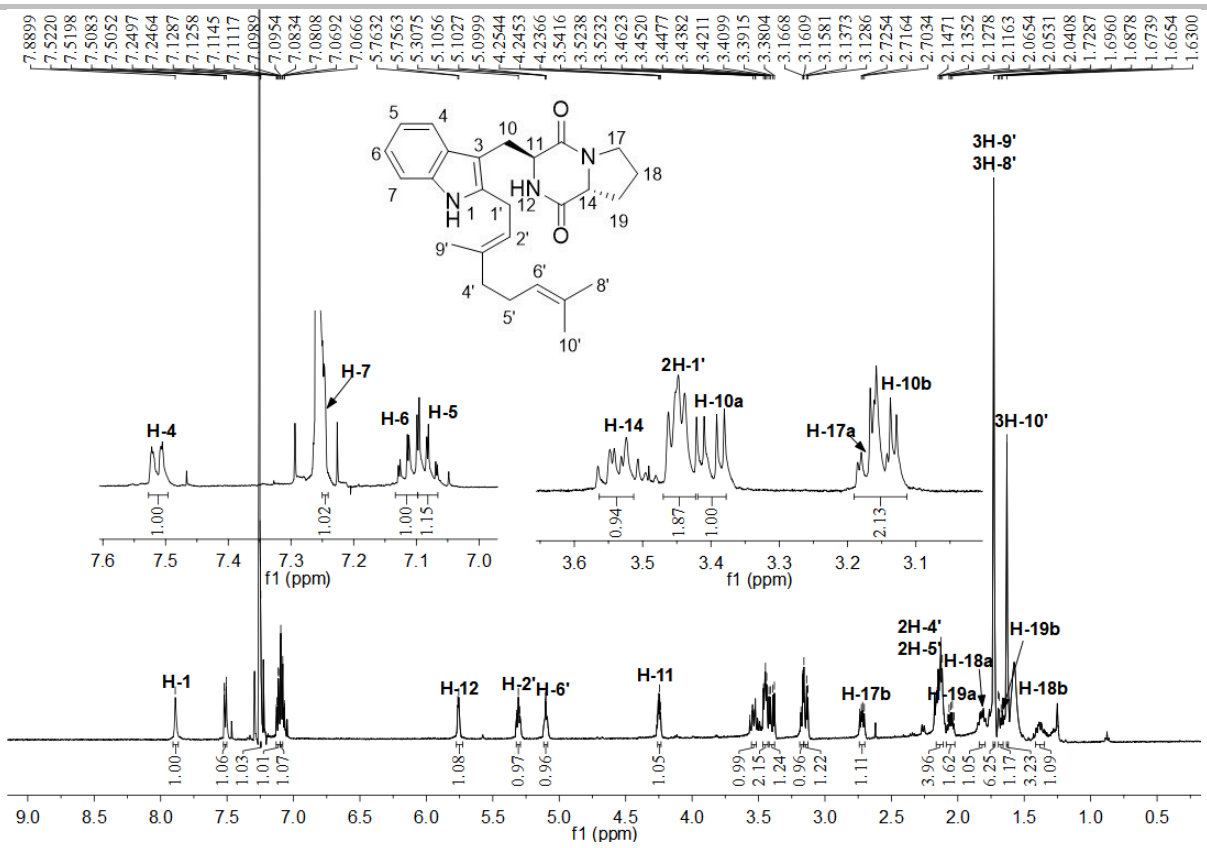

Figure S22 ^{1}H NMR spectrum of **3a2** in $CDCl_3$ (500MHz).

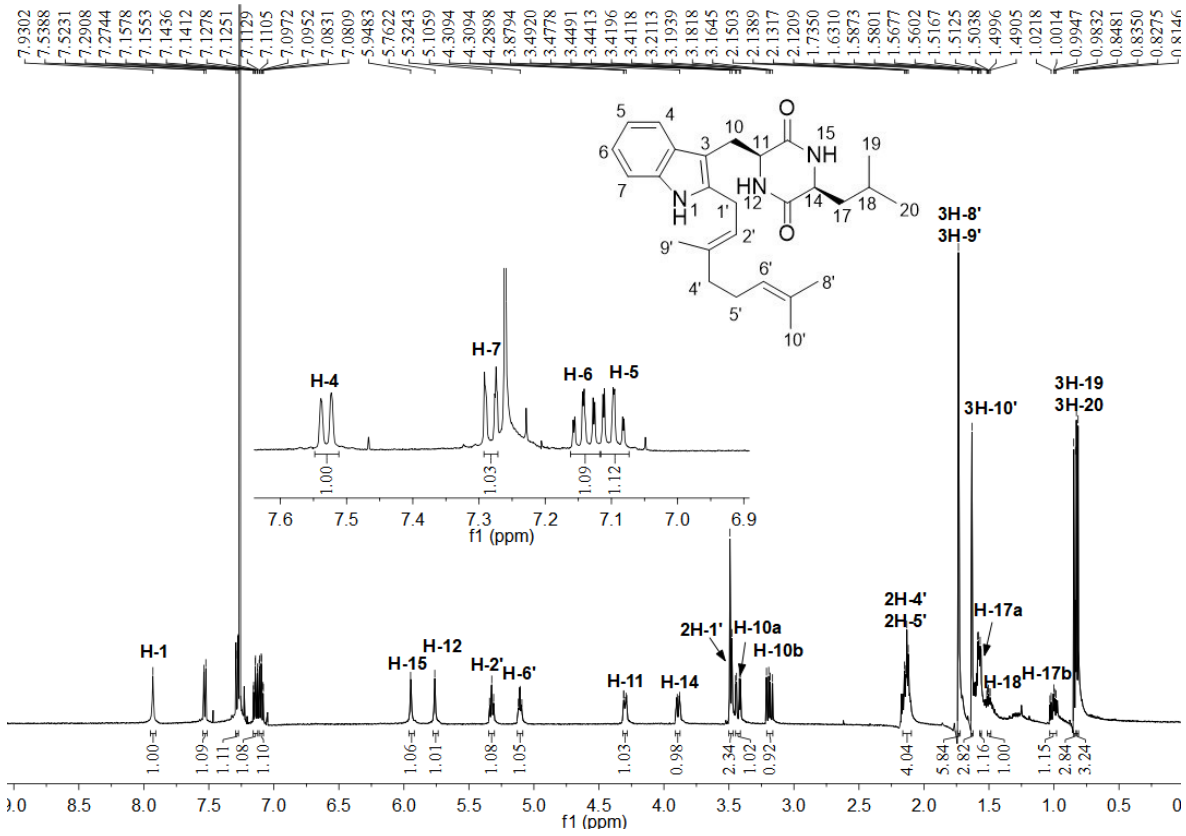

Figure S23 ^{1}H NMR spectrum of **10a2** in $CDCl_3$ (500MHz).

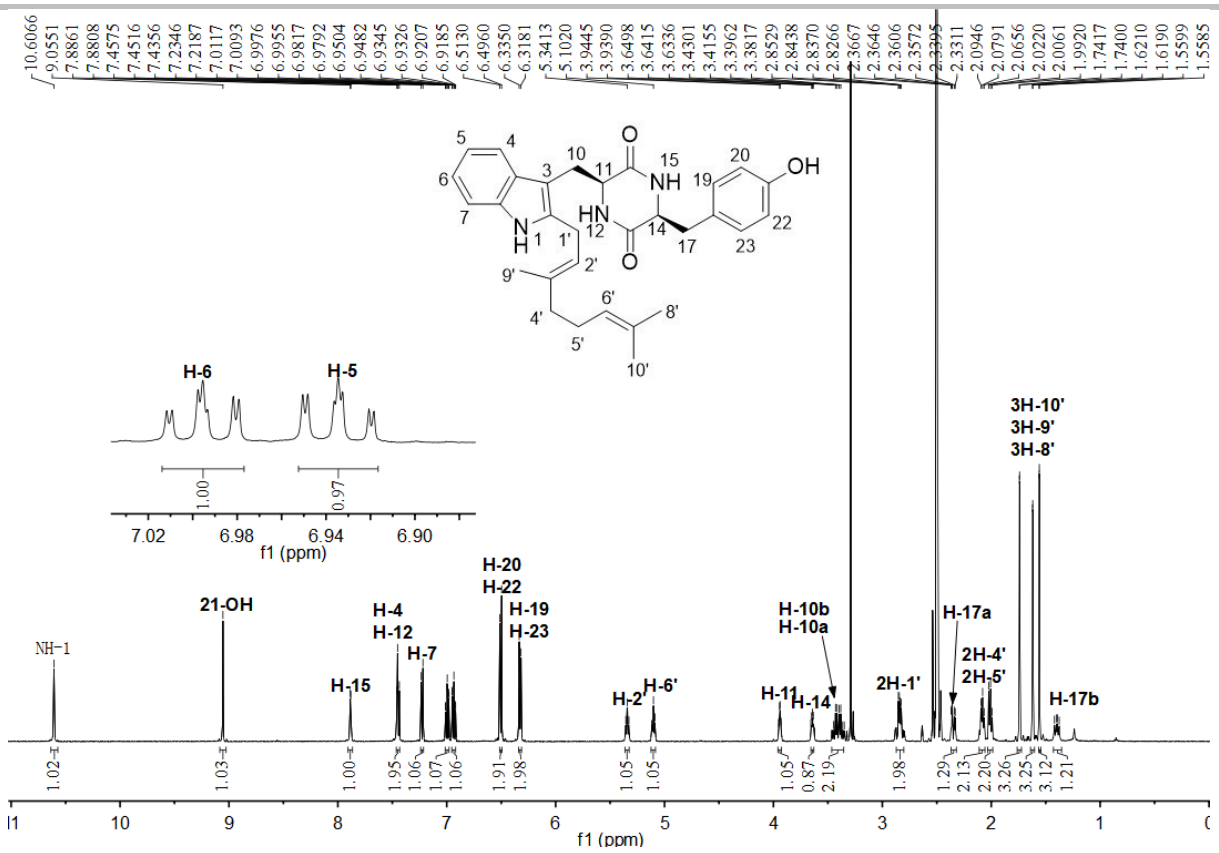

Figure S24 ^{1}H NMR spectrum of **11a2** in DMSO-d_6 (500MHz).

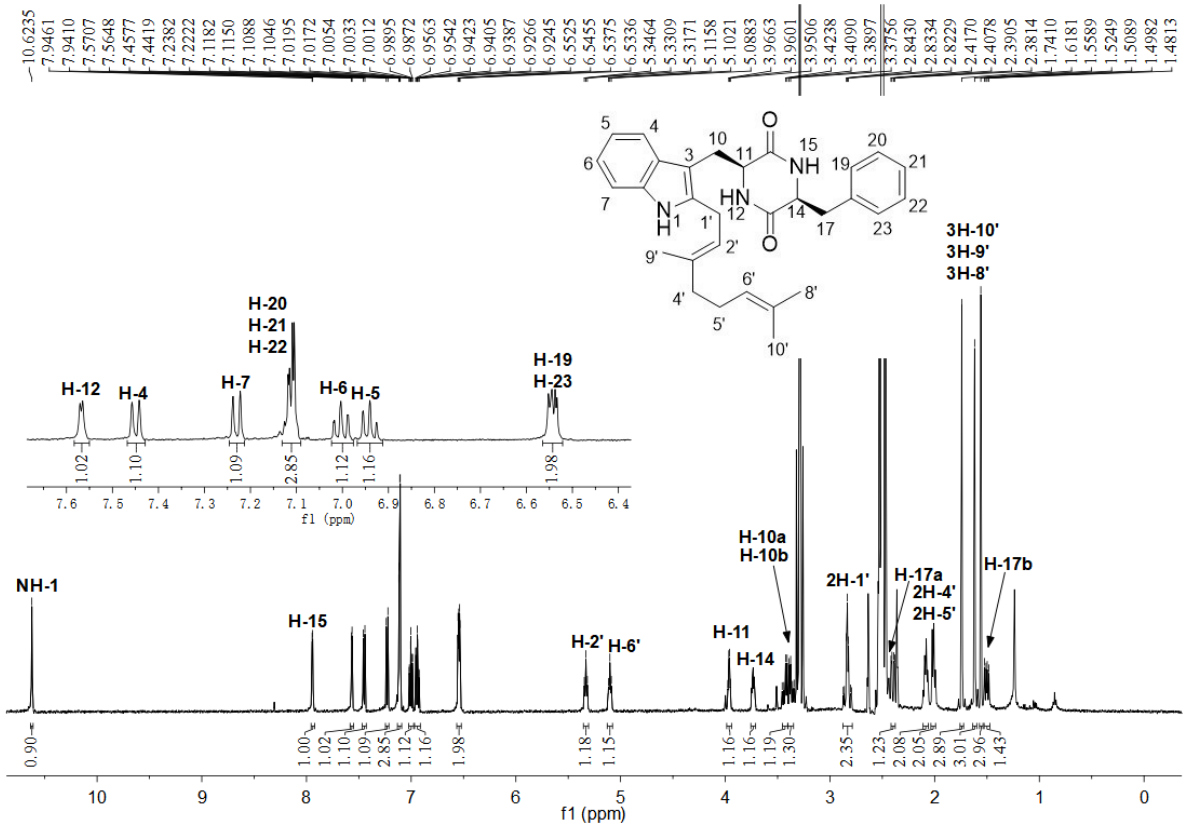

Figure S25 ^{1}H NMR spectrum of **12a2** in DMSO-d_6 (500MHz).

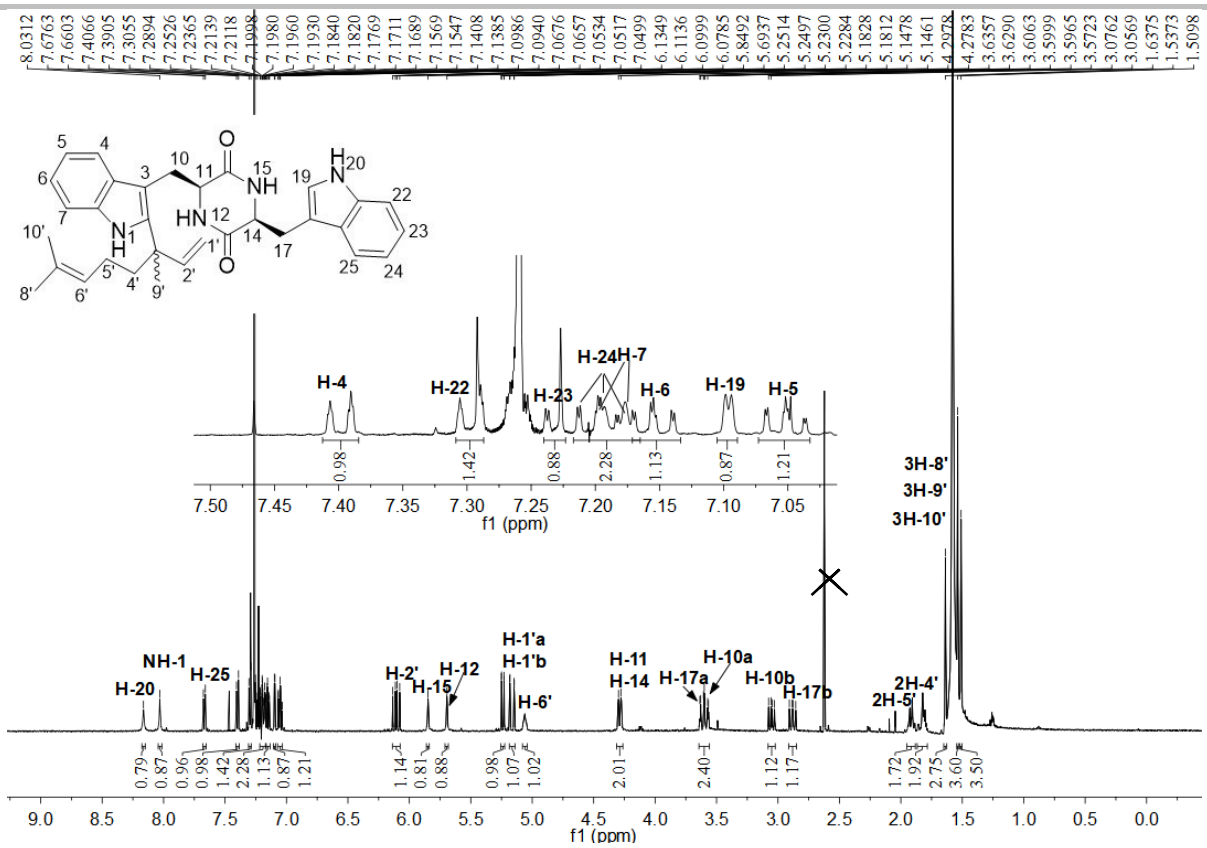

Figure S26 ^{1}H NMR spectrum of **1b2** in $CDCl_3$ (500MHz).

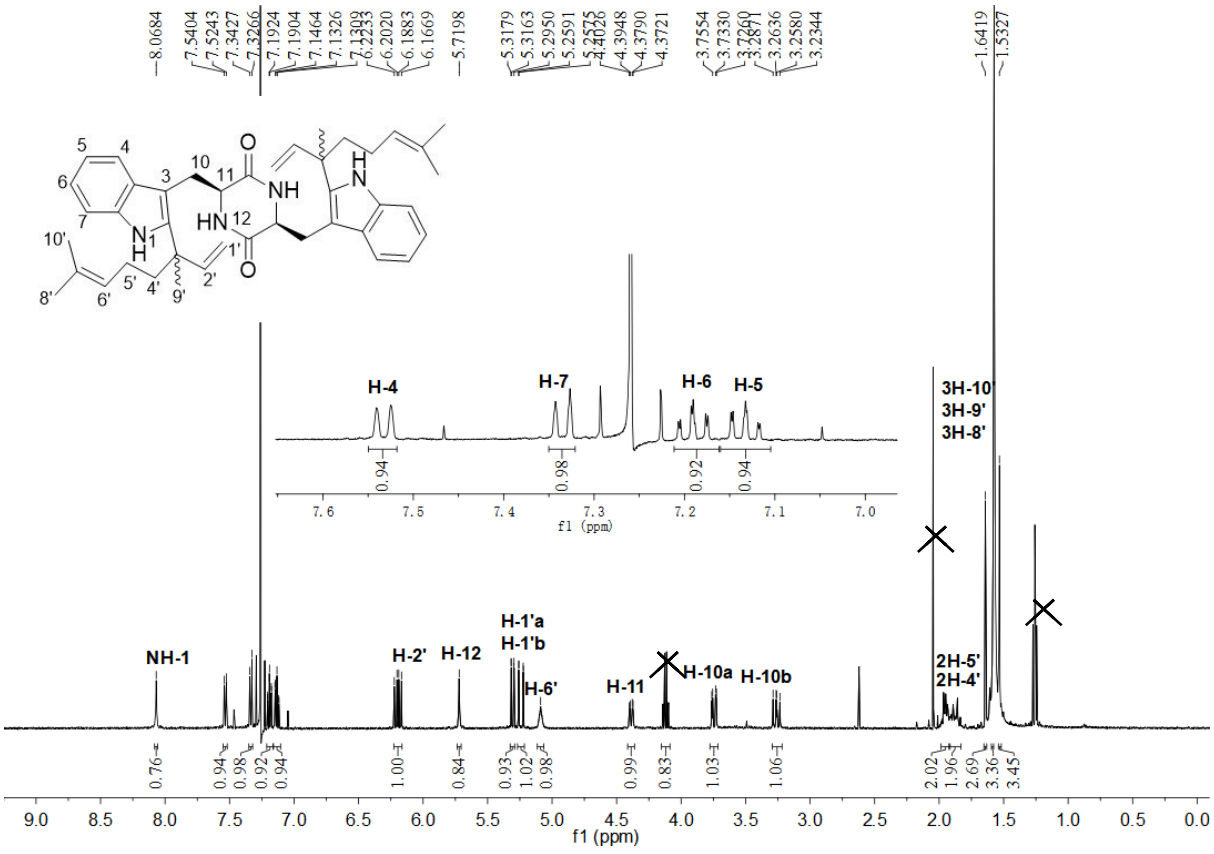

Figure S27 ^{1}H NMR spectrum of **1b2-2** in $CDCl_3$ (500MHz).

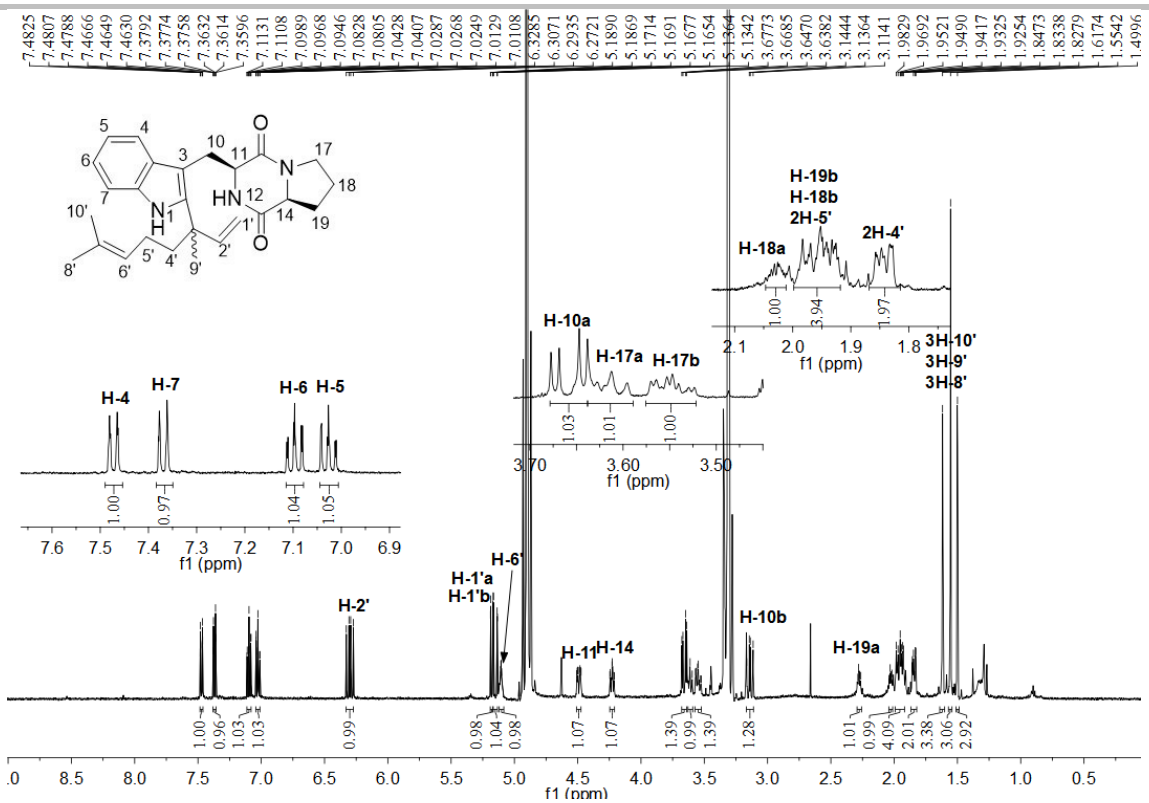

Figure S28 ^{1}H NMR spectrum of **2b2** in CD_3OD (500MHz).

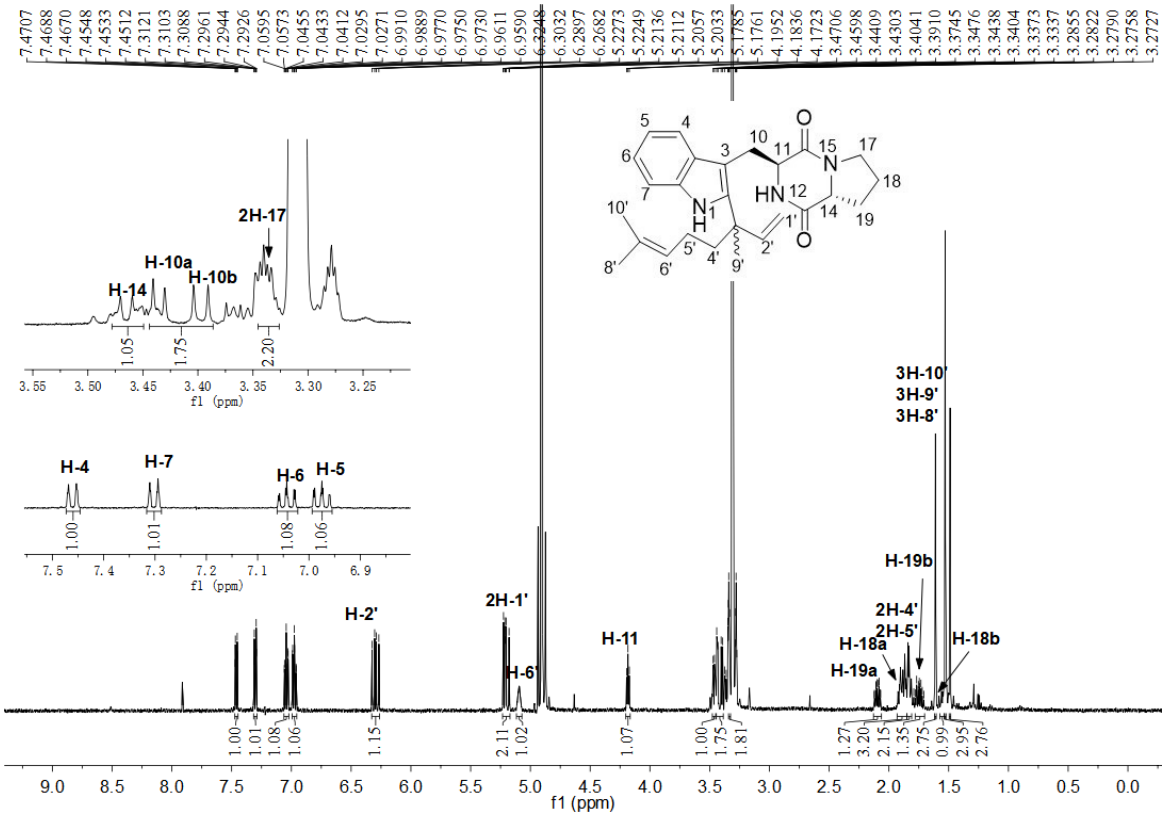

Figure S29 ^{1}H NMR spectrum of **3b2** in CD_3OD (500MHz).

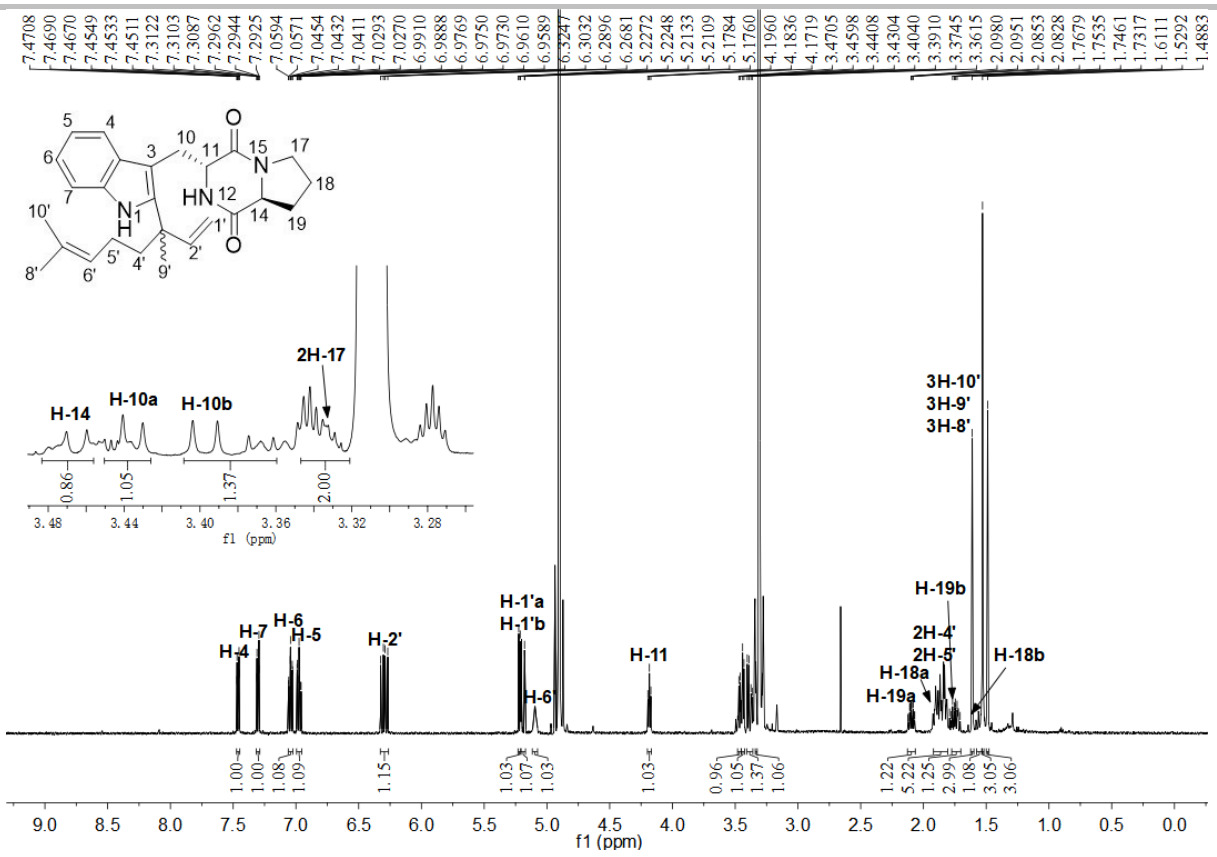

Figure S30 ^{1}H NMR spectrum of **4b2** in CD_3OD (500MHz).

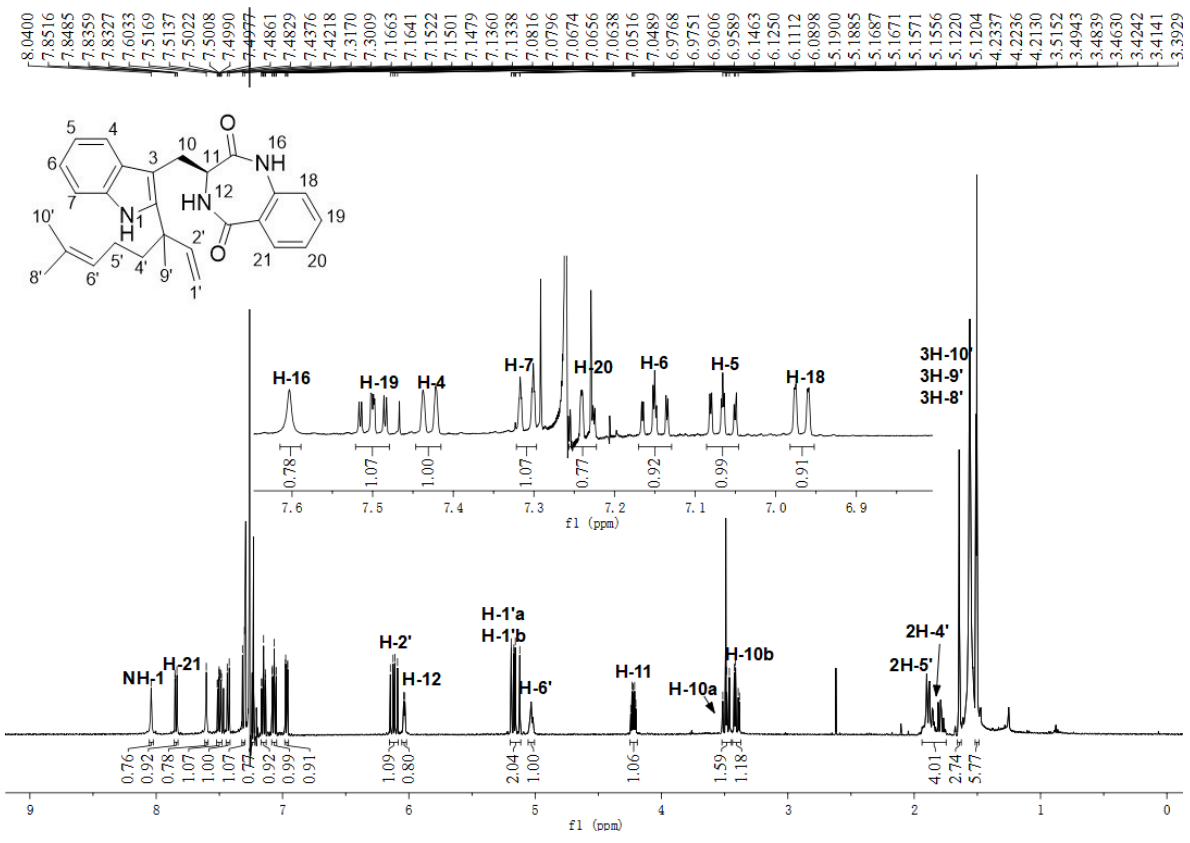

Figure S31 ^{1}H NMR spectrum of **14b2** in $CDCl_3$ (500MHz).

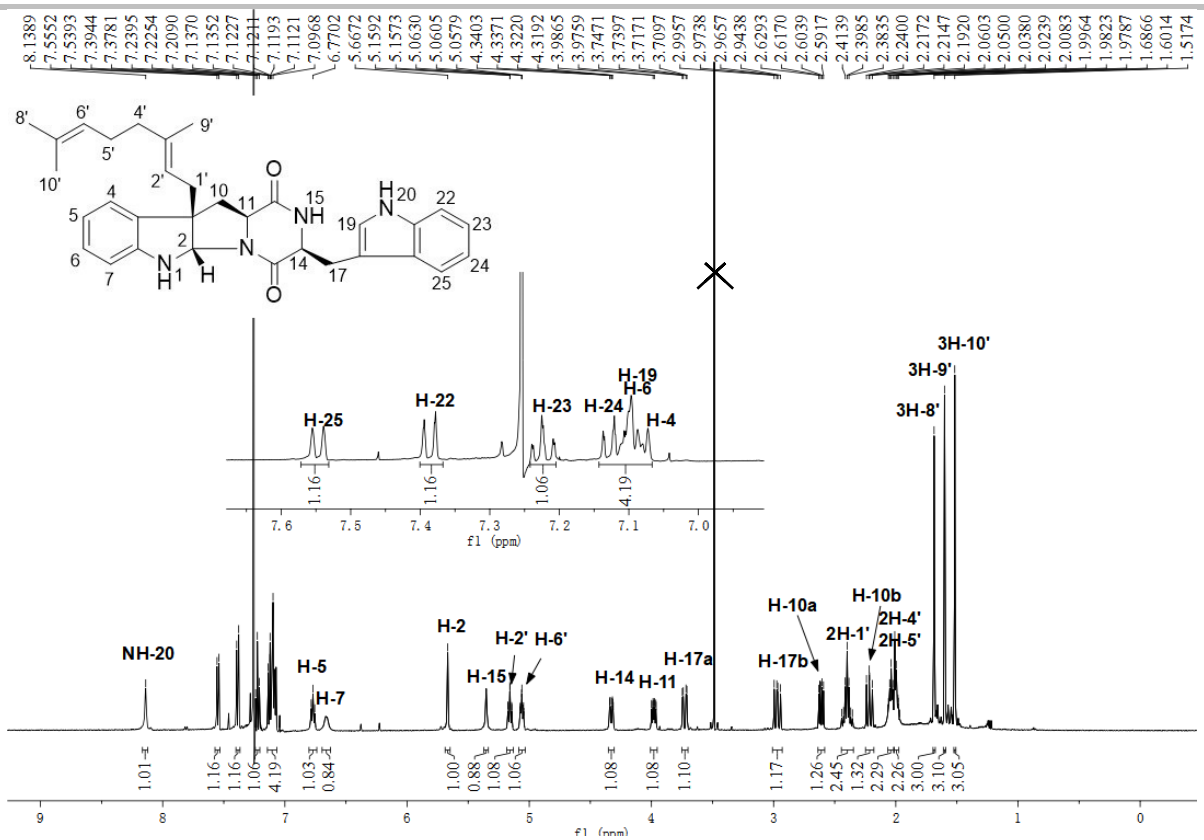

Figure S32 ^{1}H NMR spectrum of **1a3** in $CDCl_3$ (500MHz).

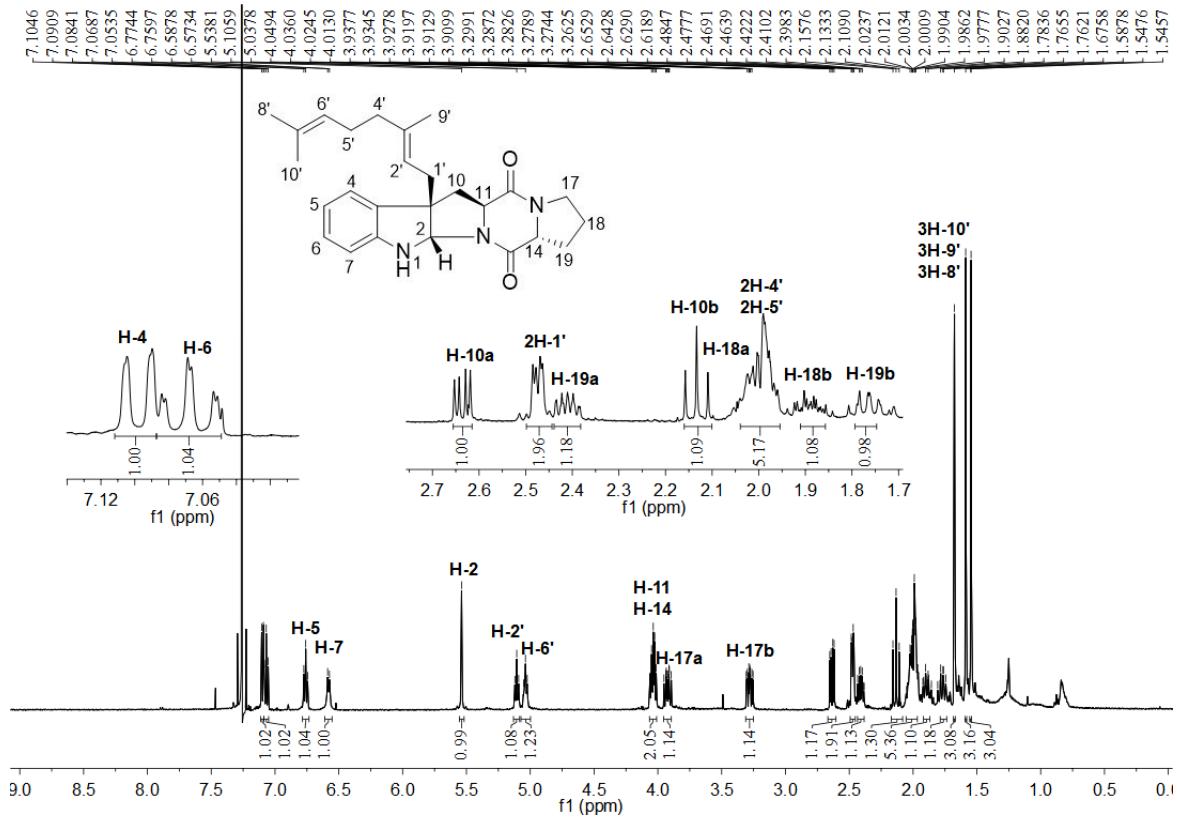

Figure S33 ^{1}H NMR spectrum of **3a3** in $CDCl_3$ (500MHz).

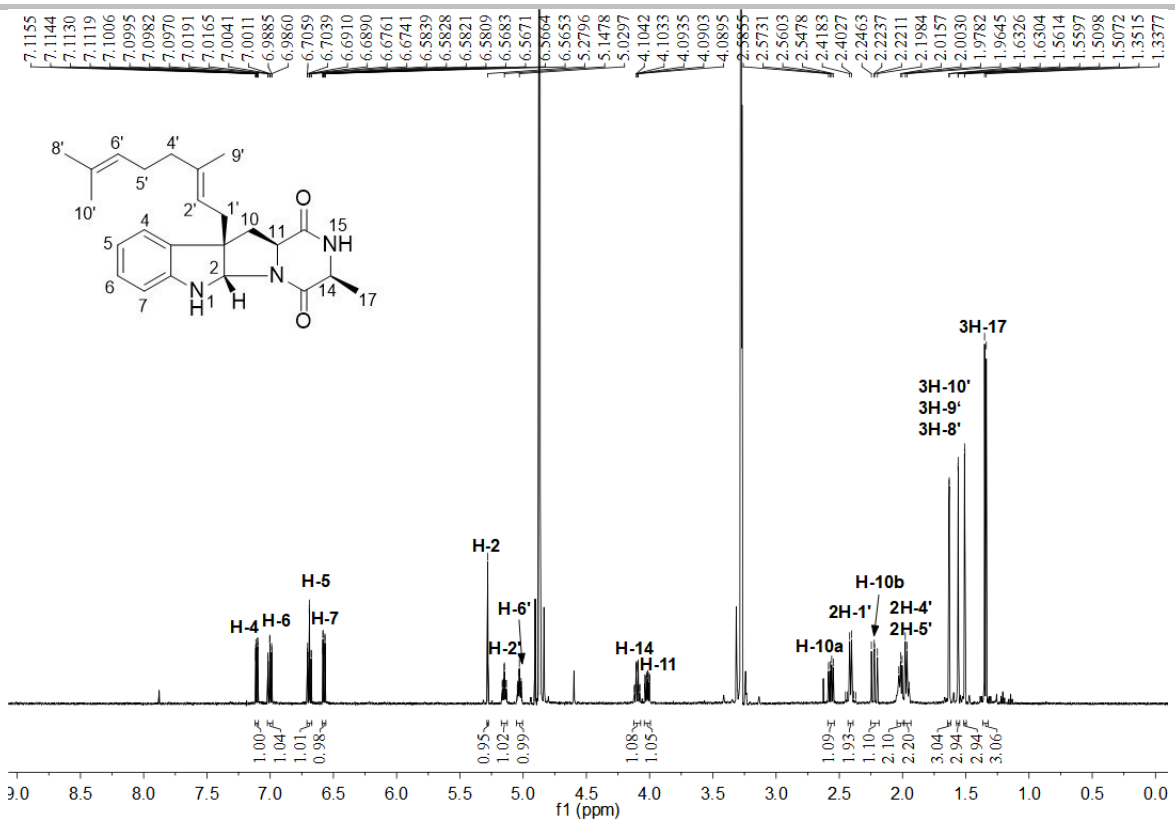

Figure S34 ^{1}H NMR spectrum of **6a3** in CD_3OD (500MHz).

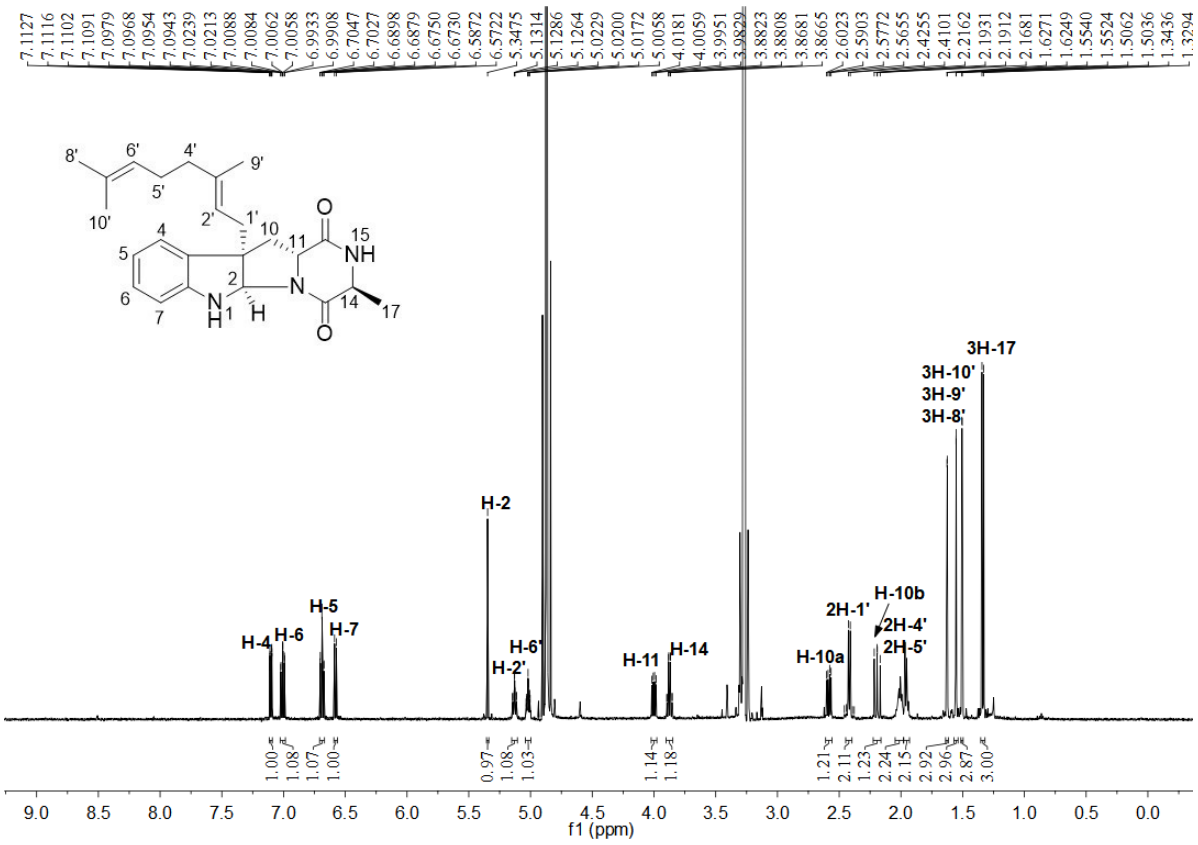

Figure S35 ^{1}H NMR spectrum of **8a3** in CD_3OD (500MHz).

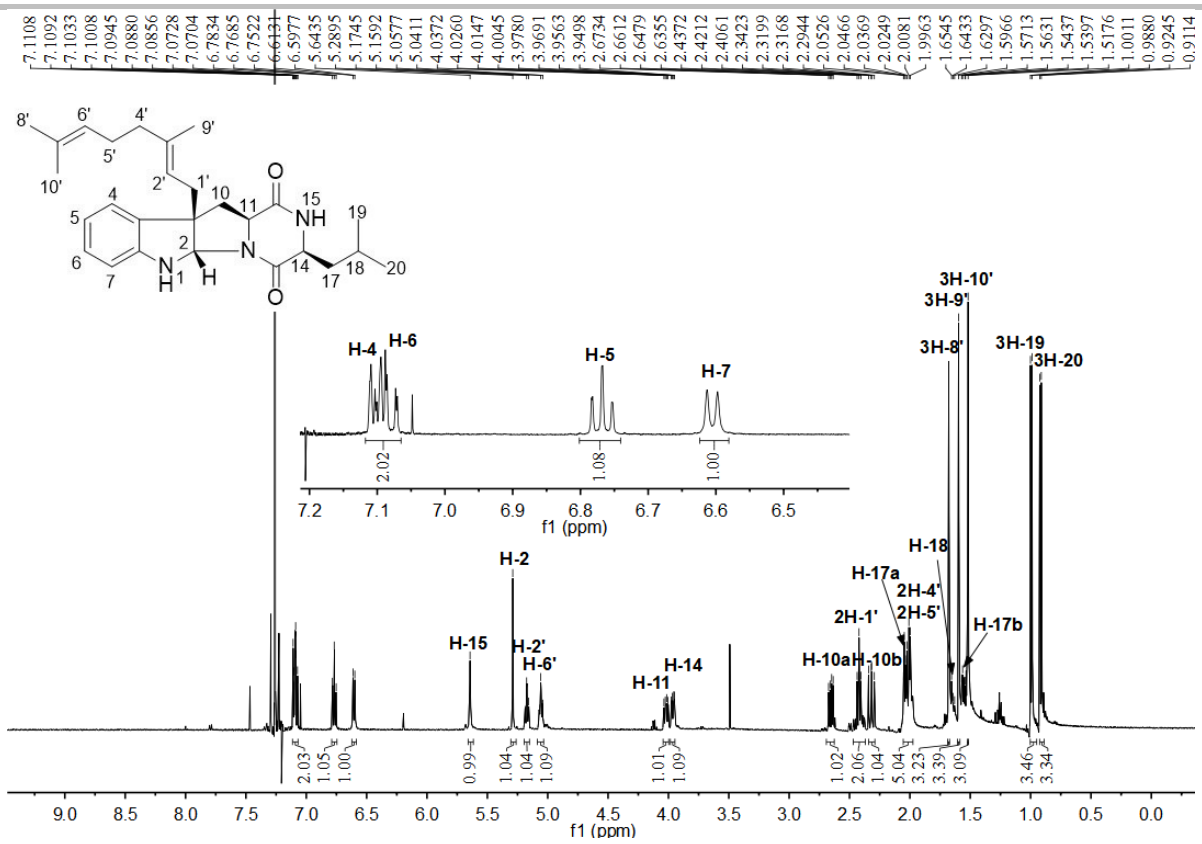

Figure S36 ^{1}H NMR spectrum of **10a3** in $CDCl_3$ (500MHz).

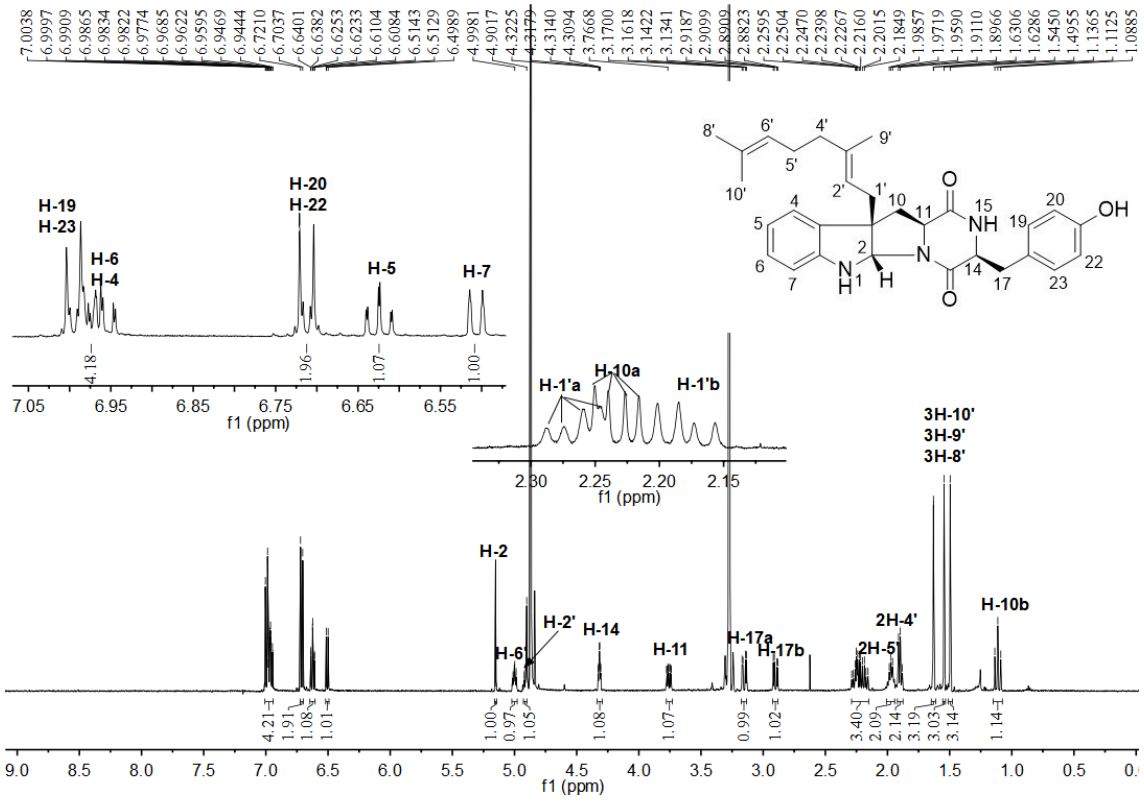

Figure S37 ^{1}H NMR spectrum of **11a3** in CD_3OD (500MHz).

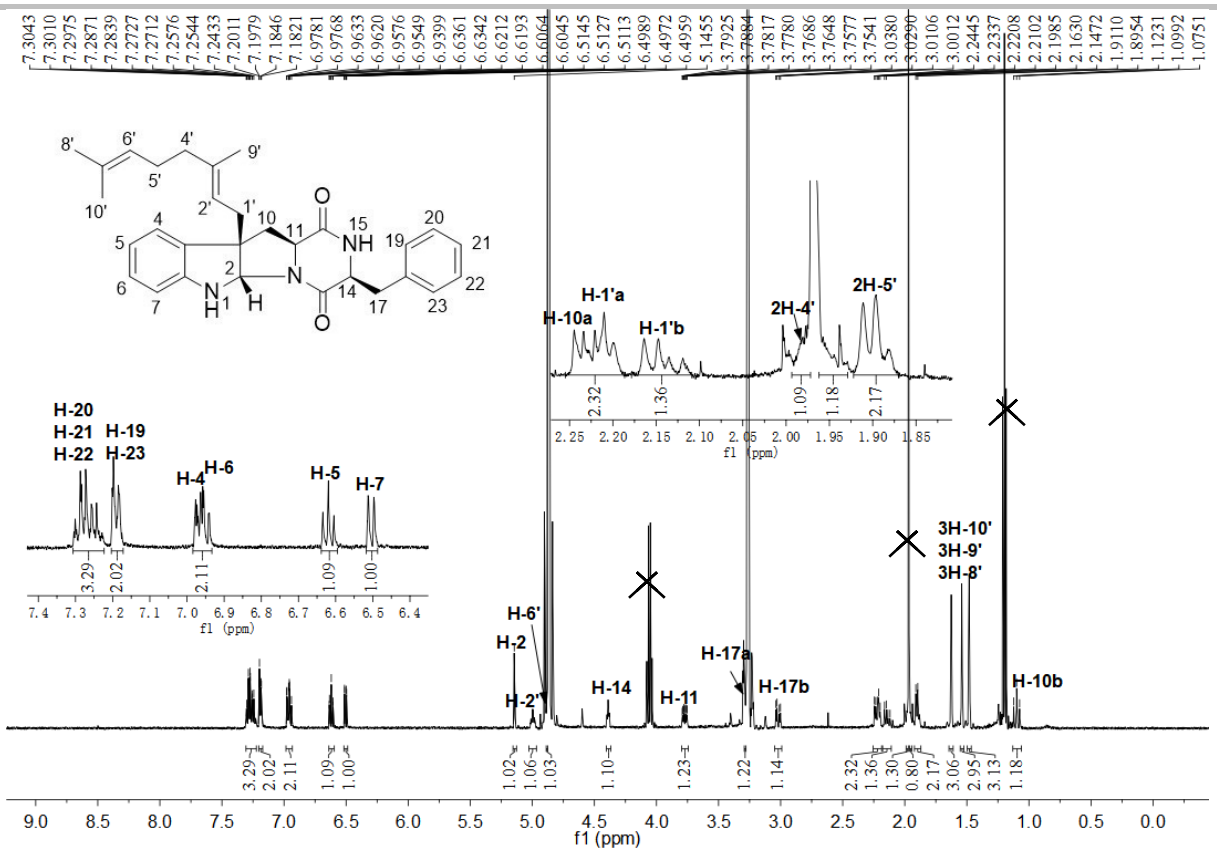

Figure S38 ^{1}H NMR spectrum of **12a3** in CD_3OD (500MHz).

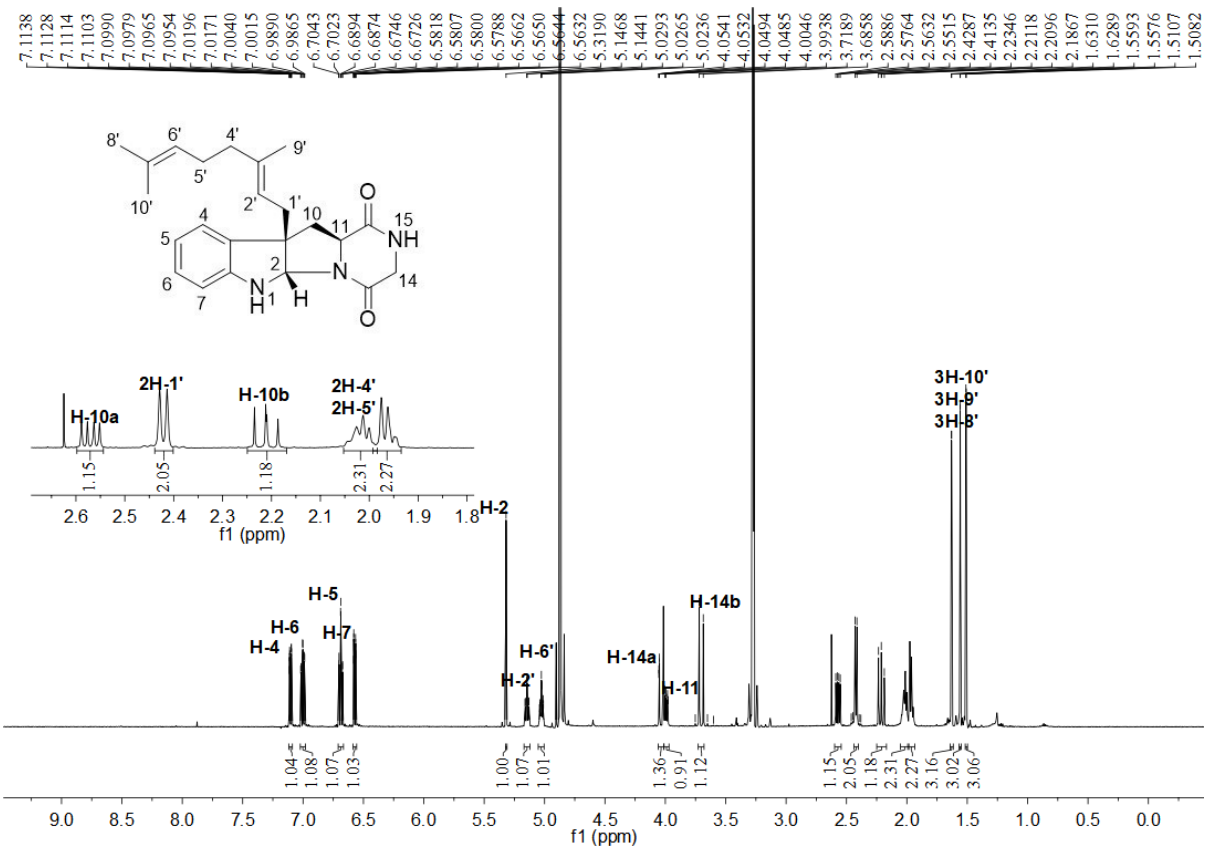

Figure S39 ^{1}H NMR spectrum of **13a3** in CD_3OD (500MHz).

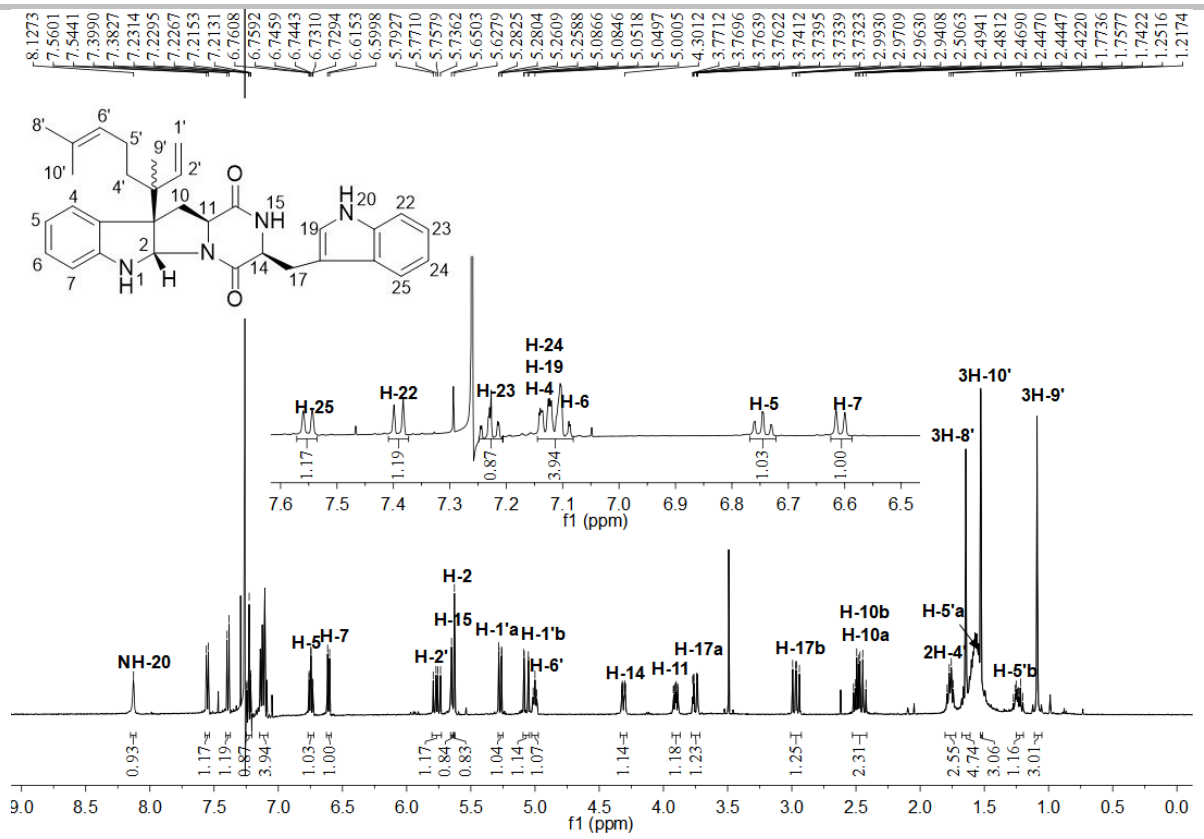

Figure S40 ^{1}H NMR spectrum of **1b3** in $CDCl_3$ (500MHz).

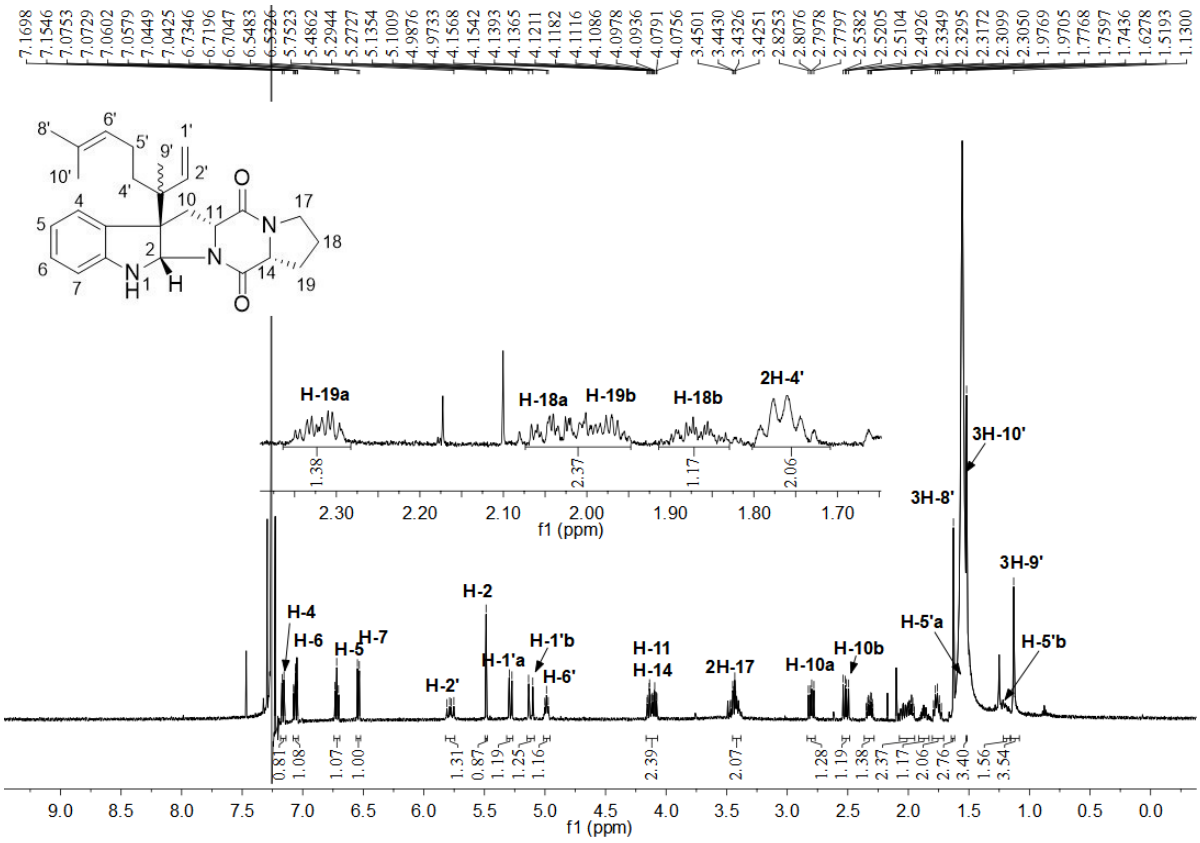

Figure S41 ^{1}H NMR spectrum of **5b3** in $CDCl_3$ (500MHz).

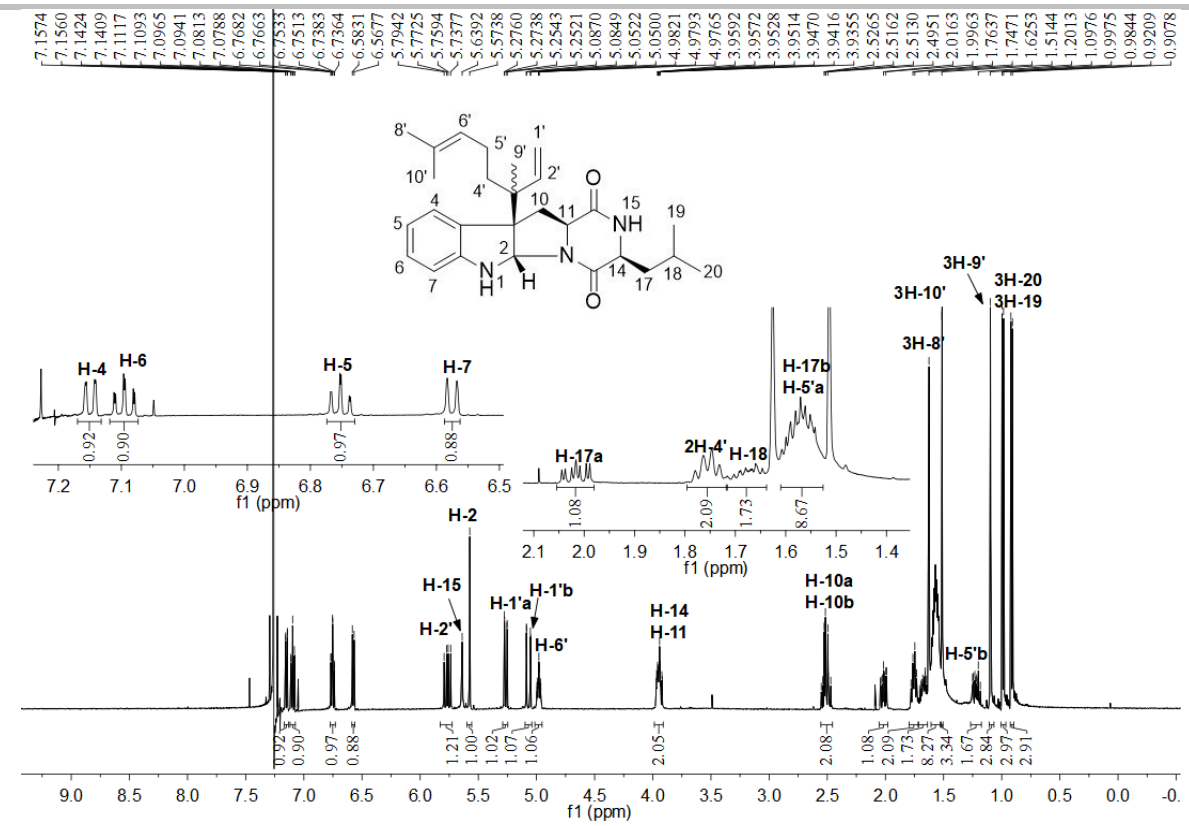

Figure S42 ^{1}H NMR spectrum of **10b3** in $CDCl_3$ (500MHz).

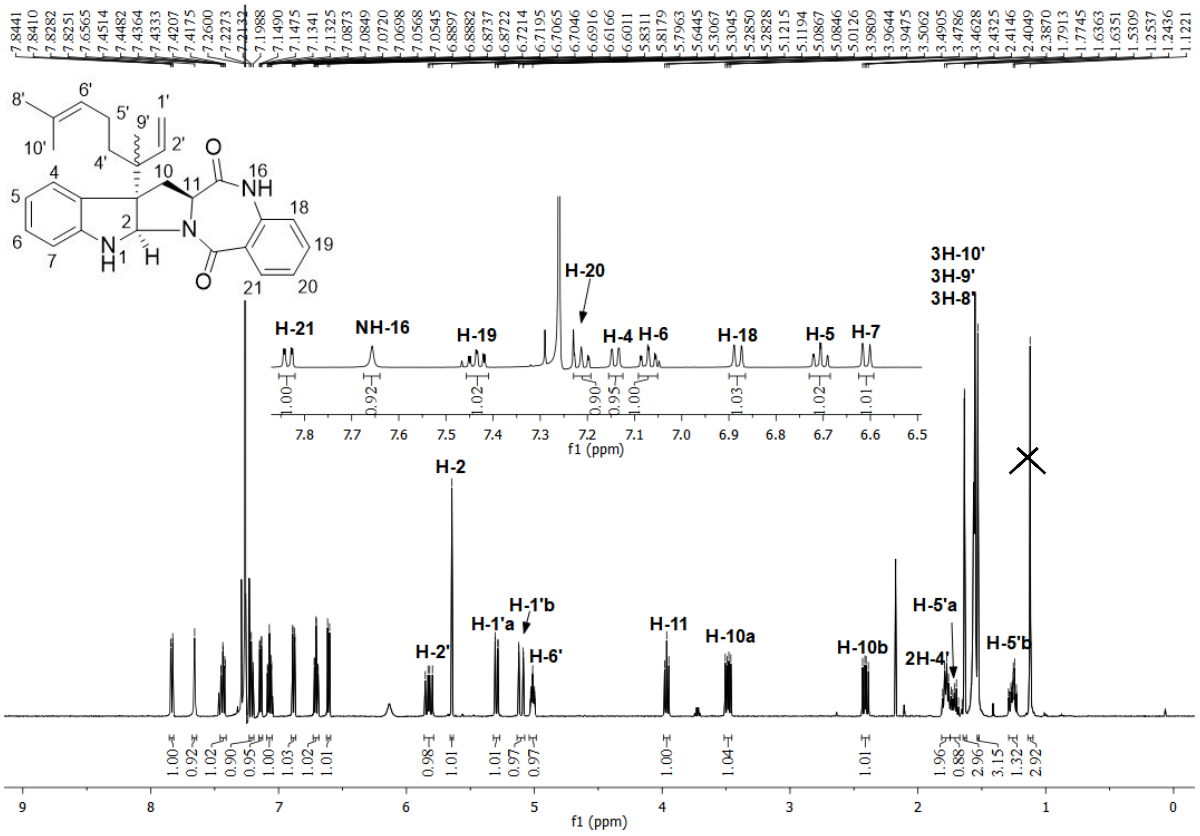

Figure S43 ^{1}H NMR spectrum of **14b3** in $CDCl_3$ (500MHz).

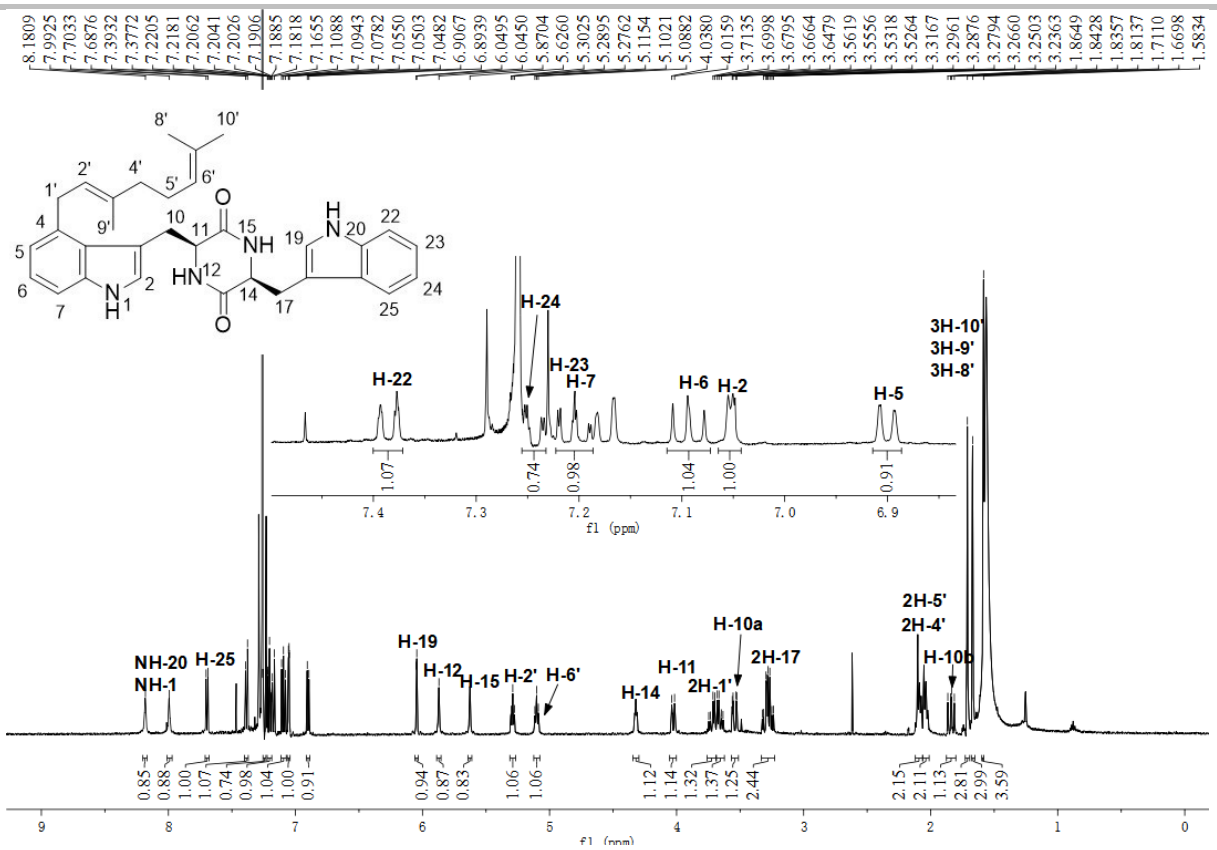

Figure S44 ^{1}H NMR spectrum of **1a4** in $CDCl_3$ (500MHz).

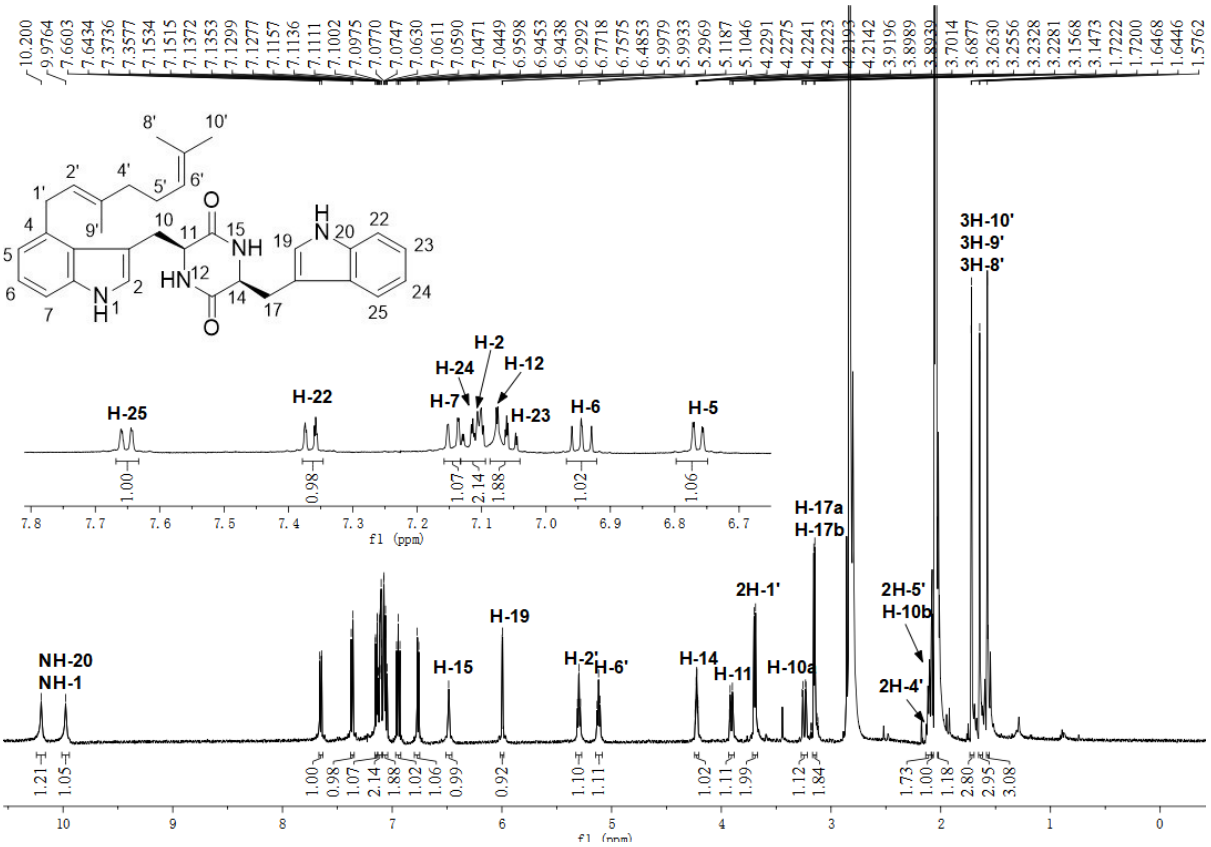

Figure S45 ^{1}H NMR spectrum of **1a4** in CD_3COCD_3 (500MHz).

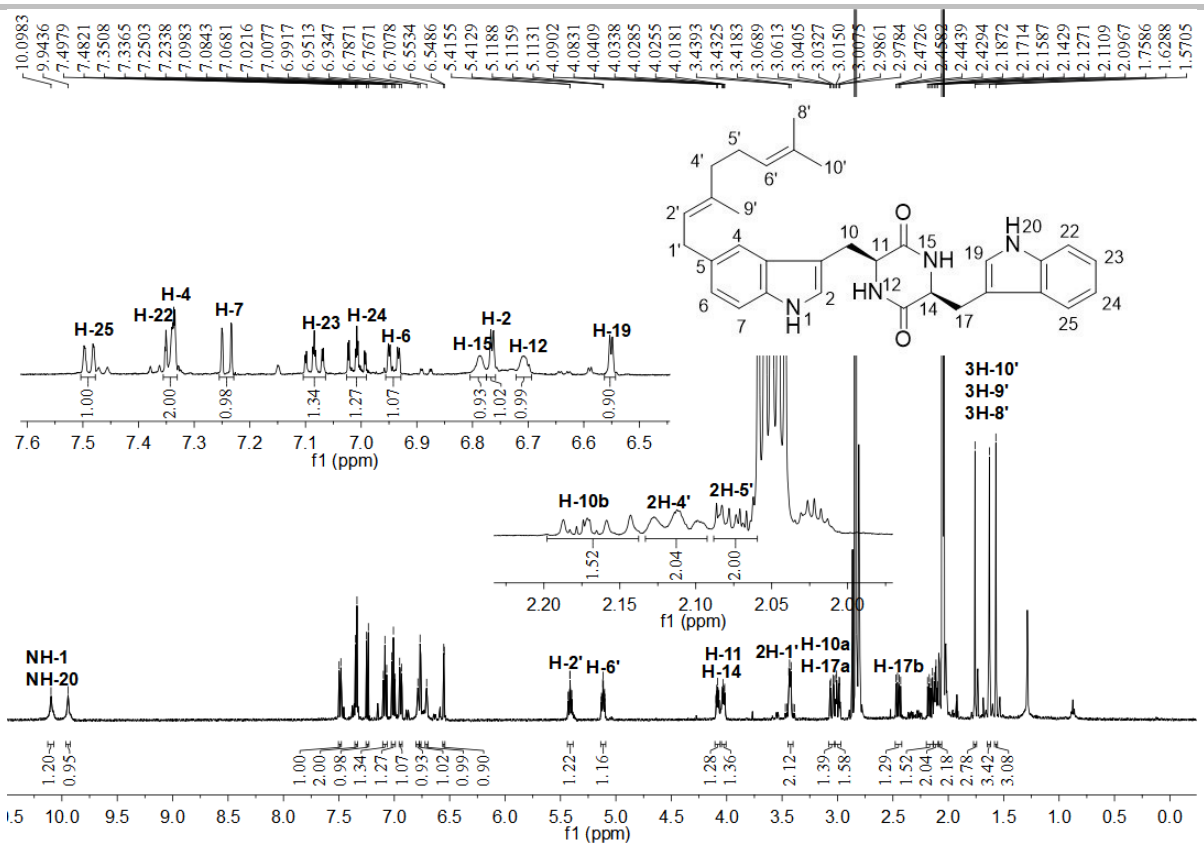

Figure S46 ^{1}H NMR spectrum of **1a5** in CD_3COCD_3 (500MHz).

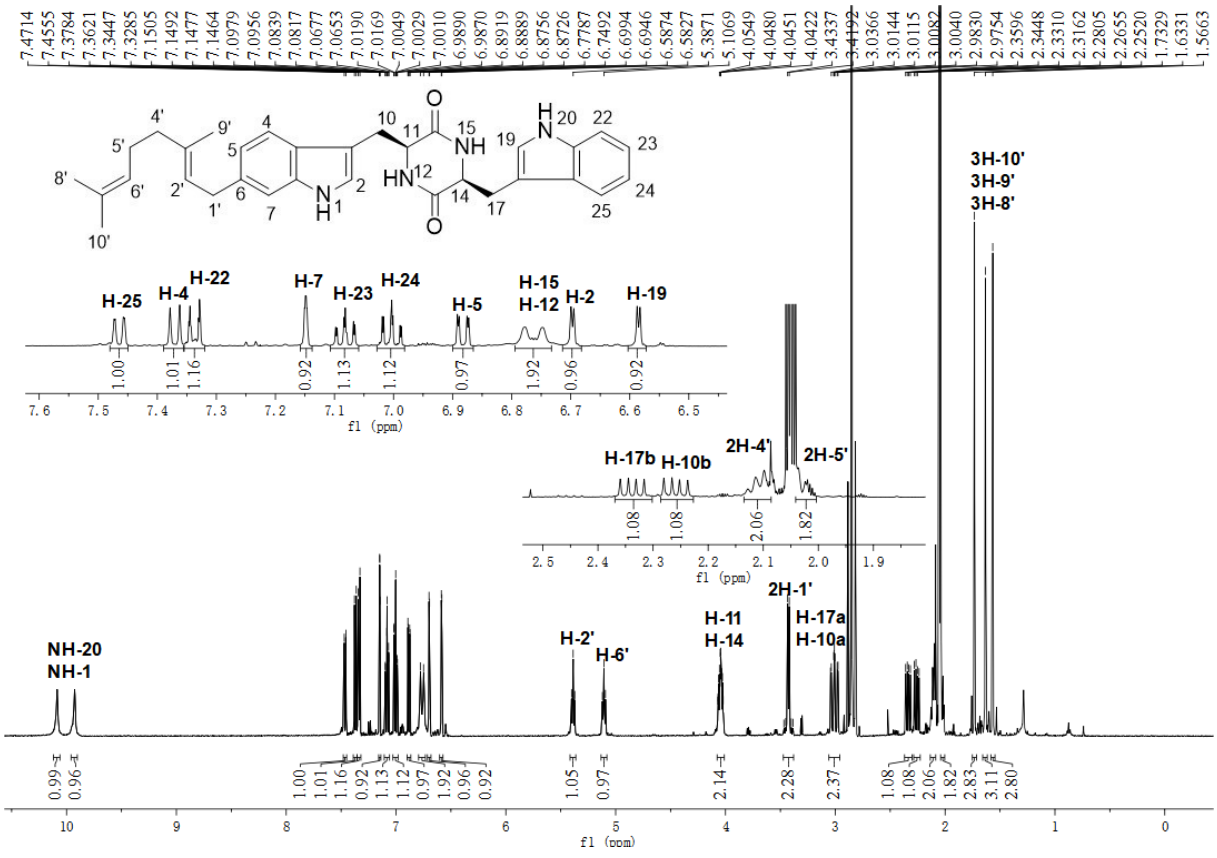

Figure S47 ^{1}H NMR spectrum of **1a6** in CD_3COCD_3 (500MHz).

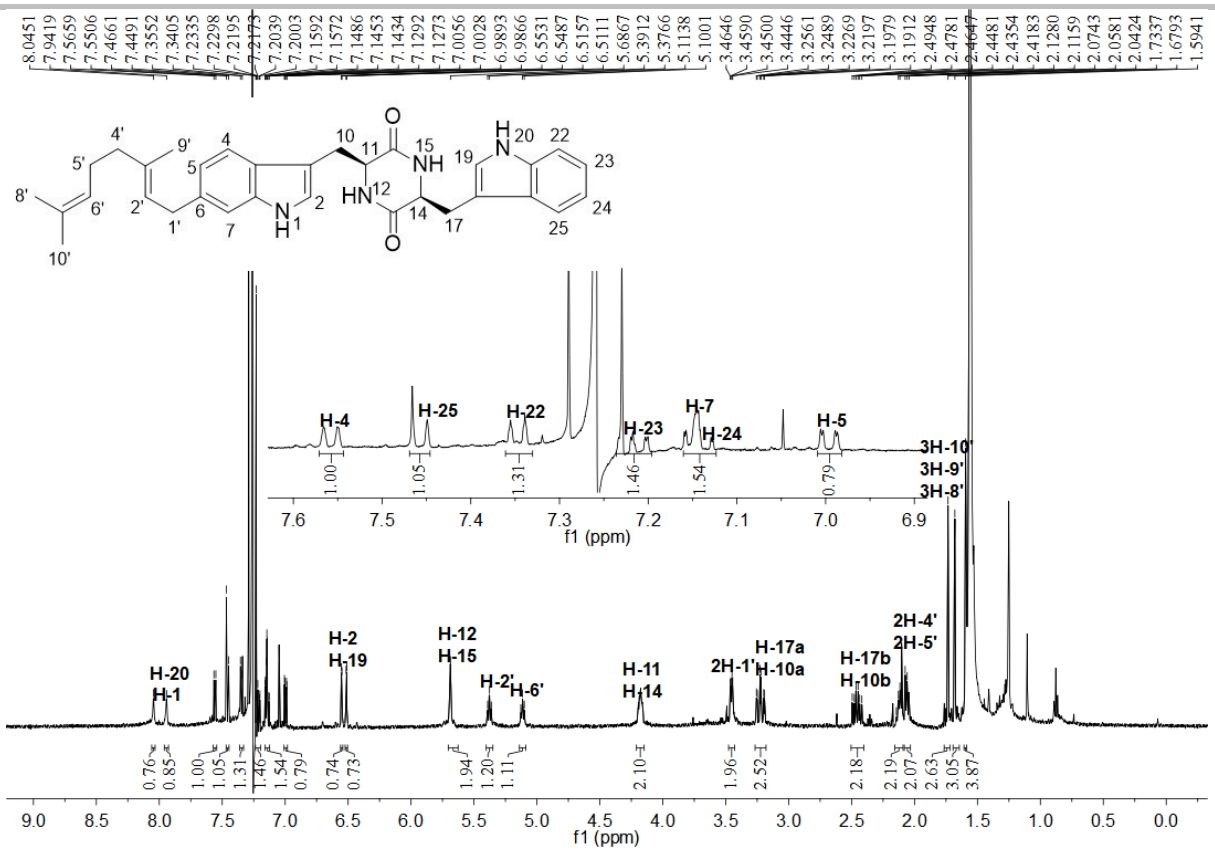

Figure S48 ^{1}H NMR spectrum of **1a6** in $CDCl_3$ (500MHz).

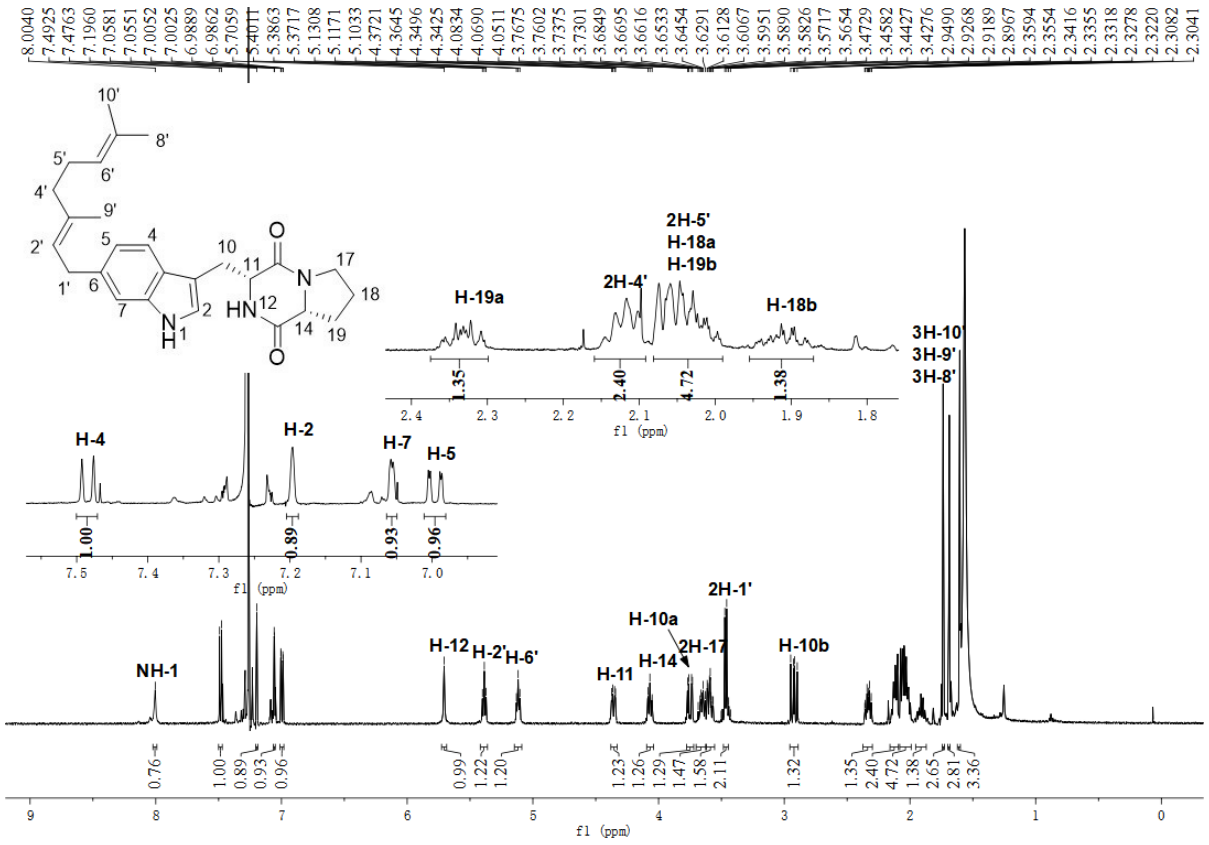

Figure S49 ^{1}H NMR spectrum of **5a6** in $CDCl_3$ (500MHz).

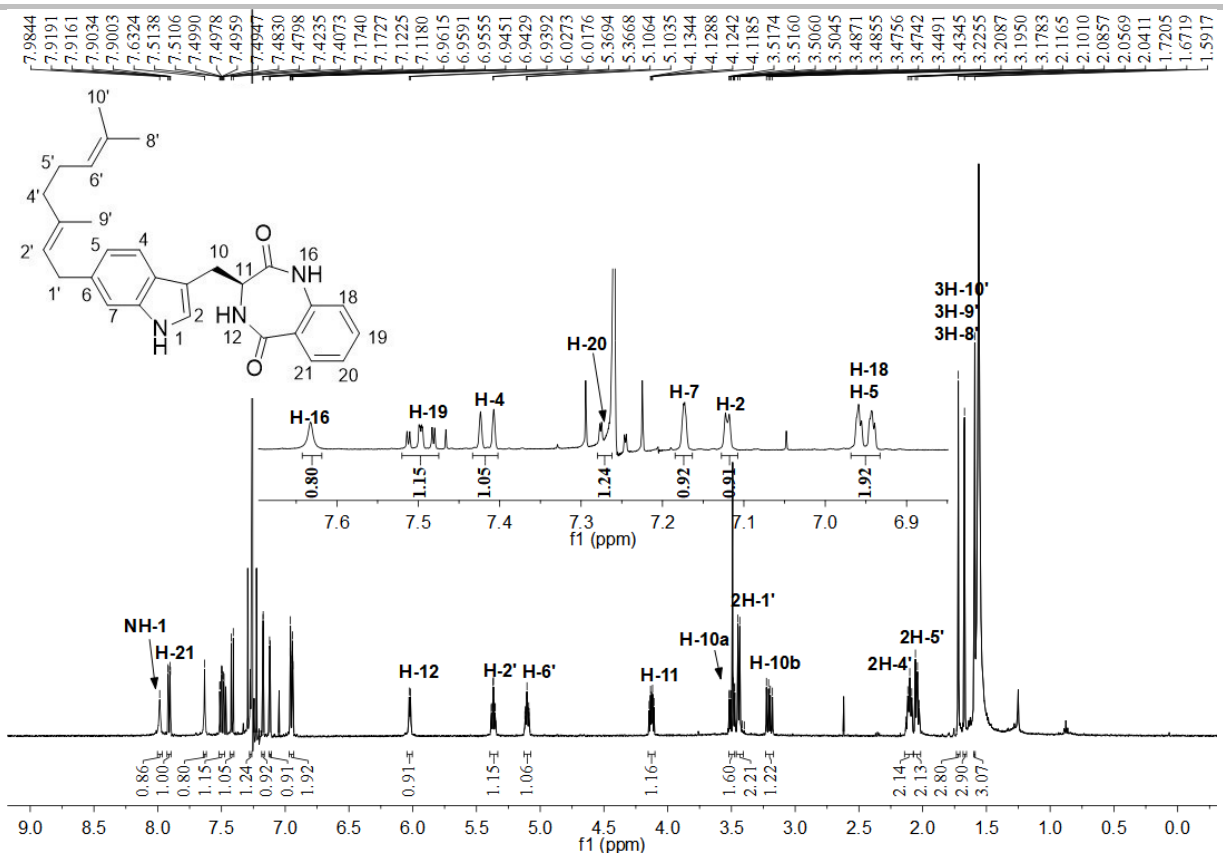

Figure S50 ^{1}H NMR spectrum of **14a6** in $CDCl_3$ (500MHz).

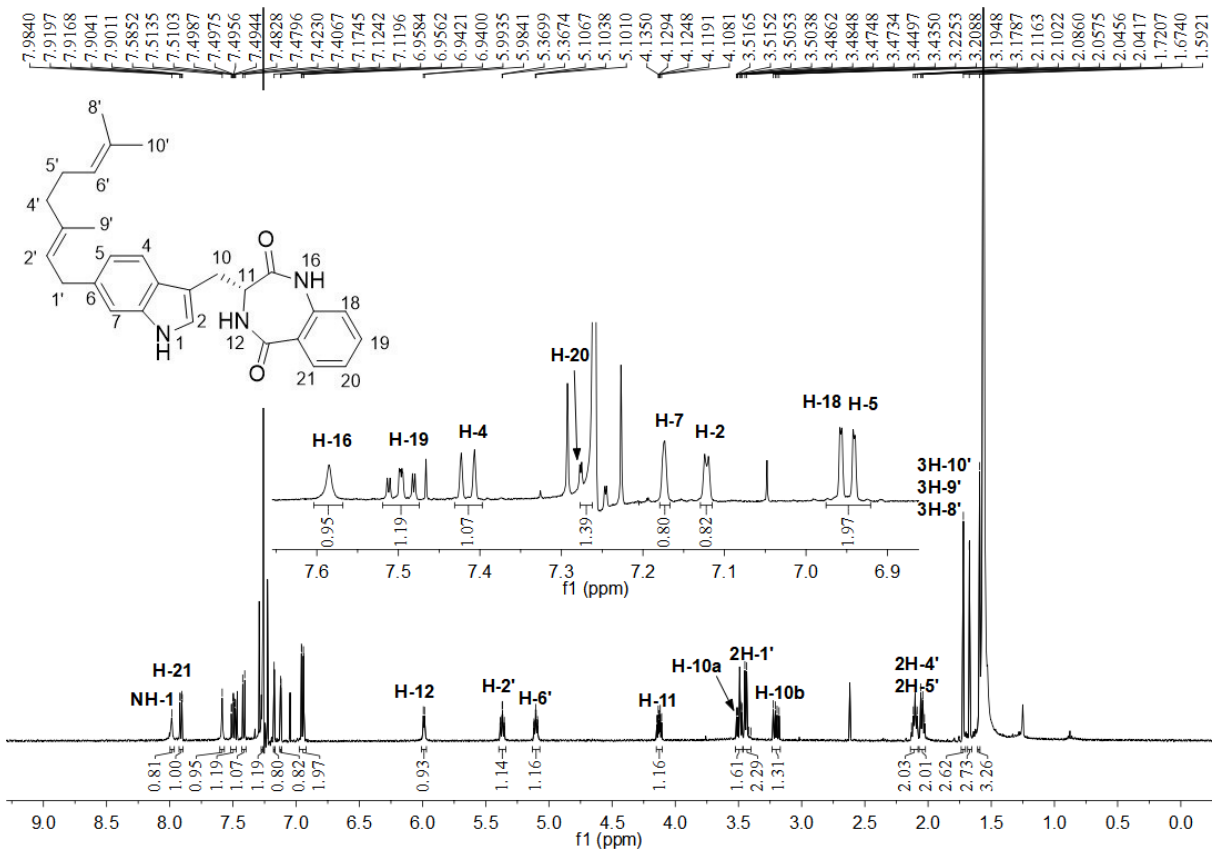

Figure S51 ^{1}H NMR spectrum of **15a6** in $CDCl_3$ (500MHz).

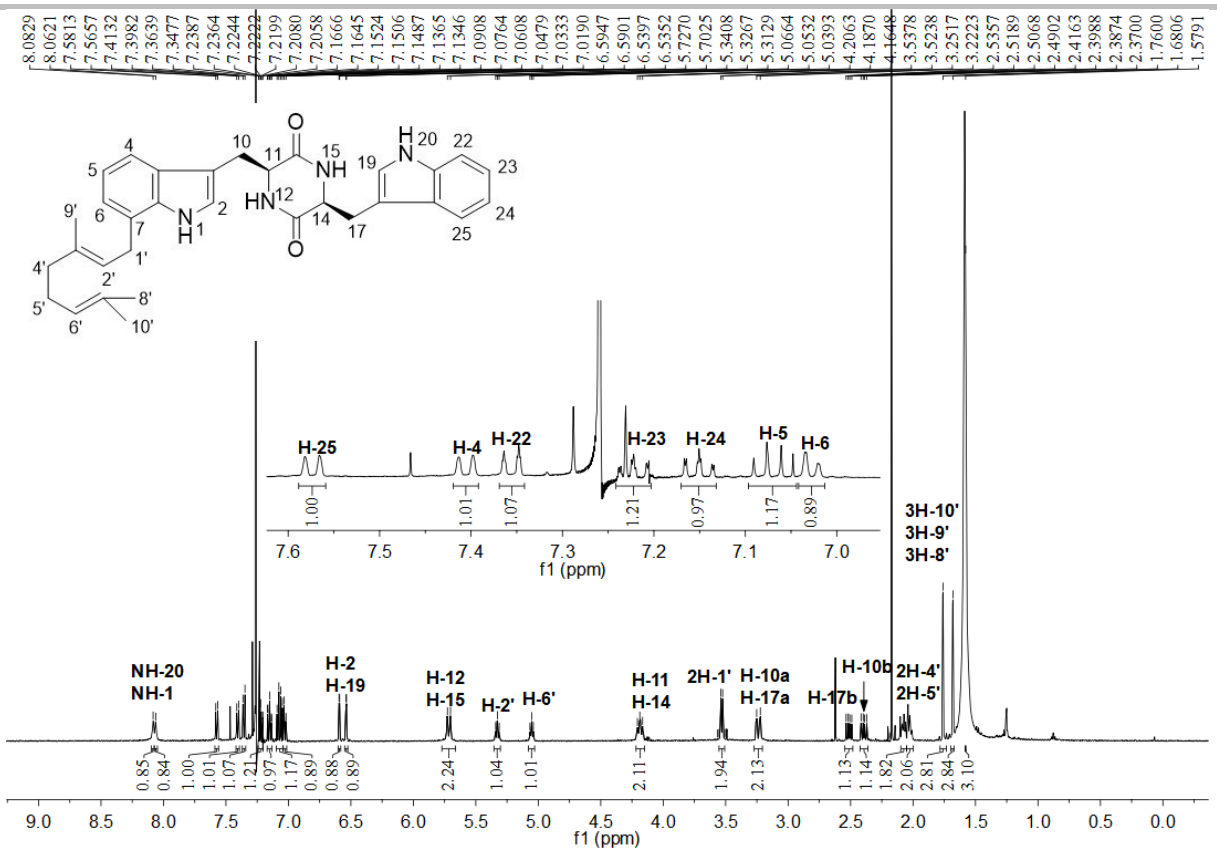

Figure S52 ^{1}H NMR spectrum of **1a7** in $CDCl_3$ (500MHz).

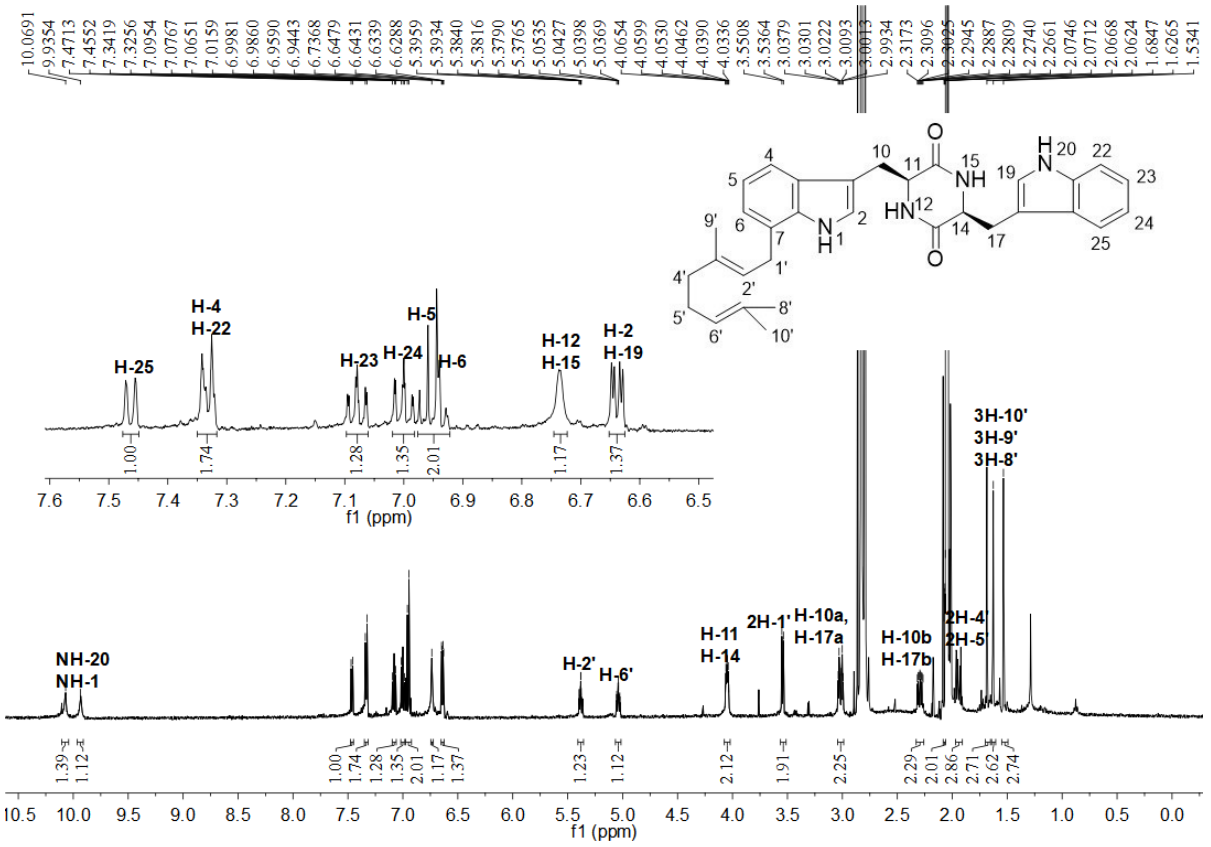

Figure S53 ^{1}H NMR spectrum of **1a7** in CD_3COCD_3 (500MHz).

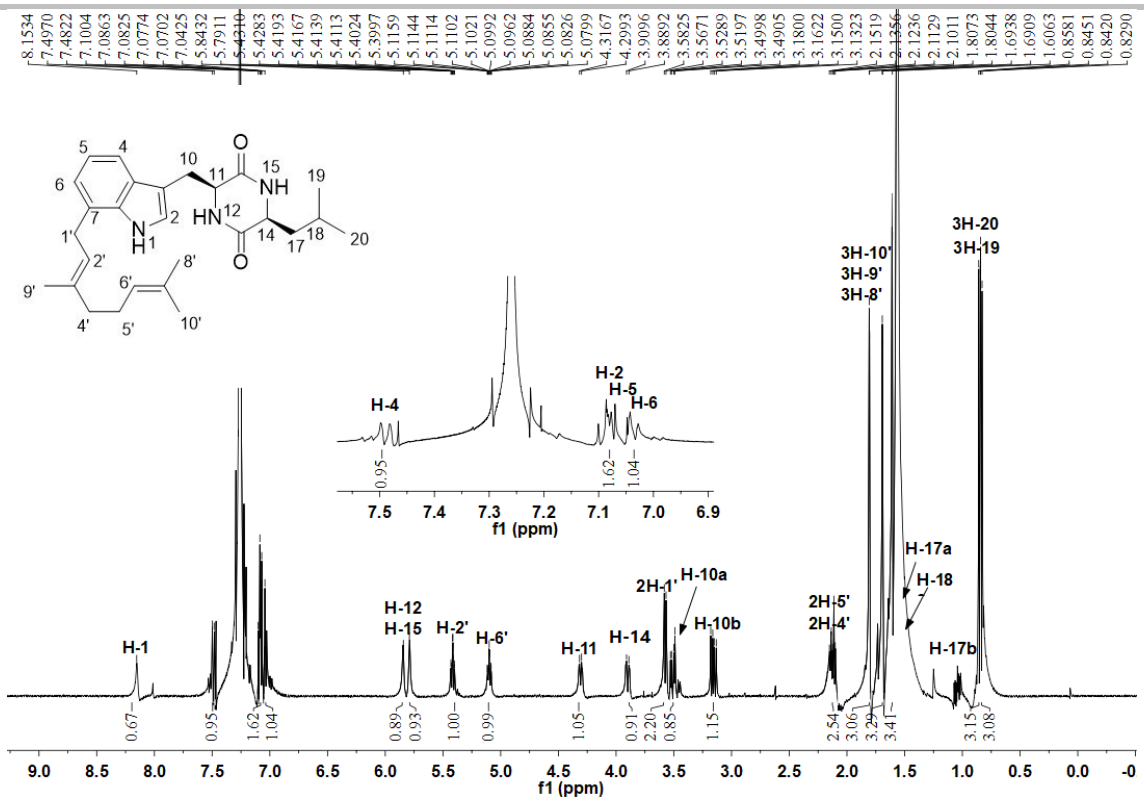

Figure S54 ^{1}H NMR spectrum of **10a7** in $CDCl_3$ (500MHz).

References

(1) Woodside, A. B.; Huang, Z.;Poulter, C. D. *Org.Synth.* **1988,** *66,* 211.

(2) Caballero, E.; Avendaño, C.;Menéndez, J. C. *Tetrahedron: Asymmetry* **1998,** *9,* 967.

(3) Cacciatore, I.; Cocco, A.; Costa, M.; Fontana, M.; Lucente, G.; Pecci, L.;Pinnen, F. *Amino Acids* **2005,** *28,* 77.

(4) Barrow, C. J. and Sun, H. H. *J Nat.Prod.* **1994,** *57,* 471.

(5) Liu, H. and Naismith, J. H. *BMC.Biotechnol.* **2008,** *8,* 91.

(6) Zheng, L.; Baumann, U.;Reymond, J. L. *Nucleic Acids Res.* **2004,** *32,* e115.

(7) Yin, W.-B.; Yu, X.; Xie, X.-L.;Li, S.-M. *Org.Biomol.Chem.* **2010,** *8,* 2430.

(8) Grundmann, A. and Li, S.-M. *Microbiology* **2005,** *151,* 2199.

(9) Yin, S.; Yu, X.; Wang, Q.; Liu, X. Q.;Li, S.-M. *Appl.Microbiol.Biotechnol.* **2013,** *97,* 1649.

(10) Yin, W.-B.; Ruan, H.-L.; Westrich, L.; Grundmann, A.;Li, S.-M. *Chembiochem* **2007,** *8,* 1154.

(11) Mundt, K. and Li, S.-M. *Microbiology* **2013,** *159,* 2169.

(12) Schymkowitz, J. W.; Rousseau, F.; Martins, I. C.; Ferkinghoff-Borg, J.; Stricher, F.;Serrano, L. *Proc.Natl.Acad.Sci.U.S.A* **2005,** *102,* 10147.

(13) Schymkowitz, J.; Borg, J.; Stricher, F.; Nys, R.; Rousseau, F.;Serrano, L. *Nucleic Acids Res.* **2005,** *33,* W382.

(14) Emsley, P.; Lohkamp, B.; Scott, W. G.;Cowtan, K. *Acta Crystallogr.D.Biol.Crystallogr.* **2010,** *66,* 486.

(15) Yu, X.; Zocher, G.; Xie, X.; Liebhold, M.; Schütz, S.; Stehle, T.;Li, S.-M. *Chem.Biol.* **2013,** *20,* 1492.

(16) Schultz, A. W.; Oh, D. C.; Carney, J. R.; Williamson, R. T.; Udwary, D. W.; Jensen, P. R.; Gould, S. J.; Fenical, W.;Moore, B. S. *J Am.Chem Soc.* **2008,** *130,* 4507.

(17) Wollinsky, B.; Ludwig, L.; Xie, X.;Li, S.-M. *Org.Biomol.Chem.* **2012,** *10,* 9262.

(18) Yin, W.-B.; Cheng, J.;Li, S.-M. *Org.Biomol.Chem.* **2009,** *7,* 2202.

(19) Yin, W.-B.; Xie, X.-L.; Matuschek, M.;Li, S.-M. *Org.Biomol.Chem.* **2010,** *8,* 1133.

(20) Pockrandt, D. and Li, S.-M. *Chembiochem.* **2013,** *14,* 2023.

(21) Chen, R.; Gao, B.; Liu, X.; Ruan, F.; Zhang, Y.; Lou, J.; Feng, K.; Wunsch, C.; Li, S.-M.; Dai, J.;Sun, F. *Nat.Chem.Biol.* **2017,** *13,* 226.

(22) Steffan, N. and Li, S.-M. *Arch.Microbiol.* **2009,** *191,* 461.

(23) Yu, X.; Liu, Y.; Xie, X.; Zheng, X.-D.;Li, S.-M. *J.Biol.Chem.* **2012,** *287,* 1371.

(24) Liebhold, M.; Xie, X.;Li, S.-M. *Org.Lett.* **2012,** *14,* 4884.

(25) Mai, P.; Zocher, G.; Stehle, T.;Li, S.-M. *Org.Biomol.Chem.* **2018,** *16,* 7461.

4.2 Peniphenone and penilactone formation in *Penicillium crustosum* via 1,4-Michael additions of *ortho*-quinone methide from hydroxyclavatol to γ-butyrolactones from crustosic acid

JACS
JOURNAL OF THE AMERICAN CHEMICAL SOCIETY
Communication
Cite This: J. Am. Chem. Soc. 2019, 141, 4225−4229
pubs.acs.org/JACS

Peniphenone and Penilactone Formation in *Penicillium crustosum* via 1,4-Michael Additions of *ortho*-Quinone Methide from Hydroxyclavatol to γ-Butyrolactones from Crustosic Acid

Jie Fan,[†,§] Ge Liao,[†,§] Florian Kindinger,[†] Lena Ludwig-Radtke,[†] Wen-Bing Yin,[‡] and Shu-Ming Li*[,†]

[†]Institut für Pharmazeutische Biologie und Biotechnologie, Philipps-Universität Marburg, Robert-Koch-Strasse 4, Marburg 35037, Germany

[‡]State Key Laboratory of Mycology, Institute of Microbiology, Chinese Academy of Sciences, Beijing 100101, China

Supporting Information

ABSTRACT: Penilactones A and B consist of a γ-butyrolactone and two clavatol moieties. We identified two separate gene clusters for the biosynthesis of these key building blocks in *Penicillium crustosum*. Gene deletion, feeding experiments, and biochemical investigations proved that a nonreducing PKS ClaF is responsible for the formation of clavatol and the PKS-NRPS hybrid TraA is involved in the formation of crustosic acid, which undergoes decarboxylation and isomerization to the predominant terrestric acid. Both acids are proposed to be converted to γ-butyrolactones with involvement of a cytochrome P_{450} ClaJ. Oxidation of clavatol to hydroxyclavatol by a nonheme Fe^{II}/2-oxoglutarate-dependent oxygenase ClaD and its spontaneous dehydration to an *ortho*-quinone methide initiate the two nonenzymatic 1,4-Michael addition steps. Spontaneous addition of the methide to the γ-butyrolactones led to peniphenone D and penilactone D, which undergo again stereospecific attacking by methide to give penilactones A/B.

Penilactones A (**1**) and B (**2**) (Figure 1A) are rare fungal metabolites and were first isolated from *Penicillium crustosum* PRB-2.[1] Together with their putative precursors peniphenone D (**3**) and penilactone D (**4**) (Figure 1A), they were also identified in other *Penicillium* species.[2−4] Feeding experiments suggested that **1** and **2** are derived from acetyl-CoA and L-malic acid (Figure 1B).[1] It was proposed that **1** and **2** are formed by 1,4-Michael additions of two clavatol (**5**) molecules in its active form *ortho*-quinone methide (**6**) with a γ-butyrolactone (tetronic acid), i.e. (*R*)-5-methyl (**7**) or (*S*)-5-carboxylmethyltetronic acid (**8**).[1,2] This hypothesis was confirmed by a biomimetic synthesis.[5−7] Acetate of hydroxyclavatol (**9**) instead of **5** was used at 110 °C for the synthesis. Hydroxyclavatol methyl ether (**10**) was also isolated from *P. crustosum*.[3]

5 can be considered as a polyketide synthase (PKS) product. However, the responsible enzyme is unknown before. Neither the direct precursor nor the biosynthesis of **7** and **8** has been reported. Michael addition as a thermodynamically controlled 1,4-addition of active methylenes to activated olefins such as α,β-unsaturated carbonyl derivatives[8] are widely used in the chemical synthesis[9−12] and also involved in the biosynthesis of natural products.[13] However, the substrates, enzymes and conditions for Michael addition involved in the formation of **1**−**4** in nature have not been reported yet.

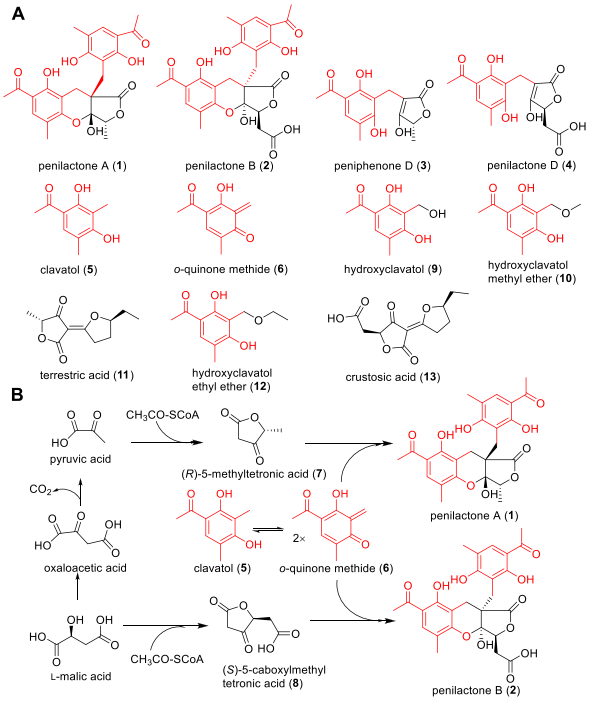

Figure 1. Metabolites from PRB-2 (A) and proposed biosynthetic routes to **1** and **2** (B).[1]

For secondary metabolite (SM) production in PRB-2, several culture conditions were tested and the extracts were analyzed on HPLC (Figure S1 in the Supplement Information (SI)). Three dominant peaks were detected in a 7 days-old PD culture (Figure S1), which were identified as **9**, **10**,[14] and terrestric acid (**11**)[15] after isolation and structure elucidation (see SI for details, NMR data and spectra are given in Tables S6−S10 and Figures S28−S45). The stereochemistry of **11** was confirmed by determination of its optical rotation and comparison with the published data.[15] **9** has not been described before and therefore

Received: January 10, 2019
Published: February 27, 2019

DOI: 10.1021/jacs.9b00110
J. Am. Chem. Soc. 2019, 141, 4225−4229

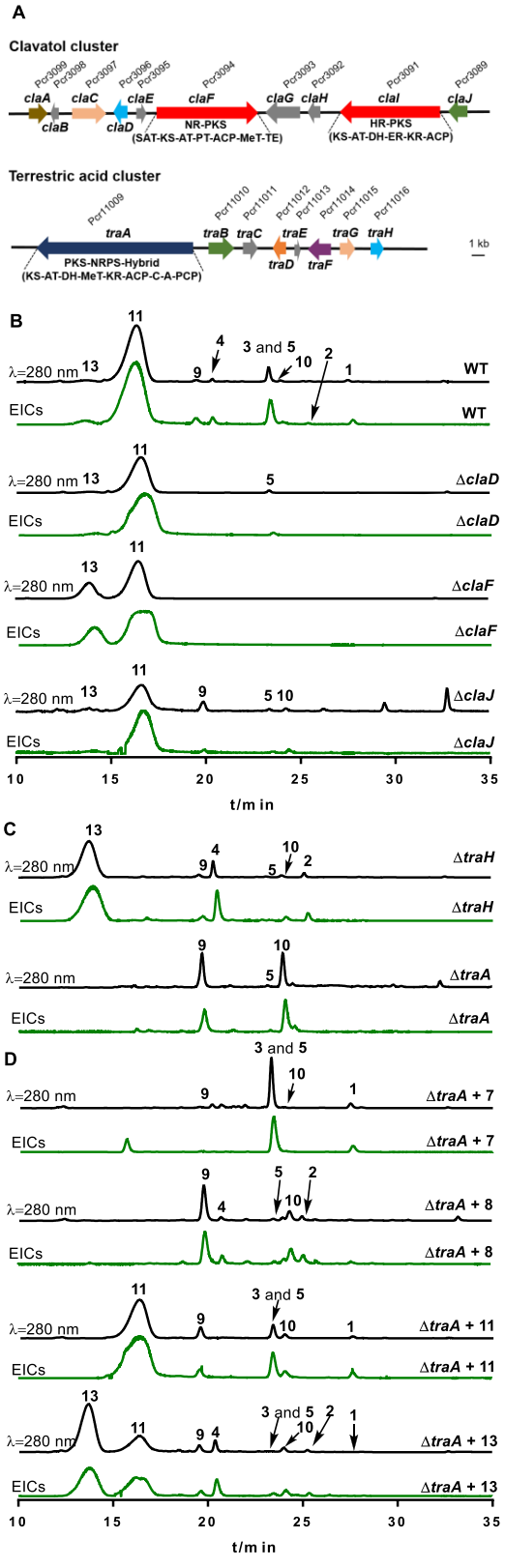

Figure 2. Schematic representation of clavatol and terrestric acid clusters in PRB-2 (A) and LC-MS results of deletion mutants (B and C) as well as of Δ*traA* mutant fed with putative precursors (D). EICs refer $[M + H]^+$ ions of **1**–**6** and **11**, **13** or $[M + Na]^+$ of **9** and **10** with tolerance ranges of ±0.005.

was confirmed by X-ray analysis (Table S11). Two additional minor peaks were proven to be **5** and hydroxyclavatol ethyl ether (**12**) (Figures 1A and S1).[14]

However, peniphenones and penilactones could only be detected in extracted ion chromatograms (EICs, data not shown). To increase their productivity, PRB-2 was cultivated in PD surface culture for 14 days. LC-MS analysis revealed clear accumulation of **1**–**4** (Figures 2, S1, and S2). A 30 days-old rice culture also accumulated **1**–**4** and was therefore used for isolation and structure elucidation by MS, NMR (Tables S6–S7 and Figures S28–S31), optical rotation, and CD spectra (Figures S46–S49).[1,3] The CD spectra of **1** and **2** (Figures S46 and S47) correspond very well to those reported previously.[1] The stereochemistry of **3** and **4** was determined by chemical synthesis from **7** and **8** with known configuration at C-5 (Figure S21, see below for the formation of **3** from **7** and **4** from **8**). Under these conditions, the production of **9** and **10** was strongly reduced. In comparison, **11** was detected as the predominant peak. Furthermore, a new peak was identified as carboxylated derivative of **11**, termed crustosic acid (**13**) hereafter (Figures 1A, S44, and S45). **13** has an $[\alpha]_D^{20}$ value of −164.1, while that of **11** at +37.1. The configuration of **13** was assigned by comparison with the optical rotation data of 5-methyl- and 5-carboxylmethyltetronic acids.[16]

For biosynthetic studies on **1** and **2**, the genome of PRB-2 was sequenced and the draft genome sequence was used for prediction of putative gene clusters by using AntiSMASH.[17] For gene inactivation, we established a gene replacement protocol using the split marker strategy and hygromycin B as selection marker, which significantly enhances the homologous recombination events at the target gene (Figure S3).[18]

Based on its aromatic character, **5** is expected to be assembled by a nonreducing PKS (NR-PKS).[19] One of the six NR-PKS genes *pcr3094* within a 36.2 kbp large cluster (Figure 2A and Table S4) has a SAT-KS-AT-PT-ACP-MeT-TE domain structure (Abbreviations for PKS and NRPS domains as given before[19,20]). It shares a sequence identity of 57.7% with CitS from *Monascus ruber*[21] and 64.4% with EAW12049.1 from *Aspergillus clavatus* (Table S4). Deletion of *pcr3094*, termed *claF* (from the clavatol cluster) hereafter, completely abolished the production of **1**–**5**, **9**, and **10** (see SI for manipulation). The two tetronic acids **11** and **13** accumulated with much higher yields in the Δ*claF* mutant than in PRB-2 (Figures 2B, S4, and S6). Feeding **5** to the mutant restored the production of **1**–**4** and **9** (Figure S15).

To provide more evidence for the function of ClaF as a clavatol synthase, *pcr3094* was cloned into pYH-wA-pyrG and expressed in *A. nidulans*.[22−24] The formation of **5** in the transformant JF11 was confirmed by LC-MS (Figure S20) and ^{1}H NMR analyses after isolation. These results proved that ClaF is responsible for **5** formation in the biosynthesis of **1**–**4** (Scheme 1).

To identify the genetic potential for **7** and **8**, we focused on PKS-NRPS hybrid enzymes, because tetronic acids like carlosic acid are usually assembled by such enzymes.[25] Analysis of the draft sequence revealed the presence of a candidate gene *pcr11009*, termed *traA* (from the terrestric acid cluster), within a 33.6 kbp large cluster. TraA with a domain structure KS-AT-DH-MeT-KR-ACP-C-A-PCP (Figure 2A) shares a sequence identity of 69.6% with CaaA in the carlosic acid biosynthesis (Table S5).[25] Deletion of *traA* completely abolished the production of **1**–**4**, indicating its involvement in the biosynthesis. As expected, **5**, **9**, and **10** were accumulated in the Δ*traA*

DOI: 10.1021/jacs.9b00110
J. Am. Chem. Soc. 2019, 141, 4225−4229

Scheme 1. Proposed Biosynthetic Pathways of Penilactones and Peniphenones in *P. crustosum*

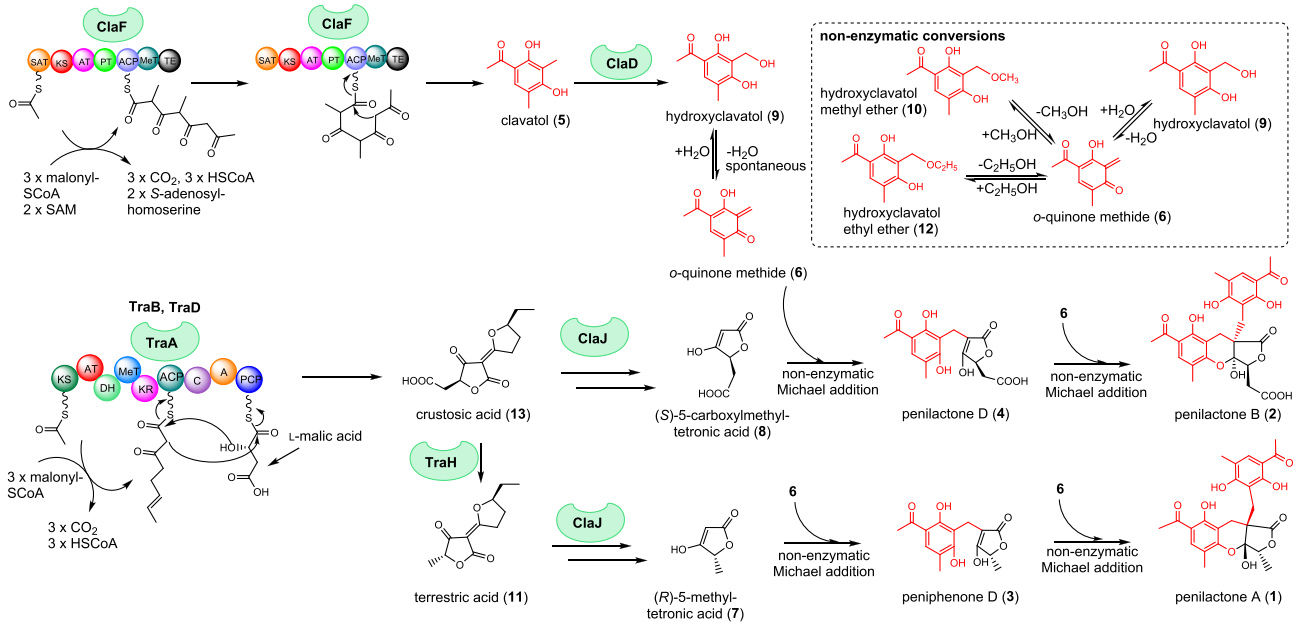

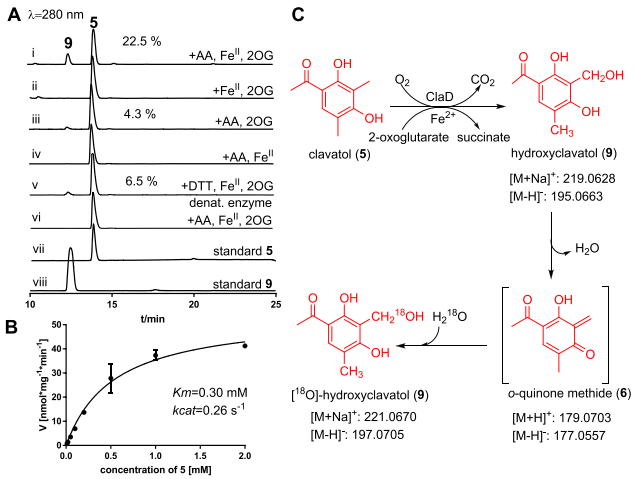

Figure 3. Functional proof of ClaD as a nonheme Fe^{II}/2-oxoglutarate-dependent clavatol oxidase (A and B) and determination of the equilibration between **9** and **6** (C).

mutant (Figures 2C and S8). Surprisingly, the production of **11** and **13** were also totally blocked. To restore the production of **1**−**4**, we chemically synthesized **7** and **8** (Figure S21)[5,7,26,27] and fed them to the Δ*traA* mutant. LC-MS analysis revealed that feeding **7** restored the production of **1** and **3**, but not **2** and **4**. In contrast, **2** and **4**, but not **1** and **3** were detected in the culture of Δ*traA* mutant fed with **8** (Figures 2C, S16, and S17). This proved that TraA is involved in the formation of **7** and **8**, which cannot be converted to each other (Scheme 1).

For understanding the role of **11** and **13** for **1**−**4**, they were isolated from Δ*claF* mutant and fed into Δ*traA* mutant. Feeding **11** only restored **1** and **3** production, while **1**−**4** were detected after feeding with **13** (Figures 2C, S18, and S19). More interestingly, **11** was also restored after feeding with **13**, but not *vice versa* (Figure 2D). This proved that **13** is the precursor of both **8** and **11**. **11** serves then as a precursor of **7** (Scheme 1).

It can be concluded that **13** is the product of TraA with or without other enzymes and mainly converted to the predominant product **11** in PRB-2. Only small amounts of **11** and **13** undergo degradation to **7** and **8** for the formation of **1**−**4** (Figure 2D and Scheme 1).

Having the both backbone genes/enzymes identified, we intended to investigate the conversion of **13** to **8** and **11**, **11** to **7**, and the metabolism of **5**. Inactivation of the oxygenase gene *traH* abolished the production of **1**, **3**, and **11**, confirming its involvement in the decarboxylation and isomerization of **13** to **11** (Figures 2C and S13). In the deletion mutants of the cytochrome P_{450} *traB* and the dehydrogenase *traD*, no accumulation of **11**, **13**, or **1**−**4** was detected (Figures S9 and S10), proving their roles in the **13** formation (Scheme 1). Deletion of *traE* and *traF* did not result in significant changes in SM production (Figures S11 and S12).

Regarding Michael addition, we presumed a more active intermediate than **5** for the formation of **6**. Detailed inspection of the *cla* cluster (Figure 2A, Table S4) revealed the presence of genes coding for an oxygenase (*claD*) and a cytochrome P_{450} (*claJ*). ClaD comprises 338 amino acids and shares a sequence identity of 53.8% with CitB in the citrinin biosynthesis.[21] It also contains the typical conserved 2-His-1-Asp ion-binding triad (His_{184}, His_{202} and Asp_{187}) of nonheme Fe^{II}/2-oxoglutarate-dependent oxygenases (Figure S22). Deletion of *claD* abolished the production of **1**−**4** and **9**, whereas **5** was clearly accumulated (Figures 2B and S5). Feeding **9** in the Δ*claD* mutant restored the production of **1**−**4** (Figure S14), proving its role in the conversion of **5** to **9**.

For biochemical characterization, *claD* was amplified and cloned into pET28a (+). The purified ClaD (Figure S23) was used for incubation with **5** in the presence of ascorbate (AA), $Fe[(NH_4)_2(SO_4)_2]$, and 2-oxoglutarate (2OG).[28,29] HPLC analysis confirmed the oxidation of **5** to **9** with a conversion yield of 22.5% after incubation with 2 μg protein at 37 °C for 30 min (Figure 3A). Nearly no consumption of **5** was detected in the assays without ascorbate or 2-oxoglutarate. Replacing ascorbate by dithiothreitol (DTT) or without additional Fe^{II} reduced the activity significantly. These results proved that ClaD acts as a nonheme Fe^{II}/2-oxoglutarate-dependent oxygenase and oxidizes **5** to yield **9**. Determination of kinetic parameters

DOI: 10.1021/jacs.9b00110
J. Am. Chem. Soc. 2019, 141, 4225−4229

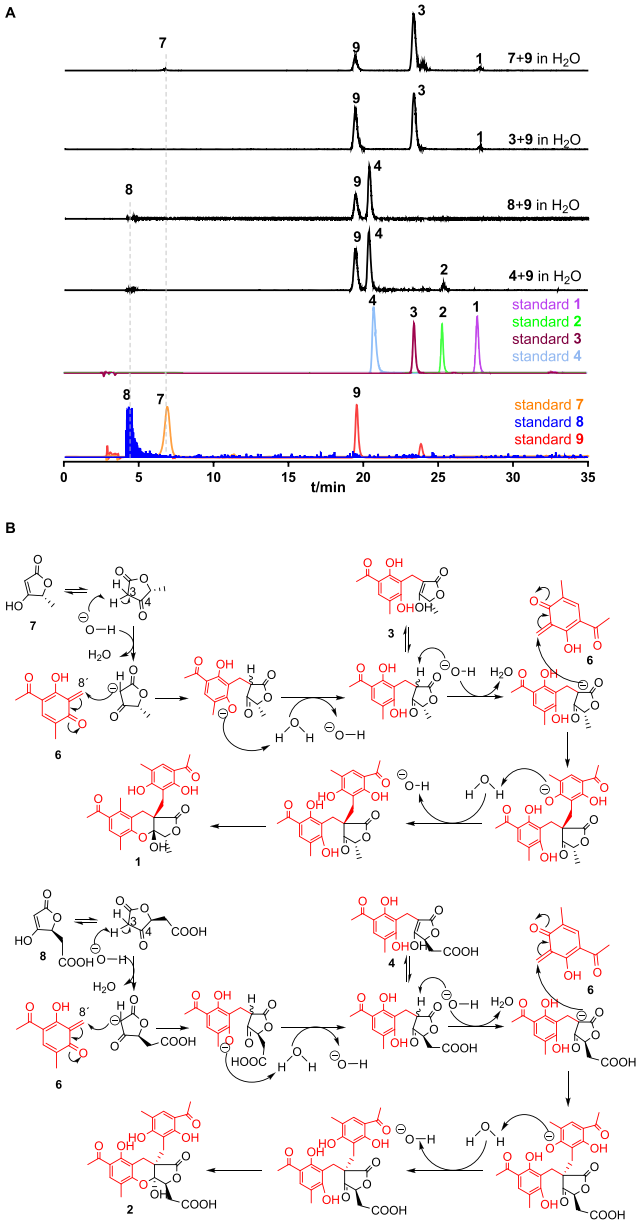

Figure 4. Nonenzymatic formation of penilactones and peniphenone. (A) LC-MS analysis of 48 h-incubation mixtures. Absorptions at 254 nm (**1**–**4**, **9**) or EICs (**7** and **8**) are illustrated. (B) Proposed mechanism of nonenzymatic formation of **1**–**4** via Michael addition.

gave a K_M of 0.30 mM toward **5** and a turnover number (k_{cat}) of 0.26 s^{-1} (Figure 3B).

To prove the conversion between **9** and **6**, **9** was incubated in H_2O and $H_2{}^{18}O$ at 25 °C for 16 h. MS data in positive and negative modes confirmed the incorporation of ^{18}O into **9** and therefore the equilibration (Figures 3C and S24).

ClaJ shares clear sequence homology with fungal cytochrome P_{450} enzymes, e.g. 42.0% identity with BAJ04372.1 from *Aspergillus oryzae*.[30] Deletion of *claJ* resulted in the abolishment of **1**–**4** (Figures 2B and S7), but still retained the production of **5**, **9**, **11**, and **13**. This indicates its role in the C–C double bond cleavage of **11** and **13** (Scheme 1). However, ClaJ could also catalyze the connection of the two building blocks via Michael addition.

For preparing feeding experiments in Δ*claJ*, we carried out control incubations of **7** with **9** and **8** with **9** in water at 25 °C, which delivered surprising results, i.e. the nonenzymatic Michael addition under these mild conditions (Figure 4A). In the first combination, **3** was detected as the major and **1** as a minor product, while **4** as the major and **2** as a minor product in the case of **8** with **9**. When **3** and **4** were incubated with **9**, **1** and **2** were detected (Figure 4A). Formation of **3** and **4** is time- and pH-dependent (Figures S25 and S26). **3** and **4** are formed under neutral or acidic conditions. When pH values were higher than 5.0, diclavatol[3] was also detected (Figure S26). It is obvious that the active intermediate **6** can be easily formed from **9** in aqueous system and initiates the Michael additions (Figure 4B), which was confirmed by incubation of **9**, **10**, and **12** in different solvents. They are stable in acetonitrile. Alcohols determined the end products of **6** (Figure S27, Scheme 1). All these results indicate that ClaJ is likely not involved in the Michael addition, probably in the conversion of **11** to **7** and **13** to **8** (Scheme 1).

Taken together, **1**–**4** are formed by enzymes from independent pathways of two separate gene clusters (Scheme 1). The *tra* cluster assembles **13**, which is converted to **11**. Both acids deliver the two γ-butyrolactones **7** and **8**. The *cla* cluster provides the highly active **6** by a spontaneous dehydration of **9**. This initiates the two step nonenzymatic Michael additions by the intermolecular nucleophile attacking of **6** to **7** or **8** and subsequent reaction with **3** and **4**. Thus, this study provides an excellent example for SMs with complex structures that are formed by enzymes from different pathways and by combination of enzymatic and nonenzymatic reactions.

■ ASSOCIATED CONTENT

Supporting Information

The Supporting Information is available free of charge on the ACS Publications website at DOI: 10.1021/jacs.9b00110.

Materials, experimental procedures, physiochemical properties and spectroscopic data (PDF)

Data for $C_{10}H_{12}O_4$ (CIF)

■ AUTHOR INFORMATION

Corresponding Author

*S.-M. Li. E-mail: shuming.li@staff.uni-marburg.de.

ORCID

Wen-Bing Yin: 0000-0002-9184-3198

Shu-Ming Li: 0000-0003-4583-2655

Author Contributions

[§]These authors contributed equally to this work.

Notes

The authors declare no competing financial interest.

■ ACKNOWLEDGMENTS

We thank Tianjiao Zhu (Ocean University of China, Qingdao) for providing strain PRB-2, Rixa Kraut, Stefan Newel, and Andreas Heine (University of Marburg) for taking MS, NMR spectra and X-ray crystal analysis, respectively. This project was financially funded in part by the Deutsche Forschungsgemeinschaft (DFG, German Research Foundation) – Li844/11-1 and INST 160/620-1 as well as the National Natural Science Foundation of China – 31861133004. Jie Fan (201507565006) and Ge Liao (201607565014) are scholarship recipients from the China Scholarship Council.

DOI: 10.1021/jacs.9b00110
J. Am. Chem. Soc. 2019, 141, 4225–4229

REFERENCES

(1) Wu, G.; Ma, H.; Zhu, T.; Li, J.; Gu, Q.; Li, D. Penilactones A and B, two novel polyketides from Antarctic deep-sea derived fungus *Penicillium crustosum* PRB-2. *Tetrahedron* **2012**, *68*, 9745.

(2) Li, H.; Jiang, J.; Liu, Z.; Lin, S.; Xia, G.; Xia, X.; Ding, B.; He, L.; Lu, Y.; She, Z. Peniphenones A-D from the mangrove fungus *Penicillium dipodomyicola* HN4−3A as inhibitors of *Mycobacterium tuberculosis* phosphatase MptpB. *J. Nat. Prod.* **2014**, *77*, 800.

(3) Wu, G. *Studies on secondary metabolites of three different marine environment-derived fungi: structures and bioactivities*. Dissertation, Ocean University of China, 2014.

(4) Sun, W.; Chen, X.; Tong, Q.; Zhu, H.; He, Y.; Lei, L.; Xue, Y.; Yao, G.; Luo, Z.; Wang, J.; Li, H.; Zhang, Y. Novel small molecule 11beta-HSD1 inhibitor from the endophytic fungus *Penicillium commune*. *Sci. Rep.* **2016**, *6*, 26418.

(5) Spence, J. T.; George, J. H. Biomimetic total synthesis of ent-penilactone A and penilactone B. *Org. Lett.* **2013**, *15*, 3891.

(6) Pantin, M.; Brimble, M. A.; Furkert, D. P. Total synthesis of (−)-peniphenone A. *J. Org. Chem.* **2018**, *83*, 7049.

(7) Spence, J. T.; George, J. H. Total synthesis of peniphenones A-D via biomimetic reactions of a common *o*-quinone methide intermediate. *Org. Lett.* **2015**, *17*, 5970.

(8) Tokoroyama, T. Discovery of the Michael reaction. *Eur. J. Org. Chem.* **2010**, *2010*, 2009.

(9) Wadhwa, P.; Kharbanda, A.; Sharma, A. Thia-Michael addition: An emerging strategy in organic synthesis. *Asian J. Org. Chem.* **2018**, *7*, 634.

(10) Mather, B. D.; Viswanathan, K.; Miller, K. M.; Long, T. E. Michael addition reactions in macromolecular design for emerging technologies. *Prog. Polym. Sci.* **2006**, *31*, 487.

(11) Zhang, Y.; Wang, W. Recent advances in organocatalytic asymmetric Michael reactions. *Catal. Sci. Technol.* **2012**, *2*, 42.

(12) Nising, C. F.; Bräse, S. The oxa-Michael reaction: from recent developments to applications in natural product synthesis. *Chem. Soc. Rev.* **2008**, *37*, 1218.

(13) Miyanaga, A. Michael additions in polyketide biosynthesis. *Nat. Prod. Rep.* **2019**, DOI: 10.1039/C8NP00071A.

(14) Astudillo, L.; Schmeda-Hirschmann, G.; Soto, R.; Sandoval, C.; Afonso, C.; Gonzalez, M. J.; Kijjoa, A. Acetophenone derivatives from Chilean isolate of *Trichoderma pseudokoningii* Rifai. *World J. Microbiol. Biotechnol.* **2000**, *16*, 585.

(15) Nukina, M. Terrestric acid as a phytotoxic metabolite from *Pyricularia oryzae* Cavara. *Agric. Biol. Chem.* **1988**, *52*, 2357.

(16) Clutterbuck, P. W.; Haworth, W. N.; Raistrick, H.; Smith, G.; Stacey, M. Studies in the biochemistry of micro-organisms: The metabolic products of *Penicillium charlesii* G. Smith. *Biochem. J.* **1934**, *28*, 94.

(17) Weber, T.; Blin, K.; Duddela, S.; Krug, D.; Kim, H. U.; Bruccoleri, R.; Lee, S. Y.; Fischbach, M. A.; Müller, R.; Wohlleben, W.; Breitling, R.; Takano, E.; Medema, M. H. antiSMASH 3.0 - a comprehensive resource for the genome mining of biosynthetic gene clusters. *Nucleic Acids Res.* **2015**, *43*, W237.

(18) Goswami, R. S. Targeted gene replacement in fungi using a split-marker approach. *Methods Mol. Biol.* **2012**, *835*, 255.

(19) Cox, R. J. Polyketides, proteins and genes in fungi: programmed nano-machines begin to reveal their secrets. *Org. Biomol. Chem.* **2007**, *5*, 2010.

(20) Miyanaga, A.; Kudo, F.; Eguchi, T. Protein-protein interactions in polyketide synthase-nonribosomal peptide synthetase hybrid assembly lines. *Nat. Prod. Rep.* **2018**, *35*, 1185.

(21) He, Y.; Cox, R. J. The molecular steps of citrinin biosynthesis in fungi. *Chem. Sci.* **2016**, *7*, 2119.

(22) Yin, W. B.; Chooi, Y. H.; Smith, A. R.; Cacho, R. A.; Hu, Y.; White, T. C.; Tang, Y. Discovery of cryptic polyketide metabolites from dermatophytes using heterologous expression in *Aspergillus nidulans*. *ACS Synth. Biol.* **2013**, *2*, 629.

(23) Li, W.; Fan, A.; Wang, L.; Zhang, P.; Liu, Z.; An, Z.; Yin, W.-B. Asperphenamate biosynthesis reveals a novel two-module NRPS system to synthesize amino acid esters in fungi. *Chem. Sci.* **2018**, *9*, 2589.

(24) Chiang, Y. M.; Ahuja, M.; Oakley, C. E.; Entwistle, R.; Asokan, A.; Zutz, C.; Wang, C. C.; Oakley, B. R. Development of genetic dereplication strains in *Aspergillus nidulans* results in the discovery of aspercryptin. *Angew. Chem., Int. Ed.* **2016**, *55*, 1662.

(25) Yang, X. L.; Awakawa, T.; Wakimoto, T.; Abe, I. Three acyltetronic acid derivatives: noncanonical cryptic polyketides from *Aspergillus niger* identified by genome mining. *ChemBioChem* **2014**, *15*, 1578.

(26) Adrian, J.; Stark, C. B. Total synthesis of muricadienin, the putative key precursor in the solamin biosynthesis. *Org. Lett.* **2014**, *16*, 5886.

(27) Stebbins, N. D.; Yu, W.; Uhrich, K. E. Enzymatic polymerization of an ibuprofen-containing monomer and subsequent drug release. *Macromol. Biosci.* **2015**, *15*, 1115.

(28) Ran, H.; Wohlgemuth, V.; Xie, X.; Li, S.-M. A non-heme FeII/2-oxoglutarate-dependent oxygenase catalyzes a double bond migration within a dimethylallyl moiety accompanied by hydroxylation. *ACS Chem. Biol.* **2018**, *13*, 2949.

(29) Steffan, N.; Grundmann, A.; Afiyatullov, A.; Ruan, H.; Li, S.-M. FtmOx1, a non heme Fe(II) and alpha-ketoglutarate-dependent dioxygenase, catalyses the endoperoxide formation of verruculogen in *Aspergillus fumigatus*. *Org. Biomol. Chem.* **2009**, *7*, 4082.

(30) Nazir, K. H. M. N. H.; Ichinose, H.; Wariishi, H. Molecular characterization and isolation of cytochrome P450 genes from the filamentous fungus *Aspergillus oryzae*. *Arch. Microbiol.* **2010**, *192*, 395.

DOI: 10.1021/jacs.9b00110
J. Am. Chem. Soc. 2019, 141, 4225−4229

SUPPORTING INFORMATION

Peniphenone and penilactone formation in *Penicillium crustosum* *via* 1,4-Michael additions of *ortho*-quinone methide from hydroxyclavatol to γ-butyrolactones from crustosic acid

Jie Fan,[1,†] Ge Liao,[1,†] Florian Kindinger,[1] Lena Ludwig-Radtke,[1] Wen-Bing Yin,[2] and Shu-Ming Li[1,*]

[1] Institut für Pharmazeutische Biologie und Biotechnologie, Philipps-Universität Marburg, Robert-Koch-Strasse 4, Marburg 35037, Germany

[2] State Key Laboratory of Mycology, Institute of Microbiology, Chinese Academy of Sciences, Beijing 100101, China

[†]These authors contributed equally to this work.

Table content

Experiment Procedures

1. Strains, media and growth conditions

The fungal strains used in this study are summarized in Table S1. *Penicillium crustosum* strain PRB-2 was isolated from a deep-sea sediment collected in Prydz Bay at a depth of -526 m.[1] For detection of secondary metabolites (SMs), the strain PRB-2 was cultivated in PD medium (potato dextrose broth, Sigma) at 25°C. *Aspergillus nidulans* strains were grown at 37°C on GMM medium (1.0% glucose, 50 mL/L salt solution, 1 mL/L trace element solution, 1.6% agar) for sporulation and transformation with appropriate nutrition as required.[2-4] The salt solution comprises (w/v) 12% $NaNO_3$, 1.04% KCl, 1.04% $MgSO_4{\cdot}7H_2O$, and 3.04% KH_2PO_4. The trace element solution contains (w/v) 2.2% $ZnSO_4{\cdot}7H_2O$, 1.1% H_3BO_3, 0.5% $MnCl_2{\cdot}4H_2O$, 0.16% $FeSO_4{\cdot}7H_2O$, 0.16% $CoCl_2{\cdot}5H_2O$, 0.16% $CuSO_4{\cdot}5H_2O$, 0.11% $(NH_4)_6Mo_7O_{24}{\cdot}4H_2O$, and 5% Na_4EDTA. *Escherichia coli* DH5α and BL21(DE3) were grown in LB medium (1% NaCl, 1% tryptone, and 0.5% yeast extract) for standard DNA manipulation. 50 μg/mL carbenicillin or kanamycin were supplemented for cultivation of recombinant *E. coli* strains.

2. Genomic DNA isolation

The mycelia of *P. crustosum* and *A. nidulans* were collected in 2 mL Eppendorf tubes by centrifugation (13,000 rpm, 10 min). Four glass beads (2.85 mm in diameter) and 400 μL of LETS buffer (10 mM Tris-HCl pH 8.0, 20 mM EDTA pH 8.0, 0.5% SDS, and 0.1 M LiCl) were added to the tubes. After vigorous mixing for 4 min, 300 μL LETS buffer was added, and then the solution was treated with 700 μL phenol: chloroform: isoamyl alcohol (25: 24: 1). The genomic DNA was precipitated by addition of 900 μL absolute ethanol. After centrifugation at 13,000 rpm for 30 min and washing with 70% ethanol, the obtained DNA was dissolved in 50 μL distillated H_2O.

3. RNA isolation and cDNA synthesis

For isolation of RNA from *P. crustosum* PRB-2, the fungus was cultivated in liquid PD medium for 7 d and the cells were collected by centrifugation. RNA extraction was performed by using Fungal RNA Mini kit (VWR OMEGA bio-tek E.Z.N.A) according to the manufacturer´s instruction. The ProtoScript II First Strand cDNA Synthesis kit (BioLabs) was used for cDNA synthesis with Oligo-dT primers.

4. Genome sequencing and sequence analysis

The genome of *P. crustosum* PRB-2 was sequenced by BerryGenomics (Beijing, China) using Nova-seq6000/X-ten (Illumina). Initial prediction and analysis of the clavatol and terrestric acid biosynthetic gene clusters were carried out by using antiSMASH (http://antismash.secondarymetabolites.org/). Prediction of the open reading frames (ORFs) was performed with the online BLAST approaches (http://blast.ncbi.nlm.nih.gov). Detailed prediction for domain structures of PKS and PKS-NRPS hybrid enzymes was performed with the PKS/NRPS analysis tool (http://nrps.igs.umaryland.edu/). The genes in clavatol and terrestric acid clusters were named as *claA-J* and *traA-H*, respectively (Figure 2A, Tables S4 and S5). The genomic DNA sequences of the clavatol and terrestric acid clusters from *P. crustosum* PRB-2 reported in this study are available at GenBank under accession numbers MK360918 and MK360919, respectively.

5. PCR amplification, gene cloning and plasmid construction

Plasmids used in this study are listed in Table S2. The oligonucleotide sequences for PCR primers are given in Table S3. Primers were designed as described for gene deletion strategy (Figure S3) and synthesized by Seqlab GmbH (Göttingen, Germany). PCR amplification was carried out by using Phusion® High-Fidelity DNA polymerase from New England Biolabs (NEB) on a T100TM Thermal cycler from Bio-Rad. PCR reaction mixtures and thermal profiles were set as recommended by the manufacturer´s instruction.

To identify the clavatol and terrestric acid biosynthetic gene clusters, we deleted genes of interest by using split-marker approach, which significantly enhances the homologous recombination events at the target genes.[5] In this approach, two DNA fragments are constructed. One fragment comprises the upstream DNA region of the target gene and the two-third of the sequence of the selection marker at its 5´-end, *e.g.* the hygromycin B resistance gene in this study. The second fragment consists of two-third at the 3´-end of the selection marker and the downstream region of the target gene (Figure S3). 1.0–1.5 kbp upstream and downstream fragments of *claD*, *claF*, *claJ*, *traA, traB*, *traD*, *traE*, *traF* and *traH* were amplified from *P. crustosum* genomic DNA using the designed primers listed in Table S3.

To construct the plasmid for heterologous expression of *claF* in *A. nidulans*, an assembly approach based on the homologous recombination in *E. coli* was used.[6] *claF* including its terminator of 480 bp was amplified from genomic DNA of *P. crustosum* by using primers A.n-claF-For/Rev (Table S3) and inserted into the corresponding sites of pYH-wA-pyrG with homologous flanking sequences of the *wA* gene.[4] To construct the plasmid for expressing *claD* in *E. coli*, the coding region of *claD* was amplified by PCR from cDNA with the primers ClaD-28-For/Rev (Table S3). The DNA fragment was digested with BamHI and EcoRI and ligated into the same site of the expression vector pET-28a (+), yielding the expression plasmid pJF37, which was confirmed by sequencing (Seqlab GmbH).

6. Genetic manipulation in *P. crustosum* and cultivation of deletion mutants

Fresh spores of *P. crustosum* were inoculated into 30 mL LMM medium (1.0% glucose, 50 mL/L salt solution, 1 mL/L trace element solution, and 0.5% yeast extract) in 100 mL flask and incubated at 25°C and 230 rpm for germination. Mycelia were harvested after 11 h by centrifugation at 5,000 rpm for 10 min, and washed with distillated H_2O. The mycelia were then transferred into a 50 mL flask with 10 mL of osmotic buffer (1.2 M $MgSO_4$ in 10 mM sodium phosphate, pH 5.8) containing 50 mg lysing enzyme from *Trichoderma harzianum* (Sigma) and 20 mg yatalase from *Corynebacterium sp.* OZ-21 (OZEKI Co., Ltd.). After shaking at 30°C and 100 rpm for 2.5 h, the cells were transferred into a 50 mL falcon tube and overlaid gently with 10 mL of trapping buffer (0.6 M sorbitol in 0.1 M Tris-HCl, pH 7.0). After centrifugation at 4°C and 5,000 rpm for 10 min, the protoplasts were collected from the interface of the two buffer systems. The protoplasts were then transferred to a sterile 15 mL falcon tube and resuspended in 200 µL of STC buffer (1.2 M sorbitol, 10 mM $CaCl_2$, and 10 mM Tris-HCl, pH 7.5) for transformation.

The *via* PCR constructed gene deletion cassettes mentioned above were transformed into *P.*

crustosum by polyethylene glycol (PEG) mediated protoplast transformation. The DNA fragments were incubated with 100 µL of the protoplasts for 50 min on ice. 1.25 mL of PEG solution (60% PEG 4000, 50 mM $CaCl_2$, 50 mM Tris-HCl, pH 7.5) was then added and gently mixed. After incubation at room temperature for 30 min, the mixture was transferred in 5 mL STC buffer and spread on plates with SMM bottom medium (1.0% glucose, 50 mL/L salt solution, 1 mL/L trace element solution, 1.2 M sorbitol, and 1.6% agar) containing 200 µg/mL hygromycin B. SMM top medium (1.0% glucose, 50 mL/L salt solution, 1 mL/L trace element solution, 1.2 M sorbitol, and 0.8% agar) containing 100 µg/mL hygromycin B was overlaid softly on the plates. Three days later, the transformants were transferred onto fresh PDA plates (PD medium with 1.6% agar) containing 200 µg/mL hygromycin B for second selection. The obtained transformants were inoculated in PD medium for isolation of genomic DNA to verify the integrity, which was carried out by PCR amplification (Figure S4). After cultivation in PD liquid medium at 25°C for 14 days, the secondary metabolites of the deletion mutants were extracted with ethyl acetate, dissolved in MeOH and analyzed on LC-MS.

7. Heterologous expression of *claF* in *A. nidulans*

A. nidulans strain LO8030 was used as the recipient host.[3] Fungal protoplast preparation and transformation were performed according to the method described previously.[3] pJF18 containing the PKS gene *claF* was transformed into *A. nidulans* strain LO8030 to create the *claF* expression strain JF11. Potential transformants were verified by PCR using the primers claF-F/R (Table S3). Rice medium was used to cultivate the transformants (25°C, 7d) for LC-MS analysis of the secondary metabolite production.

8. Precursor feeding in △*claD,* △*claF,* and △*traA*–mutants

For feeding experiments, the precursors were dissolved in DMSO to give 1 M stock solutions. Adequate volumes of such solutions were then added to 10 mL of liquid PD cultures of respective deletion mutant, △*claF*, △*claD* or △*traA*, leading to final concentrations of 0.5 mM for clavatol (**5**) and hydroxyclavatol (**9**), 0.2 mM for terrestric acid (**11**), crustosic acid (**13**), (*R*)-5-methyltetronic acid (**7**), and (*S*)-5-carboxylmethyltetronic acid (**8**). After further cultivation at 25°C for 14 d, the secondary metabolites were extracted with ethyl acetate, dissolved in MeOH and analyzed on LC-MS.

9. Chemical synthesis of tetronic acids 7 and 8

For feeding experiments in deletion mutants, two tetronic acids (*R*)-5-methyltetronic acid (**7**) and (*S*)-5-carboxylmethyltetronic acid (**8**) were synthesized chemically according to the published methods (Figure S21). **7** was synthesized in two steps from (*R*)-ethyl lactate[7] and **8** in three steps from L-malic acid.[8,9]

10. Overproduction and purification of ClaD

The expression plasmid pJF37 was constructed for *claD* expression in *E. coli* as mentioned above. The recombinant *E. coli* BL21(DE3) strain was cultivated in Terrific Broth medium (TB medium, with 2.4% yeast extract, 2.0% tryptone, 0.4% glycerol, 0.1 M phosphate buffer, pH 7.4) and *claD* expression was induced with 0.5 mM IPTG at 30°C for 6 h. The recombinant histidine-tagged ClaD was purified on Ni-NTA agaroses (Qiagen, Hilden) and proven on

SDS-PAGE (Figure S23).

11. *In vitro* assays of ClaD

To determine the enzyme activity toward clavatol (**5**), the enzyme assays (50 µL) contained phosphate buffer (20 mM, pH 7.4), ascorbic acid (1 mM), clavatol (1 mM), $Fe[(NH_4)_2(SO_4)_2]$ (1 mM), 2-oxoglutarate (1 mM), glycerol (0.5−5%), DMSO (5%), and the purified recombinant ClaD (2 µg). The enzyme assays were incubated at 37 °C for 30 min and terminated with one volume of acetonitrile. The reaction mixtures were centrifuged at 13,000 rpm for 30 min before further analysis on HPLC.

12. Proof of the existence of *ortho*-quinone methide

In order to provide evidence for the existence of *ortho*-quinone methide (**6**), hydroxyclavatol (**9**) isolated from the fungal culture was dissolved in both H_2O and in ^{18}O-enriched $H_2{}^{18}O$. After incubation at room temperature for 16 h, the samples were analyzed by MS on positive and negative modes.

To prove their conversion *via* **6**, hydroxyclavatol (**9**), hydroxyclavatol methyl ether (**10**), and hydroxyclavatol ethyl ether (**12**) were incubated in different solvents such as H_2O, acetonitrile, MeOH and EtOH at room temperature for 12 h. The mixtures were analyzed on HPLC by using method B.

13. Non-enzymatic formation of penilactones and peniphenones

To determine the non-enzymatic formation, hydroxyclavatol (**9**) was incubated with (*R*)-5-methyltetronic acid (**7**) or (*S*)-5-carboxylmethyltetronic acid (**8**) in H_2O at room temperature for 16 h. The dependence of the product formation on time (0, 5, 15, 30, 60, 120 min, and 24 h) was monitored on HPLC (method A) (Figure S25). pH dependence of the product formation was carried out by incubation in phosphate buffer saline (PBS, pH 3−10) for 12 h (Figure S26).

14. Large-scale fermentation, extraction and isolation of secondary metabolites

To isolate **5**, **9,** and **10**–**12**, *P. crustosum* PRB-2 spores were inoculated into 60x 250-mL flask containing 100 mL PD liquid medium each and incubated on a rotary shaker at 220 rpm and 25 °C for 7 d. The supernatant and mycelia were separated by filtration. The supernatant was extracted with equal volume of ethyl acetate for three times, and the mycelia were extracted with acetone. The acetone extract was concentrated under reduced pressure to afford an aqueous solution, and then extracted with ethyl acetate. The two ethyl acetate extracts were combined and evaporated under reduced pressure to give a crude extract (1.8 g). The crude extract was subjected to silica gel column chromatography by using stepwise gradient elution with the mixtures of CH_2Cl_2/MeOH (100:1 to 20:1, v/v) to give eleven fractions (1–11). Fraction 3 eluted with CH_2Cl_2/MeOH (80:1) was further purified on semi-preparative HPLC (ACN/H_2O (70:30)) to yield clavatol (**5**) (15 mg), hydroxyclavatol methyl ether (**10**) (7 mg) and hydroxyclavatol ethyl ether (**12**) (4 mg). Hydroxyclavatol (**9**) (17 mg) was obtained from fraction 7, which was eluted with CH_2Cl_2/MeOH (40:1), by semi-preparative HPLC (ACN/H_2O (60:40)). Fraction 8 eluted with CH_2Cl_2/MeOH (20:1) was chromatographed over Sephadex LH-20

column and eluted with MeOH, resulting in terrestric acid (**11**) (40 mg).

To isolate **1**–**4**, *P. crustosum* PRB-2 was cultivated in 300x 250-mL flasks each containing 20 g rice, 30 mL H_2O, and 0.75 g soy flour at 25 °C for 30 days. The rice cultures were extracted with 15 L ethyl acetate and concentrated under reduced pressure to obtain a crude extract (35 g). The crude extract was applied to silica gel column chromatography and eluted with a stepwise gradient CH_2Cl_2/acetone (100:1, 50:1, 25:1, 19:1, and 1:1), yielding eight fractions (1–8). Subsequent elution with methanol gave 10 additional fractions (9−18). Fraction 4 was separated by repeated silica gel column chromatography with CH_2Cl_2/MeOH (50:1) and petroleum ether/EtOAc (1:1 and 1:6) as solvents to afford pure peniphenone D (**3**) (12 mg). Penilactone A (**1**) (7 mg) was obtained from fraction 7 by silica gel and Sephadex LH-20 column chromatography as well as by final purification on a semi-preparative HPLC (MeOH/H_2O (70:30) with 0.1% trifluoroacetic acid). In analogy, penilactone B (**2**) (5 mg) and penilactone D (**4**) (6 mg) were purified from fractions 12 and 18, respectively.

To isolate **13**, the △*claF*-mutant was cultivated in PD medium at 25°C for 14 d. The culture was extracted with ethyl acetate using the same procedure as mentioned above. 1.0 g crude extract was obtained from 4 L culture, and subjected to silica gel column chromatography by using petroleum ether/EtOAc (10:1, 3:1, 1:1, 1:3, 1:6) as elution solvents, giving 5 fractions (1−5). Pure **13** (20 mg) was obtained from fraction 5 after purification on Sephadex LH-20 column using MeOH as eluent.

15. HPLC and LC-MS analysis of secondary metabolites

Analysis of secondary metabolites was performed on an Agilent series 1200 HPLC (Agilent Technologies, Böblingen, Germany) with an Agilent Eclipse XDB-C18 column (150 × 4.6 mm, 5 µm). Water (A) and acetonitrile (B), both with 0.1% (v/v) formic acid, were used as solvents at flow rate of 0.5 mL/min. The substances were eluted with a linear gradient from 5–100% B in 15 min, then washed with 100% (v/v) solvent B for 5 min and equilibrated with 5% (v/v) solvent B for 5 min (method A) or with a linear gradient from 5–100% B in 40 min, then washed with 100% (v/v) solvent B for 5 min and equilibrated with 5% (v/v) solvent B for 10 min (method B). Absorptions at UV 280 nm were illustrated. Semi-preparative HPLC was performed on the same equipment with an Agilent Eclipse XDB-C18 column (9.4 × 250 mm, 5 µm) column and a flow rate of 2.5 mL/min.

LC-MS analysis was performed on an Agilent 1260 HPLC system equipped with a microTOF-Q III spectrometer (Bruker, Bremen, Germany) by using Multospher 120 RP18-5µ column (250 × 2 mm, 5 µm) (CS-Chromatographie Service GmbH) and method B for separation at flow rate of 0.25 mL/min. Electrospray positive or negative ionization mode was selected for determination of the exact masses. The capillary voltage was set to 4.5 kV and a collision energy of 8.0 eV. Sodium formate was used in each run for mass calibration. The masses were scanned in the range of m/z 100–1500. Data were evaluated with the Compass DataAnalysis 4.2 software (Bruker Daltonik, Bremen, Germany).

16. NMR analysis

NMR spectra were recorded on a JOEL ECA-500 MHz spectrometer (JEOL, Tokyo, Japan). All

spectra were processed with MestReNova 6.1.0 (Metrelab). Chemical shifts are referenced to those of the solvent signals. NMR data are given in Tables S6–S10 and spectra in Figures S28–S45.

17. Measurement of optical rotations

The optical rotation was measured with the polarimeter Jasco DIP-370 at 20°C using the D-line of the sodium lamp at λ=589.3 nm. Prior to the measurement, the polarimeter was calibrated with methanol as solvent.

18. Circular dichroism (CD) spectroscopic analysis

CD spectra were taken on a J-815 CD spectrometer (Jasco Deutschland GmbH, Pfungstadt, Germany). The samples were dissolved in methanol and measured in the range of 200–400 nm by using a 1 mm path length quartz cuvette (Hellma Analytics, Müllheim, Germany). The CD spectra are given in Figures S46–S52.

19. X-ray crystallographic analysis

Colorless crystals of hydroxyclavatol (**9**) were obtained in CH_2Cl_2/MeOH. Crystallographic data for **9** (Cu Ka radiation) has been deposited in the Cambridge Crystallographic Data Centre with the deposition number CCDC 1883090 (Table S11). These data can be obtained free of charge *via* www.ccdc.cam.ac.uk/data_request/cif.

20. Physiochemical properties of the compounds described in this study

Penilactone A (**1**): Colorless solid; $[\alpha]_D^{20}$ = -14.8 (*c* 0.25, MeOH); CD (MeOH) λ_{max} ($\Delta\varepsilon$) 333 (-13.1), 295 (+28.2), 271 (-25.0), 240 (+17.2), 226 (-27.4) nm; HRMS (m/z): (ESI/$[M + H]^+$) calcd. for $C_{25}H_{27}O_9$, 471.1650, found 471.1652.

Penilactone B (**2**): Colorless solid; $[\alpha]_D^{20}$ = +12.6 (*c* 0.25, MeOH); CD (MeOH) λ_{max} ($\Delta\varepsilon$) 335 (+9.6), 292 (-28.7), 270 (+18.9), 240 (-10.5), 227 (+11.4) nm; HRMS (m/z): (ESI/$[M + H]^+$) calcd. for $C_{26}H_{27}O_{11}$, 515.1548, found 515.1570.

Peniphenone D (**3**): Colorless solid; $[\alpha]_D^{20}$ = +10.6 (*c* 0.25, MeOH); CD (MeOH) λ_{max} ($\Delta\varepsilon$) 254 (+2.4), 232 (-2.1), 200 (-3.0) nm; HRMS (m/z): (ESI/$[M + H]^+$) calcd. for $C_{15}H_{17}O_6$, 293.1020, found 293.1040.

Penilactone D (**4**): Colorless solid; $[\alpha]_D^{20}$ = -15.9 (*c* 0.20, MeOH); CD (MeOH) λ_{max} ($\Delta\varepsilon$) 280 (-1.2), 242 (-3.0), 211 (+4.9) nm; HRMS (m/z): (ESI/$[M + H]^+$) calcd. for $C_{16}H_{17}O_8$, 337.0918, found 337.0932.

Clavatol (**5**): Colorless solid; HRMS (m/z): (ESI/$[M + H]^+$) calcd. for $C_{10}H_{13}O_3$, 181.0859, found 181.0860.

(*R*)-5-Methyltetronic acid (**7**): Yellow solid; ^{1}H NMR (400 MHz, DMSO-*d6*) δ 12.60 (s, 1H, 4-OH), 4.87 (s, 1H, H-3), 4.85 (q, *J* = 6.7 Hz, 1H, H-5), 1.33 (d, *J* = 6.7 Hz, 3H, H-6); $[\alpha]_D^{20}$ = -22.8 (*c* 0.5, H_2O); CD (H_2O) λ_{max} ($\Delta\varepsilon$) 309 (-9.3), 247 (+19.4) nm; HRMS (m/z): (ESI/$[M + H]^+$) calcd. for $C_5H_7O_3$, 115.0390, found 115.0369.

(*S*)-5-carboxylmethyltetronic acid (**8**): Yellow solid; ^{1}H NMR (500 MHz, CD_3OD) δ 5.18 (dd, *J* = 8.8, 3.6 Hz, 1H, H-5), 2.94 (dd, *J* = 16.5, 3.6 Hz, 1H, H-6a), 2.53 (dd, *J* = 16.5, 8.8 Hz, 1H, H-6b); $[\alpha]_D^{20}$ = -0.8 (*c* 1.4, MeOH). HRMS (m/z): (ESI/$[M + H]^+$) calcd. for $C_6H_7O_5$, 159.0288, found 159.0272.

Hydroxyclavatol (**9**): Colorless crystal; HRMS (m/z): (ESI/$[M + Na]^+$) calcd. for $C_{10}H_{12}NaO_4$, 219.0628, found 219.0626. Crystallographic data for **9** (Cu Ka radiation) has been deposited in the Cambridge Crystallographic Data Centre with the deposition number CCDC 1883090.

Hydroxyclavatol methyl ether (**10**): Colorless solid; HRMS (m/z): (ESI/$[M + Na]^+$) calcd. for $C_{11}H_{14}NaO_4$, 233.0784, found 233.0778.

Terrestric acid (**11**): Yellow oil; $[\alpha]_D^{20}$ = +37.1 (*c* 0.80, MeOH); CD (MeOH) λ_{max} (Δε) 282 (+1.0), 234 (+2.8), 212 (+8.2) nm; HRMS (m/z): (ESI/$[M + H]^+$) calcd. for $C_{11}H_{15}O_4$, 211.0965, found 211.1003.

Hydroxyclavatol ethyl ether (**12**): Colorless solid; HRMS (m/z): (ESI/$[M + Na]^+$) calcd. for $C_{12}H_{16}NaO_4$, 247.0941, found 247.0959.

Crustosic acid (**13**): Yellow oil; $[\alpha]_D^{20}$ = -164.1 (*c* 0.50, MeOH); CD (MeOH) λ_{max} (Δε) 272 (-11.2), 207 (-12.4) nm; HRMS (m/z): (ESI/$[M + H]^+$) calcd. for $C_{12}H_{15}O_6$, 255.0863, found 255.0876.

Supplementary Tables

Table S1. Strains used in this study

Strains	Genotype
Wild type	*Penicillium crustosum* PRB-2
Δ*claD*	Δ*claD*::*hph* in *P. crustosum* PRB-2
Δ*claF*	Δ*claF*::*hph* in *P. crustosum* PRB-2
Δ*claJ*	Δ*claJ*::*hph* in *P. crustosum* PRB-2
Δ*traA*	Δ*traA*::*hph* in *P. crustosum* PRB-2
Δ*traB*	Δ*traB*::*hph* in *P. crustosum* PRB-2
Δ*traD*	Δ*traD*::*hph* in *P. crustosum* PRB-2
Δ*traE*	Δ*traE*::*hph* in *P. crustosum* PRB-2
Δ*traF*	Δ*traF*::*hph* in *P. crustosum* PRB-2
Δ*traH*	Δ*traH*::*hph* in *P. crustosum* PRB-2
Aspergillus nidulans LO8030[2,3]	*pyroA4*, *riboB2*, *pyrG89*, *nkuA::argB*, sterigmatocystin cluster (*AN7804-AN7825*)Δ, emericellamide cluster (*AN2545-AN2549*)Δ, asperfuranone cluster (*AN1039-AN1029*)Δ, monodictyphenone cluster (*AN10023-AN10021*)Δ, terrequinone cluster (*AN8512-AN8520*)Δ, austinol cluster part 1 (*AN8379-AN8384*)Δ, austinol cluster part 2 (*AN9246-AN9259*)Δ, F9775 cluster (*AN7906-AN7915*)Δ, asperthecin cluster (*AN6000-AN6002*)Δ
JF10	pYH- wA -pyrG in *A. nidulans* LO8030
JF11	*gpdA::claF::AfpyrG* in *A. nidulans* LO8030

Table S2. Plasmids used and constructed in this study

Plasmids	Description
pESC-URA	*Saccharomyces cerevisiae* shuttle vector.
pUChph	vector with hygromycin B (*hph*) resistance originate.
pET28a(+)	vector with T7 promoter, 6xHis tag, T7 terminator, kanamycin resistance.
p5HY	Two-third of the *hph* resistance gene at the 5´-end, originated from the pUChph and inserted into pESC-URA. For gene replacement using *hph* as selection marker.
p3YG	Two-third of the *hph* resistance gene at the 3´-end, originated from the pUChph and inserted into pESC-URA. For gene replacement using *hph* as selection marker.
pJF19 (p5HY-*claD*)	a 1012 bp US PCR fragment of *claD* from genomic DNA of *P. crustosum* PRB-2 inserted in p5HY.
pJF20 (p3YG-*claD*)	a 1008 bp DS PCR fragment of *claD* from genomic DNA of *P. crustosum* PRB-2 inserted in p3YG.
pJF40 (p5HY-*claF*)	a 1560 bp US PCR fragment of *claF* from genomic DNA of *P. crustosum* PRB-2 inserted in p5HY.
pJF41 (p3YG-*claF*)	a 1426 bp DS PCR fragment of *claF* from genomic DNA of *P. crustosum* PRB-2 inserted in p3YG.
pJF21 (p5HY-*claJ*)	a 1367 bp US PCR fragment of *claJ* from genomic DNA of *P. crustosum* PRB-2 inserted in p5HY.
pJF22 (p3YG-*claJ*)	a 1259 bp DS PCR fragment of *claJ* from genomic DNA of *P. crustosum* PRB-2 inserted in p3YG.
pJF38 (p5HY-*traA*)	a 1500 bp US PCR fragment of *traA* from genomic DNA of *P. crustosum* PRB-2 inserted in p5HY.
pJF39 (p3YG-*traA*)	a 1496 bp DS PCR fragment of *traA* from genomic DNA of *P. crustosum* PRB-2 inserted in p3YG.
pJF56 (p5HY-*traB*)	a 1388 bp US PCR fragment of *traB f*rom genomic DNA of *P. crustosum* PRB-2 inserted in p5HY.
pJF57 (p3YG-*traB*)	a 1067 bp DS PCR fragment of *traB* from genomic DNA of *P. crustosum* PRB-2 inserted in p3YG.
pJF54 (p5HY-*traD*)	a 1170 bp US PCR fragment of *traD* from genomic DNA of *P. crustosum* PRB-2 inserted in p5HY.
pJF55 (p3YG-*traD*)	a 1139 bp DS PCR fragment of *traD* from genomic DNA of *P. crustosum* PRB-2 inserted in p3YG.
pJF52 (p5HY-*traE*)	a 1130 bp US PCR fragment of *traE* from genomic DNA of *P. crustosum* PRB-2 inserted in p5HY.
pJF53 (p3YG-*traE*)	a 1027 bp DS PCR fragment of *traE* from genomic DNA of *P. crustosum* PRB-2 inserted in p3YG.
pJF50 (p5HY-*traF*)	a 977 bp US PCR fragment of *traF* from genomic DNA of *P. crustosum* PRB-2 inserted in p5HY.
pJF51 (p3YG-*traF*)	a 1031 bp DS PCR fragment of *traF* from genomic DNA of *P. crustosum* PRB-2 inserted in p3YG.
pJF48 (p5HY-*traH*)	a 1101 bp US PCR fragment of *traH* from genomic DNA of *P. crustosum* PRB-2 inserted in p5HY.
pJF49 (p3YG-*traH*)	a 1114 bp DS PCR fragment of *traH* from genomic DNA of *P. crustosum* PRB-2 inserted in p3YG.
pYH-wA-pyrG	*URA3*, *wA flanking*, *AfpyrG*, *Amp*
pJF18	*pYH-wA-claF*; a 8119 bp fragment of *claF* with its terminator from genomic DNA of *P. crustosum* PRB-2 inserted in *pYH-wA*
pJF37	pET-28a(+)-*claD*; a 1017 bp fragment of *claD* from cDNA of *P. crustosum* PRB-2 inserted in pET28a(+)

US: upstream; DS: downstream

Table S3. Primers used in this study

Primers	Sequence 5'-3'	Targeted amplification
P5HY-1	TGCGGCCGCCCTTTAGTGAGGGTTGAATTAGCTCTCCAAAGGGCG	Two-third of the *hph* resistance gene at the 5′-end from pUChph to construct p5HY
P5HY-2	CCTATAGTGAGTCGTATTACGGATCCAAGACCAATGCGGAGCATATAC	
P3YG-1	TGCGGCCGCCCTTTAGTGAGGGTTGAATTGATTCCGGAAGTGCTTGAC	Two-third of the *hph* resistance gene at the 3′-end from pUChph to construct p3YG
P3YG-2	CCTATAGTGAGTCGTATTACGGATCTCGCGTGGAGCCAAG	
5F-R	GCTGAAGTCGATTTGAGTCCAC	US of *hph* to verify 5F of *P. crustosum* mutant
3F-F	GCATTAATGCATTGGACCTCGC	DS of *hph* to verify 3F of *P. crustosum* mutant
claD-up-F	AAGAATTGTTAATTAAGAGCTCAGATCTGTAGAGCAGGCTGGCGGATAC	1012 bp US fragment of *claD* to construct pJF19
claD-up-R	AACCCTCACTAAAGGGCGGCCGCACTAGTGTCTTTCGCGGATGATAAAC	
claD-down-F	ATACGACTCACTATAGGGCCCGGGCGTCGACCTGGAAGGGGGAGCCTTG	1008 bp DS fragment of *claD* to construct pJF20
claD-down-R	GCTAGCCGCGGTACCAAGCTTACTCGAGCGGTGCTGGTGGTACCTATC	
claD-F	ATGCCTGTTCTAAGCAATCC	1017 bp partial fragment of *claD*
claD-R	TTAAATGGCATAACTCGCCGTC	
claD-5F-F	CTCGCAATCCATGGACGTG	US of *hph* to verify △*claD* mutant
claD-3F-R	GCGCTTTGGTTATTGCGAG	DS of *hph* to verify △*claD* mutant
claF-up-F	AAGAATTGTTAATTAAGAGCTCAGATCAGAGAACTGAGCTTTAGATTGG	1560 bp US fragment of *claF* to construct pJF40
claF-up-R	CCTCACTAAAGGGCGGCCGCACTAGCGATTGCAGCTATACCCG	
claF-down-F	ACTCACTATAGGGCCCGGGCGTCGAGCCTGATGGCCTATTGTAC	1426 bp DS of *claF* to construct pJF41
claF-down-R	TAGCCGCGGTACCAAGCTTACTCGAGATGCAGGATATACGTTTCCAC	
claF-F	GCGAATGACTGATGCAGTG	1845 bp partial fragment of *claF*
claF-R	GAAGTTCACTCGGCAGAGC	
claF-5F-F	CATCGCTATAGATGTCTGGTCC	US of *hph* to verify △*claF* mutant
claF-3F-R	CAACCCACAACTGGATCG	DS of *hph* to verify △*claF* mutant
claJ-up-F	GAATTGTTAATTAAGAGCTCAGATCTCTTGTGTAATGCCCAAATGCC	1367 bp US fragment of *claJ* to construct pJF21
claJ-up-R	CCCTCACTAAAGGGCGGCCGCACTAGTCCGTCATAGTTGAAGCGCAG	
claJ-down-F	CTCACTATAGGGCCCGGGCGTCGACATATTAAATTTCAGGTAGCACGAG	1259 bp DS fragment of *claJ* to construct pJF22
claJ-down-R	CTAGCCGCGGTACCAAGCTTACTCGAGGCTATTGCTAGGATGTCACGC	
claJ--F	ATGAAAGGTCCAATTGTCCGC	867 bp partial fragment of *claJ*
claJ-R	AAGGTATGGAAGCTTCTGGGC	
claJ-5F-F	CTAGTTAGCAGCACTCGTC	US of *hph* to verify △*claJ* mutant
claJ-3F-R	CTATAGCAGTGGTCTCAACGGC	DS of *hph* to verify △*claJ* mutant
traA-up-F	AAGAATTGTTAATTAAGAGCTCAGATCTTCGTGGTTTGTAACAACTGC	1500 bp US fragment of *traA* to construct pJF38
traA-up-R	CCTCACTAAAGGGCGGCCGCACTAGATCTTTTGAGGGTTATCTTACAGC	
traA-down-F	ACTCACTATAGGGCCCGGGCGTCGAGTTAGTTGTAGTAGCACTACTGC	1496 bp DS fragment of *traA* to construct pJF39
traA-down-R	TAGCCGCGGTACCAAGCTTACTCGACCACGTACCGTAAATATCTGG	

Table S3. Primers used in this study (continued)

traA-F	TGCATCTTGTAGAGCTCGC	1819 bp partial fragment of *traA*
traA-R	GAGGGCGGTTTTAGAATCAATTG	
traA-5F-F	GGACACACAGTTAAATGCAG	US of *hph* to verify △*traA* mutant
traA-3F-R	CCTAGGCCATGTTAGATTGC	DS of *hph* to verify △*traA* mutant
traB-up-F	GAATTGTTAATTAAGAGCTCAGATCTCTGACGAATGAGGCATTCAATG	1388 bp US fragment of *traB* to construct pJF56
traB-up-R	ACCCTCACTAAAGGGCGGCCGCACTAGCATGGCTTGACAGCGCTCTC	
traB-down-F	GACTCACTATAGGGCCCGGGCGTCGACGGGCCTCCCCTTGTCTATTC	1067 bp DS fragment of *traB* to construct pJF57
traB-down-R	CTAGCCGCGGTACCAAGCTTACTCGAGCGTCCGACGATCATGATCCC	
traB-F	GAATGCGTATTGCACTAGTATG	1037 bp partial fragment of *traB*
traB-R	CCAGTTATACCACGACACC	
traB-5F-F	CCTGCTGTACCTTCTGTATGC	US of *hph* to verify △*traB* mutant
traB-3F-R	GTGGCTACGGTTACCACTG	DS of *hph* to verify △*traB* mutant
traD-up-F	GAATTGTTAATTAAGAGCTCAGATCTGGCTCAGATCTTCCAGTGAAC	1170 bp US fragment of *traD* to construct pJF54
traD-up-R	CAACCCTCACTAAAGGGCGGCCGCACTAGGTTGCAGCTAGGTGGGTG	
traD-down-F	CTCACTATAGGGCCCGGGCGTCGACCTACCATACCTGCCTTTTCTGAC	1139 bp DS fragment of *traD* to construct pJF55
traD-down-R	GCTAGCCGCGGTACCAAGCTTACTCGAGGGACCGCTCTGCTCTCATAC	
traD--F	ATGAAAGTTTTGATTATTTTTGCCCACC	942 bp partial fragment of *traD*
traD-R	TCACGCTTCTTTGACGTCGG	
traD-5F-F	GGTAGAGCAGCGCGGTCTA	US of *hph* to verify △*traD* mutant
traD-3F-R	CAAAGGCTGAGCCAGAGACTC	DS of *hph* to verify △*traD* mutant
traE-up-F	GAATTGTTAATTAAGAGCTCAGATCTCCGCATATGCTTCAGCTGAC	1030 bp US fragment of *traE* to construct pJF52
traE-up-R	CCCTCACTAAAGGGCGGCCGCACTAGCAAATTATGCAGTGGTGCACG	
traE-down-F	CTCACTATAGGGCCCGGGCGTCGACGATAGTATGAGAGCAGAGCGGTC	1027 bp DS fragment of *traE* to construct pJF53
traE-down-R	GCTAGCCGCGGTACCAAGCTTACTCGAGGGCAGTATTCTGATGCCTGC	
traE-F	ATGGCCGCACCAGCACTTC	471 bp partial fragment of *traE*
traE-R	CTATTTGCCGAAAACTGCCCAG	
traE-5F-F	CAATGTTCCTTCTCCGTATCGGTC	US of *hph* to verify △*traE* mutant
traE-3F-R	CTGTTGACGCTGTACATGGG	DS of *hph* to verify △*traE* mutant
traF-up-F	GAAGAATTGTTAATTAAGAGCTCAGATCTCAACCGCATATCGCCAAG	977 bp US fragment of *traF* to construct pJF50
traF-up-R	CCCTCACTAAAGGGCGGCCGCACTAGCACGACAGCCTTTGTCCG	
traF-down-F	GACTCACTATAGGGCCCGGGCGTCGACAGCAATCGTCGATTTTGCAAAC	1031 bp DS of *traF* to construct pJF51
traF-down-R	CTAGCCGCGGTACCAAGCTTACTCGAGCGTATTCGGCCCCATTGAAAC	
traF-F	ATGACCTCCGGCACTGAG	1795 bp partial fragment of *traF*
traF-R	CTAATGCGCTGTAAACTTGCTC	
traF-5F-F	CAGCCAATCGAAGATCCTTGC	US of *hph* to verify △*traF* mutant
traF-3F-R	CATGTTTGCCTTGGAGCAGG	DS of *hph* to verify △*traF* mutant

Table S3. Primers used in this study (continued)

traH-up-F	GAATTGTTAATTAAGAGCTCAGATCTCCCATCCATGGTCCGATTGAG	1101 bp US fragment of *traH* to construct pJF48
traH-up-R	CCTCACTAAAGGGCGGCCGCACTAGGATTGCTTATGTGACGTGCTTTTG	
traH-down-F	CTCACTATAGGGCCCGGGCGTCGACCGTTACAGCCAAGACATTGATG	1114 bp DS fragment of *traH* to construct pJF49
traH-down-R	CTAGCCGCGGTACCAAGCTTACTCGAGCGCAGGACTCGACATGGATC	
traH-F	GCGAAGGTCATTGAGCAAGTG	1097 bp partial fragment of *traH*
traH-R	CACTACATACTGTGAATGCTATCACC	
traH-5F-F	GCGGTGGAGTTGACGGTAAG	US of *hph* to verify △*traH* mutant
traH-3F-R	GTCTCTCTCGCCCACCAC	DS of *hph* to verify △*traH* mutant
A.n-claF-For	TATTCATCTTCCCATCCAAGAACCTTTAATCATGCCGTCTGAGTCTTAC	DNA of *claF* with its 480 bp terminator from *P. crustosum* to construct pJF18
A.n-claF-Rev	CATATTTCGTCAGACACAGAATAACTCTCCATGTTATTAGGGACCATGG	
ClaD-28-For	GTGGACAGCAAATGGGTCGCGGATCCATGCCTGTTCTAAGCAATCCATC	1017 bp fragment of *claD* to construct pJF37
ClaD-28-Rev	CAAGCTTGTCGACGGAGCTCGAATTCTTAAATGGCATAACTCGCCGTCA	

US: upstream; DS: downstream

Table S4. Putative functions of the genes from clavatol gene cluster

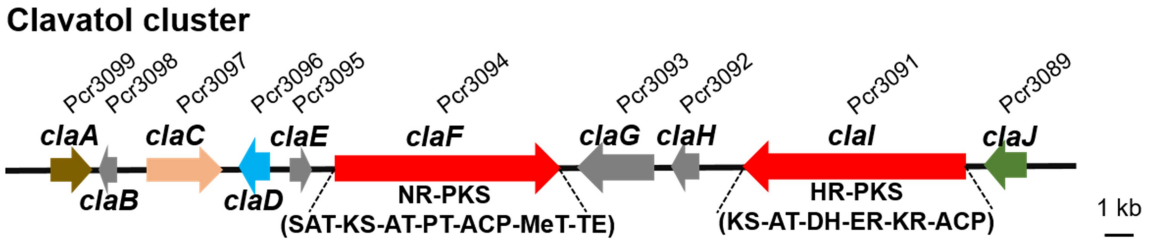

Protein	No. in genome	Size (AA)	Homologous known protein	Identity (%)	Putative function
ClaA	Pcr3099	476	C6 transcription factor (ANF07281) from *Byssochlamys fulva* [10]	53.1	transcription activator
ClaB	Pcr3098	214	hypothetical protein AUD_9432 (GAO90472) from *Aspergillus udagawae* [11]	38.8	hypothetical protein
ClaC	Pcr3097	878	enoyl-CoA hydratase/isomerase family protein (OCK96737) from *Cenococcum geophilum* [12]	53.6	enoyl-CoA hydratase/isomerase
ClaD	Pcr3096	338	Fe^{II}/2-oxoglutarate-dependent oxygenase CitB (ALI92653) from *Monascus ruber* M7 [13]	53.8	clavatol oxidase
ClaE	Pcr3095	265	citrinin biosynthesis protein CitA (ALI92654) from *Monascus ruber* M7 [13]	64.8	hypothetical protein
ClaF	Pcr3094	2587	citrinin polyketide synthase CitS (ALI92655) from *Monascus ruber* M7 [13]	57.7	clavatol synthase
ClaG	Pcr3093	743	hypothetical protein (XP_020058556.1) from *Aspergillus aculeatus* ATCC 16872	47.0	hypothetical protein
ClaH	Pcr3092	308	thiohydrolase in the brefeldin A biosynthesis (A0A068ACU9.1) from *Penicillium brefeldianum* [14]	44.0	hydrolase
ClaI	Pcr3091	2346	polyketide synthase (AFP89392) from *Cladosporium phlei* [15]	42.8	polyketide synthase
ClaJ	Pcr3089	438	cytochrome P450 monooxygenase (BAJ04372.1) from *Aspergillus oryzae*	42.0	cytochrome P450

Table S5. Putative functions of the genes from terrestric acid gene cluster

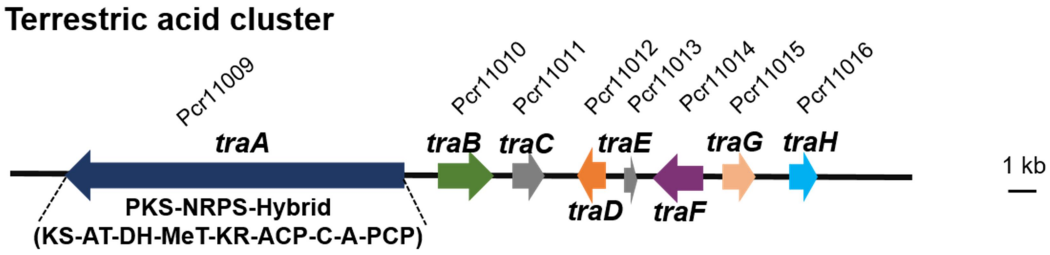

Protein	No. in genome	Size (AA)	homologous known protein	Identity (%)	Putative Function
TraA	Pcr11009	3856	NRPS/PKS hybrid enzyme (XP_001392496) from *Aspergillus niger* CBS 513.88 [16]	69.6	PKS-NRPS hybrid enzyme
TraB	Pcr11010	509	cytochrome P450 monooxygenase (XP_001392495) in toxin biosynthesis in *Aspergillus niger* CBS 513.88 [16]	65.5	cytochrome P450
TraC	Pcr11011	417	hypothetical protein (OQD61093) from *Penicillium polonicum*	81.0	hypothetical protein
TraD	Pcr11012	267	NAD(P)H dehydrogenase (AEO48230) from *Rhodospirillum rubrum* F11 [17]	63.4	flavodoxin family protein
TraE	Pcr11013	156	hypothetical protein (XP_001392493) from *Aspergillus niger* CBS 513.88 [16]	49.0	hypothetical protein
TraF	Pcr11014	482	MFS multidrug transporter (XP_001392492) from *Aspergillus niger* CBS 513.88 [16]	68.9	transporter
TraG	Pcr11015	364	enoyl reductase (XP_001392491) from *Aspergillus niger* CBS 513.88 [16]	68.9	enoyl reductase
TraH	Pcr11016	327	2-oxoglutarate-dependent oxygenase (XP_001392490) from *Aspergillus niger* CBS 513.88 [16]	66.0	2-oxoglutarate-dependent oxygenase

Table S6. ^{1}H NMR data of compounds **1** and **2**

Compound	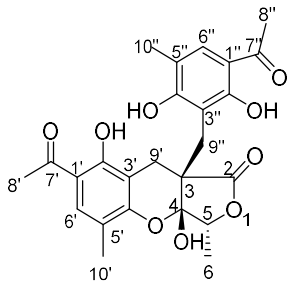	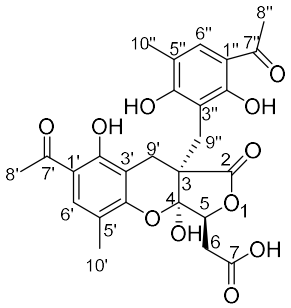
	Penilactone A (**1**, DMSO-d_6)	Penilactone B (**2**, DMSO-d_6)
Position	δ_H, multi., *J* in Hz	δ_H, multi., *J* in Hz
5	5.00, q, 6.4, 1H	5.22, dd, 9.6, 2.1, 1H
6	1.51, d, 6.4, 3H	3.18, t, 9.6, 1H
	-	2.66, dd, 16.9, 9.6, 1H
6´	7.57, s, 1H	7.59, s, 1H
8´	2.55, s, 3H	2.56, s, 3H
9´	2.97, d, 17.0, 1H	2.96, d, 17.4, 1H
	2.79, d, 17.0, 1H	2.82, d, 17.4, 1H
10´	2.13, s, 3H	2.13, s, 3H
6´´	7.61, s, 1H	7.62, s, 1H
8´´	2.52, s, 3H	2.53, s, 3H
9´´	3.25, d, 12.3, 1H	3.25, d, 13.8, 1H
	3.13, d, 12.3, 1H	3.17, d, 13.8, 1H
10´´	2.16, s, 3H	2.16, s, 3H
4-OH	8.15, s, 1H	8.32, s, 1H
2´-OH	12.82, s, 1H	12.81, s, 1H
2´´-OH	13.01, s, 1H	13.03, s, 1H
4´´-OH	9.78, s, 1H	9.84, s, 1H

Table S7. ^{1}H NMR data of compounds **3** and **4**

Compound	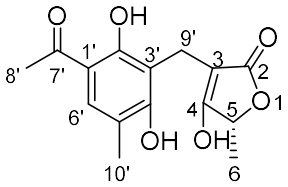	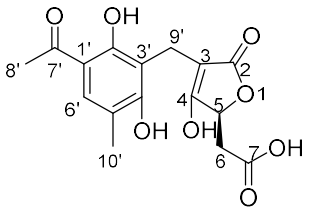
	Peniphenone D (**3**, $CDCl_3$)	Penilactone D (**4**, DMSO-d_6)
Position	δ_H, multi., *J* in Hz	δ_H, multi., *J* in Hz
5	4.83, q, 6.8, 1H	4.96, dd, 9.6, 3.0, 1H
6	1.46, d, 6.8, 3H	2.89, dd, 16.2, 3.0, 1H
	-	2.25, dd, 16.2, 9.6, 1H
6´	7.40, s, 1H	7.53, s, 1H
8´	2.56, s, 3H	2.52, s, 3H
9´	3.47, d, 15.1, 1H	3.41, d, 14.5, 1H
	3.42, d, 15.1, 1H	3.37, d, 14.5, 1H
10´	2.20, s, 3H	2.13, s, 3H
2´-OH	13.98, s, 1H	12.94, s, 1H

Table S8. ^{1}H NMR data of compounds **5, 10** and **12**

Compound	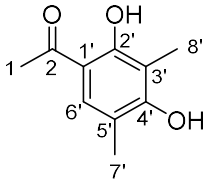 Clavatol (**5**)		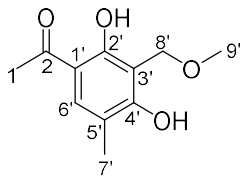 Hydroxyclavatol methyl ether (**10**, $CDCl_3$)	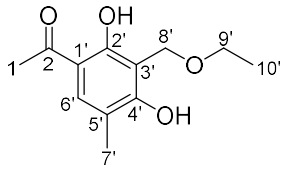 Hydroxyclavatol ethyl ether (**12**, $CDCl_3$)
Position	δ_H, multi., *J* in Hz ($CDCl_3$)	δ_H, multi., *J* in Hz (DMSO-*d6*)	δ_H, multi., *J* in Hz	δ_H, multi., *J* in Hz
1	2.56, s, 3H	2.56, s, 3H	2.54, s, 3H	2.54, s, 3H
6´	7.37, s, 1H	7.56, s, 1H	7.41, s, 1H	7.41, s, 1H
7´	2.14, s, 3H	2.05, s, 3H	2.16, s, 3H	2.16, s, 3H
8´	2.21, s, 3H	2.18, s, 3H	4.84, s, 2H	4.88, s, 2H
9´	-	-	3.50, s, 3H	3.67, q, 7.1, 2H
10´	-	-	-	1.31, t, 7.1, 3H
2´-OH	12.89, s, 1H	12.94, s, 1H	12.95, s, 1H	12.95, s, 1H
4´-OH	-	9.48, s, 1H	9.15, s, 1H	9.44, s, 1H

Table S9. NMR data of compound **9**

Compound	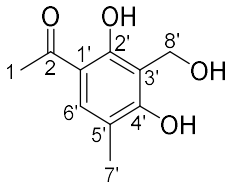 Hydroxyclavatol (**9**)	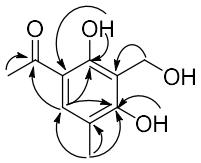		
Position	δ_H, multi., *J* in Hz ($CDCl_3$)	δ_H, multi., *J* in Hz (DMSO-d_6)	δ_C ($CDCl_3$)	Key HMBC correlations
1	2.53, s, 3H	2.53, s, 3H	26.4	C-2
2	-	-	203.0	
1´	-	-	112.6	
2´	-	-	159.8	
3´	-	-	110.3	
4´	-	-	162.4	
5´	-	-	117.2	
6´	7.40, s, 1H	7.61, s, 1H	131.9	C-2, C-2´, C-4´
7´	2.17, s, 3H	2.11, s, 3H	15.5	C-4´, C-5´, C-6´
8´	5.07, s, 2H	4.70, s, 2H	58.9	C-3´
2´-OH	12.93, s, 1H	12.98, s, 1H	-	C-1´, C-2´
4´-OH	9.13, s, 1H	10.23, s, 1H	-	C-4´
8´-OH	-	5.75, s, 1H	-	

Table S10. NMR data of **11** and **13**

Compound	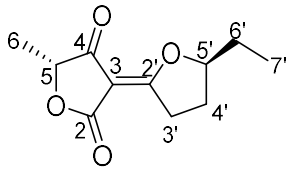 Terrestric acid (**11**, $CDCl_3$)	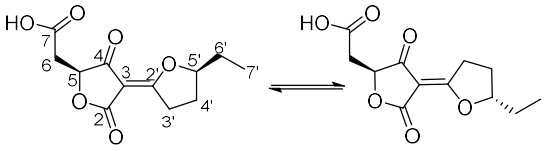 Crustosic acid (**13**, $CDCl_3$)	
Position	δ_H, multi., *J* in Hz	δ_H, multi., *J* in Hz	δ_C
2	-	-	167.5/170.7
3	-	-	95.2/95.6
4	-	-	197.4/193.8
5	4.61, q, 7.0, 1H	4.81, dd, 6.4, 4.0, 1H	78.6/78.3
6	1.46, d, 7.0, 3H	3.00, ddd, 17.2, 9.3, 4.0, 1H	35.8/35.7
	-	2.82, td, 17.2, 6.4, 1H	-
7	-	-	173.8/173.6
2´	-	-	187.6/187.0
3´	3.60, ddd, 20.1, 9.3, 1.5, 1H	3.58, ddd, 19.9, 9.3, 4.1, 1H	33.9/34.2
	3.27, ddd, 20.1, 9.7, 8.5, 1H	3.26, ddd, 19.9, 9.6, 9.0, 1H	-
4´	2.36, m, 1H	2.37, m, 1H	27.7/27.7
	1.87, m, 1H	1.86, m, 1H	-
5´	4.93, m, 1H	4.94, m, 1H	93.0/93.6
6´	1.96, m, 1H	1.94, m, 1H	26.5/26.4
	1.79, m, 1H	1.77, m, 1H	-
7´	1.06, t, 7.5, 3H	1.04, t, 7.4, 3H	9.6/9.5
7-OH	-	8.59, s, 1H	-

Table S11. Crystal data and structure refinement of **9**

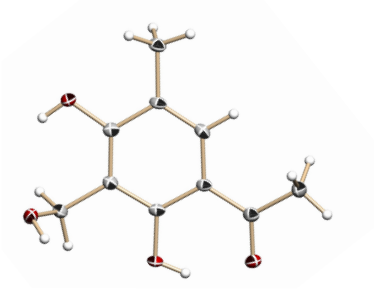

Perspective drawing of the X-ray structure of **9**

Name	Hydroxyclavatol	
Identification code	CCDC 1883090	
Empirical formula	$C_{10}H_{12}O_4$	
Formula weight	196.20	
Temperature	113(2) K	
Wavelength	1.54178 Å	
Crystal system	Triclinic	
Space group	P -1	
Unit cell dimensions	a = 7.7553(9) Å	α= 77.750(5)°.
	b = 8.2119(10) Å	β= 69.610(4)°.
	c = 8.3575(10) Å	γ= 66.847(5)°.
Volume	456.97(10) $Å^3$	
Z	2	
Density (calculated)	1.426 mg/m^3	
Absorption coefficient	0.929 mm^{-1}	
F(000)	208	
Crystal size	0.900 x 0.500 x 0.200 mm^3	
Theta range for data collection	5.669 to 64.115°.	
Index ranges	-8<=h<=9, -9<=k<=9, -9<=l<=9	
Reflections collected	3969	
Independent reflections	1409 [R(int) = 0.0585]	
Completeness to theta = 64.115°	92.6%	
Refinement method	Full-matrix least-squares on F^2	
Data / restraints / parameters	1409 / 8 / 134	
Goodness-of-fit on F^2	1.589	
Final R indices [I>2sigma(I)]	R1 = 0.0535, wR2 = 0.1801	
R indices (all data)	R1 = 0.0542, wR2 = 0.1834	
Extinction coefficient	0.044(8)	
Largest diff. peak and hole	0.391 and -0.328 $e.Å^{-3}$	

Supplementary Figures

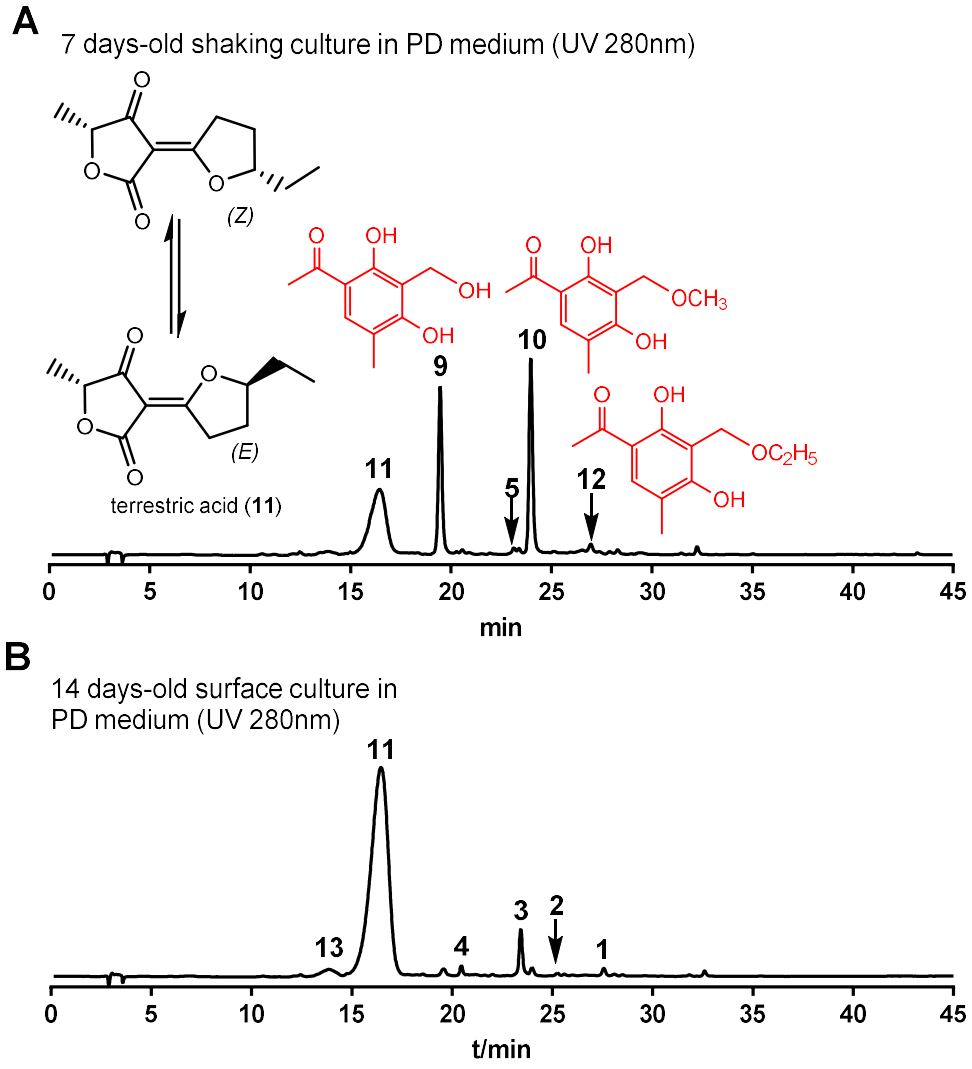

Figure S1. HPLC analysis of secondary metabolite profiles of *P. crustosum*
(A) in 7 days-old PD liquid shaking culture at 230 rpm. (B) in 14 days-old PD liquid surface culture. Absorptions at 280 nm are illustrated.

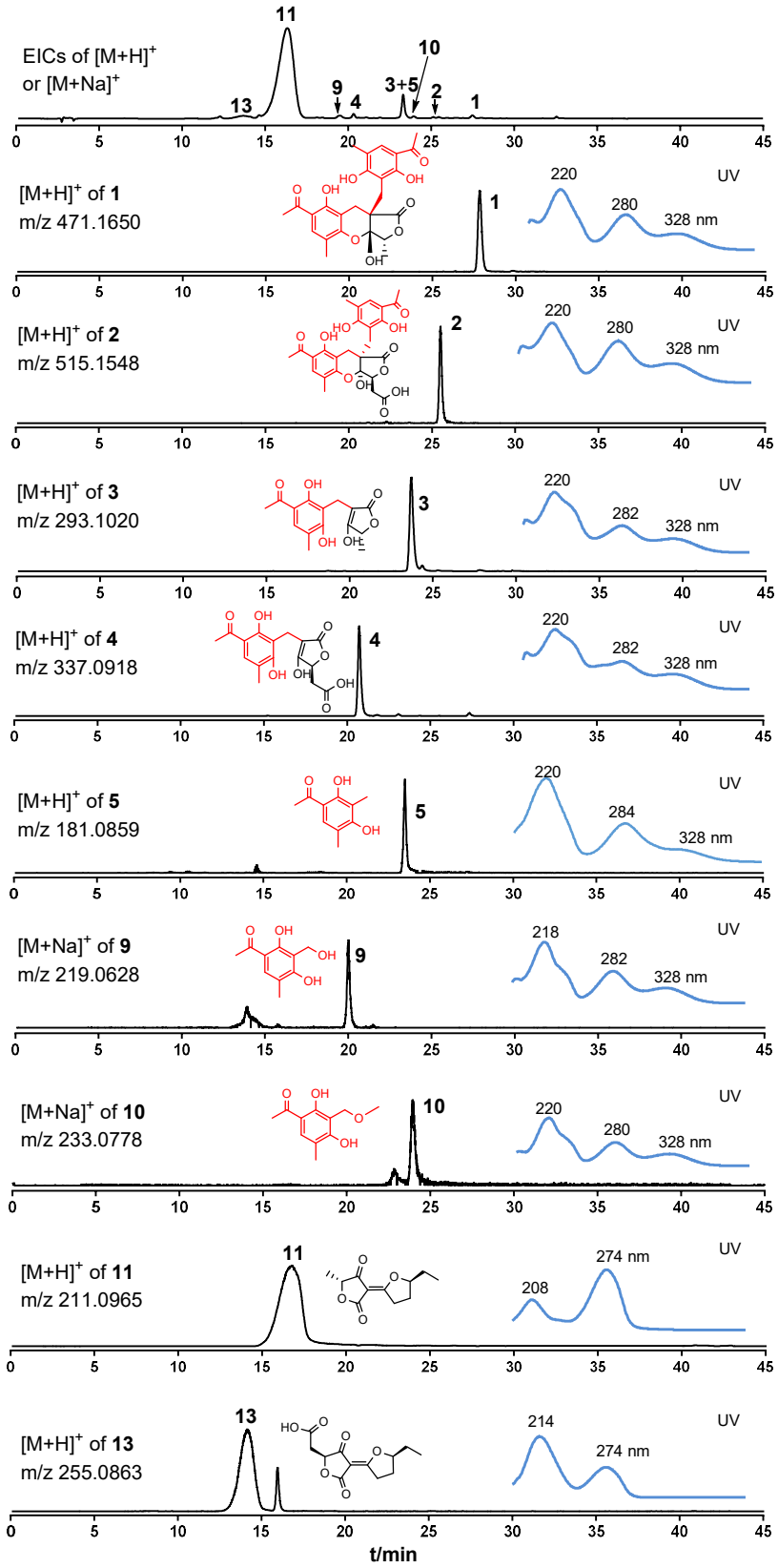

Figure S2. LC-MS analysis of secondary metabolites from a 14 days-old liquid PD surface culture of *P. crustosum*

EICs of **1**–**5**, **9**, **10**, **11**, and **13** are selected with a tolerance range of ± 0.005. UV spectra are shown in blue.

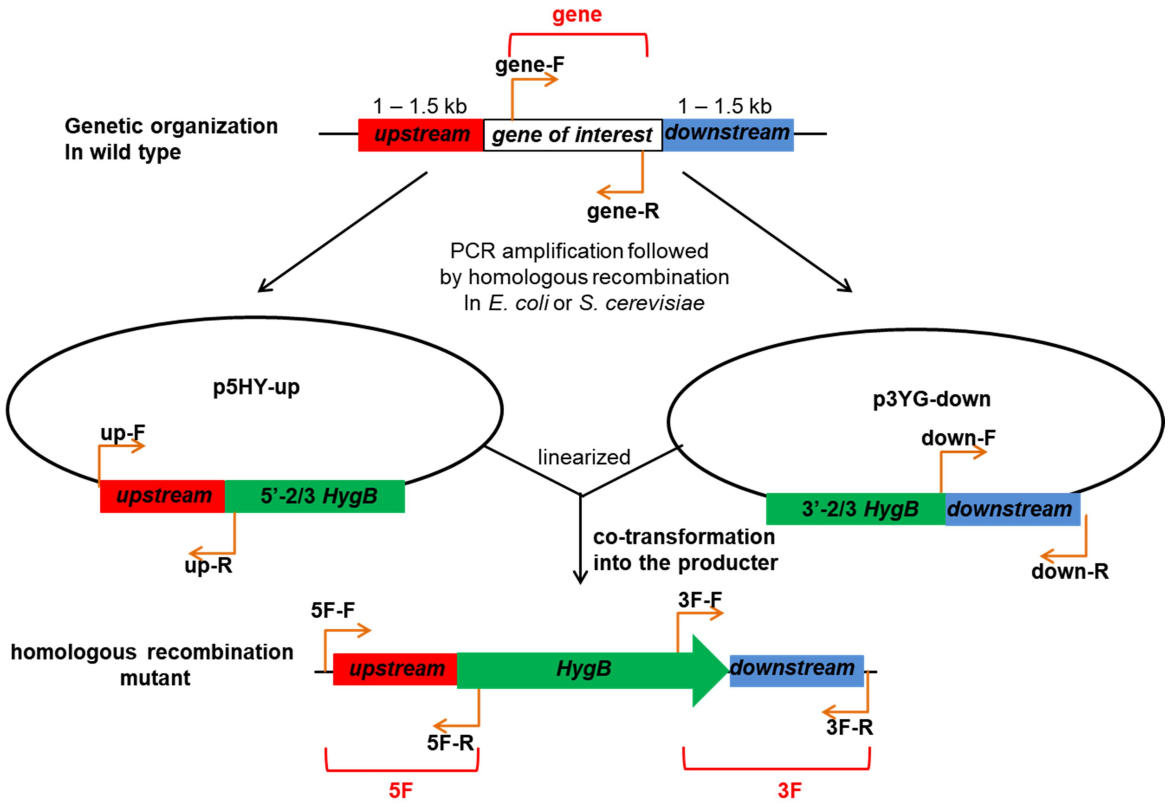

Figure S3. Schematic representation of the gene deletion strategy in *P. crustosum*

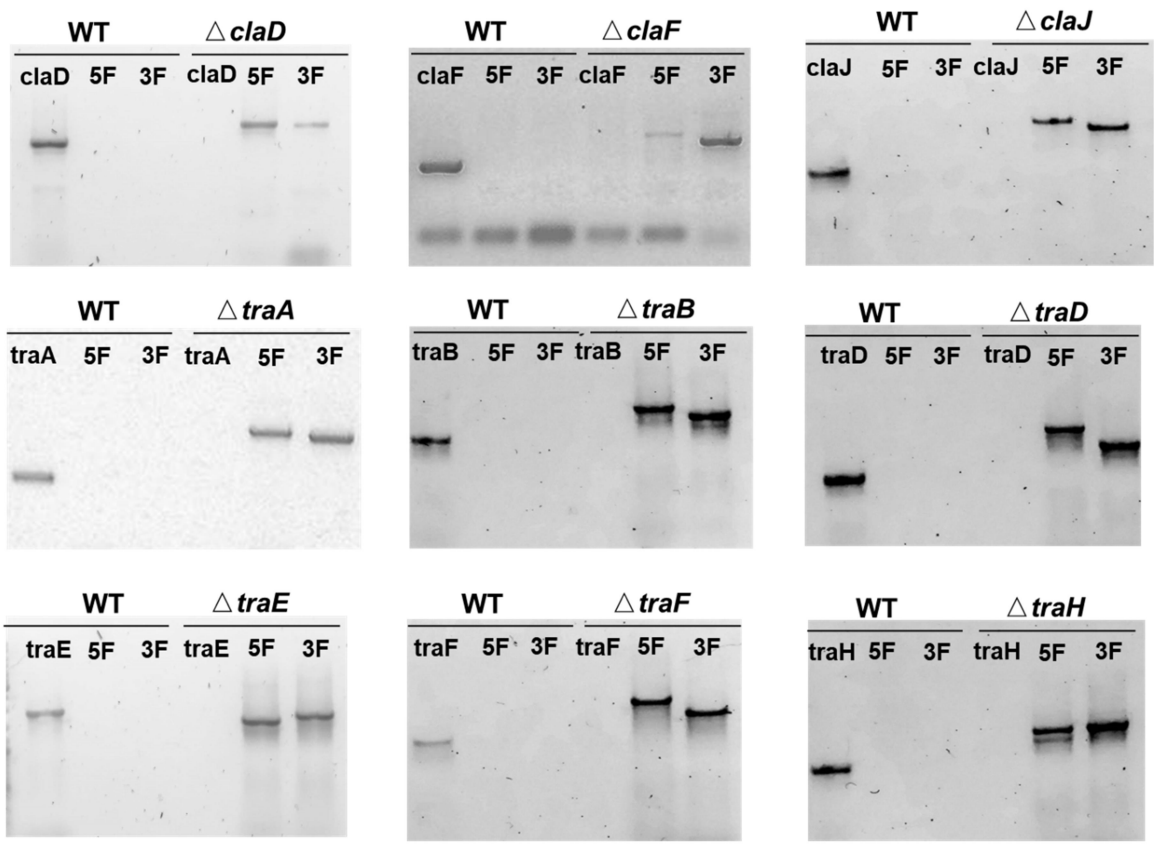

Figure S4. PCR verification of deletion mutants of *P. crustosum*
PCR amplification for three different fragments from genomic DNA of WT and deletion mutants was used to prove the presence/absence of the gene of interest and its site specific integration with the help of up- and downstream regions. The PCR primers are given in Table S3.

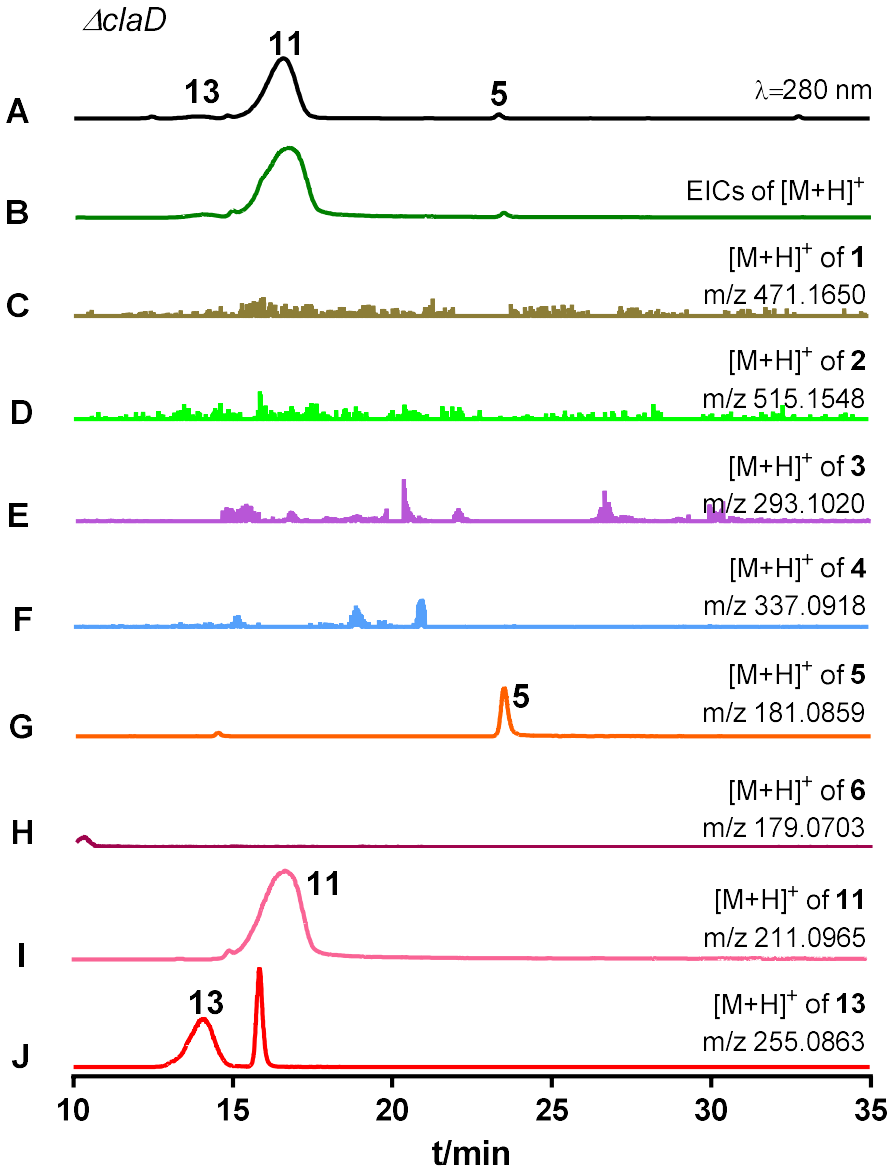

Figure S5. LC-MS analysis of the metabolite profile of the △*claD*-mutant Absorptions at 280 nm are illustrated in black (A). EICs in dark green (B) refer total $[M+H]^+$ ions of **1**–**6**, **11**, and **13** with a tolerance range of ± 0.005, and in other colors refer $[M+H]^+$ ions of **1**–**6**, **11**, and **13** (C−J), respectively.

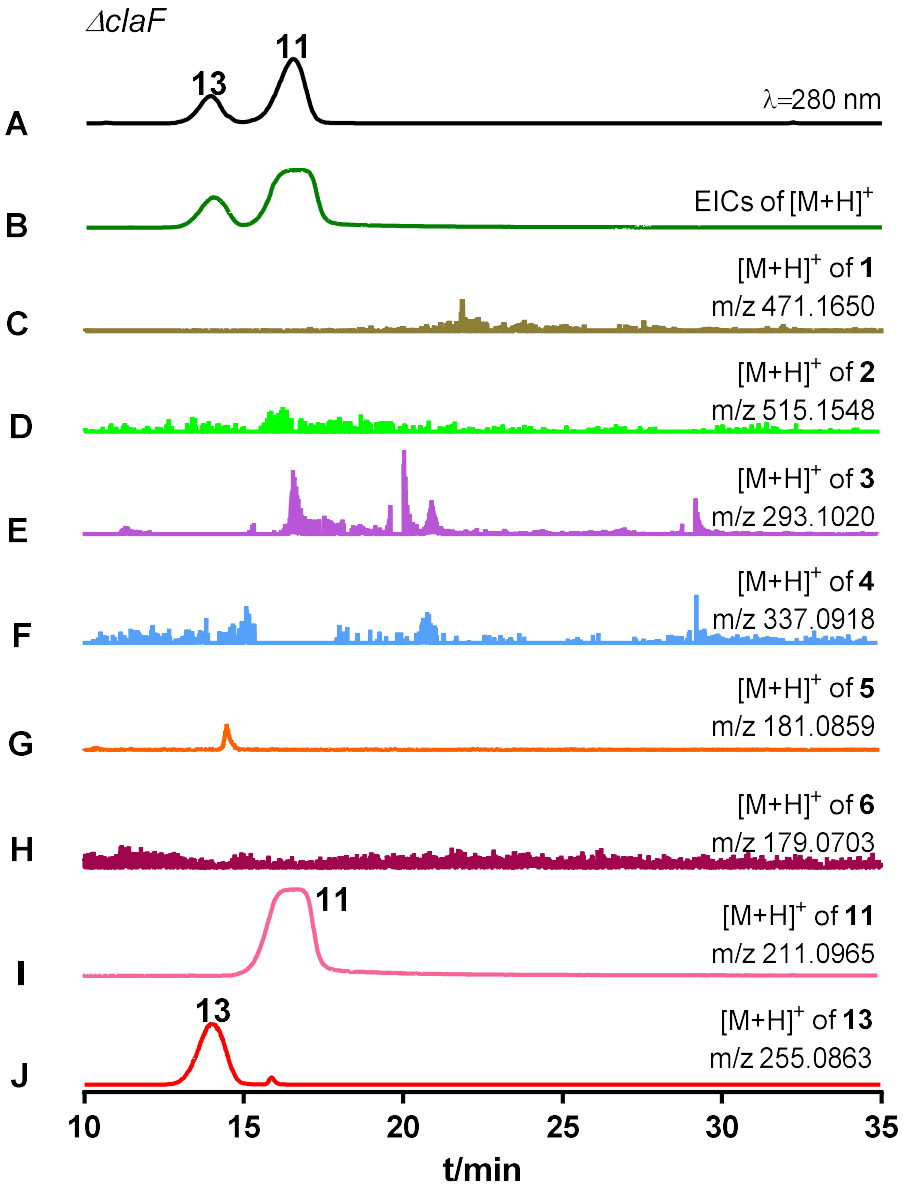

Figure S6. LC-MS analysis of the metabolite profile of the △*claF*-mutant
Absorptions at 280 nm are illustrated in black (A). EICs in dark green (B) refer total $[M+H]^+$ ions of **1**–**6**, **11**, and **13** with a tolerance range of ± 0.005, and in other colors refer $[M+H]^+$ ions of **1**–**6**, **11**, and **13** (C-J), respectively.

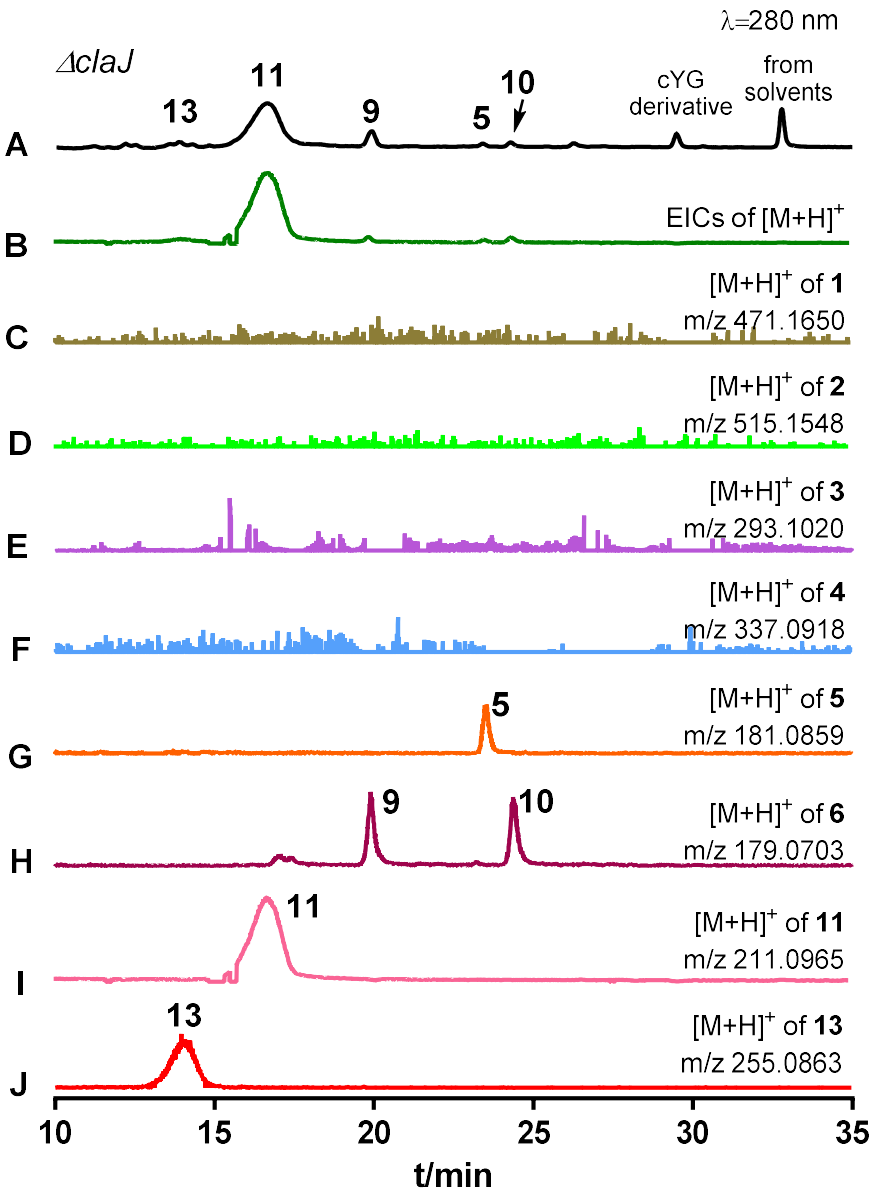

Figure S7. LC-MS analysis of the metabolite profile of the △*claJ*-mutant

Absorptions at 280 nm are illustrated in black (A). EICs in dark green (B) refer total $[M+H]^+$ ions of **1**–**6**, **11**, and **13** with a tolerance range of ± 0.005, and in other colors refer $[M+H]^+$ ions of **1**–**6**, **11**, and **13** (C-J), respectively. The peak at 29.3 min, which is very likely derived from the cyclodipeptide of tyrosine and glycine (cYG), was isolated and identified as the enantiomer of *cis*-Bis(methylthio)silvatin[18] (data not shown). The peak at 33.5 min was also detected in the control chromatogram with methanol as a sample.

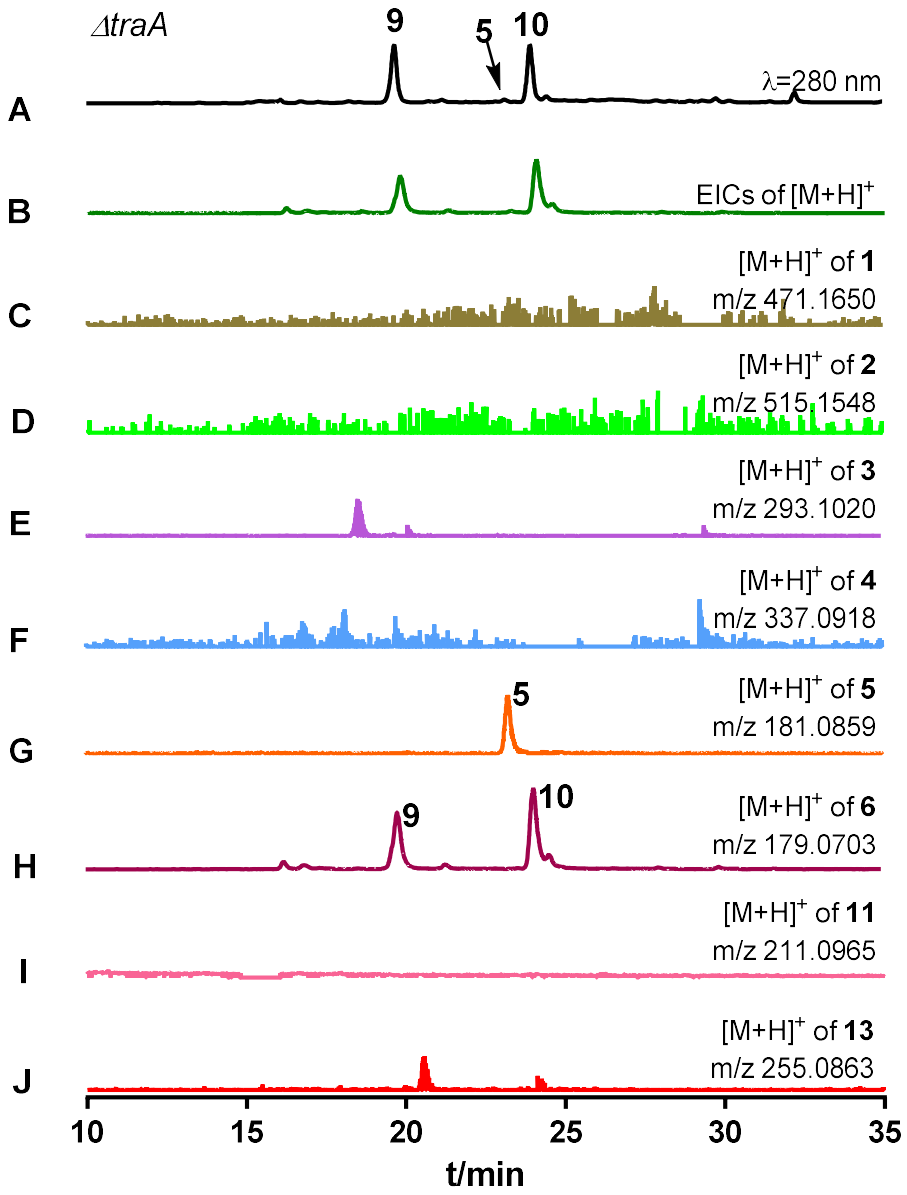

Figure S8. LC-MS analysis of the metabolite profile of the △*traA*-mutant Absorptions at 280 nm are illustrated in black (A). EICs in dark green (B) refer total $[M+H]^+$ ions of **1**–**6**, **11**, and **13** with a tolerance range of ± 0.005, and in other colors refer $[M+H]^+$ ions of **1**–**6**, **11**, and **13** (C−J), respectively.

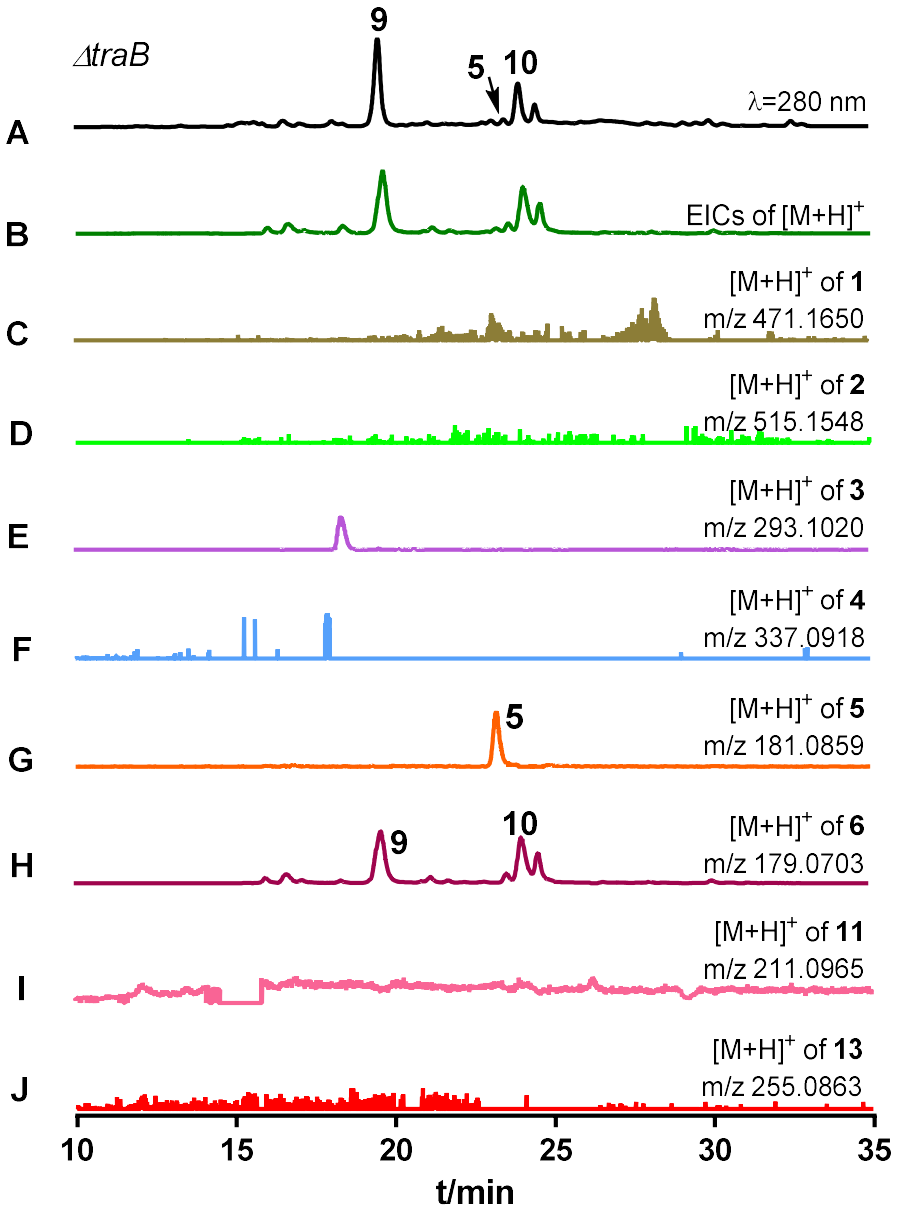

Figure S9. LC-MS analysis of the metabolite profile of the △*traB*-mutant
Absorptions at 280 nm are illustrated in black (A). EICs in dark green (B) refer total $[M+H]^+$ ions of **1**–**6**, **11**, and **13** with a tolerance range of ± 0.005, and in other colors refer $[M+H]^+$ ions of **1**–**6**, **11**, and **13** (C−J), respectively.

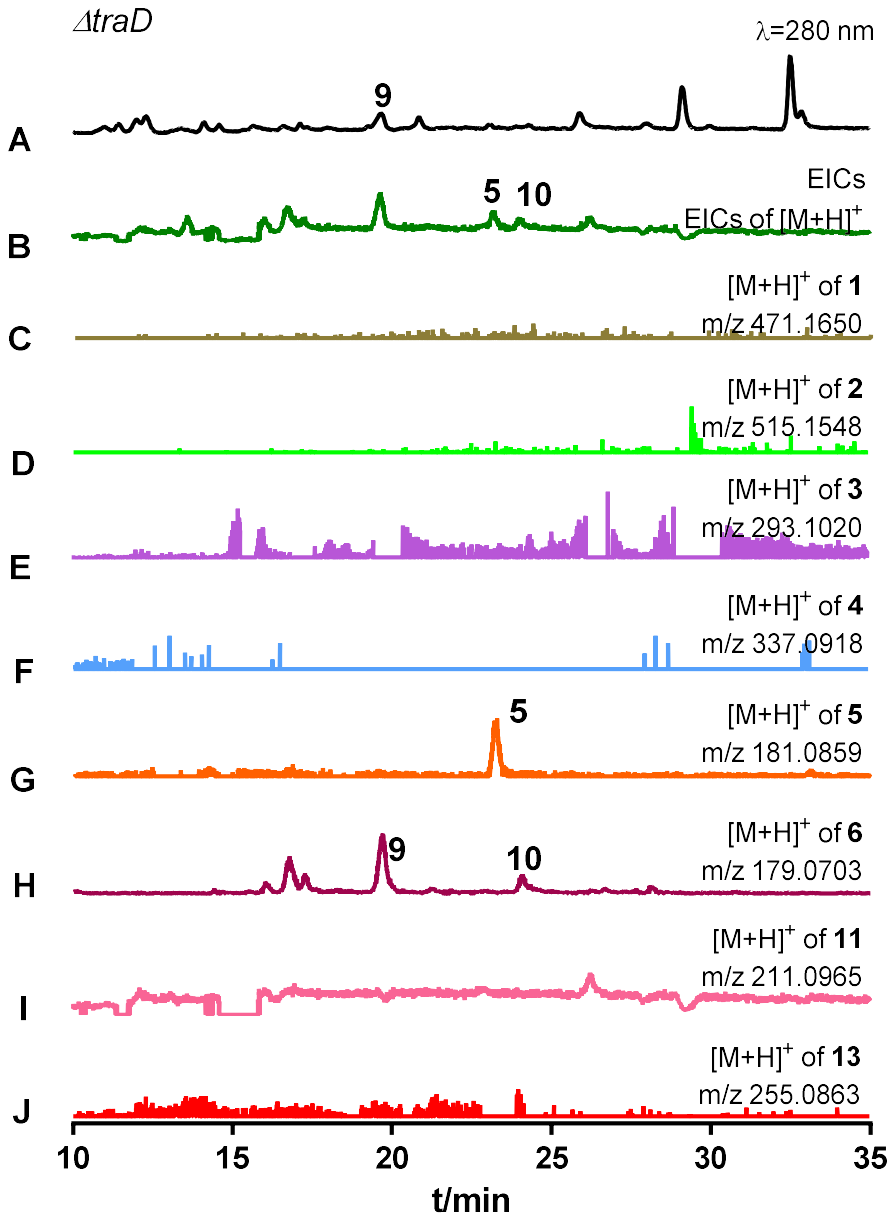

Figure S10. LC-MS analysis of the metabolite profile of the △*traD*-mutant Absorptions at 280 nm are illustrated in black (A). EICs in dark green (B) refer total $[M+H]^+$ ions of **1**–**6**, **11**, and **13** with a tolerance range of ± 0.005, and in other colors refer $[M+H]^+$ ions of **1**–**6**, **11**, and **13** (C−J), respectively.

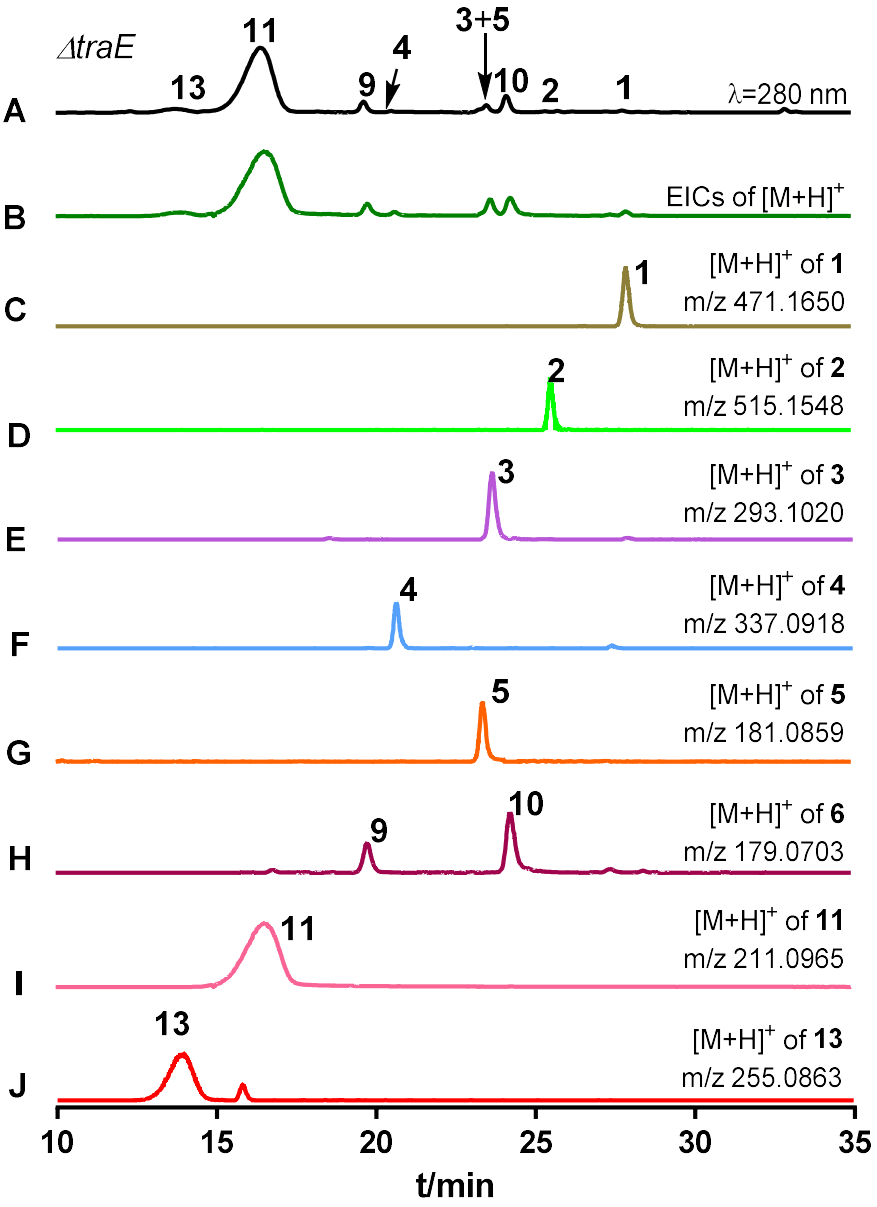

Figure S11. LC-MS analysis of the metabolite profile of the △*traE*-mutant
Absorptions at 280 nm are illustrated in black (A). EICs in dark green (B) refer total $[M+H]^+$ ions of **1**–**6**, **11**, and **13** with a tolerance range of ± 0.005, and in other colors refer $[M+H]^+$ ions of **1**–**6**, **11**, and **13** (C−J), respectively.

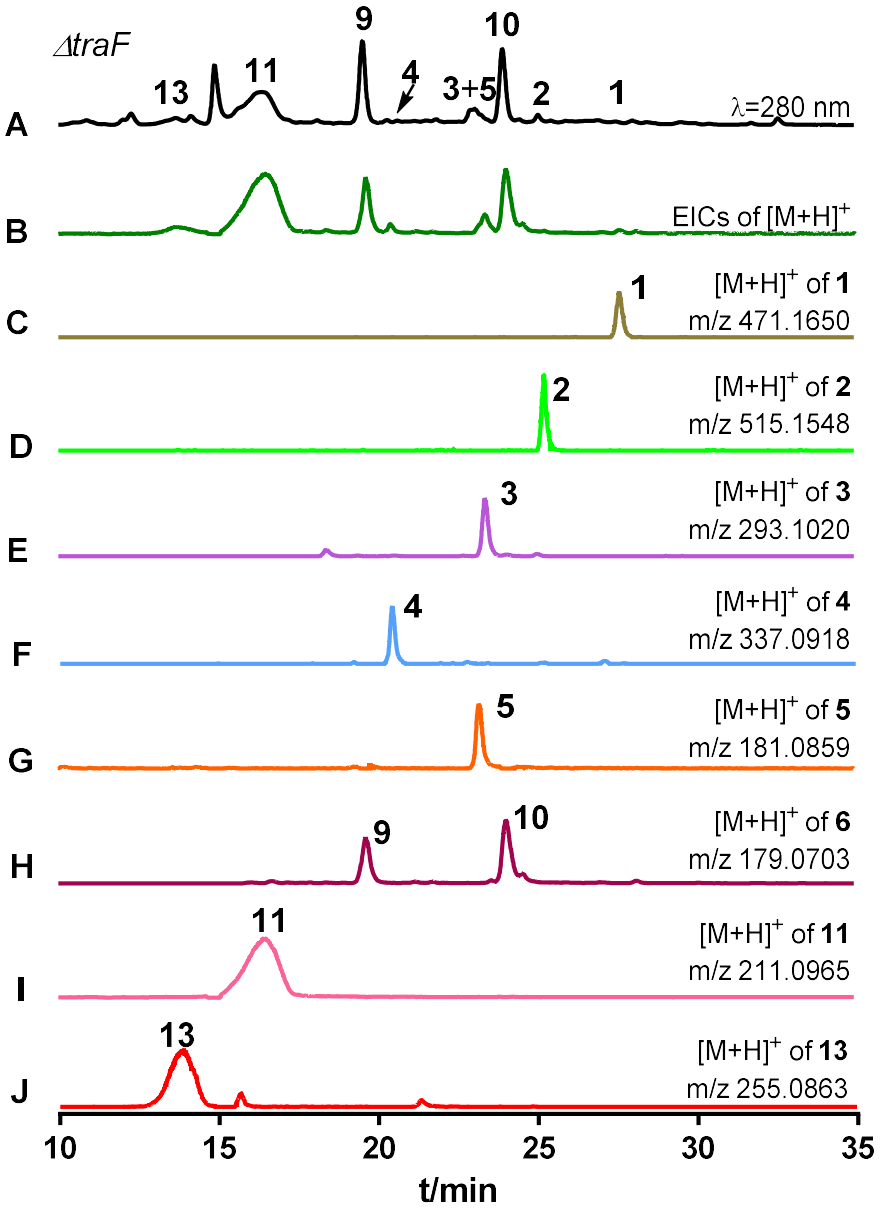

Figure S12. LC-MS analysis of the metabolite profile of the △*traF*-mutant Absorptions at 280 nm are illustrated in black (A). EICs in dark green (B) refer total $[M+H]^+$ ions of **1**–**6**, **11**, and **13** with a tolerance range of ± 0.005, and in other colors refer $[M+H]^+$ ions of **1**–**6**, **11**, and **13** (C−J), respectively.

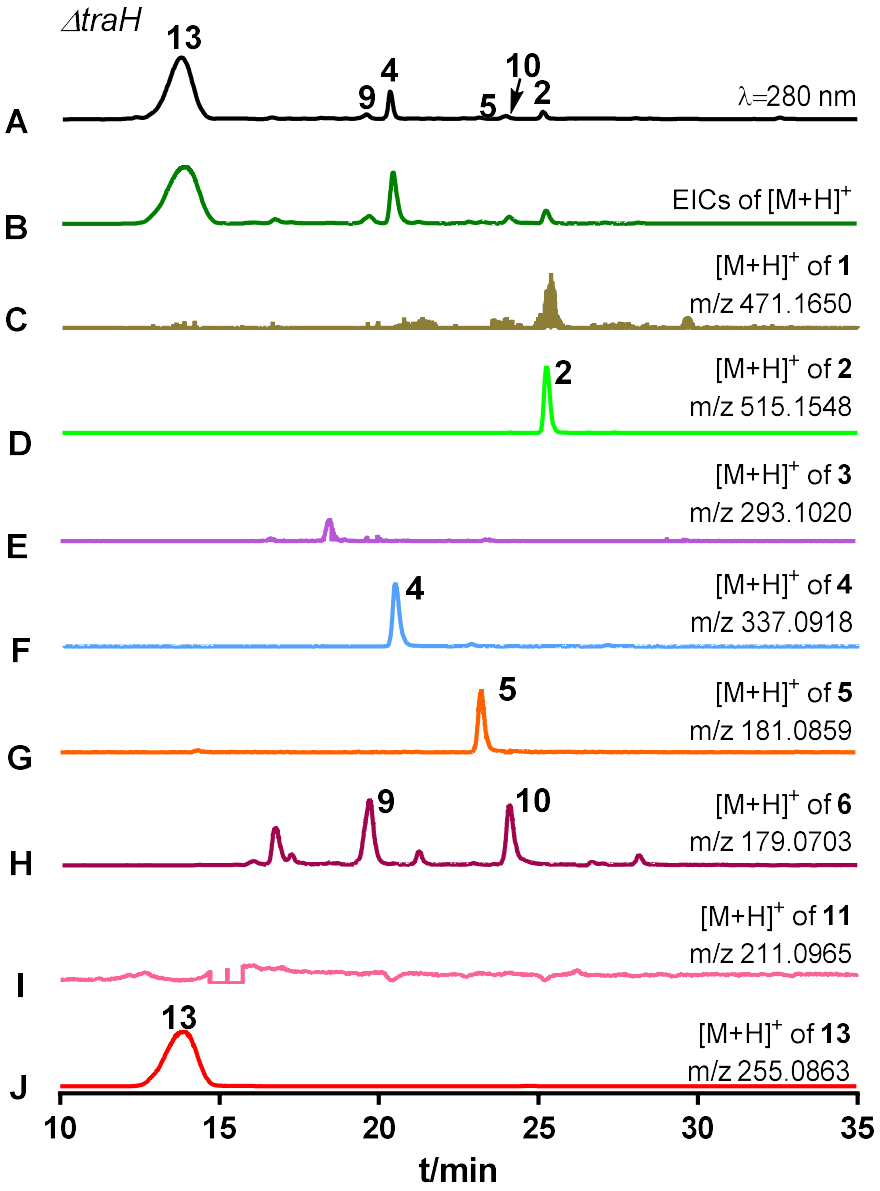

Figure S13. LC-MS analysis of the metabolite profile of the △*traH*-mutant Absorptions at 280 nm are illustrated in black (A). EICs in dark green (B) refer total $[M+H]^+$ ions of **1**–**6**, **11**, and **13** with a tolerance range of ± 0.005, and in other colors refer $[M+H]^+$ ions of **1**–**6**, **11**, and **13** (C−J), respectively.

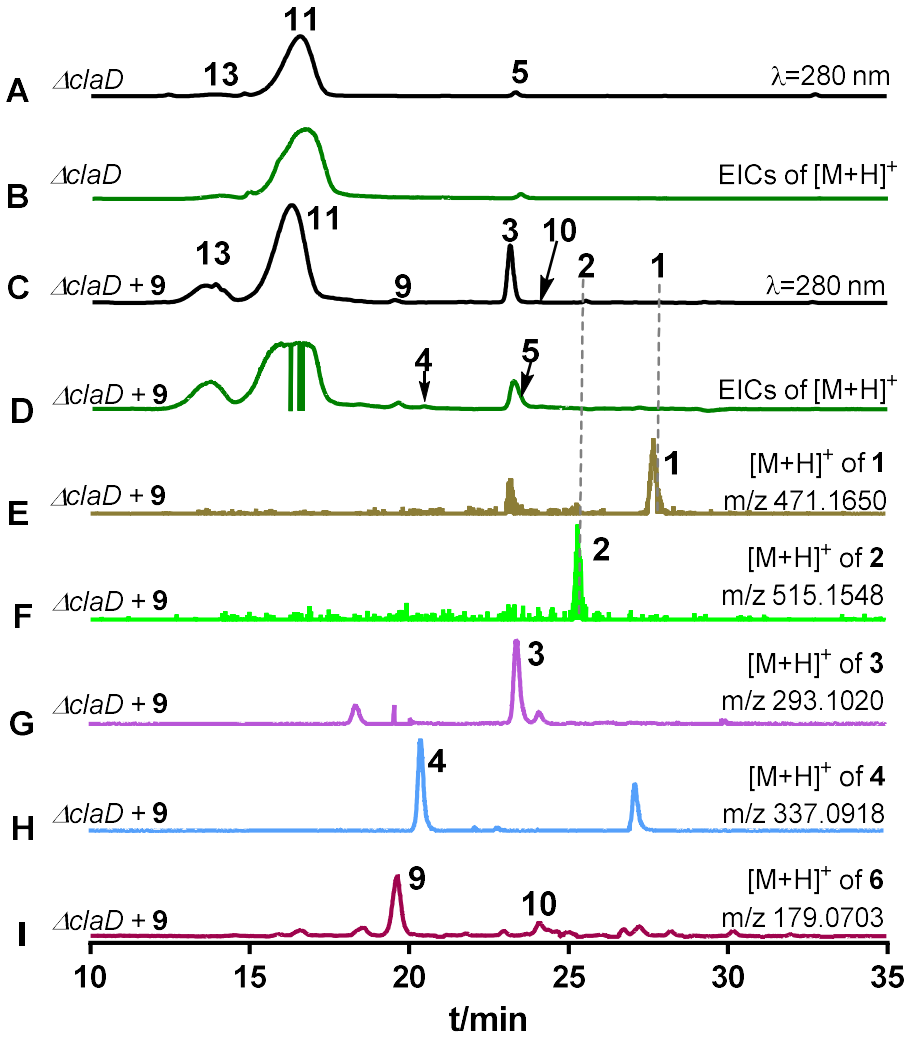

Figure S14. LC-MS analysis of the metabolite profile of the △*claD*-mutant with and without feeding with **9**

Absorptions at 280 nm are illustrated in black (A and C). EICs in dark green (B and D) refer total $[M+H]^+$ ions of **1**–**6**, **11**, and **13** with a tolerance range of ± 0.005, and in other colors refer $[M+H]^+$ ions of **1**–**4** and **6** (E−I), respectively.

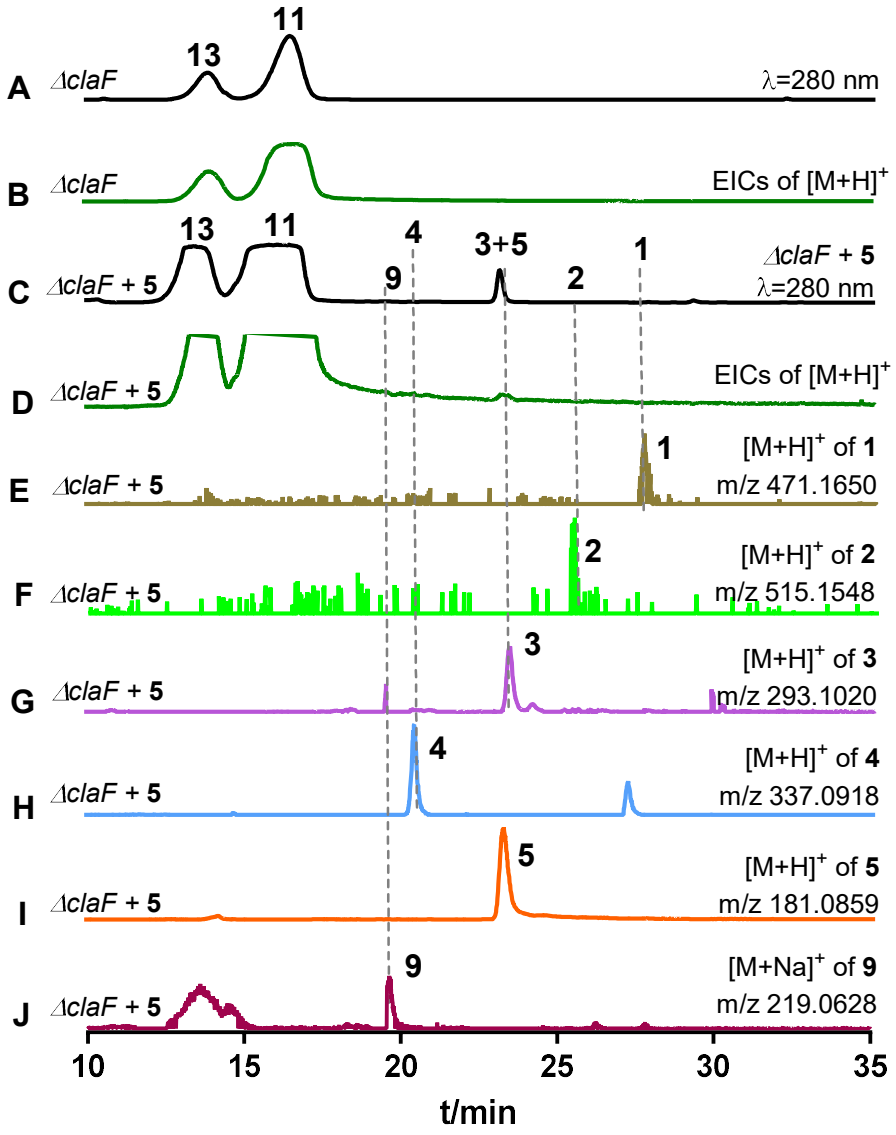

Figure S15. LC-MS analysis of the metabolite profile of the △*claF*-mutant with and without feeding with **5**

Absorptions at 280 nm are illustrated in black (A and C). EICs in dark green (B and D) refer total $[M+H]^+$ ions of **1**–**6**, **11**, and **13** with a tolerance range of ± 0.005, and in other colors refer $[M+H]^+$ ions of **1**–**5** (E−I) or $[M+Na]^+$ ion of **9** (J).

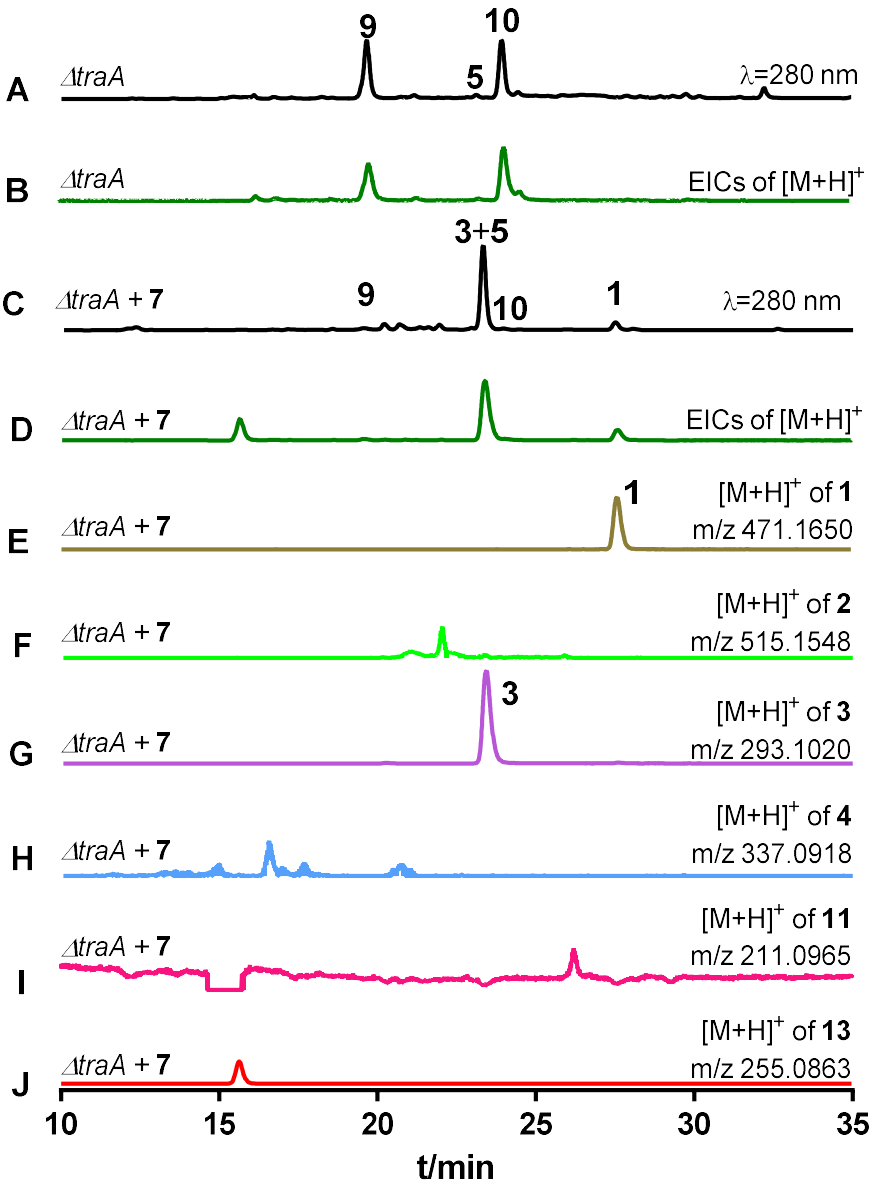

Figure S16. LC-MS analysis of the metabolite profile of the △*traA*-mutant with and without feeding with **7**

Absorptions at 280 nm are illustrated in black (A and C). EICs in dark green (B and D) refer total $[M+H]^+$ ions of **1**–**6**, **11**, and **13** with a tolerance range of ± 0.005, in other colors refer $[M+H]^+$ ions of **1**–**4**, **11**, and **13** (E–J), respectively.

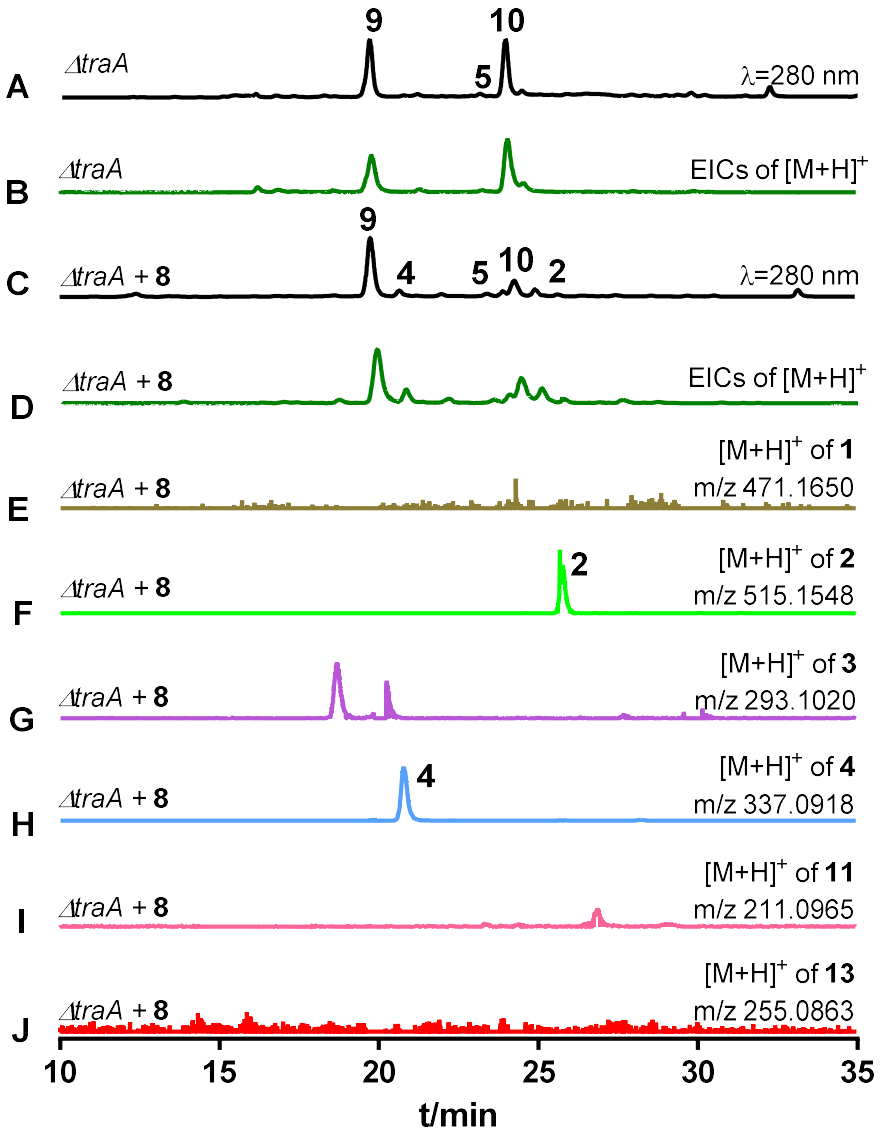

Figure S17. LC-MS analysis of the metabolite profile of the △*traA*-mutant with and without feeding with **8**

Absorptions at 280 nm are illustrated in black (A and C). EICs in dark green refer $[M+H]^+$ ions of **1–6**, **11**, and **13** (B and D) with a tolerance range of ± 0.005, and in other colors refer $[M+H]^+$ ions of **1** –**4**, **11**, and **13** (E–J), respectively.

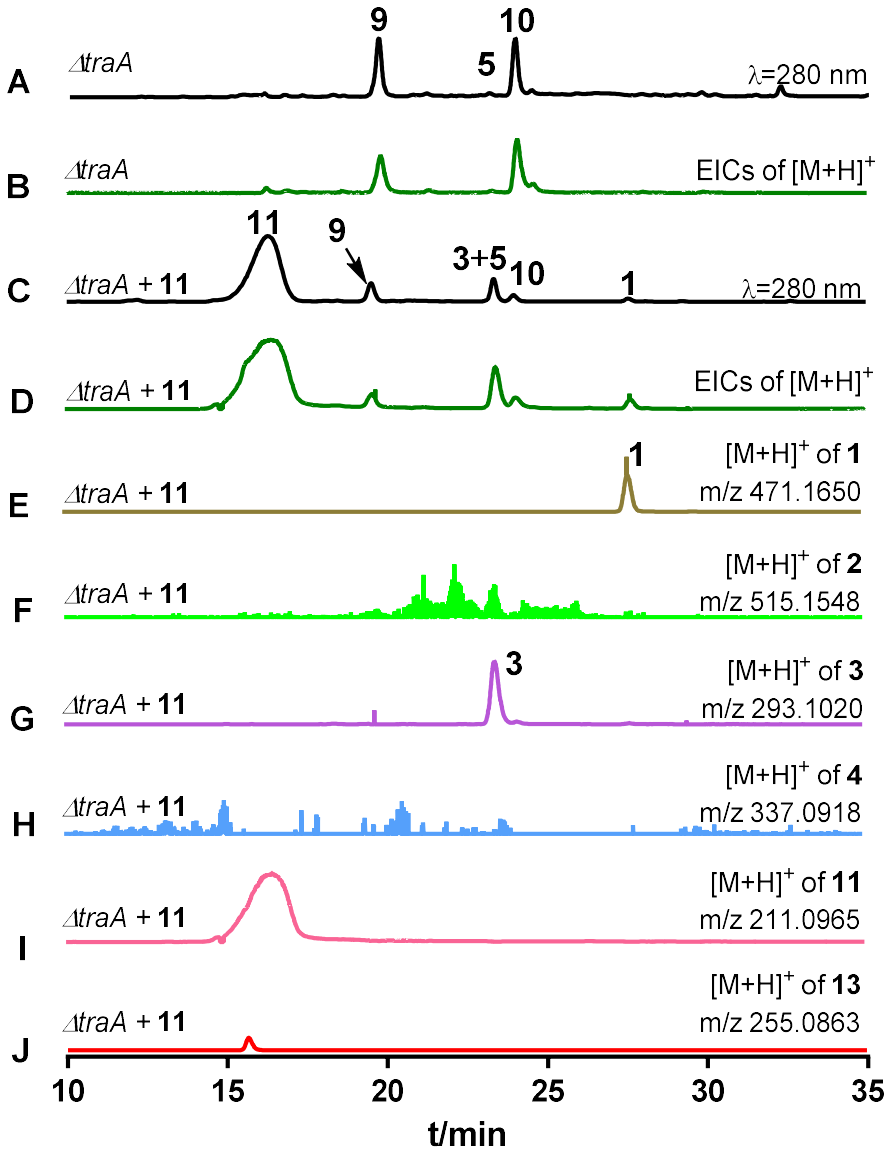

Figure S18. LC-MS analysis of the metabolite profile of the △*traA*-mutant with and without feeding with **11**

Absorptions at 280 nm are illustrated in black (A and C). EICs in dark green refer $[M+H]^+$ ions of **1–6**, **11**, and **13** (B and D with a tolerance range of ± 0.005, and in other different colors refer $[M+H]^+$ ions of **1** –**4**, **11**, and **13** (E–J), respectively.

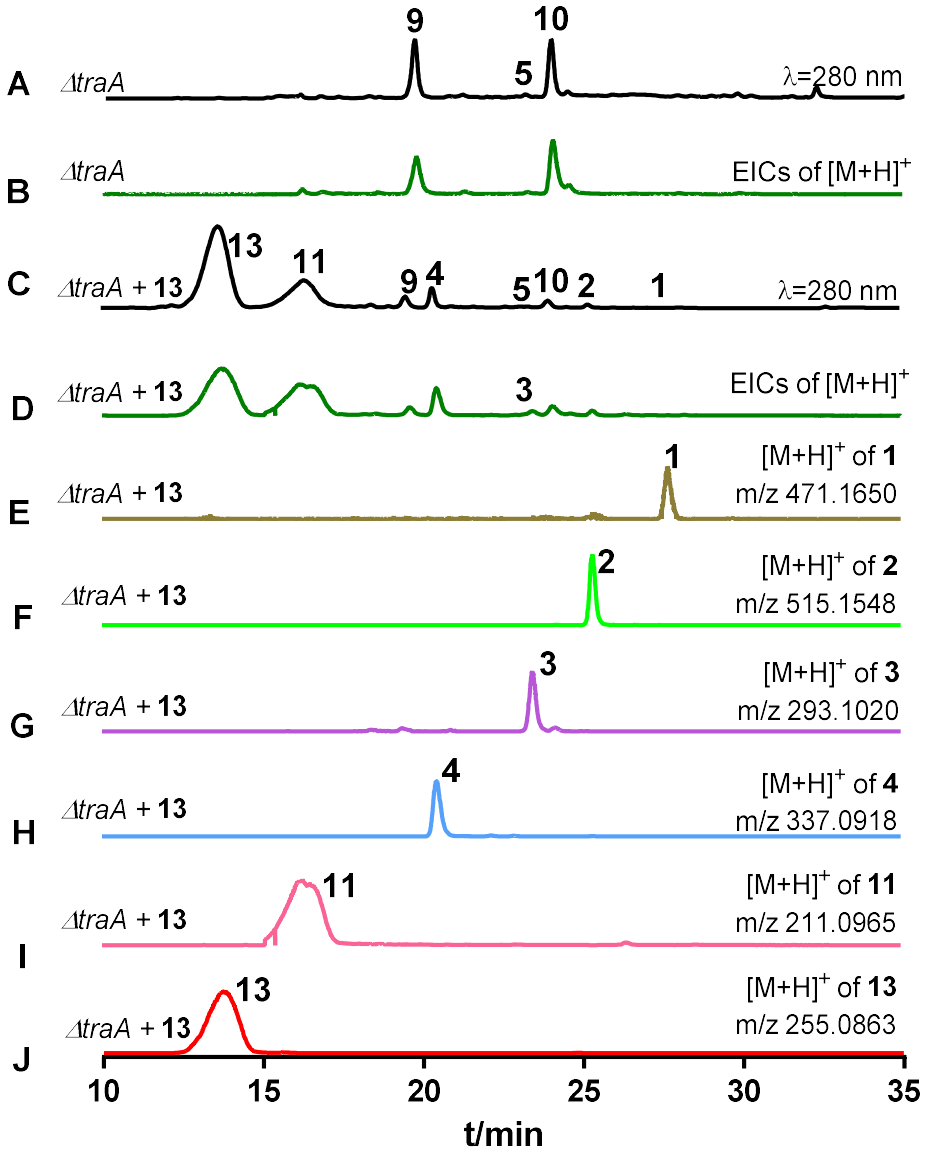

Figure S19. LC-MS analysis of the metabolite profile of the △*traA*-mutant with and without feeding with **13**

Absorptions at 280 nm are illustrated in black (A and C). EICs in dark green refer $[M+H]^+$ ions of **1**– **6**, **11**, and **13** (B and D) with a tolerance range of ± 0.005, and in other different colors refer $[M+H]^+$ ions of **1**–**4**, **11**, and **13** (E–J), respectively.

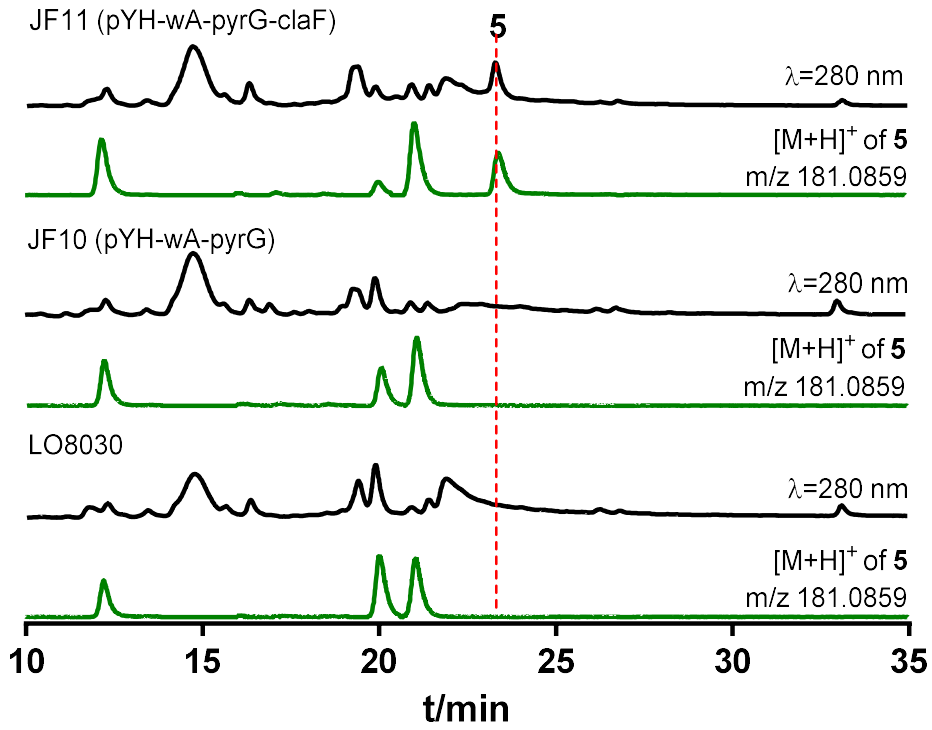

Figure S20. LC-MS analysis of the metabolite profile of different *A. nidulans* strains Absorptions at 280 nm and $[M+H]^+$ of (**5**) m/z 181.0859 are illustrated. JF11 carries the expression construct for *claF* in *A. nidulans* LO8030 and JF10 the empty vector pYH-wA-pyrG.

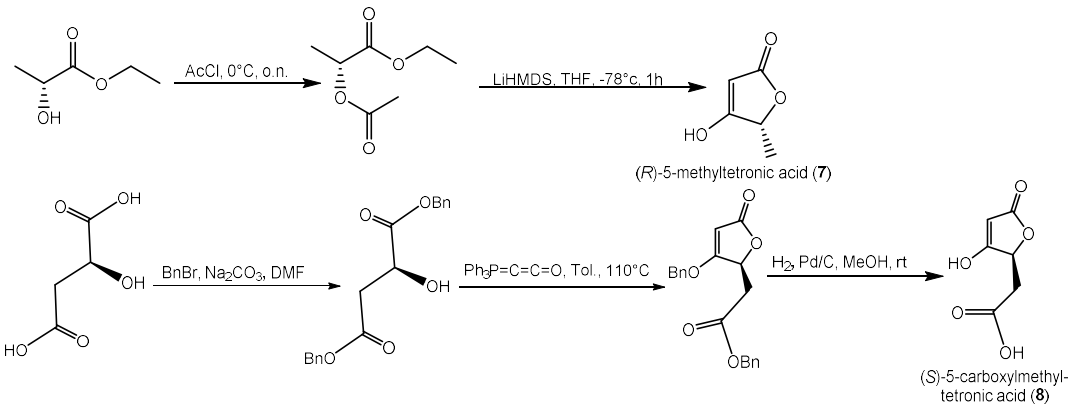

Figure S21. Chemical synthesis of the tetronic acids **7** and **8**

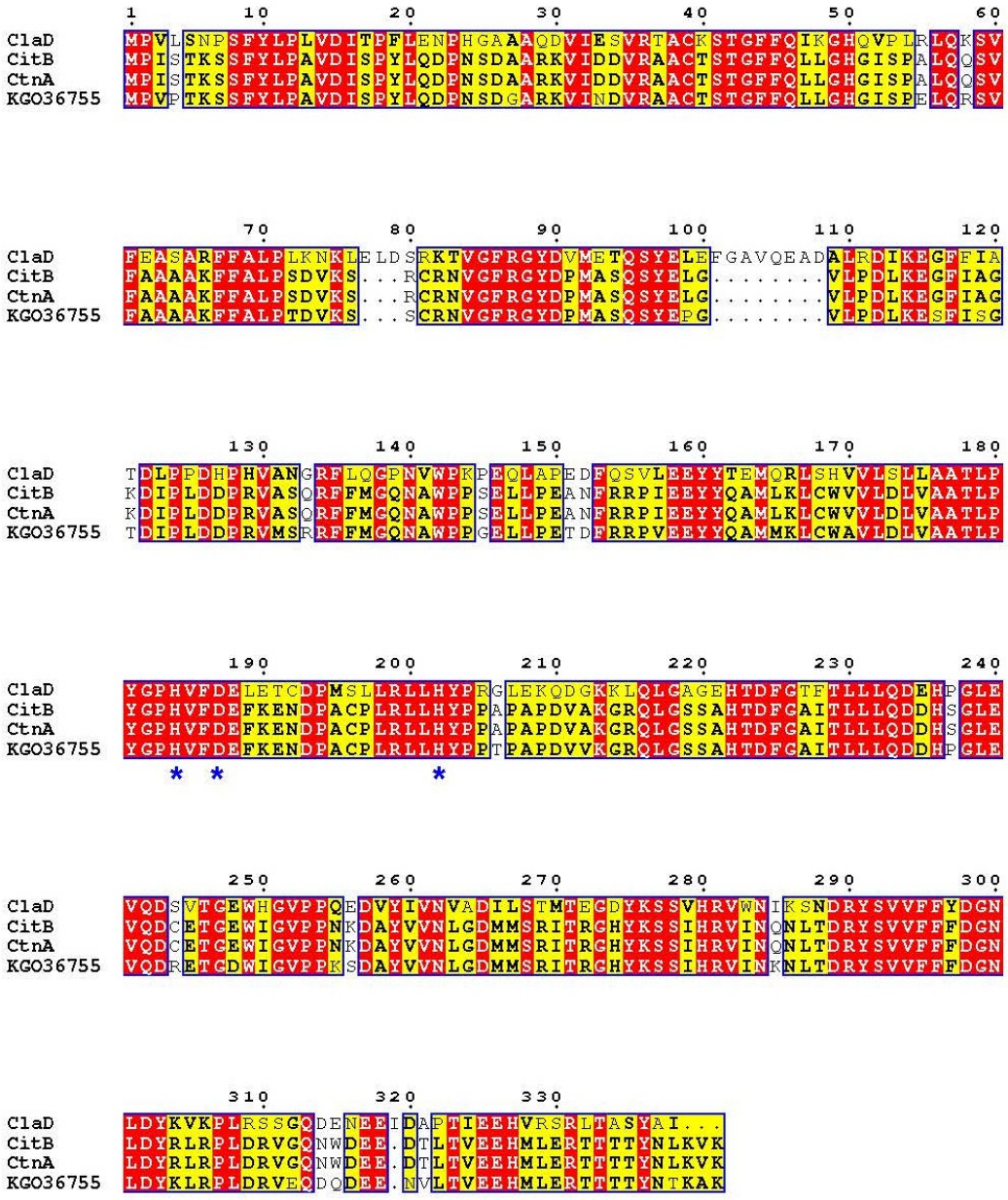

Figure S22. Sequence alignments of 2-OG-dependent oxygenases
CitB (ALI92653), CtnA (BAE95338), and KGO36755 are from *Monascus ruber* M7, *Monascus purpureus,* and *Penicillium expansum* and share sequence identities of 53.8, 53.8, and 53.6% with ClaD, respectively. ClaD also contains the typical conserved 2-His-1-Asp ion-binding triad of non-heme Fe^{II}/2-oxoglutarate-dependent oxygenases (His_{184}, His_{202} and Asp_{187}) (marked with *).[13] Protein sequence alignments were carried out by using the sequence alignment function of MEGA 5.2 and visualized with ESPript 3.0 (http://espript.ibcp.fr/ESPript/ESPript/).

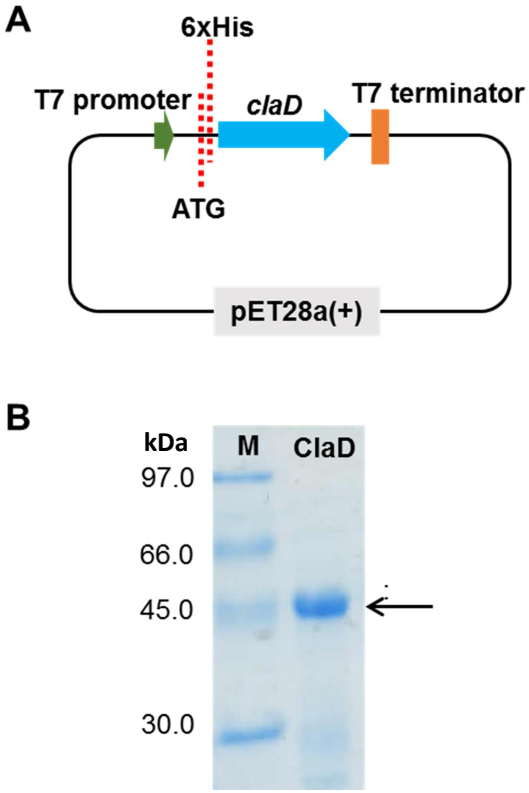

Figure S23. Analysis of ClaD on SDS PAGE

(A) *claD* was inserted into pET28a(+) with 6xHis at its *N*-terminal. (B) The recombinant histidine-tagged ClaD was purified and separated on a 12% gel after induction with 0.5 mM IPTG at 30℃ for 6 h in TB medium.

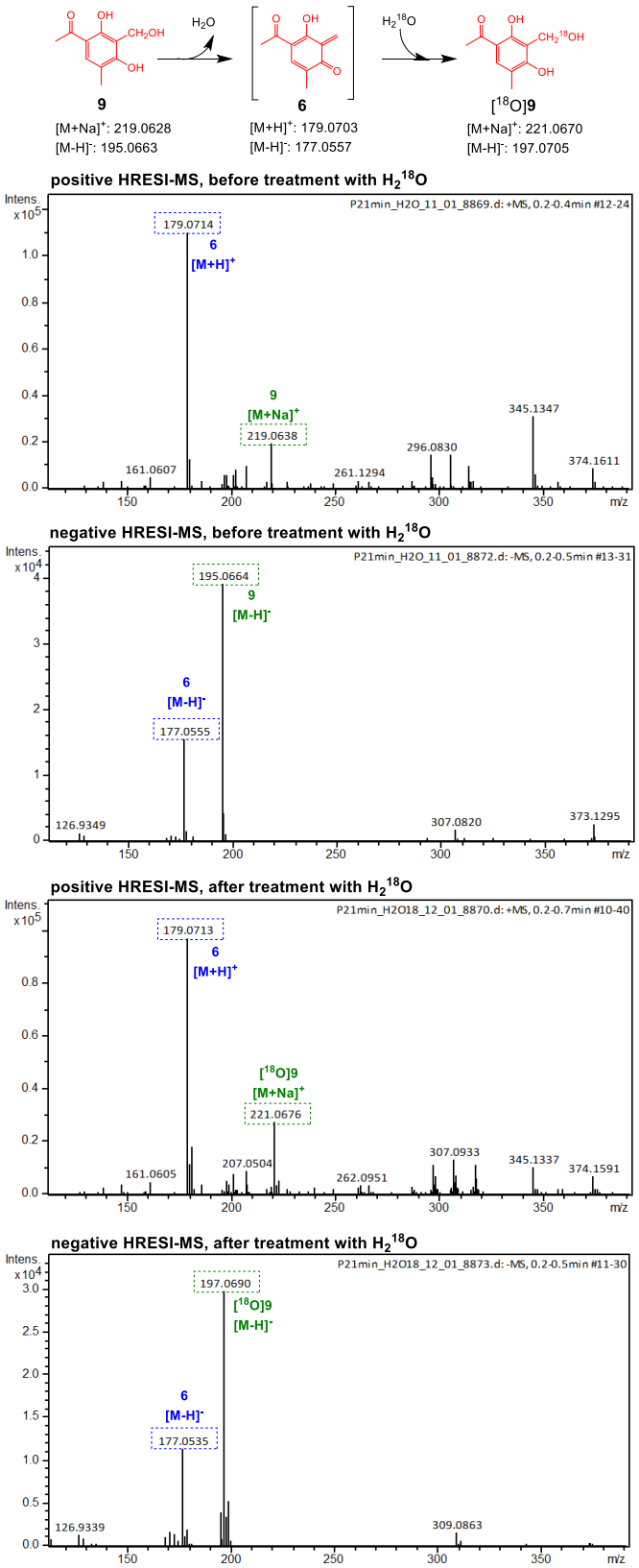

Figure S24. MS analysis of **9** after incubation in H_2O and in ^{18}O-enriched $H_2{}^{18}O$

Hydroxyclavatol (**9**) was dissolved in H_2O and ^{18}O-enriched $H_2{}^{18}O$ and incubated at room temperature for 16 h. MS data of two samples were collected in both positive and negative modes.

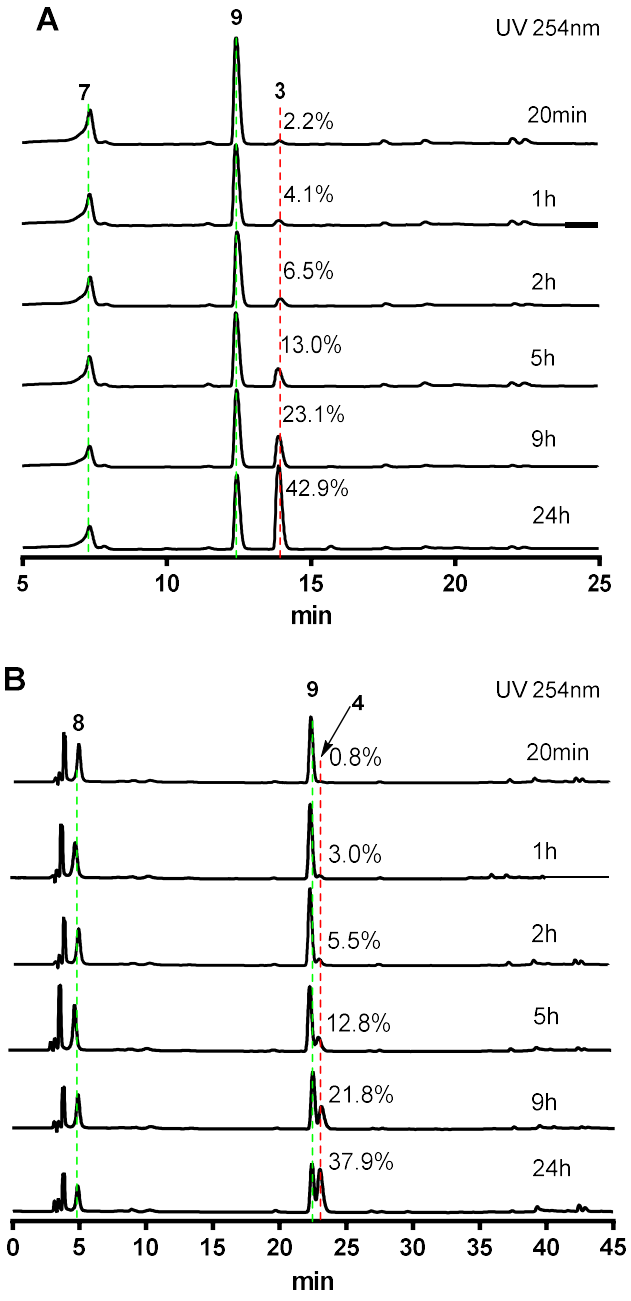

Figure S25. Time dependence of Michael addition reaction of **9** with **7** (A) or **8** (B)
The incubations were carried out at room temperature in distillated H_2O. Absorptions at 254 nm are illustrated.

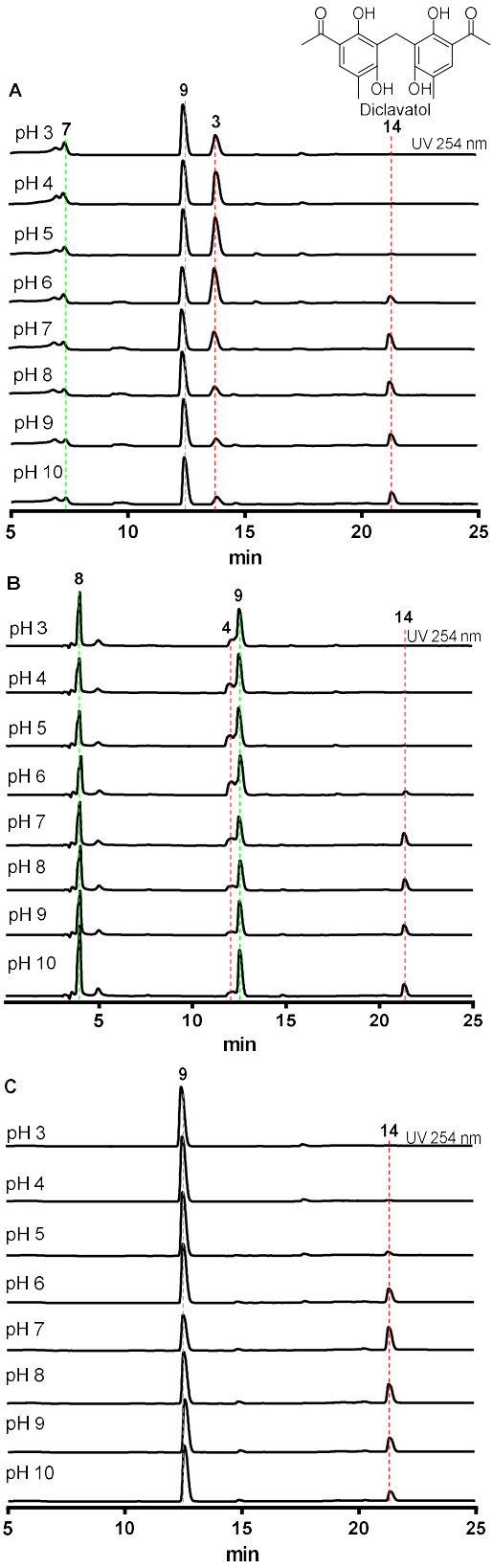

Figure S26. pH dependence on Michael addition reactions forming **3** and **4**
HPLC analysis of mixtures of **9** with **7** (A)**, 8** (B) or alone (C) in phosphate saline buffer with different pH values at room temperature for 12 h. Absorptions at 254 nm are illustrated.

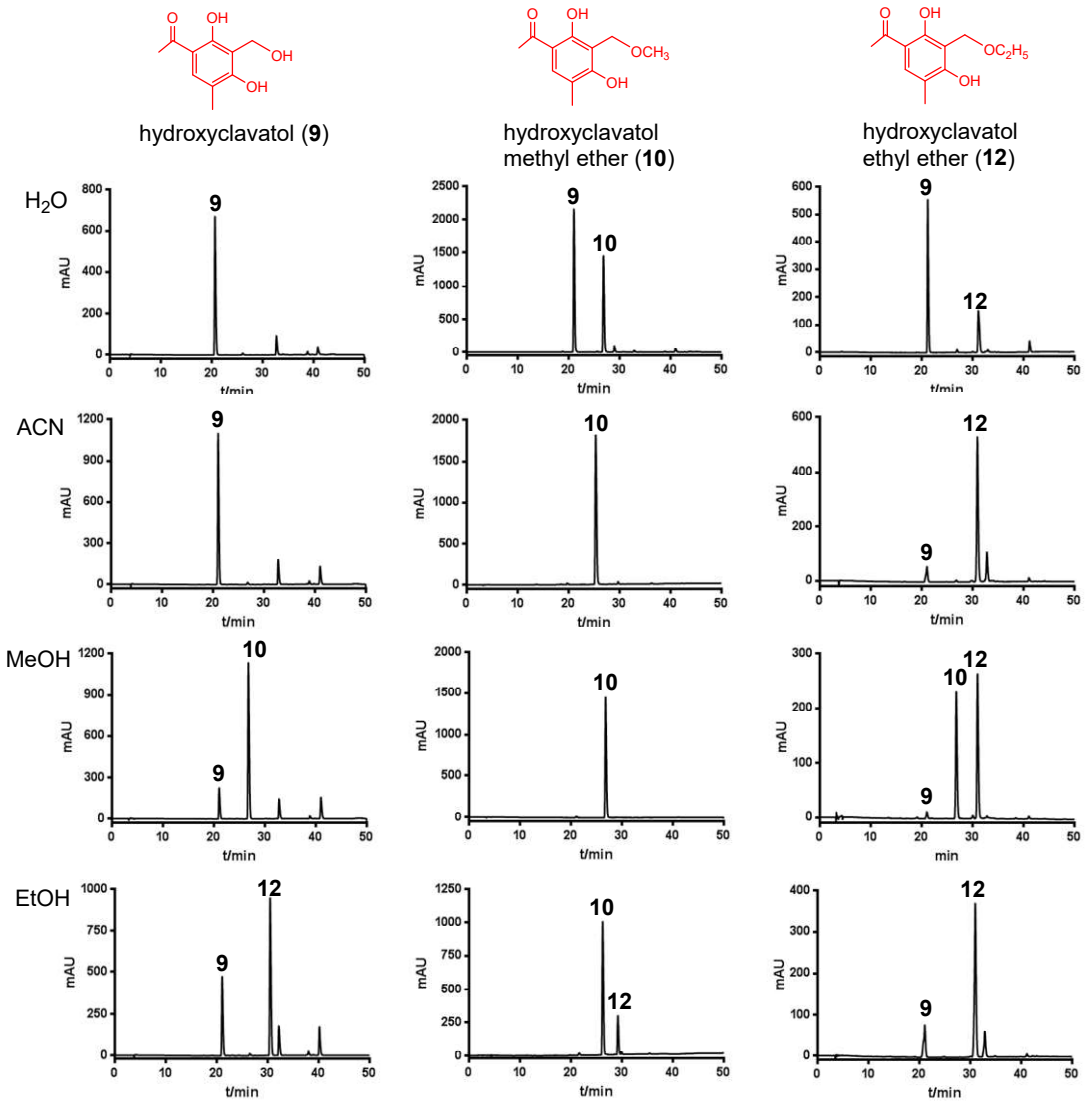

Figure S27. HPLC analysis of **9**, **10**, and **12** after incubation in different solvents
Incubation of hydroxyclavatol (**9**), hydroxyclavatol methyl ether (**10**), and hydroxyclavatol ethyl ether (**12**) in H_2O, acetonitrile, MeOH and EtOH at room temperature for 12 h. Absorptions at 280 nm are illustrated.

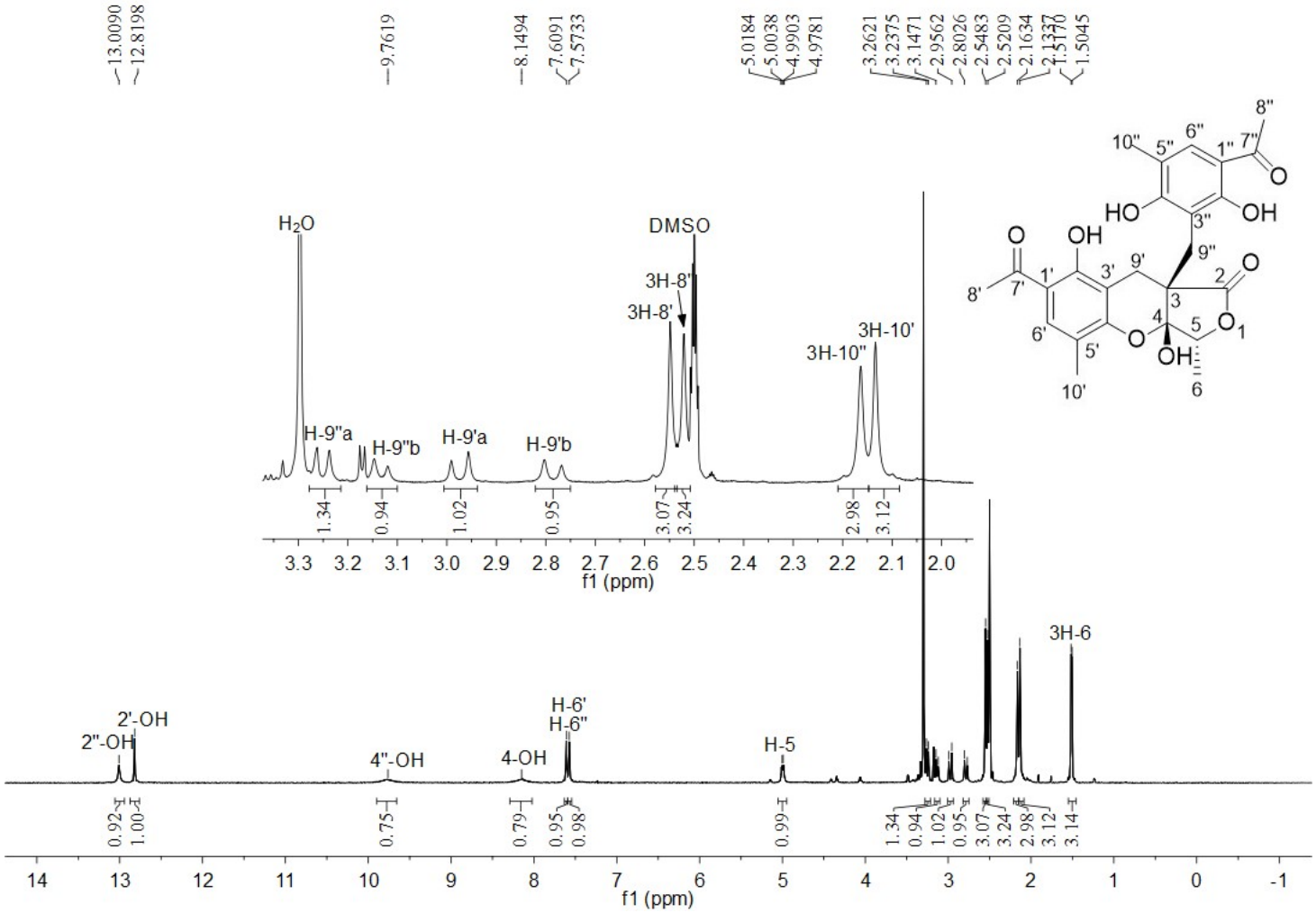

Figure S28. ^{1}H NMR spectrum of compound **1** in DMSO-*d6* (500 MHz)

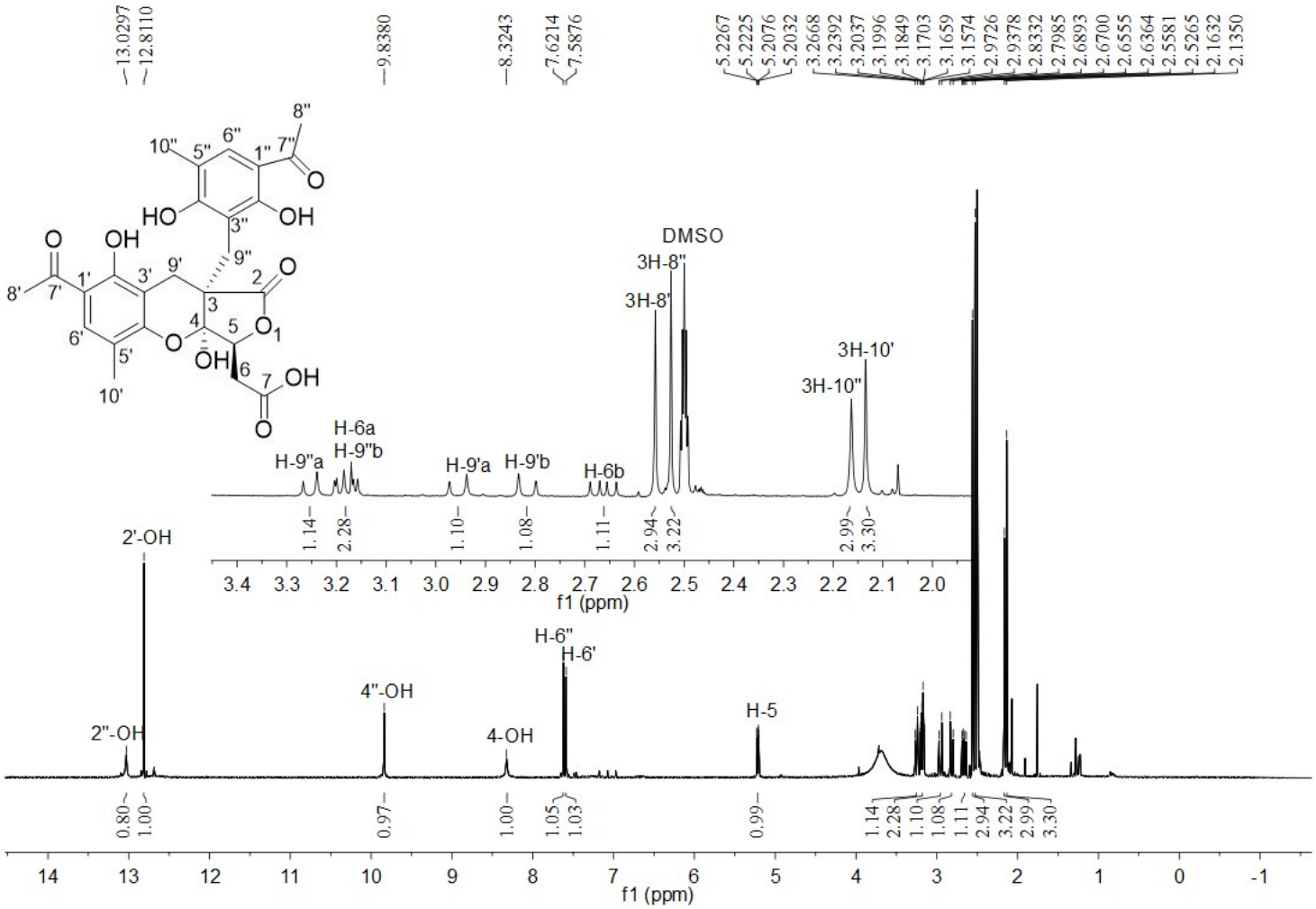

Figure S29. ^{1}H NMR spectrum of compound **2** in DMSO-*d6* (500 MHz)

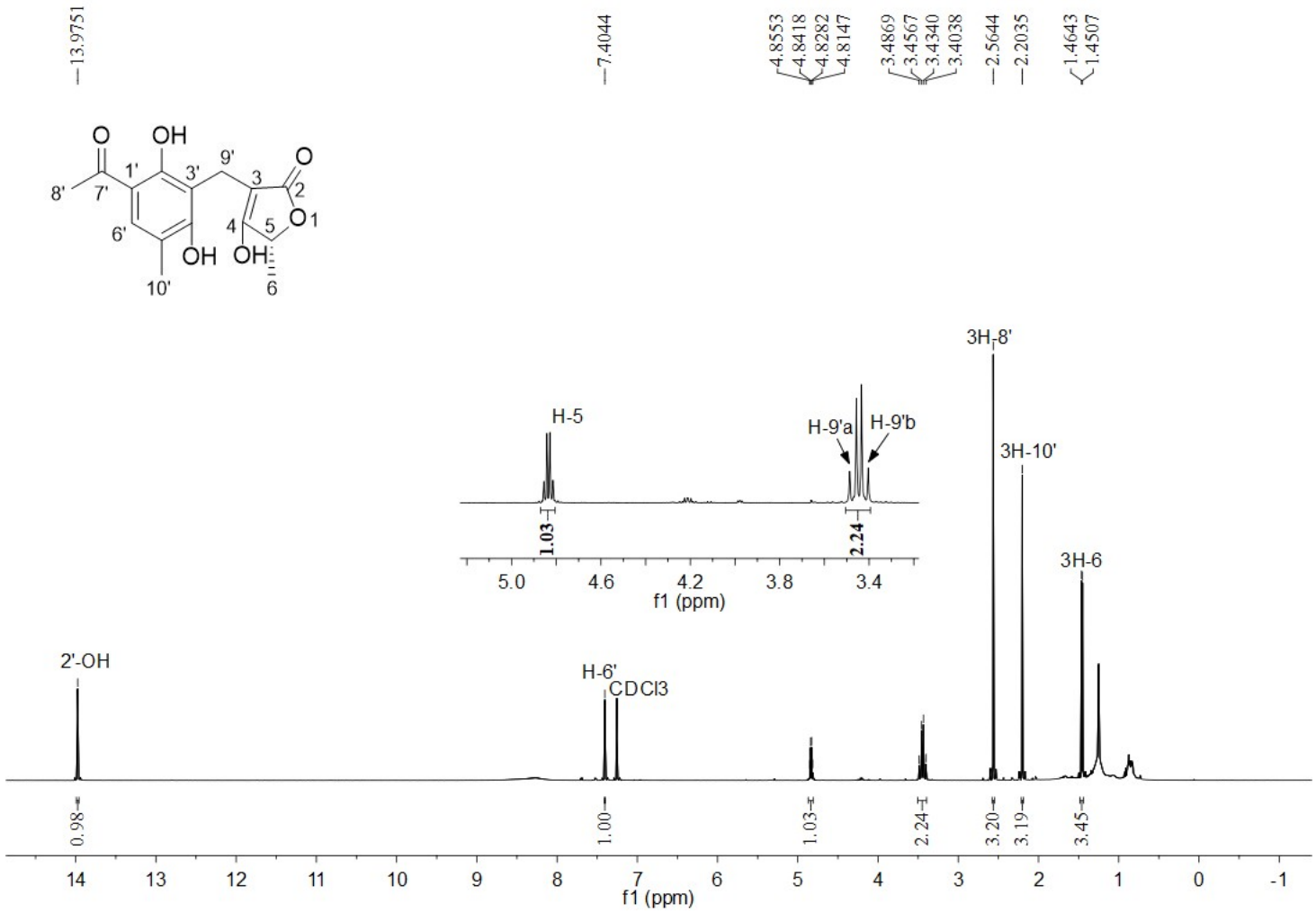

Figure S30. ^{1}H NMR spectrum of compound **3** in $CDCl_3$ (500 MHz)

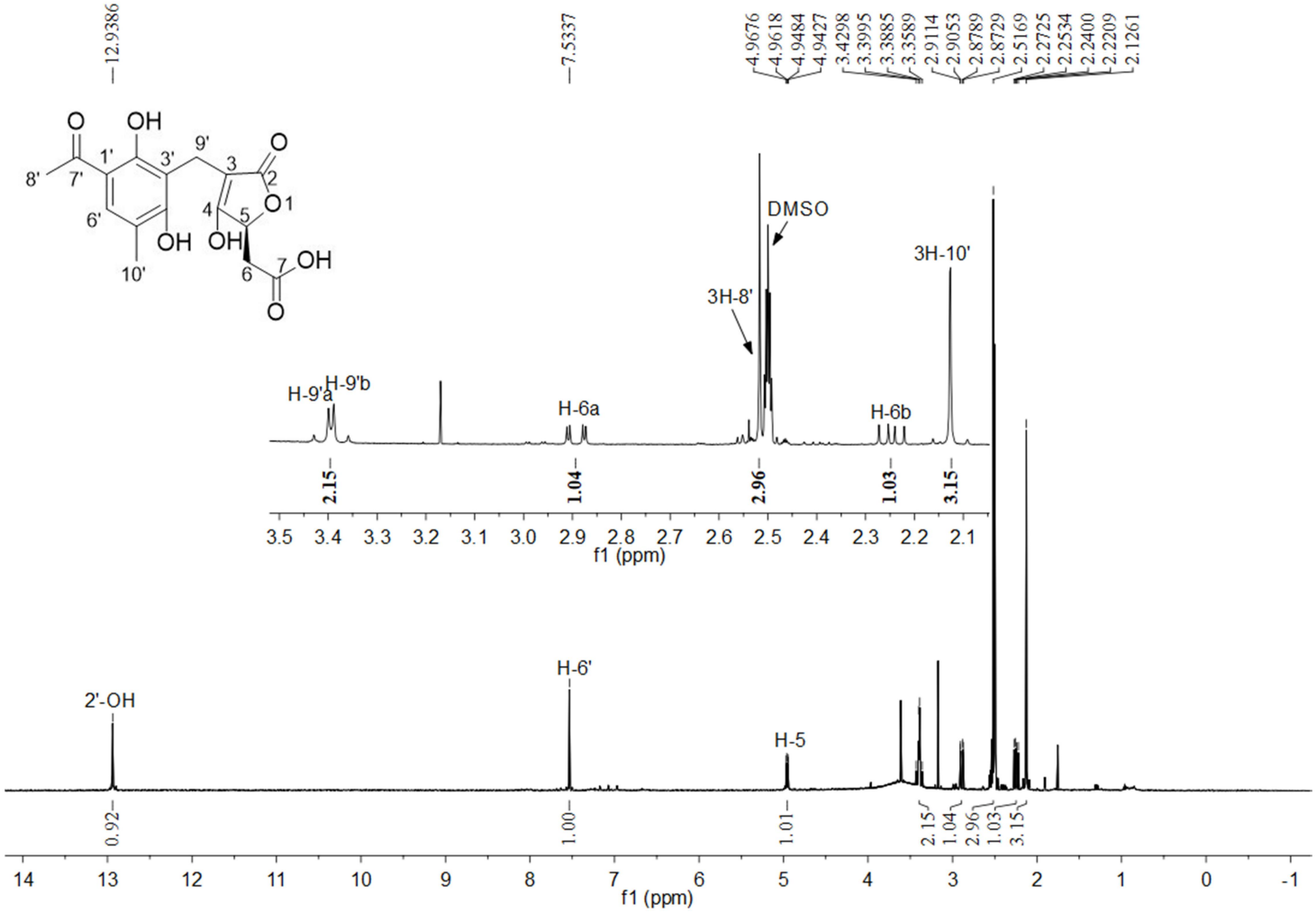

Figure S31. ^{1}H NMR spectrum of compound **4** in DMSO-*d6* (500 MHz)

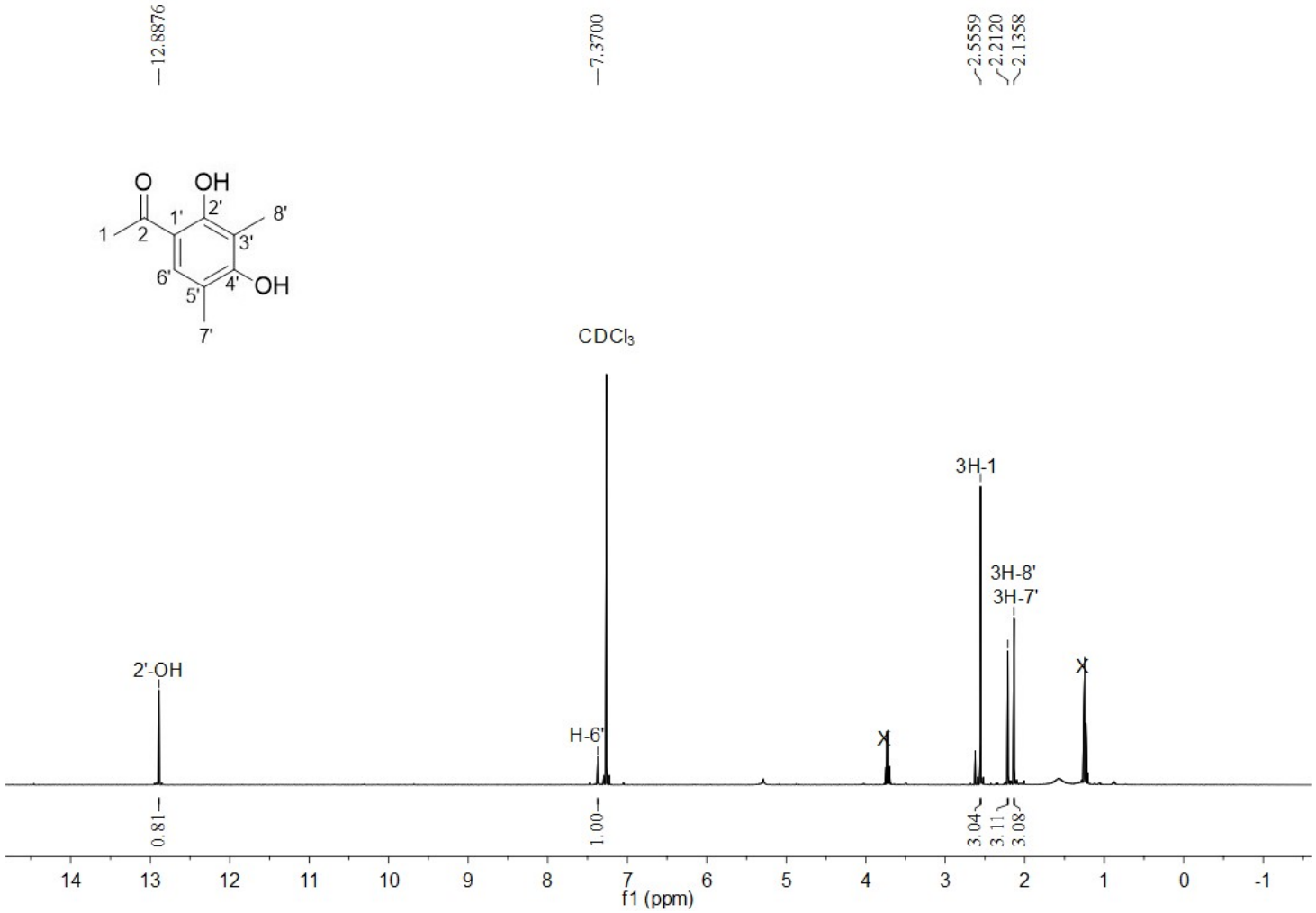

Figure S32. ^{1}H NMR spectrum of compound **5** in $CDCl_3$ (500MHz)

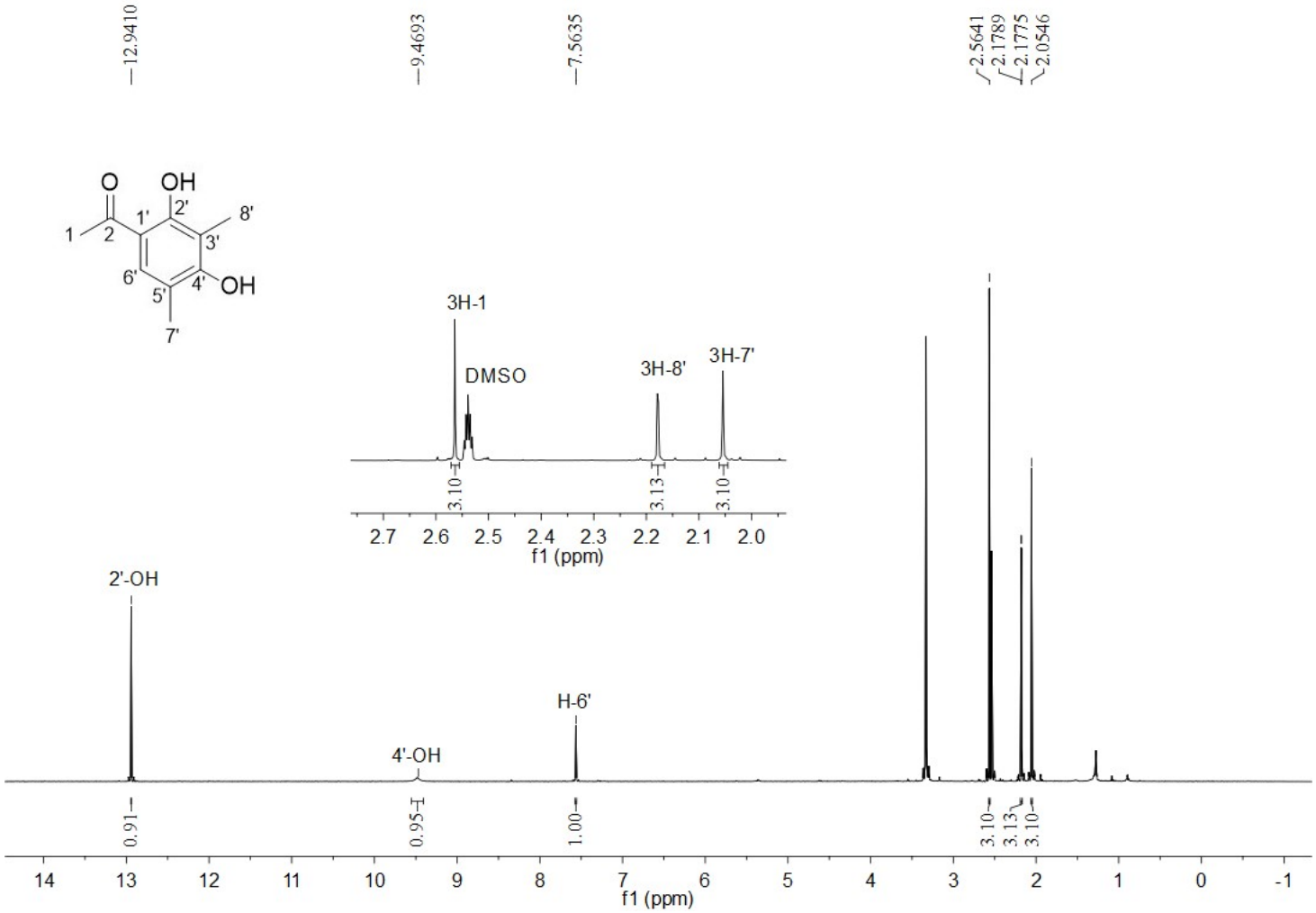

Figure S33. ^{1}H NMR spectrum of compound **5** in DMSO-d_6 (500MHz)

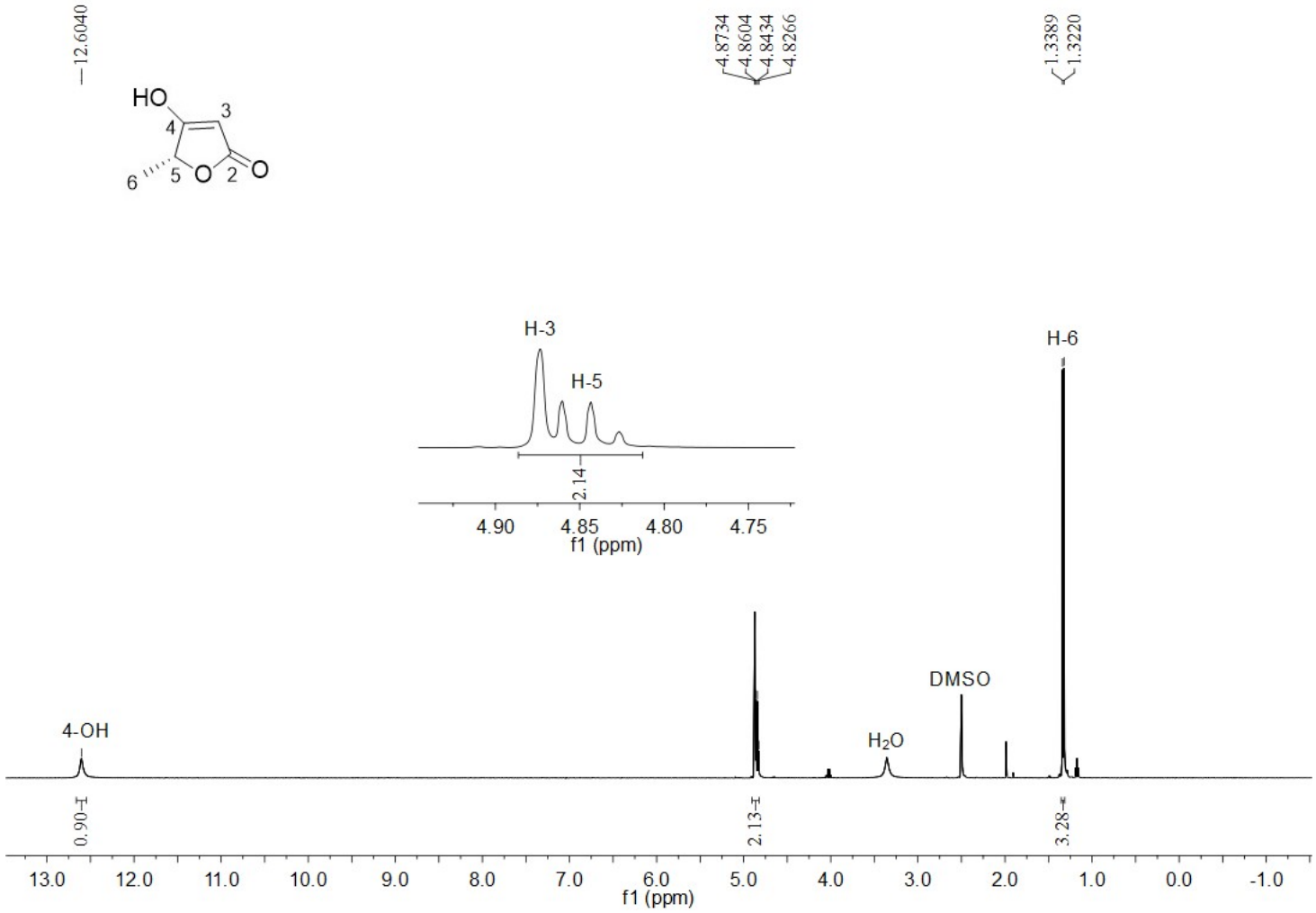

Figure S34. ^{1}H NMR spectrum of compound **7** in DMSO-d_6 (400MHz)

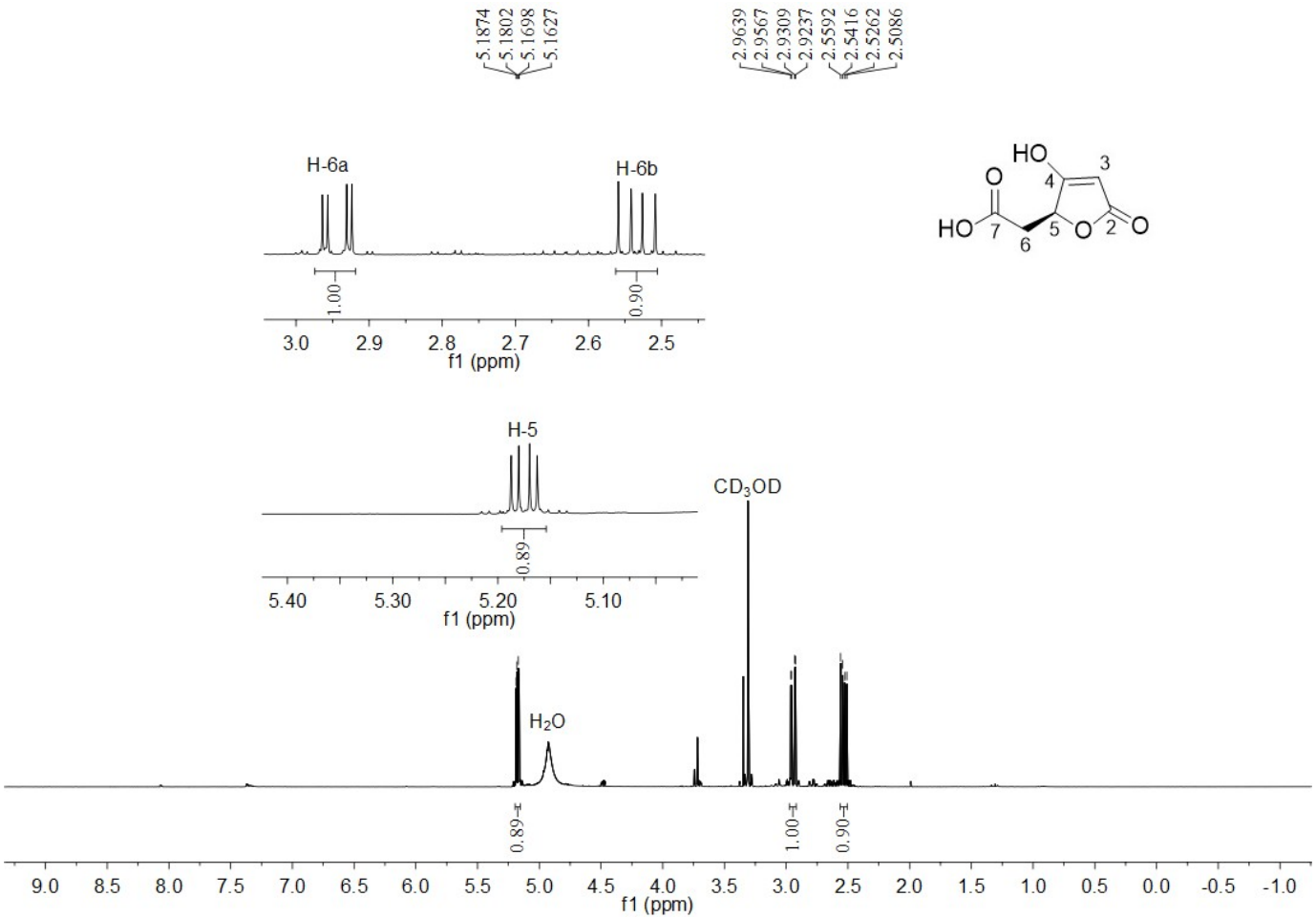

Figure S35. ^{1}H NMR spectrum of compound **8** in CD_3OD (500MHz)

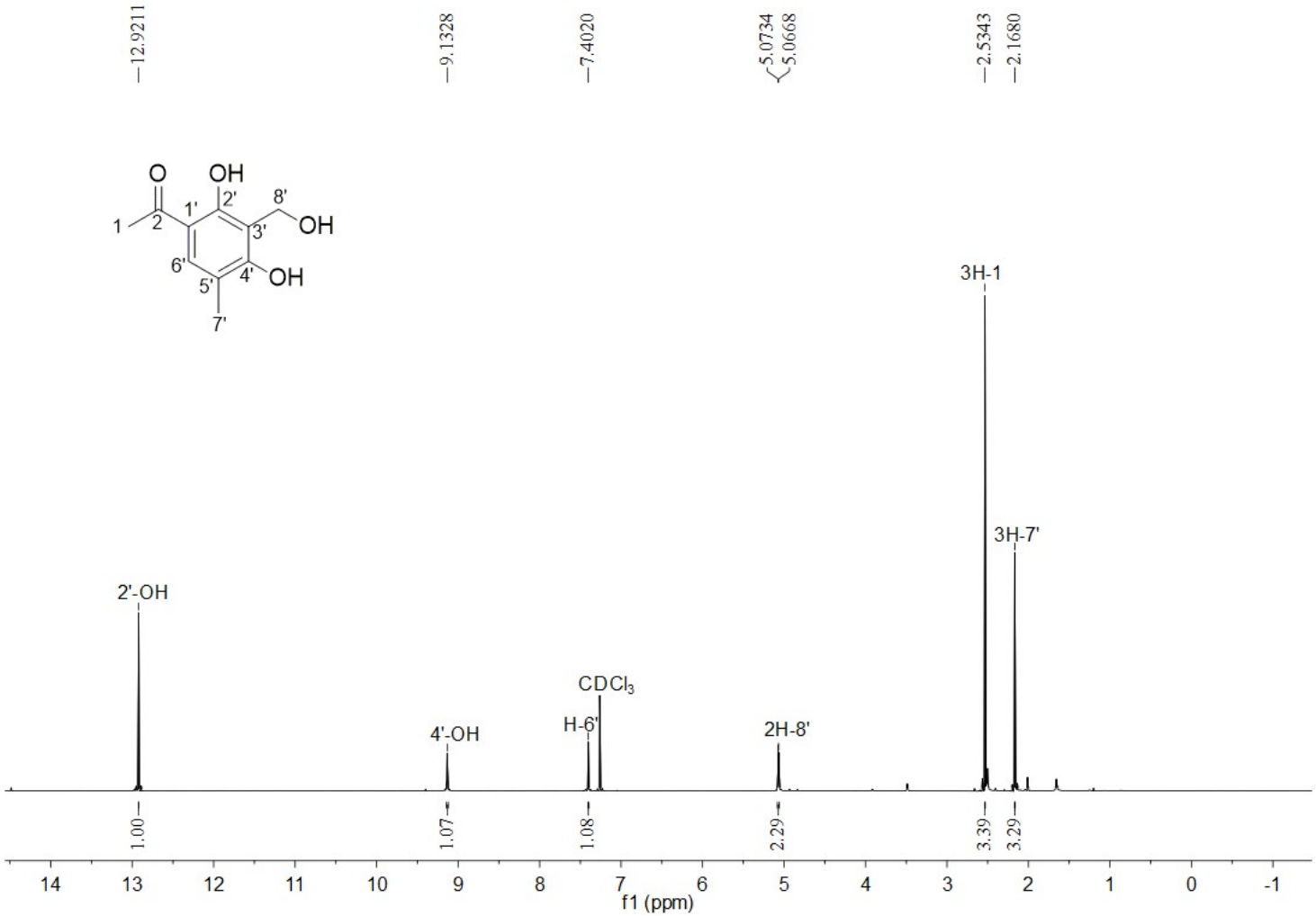

Figure S36. ^{1}H NMR spectrum of compound **9** in $CDCl_3$ (500MHz)

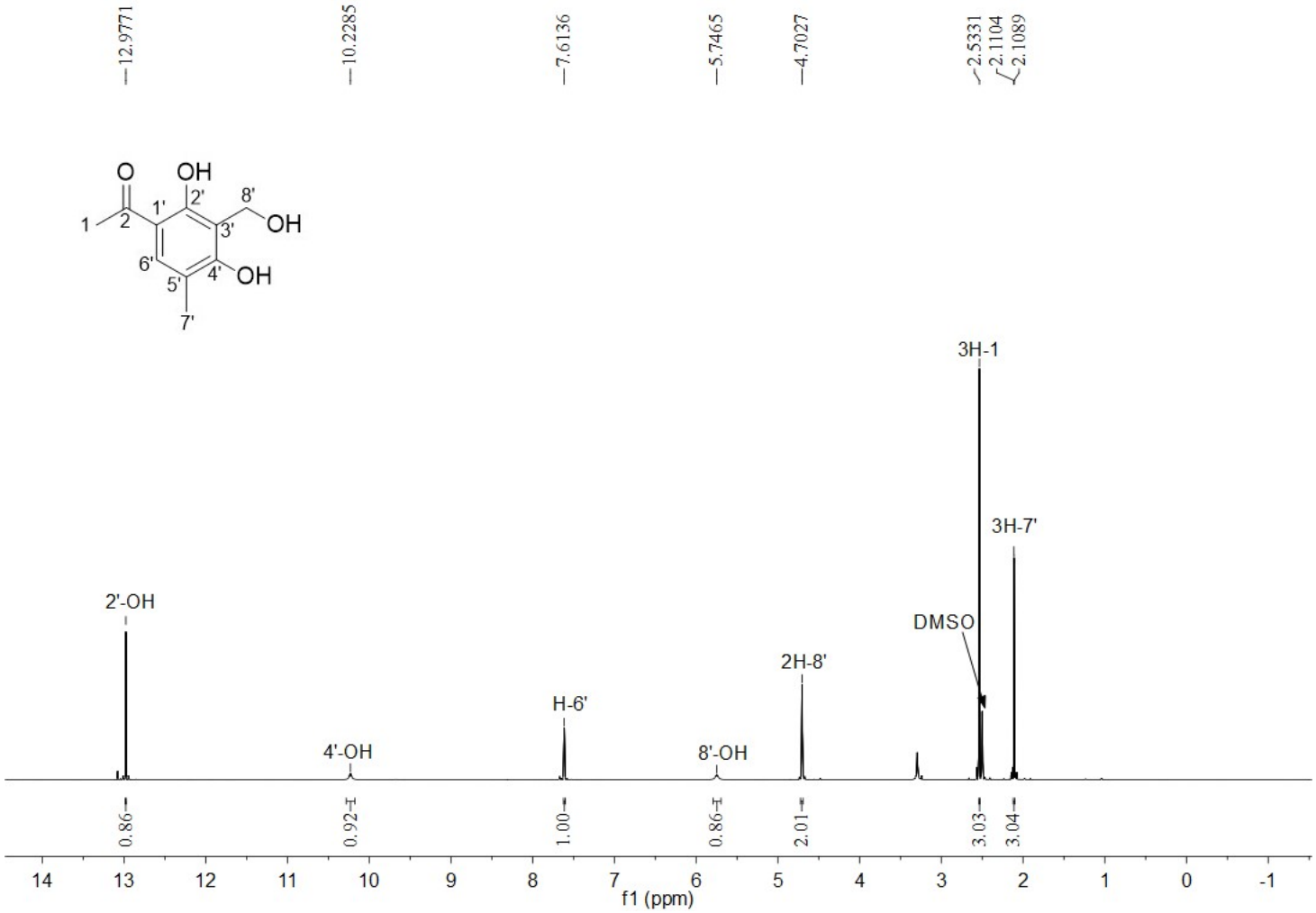

Figure S37. ^{1}H NMR spectrum of compound **9** in DMSO-*d6* (500MHz)

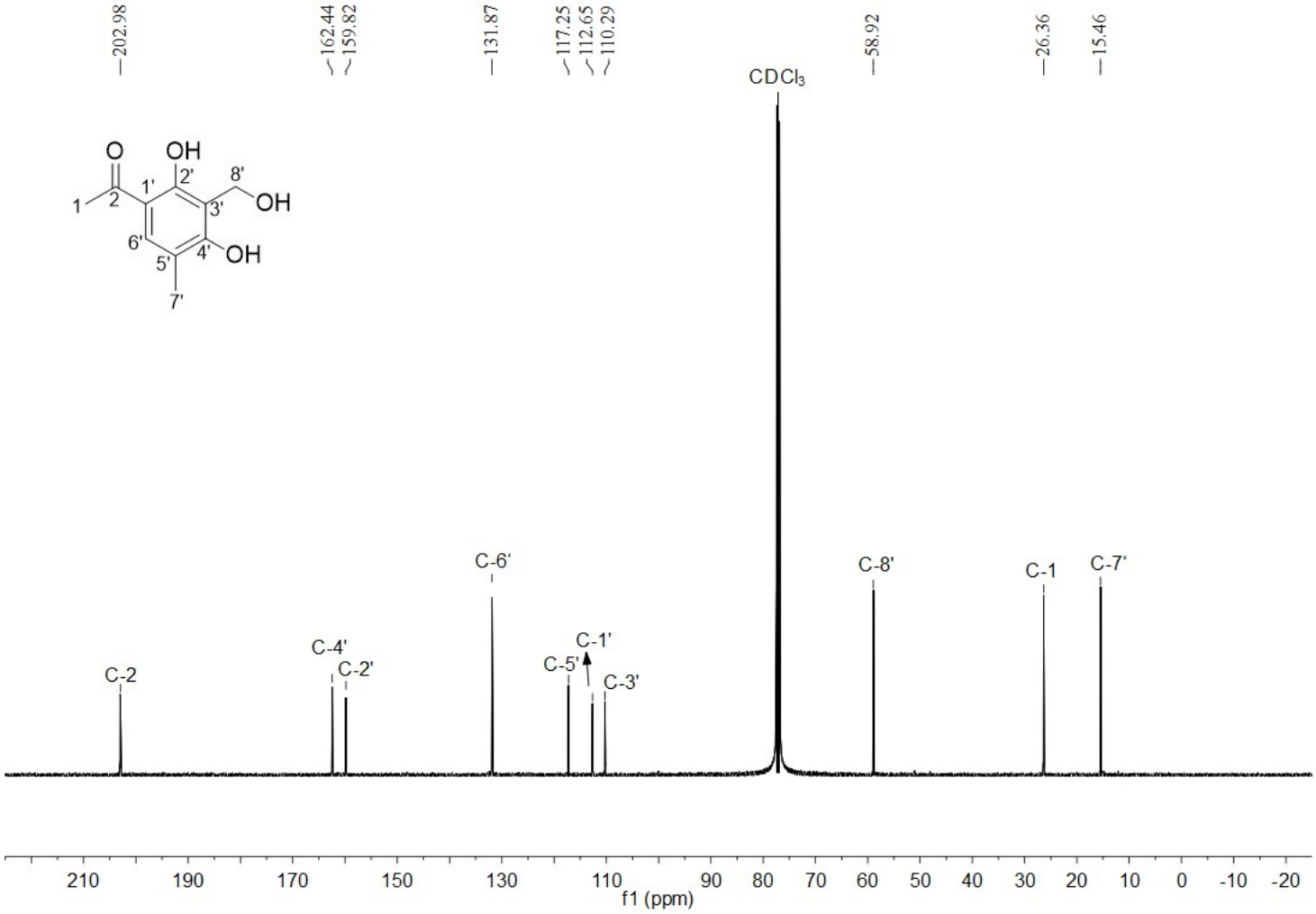

Figure S38. ^{13}C NMR spectrum of compound **9** in $CDCl_3$ (125MHz)

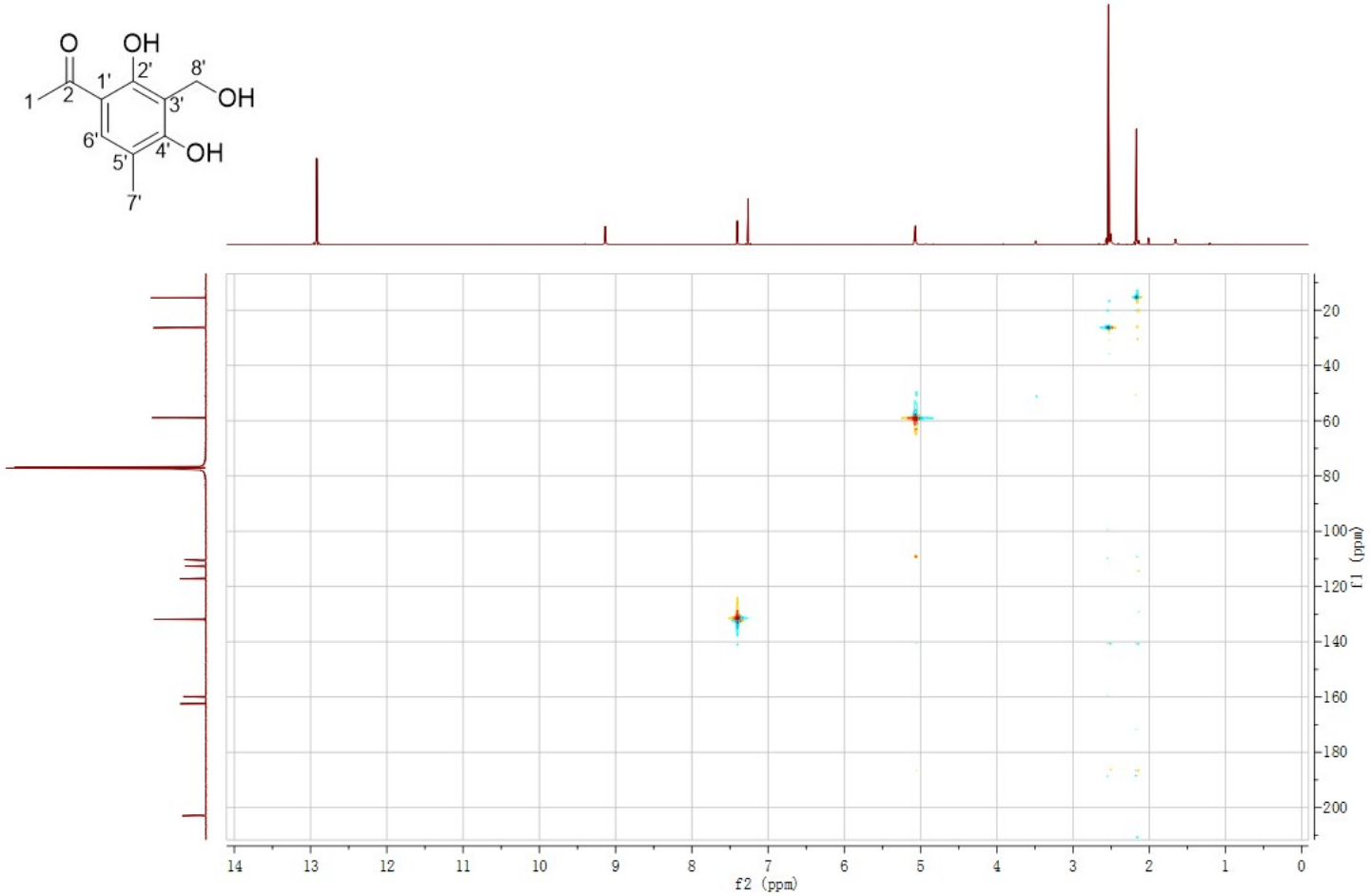

Figure S39. HMQC spectrum of compound **9** in $CDCl_3$

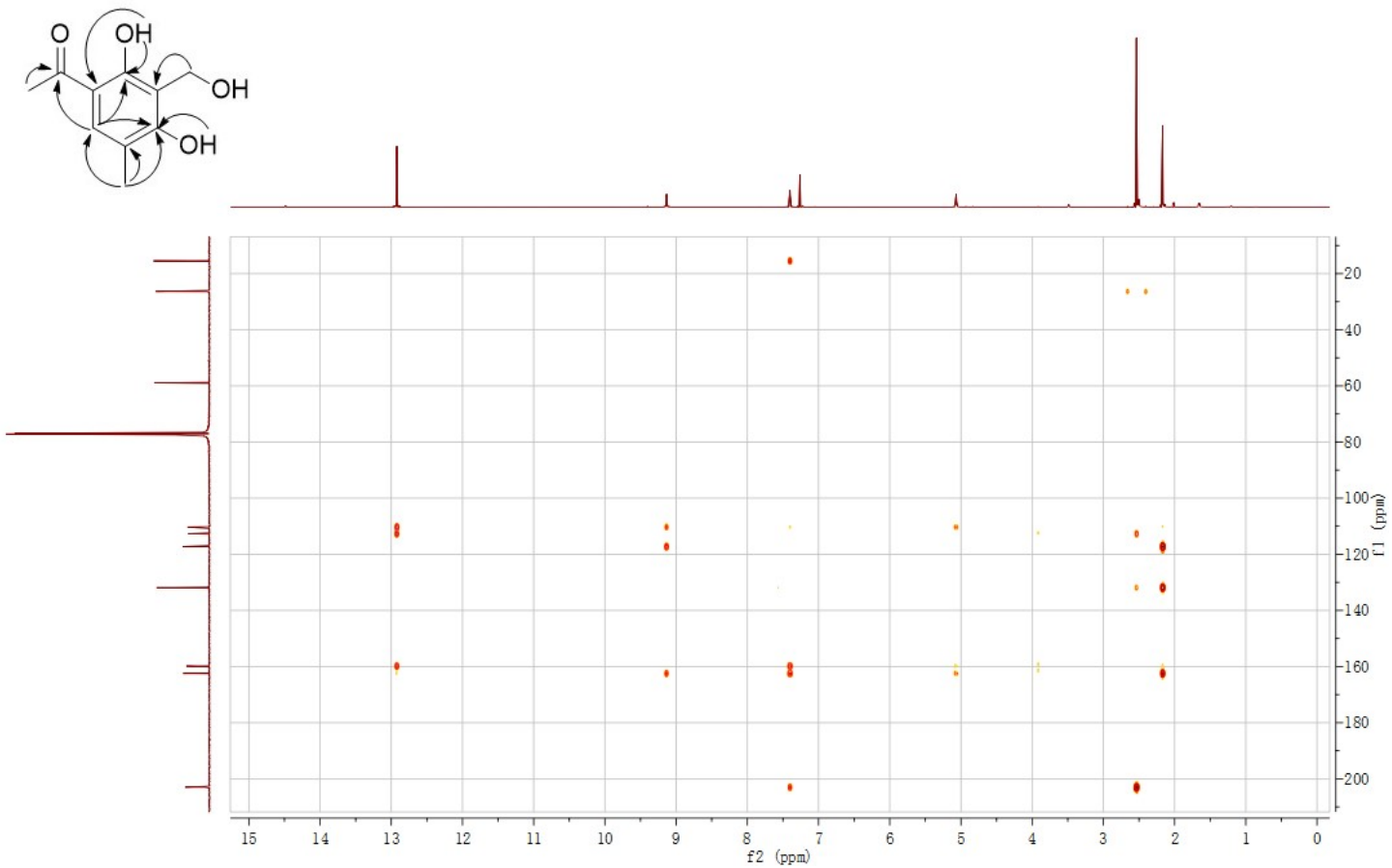

Figure S40. HMBC spectrum of compound **9** in $CDCl_3$

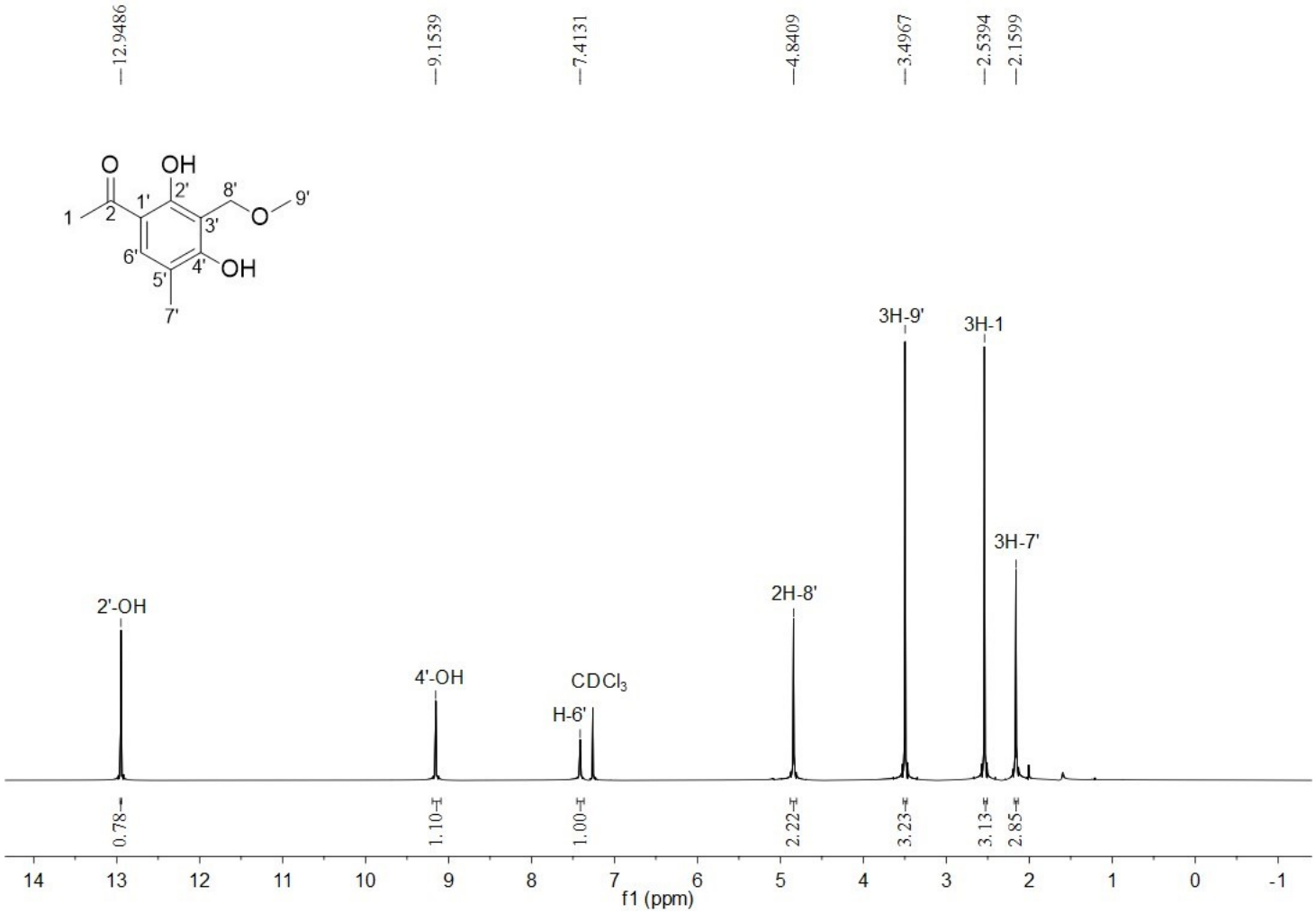

Figure S41. ^{1}H NMR spectrum of compound **10** in $CDCl_3$ (500MHz)

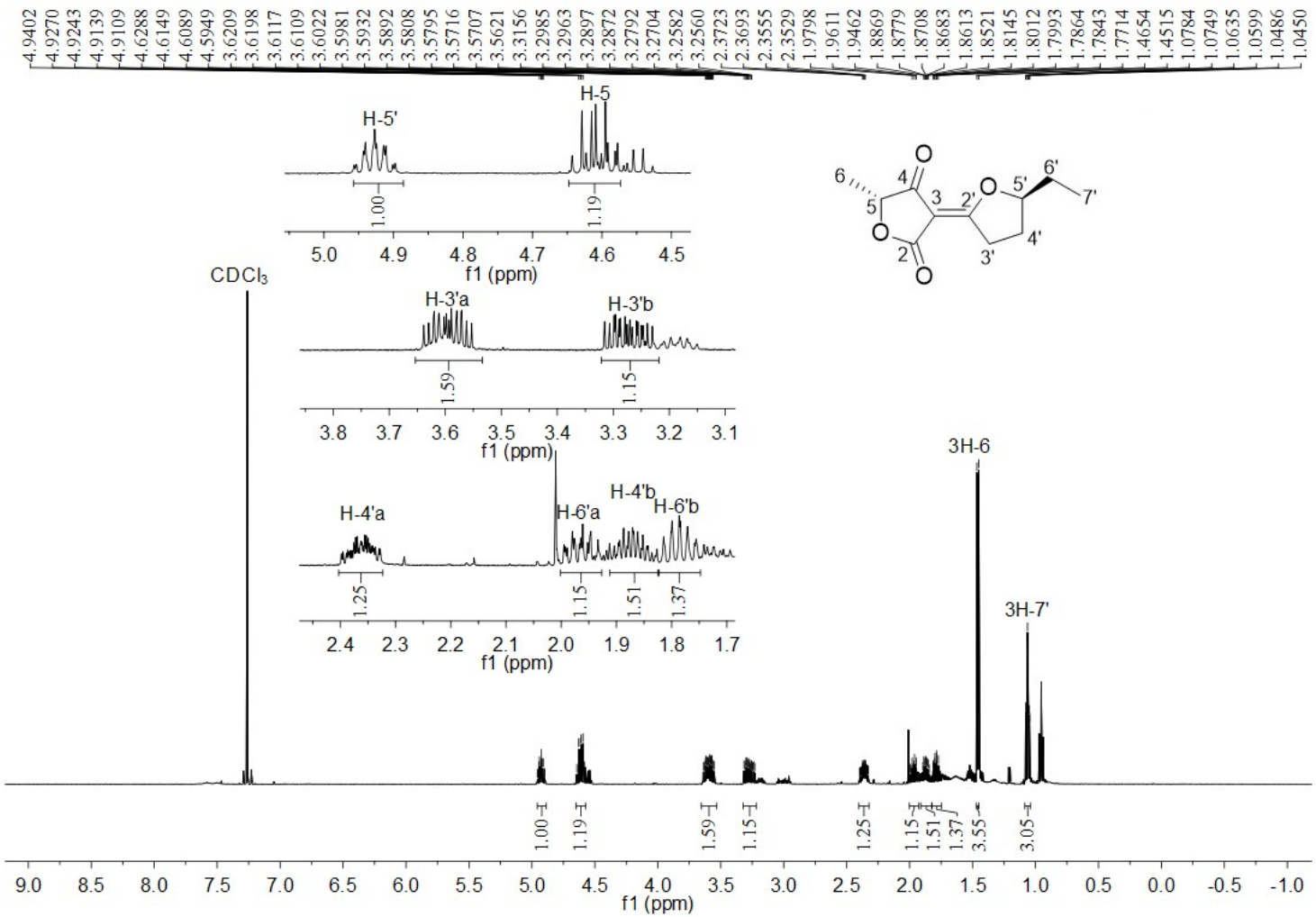

Figure S42. ^{1}H NMR spectrum of compound **11** in $CDCl_3$ (500 MHz)

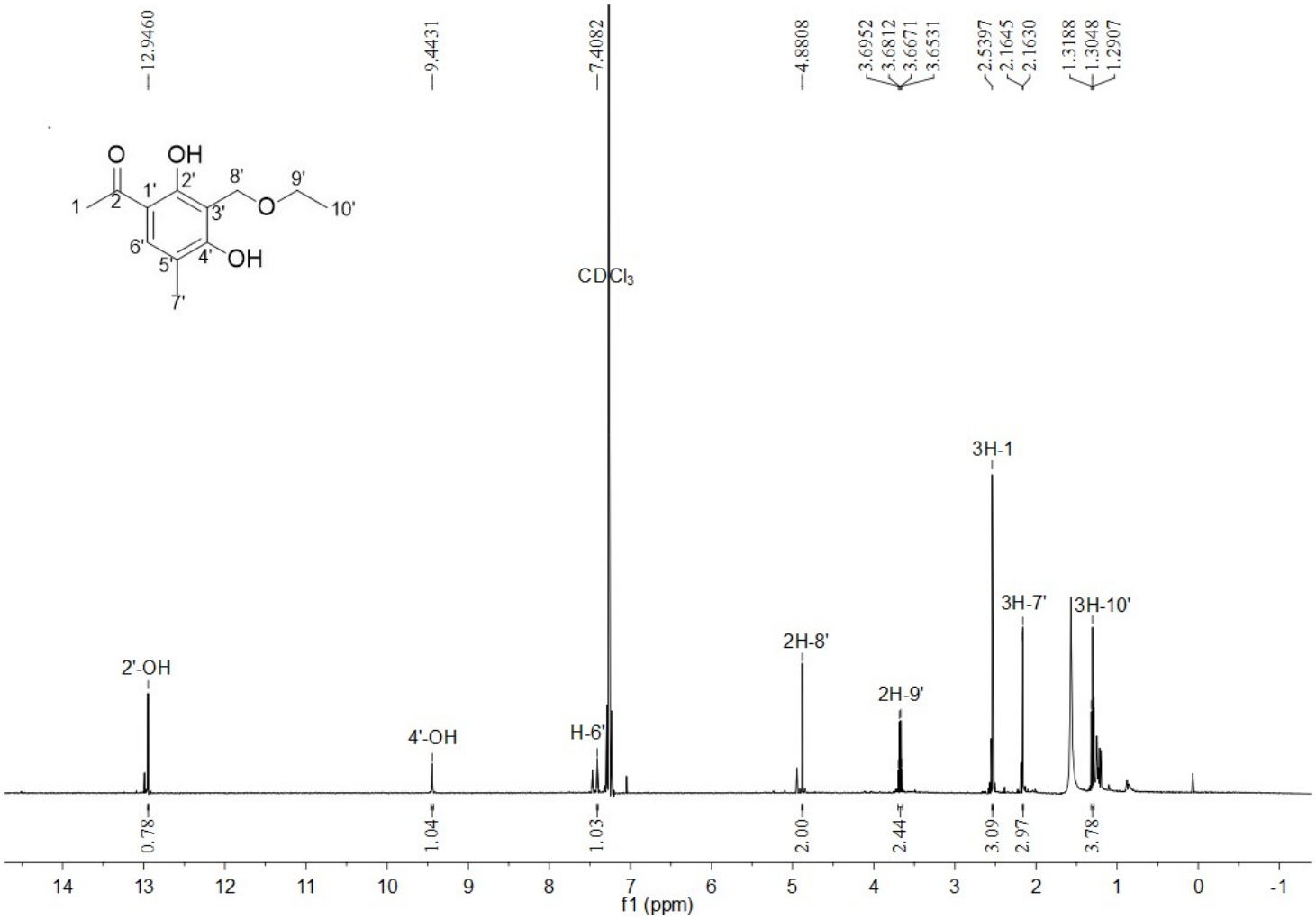

Figure S43. ^{1}H NMR spectrum of compound **12** in $CDCl_3$ (500 MHz)

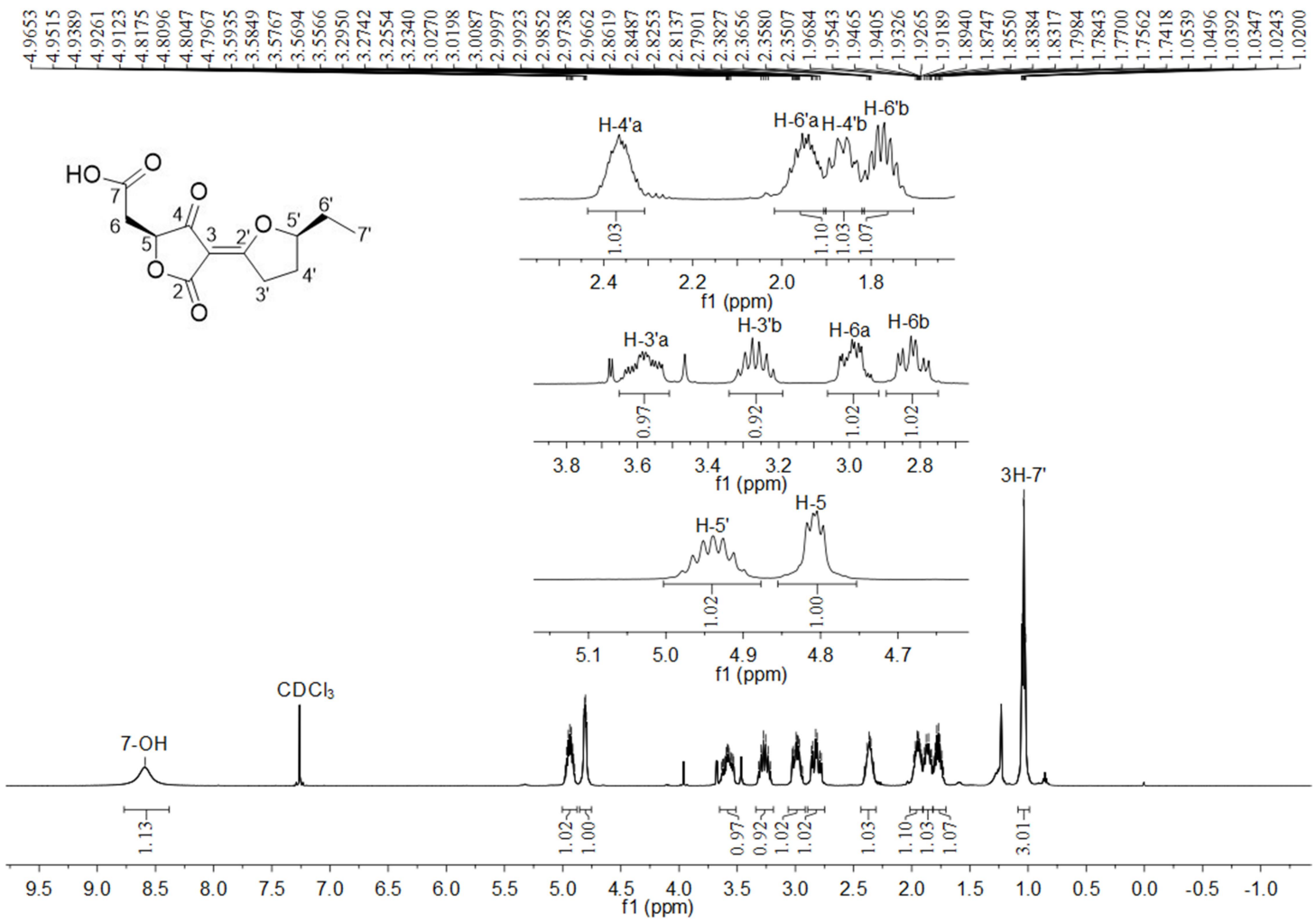

Figure S44. ^{1}H NMR spectrum of compound **13** in $CDCl_3$ (500MHz)

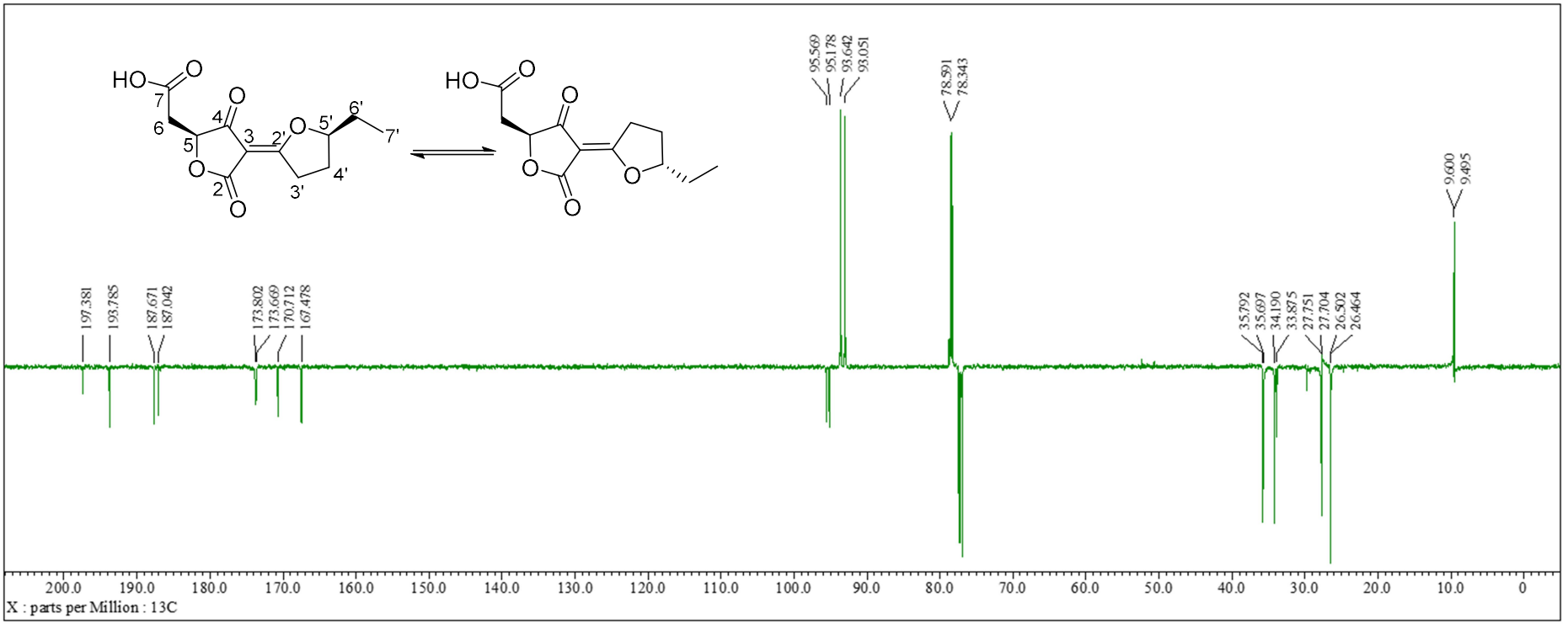

Figure S45. ^{13}C NMR spectrum of compound **13** in $CDCl_3$ (125MHz)

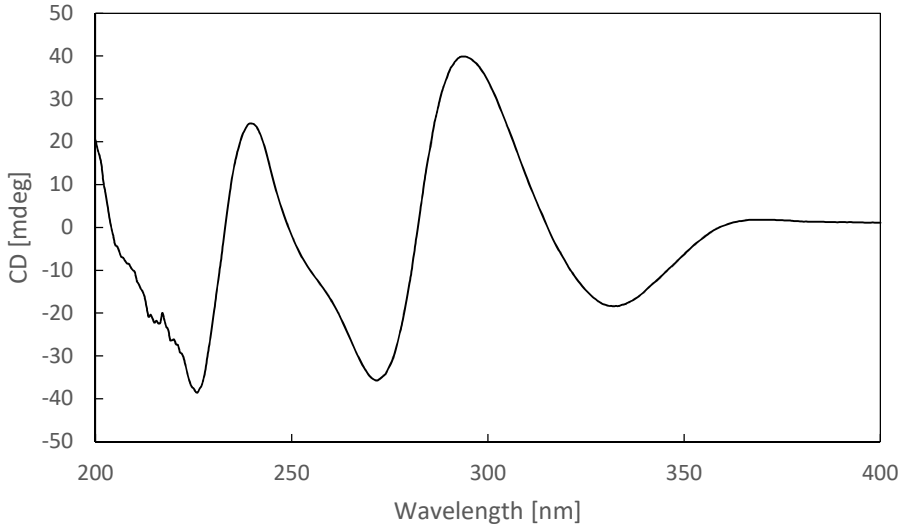

Figure S46. CD spectrum of penilactone A (**1**)

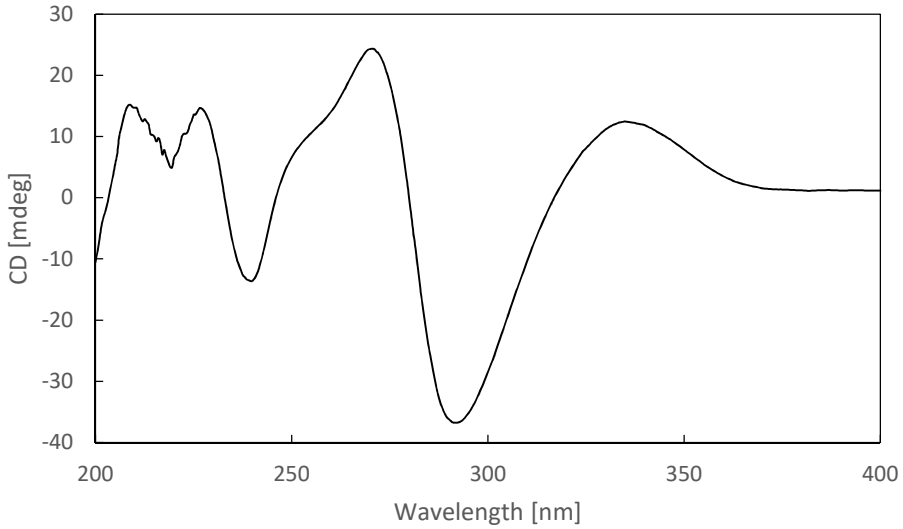

Figure S47. CD spectrum of penilactone B (**2**)

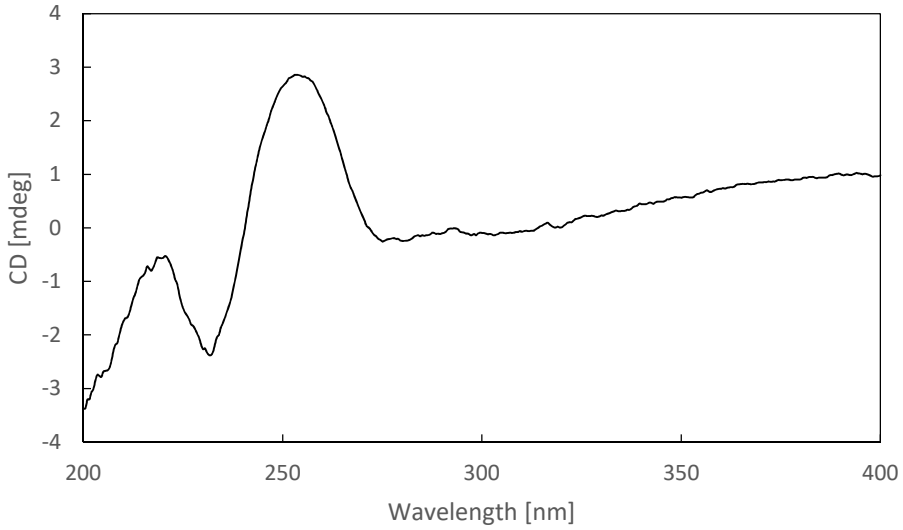

Figure S48. CD spectrum of peniphenone D (**3**)

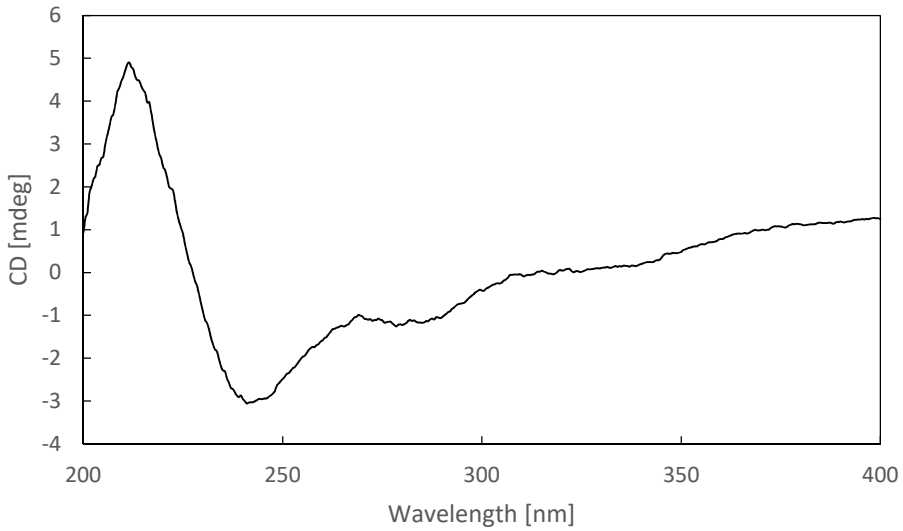

Figure S49. CD spectrum of penilactone D (**4**)

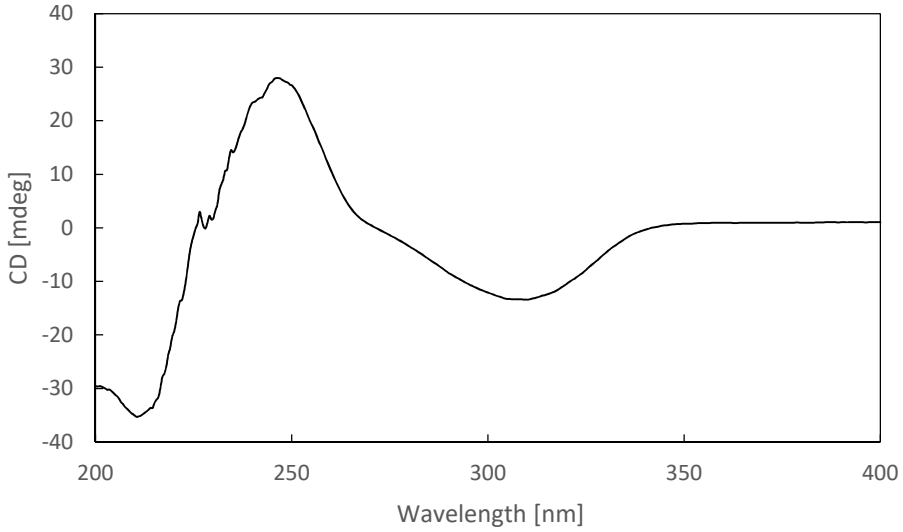

Figure S50. CD spectrum of (*R*)-5-methyltetronic acid (**7**)

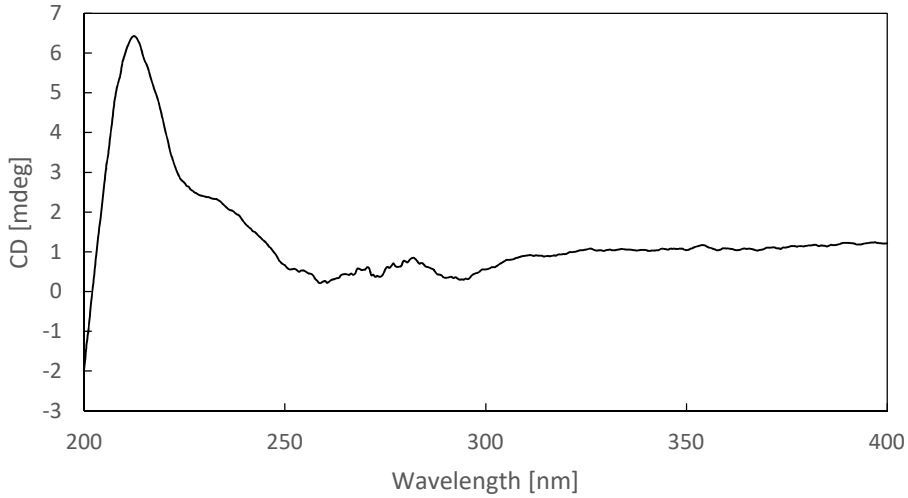

Figure S51. CD spectrum of terrestric acid (**11**)

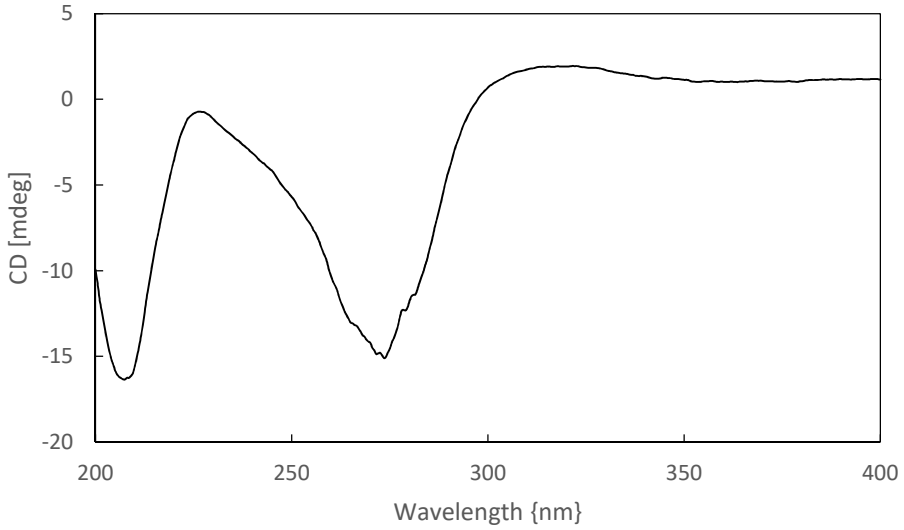

Figure S52. CD spectrum of crustosic acid (**13**)

Supplementary References

(1) Wu, G.; Ma, H.; Zhu, T.; Li, J.; Gu, Q.; Li, D. Penilactones A and B, two novel polyketides from Antarctic deep-sea derived fungus *Penicillium crustosum* PRB-2. *Tetrahedron* **2012,** *68,* 9745.

(2) Li, W.; Fan, A.; Wang, L.; Zhang, P.; Liu, Z.; An, Z.; Yin, W.-B. Asperphenamate biosynthesis reveals a novel two-module NRPS system to synthesize amino acid esters in fungi. *Chem. Sci.* **2018,** *9,* 2589.

(3) Chiang, Y. M.; Ahuja, M.; Oakley, C. E.; Entwistle, R.; Asokan, A.; Zutz, C.; Wang, C. C.; Oakley, B. R. Development of genetic dereplication strains in *Aspergillus nidulans* results in the discovery of aspercryptin. *Angew. Chem. Int. Ed. Engl.* **2016,** *55,* 1662.

(4) Yin, W. B.; Chooi, Y. H.; Smith, A. R.; Cacho, R. A.; Hu, Y.; White, T. C.; Tang, Y. Discovery of cryptic polyketide metabolites from dermatophytes using heterologous expression in *Aspergillus nidulans*. *ACS Synth. Biol.* **2013,** *2,* 629.

(5) Goswami, R. S. Targeted gene replacement in fungi using a split-marker approach. *Methods Mol. Biol.* **2012,** *835,* 255.

(6) Jacobus, A. P. and Gross, J. Optimal cloning of PCR fragments by homologous recombination in *Escherichia coli*. *PLoS. One.* **2015,** *10,* e0119221.

(7) Adrian, J. and Stark, C. B. Total synthesis of muricadienin, the putative key precursor in the solamin biosynthesis. *Org. Lett.* **2014,** *16,* 5886.

(8) Spence, J. T. and George, J. H. Biomimetic total synthesis of ent-penilactone A and penilactone B. *Org. Lett.* **2013,** *15,* 3891.

(9) Stebbins, N. D.; Yu, W.; Uhrich, K. E. Enzymatic polymerization of an ibuprofen-containing monomer and subsequent drug release. *Macromol. Biosci.* **2015,** *15,* 1115.

(10) Williams, K.; Szwalbe, A. J.; Mulholland, N. P.; Vincent, J. L.; Bailey, A. M.; Willis, C. L.; Simpson, T. J.; Cox, R. J. Heterologous production of fungal maleidrides reveals the cryptic cyclization involved in their biosynthesis. *Angew. Chem. Int. Ed Engl.* **2016,** *55,* 6784.

(11) Kusuya, Y.; Takahashi-Nakaguchi, A.; Takahashi, H.; Yaguchi, T. Draft genome sequence of the pathogenic filamentous fungus *Aspergillus udagawae* strain IFM 46973T. *Genome Announc.* **2015,** *3,* e00834-15.

(12) Peter, M.; Kohler, A.; Ohm, R. A.; Kuo, A.; Krutzmann, J.; Morin, E.; Arend, M.; Barry, K. W.; Binder, M.; Choi, C.; Clum, A.; Copeland, A.; Grisel, N.; Haridas, S.; Kipfer, T.; LaButti, K.; Lindquist, E.; Lipzen, A.; Maire, R.; Meier, B.; Mihaltcheva, S.; Molinier, V.; Murat, C.; Pöggeler, S.; Quandt, C. A.; Sperisen, C.; Tritt, A.; Tisserant, E.; Crous, P. W.; Henrissat, B.; Nehls, U.; Egli, S.; Spatafora, J. W.; Grigoriev, I. V.; Martin, F. M. Ectomycorrhizal ecology is imprinted in the genome of the dominant symbiotic fungus *Cenococcum geophilum*. *Nat. Commun.* **2016,** *7,* 12662.

(13) He, Y. and Cox, R. J. The molecular steps of citrinin biosynthesis in fungi. *Chem. Sci.* **2016,** *7,* 2119.

(14) Zabala, A. O.; Chooi, Y. H.; Choi, M. S.; Lin, H. C.; Tang, Y. Fungal polyketide synthase product chain-length control by partnering thiohydrolase. *ACS Chem. Biol.* **2014,** *9,* 1576.

(15) So, K. K.; Kim, J. M.; Nguyen, N. L.; Park, J. A.; Kim, B. T.; Park, S. M.; Hwang, K. J.; Kim, D. H. Rapid screening of an ordered fosmid library to clone multiple polyketide synthase genes of the phytopathogenic fungus *Cladosporium phlei*. *J. Microbiol. Methods* **2012,** *91,* 412.

(16) Yang, X. L.; Awakawa, T.; Wakimoto, T.; Abe, I. Three acyltetronic acid derivatives: noncanonical cryptic polyketides from *Aspergillus niger* identified by genome mining. *Chembiochem.* **2014,** *15,* 1578.

(17) Lonjers, Z. T.; Dickson, E. L.; Chu, T. P.; Kreutz, J. E.; Neacsu, F. A.; Anders, K. R.; Shepherd, J. N.

Identification of a new gene required for the biosynthesis of rhodoquinone in *Rhodospirillum rubrum*. *J. Bacteriol.* **2012,** *194,* 965.

(18) Usami, Y.; Aoki, S.; Hara, T.; Numata, A. New dioxopiperazine metabolites from a *Fusarium* species separated from a marine alga. *J. Antibiot. (Tokyo)* **2002,** *55,* 655.

4.3 Formation of terrestric acid in *Penicillium crustosum* requires redox-assisted decarboxylation and stereoisomerization

OL | Organic Letters

Letter

Cite This: *Org. Lett.* 2020, 22, 88−92

pubs.acs.org/OrgLett

Formation of Terrestric Acid in *Penicillium crustosum* Requires Redox-Assisted Decarboxylation and Stereoisomerization

Jie Fan,[†,§] Ge Liao,[†,§] Lena Ludwig-Radtke,[†] Wen-Bing Yin,[‡] and Shu-Ming Li*[,†]

[†]Institut für Pharmazeutische Biologie und Biotechnologie, Philipps-Universität Marburg, Robert-Koch-Straße 4, Marburg 35037, Germany

[‡]State Key Laboratory of Mycology, Institute of Microbiology, Chinese Academy of Sciences, Beijing 100101, China

Supporting Information

ABSTRACT: Crustosic acid (**1**) differs from terrestric acid (**2**) by a 5*β*-carboxylmethyl at the tetronate ring instead of a 5*α*-methyl group in *Penicillium crustosum*. The formation of **1** via carboxylcrustic and viridicatic acid was confirmed by gene deletion and heterologous expression. The conversion of **1** to **2** requires a decarboxylation-mediated olefination by TraH and subsequent reduction by TraD. The redox-assisted decarboxylation and stereoisomerization proved the biosynthetic relationships of fungal acyltetronates with different stereochemistry.

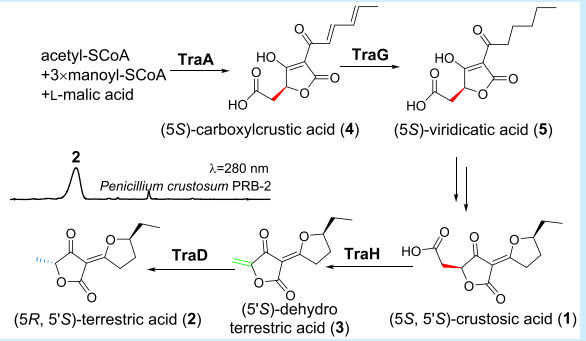

Natural products of the tetronate family with over 100 members contain a characteristic *γ*-butyrolactone ring and are mainly found in *Actinomycetes*.[1,2] Fungus-originated tetronates carry different acyl moieties at C3 and differ from each other often in substituents at C5. Representatives are crustosic acid (**1**), carlic acid, and carlosic acid with a 5*β*-carboxylmethyl moiety, terrestric acid (**2**), carolic acid, and carolinic acid with a 5*α*-methyl group, as well as dehydroterrestric acid (**3**), dehydrocarolic acid, and agglomerin F with an olefinic methylene group at the corresponding position (Figure 1A).[3−9] Despite the interesting structural features of these fungal tetronates, no detailed investigation on their biosynthesis was reported prior to this study. The biosynthesis of agglomerin F in *Aspergillus niger* was proposed after a regulator activation and product isolation (Figure 1B).[7] In this pathway, the hybrid polyketide synthase−nonribosomal peptide synthetase (PKS−NRPS) CaaA should be responsible for the formation of carlosic acid and the P450 oxygenase CaaC for the oxidative decarboxylation to install the exocyclic double bond. The nonheme Fe^{II}/2-oxoglutarate (Fe^{II}-2OG)-dependent oxygenase CaaD was speculated for the oxidation of the terminal methyl group at the acyl chain. However, no genetic and biochemical data support the hypothesis.

We recently identified the terrestric acid biosynthetic gene cluster (*traA-H, pcr11009-pcr11016*) in *Penicillium crustosum* PRB-2 and proved the involvement of the hybrid PKS−NRPS TraA in the formation of **1**. The nonheme Fe^{II}-2OG-dependent oxygenase TraH was proposed for the conversion of **1** to **2** (Figure S1, see Supporting Information (SI)).[9] In this study, we report the functions of TraA and the enoyl reductase TraG to give precursors of **1**. Biochemical investigations proved that the conversion of **1** to **2** was achieved via an oxidative decarboxylation catalyzed by TraH and a subsequent stereospecific reduction with the flavin-containing oxidoreductase TraD.

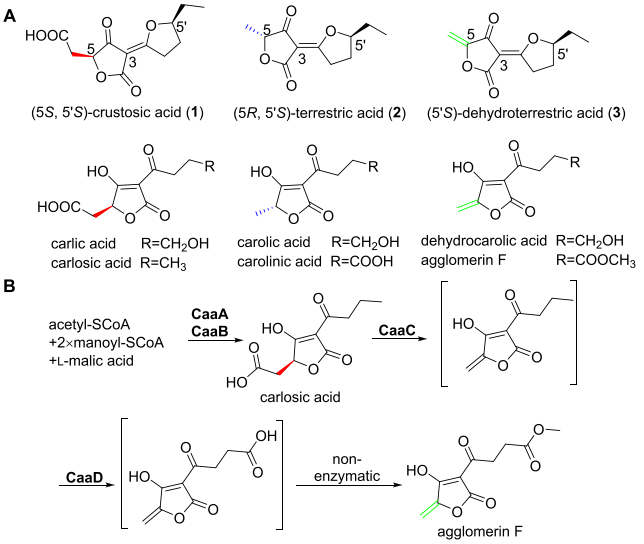

Figure 1. Representatives of acyltetronic acids in fungi (A) and proposed biosynthetic pathway of agglomerin F in *A. niger* (B).

To identify its function, the genomic sequence of *traA* was introduced into *Aspergillus nidulans* LO8030 by PEG-mediated protoplast transformation (Tables S1−S3 and Figure S2).[10−12]

Received: November 8, 2019
Published: December 13, 2019

DOI: 10.1021/acs.orglett.9b04002
Org. Lett. 2020, 22, 88−92

A transformant JF15 harboring *traA* was cultivated as a PD surface culture for 7 days. LC-MS analysis of the EtOAc extract revealed the presence of two new product peaks **4** and **4*** with $[M + H]^+$ ions at *m/z* 253.071 ± 0.005 and almost the same UV spectra (Figures 2A and S3). Both peaks were

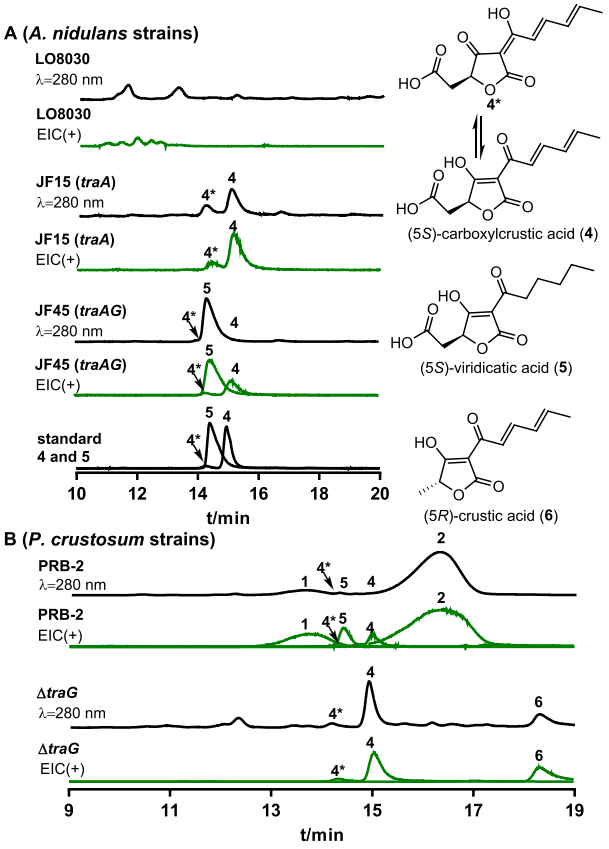

Figure 2. LC-MS analysis of extracts from *A. nidulans* (A) and *P. crustosum* (B). UV absorptions at 280 nm are illustrated. Extracted ion chromatograms (EICs) for $[M + H]^+$ ions of **1**–**6** are given with a tolerance range of ± 0.005.

interchangeable, which was observed during the isolation procedure. Isolation and structure elucidation (Table S5 and Figures S23–S26) proved **4** as the stable form in CD_3OD and identified to be a carboxylmethyltetronic acid derivative with an unsaturated acyl chain, termed carboxylcrustic acid. We proposed **4*** as a tautomer of **4** (Figures 2A and S3). Therefore, TraA, sharing 59.5% sequence identity with CaaA on the amino acid level, functions alone as a tetronate synthase and differs from other known PKS–NRPS enzymes, requiring a *trans*-acting enoyl reductase (ER) for product releasing.[13,14]

Subsequently, coexpression of *traA* and the putative ER *traG* in LO8030 led to accumulation of a predominant peak **5** with an $[M + H]^+$ ion at *m/z* 257.1038 in the obtained transformant JF45, together with the PKS–NRPS product **4** as a minor product (Figures 2A and S3). Isolation and NMR analysis proved **5** to be viridicatic acid, which was also identified in the wild-type PRB-2 (Table S6 and Figures S5 and S27–S31).[15] Obviously, TraG, with sequence identity of 68.9% with CaaB, acts as an enoyl reductase for the reduction of the two double bonds at the acyl chain. This was further confirmed by replacing *traG* with a hygromycin B cassette in PRB-2 (Figures 2B, S4, and S7).[9,16] In comparison to PRB-2, the production of **1**, **2**, and **5** was completely abolished in the Δ*traG* mutant, whereas **4** as the putative substrate of TraG was accumulated and confirmed by ^1H NMR analysis. One additional minor peak with an $[M + H]^+$ ion at *m/z* 209.0827 was identified as a decarboxylated stereoisomer of **4**, termed crustic acid (**6**), by comparing their optical rotation values and CD spectra (Table S7 and Figures S32–S34 and S38). Detection of **6** as a minor metabolite indicates that the enzyme(s) for the conversion of **1** to **2** can also use **4** as substrate, but with low activity.

To identify their metabolism in the biosynthesis, **4** and **5** were fed in the available Δ*traA* and Δ*traG* mutants, respectively (Figures S6–S9). LC-MS analysis revealed that **4** was metabolized to **2** and **6** in the Δ*traA* mutant. Feeding **5** also restored the accumulation of **2** as the predominant product in both Δ*traA* and Δ*traG* mutants, suggesting their involvement in the biosynthesis of **2**.

Structural comparison revealed that **1** is an anhydrous form of a hydroxylated derivative of **5**. Existence of the open form of **1** was confirmed by LC-MS analysis after incubation in D_2O (Figure S10). The equilibrium between the open and closed forms explains well the presence of broad peaks in the LC-MS chromatograms of **1** and **2** (Figures 2B and S5). The responsible enzyme for the hydroxylation of **5** has not been identified yet. It cannot be excluded that the responsible structure gene is located outside the *tra* cluster.

Having identified the formation of **1** with **4** and **5** as precursors, we proceeded to investigate its conversion to **2**. In our previous study, the involvement of the putative Fe^{II}-2OG-dependent oxygenase TraH in the conversion of **1** to **2** was proved by the accumulation of **1** in a Δ*traH* mutant.[9] TraH comprises 327 amino acids and shares a sequence identity of 66% with the aforementioned CaaD (Figure 1B). Sequence alignments showed the typical conserved 2-His-1-Asp ion-binding triad (His_{198}, His_{211}, and Asp_{112}) in TraH (Figure S11).[17,18] For biochemical characterization, the coding sequence of *traH* was amplified from cDNA and cloned into pET28a (+) for overexpression in *Escherichia coli*.[19,20] The recombinant N-terminally His_6-tagged protein was purified to near homogeneity as confirmed on SDS-PAGE, yielding 4.5 mg of purified TraH per liter of bacterial culture (Figure S12). TraH (5.4 μM) was then incubated with 0.5 mM of **1** in the presence of ascorbic acid (AA), $Fe[(NH_4)_2(SO_4)_2]$ (Fe^{II}), 2-oxoglutarate (2OG), and dithiothreitol (DTT) at 37 °C for 30 min.[21] Surprisingly, LC-MS analysis of the full assay showed a product peak with an $[M + H]^+$ ion at *m/z* 209.0806, corresponding to the molecular formula of $C_{11}H_{13}O_4$, but not the expected $C_{11}H_{15}O_4$ for **2** (Figures 3A and S13). Subsequent incubation of TraH with **1** in a large scale enabled us to identify this product as dehydroterrestric acid (**3**) with an exocyclic double bond at the C5-position, which had been identified in *Aspergillus hancockii* (Table S4 and Figure S22).[8] Detailed investigations demonstrated that the activity of TraH is strictly dependent on the presence of 2OG and can be enhanced by externally added Fe^{II} (Figure S14). A K_M value at 0.49 mM and a turnover number (k_{cat}) at 0.02 s^{-1} were determined for TraH reaction with **1** (Figure S13). These results proved that TraH catalyzes an oxidative decarboxylation of **1** to yield **3** instead of **2** (Scheme 1A).

Differing slightly from the previous hypothesis, conversion of **1** to **3** by TraH implies one additional enzyme required for the reduction of **3** to **2**. We took the flavin-containing oxidoreductase TraD as a top candidate for the reduction of the double bond of **3** to the α-methyl group of **2**. TraD comprises 267 amino acids with a well-known conserved FAD-

DOI: 10.1021/acs.orglett.9b04002
Org. Lett. 2020, 22, 88–92

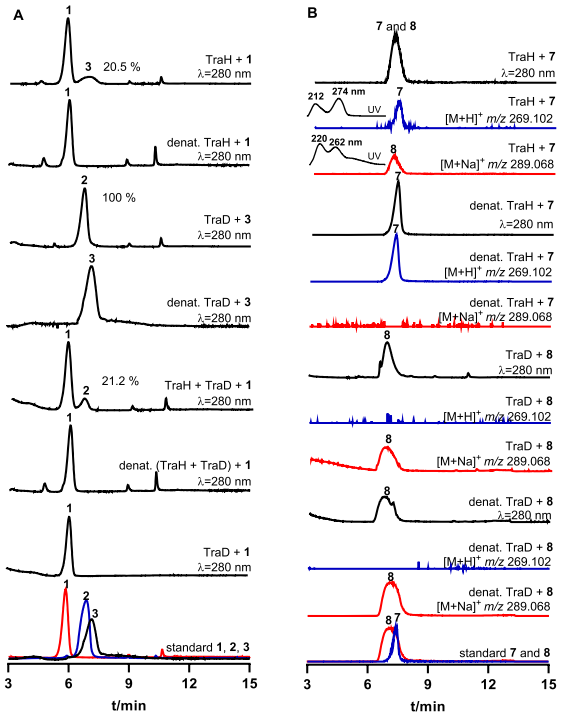

Figure 3. LC-MS analysis of enzyme assays of TraH without or together with TraD with **1**, TraD with **1** or **3** (A), TraH with **7**, and TraD with **8** (B). UV absorptions at 280 nm are illustrated. EICs refer to $[M + H]^+$ of **7** at m/z 269.102 and $[M + Na]^+$ of **8** at m/z 289.068 with a tolerance range of ± 0.005.

binding motif (GXXXGXG).[22−24] To verify its function *in vitro*, TraD was successfully overproduced in *E. coli* BL21-(DE3) in a similar way to TraH. With the aid of Ni-NTA resin, TraD was obtained in a yellow color with a yield of 10.6 mg per liter of bacterial culture (Figure S12). The enzyme assay with 0.6 μM of TraD and 0.5 mM of **3** was carried out in the presence of NADPH at 30 °C. LC-MS analysis revealed that **3** was completely converted to **2** in 10 min (Figure 3A). The high efficiency of the TraD reaction was confirmed by incubation of **3** with different protein amounts. An amount of 23% of a 0.5 mM solution of **3** was consumed by 6 nM of TraD in 10 min (Figure S15). This proved that the reduction of the exocyclic double bond at the C5-position by TraD was much more efficient than the oxidative decarboxylation of **1** by TraH, which was also confirmed by coincubation of **1** with TraH and TraD.

Incubations of 0.5 mM of **1** with TraH and TraD at different ratios in the presence of AA, Fe^{II}, 2OG, and NADPH at 30 °C for 30 min showed sequential formation of the intermediate **3** and final product **2** (Figures 3A and S16). The integrity of **2** from the enzyme assay was confirmed by isolation and comparison of its ^1H NMR and CD spectra with those of **2** from PRB-2 (Table S4 and Figures S17 and S21).[9] Therefore, it can be concluded that the flavin-containing oxidoreductase TraD is responsible for the stereospecific reduction of **3** to yield **2** with a 5α-methyl group. The product yields of **2** and **3** in different assays confirmed the high efficiency of TraD toward **3**, which was only detected at very low TraD concentration. This proved that the conversion of **1** to **2** was controlled by the TraH-catalyzed oxidative decarboxylation of **1** and provides evidence for the absence of **3** in the wild-type PRB-2.

Incubation of **4** with TraH and TraD led to the detection of a very weak peak with the same retention time and fragmentation pattern as those of **6**. The proposed intermediate dehydrocrustic acid with an $[M + H]^+$ at m/z

Scheme 1. Proposed Terrestric Acid Biosynthetic Pathway in *P. crusotusm* PRB-2 (A) and Mechanisms of TraH-Catalyzed Olefination (B)

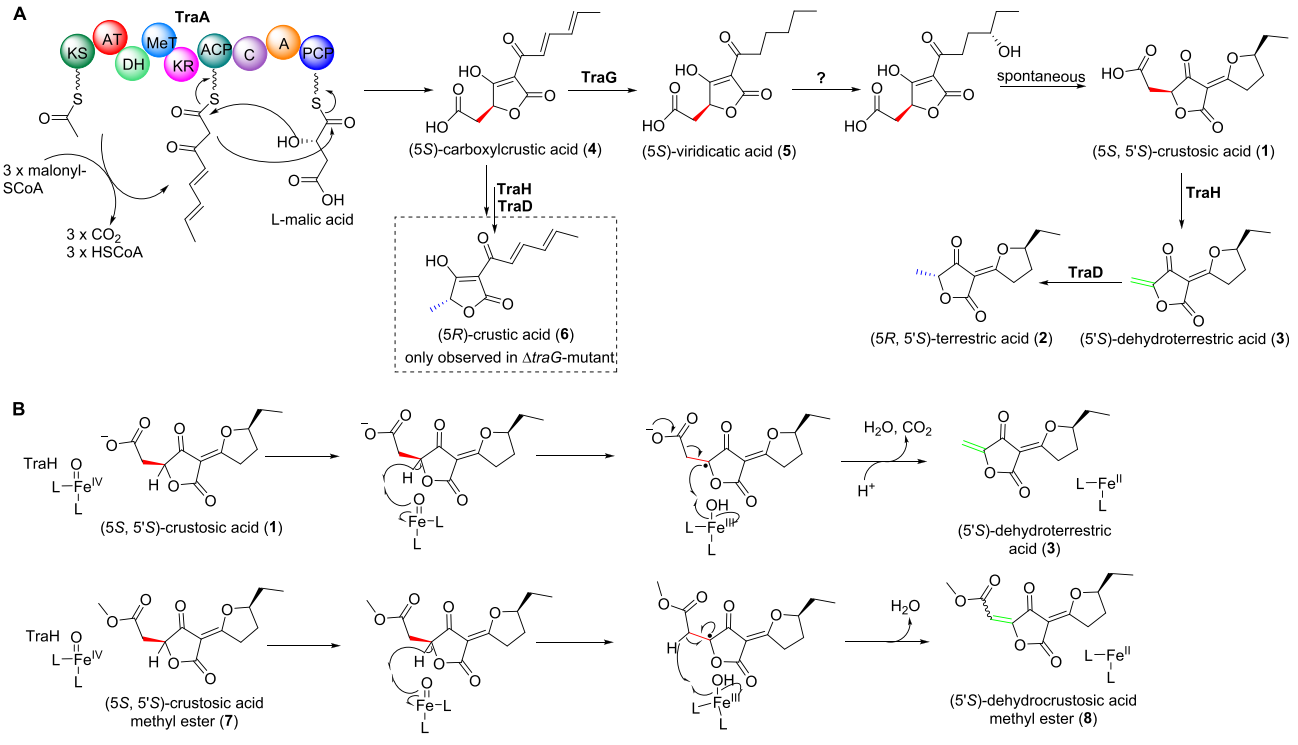

DOI: 10.1021/acs.orglett.9b04002
Org. Lett. 2020, 22, 88−92

207.0662 was also detected in the TraH assay with **4** (Figure S18). These results proved that TraH and TraD can also convert **4** to **6**, but only with very low efficiency, as observed in the Δ*traG* mutant (Scheme 1A).

Taken together, our results proved that the conversion of **1** to **2** required sequential two-step reactions, i.e., oxidative decarboxylation by the nonheme Fe^{II}-2OG-dependent oxygenase TraH and double-bond reduction by the flavin-containing oxidoreductase TraD (Scheme 1A). Oxidative decarboxylations have been reported for enzymes from different families, e.g., the cytochrome P450 OleT,[25] the FAD-dependent decarboxylase CndG,[26] and the radical *S*-adenosyl-L-methionine (SAM) enzyme HemN,[27] as well as the nonheme iron oxidase UndA[28,29] and the nonheme Fe^{II}-2OG-dependent oxygenases IsnB, AmbI3, and ScoE.[30−33] Differing from IsnB, AmbI3, and ScoE with indole vinyl isonitriles as final products, TraH provides a transient intermediate for further reduction, which accomplishes decarboxylation and stereoisomerization in the biosynthesis of fungal acyltetronates with different stereochemistry. In analogy to IsnB, the oxidative decarboxylation by TraH would very likely undergo the abstraction of a hydrogen atom from the *β*-position of COOH by Fe^{IV}-oxo species to generate the substrate radical. Subsequent radical-mediated electron transfer and C−C bond scission eventually install the exocyclic double bond in **3** accompanied by CO_2 elimination (Scheme 1B).

To probe whether the decarboxylation is required for the olefination by TraH, crustosic acid methyl ester (**7**) was prepared by spontaneous methylation of **1** in methanol (Table S8 and Figures S19, S35, and S36). The enzyme assay of **7** with TraH was carried out in a similar way as **1** with TraH. LC-MS analysis revealed the presence of an enzyme product with almost the same retention time as **7** (Figures 3B and S20). Subsequent isolation and structure elucidation by comparison of its ^{1}H NMR data with that of **7** (Tables S8 and S9 and Figures S35 and S37)) led to the unequivocal identification of dehydrocrustosic acid methyl ester (**8**) as the enzyme product, although no ^{13}C NMR data of **8** could be obtained due to low conversion. In comparison to the reported oxidative decarboxylations catalyzed by nonheme Fe^{II}-2OG-dependent oxygenases,[30−32] methylation of **1** redirected the TraH reaction from oxidative decarboxylation of **1** to the sole olefination of **7**. Conversion of **7** to the dehydrogenated product **8** by TraH seems to proceed via a second hydrogen abstraction from the *α*-position of $COOCH_3$ by Fe^{III}−OH species. In total, two consecutive cleavages of the C−H bond with H_2O elimination completed the olefin installation (Scheme 1B). **7** with a K_M at 0.11 mM and k_{cat} at 0.03 s^{-1} seem to be even a better substrate for TraH than **1** (Figure S20). However, neither **7** nor **8** was detected in *P. crustosum* PRB-2. Further incubation of TraD with **8** showed no product formation, indicating the necessity of the terminal double bond for the reduction by TraD.

In summary, our study provides new insights into the biosynthesis of fungal acyltetronic acids, especially the formation of the skeleton and the relationships between different stereoisomers. Heterologous expression and feeding experiments suggested that **4** and **5**, as the products of TraA and TraG, respectively, serve as precursors of **1**, carrying a 5*β*-carboxylmethyl group. Chemically, the conversion of **1** to **2** is a decarboxylation with epimerization. We demonstrated that **1** was first converted by the nonheme Fe^{II}-2OG-dependent oxygenase TraH, via an oxidative decarboxylation, to a transient intermediate **3** carrying an exocyclic double bond. Subsequent stereospecific reduction by the flavin-containing oxidoreductase TraD led to the formation of the final product **2** bearing a 5*α*-methyl group. Among the two-step conversion, the oxidative decarboxylation seems to be the rate-controlling reaction, and its product **3** was immediately consumed by TraD with high efficiency. Differing from other nonheme Fe^{II}-2OG-dependent oxygenases being responsible for decarboxylation-assisted olefination,[30−32] TraH is capable of catalyzing dehydrogenation with or without simultaneous decarboxylation, as demonstrated with **1** and **7** as substrates. It can be speculated that other fungal stereospecific acyltetronic acids mentioned in Figure 1A are very likely biosynthesized in a similar way.

■ ASSOCIATED CONTENT

Supporting Information

The Supporting Information is available free of charge at https://pubs.acs.org/doi/10.1021/acs.orglett.9b04002.

Experimental procedures, physiochemical properties, and NMR spectra (PDF)

■ AUTHOR INFORMATION

Corresponding Author

*E-mail: shuming.li@staff.uni-marburg.de.

ORCID

Wen-Bing Yin: 0000-0002-9184-3198

Shu-Ming Li: 0000-0003-4583-2655

Author Contributions

§J.F. and G.L. contributed equally to this work.

Notes

The authors declare no competing financial interest.

■ ACKNOWLEDGMENTS

We thank Rixa Kraut and Stefan Newel (Philipps-Universität Marburg) for taking MS and NMR spectra, respectively. This project was financially funded in part by the Deutsche Forschungsgemeinschaft (DFG, German Research Foundation)—Li844/11-1 and INST 160/620-1—as well as the National Natural Science Foundation of China—31861133004. Jie Fan (201507565006) and Ge Liao (201607565014) are scholarship recipients from the China Scholarship Council.

■ REFERENCES

(1) Vieweg, L.; Reichau, S.; Schobert, R.; Leadlay, P. F.; Sussmuth, R. D. *Nat. Prod. Rep.* **2014**, *31*, 1554.

(2) Schobert, R.; Schlenk, A. *Bioorg. Med. Chem.* **2008**, *16*, 4203.

(3) Clutterbuck, P. W.; Haworth, W. N.; Raistrick, H.; Smith, G.; Stacey, M. *Biochem. J.* **1934**, *28*, 94.

(4) Bentley, R.; Bhate, D. S.; Keil, J. G. *J. Biol. Chem.* **1962**, *237*, 859.

(5) Bracken, A.; Raistrick, H. *Biochem. J.* **1947**, *41*, 569.

(6) Nukina, M. *Agric. Biol. Chem.* **1988**, *52*, 2357.

(7) Yang, X. L.; Awakawa, T.; Wakimoto, T.; Abe, I. *ChemBioChem* **2014**, *15*, 1578.

(8) Pitt, J. I.; Lange, L.; Lacey, A. E.; Vuong, D.; Midgley, D. J.; Greenfield, P.; Bradbury, M. I.; Lacey, E.; Busk, P. K.; Pilgaard, B.; Chooi, Y. H.; Piggott, A. M. *PLoS One* **2017**, *12*, No. e0170254.

(9) Fan, J.; Liao, G.; Kindinger, F.; Ludwig-Radtke, L.; Yin, W.-B.; Li, S.-M. *J. Am. Chem. Soc.* **2019**, *141*, 4225.

(10) Yin, W. B.; Chooi, Y. H.; Smith, A. R.; Cacho, R. A.; Hu, Y.; White, T. C.; Tang, Y. *ACS Synth. Biol.* **2013**, *2*, 629.

DOI: 10.1021/acs.orglett.9b04002
Org. Lett. 2020, 22, 88−92

(11) Li, W.; Fan, A.; Wang, L.; Zhang, P.; Liu, Z.; An, Z.; Yin, W.-B. *Chem.Sci.* **2018**, *9*, 2589.
(12) Chiang, Y. M.; Ahuja, M.; Oakley, C. E.; Entwistle, R.; Asokan, A.; Zutz, C.; Wang, C. C.; Oakley, B. R. *Angew. Chem., Int. Ed.* **2016**, *55*, 1662.
(13) Halo, L. M.; Marshall, J. W.; Yakasai, A. A.; Song, Z.; Butts, C. P.; Crump, M. P.; Heneghan, M.; Bailey, A. M.; Simpson, T. J.; Lazarus, C. M.; Cox, R. J. *ChemBioChem* **2008**, *9*, 585.
(14) Xu, W.; Cai, X.; Jung, M. E.; Tang, Y. *J. Am. Chem. Soc.* **2010**, *132*, 13604.
(15) Birkinshaw, J. H.; Samant, M. S. *Biochem. J.* **1960**, *74*, 369.
(16) Goswami, R. S. *Methods Mol. Biol.* **2012**, *835*, 255.
(17) Gao, S.-S.; Naowarojna, N.; Cheng, R.; Liu, X.; Liu, P. *Nat. Prod. Rep.* **2018**, *35*, 792.
(18) Nakamura, H.; Matsuda, Y.; Abe, I. *Nat. Prod. Rep.* **2018**, *35*, 633.
(19) Yu, H.; Li, S.-M. *Org. Lett.* **2019**, *21*, 7094.
(20) Yu, X.; Li, S.-M. *Methods Enzymol.* **2012**, *516*, 259.
(21) Steffan, N.; Grundmann, A.; Afiyatullov, A.; Ruan, H.; Li, S.-M. *Org. Biomol. Chem.* **2009**, *7*, 4082.
(22) Bottoms, C. A.; Smith, P. E.; Tanner, J. J. *Protein Sci.* **2002**, *11*, 2125.
(23) Hanukoglu, I. *J. Mol. Evol.* **2017**, *85*, 205.
(24) Romeo, C.; Moriwaki, N.; Yasunobu, K. T.; Gunsalus, I. C.; Koga, H. *J. Protein Chem.* **1987**, *6*, 253.
(25) Grant, J. L.; Hsieh, C. H.; Makris, T. M. *J. Am. Chem. Soc.* **2015**, *137*, 4940.
(26) Rachid, S.; Revermann, O.; Dauth, C.; Kazmaier, U.; Müller, R. *J. Biol. Chem.* **2010**, *285*, 12482.
(27) Ji, X.; Mo, T.; Liu, W. Q.; Ding, W.; Deng, Z.; Zhang, Q. *Angew. Chem., Int. Ed.* **2019**, *58*, 6235.
(28) Rui, Z.; Li, X.; Zhu, X.; Liu, J.; Domigan, B.; Barr, I.; Cate, J. H. D.; Zhang, W. *Proc. Natl. Acad. Sci. U. S. A.* **2014**, *111*, 18237.
(29) Manley, O. M.; Fan, R.; Guo, Y.; Makris, T. M. *J. Am. Chem. Soc.* **2019**, *141*, 8684.
(30) Chang, W. C.; Sanyal, D.; Huang, J. L.; Ittiamornkul, K.; Zhu, Q.; Liu, X. *Org. Lett.* **2017**, *19*, 1208.
(31) Huang, J. L.; Tang, Y.; Yu, C. P.; Sanyal, D.; Jia, X.; Liu, X.; Guo, Y.; Chang, W. C. *Biochemistry* **2018**, *57*, 1838.
(32) Yu, C. P.; Tang, Y.; Cha, L.; Milikisiyants, S.; Smirnova, T. I.; Smirnov, A. I.; Guo, Y.; Chang, W. C. *J. Am. Chem. Soc.* **2018**, *140*, 15190.
(33) Harris, N. C.; Born, D. A.; Cai, W.; Huang, Y.; Martin, J.; Khalaf, R.; Drennan, C. L.; Zhang, W. *Angew. Chem., Int. Ed.* **2018**, *57*, 9707.

DOI: 10.1021/acs.orglett.9b04002
Org. Lett. 2020, 22, 88−92

Supporting Information

Formation of terrestric acid in *Penicillium crustosum* requires redox-assisted decarboxylation and stereoisomerization

Jie Fan,[1,†] Ge Liao,[1,†] Lena Ludwig-Radtke,[1] Wen-Bing Yin,[2] and Shu-Ming Li[1,*]

[1]Institut für Pharmazeutische Biologie und Biotechnologie, Philipps-Universität Marburg, Robert-Koch-Straße 4, Marburg 35037, Germany

[2]State Key Laboratory of Mycology, Institute of Microbiology, Chinese Academy of Sciences, Beijing 100101, China

[†]These authors contributed equally to this work.

Table of content

Experiment Procedures

1. Computer-assisted sequence analysis

Sequence analysis of terrestric acid gene cluster was carried out by antiSMASH (http://antismash.secondarymetabolites.org/) and by comparison with known entries in database. The genomic DNA sequence of the terrestric acid cluster from *P. crustosum* PRB-2 reported in this study is available at GenBank under the accession number MK360919. Multiple sequence alignments for TraH and analogues were carried out with the program ClustalW and visualized with ESPript 3.2 (http://espript.ibcp.fr/ESPript/cgi-bin/ESPript.cgi) to identify strictly conserved amino acid residues.

2. Strains, media and growth conditions

The fungal strains used in this study are summarized in Table S1. *Penicillium crustosum* strain PRB-2 was isolated from a deep-sea sediment collected in Prydz Bay at a depth of -526 m.[1] The wild type strain PRB-2 and deletion mutants *ΔtraA* and *ΔtraG* were cultivated on PDA plates (potato dextrose broth, Sigma) with 1.6% agar at 25°C for sporulation and in PD surface culture at 25°C for 7 days for detection of secondary metabolites (SMs).

Aspergillus nidulans strains were grown at 37°C on GMM medium (1.0% glucose, 50 mL/L salt solution, 1 mL/L trace element solution, 1.6% agar) for sporulation and transformation with appropriate nutrition as required, and incubated at 25°C in PD medium for 7 days for SM detection.[2-4] The salt solution contains (*w/v*) 12% $NaNO_3$, 1.04% KCl, 1.04% $MgSO_4{\cdot}7H_2O$, and 3.04% KH_2PO_4. The trace element solution comprises (*w/v*) 2.2% $ZnSO_4{\cdot}7H_2O$, 1.1% H_3BO_3, 0.5% $MnCl_2{\cdot}4H_2O$, 0.16% $FeSO_4{\cdot}7H_2O$, 0.16% $CoCl_2{\cdot}5H_2O$, 0.16% $CuSO_4{\cdot}5H_2O$, 0.11% $(NH_4)_6Mo_7O_{24}{\cdot}4H_2O$, and 5% Na_4EDTA.

Escherichia coli DH5α and BL21(DE3) were grown in liquid or on solid Luria-Bertani (LB) medium (1% NaCl, 1% tryptone, and 0.5% yeast extract) for standard DNA manipulation. 50 μg/mL carbenicillin or 25 μg/mL kanamycin were supplemented for cultivation of recombinant *E. coli* strains.

3. Genomic DNA isolation

The mycelia of *P. crustosum* and *A. nidulans* were collected on sterilized filter paper and then suspended in 400 μL of LETS buffer (10 mM Tris-HCl pH 8.0, 20 mM EDTA pH 8.0, 0.5% SDS, and 0.1 M LiCl) in 2 mL Eppendorf tubes and vigorous vortexed with four glass beads (2.85 mm in diameter). 300 μL LETS buffer were added in the solution, which was subsequently treated with 700 μL phenol: chloroform: isoamylol (25:24:1). The genomic DNA (gDNA) was precipitated by addition of 900 μL absolute ethanol and centrifugation at 17,000 x *g* for 30 min. After washing with 70% ethanol and drying, the obtained DNA was dissolved in 50 μL distillated H_2O.

4. RNA isolation and cDNA synthesis

For isolation of RNA from *P. crustosum* PRB-2, the fungus was cultivated in liquid PD medium shaking at 230 rpm for 7 days and the cells were collected by centrifugation. RNA extraction was performed by using Fungal RNA Mini kit (VWR OMEGA bio-tek E.Z.N.A) according to the standard manufacturer´s instruction. The ProtoScript II First Strand cDNA Synthesis kit (BioLabs) was used for cDNA synthesis with Oligo-dT primers.

5. PCR amplification, gene cloning and plasmid construction

Plasmids used in this study are listed in Table S2. The oligonucleotide sequences for PCR amplification are given in Table S3. Genetic manipulation in *E. coli* was carried out according to the protocol by Sambrook and Russell.[5] All primers were synthesized by Seqlab GmbH (Göttingen, Germany). PCR amplification was carried out by using Phusion® High-Fidelity DNA polymerase from New England Biolabs (NEB) on a T100TM Thermal cycler from Bio-Rad. PCR reaction mixtures and thermal profiles were set as recommended by the manufacturer´s instruction.

To construct pJF80 and pJF81 for *traG* deletion, primers were designed with split-marker strategy by using p5HY and p3YG vectors (Figure S4).[6,7] To construct the plasmids for heterologous expression of *traA* and *traAG* in *A. nidulans*, an assembly approach based on the homologous recombination in *E. coli* was used (Figure S2).[8] Full length of *traA* including its terminator of 497 bp was amplified from gDNA of *P. crustosum* PRB-2 as the template by PCR with primer pairs A.n-traA-1F-For/1F-Rev and A.n-traA-2F-For/2F-Rev (Table S3) and inserted into the corresponding sites of pYH-wA-pyrG with homologous flanking sequences of the *wA* gene to create pJF27.[4] For co-expression of *traA* and *traG*, *traA* including *gpdA* promoter and its terminator of 497 bp from pJF27, and *traG* with its 778 bp promoter and 568 bp terminator from *P. crustosum* PRB-2 were cloned into pYWB2 by homologous recombination with flanking sequences of the *wA* gene to create pJF91.[9] Herein, primers A.n-traAG-1F-For/traA-1F-Rev, A.n-traA-2F-For/traAG-1F-Rev and A.n-traAG-2F-For/2F-Rev (Table S3) were used for PCR amplification.

To construct the plasmid for expressing *traD* and *traH* in *E. coli*, the coding region of *traD* and *traH* were amplified by PCR from cDNA with the primer pairs TraD-28-For/Rev and TraH-28-For/Rev (Table S3). The expression vector pET-28a (+) was digested with BamHI and EcoRI, and ligated with DNA fragments by homologous recombination yielding the expression plasmid pJF72 for TraD and pJF74 for TraH, which were confirmed by sequencing (Seqlab GmbH).

6. Deletion of *traG* in *P. crustosum* and cultivation of deletion mutants.

Fresh conidia from 7-day PDA culture of *P. crustosum* PRB-2 were inoculated into 30 mL LMM medium (1.0% glucose, 50 mL/L salt solution, 1 mL/L trace element solution, and 0.5% yeast extract) in 100 mL flask and incubated at 25°C and 230 rpm for germination. Mycelia were harvested after 11 h by centrifugation at 2,800 x *g* for 10 min, and washed with distillated H_2O. The mycelia were then transferred into a 50 mL flask with 10 mL of osmotic buffer (1.2 M $MgSO_4$ in 10 mM sodium phosphate, pH 5.8) containing 50 mg lysing enzyme from *Trichoderma harzianum* (Sigma) and 20 mg yatalase from *Corynebacterium sp.* OZ-21 (OZEKI Co., Ltd.). After shaking at 30°C and 100 rpm for 2.5 h, the cells were transferred into a 50 mL falcon tube and overlaid gently with 10 mL of trapping buffer (0.6 M sorbitol in 0.1 M Tris-HCl, pH 7.0). After centrifugation at 4°C and 2,800 x *g* for 10 min, the protoplasts were collected from the interface of the two buffer systems. The protoplasts were then transferred to a sterile 15 mL falcon tube and resuspended in 200 μL of STC buffer (1.2 M sorbitol, 10 mM $CaCl_2$, and 10 mM Tris-HCl, pH 7.5) for transformation.

The *via* PCR constructed gene deletion cassettes mentioned above were transformed into *P. crustosum* by polyethylene glycol (PEG) mediated protoplast transformation. The DNA fragments (2 μg) were incubated with 100 μL of the protoplasts for 50 min on ice. 1.25 mL of PEG solution (60% PEG 4000, 50 mM $CaCl_2$, 50 mM Tris-HCl, pH 7.5) was then added and gently mixed. After incubation at room temperature for 30 min, the mixture was transferred in 5 mL STC buffer and spread on plates with SMM bottom medium (1.0% glucose, 50 mL/L salt solution, 1 mL/L trace element solution, 1.2 M sorbitol, and 1.6% agar) containing 200 μg/mL hygromycin B. SMM top medium (1.0% glucose, 50 mL/L salt solution, 1 mL/L trace element solution, 1.2 M sorbitol, and 0.8% agar) containing 100 μg/mL hygromycin B was overlaid softly on the plates. Three days later, the transformants were transferred onto fresh PDA plates containing 200 μg/mL hygromycin B for second round selection. The obtained transformants were inoculated in PD medium for isolation of genomic DNA to verify the integrity, which was carried out by PCR amplification (Figure S4). The obtained Δ*traG* mutant was cultivated in PD liquid medium at 25 °C for 7 days, together with Δ*traA* mutant in a previous study.[6] For SM detection of the deletion mutants, cultures were extracted with ethyl acetate, dissolved in a mixture of MeOH and H_2O (8 : 2) and analyzed on LC-MS by method B (see below for methods of HPLC and LC-MS analysis).

7. Heterologous expression of *traA* and *traG* in *A. nidulans*

A. nidulans strain LO8030 was used as the recipient host.[3] Fungal protoplast preparation and transformation were performed according to the method described previously.[3] pJF27 containing the PKS-NRPS gene *traA* was transformed into LO8030 to create the *traA* expression strain JF15. pJF91 containing both *traA* and *traG* was transformed into LO8030 to create the *traAG* expression strain JF45. Potential transformants were verified by PCR using the primers traA-F/R or traG-F/R (Table S3). Differing from *P. crustosum*, germination condition was at 37°C with appropriate nutrition as supplements (0.75 μM riboflavin and 0.5 μM pyridoxine for JF15, 5% uracil, 6% uridine and 0.5 μM pyridoxine for JF45) for 6 h. Protoplastation condition was at 37°C for 2.5 h. *A. nidulans* strains were cultivated in PD liquid medium at 25°C for 7 days for LC-MS analysis (method B) of the SM production.

8. Precursor feeding in *P. crustosum* deletion mutants

For feeding experiments, the precursors (5*S*)-carboxylcrustic acid (**4**) and (5*S*)-viridicatic acid (**5**) were dissolved in DMSO to give 1 M stock solution, and added to 10 mL of PD cultures of respective deletion mutants, **4** to Δ*traA* mutant, and **5** to Δ*traA* and Δ*traG*, leading to final concentrations of 0.4 mM. After further cultivation at 25°C for 7 d in PD medium, the secondary metabolites were extracted with ethyl acetate, dissolved in a mixture of MeOH and H_2O (8 : 2) and analyzed on LC-MS by method B (see below for methods of HPLC and LC-MS analysis).

9. Overproduction and purification of TraD and TraH

The expression plasmids pJF72 and pJF74 were constructed for TraD and TraH expression in *E. coli* as mentioned above. The recombinant *E. coli* BL21(DE3) strains were cultivated in Terrific Broth (TB) medium (2.4% yeast extract, 2.0% tryptone, 0.4% glycerol, 0.1 M phosphate buffer, pH 7.4). TraH expression was induced with 0.5 mM IPTG at 20°C for 16 h and TraD at 16°C for 16 h. The recombinant His_6-tagged protein were purified on Ni-NTA affinity chromatography

(Qiagen, Hilden) using the published procedures.[10,11] The purity for TraH and TraD were confirmed on sodium dodecyl sulfate-polyacrylamide gel electrophoresis (SDS-PAGE) (Figure S12). The protein concentration was determined on Nanodrop 2000c spectrophotometer (Thermo Scientific, Braunschweig, Germany). 4.5 mg/L of protein can be obtained for TraH, 10.6 mg/L of protein can be obtained for TraD from the bacterial culture.

10. *In vitro* assays of TraD and TraH

To determine the enzyme activity of TraH toward (5*S*, 5'*S*)-crustosic acid (**1**) or (5*S*, 5'*S*)-crustosic acid methyl ester (**7**), the enzyme assays (50 μL) contained phosphate buffer (20 mM, pH 7.4), ascorbic acid (1 mM), (5*S*, 5'*S*)-crustosic acid (**1**, 0.5 mM) or (5*S*, 5'*S*)-crustosic acid methyl ester (**7**, 0.5 mM), DTT (1 mM), $Fe[(NH_4)_2(SO_4)_2]$ (1 mM), 2-oxoglutarate (1 mM), glycerol (0.5 − 5%), DMSO (5%), and the purified recombinant TraH (5.4 μM). The enzyme assays were carried out at 37 °C for 30 min and terminated with one volume of acetonitrile. The reaction mixtures were centrifuged at 17,000 x *g f*or 30 min before further analysis on HPLC and LC-MS by method A (see below for methods of HPLC and LC-MS analysis).

To determine the enzyme activity of TraD toward dehydroterrestric acid (**3**), the enzyme assays (50 μL) contained phosphate buffer (20 mM, pH 7.4), NAD(P)H (2 mM), glycerol (0.5 − 5%), DMSO (5%), dehydroterrestric acid (**3**, 0.5 mM), and the purified recombinant TraD (0.6 μM). The enzyme assays were incubated at 30 °C for 10 min and terminated with one volume of acetonitrile. The reaction mixtures were centrifuged at 17,000 x *g* for 30 min before further analysis on HPLC and LC-MS by method A. The same reaction condition was used for the enzyme assay of TraD with (5'*S*)-dehydrocrustosic acid methyl ester (**8**).

To prove the conversion of (5*S*, 5'*S*)-crustosic acid (**1**) by TraH and TraD, the enzyme assays (50 μL) contained phosphate buffer (20 mM, pH 7.4), ascorbic acid (1 mM), (5*S*, 5'*S*)-crustosic acid (**1**, 0.5 mM), $Fe[(NH_4)_2(SO_4)_2]$ (1 mM), 2-oxoglutarate (1 mM), NADPH (2 mM), glycerol (0.5 − 5%), DMSO (5%), and the purified recombinant TraH (5.4 μM) and TraD (0.6 μM). The enzyme assays were incubated at 30 °C for 30 min and terminated with one volume of acetonitrile. The reaction mixtures were centrifuged at 17,000 x *g* for 30 min before further analysis on HPLC and LC-MS by method A.

To prove the conversion of (5*S*)-carboxylcrustic acid (**4**) to (5*R*)-crustic acid (**6**) by TraH and TraD, the enzyme assays (50 μL) containing phosphate buffer (20 mM, pH 7.4), ascorbic acid (1 mM), (5*S*)-carboxylcrustic acid (**4**, 0.5 mM), DTT (1 mM), $Fe[(NH_4)_2(SO_4)_2]$ (1 mM), 2-oxoglutarate (1 mM), NAD(P)H (2 mM), glycerol (0.5 − 5%), DMSO (5%), and the purified recombinant TraH (12 μM) and TraD (6 μM) were incubated at 30°C for 16 h and terminated with one volume of acetonitrile. The reaction mixtures were centrifuged at 17,000 x *g* for 30 min before further analysis on HPLC and LC-MS by method A. In addition, (5*S*)-carboxylcrustic acid (**4**, 0.5 mM) was incubated with TraH (12 μM) in the presence of ascorbic acid (1 mM), DTT (1 mM), $Fe[(NH_4)_2(SO_4)_2]$ (1 mM), 2-oxoglutarate (1 mM) at 37°C for 16 h. After terminated with acetonitrile and centrifugation, the enzyme assay was further analyzed on HPLC and LC-MS by method A.

11. Large-scale fermentation, extraction and isolation of secondary metabolites

To isolate **4** from *A. nidulans* carrying *traA*, the transformant JF15 was cultivated in 60 x 250 mL flasks each containing 50 mL PD liquid medium with appropriate nutrition as supplement at 25°C for 7 days. The supernatant and mycelia were separated, and extracted with ethyl acetate and acetone, separately. The acetone extract was concentrated under reduced pressure to afford an aqueous solution, and then extracted with ethyl acetate. The two ethyl acetate extracts were combined and evaporated under reduced pressure to give a crude extract (0.8 g). The crude extract was applied to Sephadex LH-20 column eluted with methanol, yielding twenty fractions (1 – 20). Fraction 8 was purified on a semi-preparative HPLC (acetonitrile / H_2O (40 : 60) with 0.1% trifluoroacetic acid) yielding compound **4** (8 mg).

To isolate **5** from *A. nidulans* carrying *traA* and *traG*, the transformant JF45 was cultivated in 10 x 1 L flasks each containing 100 g rice and 150 mL H_2O (with appropriate nutrition as supplement) at 25°C for 7 days. After extracting with 15 L ethyl acetate and concentrated under reduced pressure, the crude extract (2.5 g) obtained from JF45 cultivation was applied to silica gel column chromatography by using petroleum ether / EtOAc (1 : 1, 1 : 3, and 1 : 5, *v/v*) as elution solvents, giving fractions 1 − 10. **5** (15 mg) was obtained from fraction 3 after purification on Sephadex LH-20 column using MeOH as eluent.

To isolate **5** from *P. crustosum* PRB-2, spores were inoculated in 4 L PD liquid medium and cultivated at 25°C for 14 days. 1.0 g crude extract was obtained after extraction, and subjected to silica gel column chromatography by using petroleum ether / EtOAc (10 : 1, 3 : 1, 1 : 1, 1 : 3, 1 : 6, *v/v*) as elution solvents, giving fractions 1 − 5. **5** (3 mg) was obtained from fraction 3 by applying to Sephadex LH-20 column using MeOH as eluent.

To isolate the accumulated products **4** and **6** from Δ*traG* mutant, the strain was cultivated in 6 L PD liquid medium at 25°C for 14 days and extracted as mentioned above. The resulted crude extract (2.5 g) was subjected to silica gel column chromatography by using stepwise gradient elution with the mixtures of petroleum ether / EtOAc (10 : 1, 5 : 1, 3 : 1, and 1 : 1, *v/v*) to give 25 fractions. Subsequent purification on semi-preparative HPLC with isocratic elution using acetonitrile / H_2O (40 : 60) supplied with 0.1% trifluoroacetic acid yielded 3 mg of **4**, using acetonitrile / H_2O (70 : 30) with 0.1% trifluoroacetic acid yielded 5 mg of **6**.

To prepare the enzyme products for structural elucidation, assays were carried out in large scales (10 − 20 mL) using the reaction conditions mentioned above. The reaction mixtures were extracted with double volume of ethyl acetate for three times. The organic phases were combined and concentrated under vacuum. The resulted residues were dissolved in acetonitrile and centrifuged at 17,000 x *g* for 20 min. After isolation on semi-preparative HPLC eluted with 40% acetonitrile containing 0.1% trifluoroacetic acid, compound **2** from the incubation mixture of TraH, TraD and **1**, compound **3** from TraH and **1**, and **5** from TraH and **4**, were obtained.

12. Determination of kinetic parameters

For determination of kinetic parameters of TraH toward **1** or **7**, the enzyme assays were carried out in a similar way as mentioned above, excepting that substrates at final concentrations of

0.01, 0.02, 0.05, 0.1, 0.2, 0.5, 1, 2, 5 mM, respectively. The enzyme assays were incubated at 37°C for 30 min and terminated with one volume of acetonitrile. The supernatants were subjected to HPLC analysis by method A after centrifuging at 17,000 *x g* for 30 min. The K_M and *kcat* values were obtained by analysis with GraphPad Prism 8.

13. HPLC and LC-MS analysis of secondary metabolites

Analysis of SMs was performed on an Agilent series 1200 HPLC (Agilent Technologies, Böblingen, Germany) with an Agilent Eclipse XDB-C18 column (150 × 4.6 mm, 5 μm). Water (A) and acetonitrile (B), both with 0.1% (*v/v*) formic acid, were used as solvents at flow rate of 0.5 mL/min. The substances were eluted with a linear gradient from 5 – 100% B in 15 min, then washed with 100% (*v/v*) solvent B for 5 min and equilibrated with 5% (*v/v*) solvent B for 5 min (method A) or with a linear gradient from 5 – 100% B in 40 min, then washed with 100% (*v/v*) solvent B for 5 min and equilibrated with 5% (*v/v*) solvent B for 10 min (method B). UV absorptions at 280 nm were illustrated in this study. Semi-preparative HPLC was performed on the same equipment with an Agilent Eclipse XDB-C18 column (9.4 × 250 mm, 5 μm) column and a flow rate of 2 mL/min.

LC-MS analysis was performed on an Agilent 1260 HPLC system equipped with a microTOF-Q III spectrometer (Bruker, Bremen, Germany) by using Multospher 120 RP18-5μ column (250 × 2 mm, 5 μm) (CS-Chromatographie Service GmbH) and method A or method B for separation at flow rate of 0.25 mL/min. Electrospray positive or negative ionization mode was selected for determination of the exact masses. The capillary voltage was set to 4.5 kV and a collision energy of 8.0 eV. Sodium formate was used in each run for mass calibration. The masses were scanned in the range of *m/z* 100 – 1500. Data were evaluated with the Compass DataAnalysis 4.2 software (Bruker Daltonik, Bremen, Germany).

14. NMR analysis

NMR spectra were recorded on a JEOL ECA-500 MHz spectrometer (JEOL, Tokyo, Japan). The spectra were processed with MestReNova 6.1.0 (Metrelab) or Delta 5.0.4 (JEOL). Chemical shifts are referenced to those of the solvent signals. NMR data are given in Tables S4 – S8 and spectra in Figures S21 – S35.

15. Circular dichroism (CD) spectroscopic analysis

CD spectra were taken on a J-815 CD spectrometer (Jasco Deutschland GmbH, Pfungstadt, Germany). The samples were dissolved in methanol and measured in the range of 200–400 nm by using a 1 mm path length quartz cuvette (Hellma Analytics, Müllheim, Germany). The CD spectra are given in Figures S36.

16. Measurement of optical rotations

The optical rotation was measured with the polarimeter Jasco DIP-370 at 20°C using the D-line of the sodium lamp at λ=589.3 nm. Prior to the measurement, the polarimeter was calibrated with methanol or ethanol as solvent.

17. Physiochemical properties of the compounds described in this study

(5*R*, 5'*S*)-terrestric acid (**2**): Yellow oil; CD (MeOH): λ_{max} ($\Delta\varepsilon$) 282 (+0.9) nm, 228 (+2.8), 212

(+7.5); HRMS (*m/z*): (ESI/$[M+H]^+$) calcd. for $C_{11}H_{15}O_4$, 211.0965, found 211.0963.

(5'*S*)-dehydroterrestric acid (**3**): White powder; HRMS (*m/z*): (ESI/$[M+H]^+$) calcd. for $C_{11}H_{13}O_4$, 209.0808, found 209.0806.

(5*S*)-carboxylcrustic acid (**4**): Yellow oil; $[\alpha]_D^{20}$ = -46.5 (*c* 0.40, MeOH); HRMS (*m/z*): (ESI/$[M+H]^+$) calcd. for $C_{12}H_{13}O_6$, 253.0707, found 253.0719
CD spectrum (MeOH) of sample isolated from a *A. nidulans* strain JF15 harboring *traA*: λ_{max} ($\Delta\varepsilon$) 332 (-1.9), 268 (-1.7), 228 (-4.1) nm .
CD spectrum (MeOH) of sample isolated from Δ*traG* mutant of *P. crustosum*: λ_{max} ($\Delta\varepsilon$) 346 (-2.8), 279 (-3.9), 223 (-6.0) nm.

(5*S*)-viridicatic acid (**5**): Yellow oil; $[\alpha]_D^{20}$ = -73.6 (*c* 1.0, EtOH); HRMS (*m/z*): (ESI/$[M+H]^+$) calcd. for $C_{12}H_{17}O_6$, 257.1020, found 257.1038.
CD spectrum (MeOH) of sample isolated from a *A. nidulans* strain JF45 harboring *traA* and *traG*: λ_{max} ($\Delta\varepsilon$) 258 (-11.4), 230 (-11.3) nm.
CD spectrum (MeOH) of sample isolated from *P. crustosum* PRB-2: λ_{max} ($\Delta\varepsilon$) 259 (-7.0), 230 (-7.6) nm.

(5*R*)-crustic acid (**6**): Yellow oil; $[\alpha]_D^{20}$ = +19.1 (*c* 0.25, MeOH); CD (MeOH) λ_{max} ($\Delta\varepsilon$) 317 (+0.2), 258 (+2.1), 228 (+5.2) nm; HRMS (*m/z*): (ESI/$[M+H]^+$) calcd. for $C_{11}H_{13}O_4$, 209.0808, found 209.0827.

(5*S*, 5'*S*)-custosic acid methyl ester (**7**): Yellow oil; HRMS (*m/z*): (ESI/$[M+H]^+$) calcd. for $C_{13}H_{17}O_6$, 269.1020, found 269.1037.

(5'*S*)-dehydrocrustosic acid methyl ester (**8**): White powder; HRMS (*m/z*): (ESI/$[M+Na]^+$) calcd. for $C_{13}H_{14}NaO_6$, 289.0683, found 289.0700.

Supplementary Tables

Table S1. Strains used in this study

Strains	Genotype	Source/Ref.
Penicillium crustosum		
PRB-2	Wild type	[1]
Δ*traA*	Δ*traA*::*hph* in *P. crustosum* PRB-2	[6]
Δ*traG*	Δ*traG*::*hph* in *P. crustosum* PRB-2	This study
Aspergillus nidulans		
LO8030	*pyroA4*, *riboB2*, *pyrG89*, *nkuA::argB*, sterigmatocystin cluster (*AN7804-AN7825*)Δ, emericellamide cluster (*AN2545-AN2549*) Δ, asperfuranone cluster (*AN1039-AN1029*) Δ, monodictyphenone cluster (*AN10023-AN10021*) Δ, terrequinone cluster (*AN8512-AN8520*) Δ, austinol cluster part 1 (*AN8379-AN8384*) Δ, austinol cluster part 2 (*AN9246-AN9259*) Δ, F9775 cluster (*AN7906-AN7915*) Δ, asperthecin cluster (*AN6000-AN6002*) Δ	[2,3]
JF15	*gpdA::traA::AfpyrG* in *A. nidulans* LO8030	This study
JF45	*gpdA::traA::traG::Ribo* in *A. nidulans* LO8030	This study

Table S2. Plasmids used and constructed in this study

Plasmids	Description	Source/Ref.
p5HY	Two-third of the *hph* resistance gene at the 5´-end, originated from the pUChph and inserted into pESC-URA. For gene replacement using *hph* as selection marker.	6
p3YG	Two-third of the *hph* resistance gene at the 3´-end, originated from the pUChph and inserted into pESC-URA. For gene replacement using *hph* as selection marker.	6
pJF80	A 1054 bp US PCR fragment of *traG* from genomic DNA of *P. crustosum* PRB-2 inserted in p5HY.	This study
pJF81	A 939 bp DS PCR fragment of *traG* from genomic DNA of *P. crustosum* PRB-2 inserted in p3YG.	This study
pYH-wA-pyrG	*URA3*, *wA flanking*, *AfpyrG*, *Amp*	4
pYWB2	*URA3*, *wA flanking*, *Afribo*, *Amp*	9
pJF27	*pYH-wA-traA*; a 12068 bp fragment of *traA* with its terminator from genomic DNA of *P. crustosum* PRB-2 inserted in *pYH-wA-gpdA*	This study
pJF91	*pYH-wA-traAG*; a 12788 bp fragment of *traA* with *gpdA* promoter and its terminator from pJF27, and a 2528 bp fragment of *traG* with its promoter and terminator from genomic DNA of *P. crustosum* PRB-2 inserted in *pYWB2*	This study
pJF72	pET-28a(+)-*traD*; a 804 bp fragment of *traD* from cDNA of *P. crustosum* PRB-2 with BamHI and EcoRI inserted in pET28a(+)	This study
pJF74	pET-28a(+)-*traH*; a 984 bp fragment of *traH* from cDNA of *P. crustosum* PRB-2 with BamHI and EcoRI inserted in pET28a(+)	This study

US: upstream; DS: downstream

Table S3. Primers used in this study

Primers	Sequence 5'-3'	Targeted amplification
5F-R	GCTGAAGTCGATTTGAGTCCAC	US of *hph* to verify 5F of *P. crustosum* mutant
3F-F	GCATTAATGCATTGGACCTCGC	DS of *hph* to verify 3F of *P. crustosum* mutant
traA-F	TGCATCTTGTAGAGCTCGC	1819 bp partial fragment of *traA*
traA-R	GAGGGCGGTTTTAGAATCAATTG	
traG-up-F	GAATTGTTAATTAAGAGCTCAGATCTCTAGCAGGACTCATCACAGACG	1054 bp upstream fragment of *traG* to construct pJF80
traG-up-R	CAACCCTCACTAAAGGGCGGCCGCACTAGCCGGGCTTCAGGGAAATTC	
traG-down-F	CGACTCACTATAGGGCCCGGGCGTCGACCCATGGTCCGATTGAGCTGG	939 bp downstream fragment of *traG* to construct pJF81
traG-down-R	CTAGCCGCGGTACCAAGCTTACTCGAGGCATGATTTGCCTCTAGACCCC	
traG-F	CAACACAATGTCACGGTACC	1071 bp partial fragment of *traG*
traG-R	CAGACATGGCCTGGGTACG	
traG-5F-F	CCGACAGACGAATATGGTGGC	US of *hph* to verify Δ*traG* mutant
traG-3F-R	CAGACATGCTTTCCGCAC	DS of *hph* to verify Δ*traG* mutant
A.n-traA-1F-For	CATCTTCCCATCCAAGAACCTTTAATCATGGTTCTACCCCAGCCC	DNA of 1st *traA* fragment 5442 bp from *P. crustosum* to construct pJF27
A.n-traA-1F-Rev	CTCATCAAGCCCGTGGACGAGCAAATGACTGTGAGCAACCACCATAG	
A.n-traA-2F-For	CTATGGTGGTTGCTCACAGTCATTTGCTCGTCCACGGGCTTGATGAG	DNA of 2nd *traA* fragment 6176 bp with its 497 bp terminator from *P. crustosum* to construct pJF27
A.n-traA-2F-Rev	GACACAGAATAACTCTCGCTAGCGTAGCTGGCAAATATAGTTACCT	
A.n-traAG-1F-For	CTTGACTCTCCTTCTCCTGATCGGATCCCATGCGGAGAGACGGACG	DNA of 6190 bp from pJF27 with A.n-traA-1F-Rev to construct pJF91
A.n-traAG-1R-Rev	TTAGTTTGCAAAATCGACGATTGCTGTAGCTGGCAAATATAGTTACCTA	DNA of 6673 bp from pJF27 with A.n-traA-2F-For to construct pJF91
A.n-traAG-2F-For	GATAGGTAACTATATTTGCCAGCTACAGCAATCGTCGATTTTGCAAAC	DNA of *traG* with its 788 bp promoter and 568 bp terminator from *P. crustosum* to construct pJF91
A.n-traAG-2R-Rev	CAACACCATATTTTAATCCCATGTGCATGGATACTCAGGTGGTATAATT	
TraD-28-For	GTGGACAGCAAATGGGTCGCGGATCCATGAAAGTTTTGATTATTTTTGC	804 bp fragment of *traD* to construct pJF72
TraD-28-Rev	GCAAGCTTGTCGACGGAGCTCGAATTCTCACGCTTCTTTGACGTCG	
TraH-28-For	CTGGTGGACAGCAAATGGGTCGCGGATCCATGTCTGTCGATGCGGCC	984 bp fragment of *traH* to construct pJF74
TraH-28-Rev	CAAGCTTGTCGACGGAGCTCGAATTCCTACAATGAAGTATCATCCGTCA	

US: upstream; DS: downstream

Table S4. ^{1}H NMR data of compounds **2** and **3**

Compound	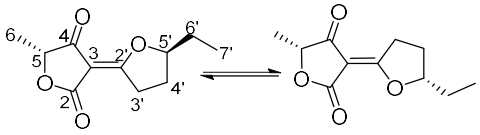 (5*R*, 5'*S*)-terrestric acid (**2**, $CDCl_3$)[12]	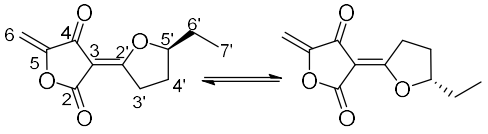 (5'*S*)-dehydroterrestric acid (**3**, DMSO-d_6)[13]
Position	δ_H, multi., *J* in Hz	δ_H, multi., *J* in Hz
5	4.62, q, 7.0, 1H	-
6	1.48, d, 7.0, 3H	5.18, d, 2.5, 1H
	-	5.01, d, 2.5, 1H
3´	3.60, ddd, 20.0, 9.6, 4.5, 1H	3.56, ddd, 19.9, 9.4, 4.2, 1H[a]
	3.27, ddd, 20.0, 9.6, 5.1, 1H	3.48, ddd, 19.9, 9.4, 4.2, 1H[a]
4´	2.36, m, 1H	2.33, m, 1H
	1.87, m, 1H	1.84, m, 1H
5´	4.93, m, 1H	5.02, m, 1H
6´	1.97, m, 1H	1.81, m, 1H
	1.79, m, 1H	1.74, m, 1H
7´	1.07, t, 7.5, 3H	0.97, t, 7.4, 3H

Note: Due to the *Z*/*E* isomerization, there were two sets of signals in a ratio of 1:1 showed in the ^{1}H NMR spectra. The corresponding signals are overlapping in most cases with each other. Therefore, only one set of the NMR data was listed in the table. The *Z*/*E* isomerization was proved by deuterium incorporation after incubation of (5*S*, 5'*S*)-crustosic acid (**1**) in D_2O-enriched milieu (Figure S10).

[a] signals overlapped with those of water.

Compounds **3** and **2** were isolated from incubation mixtures of **1** with TraH alone and with TraH and TraD, respectively. Their NMR data correspond very well to those reported previously.[12,13]

Table S5. NMR data of compound **4**

Compound	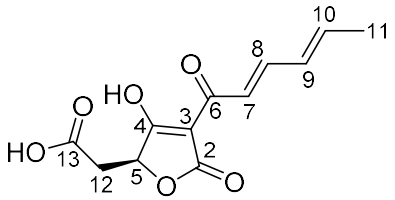	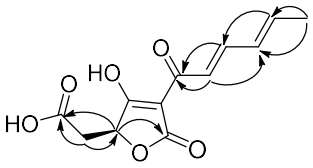
	(5*S*)-carboxylcrustic acid (**4**, CD_3OD)	

Position	δ_H, multi., *J* in Hz	δ_C	Key HMBC correlations
2	-	167.8[a]	
3	-	n.d.[b]	
4	-	n.d.[b]	
5	4.95, dd, 5.9, 4.1, 1H	80.2	C-2, C-13
6	-	178.5	
7	7.10, d, 15.3, 1H	119.0	C-6, C-9
8	7.68, dd, 15.3, 9.9, 1H	149.5	C-6, C-10
9	6.50, m, 1H	132.2	C-8, C-11
10	6.50, m, 1H	146.5	C-8, C-11
11	1.96, d, 5.5, 3H	19.3	C-9, C-10
12	2.99, dd, 17.4, 4.1, 1H	35.8	C-5, C-13
	2.88, dd, 17.4, 5.9, 1H	-	
13	-	172.2	

Note: [a] Signals acquired from HMBC correlations.

[b] Signals not detected in neither ^{13}C NMR nor HMBC spectrum.

Compound **4** was isolated from *A. nidulans* JF15 harboring pJF27 with *traA*.

Table S6. NMR data of compound **5**

Compound	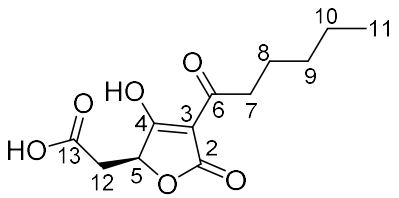	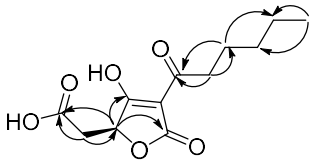
	(5*S*)-viridicatic acid (**5**, DMSO-d_6)	

Position	δ_H, multi., *J* in Hz	δ_C	Key HMBC correlations
2	-	174.2	
3	-	94.2	
4	-	171.8	
5	4.37, dd, 9.3, 3.5, 1H	75.7	C-2, C-4, C-13
6	-	194.2	
7	2.61, dd, 8.5, 6.9, 2H	40.1[a]	C-6, C-8, C-9
8	1.45, m, 2H	24.2	C-6, C-9, C-10
9	1.25, m, 2H	31.3	C-10
10	1.25, m, 2H	22.0	C-9
11	0.85, t, 7.0, 3H	13.9	C-9, C-10
12	2.69, dd, 16.0, 3.5, 1H	37.6	C-5, C-13
	2.20, dd, 16.0, 9.3, 1H	-	
13	-	193.7	
13-OH	12.44, s, 1H	-	

Note: [a] signals overlapped with those of solvents.

Compound **5** was isolated from *A. nidulans* JF45 harboring pJF91 with *traA* and *traG*.

Table S7. NMR data of compound **6**

Compound	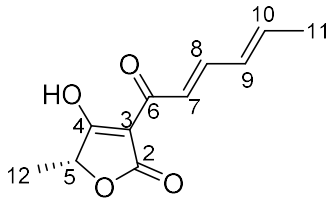 (5*R*)-crustic acid (**6**, CD_3OD)	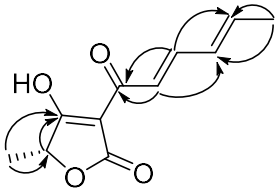	
Position	δ_H, multi., *J* in Hz	δ_C	Key HMBC correlations
2	-	173.7	
3	-	96.8	
4	-	201.4[a]	
5	4.79, q, 7.0, 1H	80.8	C-2, C-4
6	-	179.4	
7	7.11, d, 15.2, 1H	119.0	C-6, C-9
8	7.69, dd, 15.2, 9.9, 1H	149.9	C-6, C-10
9	6.50, m, 1H	132.2	C-7, C-11
10	6.50, m, 1H	146.9	C-8, C-11
11	1.96, d, 5.6, 3H	19.4	C-9, C-10
12	1.45, d, 7.0, 3H	17.0	C-4, C-5

Note: [a] Signal acquired from HMBC correlations.

Compound **6** was isolated from a Δ*traG*-mutant.

Table S8. NMR data of compound **7**

Compound	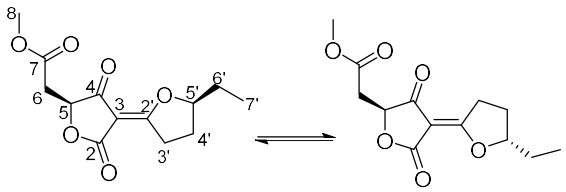
	(5*S*, 5'*S*)-crustosic acid methyl ester (**7**, $CDCl_3$)

Position	δ_H, multi., *J* in Hz	δ_C
2	-	170.6/167.2
3	-	95.8/95.3
4	-	197.5/193.7
5	4.83, dd, 6.9, 4.1, 1H	78.8/78.6
6	3.00, dd, 9.0, 4.1, 1H	35.9/35.9
	2.85, dd, 9.0, 6.9, 1H	-
7	-	169.8/169.8
8	3.70, s, 3H	52.3/52.3
9	-	-
10	-	-
11	-	-
12	-	-
2´	-	187.0/186.3
3´	3.61, ddd, 14.0, 8.7, 4.2, 1H	34.1/33.8
	3.28, ddd, 14.0, 9.5, 8.6, 1H	-
4´	2.37, m, 1H	27.9/27.8
	1.87, m, 1H	-
5´	4.93, m, 1H	93.3/92.8
6´	1.98, m, 1H	26.6/26.6
	1.79, m, 1H	-
7´	1.06, t, 7.5, 3H	9.7/9.5

Note: due to the *Z*/*E* isomerization, there were two sets of signals in a ratio of 1:1 showed in the ^{1}H NMR spectra. The corresponding signals are overlapping in most cases with each other. Therefore, only one set of the NMR data was listed in the table.

Compound **7** was isolated from a methanol solution of **1**.

Table S9. ^{1}H NMR data of compound **8**

Compound	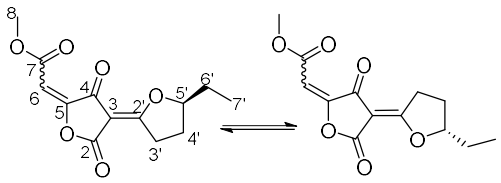
	(5'*S*)-dehydrocrustosic acid methyl ester (**8**, $CDCl_3$)
Position	δ_H, multi., *J* in Hz
6	5.91, s, 1H
8	3.81, s, 3H
3´	3.68, ddd, 20.3, 9.4, 4.0, 1H
	3.35, m, 1H
4´	2.43, m, 1H
	2.01, m, 1H[a]
5´	5.02, m, 1H
6´	1.93, m, 1H[a]
	1.83, m, 1H
7´	1.08, t, 7.4, 3H

Note: due to the *Z*/*E* isomerization, there were two sets of signals in a ratio of 1:1 showed in the ^{1}H NMR spectra. The corresponding signals are overlapping in most cases with each other. Therefore, only one set of the NMR data was listed in the table.

[a] signals overlapped with those of water.

Compound **8** was isolated from incubation mixture of **7** with TraH.

Supplementary Figures

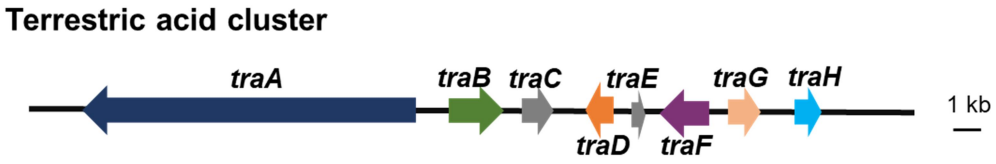

Protein	Putative function
TraA	carboxylcrustic acid synthase
	KS-AT-DH-MeT-KR-ACP-C-A-PCP
TraB	cytochrome P450
TraC	hypothetical protein
TraD	flavin containing dehydroterrestric acid hydrogenase
TraE	hypothetical protein
TraF	transporter
TraG	crustic acid reductase
TraH	2-oxoglutarate-dependent crustosic acid decarboxylase

The domain organization of TraA was deduced as ketosynthase (KS), acyltransferase (AT), dehydratase (DH), methyltransferase (MeT), ketoreductase (KR), and acyl carrier protein (ACP) domains of PKS, and the condensation (C), adenylation (A), peptidyl carrier protein (PCP) domains of NRPS.[14,15]

Figure S1. Deduced functions of ORFs in terrestric acid gene cluster of *P. crustosum* PRB-2[6]

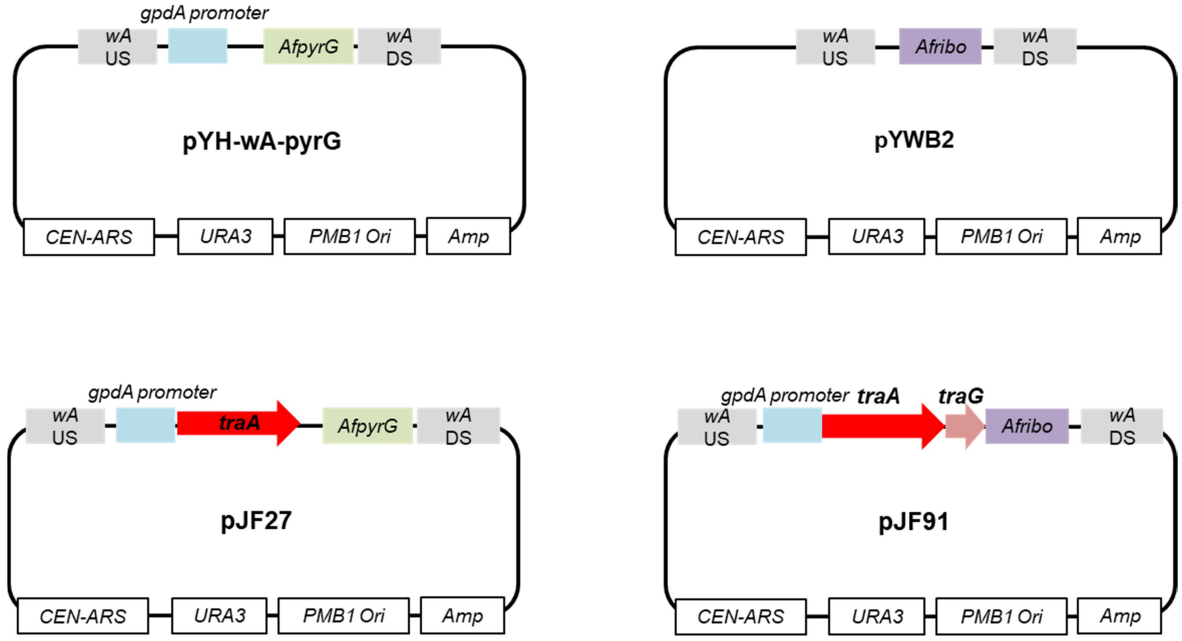

Figure S2. Constructs used for heterologous expression of *traA* and *traAG* in *A. nidulans*

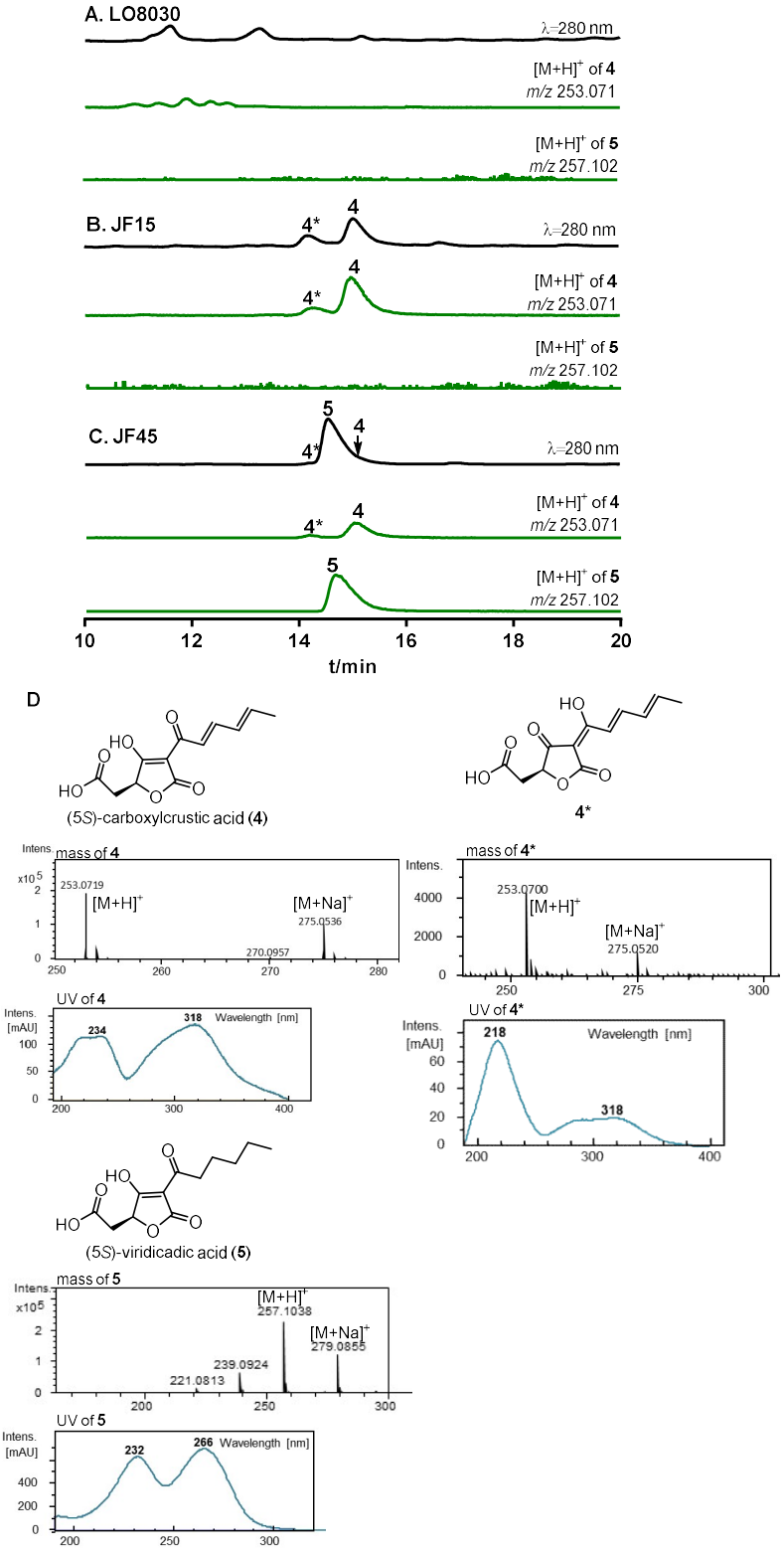

Figure S3. LC-MS analysis of the metabolite profile of different *A. nidulans* strains LO8030 as an expression host in (A), JF15 carrying the expression construct for *traA* (B), JF45 for co-expression of *traA* and *traG* (C) were cultivated in PD medium at 25 °C for 7 days. UV absorptions at 280 nm, $[M+H]^+$ of **4** at *m/z* 253.071 ± 0.005 and $[M+H]^+$ of **5** at *m/z* 257.102 ± 0.005 are illustrated. Structures, mass, and UV spectra of **4**, **4*** and **5** are shown in (D).

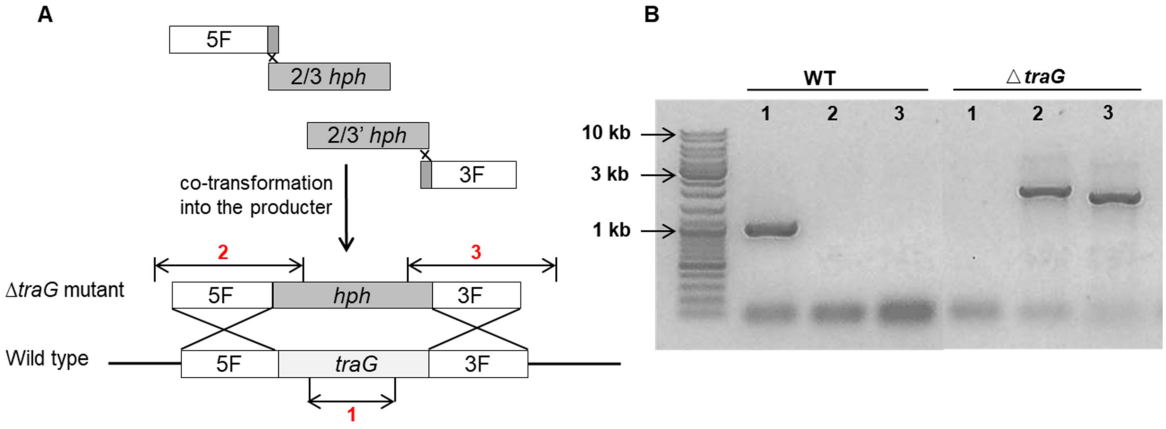

Figure S4. Verification of Δ*traG*-mutant from *P. crustosum* PRB-2
Gene deletion strategy in *P. crustosum* was schematically represented in (A). PCR amplification for three different fragments from genomic DNA of WT and Δ*traG*-mutant was used to prove the presence/absence of *traG* and its site specific integration with the help of up- and downstream regions (B). The PCR primers are given in Table S3.

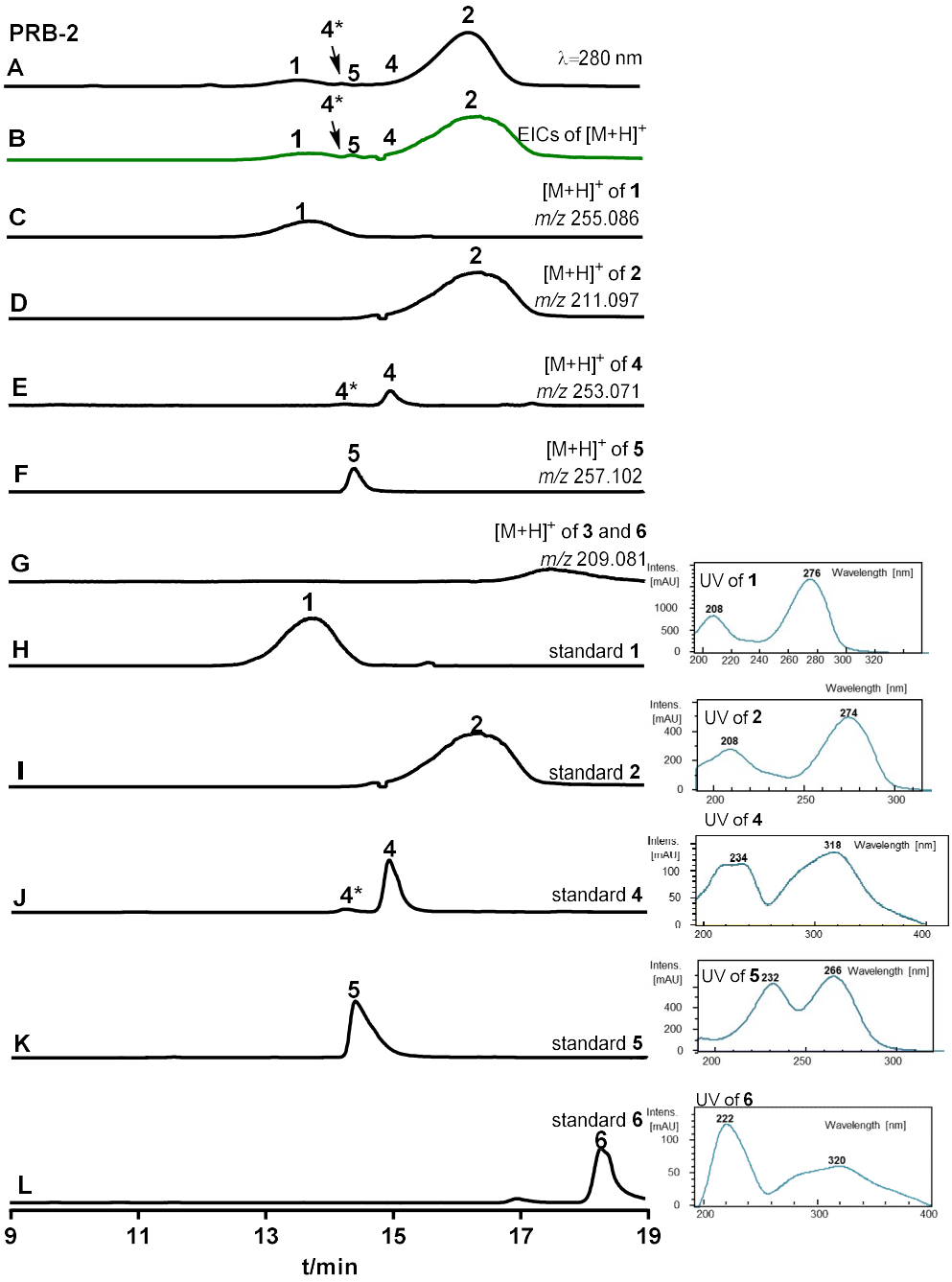

Figure S5. LC-MS detection of secondary metabolites from a 7 days-old liquid PD surface culture of *P. crustosum* PRB-2

UV absorptions at 280 nm are illustrated in (A). EICs in dark green refer total $[M+H]^+$ ions of **1** – **6** with a tolerance range of ± 0.005 (B), and in black refer $[M+H]^+$ ions of **1** – **6** (C – G), respectively. Standards of **1**, **2**, **4** – **6** are shown in H – L.

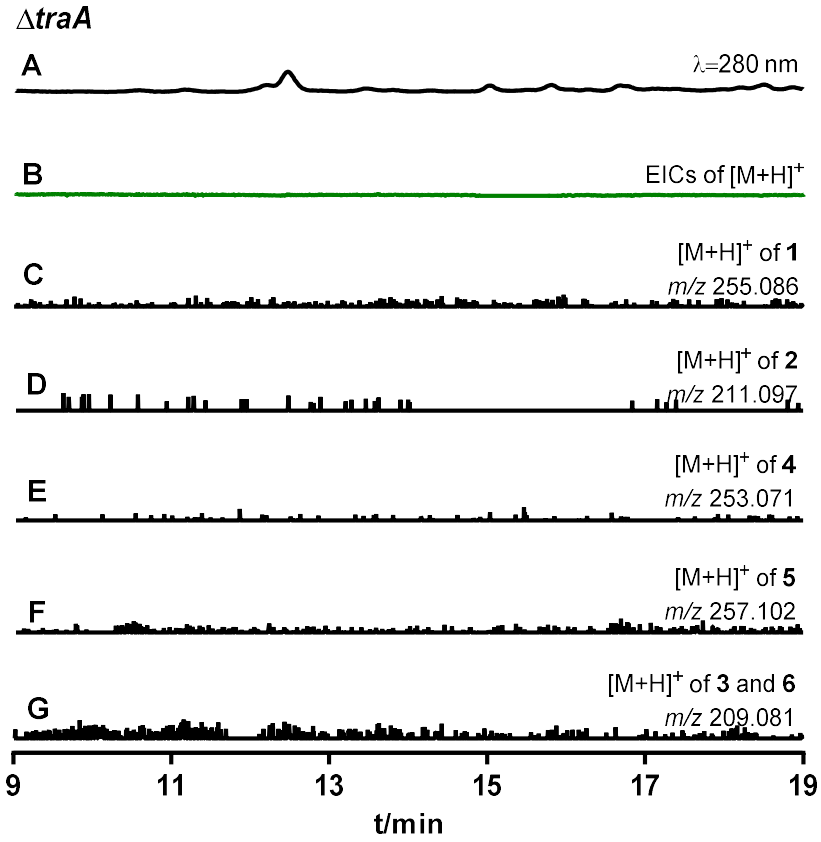

Figure S6. LC-MS detection of the metabolites in the terrestric acid biosynthesis in Δ*traA*-mutant obtained from a previous study[6]

UV absorptions at 280 nm are illustrated in (A). EICs in dark green refer total $[M+H]^+$ ions of **1** – **6** with a tolerance range of ± 0.005 (B), and in black refer $[M+H]^+$ ions of **1** – **6** (C − G), respectively.

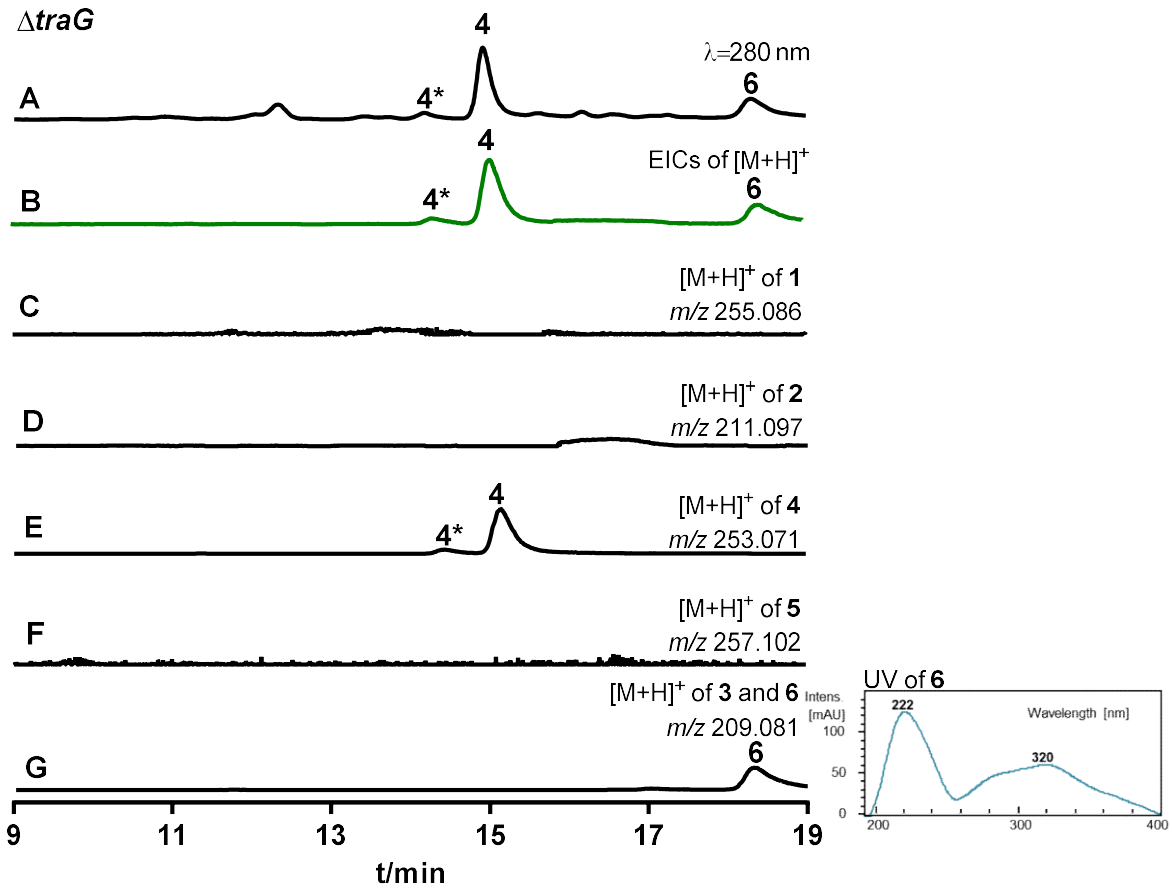

Figure S7. LC-MS detection of the metabolites in the terrestric acid biosynthesis in Δ*traG*-mutant UV absorptions at 280 nm are illustrated in (A). EICs in dark green refer total $[M+H]^+$ ions of **1** – **6** with a tolerance range of ± 0.005 (B), and in black refer $[M+H]^+$ ions of **1** – **6** (C−G), respectively.

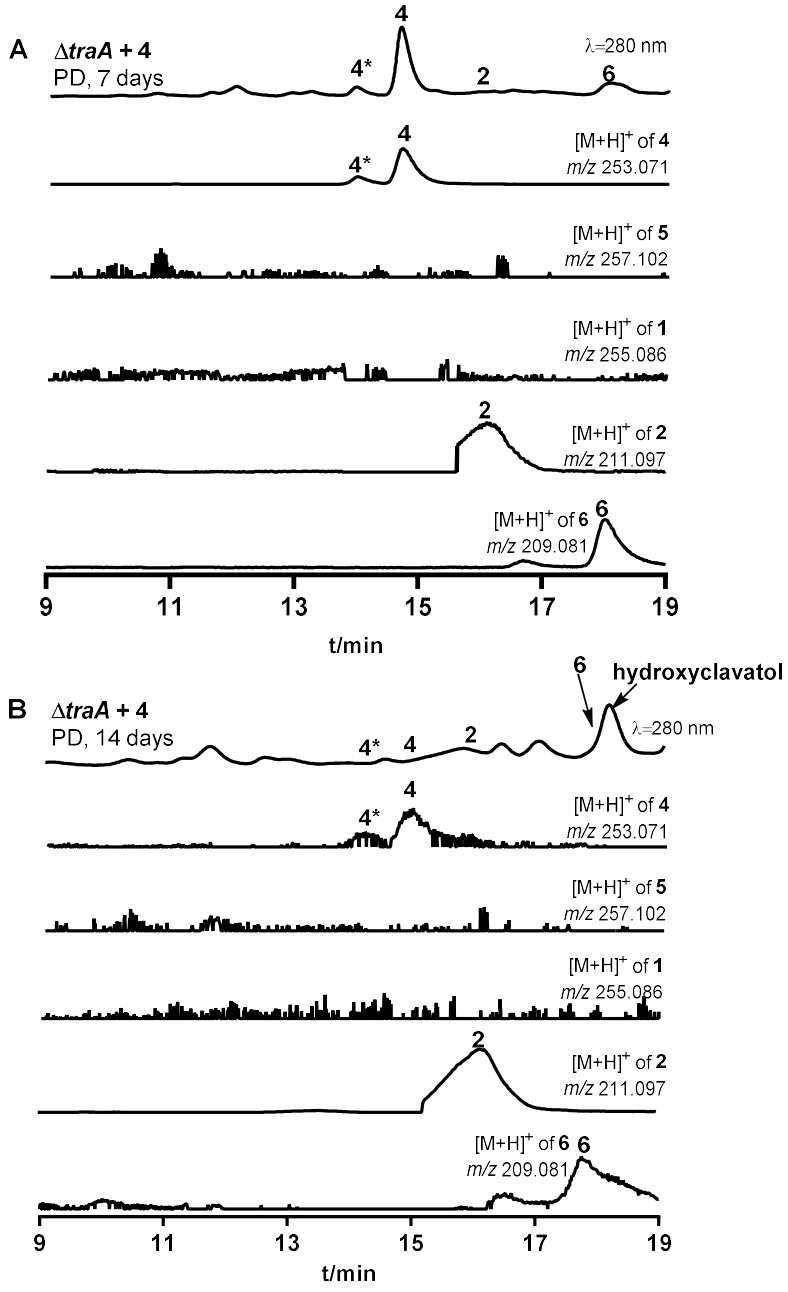

Figure S8. LC-MS detection of the metabolite profile of Δ*traA* mutant after feeding with **4** Δ*traA* culture were fed with **4** and maintained for 7 days (A) and 14 days (B). UV absorptions at 280 nm are illustrated. EICs refer $[M+H]^+$ ions of **1**, **2**, **4**, **5** and **6** with a tolerance range of ± 0.005.

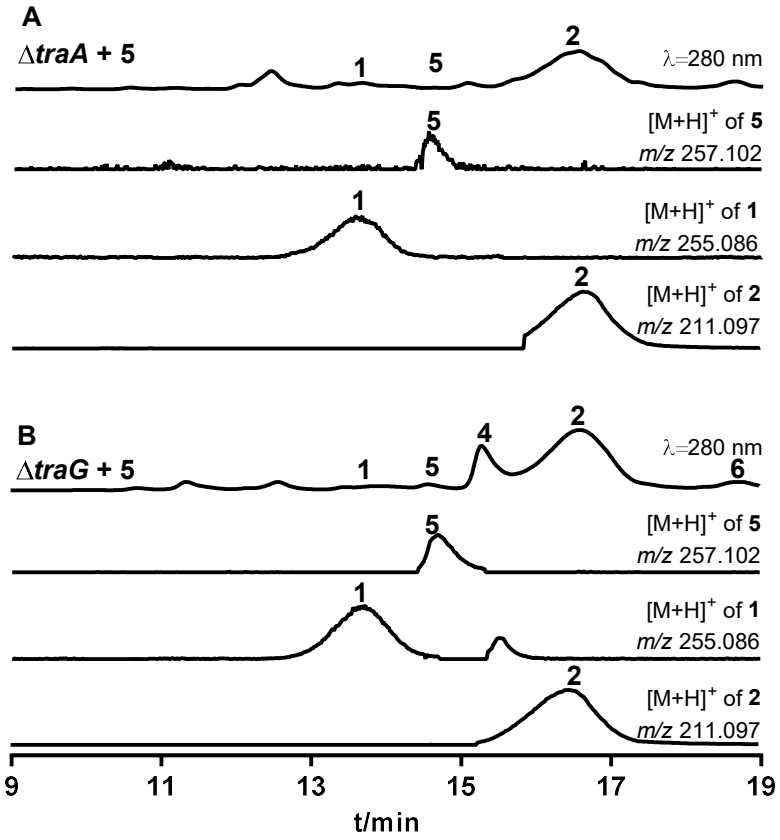

Figure S9. LC-MS detection of the metabolite profile of Δ*traA* and Δ*traG* mutants after feeding with **5**

Δ*traA* (A) and Δ*traG* (B) cultures were fed with **5** and maintained for 7 days. UV absorptions at 280 nm are illustrated. EICs refer $[M+H]^+$ ions of **1**, **2** and **5** with a tolerance range of ± 0.005.

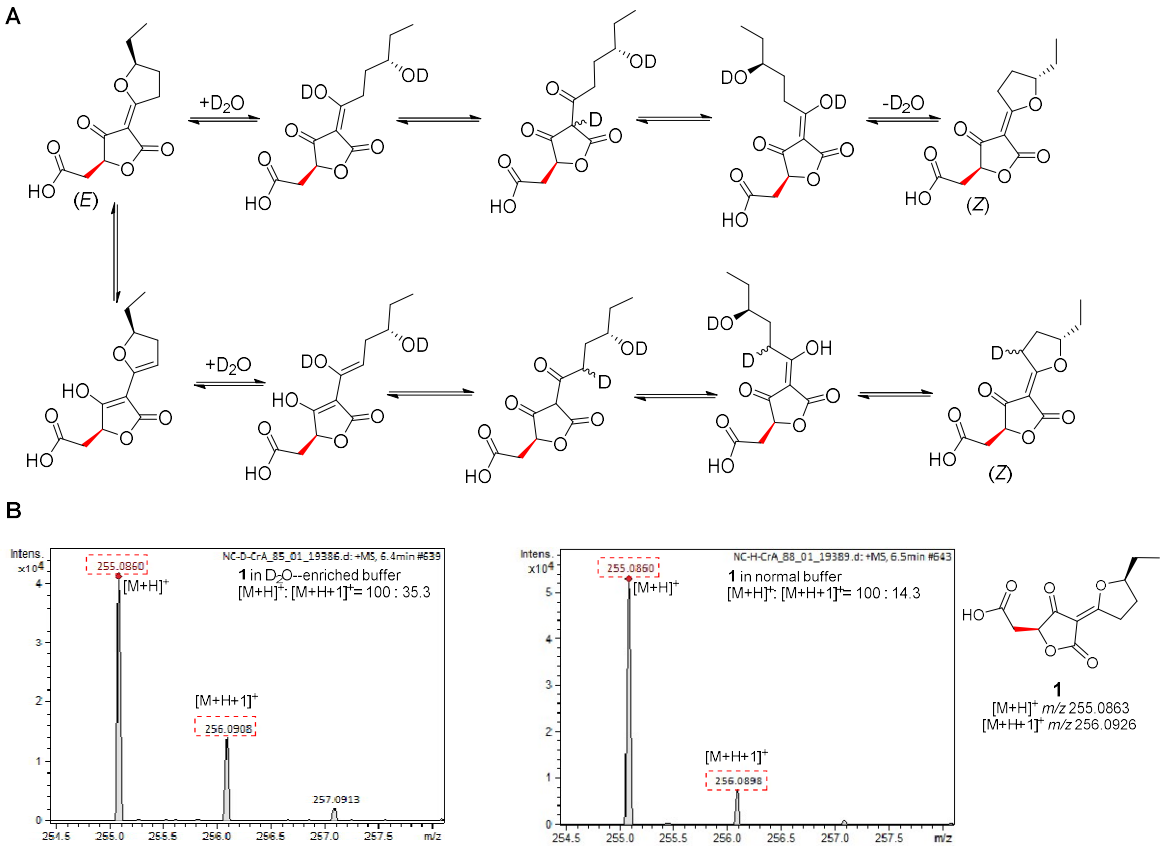

Figure S10. Incorporation of deuterium in **1** *via E/Z*-isomerization in D_2O-enriched milieu

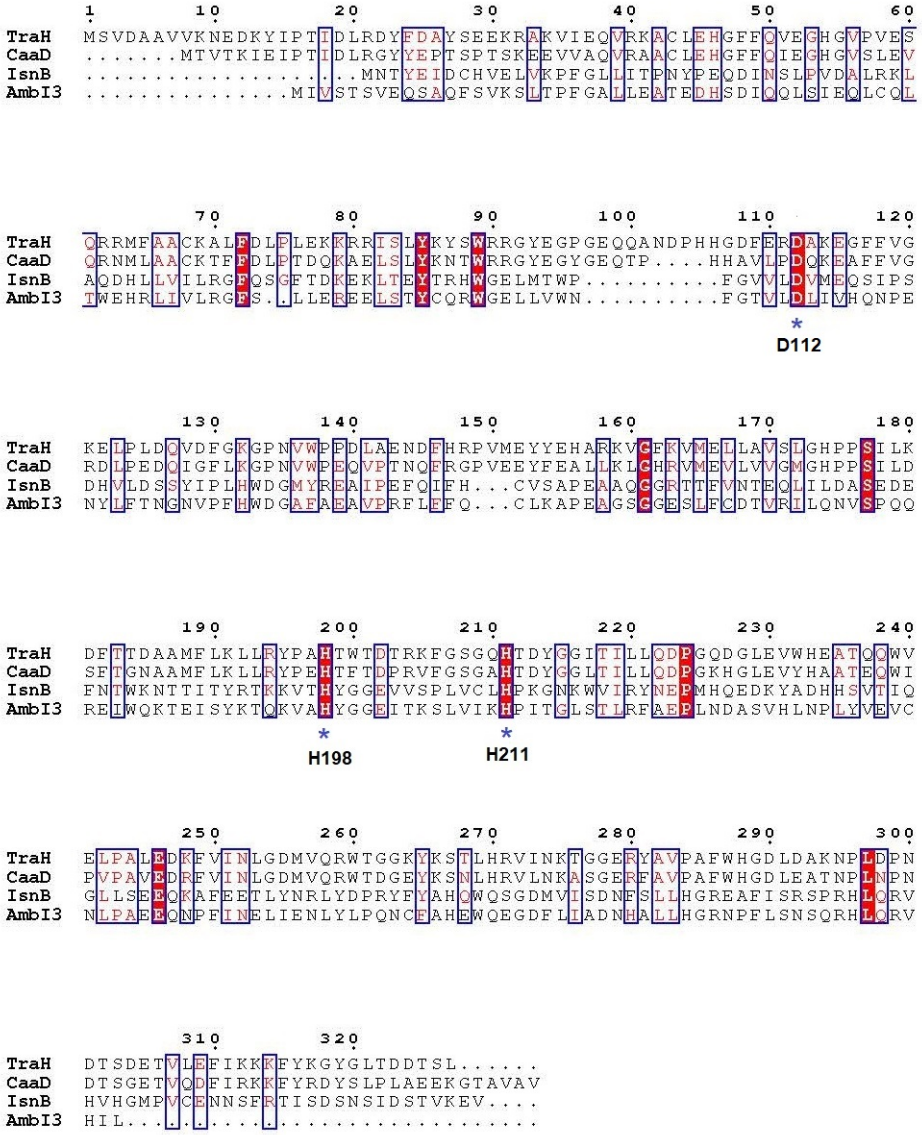

Figure S11. Sequence alignments of non-heme Fe^{II}-2OG-dependent decarboxylases CaaD (XP_001392490), IsnB (CEK22194.1), and AmbI3 (AIJ28554.1) are from *Aspergillus niger*, *Xenorhabdus nematophila,* and *Fischerella ambigua*, respectively.[16-18] TraH also contains the typical conserved 2-His-1-Asp ion-binding triad of non-heme Fe^{II}/2-oxoglutarate-dependent enzyme (His_{198}, His_{211} and Asp_{112}) (marked with *). Protein sequence alignments were carried out by using the sequence alignment function of ClustalW and visualized with ESPript 3.0 (http://espript.ibcp.fr/ESPript/ESPript/).

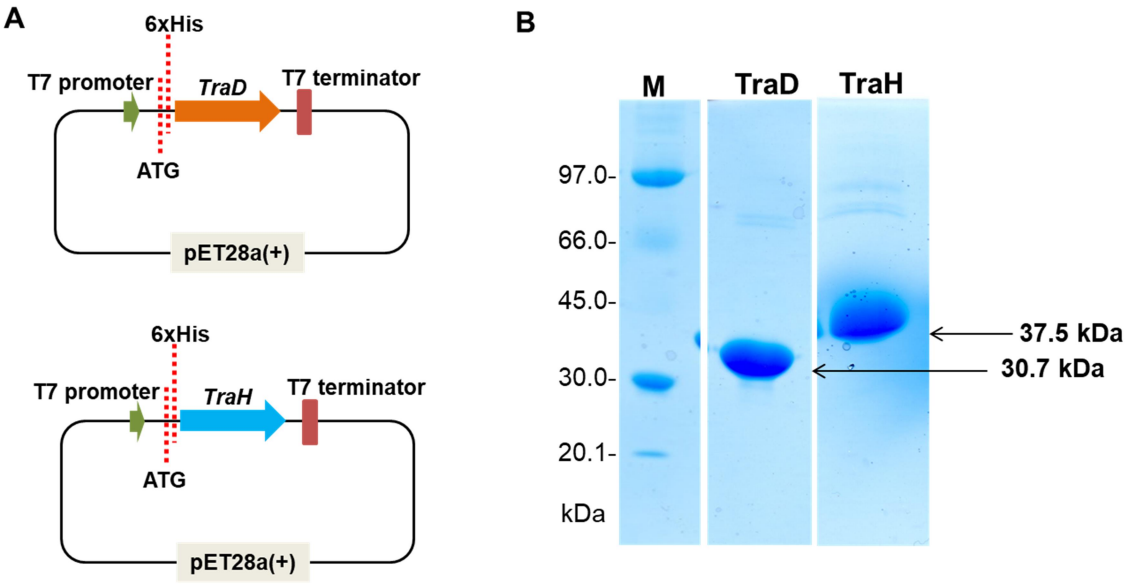

Figure S12. Analysis of recombinant TraD and TraH on SDS-PAGE

TraD and *traH* were separately inserted into pET28a(+) with 6xHis-tag at its *N*-terminal (A). The purified recombinant histidine-tagged TraD and TraH were separated on a 12% SDS-PAGE (B).

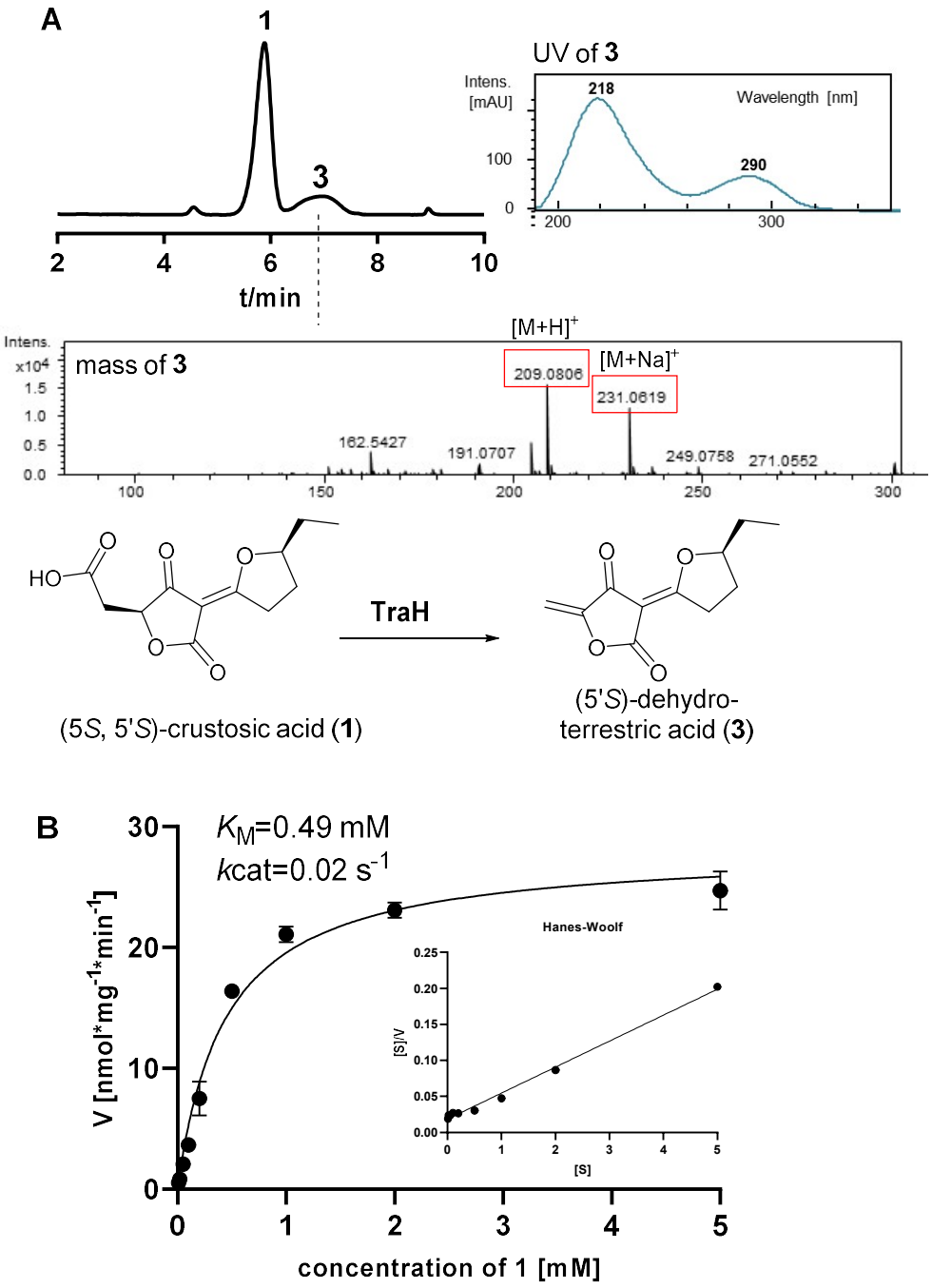

Figure S13. Oxidative decarboxylation of **1** catalyzed by TraH
LC-MS analysis of incubation mixture of **1** with TraH (A), determination of kinetic parameter of the TraH toward **1** (B).

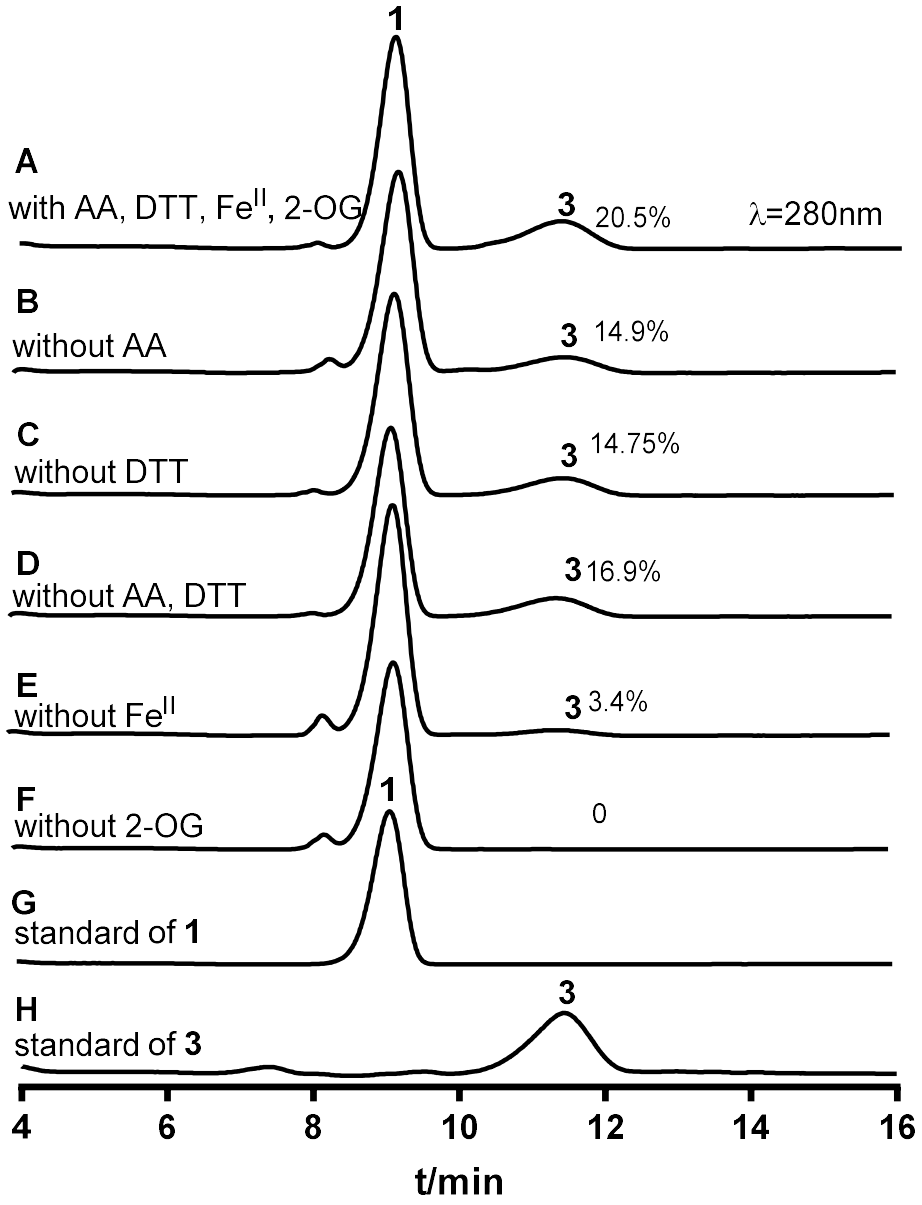

Figure S14. HPLC analysis of the incubation mixtures of **1** with TraH
5.4 μM TraH in the full assay with ascorbic acid (AA), dithiothreitol (DTT), $Fe[(NH_4)_2(SO_4)_2]$ (Fe^{II}) and 2-oxoglutarate (2OG) (A); full assay without AA (B); full assay without DTT (C); full assay without AA and DTT (D); full assay without exogenous Fe^{II} (E); full assay without 2OG (F), standards of **1** (G) and **3** (H). UV absorptions at 280 nm are illustrated.

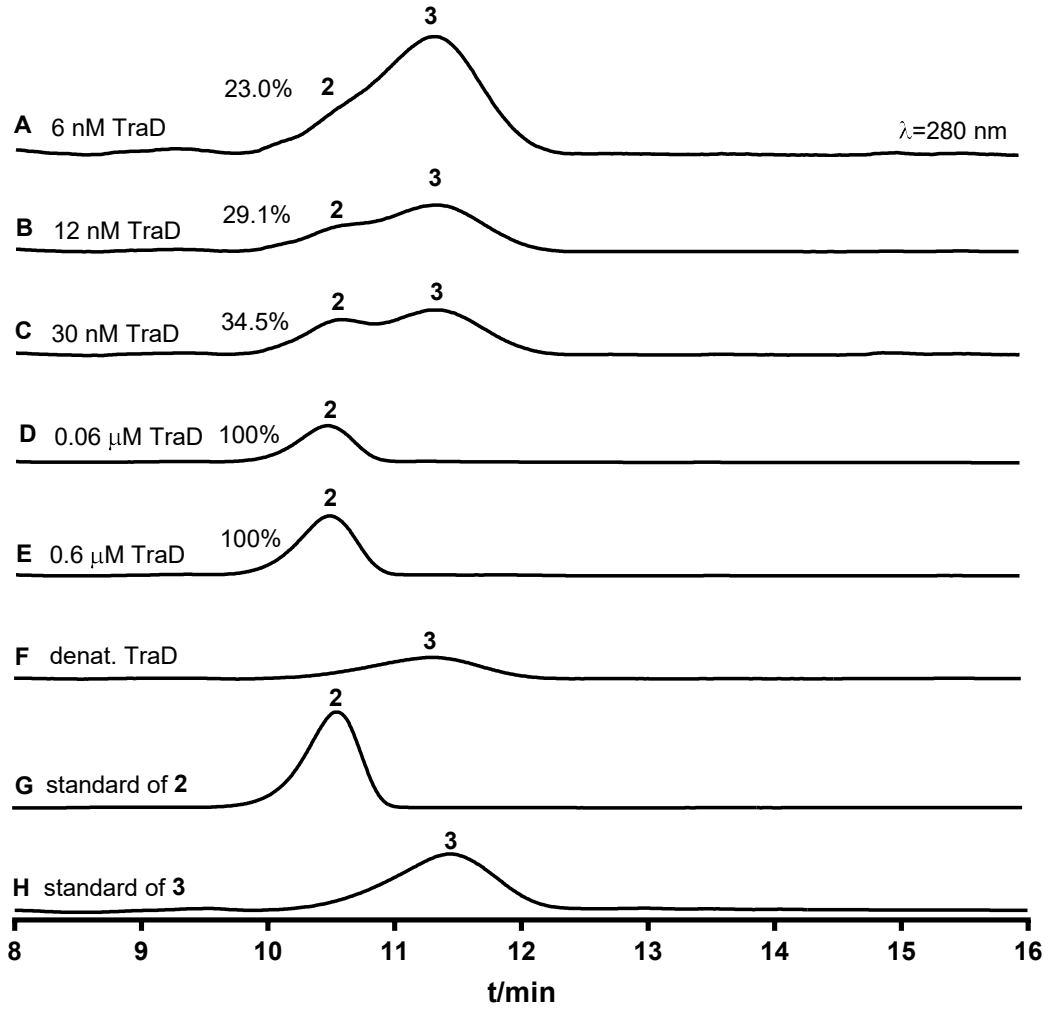

Figure S15. HPLC analysis of incubation mixtures of **3** with TraD at different concentrations

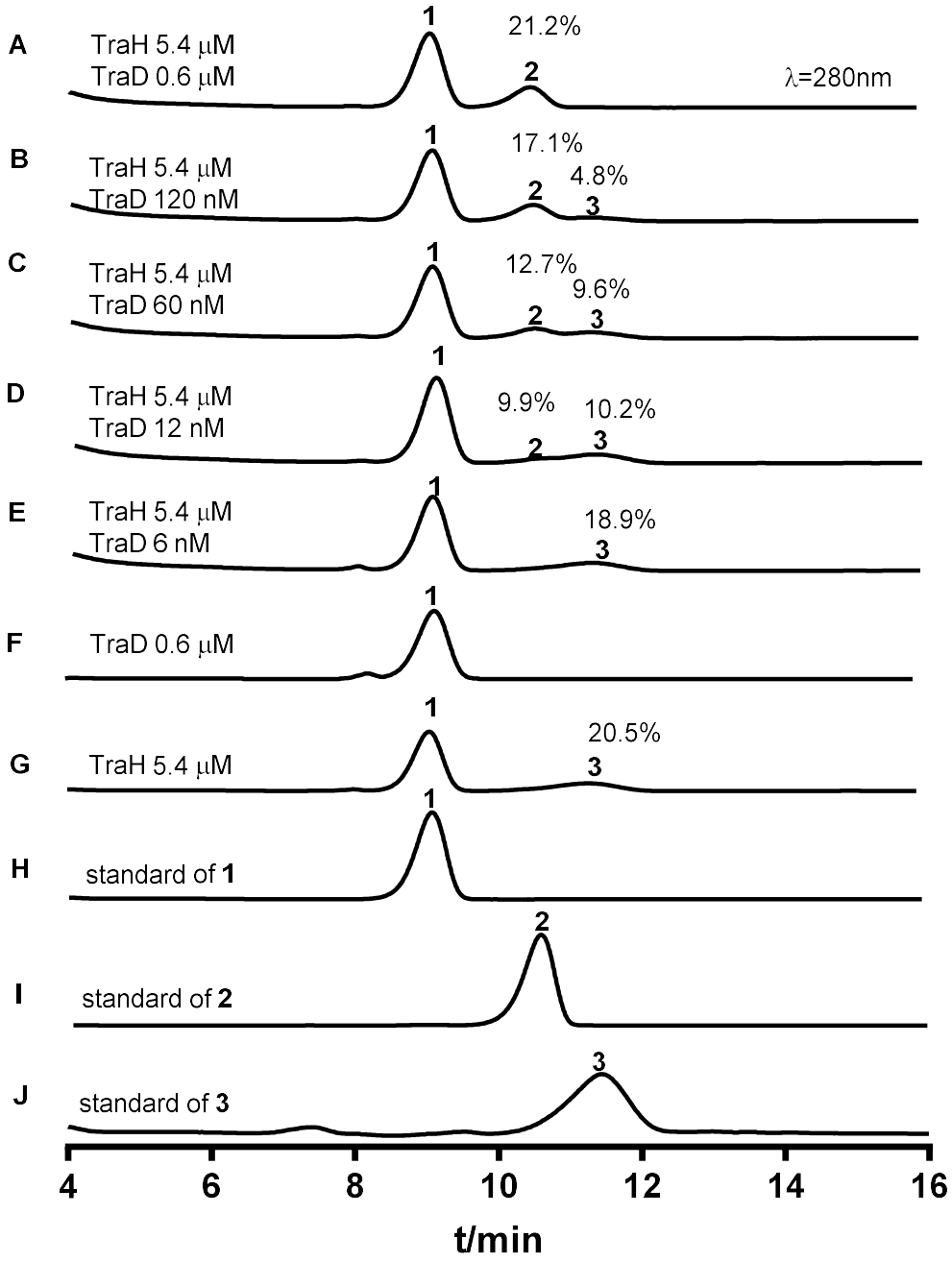

Figure S16. HPLC analysis of sequential reaction products in enzyme assays of TraH and TraD with **1**

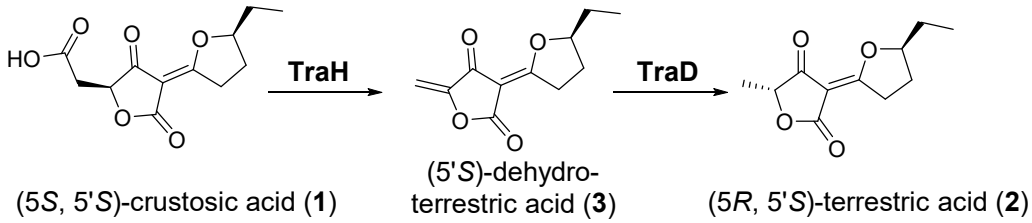

(5*S*, 5'*S*)-crustosic acid (**1**) (5*R*, 5'*S*)-terrestric acid (**2**)

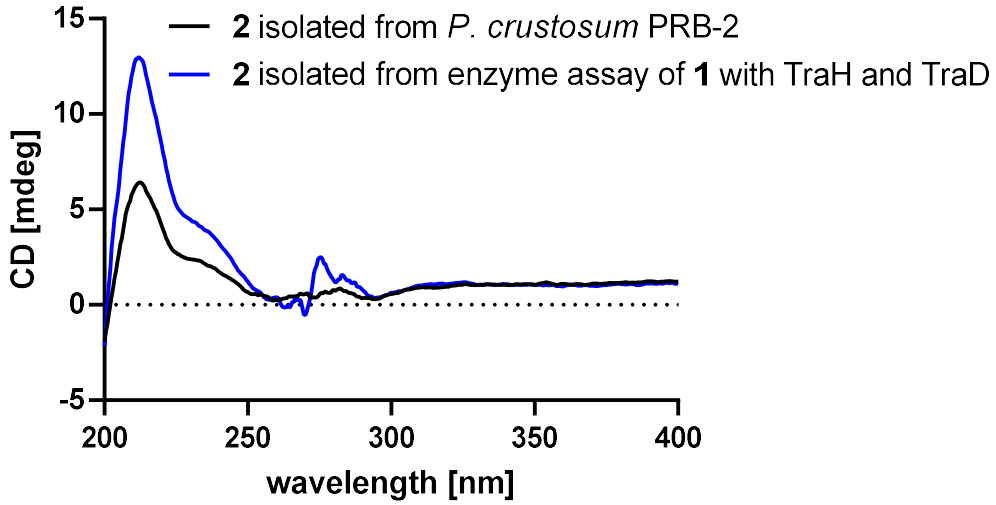

Figure S17. Comparison of CD spectra of two terrestric acid samples

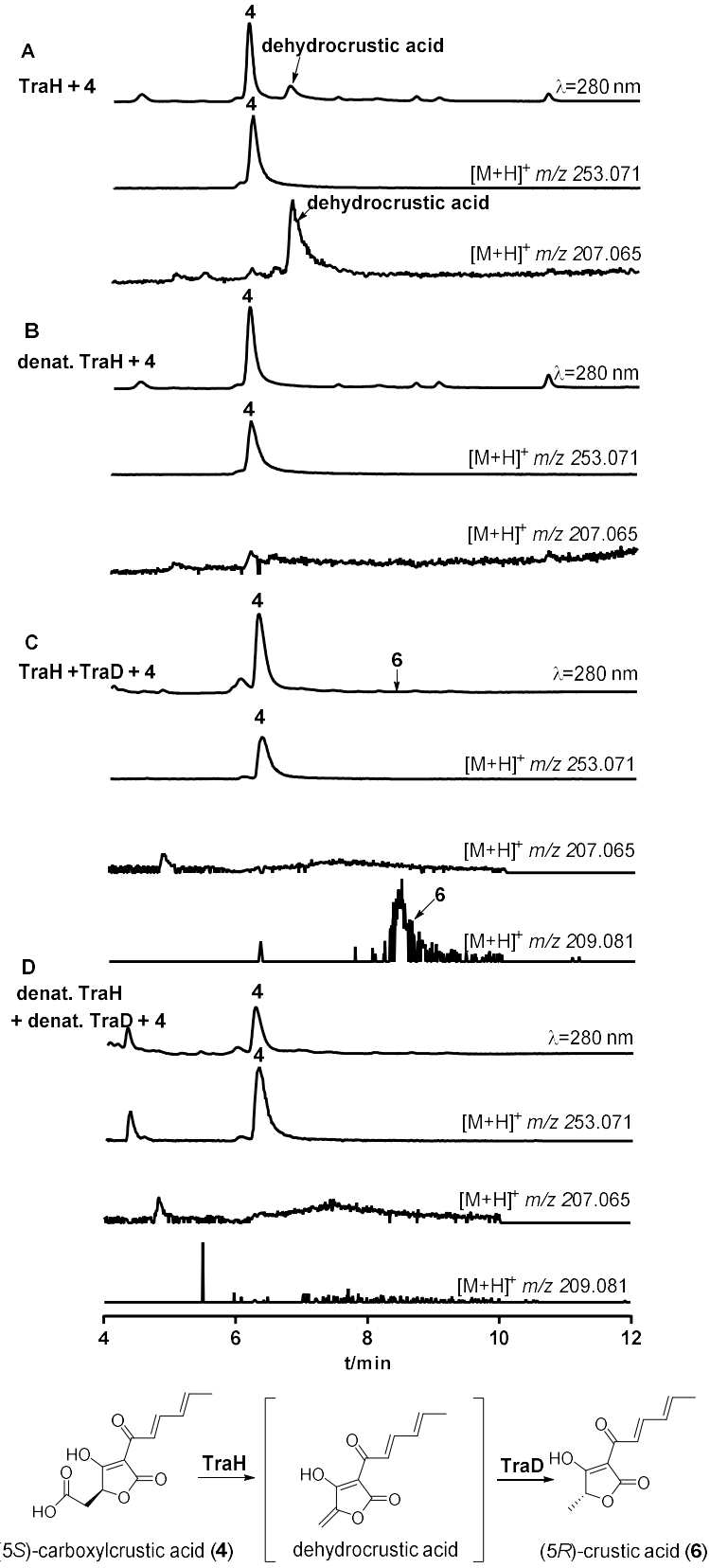

Figure S18. LC-MS analysis of enzyme assays of **4** with TraH without or together with TraD Incubation mixtures of **4** with TraH (A), **4** with denat TraH (B) at 37℃ for 16 h, **4** with TraH and TraD (C), and **4** with denat TraH and TraD (D) at 30℃ for 16 h. EICs refer $[M+H]^+$ ions of **4**, **6** and dehydrocrustic acid with a tolerance range of ± 0.005.

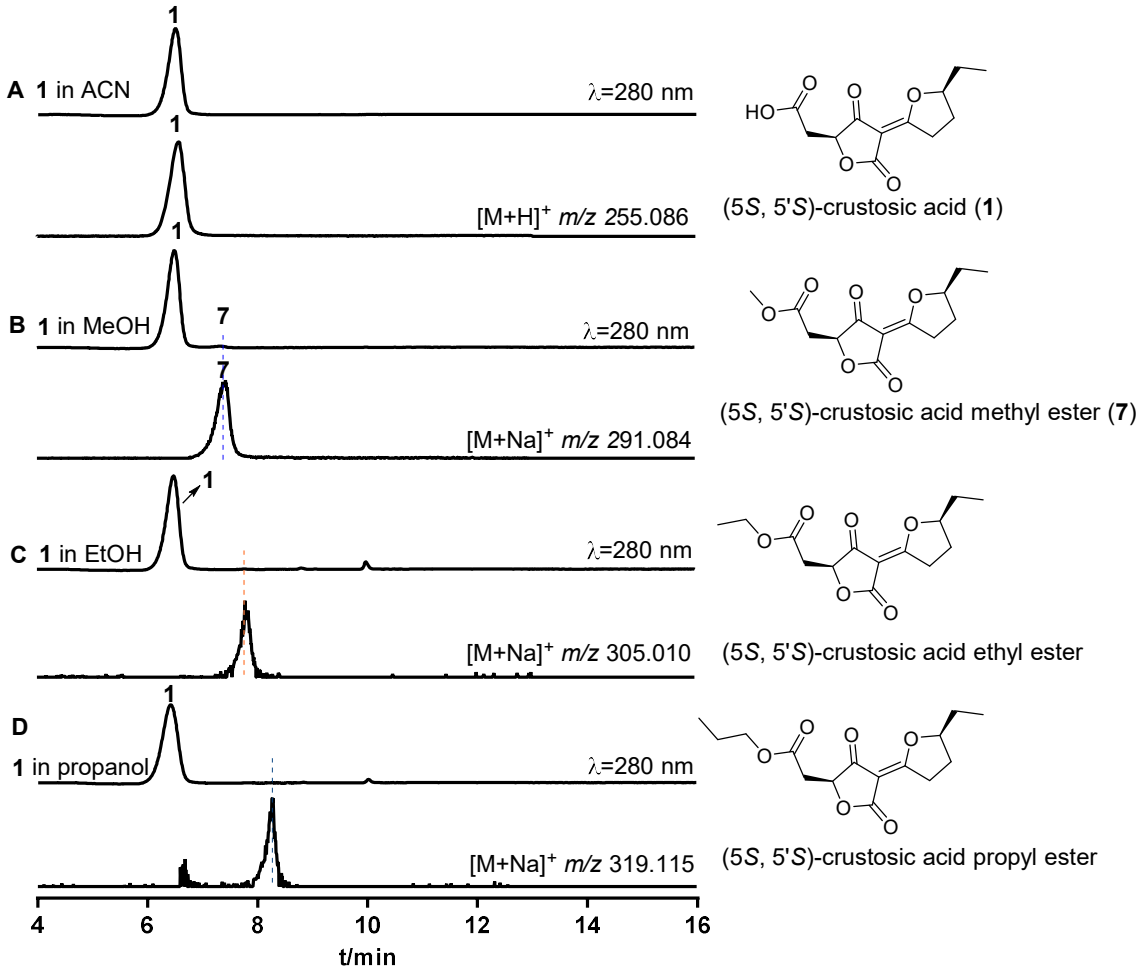

Figure S19. LC-MS analysis of spontaneous ester formation of **1** with different alcohols
0.4 mM solutions of crustosic acid (**1**) in ACN, MeOH, EtOH or n-propanol were kept at 25℃ for 24 h and subjected directly to LC-MS analysis. UV absorptions at 280 nm are illustrated. EIC at *m/z* 255.086 ± 0.005 refer $[M+H]^+$ ion of (5*S*, 5'*S*)-crustosic acid (**1**), EICs at *m/z* 291.084 ± 0.005, 305.010 ± 0.005, 319.115 ± 0.005 refer $[M+Na]^+$ ion of its methyl ester (**7**), ethyl ester, propyl ester, respectively.

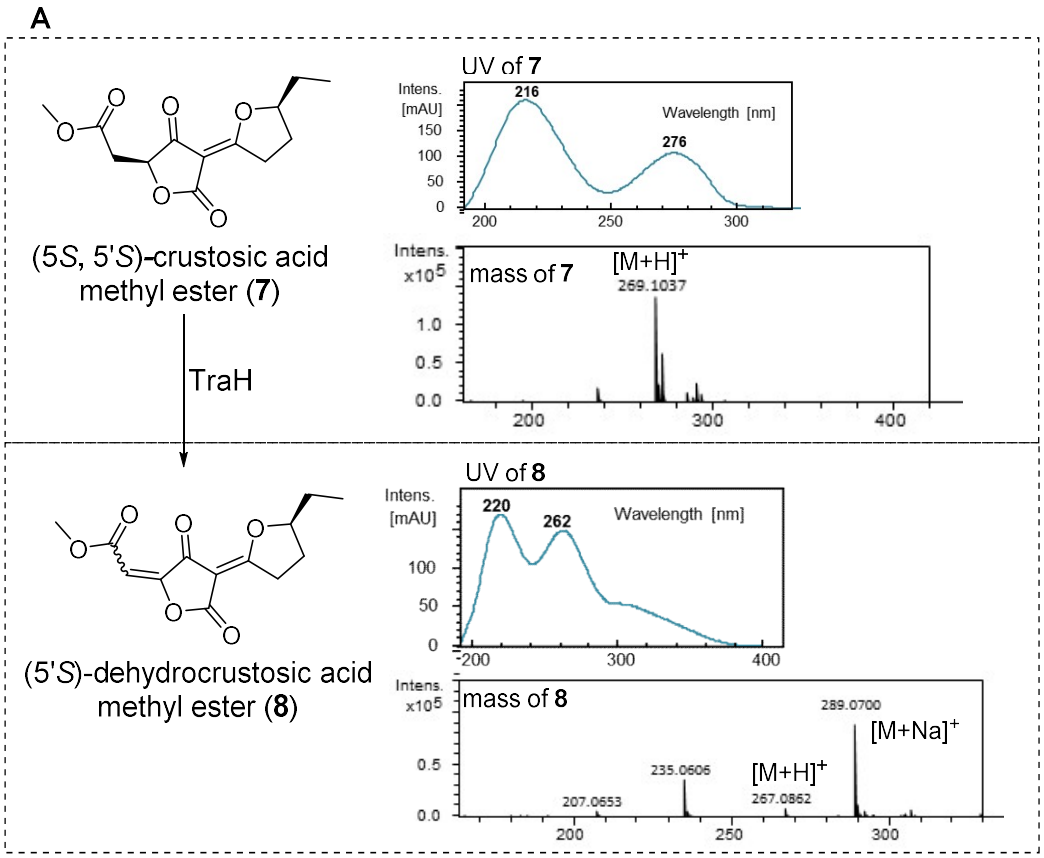

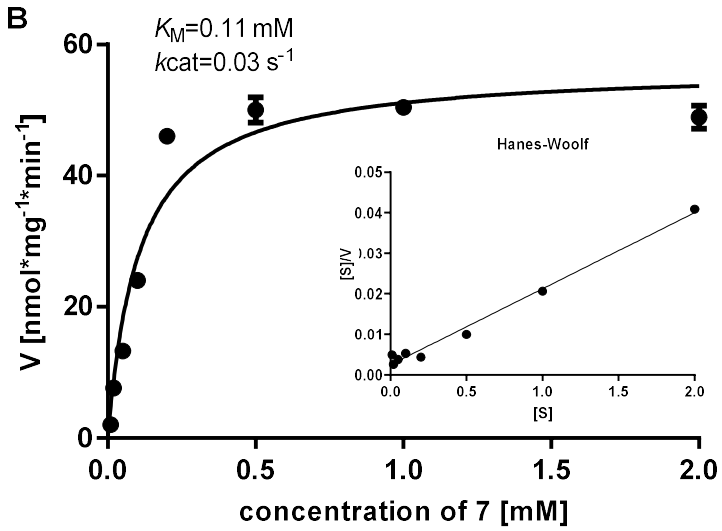

Figure S20. Conversion of **7** to **8** catalyzed by TraH
LC-MS analysis of incubation mixture of **7** with TraH (A), determination of kinetic parameter of the TraH toward **7** (B).

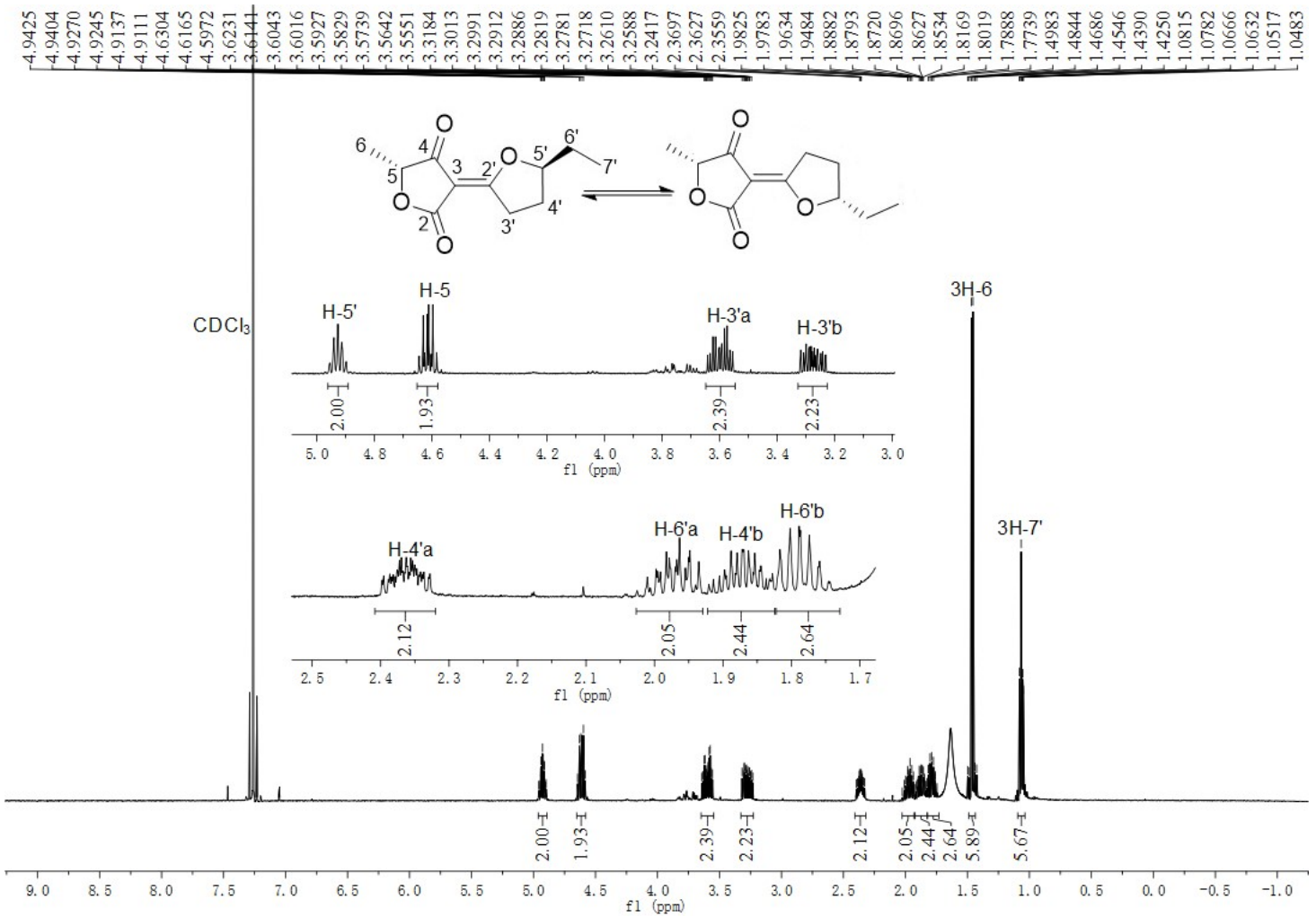

Figure S21. ^{1}H NMR spectrum of compound **2** isolated from an incubation mixture of **1** with TraH and TraD in $CDCl_3$ (500MHz)

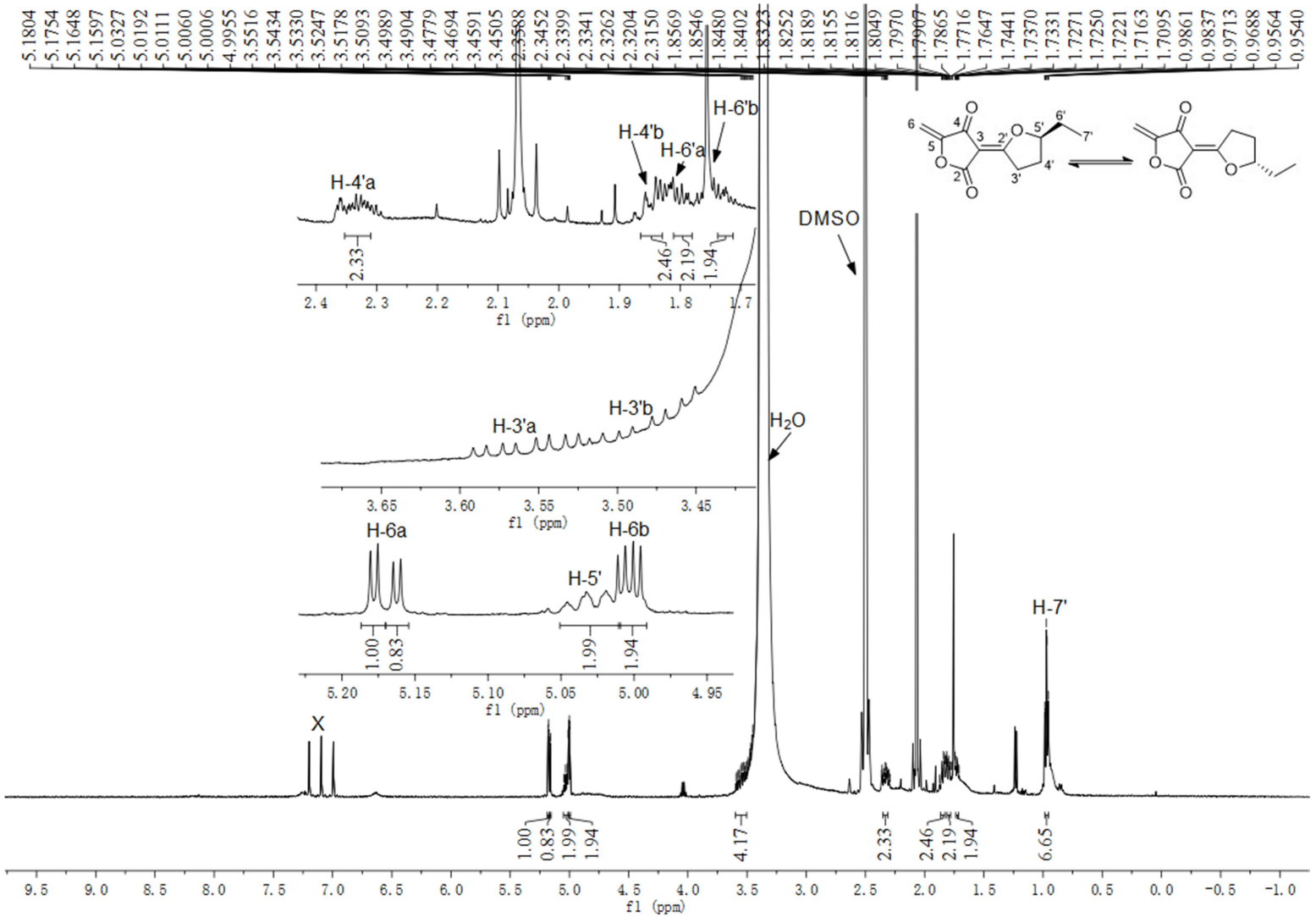

Figure S22. ^{1}H NMR spectrum of compound **3** in DMSO-d_6 (500MHz)

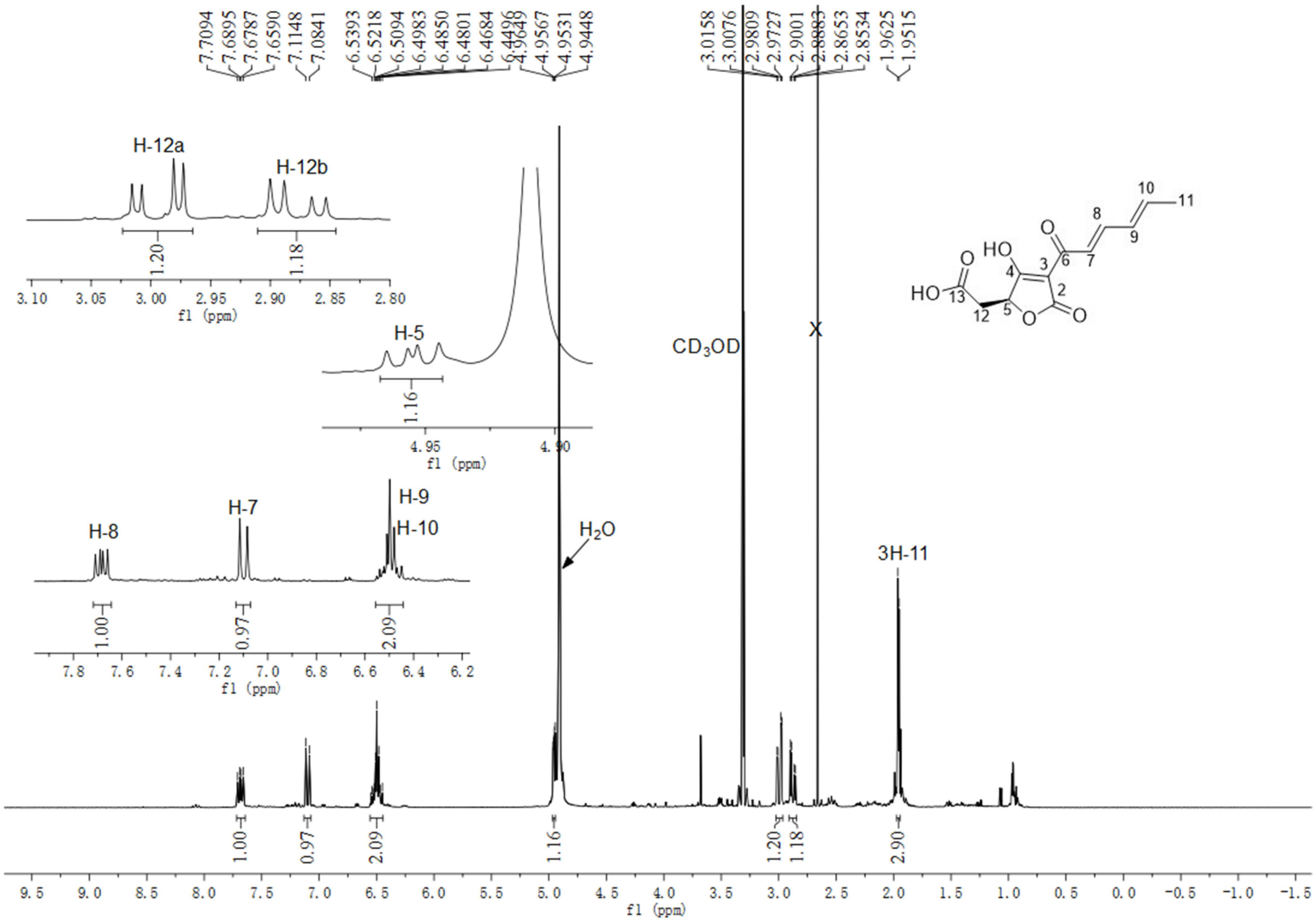

Figure S23. ^{1}H NMR spectrum of compound **4** isolated from *A. nidulans* JF15 harboring *traA* in CD_3OD (500MHz)

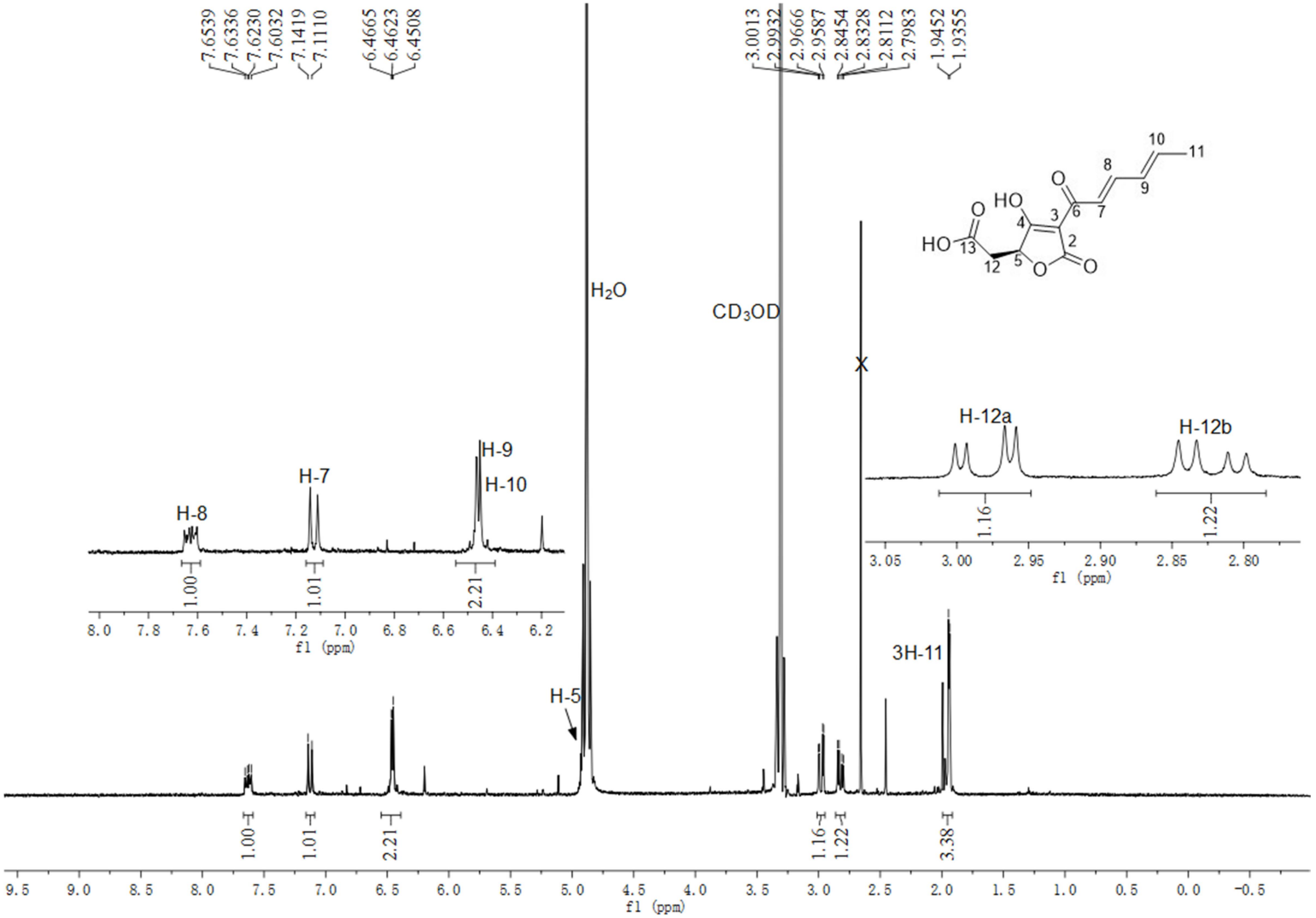

Figure S24. ^{1}H NMR spectrum of compound **4** isolated from Δ*traG*-mutant in CD_3OD (500MHz)

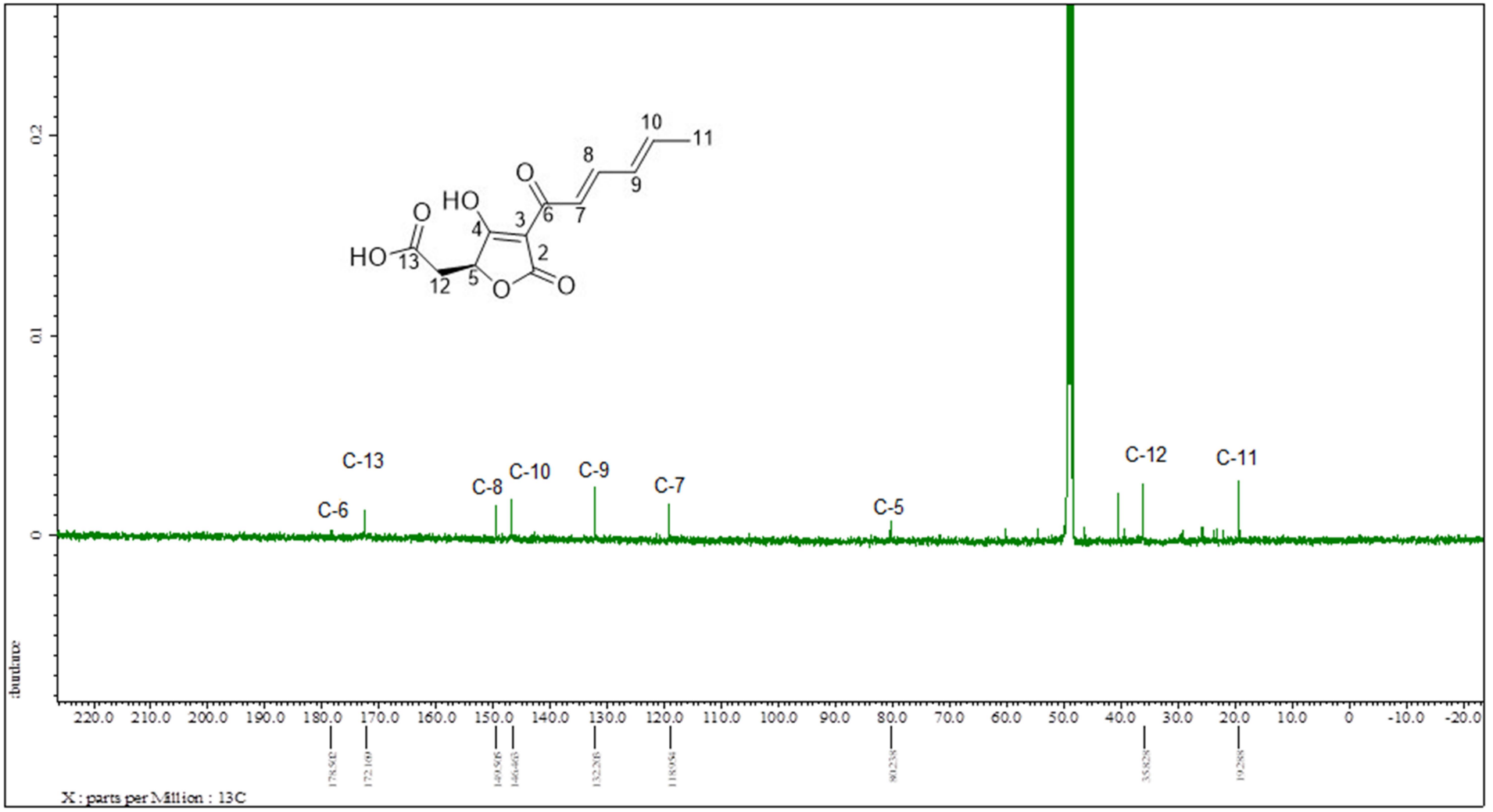

Figure S25. ^{13}C NMR spectrum of compound **4** isolated from *A. nidulans* JF15 harboring *traA* in CD_3OD (125MHz)

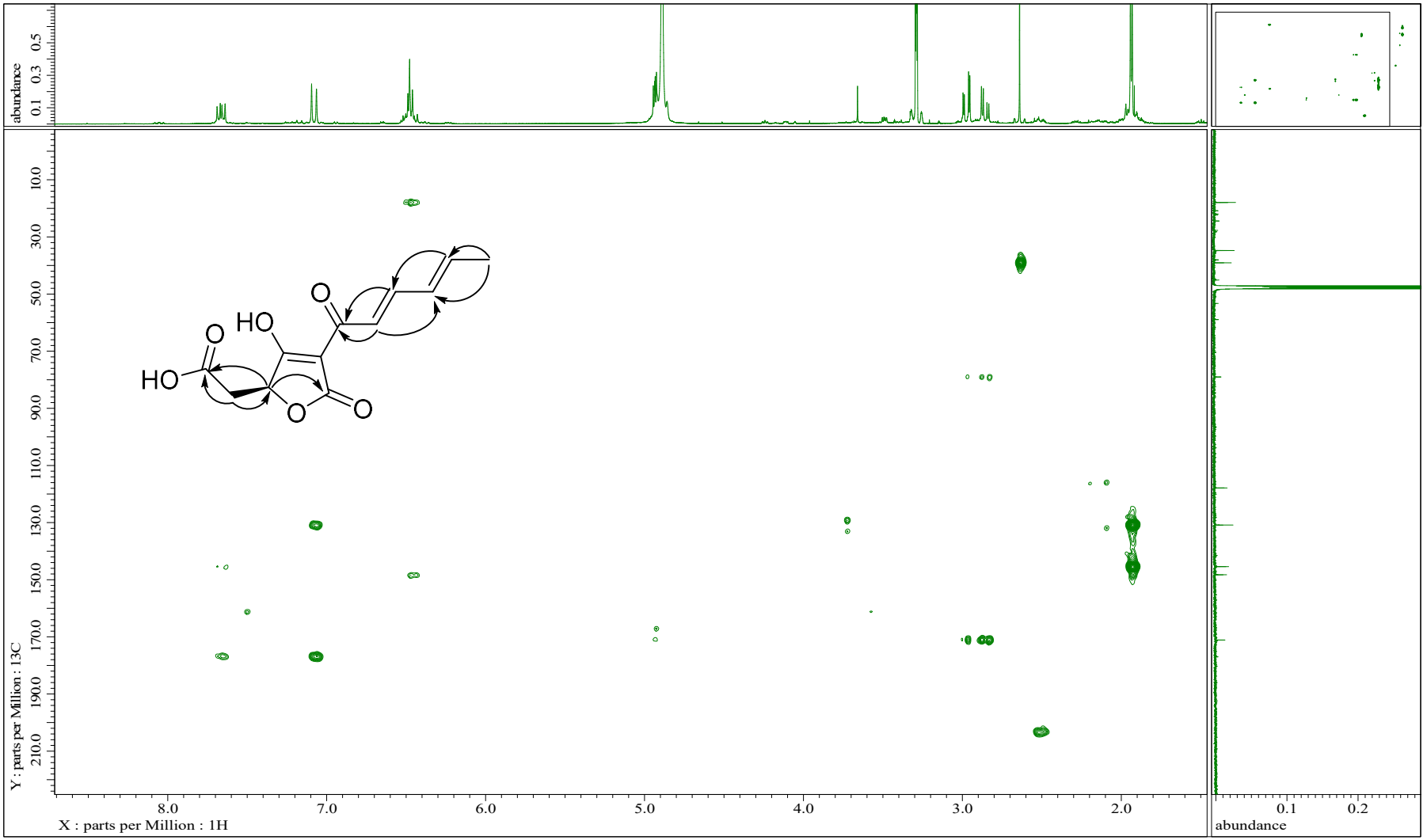

Figure S26. HMBC spectrum of compound **4** isolated from *A. nidulans* JF15 harboring *traA* in CD_3OD

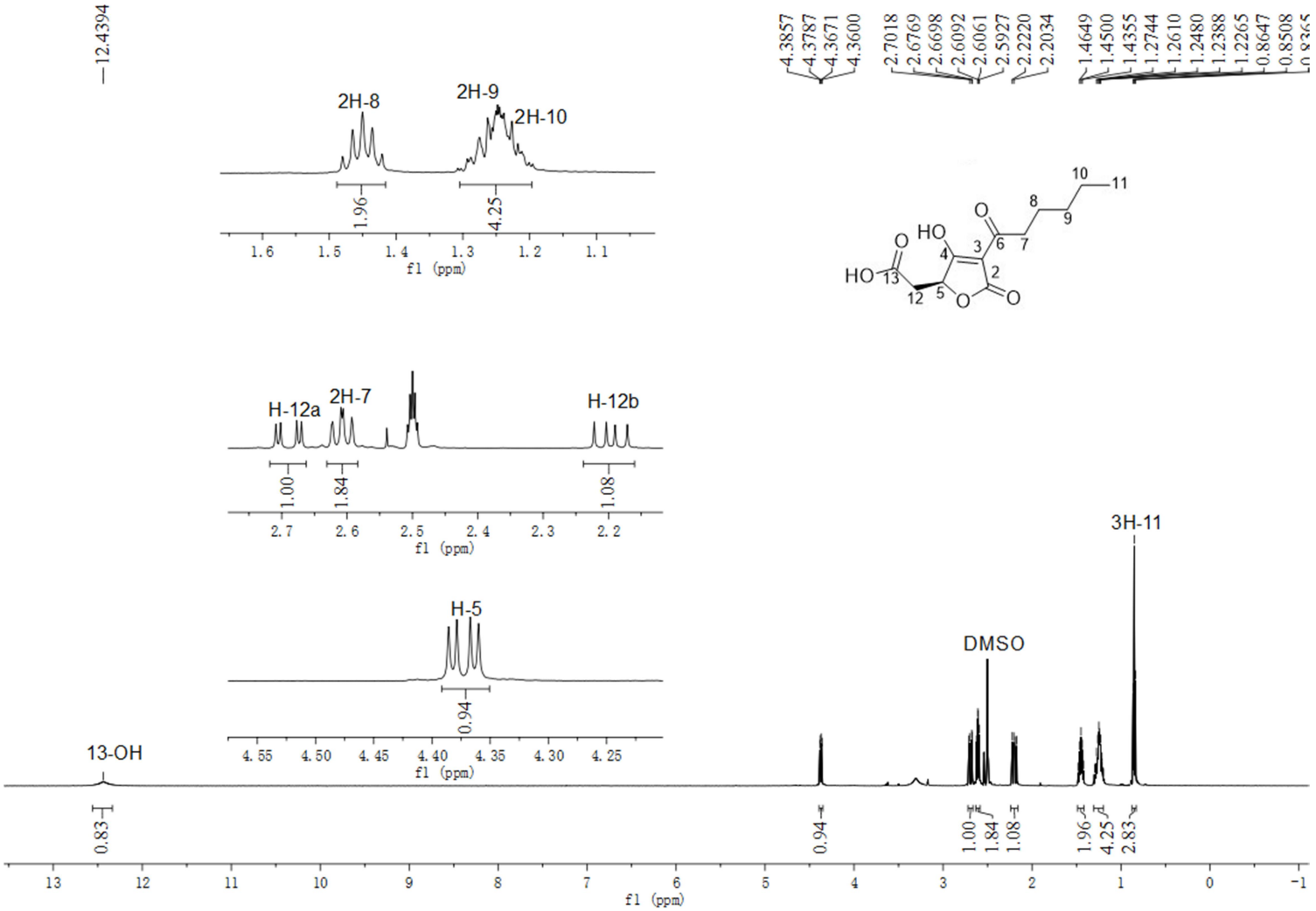

Figure S27. [1]H NMR spectrum of compound **5** isolated from *P. crustosum* PRB-2 in DMSO-d_6 (500MHz)

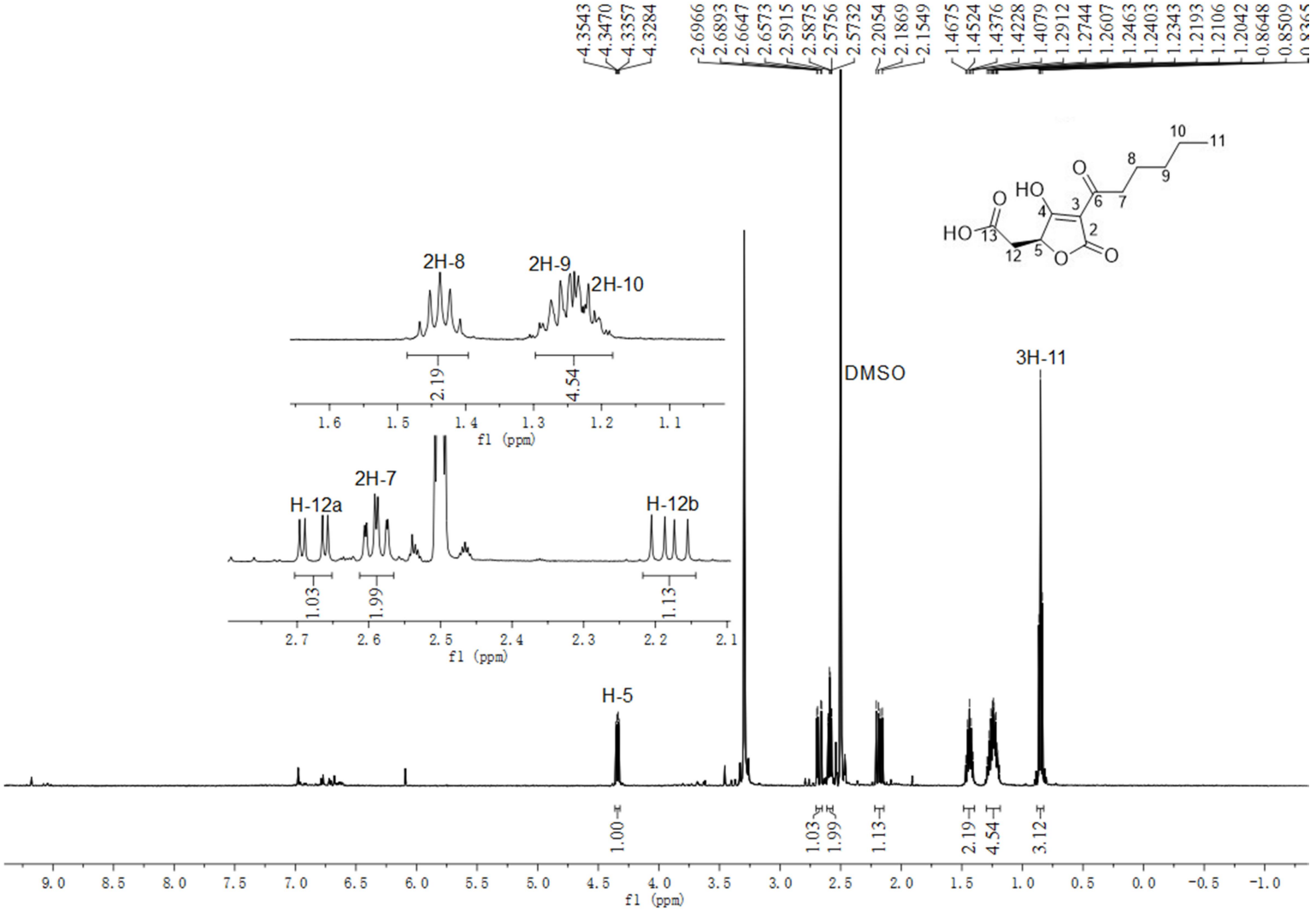

Figure S28. ^{1}H NMR spectrum of compound **5** isolated from *A. nidulans* JF45 harboring *traAG* in DMSO-d_6 (500MHz)

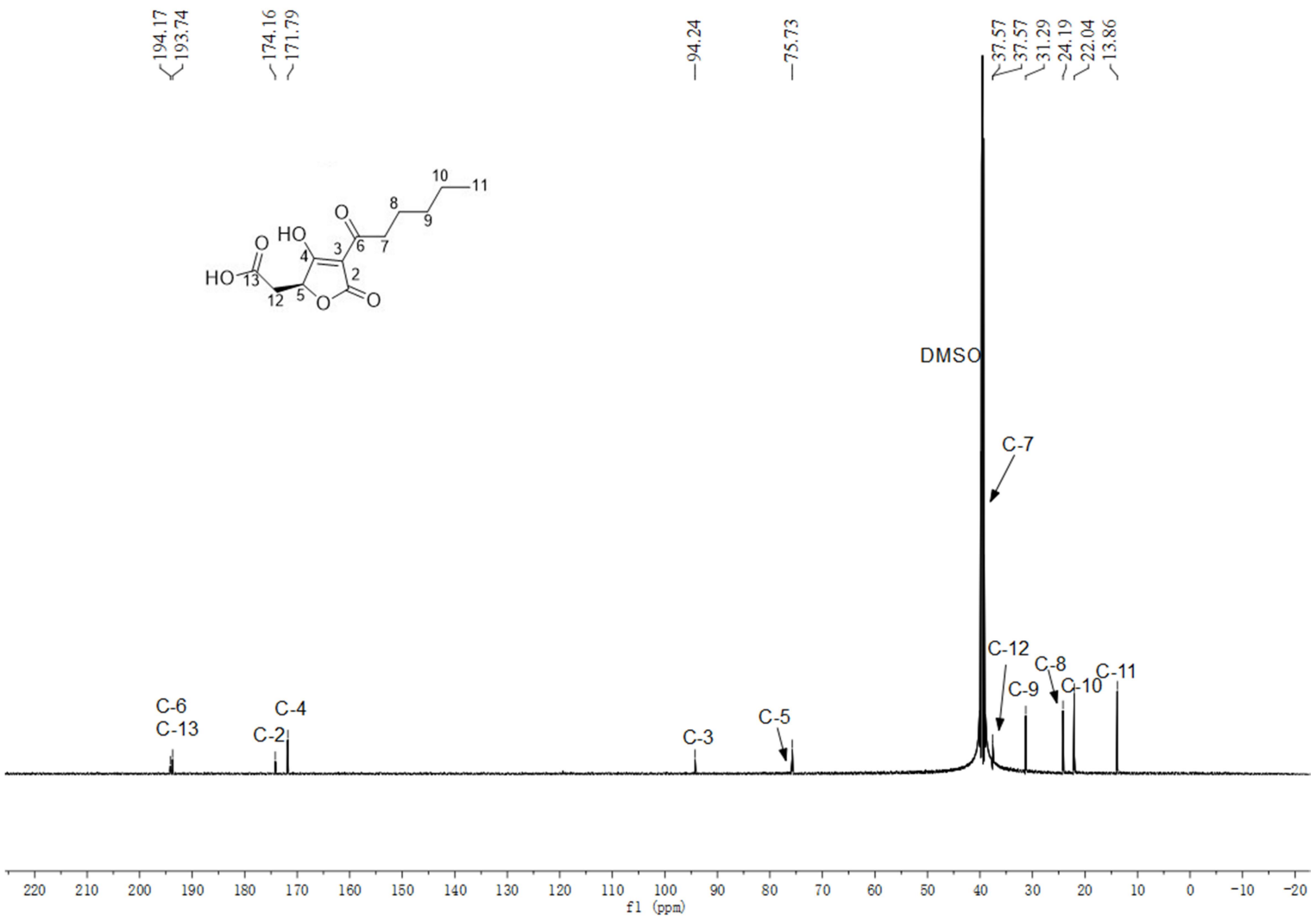

Figure S29. ^{13}C NMR spectrum of compound **5** isolated from *A. nidulans* JF45 harboring *traAG* in DMSO-d_6 (125MHz)

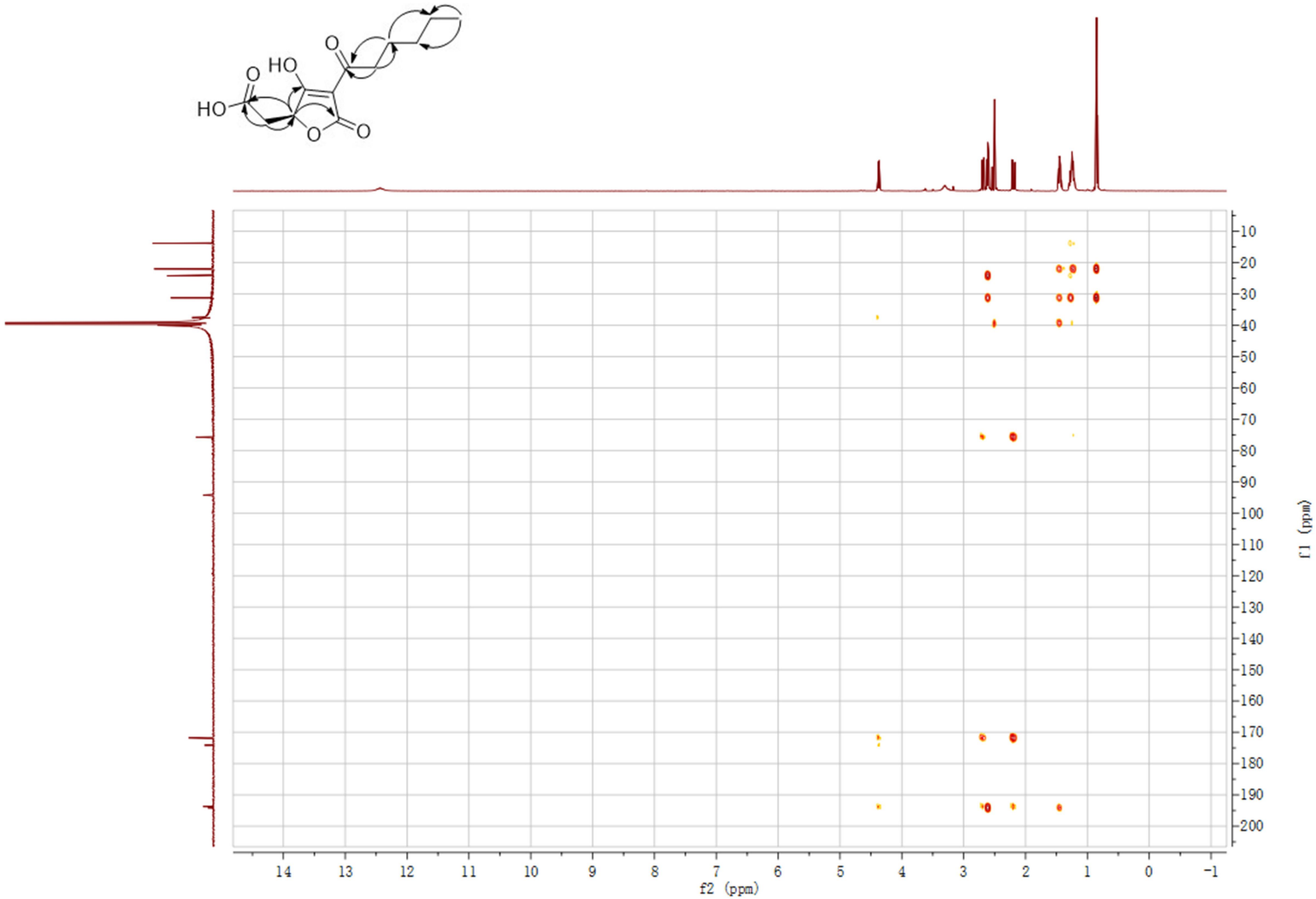

Figure S30. HMBC spectrum of compound **5** isolated from *A. nidulans* JF45 harboring *traAG* in DMSO-d_6

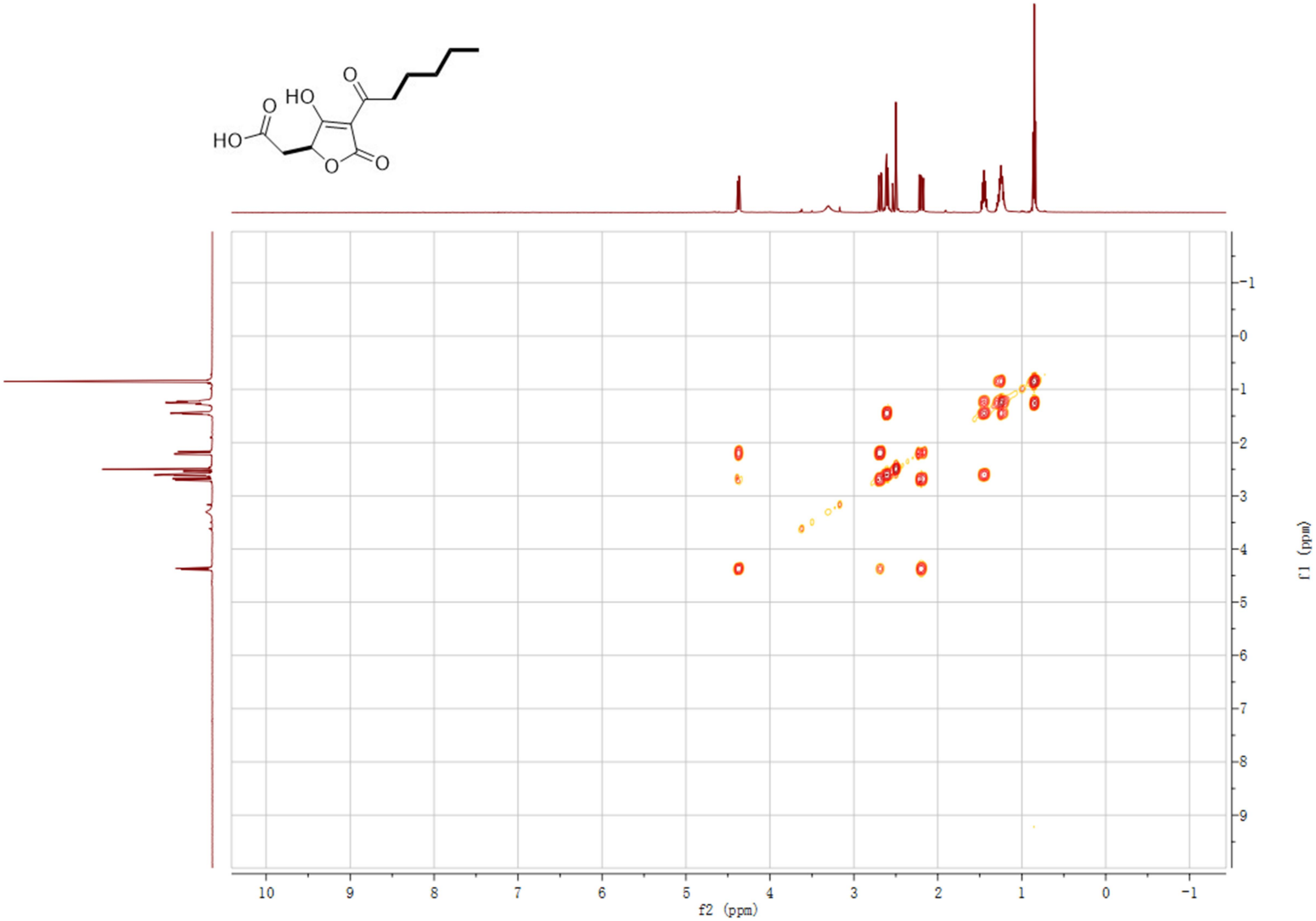

Figure S31. ^{1}H-^{1}H COSY spectrum of compound **5** isolated from *A. nidulans* JF45 harboring *traAG* in DMSO-d_6

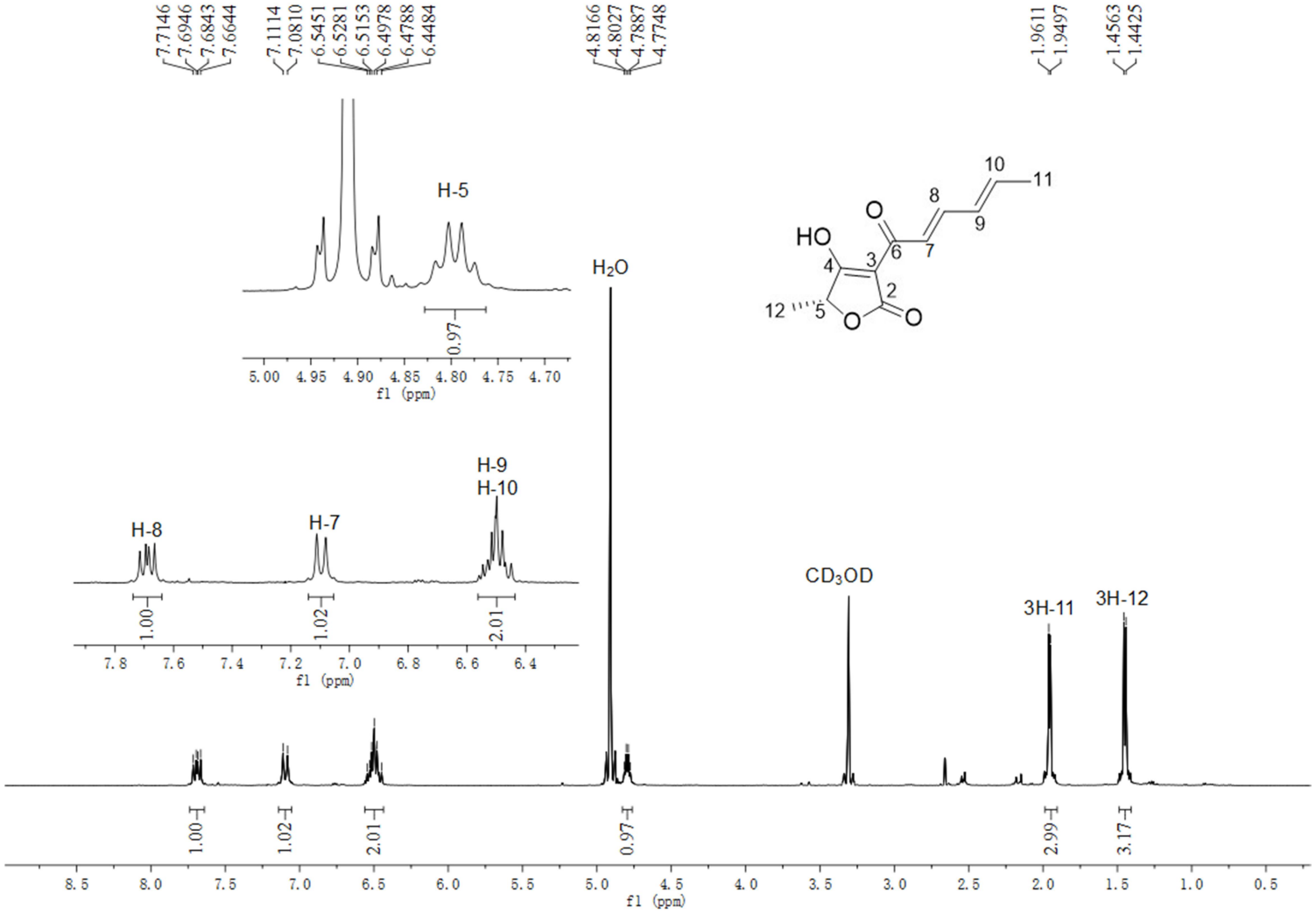

Figure S32. ^{1}H NMR spectrum of compound **6** in CD_3OD (500MHz)

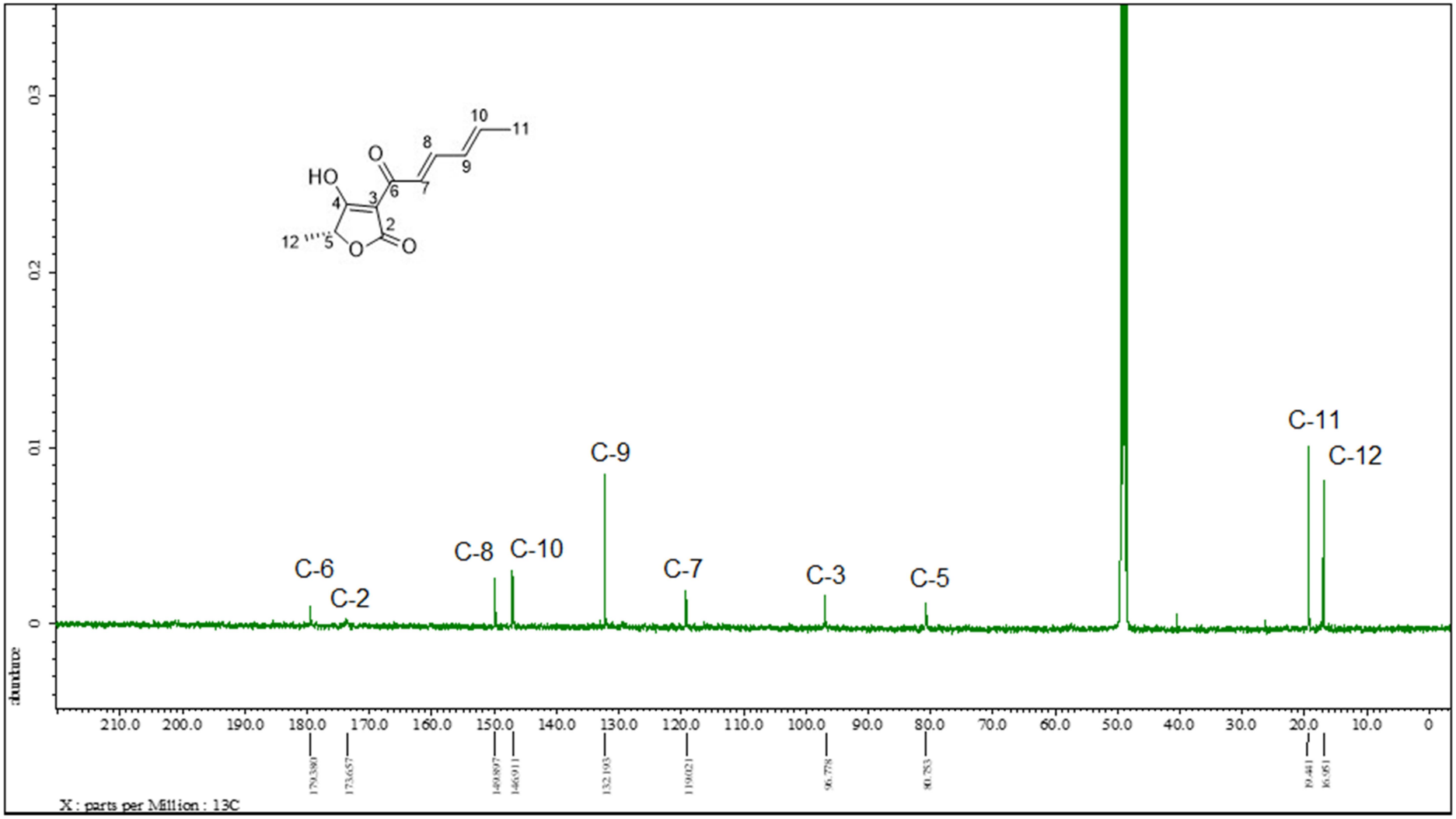

Figure S33. ^{13}C NMR spectrum of compound **6** in CD_3OD (125MHz)

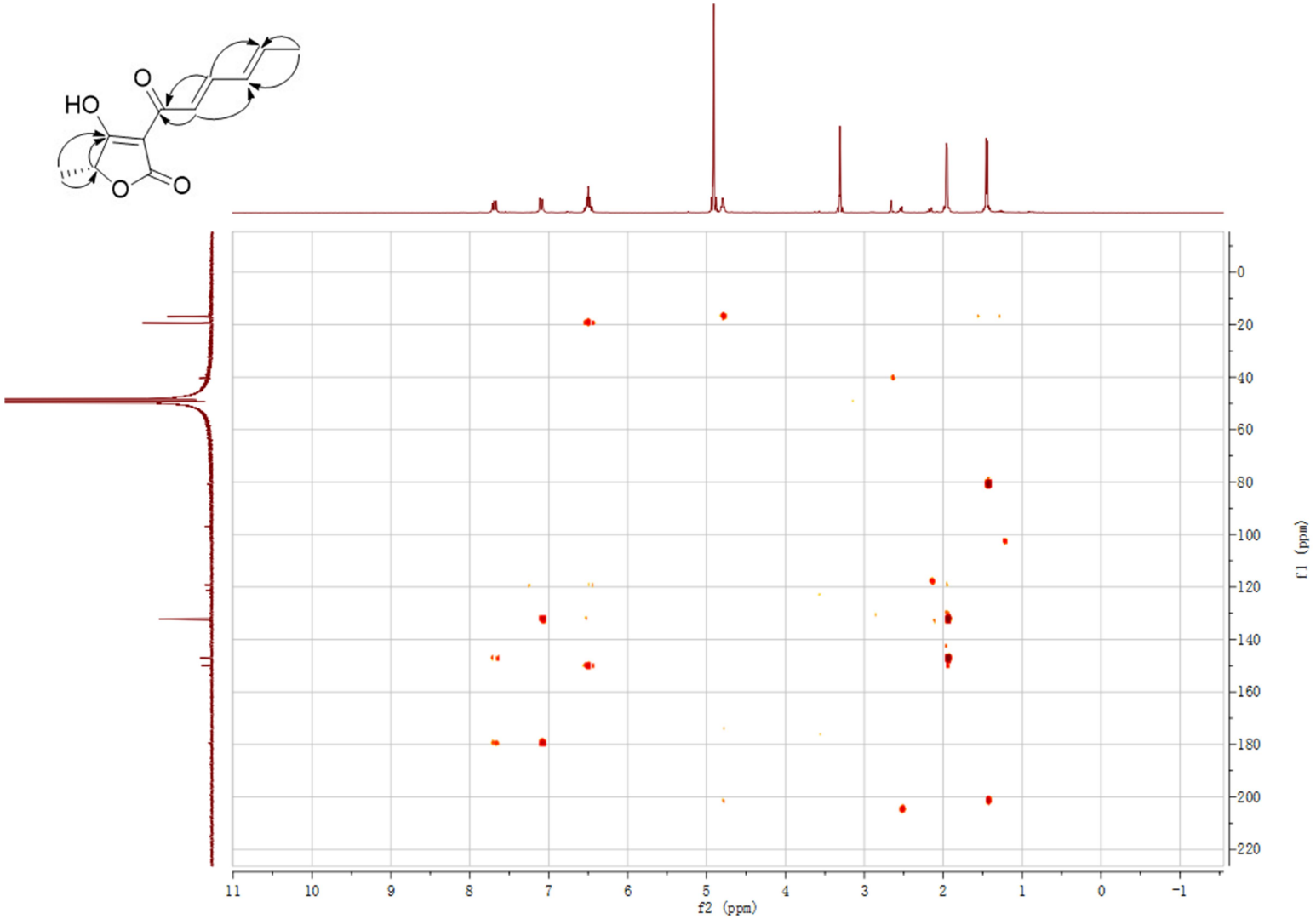

Figure S34. HMBC spectrum of compound **6** in CD_3OD

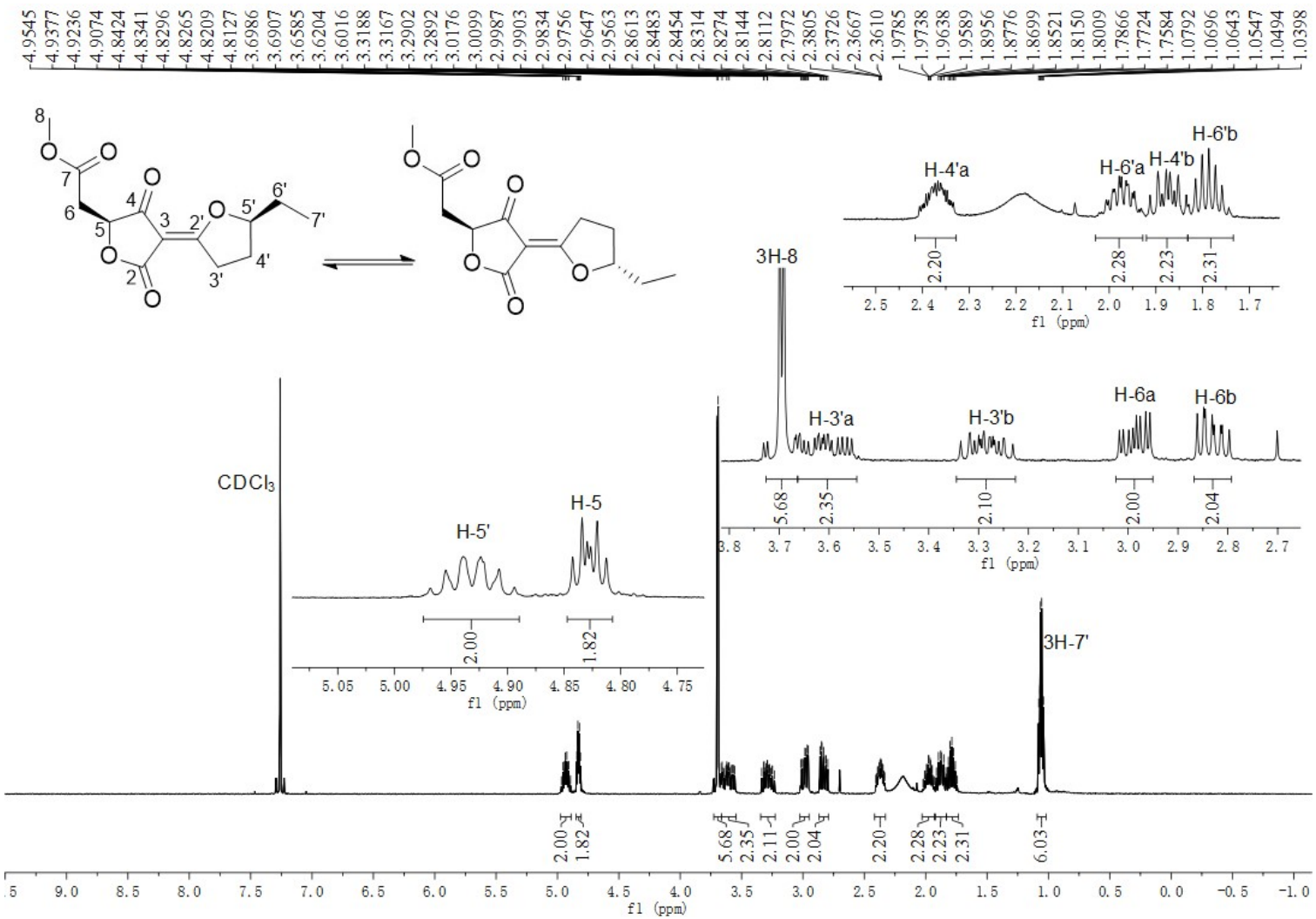

Figure S35. ^{1}H NMR spectrum of compound **7** in $CDCl_3$ (500MHz)

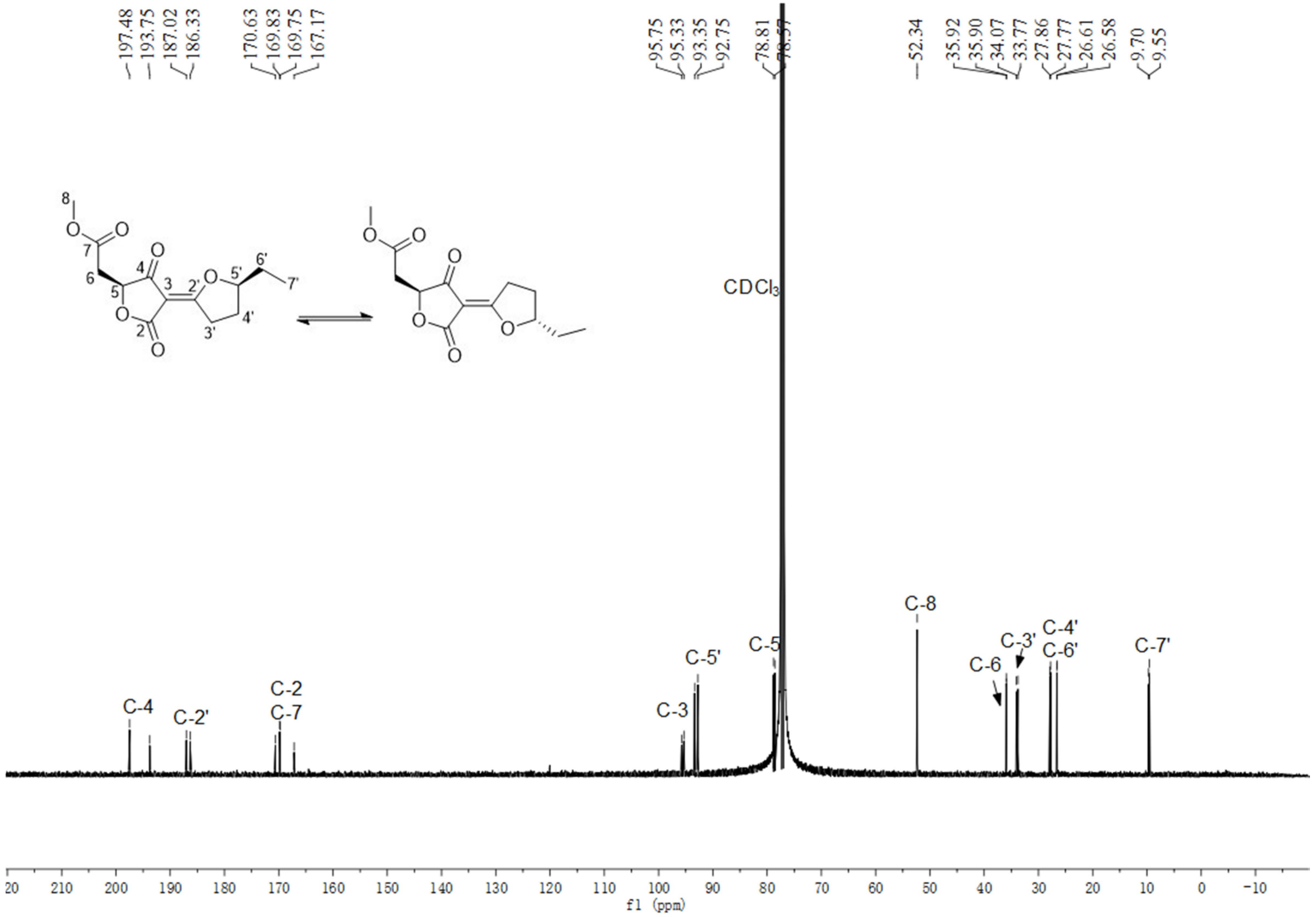

Figure S36. ^{13}C NMR spectrum of compound **7** in $CDCl_3$ (125MHz)

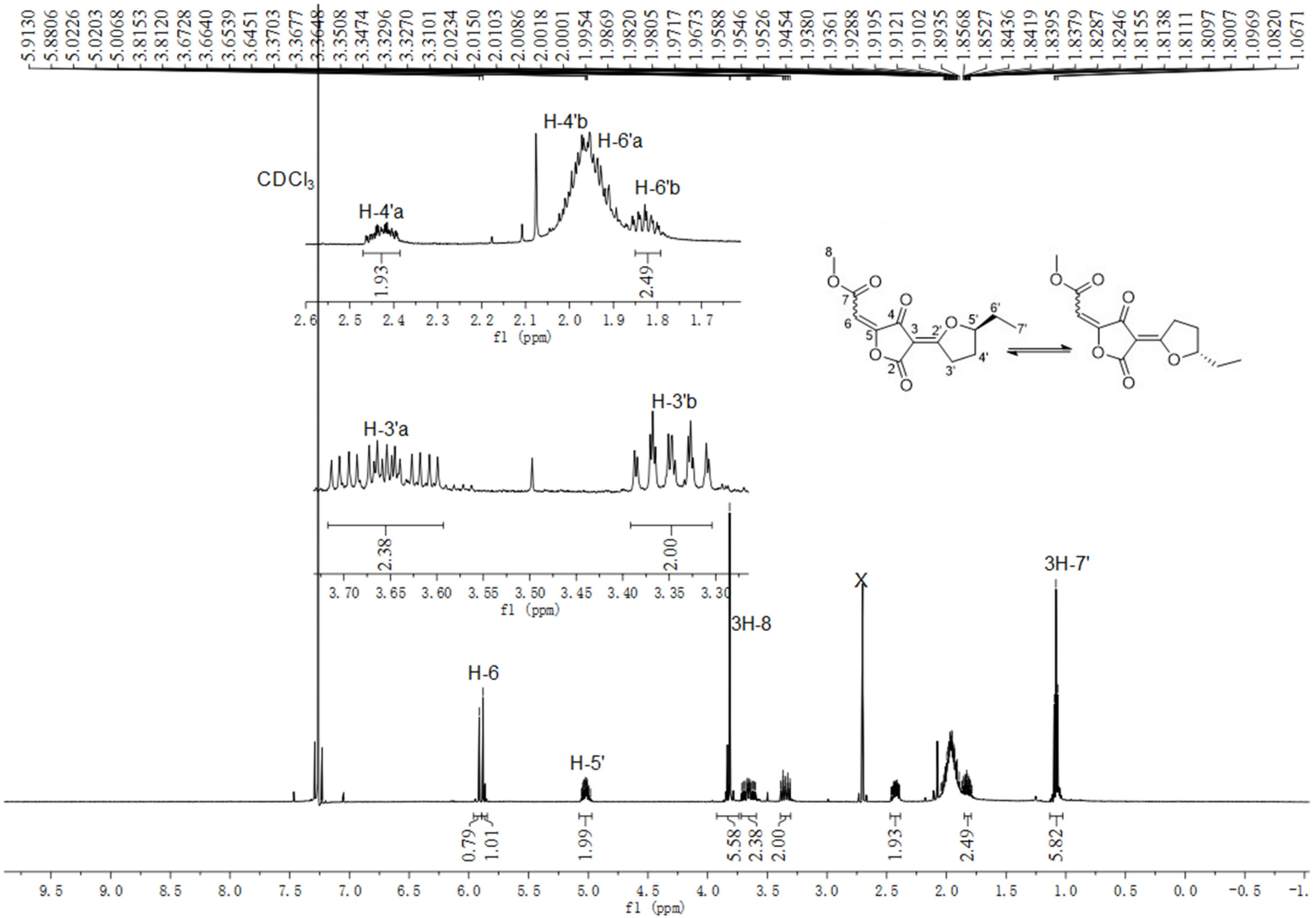

Figure S37. ^{1}H NMR spectrum of compound **8** in $CDCl_3$ (500MHz)

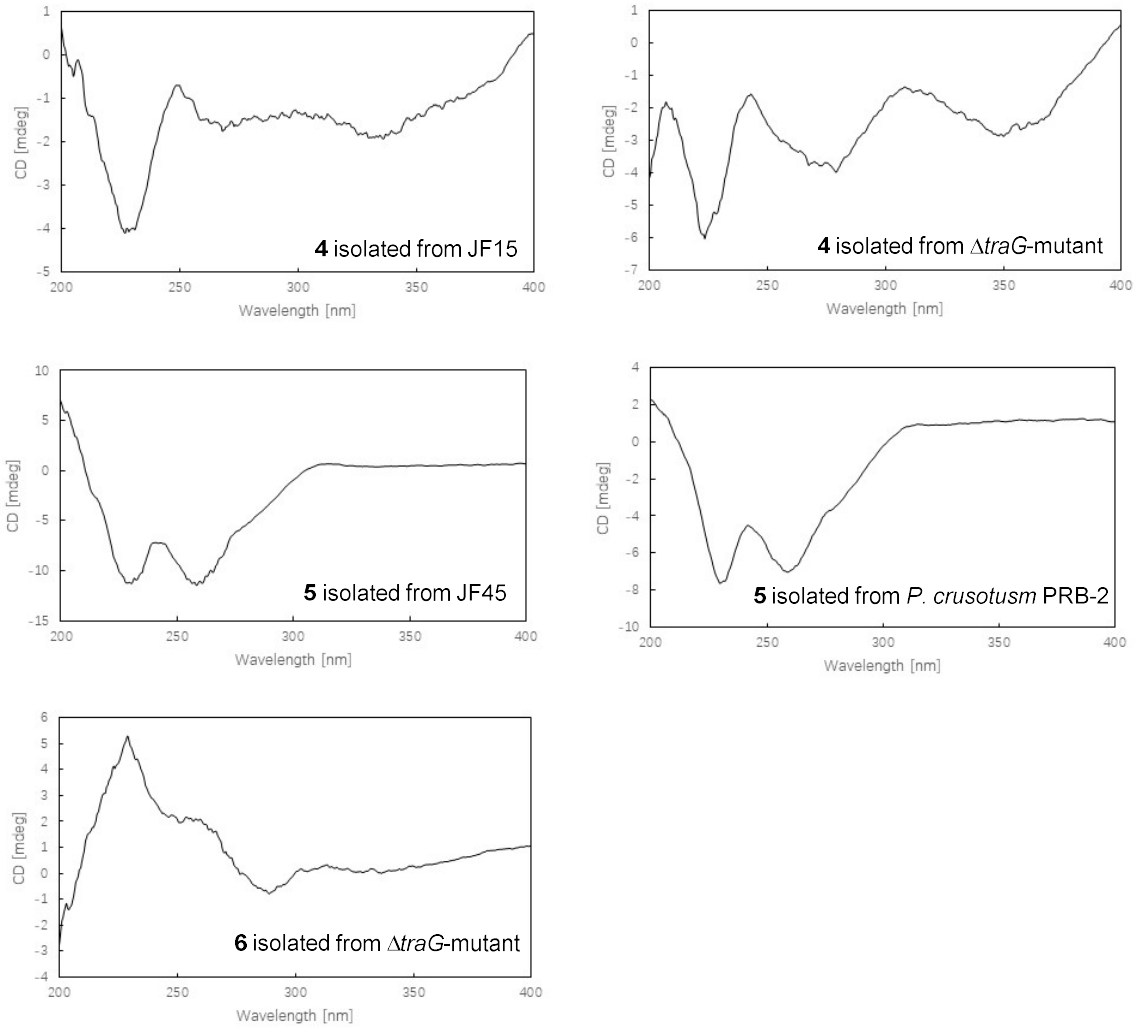

Figure S38. CD spectra of compounds **4** – **6**

Supplementary References

(1) Wu, G.; Ma, H.; Zhu, T.; Li, J.; Gu, Q.; Li, D. Penilactones A and B, two novel polyketides from Antarctic deep-sea derived fungus *Penicillium crustosum* PRB-2. *Tetrahedron* **2012**, *68,* 9745.

(2) Li, W.; Fan, A.; Wang, L.; Zhang, P.; Liu, Z.; An, Z.; Yin, W.-B. Asperphenamate biosynthesis reveals a novel two-module NRPS system to synthesize amino acid esters in fungi. *Chem. Sci.* **2018**, *9,* 2589.

(3) Chiang, Y. M.; Ahuja, M.; Oakley, C. E.; Entwistle, R.; Asokan, A.; Zutz, C.; Wang, C. C.; Oakley, B. R. Development of genetic dereplication strains in *Aspergillus nidulans* results in the discovery of aspercryptin. *Angew. Chem. Int. Ed. Engl.* **2016**, *55,* 1662.

(4) Yin, W. B.; Chooi, Y. H.; Smith, A. R.; Cacho, R. A.; Hu, Y.; White, T. C.; Tang, Y. Discovery of cryptic polyketide metabolites from dermatophytes using heterologous expression in *Aspergillus nidulans*. *ACS Synth. Biol.* **2013**, *2,* 629.

(5) Sambrook, J.; Russell, D. W. *Molecular cloning: a laboratory manual;* 3rd ed.; Cold Spring Harbor Laboratory Press, Cold Spring Harbor: New York, 2001.

(6) Fan, J.; Liao, G.; Kindinger, F.; Ludwig-Radtke, L.; Yin, W.-B.; Li, S.-M. Peniphenone and penilactone formation in *Penicillium crustosum via* 1,4-Michael additions of *ortho*-quinone methide from hydroxyclavatol to γ-butyrolactones from crustosic acid. *J. Am. Chem. Soc.* **2019**, *141,* 4225.

(7) Goswami, R. S. Targeted gene replacement in fungi using a split-marker approach. *Methods Mol. Biol.* **2012**, *835,* 255.

(8) Jacobus, A. P. and Gross, J. Optimal cloning of PCR fragments by homologous recombination in *Escherichia coli*. *PLoS. One.* **2015**, *10,* e0119221.

(9) Zhang, P.; Wang, X.; Fan, A.; Zheng, Y.; Liu, X.; Wang, S.; Zou, H.; Oakley, B. R.; Keller, N. P.; Yin, W. B. A cryptic pigment biosynthetic pathway uncovered by heterologous expression is essential for conidial development in *Pestalotiopsis fici*. *Mol. Microbiol.* **2017**, *105,* 469.

(10) Yu, X. and Li, S.-M. Prenyltransferases of the dimethylallyltryptophan synthase superfamily. *Methods Enzymol.* **2012**, *516,* 259.

(11) Yu, H. and Li, S.-M. Two cytochrome P450 enzymes from *Streptomyces* sp. NRRL S-1868 catalyze distinct dimerization of tryptophan-containing cyclodipeptides. *Org. Lett.* **2019**, *21,* 7094.

(12) Jacobsen, J. P.; Reffstrup, T.; Cox, R. E.; Holker, J. S. E.; Boll, P. M. Revision of the structures of the naturally occurring acyl tetronic acids: dehydrocarolic acid, terrestric acid and carlic acid. *Tetrahedron Lett.* **1978**, *19,* 1081.

(13) Pitt, J. I.; Lange, L.; Lacey, A. E.; Vuong, D.; Midgley, D. J.; Greenfield, P.; Bradbury, M. I.; Lacey, E.; Busk, P. K.; Pilgaard, B.; Chooi, Y. H.; Piggott, A. M. *Aspergillus hancockii* sp. nov., a biosynthetically talented fungus endemic to southeastern Australian soils. *PLoS. One.* **2017**, *12,* e0170254.

(14) Cox, R. J. Polyketides, proteins and genes in fungi: programmed nano-machines begin to reveal their secrets. *Org. Biomol. Chem.* **2007**, *5,* 2010.

(15) Miyanaga, A.; Kudo, F.; Eguchi, T. Protein-protein interactions in polyketide synthase-nonribosomal peptide synthetase hybrid assembly lines. *Nat. Prod. Rep.* **2018**, *35,* 1185.

(16) Huang, J. L.; Tang, Y.; Yu, C. P.; Sanyal, D.; Jia, X.; Liu, X.; Guo, Y.; Chang, W. C. Mechanistic investigation of oxidative decarboxylation catalyzed by two iron(II)- and 2-oxoglutarate-dependent enzymes. *Biochemistry* **2018**, *57,* 1838.

(17) Yu, C. P.; Tang, Y.; Cha, L.; Milikisiyants, S.; Smirnova, T. I.; Smirnov, A. I.; Guo, Y.; Chang, W. C. Elucidating the reaction pathway of decarboxylation-assisted olefination catalyzed by a mononuclear non-heme iron enzyme. *J Am. Chem. Soc.* **2018**, *140,* 15190.

(18) Yang, X. L.; Awakawa, T.; Wakimoto, T.; Abe, I. Three acyltetronic acid derivatives: noncanonical cryptic polyketides from *Aspergillus niger* identified by genome mining. *Chembiochem* **2014**, *15,* 1578.

4.4 Increasing structural diversity of natural products by Michael addition with *ortho*-quinone methide as the acceptor

JOC The Journal of Organic Chemistry
Cite This: J. Org. Chem. 2020, 85, 1298−1307
Note
pubs.acs.org/joc

Increasing Structural Diversity of Natural Products by Michael Addition with *ortho*-Quinone Methide as the Acceptor

Ge Liao,[†] Jie Fan,[†] Lena Ludwig-Radtke, Katja Backhaus, and Shu-Ming Li*

Institut für Pharmazeutische Biologie und Biotechnologie, Philipps-Universität Marburg, Robert-Koch Straße 4, Marburg 35037, Germany

Supporting Information

ABSTRACT: The active form of clavatol, *ortho*-quinone methide, can be generated from hydroxyclavatol in an aqueous system and used as a highly reactive intermediate for coupling with diverse natural products under very mild conditions. These include flavonoids, hydroxynaphthalenes, coumarins, xanthones, anthraquinones, phloroglucinols, phenolic acids, indole derivatives, tyrosine analogues, and quinolines. The clavatol moiety was mainly attached via C−C bonds to the *ortho*- or *para*-positions of phenolic hydroxyl/amino groups and the C2-position of the indole ring.

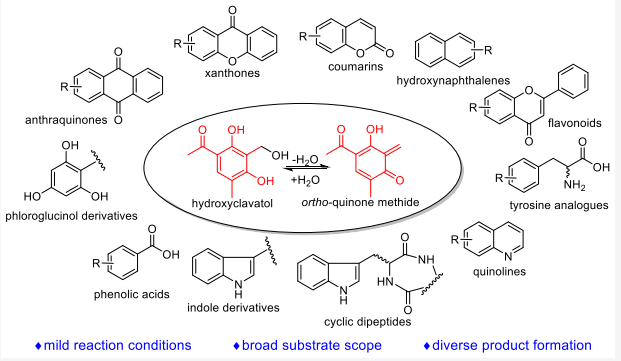

Ortho-quinone methides (*o*-QMs), as transient intermediates with remarkable reactivity, have been utilized as useful reactants in chemical synthesis.[1−5] A wide range of strategies, e.g., thermally driven,[6,7] photolytically induced tautomerization,[8,9] and benzylic oxidation,[10,11] were developed to generate *o*-QMs. However, *o*-QMs can also be formed by spontaneous elimination of a stable molecule with concomitant dearomatization.[12,13]

Recently, we reported the formation of penilactones A and B by two-step nonenzymatic Michael additions between a γ-butyrolactone and two *o*-QM molecules. The key precursor hydroxyclavatol was the oxidation product of clavatol by the nonheme Fe^{II}/2-oxoglutarate dependent oxygenase ClaD and undergoes spontaneous water elimination, resulting in the active *o*-QM intermediate (Figure 1i).[12]

In addition to penilactones A and B from *Penicillium crustosum*,[14] a number of natural products containing a clavatol unit are found in fungi, especially in *Penicillium* species.[14−20] These include a clavatol−flavanone adduct from *Penicillium griseoroseum*[16] as well as coupling products of clavatol with α-pyrone (communol A) and indole (communol B) from *Penicillium commune*[17] (Figure 1ii). More coupling products of clavatol with diverse lactones, phenols, and quinones are listed in Figure S1 (see Supporting Information (SI)).

The occurrence of these natural products implies the involvement of clavatol, very likely via the *o*-QM intermediate, in their formation. Inspired by the postbiosynthetic nonenzymatic event in the formation of penilactones A and B, we wondered whether these clavatol-containing compounds are also pseudonatural products.

This hypothesis triggered our interest to prove the reactivity of the *o*-QM intermediate derived from hydroxyclavatol with

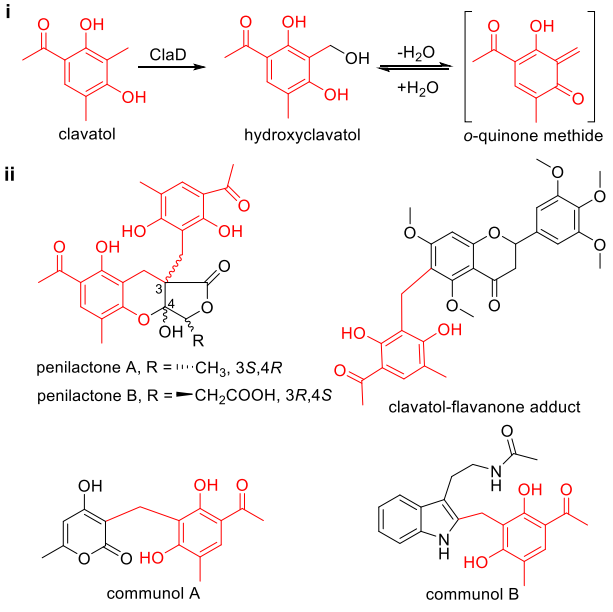

Figure 1. Formation of hydroxyclavatol and its equilibration with the *o*-QM intermediate (i). Representative examples of clavatol-containing natural products (ii). See Figure S1 for more examples.

diverse natural products. Encouraged by accumulation of the clavatol−flavanone adduct in *P. griseoroseum*,[16] we synthesized hydroxyclavatol chemically (Scheme S1)[6,21] and screened its reactivity with 16 flavonoids including catechin (**1a**−**16a**)

Received: November 1, 2019
Published: December 20, 2019

DOI: 10.1021/acs.joc.9b02971
J. Org. Chem. 2020, 85, 1298−1307

under mild conditions (Figures S2–S4). Both hydroxyclavatol and reactants at a final concentration of 0.4 mM in 50 μL of H_2O were incubated at 25 °C for 16 h without pH adjustment. LC–MS analysis of the incubation mixtures showed that, with the exception for **10a**, $[M + H]^+$ ions being 178 Da larger than the corresponding reactants were detected. These proved the formation of the coupling products of flavonoids with clavatol. Masses of products harboring two clavatol units were also detected when using **4a**, **5a**, **8a**, **9a**, and **12a**–**15a** as reactants.

Subsequent assays of hydroxyclavatol with other phenolic substances, including hydroxynaphthalenes (**17a**–**27a**), coumarins (**28a**–**32a**), xanthones (**33a**–**38a**), anthraquinones (**39a**–**42a**), phloroglucinol derivatives (**43a**–**51a**), and phenolic acids (**52a**–**60a**) were carried out in a similar way as mentioned above. Products were detected in incubation mixtures of hydroxyclavatol with 9 of 11 tested hydroxynaphthalenes. This proved hydroxynaphthalenes as suitable reactants for coupling with the *o*-QM (Figures S2–S4). Coumarins with **29a** as an exception, xanthones, and anthraquinones were relatively poor reaction partners for the *o*-QM and gave no product or only trace amount of products in their reaction mixtures (Figures S2–S5). Among all the tested phenolic substances, phloroglucinol derivatives were found to be the most favorable Michael donors for the *o*-QM intermediate, with 10 to 55% conversion (Figures S2 and S6). In addition, coupling products of benzoic acids (**52a**–**54a**) were also observed by LC–MS analysis, while products from hydroxyphenyl acetic acid (**55a**), propionic acids (**56a** and **57a**), and acrylic acids (**58a** – **60a**) were not detectable (Figures S2–S4).

We speculated that the formation of the clavatol–indole adduct communol B from *P. commune*[17] was also a non-enzymatic event and therefore investigated the reaction activity of hydroxyclavatol with indole derivatives (**61a**–**72a**). The incubation mixture of L-tryptophan (**61a**) with hydroxyclavatol showed a coupling product with a conversion of 20%, while replacement of the nitrogen of the indole ring by sulfur (**62a**) and methylation at the N1 position (**63a**) significantly reduced the activity. Other indole derivatives carrying different side chains at C3 coupled with clavatol with up to 49% conversion (Figures S2, S3, and S7).

Subsequently, cyclic dipeptides (**73a**–**82a**) were tested by coincubation with hydroxyclavatol. All tryptophan-containing cyclic dipeptides (**73a**–**80a**) showed UV detectable product formation with 9 to 29% conversion. No product formation was detected for the incubation mixtures of *cyclo*-L-Tyr–L-Tyr (**81a**) and *cyclo*-L-Ser–L-Tyr (**82a**) (Figures S2–4, S7, and S8). In contrast to the easy coupling of L-tryptophan with the *o*-QM, L-tyrosine and its analogues (**83a** – **87a**) were generally poorly converted to their clavatol adducts. **88a**–**90a** with an amino group at the benzene ring showed UV detectable product formation (Figures S2 and S3). All selected quinolines (**91a**–**99a**) served as Michael donors to couple with the *o*-QM, especially **92a**, **94a**, **95a**, and **98a** with obvious product peaks in UV chromatograms (Figures S2, S3, and S8).

In addition, clear product formation was also detected for the *o*-QM with other nitrogen-containing reactants, including 2-aminobenzyl alcohol (**100a**), 2-aminobenzoic acid (**101a**), and even tris(hydroxymethyl)aminomethane (Tris, **102a**) prepared as Tris–HCl buffer (pH 7.5) (Figures S2 and S8).

In summary, we demonstrated in a previous study that Michael additions between the *o*-QM and γ-butyrolactones took place easily under neutral or acidic conditions.[12] Therefore, hydroxyclavatol was incubated in this study with 101 natural products or natural-product-like compounds at 25 °C and a nearly neutral pH value, which led to the detection of coupling products in 85 cases. Product formation with 10 to 55% conversion was detected for 49 reactants (Schemes 1 and 2 and Figures S5–S10). To facilitate the isolation of the

Scheme 1. Reactions of Hydroxyclavatol with Nitrogen-Free Reactants

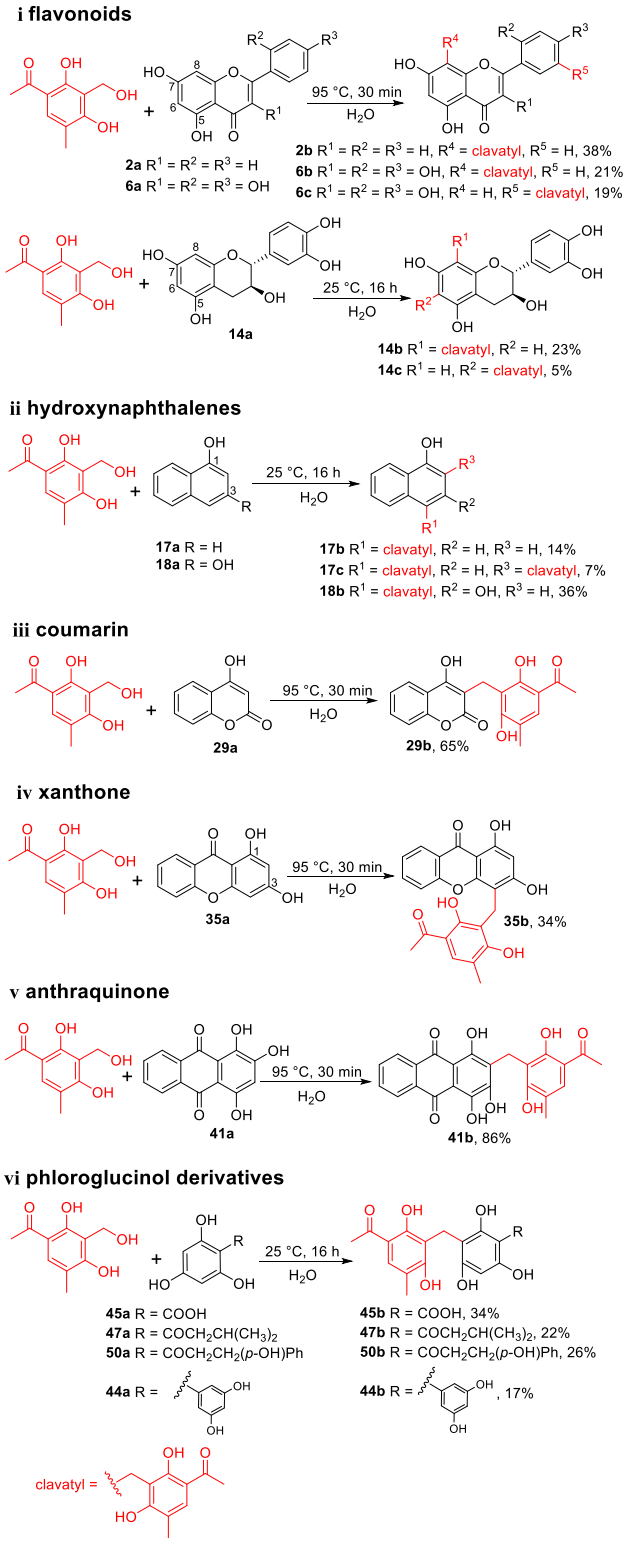

DOI: 10.1021/acs.joc.9b02971
J. Org. Chem. 2020, 85, 1298–1307

Scheme 2. Reactions of Hydroxyclavatol with Nitrogen-Containing Reactants

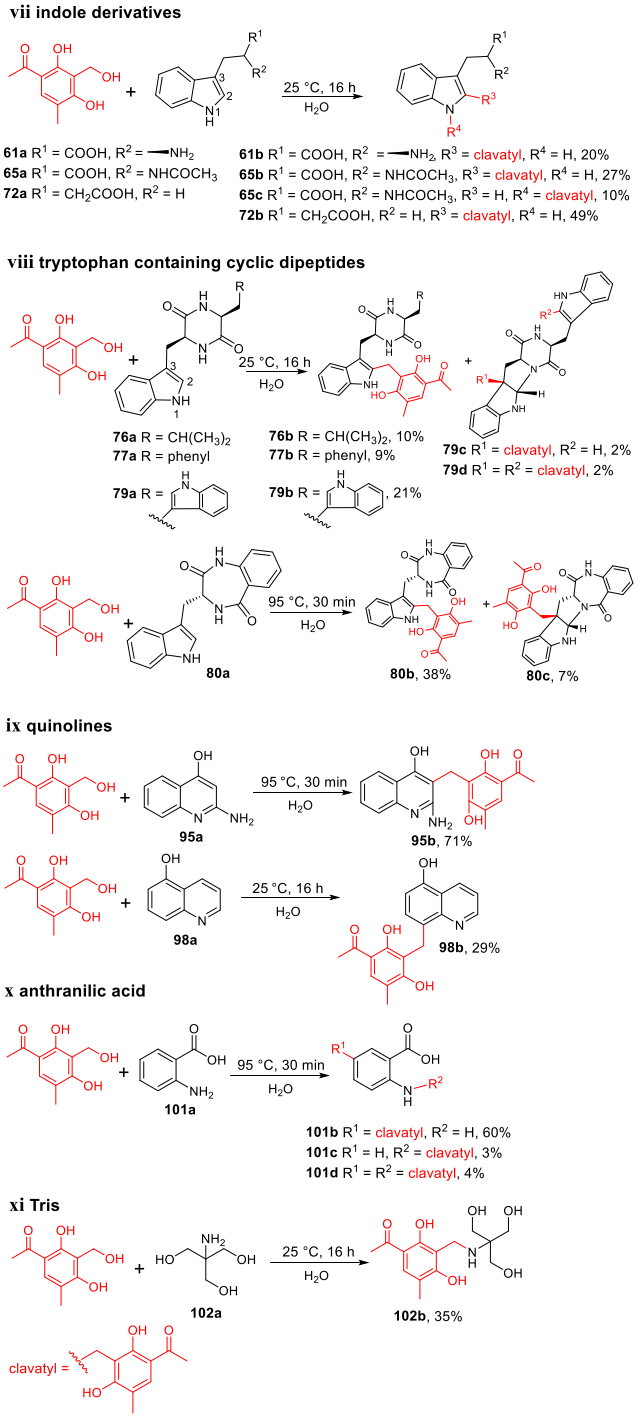

products for structural elucidation, we changed the reaction temperature for all the incubations to 95 °C for 30 min to improve the product yields. As shown in Figures S5−S10, the majority of the reactions was promoted by increased temperature, leading to generally 2 to 10-fold higher accumulation of the coupling products. Taking purpurin (**41a**) as an example, its coupling with clavatol was improved dramatically from a trace amount to 86%. In total, product formation with 30 to 99% conversion was achieved for 58 reactants at 95 °C for 30 min. However, in a few cases, no significant change was observed for reactions performed at 25 and 95 °C (Figures S5−S10). Therefore, large scaled reactions of hydroxyclavatol with 23 reactants of different structural skeletons were carried out at either 25 or 95 °C, resulting in the isolation of 32 products, which were further subjected to HR-ESI-MS and NMR analyses (Figures S12−S86).

Structural elucidation of the coupling products of phenolic reactants confirmed the attachment of the clavatol unit to the *ortho*- or *para*-positions of the hydroxyl group at the benzene ring. Herein, the *o*-QM formed from hydroxyclavatol in an aqueous system was proposed to act as the Michael acceptor for the phenolic substances (Figure S11i,ii). The formation of **17b** and **98b** represents examples for the attachment of a clavatol moiety onto the *para*-position of the hydroxyl group (Schemes 1 and 2 and Figures S5 and S8). For flavan derivatives with a 5,7-dihydroxyl feature (**2a**, **6a**, and **14a**), C8-adducts (**2b**, **6b**, and **14b**) were identified as main products, and the C6-adduct (**14c**) was identified as a byproduct (Scheme 1 and Figure S5). The clavatol-containing flavanone from *P. griseoroseum* (Figure 1) was identified by feeding 5,7,3′,4′,5′-pentamethoxyflavanone into the culture.[16] The incorporation of the clavatol unit into the exogenous flavanone might be also a nonenzymatic product. In analogy, **18b** and **35b** were identified as products of hydroxyclavatol with 1,3-dihydroxynaphthalene (**18a**) and 1,3-dihydroxyxanthone (**35a**) (Scheme 1 and Figures S5 and S6). Additionally, formation of **29b** by the linkage between the clavatol unit and the *α*-pyrone moiety of **29a** suggests that communol A from *P. commune* could be formed in a similar way (Scheme 1 and Figure S5). Phloroglucinol derivatives harboring three hydroxyl groups at the benzene ring conjugated with a clavatol also via C−C bonds (**44b**, **45b**, **47b**, and **50b**) (Scheme 1 and Figure S6).

The indole ring in the tryptophanyl moiety contributes greatly to structural complexity by enzymatic modifications and spontaneous rearrangement.[22,23] Communol B mentioned above represents a coupling example of a clavatol moiety with an indole skeleton.[17] Accordingly, incubation of L-tryptophan (**61a**) with hydroxyclavatol enabled us to obtain the product (**61b**) with a similar structure to communol B (Scheme 2 and Figure S7). Subsequent isolation of clavatol adducts with different indole derivatives ((±)-**65b** and **72b**) confirmed the spontaneous addition of the indole moiety via C2 to the *o*-QM (Scheme 2 and Figure S7). Furthermore, a number of coupling products of clavatol with tryptophan-containing cyclic dipeptides were also identified. Among them, C2-adducts were obtained as main products (**76b**, **77b**, **79b**, and **80b**), and C3-adducts (**79c** and **80c**) were obtained as byproducts (Scheme 2 and Figures S7 and S8). In addition, a *cyclo*-L-Trp−L-Trp derivative carrying two clavatol units (**79d**) was also identified (Scheme 2 and Figure S7). The conjugation between the clavatol unit and indole skeleton indicates that the electron transfer in the indole ring enabled the Michael addition from C2 to the electrophilic methylene group of the *o*-QM (Figure S11iii).

Steinmetz et al.[24] reported C−N coupling compounds as Michael addition products of different nucleophiles via their amino groups to the *p*-quinone methide, i.e., elansolid A3. However, only a few coupling products were obtained via C−N bond formation in this study. Examples are (±)-**65c** as a byproduct from the incubation of hydroxyclavatol with *N*-acetyl-DL-tryptophan ((±)-**65a**), **101c**, and **101d** from 2-aminobenzoic acid (**101a**) and **102b** from Tris (**102a**) (Scheme 2 and Figures S7, S8, and S11iv). It can be concluded

DOI: 10.1021/acs.joc.9b02971
J. Org. Chem. 2020, 85, 1298−1307

that the cross-coupling between the nucleophiles tested above and the *o*-QM from hydroxyclavatol occurs preferentially via C−C bond formation. In addition, the C−N bond in **101d** seems unstable and can be easily hydrolyzed, which was observed by inspection of the ^{1}H NMR spectrum of **101d** (Figure S83) and comparison of the impurity signals with those of **101b** (Figure S79).

After structure elucidation, the obtained clavatol-containing products were screened for their antibacterial, acetylcholinesterase, and α-glucosidase inhibition activities. Detailed evaluation of the α-glucosidase inhibitory activity revealed the clavatol-coupling products **2b**, **17b**, **18b**, **35b**, **72b**, and **95b** showed clear inhibition with IC_{50} values ranging from 43.8 ± 1.0 to 231.0 ± 7.5 μM, while their precursors showed no activity. These concentrations are significantly lower than that of the control substance acarbose with an IC_{50} at 766.2 ± 37.8 μM (Table 1), indicating that conjugation of low-molecular-weight compounds with clavatol has the potential to increase the biological activity.

Table 1. Inhibitory Effects of the Selected Compounds against α-Glucosidase

reactants	IC_{50} (μM)	products	IC_{50} (μM)
2a	n.i.	**2b**	60.1 ± 0.6
17a	n.i.	**17b**	167.8 ± 2.3
18a	n.i.	**18b**	231.0 ± 7.5
35a	n.i.	**35b**	43.8 ± 1.0
72a	n.i.	**72b**	140.1 ± 1.3
95a	n.i.	**95b**	52.0 ± 2.4
acarbose[a]	766.2 ± 37.8		

[a]Positive control. n.i.: no inhibition. The IC_{50} data with standard deviation are mean values of three independent experiments.

In summary, our extended study on the utility of hydroxyclavatol proved that the *o*-QM generated from hydroxyclavatol can be considered as an excellent Michael acceptor for a variety of substances. The coupling reactions occurred under very mild conditions, i.e., overnight incubation at 25 °C in water. Increasing the reaction temperature can accelerate the reaction rate and promote the product accumulation. Diverse clavatol-containing products were identified in this study by incorporation of a clavatol unit onto the *ortho*- or *para*-positions of the hydroxyl group of different phenolic compounds as well as connection between the methylene group of the clavatol unit and the C2 of indole skeletons. Additional C−N bond formation of clavatol-coupling products was also observed in a few cases.

Despite of the wide application of QMs in chemical synthesis,[1−5] QMs have also been reported to be involved in the assembly of natural products in recent years. For example, elansolid A3 acts as a key intermediate in the biosynthesis of elansolids.[25,26] Spontaneous Diels−Alder addition via an *o*-QM intermediate was suggested for the formation of leprins.[27] Another QM-like intermediate is likely responsible for the dimerization of benzofluorene-containing angucyclines.[13] In analogy, it is plausible that the clavatol-containing natural products listed in Figures 1 and S1 are formed by nonenzymatic Michael addition with involvement of the *o*-QM derived from hydroxyclavatol. Furthermore, it can be expected that more clavatol-coupling natural products will be discovered in the near future.

EXPERIMENTAL SECTION

Chemicals. **35a−38a**, **46a−48a**, **73a**, **75a**, **79a**, and **80a** were chemically synthesized as previously reported.[28−34] Other chemicals used in this study were purchased from Bachem (Bubendorf, Switzerland), ABCR (Karlsruhe, Germany), TCI Europe (Zwijndrecht, Belgium), Alfa Aesar (Kandel, Germany), Carl Roth (Karlsruhe, Germany), Sigma-Aldrich (St. Louis, USA), or Acros (Merelbeke, Belgium).

Reaction Conditions of Hydroxyclavatol with the Tested Aromatic Compounds. Stock solutions of the tested compounds were prepared at 20 mM in DMSO or DMSO/H_2O (*v*/*v*, 1:1). Reactions were initiated by adding hydroxyclavatol (0.4 mM) and reactants (0.4 mM) into 50 μL of distilled H_2O without pH adjustment. As a result, the reactions generally took place in the pH environment of 5.0−7.5. After incubation at 25 °C for 16 h, 50 μL of ACN was added into the reaction mixture. A 5 μL aliquot of supernatant was injected into LC−MS for analysis after centrifugation at 13 000 rpm for 30 min. Conversions were calculated from peak areas of products and reactants with UV detection. Two independent experiments were performed. In addition, reactions of all reactants were also carried out at 95 °C for 30 min.

LC−MS Analysis of Reaction Mixtures. LC−MS analysis was performed on a microTOF-Q III spectrometer (Bruker, Bremen, Germany) with an Agilent 1260 HPLC system (Agilent Technologies, Böblingen, Germany), using the Multospher 120 RP18-5μ column (250 × 2 mm, 5 μm) (CS-Chromatographie Service GmbH). H_2O (A) and ACN (B), both with 0.1% (*v*/*v*) HCOOH, were used as solvents at flow rate of 0.25 mL/min. The substances were eluted with a linear gradient from 5−100% (*v*/*v*) B in 15 min. The column was then washed with 100% (*v*/*v*) solvent B for 5 min and equilibrated with 5% (*v*/*v*) solvent B for 5 min. Detection was carried out on a photodiode array detector, and UV absorptions at 280 nm are illustrated in this study. Electrospray ionization in positive or negative mode was set for the determination of the accuracy masses. HCOONa was used in each run for mass calibration. The capillary voltage was set to 4.5 kV, and collision energy was set to 8.0 eV. Data were evaluated with the Compass DataAnalysis 4.2 software (Bruker Daltonik, Bremen, Germany). The masses were scanned in the range of *m*/*z* 100−1500.

Isolation and Identification of the Reaction Products. To isolate the reaction products for structural elucidation, reactions were carried out in large scaled incubations (40 or 200 mL) containing hydroxyclavatol (0.4 mM), different reactants (0.4−0.8 mM), and up to 2% (*v*/*v*) DMSO. After incubation at 25 °C for 16 h or heating at 95 °C for 30 min, the reaction mixtures were extracted with a double volume of EtOAc three times. The organic phases were combined and concentrated under vacuum. The resulted residues were dissolved in MeOH and centrifuged at 13 000 rpm for 20 min. The products were then purified by silica gel column chromatography with a stepwise gradient of petroleum ether/EtOAc or on a Sephadex LH20 column with MeOH as elution solvent. A semipreparative HPLC equipped with an Agilent ZORBAX Eclipse XDB-C18 HPLC column (250 × 9.4 mm, 5 μm) was also applied for purification by using isocratic elution with H_2O and ACN containing 0.1% trifluoroacetic acid (TFA). NMR spectra were recorded on a JEOL ECA-500 MHz spectrometer (JEOL, Tokyo, Japan). The spectra were processed with MestReNova 6.1.0 (Metrelab). Chemical shifts are referenced to those of the solvent signals.

Structural Elucidation. Characteristic signals of the clavatol moiety were observed in ^{1}H NMR spectra of all the isolated products as a set of signals for an aromatic proton at approximately 7.5 ppm, a singlet between 12−14 ppm, a methylene group mostly between 3−4 ppm, and two methyl groups at around 2.5 and 2.1 ppm. The clavatol-coupling products generally belong to two major groups. The majority is with the clavatol unit attached to the *ortho*- or *para*-position of a phenolic hydroxyl group at the benzene ring and other products carrying clavatol moieties attached to C2 or C3 of the indole skeleton.

In the cases of **17b** and **98b**, the linkage between the methylene group of the clavatol unit and the *para*-position of the hydroxy group

DOI: 10.1021/acs.joc.9b02971
J. Org. Chem. 2020, 85, 1298−1307

was proven by HMBC correlations (Figures S27−S30 and S76−S78). In analogy, correlations of the methylene group to different aromatic carbons in the HMBC spectra supported the linkage between the clavatol part and meta-dihydroxylated benzene ring, such as **2b** (Figures S12−S14), **6b** (Figures S15−S17), **6c** (Figures S18−S20), **14b** (Figures S21−S25), **18b** (Figures S32−S34), **35b** (Figures S38−S40), and **41b** (Figures S41−S43). **14c** obtained as the byproduct from the reaction mixture of (+)-catechin (**14a**) with hydroxyclavatol is an analogue of isopilosanols A−C. Its structure was confirmed by comparison of ^{1}H NMR spectra with those of reported data (Figure S26).[35,36] Since **44b**, **45b**, **47b**, and **50b** are formed via coupling of clavatol unit with phloroglucinol derivatives, the attachment of clavatol to the phloroglucinol moiety in **44b** and **47b** was proven by HMBC correlations as examples (Figures S44−S46 and S48−S50). The structures of **45b** and **50b** are deduced according to their molecular weight and ^{1}H NMR data (Figures S47 and S51). **29b** and **95b** showed two sets of signals in their ^{1}H NMR, one set for the clavatol subunit and one set of four coupling aromatic protons for the ortho-disubstituted benzene ring, suggesting the attachment of the clavatol unit to the α-pyrone ring in **29b** (Figures S35−S37) and to the pyridine ring in **95b** (Figures S73−S75).

61b, (±)-**65b**, and **72b** are indole derivatives with the clavatol unit linked at C2-position and differ only at the side chain of the C3-position. Therefore, their structures were determined by comparison of the NMR data (Figures S52−S54 and S60) with the known compound communol B.[17] (±)-**65c** is an example of C−N bond formation between the clavatol moiety and the indole skeleton, which was confirmed by HMBC correlations (Figures S55−S59). **76b**, **77b**, **79b**, **79c**, **79d**, **80b**, and **80c** are coupling products of clavatol with tryptophan-containing cyclic dipeptides (Figures S61−S72). The structures of **79b** and **80b** were unequivocally confirmed by ^{1}H and ^{13}C NMR data as well as HMBC correlations (Figures S63−S66 and S69−S71). Other products are analogues of **79b**, and their structures were determined according to the C2- and C3-substitution patterns of the indole ring as reported before.[37]

In the cases of **101b−101d** obtained from 2-aminobenzoic acid (**101a**), detailed inspection of the ^{1}H NMR revealed that **101b** and **101c** are products with one clavatol moiety, and **101d** is a product harboring two clavatol units. The presence of one set of characteristic signals for an ABX system in the ^{1}H NMR spectrum of **101b** revealed a para-substitution of the amino group at the benzene ring. The structure of **101b** was further confirmed by ^{13}C NMR and HMBC analyses (Figures S79−S81). In the ^{1}H NMR spectrum of **101c**, the coupling pattern consisting of four protons at the benzene ring, and a downfield shift of the methylene group from 3.95 to 4.51 ppm (Figure S82) indicated clavatol attachment to the amino group of **101a**. Similarly, one clavatol at the *para*-position of the amino group and one at the amino group can be concluded for the structure of **101d** (Figure S83). **102b** is another clavatol-coupling derivative via a C−N linkage, which was supported by the slightly downfield shifts of the methylene group at 4.49 ppm in the ^{1}H NMR spectrum and confirmed by HMBC correlations (Figure S84−S86).

Characterization Data. *8-(3-Acetyl-2,6-dihydroxy-5-methylbenzyl)-5,7-dihydroxy-2-phenyl-4H-chromen-4-one (**2b**).* The title compound was prepared using **2a** (0.106 mmol, 32.0 mg) and hydroxyclavatol (0.102 mmol, 20.0 mg) as reactants. The product was isolated in 39% yield (17.3 mg) as yellow amorphous solid. Eluent: petroleum ether/EtOAc (5:1, *v*/*v*). ^{1}H NMR (500 MHz, DMSO-d_6) δ 13.00 (s, 1H), 8.00 (dd, J = 8.4, 1.5 Hz, 2H), 7.59 (tt, J = 7.5, 1.5 Hz, 1H), 7.54−7.49 (m, 2H), 7.52 (s, 1H), 6.91 (s, 1H), 6.25 (s, 1H), 4.10 (s, 2H), 2.49 (s, 3H), 2.11 (s, 3H). ^{13}C{^{1}H} NMR (125 MHz, DMSO-d_6) δ 203.2, 182.2, 163.4, 162.2, 160.9, 160.9, 159.1, 155.0, 131.8, 131.1, 130.8, 128.9, 128.9, 126.5, 126.5, 115.8, 113.1, 112.1, 105.5, 104.8, 103.8, 98.4, 26.1, 16.6, 16.2. HRMS (ESI-TOF) m/z: [M + H]$^+$ Calcd for $C_{25}H_{21}O_7$ 433.1282; Found 433.1272.

*8-(3-Acetyl-2,6-dihydroxy-5-methylbenzyl)-2-(2,4-dihydroxyphenyl)-3,5,7-trihydroxy-4H-chromen-4-one (**6b**).* The title compound was prepared using **6a** (0.108 mmol, 32.9 mg) and hydroxyclavatol (0.066 mmol, 12.9 mg) as reactants. The product was isolated in 17% yield (5.5 mg) as yellow amorphous solid. Eluent: ACN/H_2O (55:45, *v*/*v*) supplied with 0.1% TFA. ^{1}H NMR (500 MHz, DMSO-d_6) δ 12.82 (s, 1H), 12.64 (s, 1H), 9.74 (s, 1H), 7.48 (s, 1H), 7.09 (d, J = 8.5 Hz, 1H), 6.37 (d, J = 2.3 Hz, 1H), 6.30 (dd, J = 8.5, 2.3 Hz, 1H), 6.20 (s, 1H), 3.95 (s, 2H), 2.49 (s, 3H), 2.07 (s, 3H). ^{13}C{^{1}H} NMR (125 MHz, DMSO-d_6) δ 202.8, 176.3, 160.9, 160.9, 160.4, 160.4, 158.4, 156.5, 154.5, 148.7, 135.4, 131.1, 130.5, 115.6, 113.1, 112.0, 109.5, 107.0, 104.7, 103.4, 102.9, 97.5, 26.1, 16.2, 16.2. HRMS (ESI-TOF) m/z: [M + H]$^+$ Calcd for $C_{25}H_{21}O_{10}$ 481.1129; Found 481.1151.

*2-(5-(3-Acetyl-2,6-dihydroxy-5-methylbenzyl)-2,4-dihydroxyphenyl)-3,5,7-trihydroxy-4H-chromen-4-one (**6c**).* The title compound was prepared using **6a** (0.108 mmol, 32.9 mg) and hydroxyclavatol (0.066 mmol, 12.9 mg) as reactants. The product was isolated in 21% yield (6.7 mg) as yellow amorphous solid. Eluent: ACN/H_2O (55:45, *v*/*v*) supplied with 0.1% TFA. ^{1}H NMR (500 MHz, DMSO-d_6) δ 12.95 (s, 1H), 10.66 (s, 1H), 7.58 (s, 1H), 6.79 (s, 1H), 6.50 (s, 1H), 6.18 (d, J = 2.2 Hz, 1H), 6.14 (d, J = 2.2 Hz, 1H), 3.78 (s, 2H), 2.52 (s, 3H), 2.15 (s, 3H). ^{13}C{^{1}H} NMR (125 MHz, DMSO-d_6) δ 203.2, 176.0, 163.6, 160.9, 160.7, 160.6, 157.4, 156.7, 154.4, 148.9, 136.0, 131.1, 129.9, 117.6, 116.0, 113.2, 112.3, 109.0, 103.4, 102.6, 98.0, 93.1, 26.1, 21.1, 16.1. HRMS (ESI-TOF) m/z: [M + H]$^+$ Calcd for $C_{25}H_{21}O_{10}$ 481.1129; Found 481.1147.

*1-(3-(((2R,3S)-2-(3,4-Dihydroxyphenyl)-3,5,7-trihydroxychroman-8-yl)methyl)-2,4-dihydroxy-5-methylphenyl)ethan-1-one (**14b**).* The title compound was prepared using **14a** (0.106 mmol, 30.8 mg) and hydroxyclavatol (0.066 mmol, 12.9 mg) as reactants. The product was isolated in 28% yield (8.6 mg) as brown oil. Eluent: ACN/H_2O (55:45, *v*/*v*) supplied with 0.1% TFA. ^{1}H NMR (500 MHz, acetone-d_6) δ 14.26 (s, 1H), 7.59 (s, 1H), 6.99 (d, J = 1.2 Hz, 1H), 6.86 (s, 1H), 6.86 (s, 1H), 6.11 (s, 1H), 4.81 (d, J = 7.8 Hz, 1H), 4.15 (ddd, J = 8.5, 7.8, 5.5 Hz, 1H), 3.81 (d, J = 15.6 Hz, 1H), 3.77 (d, J = 15.6 Hz, 1H), 2.97 (dd, J = 16.3, 5.5 Hz, 1H), 2.61 (dd, J = 16.3, 8.5 Hz, 1H), 2.53 (s, 3H), 2.09 (s, 3H). ^{1}H NMR (500 MHz, pyridine-d_6) δ 7.62 (d, J = 2.1 Hz, 1H), 7.47 (s, 1H), 7.30 (d, J = 8.1 Hz, 1H), 7.25 (dd, J = 8.1, 2.1 Hz, 1H), 6.67 (s, 1H), 5.31 (d, J = 7.7 Hz, 1H), 4.57 (ddd, J = 8.4, 7.7, 5.4 Hz, 1H), 4.47 (d, J = 15.1 Hz, 1H), 4.35 (d, J = 15.1 Hz, 1H), 3.63 (dd, J = 16.1, 5.4 Hz, 1H), 3.31 (dd, J = 16.1, 8.4 Hz, 1H), 2.46 (s, 3H), 2.20 (s, 3H). ^{1}H NMR (500 MHz, DMSO-d_6) δ 12.90 (s, 1H), 9.67 (s, 1H), 9.11 (s, 1H), 8.95 (s, 1H), 7.48 (s, 1H), 6.66 (d, J = 2.0 Hz, 1H), 6.60 (d, J = 8.1 Hz, 1H), 6.46 (dd, J = 8.1, 2.0 Hz, 1H), 6.03 (s, 1H), 4.54 (d, J = 7.1 Hz, 1H), 3.82−3.78 (m, 1H), 3.76 (d, J = 14.8 Hz, 1H), 3.68 (d, J = 14.8 Hz, 1H), 2.62 (dd, J = 16.2, 5.3 Hz, 1H), 2.49 (s, 3H), 2.37 (dd, J = 16.2, 7.7 Hz, 1H), 2.04 (s, 3H). ^{13}C{^{1}H} NMR (125 MHz, DMSO-d_6) δ 202.6, 160.6, 160.4, 154.0, 153.0, 152.8, 144.6, 144.5, 130.3, 130.2, 117.9, 115.6, 114.9, 114.4, 113.5, 112.2, 103.2, 99.8, 94.8, 81.2, 66.0, 30.6, 27.7, 26.2, 15.8. $[\alpha]_D^{20}$ = +25 (c 0.1, MeOH); HRMS (ESI-TOF) m/z: [M + H]$^+$ Calcd for $C_{25}H_{25}O_9$ 469.1493; Found 469.1493.

*1-(3-(((2R,3S)-2-(3,4-Dihydroxyphenyl)-3,5,7-trihydroxychroman-6-yl)methyl)-2,4-dihydroxy-5-methylphenyl)ethan-1-one (**14c**).* The title compound was prepared using **14a** (0.106 mmol, 30.8 mg) and hydroxyclavatol (0.066 mmol, 12.9 mg) as reactants. The product was isolated in 6% yield (1.8 mg) as brown oil. Eluent: ACN/H_2O (55:45, *v*/*v*) supplied with 0.1% TFA. ^{1}H NMR (500 MHz, acetone-d_6) δ 14.5 (s, 1H), 7.67 (s, 1H), 6.85 (d, J = 2.0 Hz, 1H), 6.77 (d, J = 8.1 Hz, 1H), 6.71 (dd, J = 8.1, 2.0 Hz, 1H), 6.10 (s, 1H), 4.57 (d, J = 7.5 Hz, 1H), 3.98 (ddd, J = 8.5, 7.5, 5.3 Hz, 1H), 3.86 (s, 2H), 2.87 (dd, J = 16.2, 5.3 Hz, 1H), 2.60 (s, 3H), 2.54 (dd, J = 16.2, 8.5 Hz, 1H), 2.15 (s, 3H). $[\alpha]_D^{20}$ = +23 (c 0.1, MeOH); HRMS (ESI-TOF) m/z: [M + H]$^+$ Calcd for $C_{25}H_{25}O_9$ 469.1493; Found 469.1496.

*1-(2,4-Dihydroxy-3-((4-hydroxynaphthalen-1-yl)methyl)-5-methylphenyl)ethan-1-one (**17b**).* The title compound was prepared using **17a** (0.179 mmol, 25.9 mg) and hydroxyclavatol (0.076 mmol, 14.9 mg) as reactants. The product was isolated in 21% yield (5.0 mg) as yellow amorphous solid. Eluent: ACN/H_2O (70:30, *v*/*v*). ^{1}H NMR (500 MHz, acetone-d_6) δ 13.09 (s, 1H), 8.28 (dd, J = 8.6, 1.5, Hz, 1H), 8.23 (dd, J = 8.6, 1.5, Hz, 1H), 7.71 (s, 1H), 7.56 (ddd, J = 8.6, 7.0, 1.5 Hz, 1H), 7.48 (ddd, J = 8.6, 7.0, 1.5 Hz, 1H), 6.71 (s, 2H),

DOI: 10.1021/acs.joc.9b02971
J. Org. Chem. 2020, 85, 1298−1307

4.38 (s, 2H), 2.60 (s, 3H), 2.25 (s, 3H). ^{1}H NMR (500 MHz, DMSO-d_6) δ 12.95 (s, 1H), 9.78 (s, 1H), 9.54 (s, 1H), 8.22 (d, J = 8.5 Hz, 1H), 8.16 (d, J = 8.5 Hz, 1H), 7.66 (s, 1H), 7.55 (dd, J = 8.5, 6.8 Hz, 1H), 7.46 (dd, J = 8.5, 6.8 Hz, 1H), 6.67 (d, J = 8.0 Hz, 1H), 6.63 (d, J = 8.0 Hz, 1H), 4.26 (s, 2H), 2.57 (s, 3H), 2.19 (s, 3H). ^{13}C{^{1}H} NMR (125 MHz, DMSO-d_6) δ 203.2, 161.1, 160.9, 151.4, 132.8, 131.3, 125.8, 125.6, 124.8, 124.1, 124.0, 123.6, 122.4, 116.0, 113.1, 112.3, 107.3, 26.2, 24.3, 16.2. HRMS (ESI-TOF) m/z: $[M - H]^-$ Calcd for $C_{20}H_{17}O_4$ 321.1132; Found 321.1159.

*1,1′-(((4-Hydroxynaphthalene-1,3-diyl)bis(methylene))bis(2,4-dihydroxy-5-methyl-3,1-phenylene))bis(ethan-1-one) (**17c**).* The title compound was prepared using **17a** (0.179 mmol, 25.9 mg) and hydroxyclavatol (0.076 mmol, 14.9 mg) as reactants. The product was isolated in 6% yield (1.5 mg) as yellow amorphous solid. Eluent: ACN/H_2O (70:30, v/v). ^{1}H NMR (500 MHz, acetone-d_6) δ 13.11 (s, 1H), 13.00 (s, 1H), 8.27 (d, J = 8.4 Hz, 1H), 8.16 (d, J = 8.4 Hz, 1H), 7.69 (s, 1H), 7.54 (s, 1H), 7.50 (dd, J = 8.4, 6.8 Hz, 1H), 7.47 (dd, J = 8.4, 6.8 Hz, 1H), 7.00 (s, 1H), 4.30 (s, 2H), 3.98 (s, 2H), 2.63 (s, 3H), 2.55 (s, 3H), 2.24 (s, 3H), 2.15 (s, 3H). HRMS (ESI-TOF) m/z: $[M - H]^-$ Calcd for $C_{30}H_{27}O_7$ 499.1762; Found 499.1773.

*1-(3-((2,4-Dihydroxynaphthalen-1-yl)methyl)-2,4-dihydroxy-5-methylphenyl)ethan-1-one (**18b**).* The title compound was prepared using **18a** (0.161 mmol, 25.9 mg) and hydroxyclavatol (0.089 mmol, 17.4 mg) as reactants. The product was isolated in 24% yield (7.3 mg) as white amorphous solid. Eluent: ACN/H_2O (65:35, v/v) supplied with 0.1% TFA. ^{1}H NMR (500 MHz, DMSO-d_6) δ 13.66 (s, 1H), 10.11 (s, 1H), 8.32 (d, J = 8.9 Hz, 1H), 8.00 (d, J = 8.9 Hz, 1H), 7.55 (s, 1H), 7.37 (dd, J = 8.9, 6.7 Hz, 1H), 7.19 (dd, J = 8.9, 6.7 Hz, 1H), 6.71 (s, 1H), 4.18 (s, 2H), 2.54 (s, 3H), 2.04 (s, 3H). ^{13}C{^{1}H} NMR (125 MHz, DMSO-d_6) δ 203.4, 160.9, 159.9, 153.1, 150.9, 134.1, 131.0, 126.6, 123.5, 122.2, 121.5, 120.8, 116.1, 113.3, 112.1, 107.9, 99.6, 26.2, 17.1, 15.7. HRMS (ESI-TOF) m/z: $[M - H]^-$ Calcd for $C_{20}H_{17}O_5$ 337.1081; Found 337.1097.

*3-(3-Acetyl-2,6-dihydroxy-5-methylbenzyl)-4-hydroxy-2H-chromen-2-one (**29b**).* The title compound was prepared using **29a** (0.173 mmol, 28.1 mg) and hydroxyclavatol (0.076 mmol, 14.9 mg) as reactants. The product was isolated in 43% yield (11.2 mg) as white amorphous solid. Eluent: ACN/H_2O (90:10, v/v) supplied with 0.1% TFA. ^{1}H NMR (500 MHz, $CDCl_3$) δ 14.70 (s, 1H), 10.28 (s, 1H), 10.23 (s, 1H), 7.93 (dd, J = 8.5, 1.6 Hz, 1H), 7.56 (ddd, J = 8.5, 7.0, 1.6 Hz, 1H), 7.43 (s, 1H), 7.35 (dd, J = 8.5, 1.6 Hz, 1H), 7.33 (ddd, J = 8.5, 7.0, 1.6 Hz, 1H), 3.87 (s, 2H), 2.58 (s, 3H), 2.21 (s, 3H). ^{13}C{^{1}H} NMR (125 MHz, $CDCl_3$) δ 203.6, 168.4, 163.4, 162.0, 158.9, 152.3, 132.6, 131.1, 124.8, 123.9, 119.8, 116.7, 116.3, 112.6, 112.3, 103.5, 26.0, 18.2, 16.2. HRMS (ESI-TOF) m/z: $[M + H]^+$ Calcd for $C_{19}H_{17}O_6$ 341.1020; Found 341.1013.

*4-(3-Acetyl-2,6-dihydroxy-5-methylbenzyl)-1,3-dihydroxy-9H-xanthen-9-one (**35b**).* The title compound was prepared using **35a** (0.122 mmol, 27.9 mg) and hydroxyclavatol (0.071 mmol, 13.9 mg) as reactants. The product was isolated in 31% yield (9.1 mg) as white amorphous solid. Eluent: ACN/H_2O (80:20, v/v) supplied with 0.1% TFA. ^{1}H NMR (500 MHz, DMSO-d_6) δ 13.04 (s, 1H), 12.76 (s, 1H), 8.08 (dd, J = 8.0, 1.6 Hz, 1H), 7.83 (ddd, J = 8.0, 7.2, 1.6 Hz, 1H), 7.52 (s, 1H), 7.42 (ddd, J = 8.0, 7.2, 1.6 Hz, 1H), 7.39 (dd, J = 8.0, 1.6 Hz, 1H), 6.28 (s, 1H), 4.06 (s, 2H), 2.50 (s, 3H), 2.16 (s, 3H). ^{13}C{^{1}H} NMR (125 MHz, DMSO-d_6) δ 203.1, 179.9, 161.0, 161.0, 160.3, 160.3, 155.3, 154.8, 135.5, 130.7, 125.1, 124.1, 119.4, 117.3, 115.7, 113.4, 112.0, 105.5, 102.1, 97.5, 26.1, 16.3, 16.2. HRMS (ESI-TOF) m/z: $[M + H]^+$ Calcd for $C_{23}H_{19}O_7$ 407.1125; Found 407.1116.

*2-(3-Acetyl-2,6-dihydroxy-5-methylbenzyl)-1,3,4-trihydroxyanthracene-9,10-dione (**41b**).* The title compound was prepared using **41a** (0.094 mmol, 24.1 mg) and hydroxyclavatol (0.058 mmol, 11.4 mg) as reactants. The product was isolated in 33% yield (8.3 mg) as red amorphous solid. Eluent: ACN/H_2O (75:25, v/v) supplied with 0.1% TFA. ^{1}H NMR (500 MHz, DMSO-d_6) δ 14.24 (s, 1H), 13.46 (s, 1H), 12.95 (s, 1H), 8.27 (dd, J = 7.6, 1.3 Hz, 1H), 8.26 (dd, J = 7.6, 1.3 Hz, 1H), 7.93 (td, J = 7.6, 1.3 Hz, 1H), 7.89 (td, J = 7.6, 1.3 Hz, 1H), 7.51 (s, 1H), 3.99 (s, 2H), 2.50 (s, 3H), 2.11 (s, 3H). ^{13}C{^{1}H} NMR (125 MHz, DMSO-d_6) δ 202.9, 184.8, 181.8, 161.2, 160.9, 160.9, 155.8, 134.7, 133.7, 133.6, 132.4, 130.7, 126.3, 126.2, 123.2, 115.8, 112.5, 112.2, 112.0, 109.8, 26.2, 17.5, 16.2. HRMS (ESI-TOF) m/z: $[M + H]^+$ Calcd for $C_{24}H_{19}O_8$ 435.1074; Found 435.1069.

*1-(2,4-Dihydroxy-5-methyl-3-((2,3′,4,5′,6-pentahydroxy-[1,1′-biphenyl]-3-yl)methyl)phenyl)ethan-1-one (**44b**).* The title compound was prepared using **44a** (0.128 mmol, 30.0 mg) and hydroxyclavatol (0.076 mmol, 14.9 mg) as reactants. The product was isolated in 28% yield (8.9 mg) as brown oil. Eluent: ACN/H_2O (60:40, v/v) supplied with 0.1% TFA. ^{1}H NMR (500 MHz, DMSO-d_6) δ 13.96 (s, 1H), 8.90 (s, 1H), 8.87 (s, 1H), 7.64 (s, 1H), 6.10 (s, 1H), 6.06–6.04 (m, 3H), 3.73 (s, 2H), 2.56 (s, 3H), 2.12 (s, 3H). ^{13}C{^{1}H} NMR (125 MHz, DMSO-d_6) δ 203.8, 160.6, 158.7, 157.4, 157.4, 154.2, 152.9, 152.8, 136.3, 131.1, 117.2, 113.2, 112.2, 110.1, 109.4, 109.4, 103.4, 100.5, 94.9, 48.6, 26.1, 15.7. HRMS (ESI-TOF) m/z: $[M + H]^+$ Calcd for $C_{22}H_{21}O_8$ 413.1231; Found 413.1242.

*3-(3-Acetyl-2,6-dihydroxy-5-methylbenzyl)-2,4,6-trihydroxybenzoic acid (**45b**).* The title compound was prepared using **45a** (0.024 mmol, 4.2 mg) and hydroxyclavatol (0.016 mmol, 3.1 mg) as reactants. The product was isolated in 44% yield (2.5 mg) as white amorphous solid. Eluent: ACN/H_2O (60:40, v/v) supplied with 0.1% TFA. ^{1}H NMR (500 MHz, acetone-d_6) δ 14.42 (s, 1H), 7.64 (s, 1H), 6.04 (s, 1H), 3.82 (s, 2H), 2.59 (s, 3H), 2.13 (s, 3H). HRMS (ESI-TOF) m/z: $[M + H]^+$ Calcd for $C_{17}H_{17}O_8$ 349.0918; Found 349.0925.

*1-(3-(3-Acetyl-2,6-dihydroxy-5-methylbenzyl)-2,4,6-trihydroxyphenyl)-3-methylbutan-1-one (**47b**).* The title compound was prepared using **29a** (0.142 mmol, 30.0 mg) and hydroxyclavatol (0.076 mmol, 14.9 mg) as reactants. The product was isolated in 31% yield (9.1 mg) as yellow amorphous solid. Eluent: ACN/H_2O (90:10, v/v) supplied with 0.1% TFA. ^{1}H NMR (500 MHz, DMSO-d_6) δ 13.09 (s, 1H), 10.69 (s, 1H), 7.51 (s, 1H), 5.96 (s, 1H), 3.74 (s, 2H), 2.87 (d, J = 6.7 Hz, 1H), 2.51 (s, 3H), 2.14 (m, 1H), 2.08 (s, 3H), 0.90 (d, J = 6.7 Hz, 3H), 0.90 (d, J = 6.7 Hz, 3H). ^{13}C{^{1}H} NMR (125 MHz, DMSO-d_6) δ 205.1, 203.0, 163.4, 162.3, 160.8, 160.7, 160.3, 130.4, 115.7, 113.3, 112.0, 104.4, 103.7, 94.4, 51.8, 48.6, 26.1, 24.8, 22.6, 22.6, 15.9. HRMS (ESI-TOF) m/z: $[M + H]^+$ Calcd for $C_{21}H_{25}O_7$ 389.1595; Found 389.1597.

*1-(3-(3-Acetyl-2,6-dihydroxy-5-methylbenzyl)-2,4,6-trihydroxyphenyl)-3-(4-hydroxyphenyl)propan-1-one (**50b**).* The title compound was prepared using **50a** (0.028 mmol, 7.9 mg) and hydroxyclavatol (0.024 mmol, 4.7 mg) as reactants. The product was isolated in 19% yield (2.0 mg) as white amorphous solid. Eluent: ACN/H_2O (80:20, v/v) supplied with 0.1% TFA. ^{1}H NMR (500 MHz, acetone-d_6) δ 14.53 (s, 1H), 7.66 (s, 1H), 7.10 (d, J = 8.6 Hz, 2H), 6.75 (d, J = 8.6 Hz, 2H), 6.08 (s, 1H), 3.85 (s, 2H), 3.39 (t, J = 7.5 Hz, 2H), 2.90 (t, J = 7.5 Hz, 2H), 2.59 (s, 3H), 2.14 (s, 3H). HRMS (ESI-TOF) m/z: $[M + H]^+$ Calcd for $C_{25}H_{25}O_8$ 453.1544; Found 453.1561.

*(S)-3-(2-(3-Acetyl-2,6-dihydroxy-5-methylbenzyl)-1H-indol-3-yl)-2-aminopropanoic acid (**61b**).* The title compound was prepared using **61a** (0.160 mmol, 44.0 mg) and hydroxyclavatol (0.102 mmol, 20.0 mg) as reactants. The product was isolated in 27% yield (10.4 mg) as yellow amorphous solid. Eluent: CH_2Cl_2. ^{1}H NMR (500 MHz, DMSO-d_6) δ 10.19 (s, 1H), 7.56 (s, 1H), 7.51 (d, J = 8.0 Hz, 1H), 7.26 (d, J = 8.0 Hz, 1H), 6.94 (dd, J = 8.0, 6.8 Hz, 1H), 6.90 (dd, J = 8.0, 6.8 Hz, 1H), 4.14 (d, J = 15.2 Hz, 1H), 4.07 (d, J = 15.2 Hz, 1H), 3.41 (dd, J = 6.8, 5.8, 1H), 3.18 (dd, J = 14.7, 5.8 Hz, 1H), 3.03 (dd, J = 14.7, 6.8 Hz, 1H), 2.52 (s, 3H), 2.11 (s, 3H). ^{13}C{^{1}H} NMR (125 MHz, DMSO-d_6) δ 202.1, 171.2, 161.5, 136.1, 134.9, 130.8, 128.4, 119.8, 118.2, 118.0, 117.2, 111.9, 111.4, 110.9, 105.1, 55.0, 26.1, 25.9, 20.0, 16.5. $[\alpha]_D^{20} = -6$ (c 0.2, acetone); HRMS (ESI-TOF) m/z: $[M + H]^+$ Calcd for $C_{21}H_{23}N_2O_5$ 383.1601; Found 383.1609.

*2-Acetamido-3-(2-(3-acetyl-2,6-dihydroxy-5-methylbenzyl)-1H-indol-3-yl)propanoic acid ((±)-**65b**).* The title compound was prepared using (±)-**65a** (0.178 mmol, 44.0 mg) and hydroxyclavatol (0.069 mmol, 13.5 mg) as reactants. The product was isolated in 29% yield (8.6 mg) as brown oil. Eluent: ACN/H_2O (55:45, v/v) supplied with 0.1% TFA. ^{1}H NMR (500 MHz, acetone-d_6) δ 13.26 (s, 1H), 7.66 (s, 1H), 7.53 (d, J = 7.4 Hz, 1H), 7.23 (d, J = 7.4 Hz, 1H), 6.96 (t, J = 7.4 Hz, 1H), 6.92 (t, J = 7.4 Hz, 1H), 4.81 (ddd, J = 8.2, 7.7,

DOI: 10.1021/acs.joc.9b02971
J. Org. Chem. 2020, 85, 1298–1307

6.0 Hz, 1H), 4.21 (d, *J* = 15.0 Hz, 1H), 4.18 (d, *J* = 15.0 Hz, 1H), 3.45 (dd, *J* = 14.7, 6.0 Hz, 1H), 3.33 (dd, *J* = 14.7, 7.7 Hz, 1H), 2.57 (s, 3H), 2.26 (s, 3H), 1.85 (s, 3H). HRMS (ESI-TOF) *m/z*: $[M + H]^+$ Calcd for $C_{23}H_{25}N_2O_6$ 425.1707; Found 425.1713.

*N^a-Acetyl-1-(3-acetyl-2,6-dihydroxy-5-methylbenzyl)tryptophan ((±)-**65c**).* The title compound was prepared using (±)-**65a** (0.178 mmol, 44.0 mg) and hydroxyclavatol (0.069 mmol, 13.5 mg) as reactants. The product was isolated in 14% yield (4.3 mg) as brown oil. Eluent: ACN/H_2O (55:45, *v/v*) supplied with 0.1% TFA. ^1H NMR (500 MHz, acetone-d_6) δ 13.31 (s, 1H), 7.71 (s, 1H), 7.70 (d, *J* = 8.2 Hz, 1H), 7.51 (d, *J* = 8.2 Hz, 1H), 7.29 (s, 1H), 7.09 (dd, *J* = 8.2, 7.0 Hz, 1H), 6.97 (dd, *J* = 8.2, 7.0 Hz, 1H), 5.33 (s, 2H), 4.68 (ddd, *J* = 8.2, 7.5, 5.6 Hz, 1H), 3.27 (dd, *J* = 14.7, 5.6 Hz, 1H), 3.10 (dd, *J* = 14.7, 7.5 Hz, 3H), 2.56 (s, 3H), 2.27 (s, 3H), 1.83 (s, 3H). ^1H NMR (500 MHz, DMSO-d_6) δ 13.19 (s, 1H), 8.06 (d, *J* = 8.4 Hz, 1H), 7.69 (s, 1H), 7.65 (d, *J* = 8.2 Hz, 1H), 7.48 (d, *J* = 8.2 Hz, 1H), 7.15 (s, 1H), 7.10 (dd, *J* = 8.2, 7.0 Hz, 1H), 6.98 (dd, *J* = 8.2, 7.0 Hz, 1H), 5.25 (s, 2H), 4.38 (td, *J* = 9.2, 5.1 Hz, 1H), 3.11 (dd, *J* = 15.0, 5.1 Hz, 1H), 2.90 (dd, *J* = 15.0, 9.2 Hz, 1H), 2.54 (s, 3H), 2.17 (s, 3H), 1.75 (s, 3H). $^{13}C\{^1H\}$ NMR (125 MHz, DMSO-d_6) δ 203.4, 173.4, 169.0, 161.0, 161.0, 136.0, 133.1, 127.3, 127.2, 120.8, 118.3, 118.1, 116.1, 112.4, 111.1, 110.2, 109.1, 52.8, 37.5, 26.9, 26.2, 22.2, 16.2. HRMS (ESI-TOF) *m/z*: $[M + H]^+$ Calcd for $C_{23}H_{25}N_2O_6$ 425.1707; Found 425.1708.

*4-(2-(3-Acetyl-2,6-dihydroxy-5-methylbenzyl)-1H-indol-3-yl)-butanoic acid (**72b**).* The title compound was prepared using **72a** (0.008 mmol, 1.6 mg) and hydroxyclavatol (0.008 mmol, 1.6 mg) as reactants. The product was isolated in 46% yield (1.4 mg) as brown oil. Eluent: ACN/H_2O (65:35, *v/v*) supplied with 0.1% TFA. ^1H NMR (500 MHz, $CDCl_3$) δ 13.30 (s, 1H), 8.57 (s, 1H), 7.49 (d, *J* = 8.0 Hz, 1H), 7.40 (s, 1H), 7.24 (d, *J* = 8.0 Hz, 1H), 7.08 (dd, *J* = 8.0, 7.0 Hz, 1H), 7.03 (dd, *J* = 8.0, 7.0 Hz, 1H), 4.14 (s, 2H), 2.95 (t, *J* = 7.0 Hz, 2H), 2.57 (s, 3H), 2.50 (t, *J* = 7.0 Hz, 2H), 2.18 (s, 3H), 2.07−2.01 (m, 2H). HRMS (ESI-TOF) *m/z*: $[M + H]^+$ Calcd for $C_{22}H_{24}NO_5$ 382.1649; Found 382.1662.

*(3S,6S)-3-((2-(3-Acetyl-2,6-dihydroxy-5-methylbenzyl)-1H-indol-3-yl)methyl)-6-isobutylpiperazine-2,5-dione (**76b**).* The title compound was prepared using **76a** (0.016 mmol, 4.8 mg) and hydroxyclavatol (0.016 mmol, 3.2 mg) as reactants. The product was isolated in 13% yield (1.0 mg) as white amorphous solid. Eluent: ACN/H_2O (60:40, *v/v*). ^1H NMR (500 MHz, $CDCl_3$) δ 13.40 (s, 1H), 8.77 (s, 1H), 7.51 (d, *J* = 8.0 Hz, 1H), 7.46 (s, 1H), 7.25 (d, *J* = 8.0 Hz, 1H), 7.12 (dd, *J* = 8.0, 7.1 Hz, 1H), 7.07 (dd, *J* = 8.0, 7.1 Hz, 1H), 6.39 (s, 1H), 5.99 (s, 1H), 4.40 (d, *J* = 8.9 Hz, 1H), 4.16 (d, *J* = 15.0 Hz, 1H), 4.13 (d, *J* = 15.0 Hz, 1H), 3.94 (d, *J* = 10.0 Hz, 1H), 3.65 (dd, *J* = 14.8, 3.2 Hz, 1H), 3.28 (dd, *J* = 14.8, 8.9 Hz, 1H), 2.60 (s, 3H), 2.23 (s, 3H), 1.68−1.60 (m, 1H), 1.61−1.56 (m, 1H), 1.17 (ddd, 13.7, 10.0, 4.5 Hz, 1H), 0.86 (d, *J* = 6.2 Hz, 1H), 0.85 (d, *J* = 6.2 Hz, 1H). $[\alpha]_D^{20}$ = −41 (*c* 0.1, $CHCl_3$); HRMS (ESI-TOF) *m/z*: $[M + H]^+$ Calcd for $C_{27}H_{32}N_3O_5$ 478.2336; Found 478.2339.

*(3S,6S)-3-((2-(3-Acetyl-2,6-dihydroxy-5-methylbenzyl)-1H-indol-3-yl)methyl)-6-benzylpiperazine-2,5-dione (**77b**).* The title compound was prepared using **77a** (0.032 mmol, 10.7 mg) and hydroxyclavatol (0.016 mmol, 3.1 mg) as reactants. The product was isolated in 24% yield (2.0 mg) as white amorphous solid. Eluent: ACN/H_2O (55:45, *v/v*). ^1H NMR (500 MHz, DMSO-d_6) δ 13.04 (s, 1H), 9.96 (s, 1H), 9.63 (s, 1H), 7.94 (d, *J* = 3.0 Hz, 1H), 7.64 (d, *J* = 3.3 Hz, 1H), 7.62 (s, 1H), 7.43 (d, *J* = 7.6 Hz, 1H), 7.22 (d, *J* = 7.6 Hz, 1H), 7.16−7.10 (m, 3H), 6.95 (dd, *J* = 7.6, 6.5 Hz, 1H), 6.92 (dd, *J* = 7.6, 6.5 Hz, 1H), 6.62 (dd, *J* = 7.5, 2.3 Hz, 2H), 4.05 (d, *J* = 15.7 Hz, 1H), 4.07−4.04 (m, 1H), 4.01 (d, *J* = 15.7 Hz, 1H), 3.80−3.76 (m, 1H), 3.05 (dd, *J* = 14.7, 4.7 Hz, 1H), 2.98 (dd, *J* = 14.7, 5.4 Hz, 1H), 2.55 (s, 3H), 2.47 (m, 1H), 2.18 (s, 3H), 1.61 (dd, *J* = 13.7, 7.9 Hz, 1H). $[\alpha]_D^{20}$ = −49 (*c* 0.2, MeOH); HRMS (ESI-TOF) *m/z*: $[M + H]^+$ Calcd for $C_{30}H_{30}N_3O_5$ 512.2180; Found 512.2200.

*3-((1H-Indol-3-yl)methyl)-6-((2-(3-acetyl-2,6-dihydroxy-5-methylbenzyl)-1H-indol-3-yl)methyl)piperazine-2,5-dione (**79b**).* The title compound was prepared using **79a** (0.040 mmol, 14.9 mg) and hydroxyclavatol (0.033 mmol, 6.5 mg) as reactants. The product was isolated in 30% yield (5.4 mg) as white amorphous solid. Eluent: ACN/H_2O (65:35, *v/v*). ^1H NMR (500 MHz, $CDCl_3$) δ 13.40 (s, 1H), 8.74 (s, 1H), 8.01 (s, 1H), 7.48 (s, 1H), 7.47 (d, *J* = 8.0, 1H), 7.46 (d, *J* = 8.2, 1H), 7.34 (d, *J* = 8.2 Hz, 1H), 7.24 (d, *J* = 8.0 Hz, 1H), 7.17 (dd, *J* = 8.2, 7.2 Hz, 1H), 7.11 (dd, *J* = 8.2, 7.2 Hz, 1H), 7.08 (dd, *J* = 8.0, 7.1 Hz, 1H), 7.05 (dd, *J* = 8.0, 7.1 Hz, 1H), 6.58 (s, 1H), 6.48 (s, 1H), 5.84 (s, 1H), 4.36 (d, *J* = 7.7 Hz, 1H), 4.20 (d, *J* = 10.1 Hz, 1H), 4.08 (d, *J* = 15.1 Hz, 1H), 4.04 (d, *J* = 15.1 Hz, 1H), 3.45 (dd, *J* = 14.7, 3.2 Hz, 1H), 3.30 (dd, *J* = 14.5, 3.2 Hz, 1H), 3.08 (dd, *J* = 14.5, 7.7 Hz, 1H), 2.61 (s, 3H), 2.27−2.24 (m, 1H), 2.23 (s, 3H). ^1H NMR (500 MHz, DMSO-d_6) δ 13.04 (s, 1H), 10.75 (d, *J* = 1.9 Hz, 1H), 9.92 (s, 1H), 9.61 (s, 1H), 7.85 (d, *J* = 2.5 Hz, 1H), 7.62 (s, 1H), 7.60 (d, *J* = 2.7 Hz, 1H), 7.30 (d, *J* = 8.0 Hz, 1H), 7.27 (d, *J* = 8.2 Hz, 1H), 7.25 (d, *J* = 8.2 Hz, 1H), 7.21 (d, *J* = 8.0 Hz, 1H), 6.98 (dd, *J* = 8.0, 7.0 Hz, 1H), 6.93 (dd, *J* = 8.0, 7.0 Hz, 1H), 6.90 (dd, *J* = 8.0, 7.0 Hz, 1H), 6.88 (dd, *J* = 8.0, 7.0 Hz, 1H), 6.37 (d, *J* = 2.1 Hz, 1H), 4.02 (dd, *J* = 8.1, 3.8 Hz, 1H), 3.97 (d, *J* = 15.4 Hz, 1H), 3.91 (d, *J* = 15.4 Hz, 1H), 3.81−3.76 (m, 1H), 2.99 (dd, *J* = 14.4, 4.6 Hz, 1H), 2.88 (dd, *J* = 14.4, 5.4 Hz, 1H), 2.71 (dd, *J* = 14.4, 3.8 Hz, 1H), 2.55 (s, 3H), 2.17 (s, 3H), 1.85 (dd, *J* = 14.4, 8.1 Hz, 1H). $^{13}C\{^1H\}$ NMR (125 MHz, DMSO-d_6) δ 203.1, 167.0, 166.5, 160.7, 160.6, 136.1, 136.1, 135.2, 131.4, 128.4, 127.0, 124.2, 120.7, 119.8, 119.4, 118.2, 118.1, 118.0, 115.9, 112.5, 112.5, 111.1, 110.8, 108.8, 104.9, 55.9, 55.3, 30.6, 30.6, 26.2, 19.3, 16.2. $[\alpha]_D^{20}$ = −38 (*c* 0.1, $CHCl_3$); HRMS (ESI-TOF) *m/z*: $[M + H]^+$ Calcd for $C_{32}H_{31}N_4O_5$ 551.2289; Found 551.2313.

*(3S,5aS,10bS,11aS)-3-((1H-Indol-3-yl)methyl)-10b-(3-acetyl-2,6-dihydroxy-5-methylbenzyl)-2,3,6,10b,11,11a-hexahydro-4H-pyrazino[1′,2′:1,5]pyrrolo[2,3-b]indole-1,4(5aH)-dione (**79c**).* The title compound was prepared using **79a** (0.040 mmol, 14.9 mg) and hydroxyclavatol (0.033 mmol, 6.5 mg) as reactants. The product was isolated in 3% yield (0.6 mg) as white amorphous solid. Eluent: ACN/H_2O (65:35, *v/v*). ^1H NMR (500 MHz, $CDCl_3$) δ 13.01 (s, 1H), 8.11 (s, 1H), 7.51 (d, *J* = 8.0 Hz, 1H), 7.44 (s, 1H), 7.38 (d, *J* = 8.0 Hz, 1H), 7.21 (dd, *J* = 8.0, 7.0 Hz, 1H), 7.15 (dd, *J* = 8.0, 7.0 Hz, 1H), 7.11 (d, *J* = 8.0 Hz, 1H), 7.10 (dd, *J* = 8.0, 7.0 Hz, 1H), 7.06 (s, 1H), 6.82 (dd, *J* = 8.0, 7.0 Hz, 1H), 6.72 (d, *J* = 8.0 Hz, 1H), 5.60 (s, 1H), 5.47 (s, 1H), 4.29 (d, *J* = 11.0 Hz, 1H), 3.92 (dd, *J* = 11.3, 5.8 Hz, 1H), 3.69 (dd, *J* = 15.0, 3.5 Hz, 1H), 3.21 (d, *J* = 14.0 Hz, 1H), 2.97 (d, *J* = 14.0 Hz, 1H), 2.90 (dd, *J* = 15.0, 11.0 Hz, 1H), 2.74 (dd, *J* = 13.2, 5.8 Hz, 1H), 2.57 (s, 3H), 2.37 (dd, *J* = 13.2, 11.3 Hz, 1H), 2.18 (s, 3H). $[\alpha]_D^{20}$ = −58 (*c* 0.06, $CHCl_3$); HRMS (ESI-TOF) *m/z*: $[M + H]^+$ Calcd for $C_{32}H_{31}N_4O_5$ 551.2289; Found 551.2314.

*(3S,5aS,10bS,11aS)-10b-(3-Acetyl-2,6-dihydroxy-5-methylbenzyl)-3-((2-(3-acetyl-2,6-dihydroxy-5-methylbenzyl)-1H-indol-3-yl)-methyl)-2,3,6,10b,11,11a-hexahydro-4H-pyrazino[1′,2′:1,5]pyrrolo-[2,3-b]indole-1,4(5aH)-dione (**79d**).* The title compound was prepared using **79a** (0.040 mmol, 14.9 mg) and hydroxyclavatol (0.033 mmol, 6.5 mg) as reactants. The product was isolated in 4% yield (1.0 mg) as white amorphous solid. Eluent: ACN/H_2O (65:35, *v/v*). ^1H NMR (500 MHz, $CDCl_3$) δ 12.98 (s, 1H), 12.92 (s, 1H), 8.18 (s, 1H), 7.59 (d, *J* = 8.0 Hz, 1H), 7.42 (s, 1H), 7.40 (d, *J* = 8.0 Hz, 1H), 7.24−7.21 (m, 1H), 7.19 (t, *J* = 7.5, 1H), 7.12 (dd, *J* = 8.0, 7.0 Hz, 1H) 7.12 (s, 1H), 6.89 (d, *J* = 7.5 Hz, 1H), 6.79 (d, *J* = 7.5 Hz, 1H), 6.71 (t, *J* = 7.5 Hz, 1H), 5.69 (s, 1H), 5.52 (s, 1H), 4.76 (d, *J* = 15.2 Hz, 1H), 4.54 (d, *J* = 15.2 Hz, 1H), 4.46 (dd, *J* = 10.0, 3.4 Hz, 1H), 3.99 (dd, *J* = 11.9, 5.5 Hz, 1H), 3.70 (dd, *J* = 15.0, 3.4 Hz, 1H), 3.12 (dd, *J* = 15.0, 10.0 Hz, 1H), 2.78 (s, 2H), 2.69 (dd, *J* = 13.0, 5.5 Hz, 1H), 2.55 (s, 3H), 2.51 (s, 3H), 2.28 (s, 3H), 2.04 (dd, *J* = 13.0, 11.9 Hz, 1H), 1.99 (s, 3H). $[\alpha]_D^{20}$ = −63 (*c* 0.1, $CHCl_3$); HRMS (ESI-TOF) *m/z*: $[M + H]^+$ Calcd for $C_{42}H_{41}N_4O_8$ 729.2919; Found 729.2932.

*(R)-3-((2-(3-Acetyl-2,6-dihydroxy-5-methylbenzyl)-1H-indol-3-yl)methyl)-3,4-dihydro-1H-benzo[e][1,4]diazepine-2,5-dione (**80b**).* The title compound was prepared using **80a** (0.080 mmol, 24.5 mg) and hydroxyclavatol (0.051 mmol, 10.0 mg) as reactants. The product was isolated in 21% yield (5.3 mg) as white amorphous solid. Eluent: ACN/H_2O (55:45, *v/v*). ^1H NMR (500 MHz, acetone-d_6) δ 13.30 (s, 1H), 9.71 (s, 1H), 9.52 (s, 1H), 7.71 (d, *J* = 8.0 Hz, 1H), 7.62 (s, 1H), 7.52 (dd, *J* = 8.0, 7.2 Hz, 1H), 7.45 (d, *J* = 8.0 Hz, 1H), 7.23 (d, *J* = 8.0 Hz, 1H), 7.21 (d, *J* = 8.0 Hz, 1H), 7.20 (dd, *J* = 8.0, 7.2 Hz,

DOI: 10.1021/acs.joc.9b02971
J. Org. Chem. 2020, 85, 1298−1307

1H), 6.93 (dd, J = 8.0, 7.0 Hz, 1H), 6.84 (dd, J = 8.0, 7.0 Hz, 1H), 4.28 (d, J = 15.0 Hz, 1H), 4.25 (dd, J = 9.0, 5.9 Hz, 1H), 4.22 (d, J = 15.0 Hz, 1H), 3.51 (dd, J = 15.0, 5.9 Hz, 1H), 3.34 (dd, J = 15.0, 9.0 Hz, 1H), 2.56 (s, 3H), 2.24 (s, 3H). $^{13}C\{^1H\}$ NMR (125 MHz, acetone-d_6) δ 203.9, 172.7, 168.5, 161.4, 161.4, 137.5, 136.6, 136.5, 133.3, 132.4, 131.8, 128.9, 127.1, 125.1, 121.9, 121.6, 119.5, 118.5, 117.0, 114.2, 113.8, 111.7, 106.3, 53.2, 26.4, 24.4, 20.2, 16.3. $[\alpha]_D^{20}$ = −52 (c 0.1, acetone); HRMS (ESI-TOF) m/z: $[M + H]^+$ Calcd for $C_{28}H_{26}N_3O_5$ 484.1867; Found 484.1870.

*(5aS,13aR,14aS)-14a-(3-Acetyl-2,6-dihydroxy-5-methylbenzyl)-5a,13a,14,14a-tetrahydrobenzo[5′,6′][1,4]diazepino[1′,2′:1,5]-pyrrolo[2,3-b]indole-7,13(5H,12H)-dione (**80c**).* The title compound was prepared using **80a** (0.080 mmol, 24.5 mg) and hydroxyclavatol (0.051 mmol, 10.0 mg) as reactants. The product was isolated in 4% yield (1.0 mg) as white amorphous solid. Eluent: ACN/H_2O (55:45, v/v). ^1H NMR (500 MHz, acetone-d_6) δ 13.14 (s, 1H), 9.54 (s, 1H), 8.63 (s, 1H), 7.76 (d, J = 8.0 Hz, 1H), 7.64 (d, J = 8.0 Hz, 1H), 7.48 (dd, J = 8.0, 7.3 Hz, 1H), 7.20 (dd, J = 8.0, 7.3 Hz, 1H), 7.16 (dd, J = 8.2 Hz, 1H), 7.12 (d, J = 8.0 Hz, 1H), 6.97 (dd, J = 8.2, 7.7 Hz, 1H), 6.67 (d, J = 8.2 Hz, 1H), 6.61 (dd, J = 8.2, 7.7 Hz, 1H), 6.31 (s, 1H), 5.65 (s, 1H), 4.01 (dd, J = 8.2, 7.0 Hz, 1H), 3.22 (d, J = 14.0 Hz, 1H), 3.17 (d, J = 14.0 Hz, 1H), 3.17 (dd, J = 14.0, 7.0 Hz, 1H), 2.56 (s, 3H), 2.47 (dd, J = 14.0, 8.2 Hz, 1H), 2.25 (s, 1H). $[\alpha]_D^{20}$ = −47 (c 0.1, acetone); HRMS (ESI-TOF) m/z: $[M + H]^+$ Calcd for $C_{28}H_{26}N_3O_5$ 484.1867; Found 484.1874.

*1-(3-((2-Amino-4-hydroxyquinolin-3-yl)methyl)-2,4-dihydroxy-5-methylphenyl)ethan-1-one (**95b**).* The title compound was prepared using **95a** (0.128 mmol, 20.6 mg) and hydroxyclavatol (0.058 mmol, 11.3 mg) as reactants. The product was isolated in 46% yield (9.0 mg) as brown amorphous solid. Eluent: ACN/H_2O (75:25, v/v) supplied with 0.1% TFA. ^1H NMR (500 MHz, DMSO-d_6) δ 13.93 (s, 1H), 11.52 (s, 1H), 8.05 (d, J = 8.2 Hz, 1H), 7.56 (s, 1H), 7.55 (dd, J = 8.2, 7.1, 1H), 7.36 (d, J = 8.2 Hz, 1H), 7.25 (dd, J = 8.2, 7.1 Hz, 1H), 6.67 (s, 2H), 3.70 (s, 2H), 2.53 (s, 3H), 2.08 (s, 3H). $^{13}C\{^1H\}$ NMR (125 MHz, DMSO-d_6) δ 202.9, 174.0, 164.1, 159.4, 153.0, 136.9, 130.9, 130.8, 124.4, 122.3, 120.6, 117.7, 116.3, 113.1, 111.0, 101.0, 25.8, 17.6, 15.9. HRMS (ESI-TOF) m/z: $[M + H]^+$ Calcd for $C_{19}H_{19}N_2O_4$ 339.1339; Found 339.1357.

*1-(2,4-Dihydroxy-3-((5-hydroxyquinolin-8-yl)methyl)-5-methyl phenyl)ethan-1-one (**98b**).* The title compound was prepared using **98a** (0.157 mmol, 22.9 mg) and hydroxyclavatol (0.059 mmol, 11.5 mg) as reactants. The product was isolated in 38% yield (7.1 mg) as yellow amorphous solid. Eluent: ACN/H_2O (80:20, v/v) supplied with 0.1% TFA. ^1H NMR (500 MHz, DMSO-d_6) δ 13.19 (s, 1H), 10.59 (s, 1H), 9.01 (dd, J = 4.5, 1.7 Hz, 1H), 8.69 (dd, J = 8.4, 1.7 Hz, 1H), 7.75 (d, J = 8.0 Hz, 1H), 7.63 (dd, J = 8.4, 4.5 Hz, 1H), 7.55 (s, 1H), 6.96 (d, J = 8.0 Hz, 1H), 4.23 (s, 2H), 2.51 (s, 3H), 2.12 (s, 3H). $^{13}C\{^1H\}$ NMR (125 MHz, DMSO-d_6) δ 203.1, 161.2, 160.9, 152.0, 148.6, 144.4, 133.7, 132.1, 130.7, 126.9, 120.2, 120.1, 117.3, 114.1, 112.0, 109.0, 26.1, 24.5, 15.9. HRMS (ESI-TOF) m/z: $[M + H]^+$ Calcd for $C_{19}H_{18}NO_4$ 324.1230; Found 324.1235.

*5-(3-Acetyl-2,6-dihydroxy-5-methylbenzyl)-2-aminobenzoic acid (**101b**).* The title compound was prepared using **101a** (0.167 mmol, 23.0 mg) and hydroxyclavatol (0.066 mmol, 12.9 mg) as reactants. The product was isolated in 23% yield (4.7 mg) as brown amorphous solid. Eluent: ACN/H_2O (65:35, v/v) supplied with 0.1% TFA. ^1H NMR (500 MHz, acetone-d_6) δ 13.08 (s, 1H), 7.72 (d, J = 2.1 Hz, 1H), 7.62 (s, 1H), 7.37 (dd, J = 8.4, 2.1 Hz, 1H), 6.68 (d, J = 8.4 Hz, 1H), 3.95 (s, 2H), 2.56 (s, 3H), 2.24 (s, 3H). $^{13}C\{^1H\}$ NMR (125 MHz, acetone-d_6) δ 204.0, 163.7, 162.0, 161.6, 146.0, 136.8, 132.2, 132.1, 129.8, 116.4, 115.5, 114.0, 114.0, 112.6, 27.9, 26.4, 16.3. HRMS (ESI-TOF) m/z: $[M + H]^+$ Calcd for $C_{17}H_{18}NO_5$ 316.1179; Found 316.1169.

*2-((3-Acetyl-2,6-dihydroxy-5-methylbenzyl)amino)benzoic acid (**101c**).* The title compound was prepared using **101a** (0.167 mmol, 23.0 mg) and hydroxyclavatol (0.066 mmol, 12.9 mg) as reactants. The product was isolated in 6% yield (1.2 mg) as brown amorphous solid. Eluent: ACN/H_2O (65:35, v/v) supplied with 0.1% TFA. ^1H NMR (500 MHz, acetone-d_6) δ 13.23 (s, 1H), 7.89 (d, J = 8.0 Hz, 1H), 7.68 (s, 1H), 7.37 (dd, J = 8.0, 7.1 Hz, 1H), 7.05 (d, J = 8.0 Hz, 1H), 6.59 (dd, J = 8.0, 7.1 Hz, 1H), 4.51 (s, 2H), 2.56 (s, 3H), 2.21 (s, 3H). HRMS (ESI-TOF) m/z: $[M + H]^+$ Calcd for $C_{17}H_{18}NO_5$ 316.1179; Found 316.1181.

*5-(3-Acetyl-2,6-dihydroxy-5-methylbenzyl)-2-((3-acetyl-2,6-dihydroxy-5-methylbenzyl)amino)benzoic acid (**101d**).* The title compound was prepared using **101a** (0.167 mmol, 23.0 mg) and hydroxyclavatol (0.066 mmol, 12.9 mg) as reactants. The product was isolated in 3% yield (0.9 mg) as yellow amorphous solid. Eluent: ACN/H_2O (65:35, v/v) supplied with 0.1% TFA. ^1H NMR (500 MHz, acetone-d_6) δ 13.21 (s, 1H), 13.06 (s, 1H), 7.89 (d, J = 2.1 Hz, 1H), 7.64 (s, 1H), 7.59 (s, 1H), 7.32 (dd, J = 8.6, 2.1 Hz, 1H), 6.92 (d, J = 8.6 Hz, 1H), 4.49 (s, 2H), 3.91 (s, 2H), 2.55 (s, 3H), 2.54 (s, 3H), 2.22 (s, 3H), 2.17 (s, 3H). HRMS (ESI-TOF) m/z: $[M + H]^+$ Calcd for $C_{27}H_{28}NO_8$ 494.1809; Found 494.1823.

*1-(3-(((1,3-Dihydroxy-2-(hydroxymethyl)propan-2-yl)amino)-methyl)-2,4-dihydroxy-5-methylphenyl)ethan-1-one (**102b**).* The title compound was prepared by using **102a** (1.0 mmol, 122.0 mg, prepared as Tris−HCl buffer, pH 7.5) and hydroxyclavatol (0.066 mmol, 12.9 mg) as reactants. The product was isolated in 16% yield (3.2 mg) as brown oil. Eluent: ACN/H_2O (70:30, v/v) supplied with 0.1% TFA. ^1H NMR (500 MHz, CD_3OD) δ 7.72 (s, 1H), 4.49 (s, 2H), 3.82 (s, 6H), 2.56 (s, 3H), 2.22 (s, 3H). $^{13}C\{^1H\}$ NMR (125 MHz, CD_3OD) δ 204.9, 162.5, 162.4, 135.5, 117.3, 114.4, 107.3, 67.5, 59.7, 59.7, 59.7, 36.5, 26.3, 16.1. HRMS (ESI-TOF) m/z: $[M + H]^+$ Calcd for $C_{14}H_{22}NO_6$ 300.1442; Found 300.1445.

α-Glucosidase Inhibition Assay. The α-glucosidase inhibition activity was evaluated by modified procedures reported previously.[38,39] The assays contained 100 mM phosphate buffer (pH 6.8), α-glucosidase (1.3 U/mL) (Sigma-Aldrich, St. Louis, USA), and 10 μL of a 2 mM DMSO solution of compounds to be tested. After preincubation at 37 °C for 15 min, the assays were initiated by addition of 40 μL of 2.5 mM p-nitrophenyl-α-D-glucopyranoside solution (Sigma-Aldrich, St. Louis, USA) to a final volume of 150 μL. After incubation at 37 °C for a further 15 min, the absorbance at 405 nm was recorded on a microplate reader (BMG Labtech, Offenburg, Germany). DMSO was used as a negative control, and acarbose (TCI Europe, Zwijndrecht, Belgium) was used as positive control. All assays were performed in triplicate. The IC_{50} value was determined by regression analysis.[40,41]

■ ASSOCIATED CONTENT

Supporting Information

The Supporting Information is available free of charge at https://pubs.acs.org/doi/10.1021/acs.joc.9b02971.

Chemical synthesis of hydroxyclavatol, structural overview of all reactants, LC−MS chromatograms of selected reactions, NMR spectra of coupling products (PDF)

■ AUTHOR INFORMATION

Corresponding Author

*E-mail: shuming.li@staff.uni-marburg.de.

ORCID

Shu-Ming Li: 0000-0003-4583-2655

Author Contributions

†G.L. and J.F. contributed equally to this work.

Notes

The authors declare no competing financial interest.

■ ACKNOWLEDGMENTS

We thank Rixa Kraut and Stefan Newel (University of Marburg) for taking MS and NMR spectra, respectively. S.-M.L. acknowledges the DFG for funding the Bruker microTOF QIII mass spectrometer (INST 160/620-1). G.L. (201607565014) and J.F. (201507565006) are scholarship recipients from the China Scholarship Council.

REFERENCES

(1) Van De Water, R. W.; Pettus, T. R. R. *o*-Quinone methides: intermediates underdeveloped and underutilized in organic synthesis. *Tetrahedron* **2002**, *58* (27), 5367−5406.

(2) Bai, W. J.; David, J. G.; Feng, Z. G.; Weaver, M. G.; Wu, K. L.; Pettus, T. R. R. The domestication of *ortho*-quinone methides. *Acc. Chem. Res.* **2014**, *47* (12), 3655−3664.

(3) Nielsen, C. D. T.; Abas, H.; Spivey, A. C. Stereoselective reactions of *ortho*-quinone methide and *ortho*-quinone methide imines and their utility in natural product synthesis. *Synthesis* **2018**, *50* (20), 4008−4018.

(4) Pathak, T. P.; Sigman, M. S. Applications of *ortho*-quinone methide intermediates in catalysis and asymmetric synthesis. *J. Org. Chem.* **2011**, *76* (22), 9210−9215.

(5) Willis, N. J.; Bray, C. D. *ortho*-Quinone methides in natural product synthesis. *Chem. - Eur. J.* **2012**, *18* (30), 9160−9173.

(6) Spence, J. T.; George, J. H. Biomimetic total synthesis of *ent*-penilactone A and penilactone B. *Org. Lett.* **2013**, *15* (15), 3891−3893.

(7) Spence, J. T.; George, J. H. Total synthesis of peniphenones A-D *via* biomimetic reactions of a common *o*-quinone methide intermediate. *Org. Lett.* **2015**, *17* (24), 5970−5973.

(8) Forest, K.; Wan, P.; Preston, C. M. Catechin and hydroxybenzhydrols as models for the environmental photochemistry of tannins and lignins. *Photochem. Photobiol. Sci.* **2004**, *3* (5), 463−472.

(9) Chen, Y.; Steinmetz, M. G. Photoactivation of amino-substituted 1,4-benzoquinones for release of carboxylate and phenolate leaving groups using visible light. *J. Org. Chem.* **2006**, *71* (16), 6053−6060.

(10) Bishop, L. M.; Winkler, M.; Houk, K. N.; Bergman, R. G.; Trauner, D. Mechanistic investigations of the acid-catalyzed cyclization of a vinyl *ortho*-quinone methide. *Chem. - Eur. J.* **2008**, *14* (18), 5405−5408.

(11) Patel, A.; Netscher, T.; Rosenau, T. Stabilization of *ortho*-quinone methides by a bis (sulfonium ylide) derived from 2, 5-dihydroxy-[1, 4] benzoquinone. *Tetrahedron Lett.* **2008**, *49* (15), 2442−2445.

(12) Fan, J.; Liao, G.; Kindinger, F.; Ludwig-Radtke, L.; Yin, W.-B.; Li, S.-M. Peniphenone and penilactone formation in *Penicillium crustosum via* 1,4-Michael additions of *ortho*-quinone methide from hydroxyclavatol to γ-butyrolactones from crustosic acid. *J. Am. Chem. Soc.* **2019**, *141*, 4225−4229.

(13) Huang, C.; Yang, C.; Zhang, W.; Zhang, L.; De, B. C.; Zhu, Y.; Jiang, X.; Fang, C.; Zhang, Q.; Yuan, C. S.; Liu, H. W.; Zhang, C. Molecular basis of dimer formation during the biosynthesis of benzofluorene-containing atypical angucyclines. *Nat. Commun.* **2018**, *9* (1), 2088.

(14) Wu, G.; Ma, H.; Zhu, T.; Li, J.; Gu, Q.; Li, D. Penilactones A and B, two novel polyketides from Antarctic deep-sea derived fungus *Penicillium crustosum* PRB-2. *Tetrahedron* **2012**, *68*, 9745−9749.

(15) Tomoda, H.; Tabata, N.; Masuma, R.; Si, S. Y.; Omura, S. Erabulenols, inhibitors of cholesteryl ester transfer protein produced by *Penicillium* sp. FO-5637. I. Production, isolation and biological properties. *J. Antibiot.* **1998**, *51* (7), 618−623.

(16) da Silva, B. F.; Rodrigues-Fo, E. Production of a benzylated flavonoid from 5,7,3′,4′,5′-pentamethoxyflavanone by *Penicillium griseoroseum*. *J. Mol. Catal. B: Enzym.* **2010**, *67* (3−4), 184−188.

(17) Wang, J.; Liu, P.; Wang, Y.; Wang, H.; Li, J.; Zhuang, Y.; Zhu, W. Antimicrobial aromatic polyketides from Gorgonian-associated fungus, *Penicillium commune* 518. *Chin. J. Chem.* **2012**, *30*, 1236−1242.

(18) Li, H.; Jiang, J.; Liu, Z.; Lin, S.; Xia, G.; Xia, X.; Ding, B.; He, L.; Lu, Y.; She, Z. Peniphenones A-D from the mangrove fungus *Penicillium dipodomyicola* HN4−3A as inhibitors of *Mycobacterium tuberculosis* phosphatase MptpB. *J. Nat. Prod.* **2014**, *77* (4), 800−806.

(19) Sun, W.; Chen, X.; Tong, Q.; Zhu, H.; He, Y.; Lei, L.; Xue, Y.; Yao, G.; Luo, Z.; Wang, J.; Li, H.; Zhang, Y. Novel small molecule 11beta-HSD1 inhibitor from the endophytic fungus *Penicillium commune*. *Sci. Rep.* **2016**, *6*, 26418.

(20) Yu, G.; Sun, Z.; Peng, J.; Zhu, M.; Che, Q.; Zhang, G.; Zhu, T.; Gu, Q.; Li, D. Secondary metabolites produced by combined culture of *Penicillium crustosum* and a *Xylaria* sp. *J. Nat. Prod.* **2019**, *82* (7), 2013−2017.

(21) Davies, M. W.; Maskell, L.; Shipman, M.; Slawin, A. M.; Vidot, S. M.; Whatmore, J. L. Studies toward the synthesis of luminacin D: assembly of simplified analogues devoid of the epoxide displaying antiangiogenic activity. *Org. Lett.* **2004**, *6* (22), 3909−3912.

(22) Walsh, C. T. Biological matching of chemical reactivity: pairing indole nucleophilicity with electrophilic isoprenoids. *ACS Chem. Biol.* **2014**, *9* (12), 2718−2728.

(23) Alkhalaf, L. M.; Ryan, K. S. Biosynthetic manipulation of tryptophan in bacteria: Pathways and mechanisms. *Chem. Biol.* **2015**, *22* (3), 317−328.

(24) Steinmetz, H.; Zander, W.; Shushni, M. A. M.; Jansen, R.; Gerth, K.; Dehn, R.; Dräger, G.; Kirschning, A.; Müller, R. Precursor-directed syntheses and biological evaluation of new elansolid derivatives. *ChemBioChem* **2012**, *13* (12), 1813−1817.

(25) Jansen, R.; Gerth, K.; Steinmetz, H.; Reinecke, S.; Kessler, W.; Kirschning, A.; Müller, R. Elansolid A3, a unique *p*-quinone methide antibiotic from *Chitinophaga sancti*. *Chem. - Eur. J.* **2011**, *17* (28), 7739−7744.

(26) Dehn, R.; Katsuyama, Y.; Weber, A.; Gerth, K.; Jansen, R.; Steinmetz, H.; Höfle, G.; Müller, R.; Kirschning, A. Molecular basis of elansolid biosynthesis: evidence for an unprecedented quinone methide initiated intramolecular Diels-Alder cycloaddition/macrolactonization. *Angew. Chem., Int. Ed.* **2011**, *50* (17), 3882−3887.

(27) Ohashi, M.; Liu, F.; Hai, Y.; Chen, M.; Tang, M. C.; Yang, Z.; Sato, M.; Watanabe, K.; Houk, K. N.; Tang, Y. SAM-dependent enzyme-catalysed pericyclic reactions in natural product biosynthesis. *Nature* **2017**, *549* (7673), 502−506.

(28) Liu, Y.; Zou, L.; Ma, L.; Chen, W.-H.; Wang, B.; Xu, Z.-L. Synthesis and pharmacological activities of xanthone derivatives as α-glucosidase inhibitors. *Bioorg. Med. Chem.* **2006**, *14* (16), 5683−5690.

(29) Grover, P. K.; Shah, G. D.; Shah, R. C. Xanthones. Part IV. A new synthesis of hydroxyxanthones and hydroxybenzophenones. *J. Chem. Soc.* **1955**, 3982−3985.

(30) Morkunas, M.; Dube, L.; Gotz, F.; Maier, M.-E. Synthesis of the acylphloroglucinols rhodomyrtone and rhodomyrtosone B. *Tetrahedron* **2013**, *69* (40), 8559−8563.

(31) Pepper, H. P.; Lam, H. C.; Bloch, W. M.; George, J. H. Biomimetic total synthesis of (±)-garcibracteatone. *Org. Lett.* **2012**, *14* (19), 5162−5164.

(32) Caballero, E.; Avendaño, C.; Menéndez, J. C. Stereochemical issues related to the synthesis and reactivity of pyrazino[2′,1′-5,1]pyrrolo[2,3-b]indole-1,4-diones. *Tetrahedron: Asymmetry* **1998**, *9* (6), 967−981.

(33) Cacciatore, I.; Cocco, A.; Costa, M.; Fontana, M.; Lucente, G.; Pecci, L.; Pinnen, F. Biochemical properties of new synthetic carnosine analogues containing the residue of 2,3-diaminopropionic acid: the effect of N-acetylation. *Amino Acids* **2005**, *28* (1), 77−83.

(34) George, J.-H.; Hesse, M.-D.; Baldwin, E.; Adlington, R.-M. Biomimetic synthesis of polycyclic polyprenylated acylphloroglucinol natural products isolated from *Hypericum papuanum*. *Org. Lett.* **2010**, *12* (15), 3532−3535.

(35) Kasai, S.; Watanabe, S.; Kawabata, J.; Tahara, S.; Mizutani, J. Antimicrobial catechin derivatives of *Agrimonia pilosa*. *Phytochemistry* **1992**, *31* (3), 787−789.

(36) Kim, H. W.; Park, J.; Kang, K. B.; Kim, T. B.; Oh, W. K.; Kim, J.; Sung, S. H. Acylphloroglucinolated catechin and phenylethyl isocoumarin derivatives from *Agrimonia pilosa*. *J. Nat. Prod.* **2016**, *79* (9), 2376−2383.

(37) Liao, G.; Mai, P.; Fan, J.; Zocher, G.; Stehle, T.; Li, S.-M. Complete decoration of the indolyl residue in *cyclo*-L-Trp-L-Trp with geranyl moieties by using engineered dimethylallyl transferases. *Org. Lett.* **2018**, *20*, 7201−7205.

(38) Matsui, T.; Yoshimoto, C.; Osajima, K.; Oki, T.; Osajima, Y. *In vitro* survey of α-glucosidase inhibitory food components. *Biosci., Biotechnol., Biochem.* **1996**, *60* (12), 2019−2022.

DOI: 10.1021/acs.joc.9b02971
J. Org. Chem. 2020, 85, 1298−1307

(39) Matsui, T.; Oki, T.; Osajima, Y. Isolation and identification of peptidic α-glucosidase inhibitors derived from sardine muscle hydrolyzate. *Z. Naturforsch., C: J. Biosci.* **1999**, *54* (3−4), 259−263.
(40) Rivera-Chávez, G.; González-Andrade, M.; González, M. d. C.; Glenn, A. E.; Mata, R. Thielavins A, J and K: α-glucosidase inhibitors from MEXU 27095, an endophytic fungus from *Hintonia latiflora*. *Phytochemistry* **2013**, *94*, 198−205.
(41) Rivera-Chávez, G.; Figueroa, M.; González, M. d. C.; Glenn, A. E.; Mata, R. α-Glucosidase inhibitors from a *Xylaria feejeensis* associated with *Hintonia latiflora*. *J. Nat. Prod.* **2015**, *78* (4), 730−735.

DOI: 10.1021/acs.joc.9b02971
J. Org. Chem. 2020, 85, 1298−1307

Supporting Information

Increasing structural diversity of natural products by Michael addition with *ortho*-quinone methide as the acceptor

Ge Liao,† Jie Fan,† Lena Ludwig-Radtke, Katja Backhaus, and Shu-Ming Li*

Institut für Pharmazeutische Biologie und Biotechnologie, Philipps-Universität Marburg, Robert-Koch Straße 4, Marburg 35037, Germany

Corresponding Author
*E-mail: shuming.li@staff.uni-marburg.de

†These authors contributed equally to this work.

Table of contents

Scheme S1. Chemical synthesis of hydroxyclavatol.

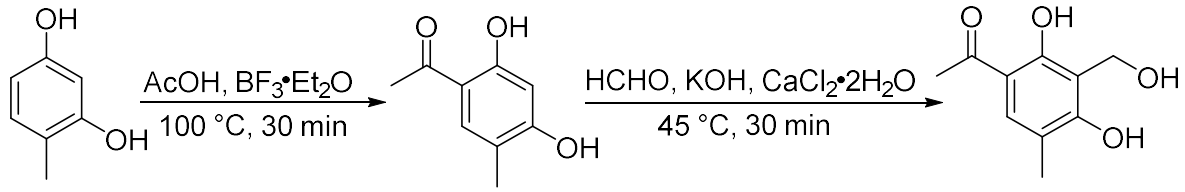

4-Methyl-6-acetylresorcinol was firstly synthesized by a Friedel-Craft acylation of 4-methylbenzene-1,3-diol (BLDpharm, Shanghai, China) as reported.[1] Introducing the hydroxymethylene group onto 4-methyl-6-acetylresorcinol was achieved by using a modified method reported for the synthesis of luminacin D.[2]

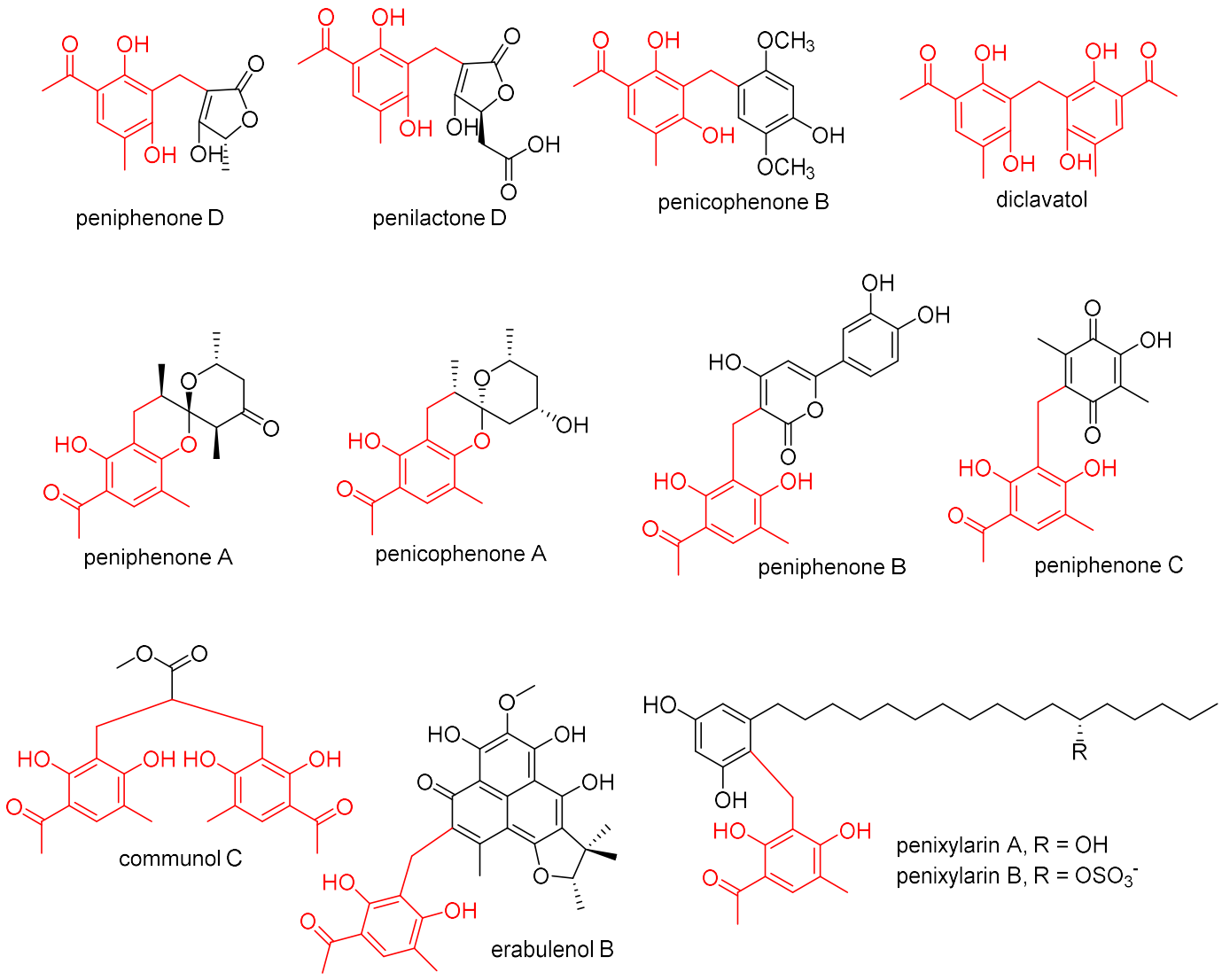

Figure S1. Examples of fungal clavatol-containing natural products.[3-9]

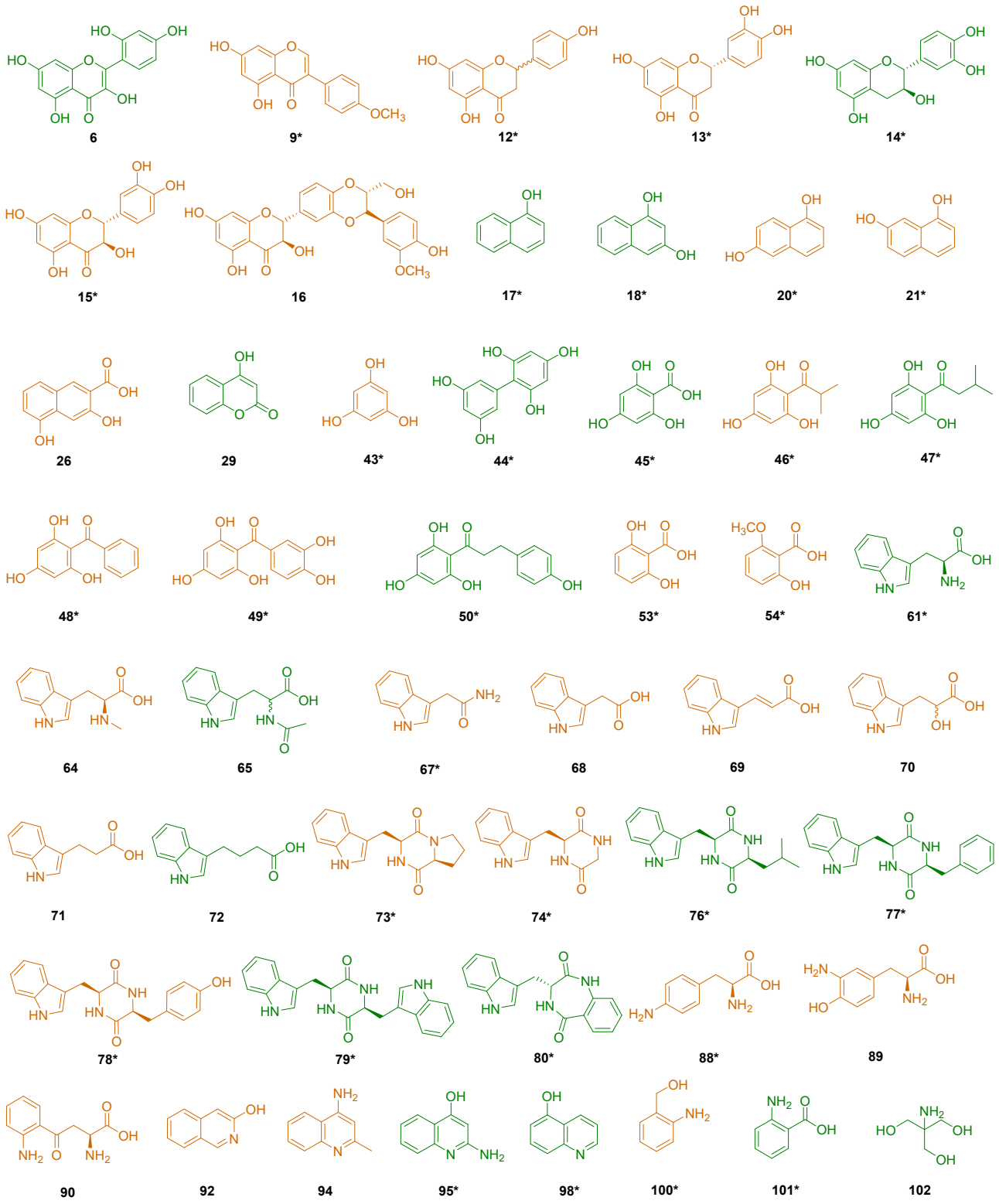

Figure S2. Structures of tested reactants with conversions between 10% – 55%.
Products of reactants in green were further identified by NMR after isolation. Products of reactants in orange were only identified by LC-MS analysis. Products with two clavatol moieties were detected from reactants labled with *. Reaction mixtures (50 μL) containing 0.4 mM hydroxyclavatol and 0.4 mM reactants were incubated at 25 °C for 16 h before sent to LC-MS analysis. The conversion (%) was calculated by peak areas with UV detection.

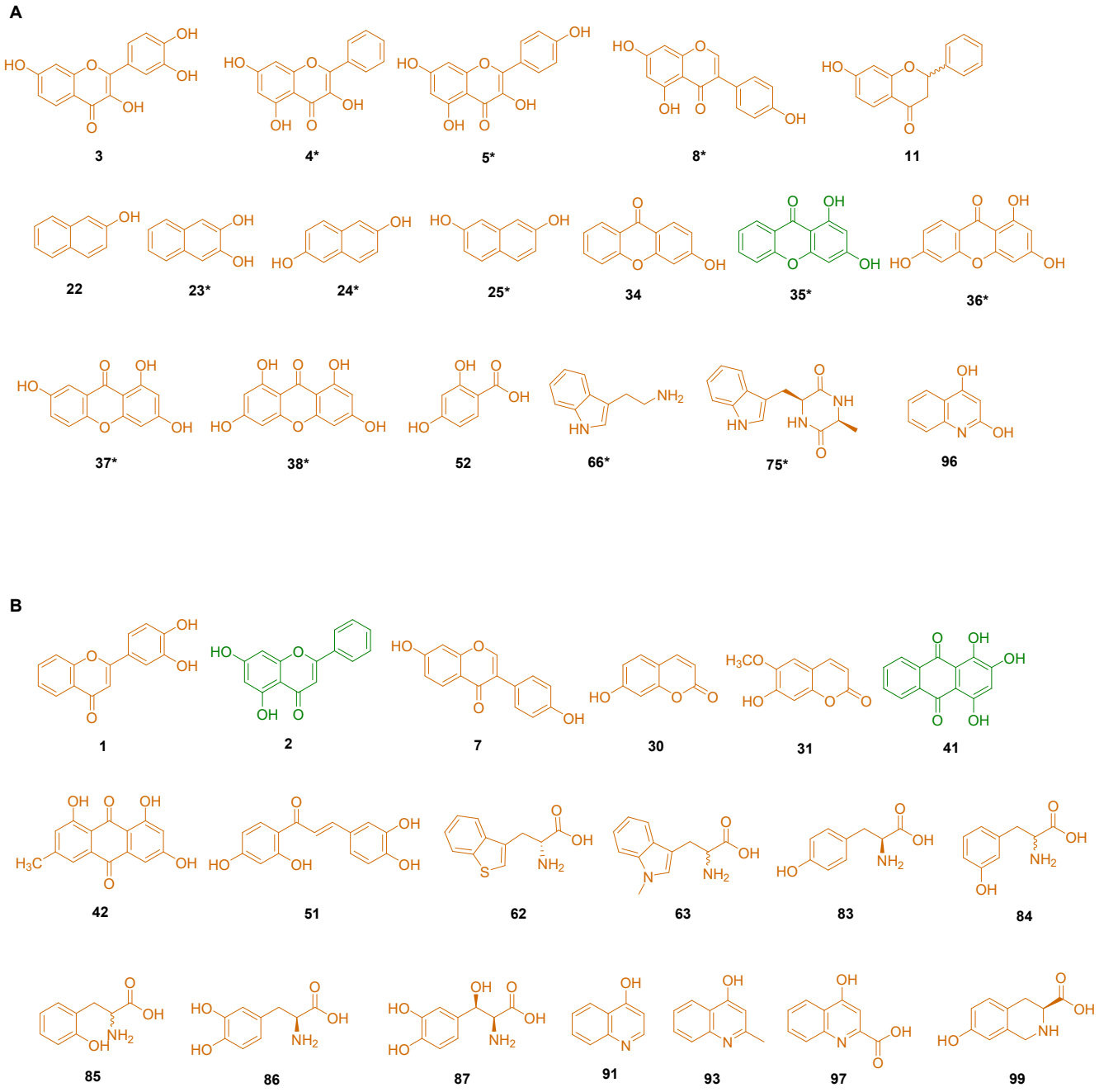

Figure S3. Structures of tested reactants with conversions between 1% – 10% (A), and only detected by EIC of $[M+H]^+$/$[M-H]^-$ ions (B).

Reaction mixtures (50 μL) containing 0.4 mM hydroxyclavatol and 0.4 mM reactants were incubated at 25 °C for 16 h before sent to LC-MS analysis. Products of reactants in green were isolated from incubations at 95 °C for 30 min. Products of reactants in orange were only identified by LC-MS analysis. Products with two clavatol moieties were detected from reactants labled with *. The conversion (%) was calculated by peak areas with UV detection.

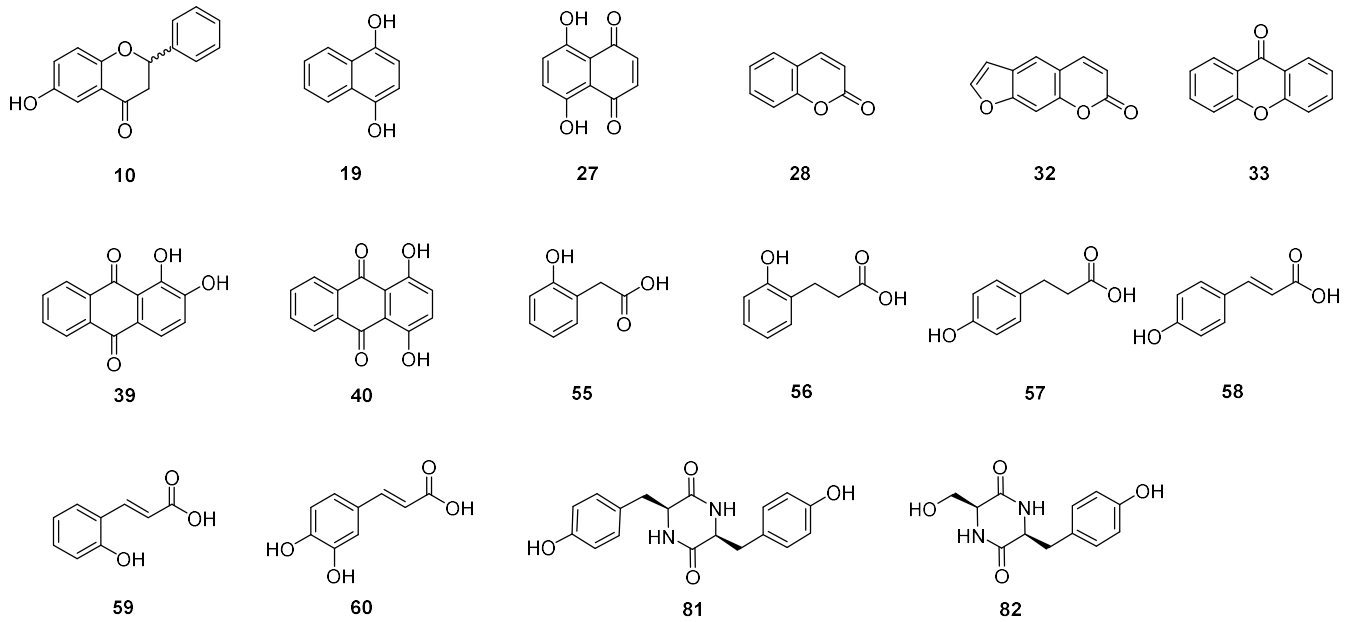

Figure S4. Structures of tested reactants with no detectable product by EIC of $[M+H]^+$/$[M-H]^-$ ions.
Reaction mixtures (50 μL) containing 0.4 mM hydroxyclavatol and 0.4 mM reactants were incubated at 25 °C for 16 h before sent to LC-MS analysis.

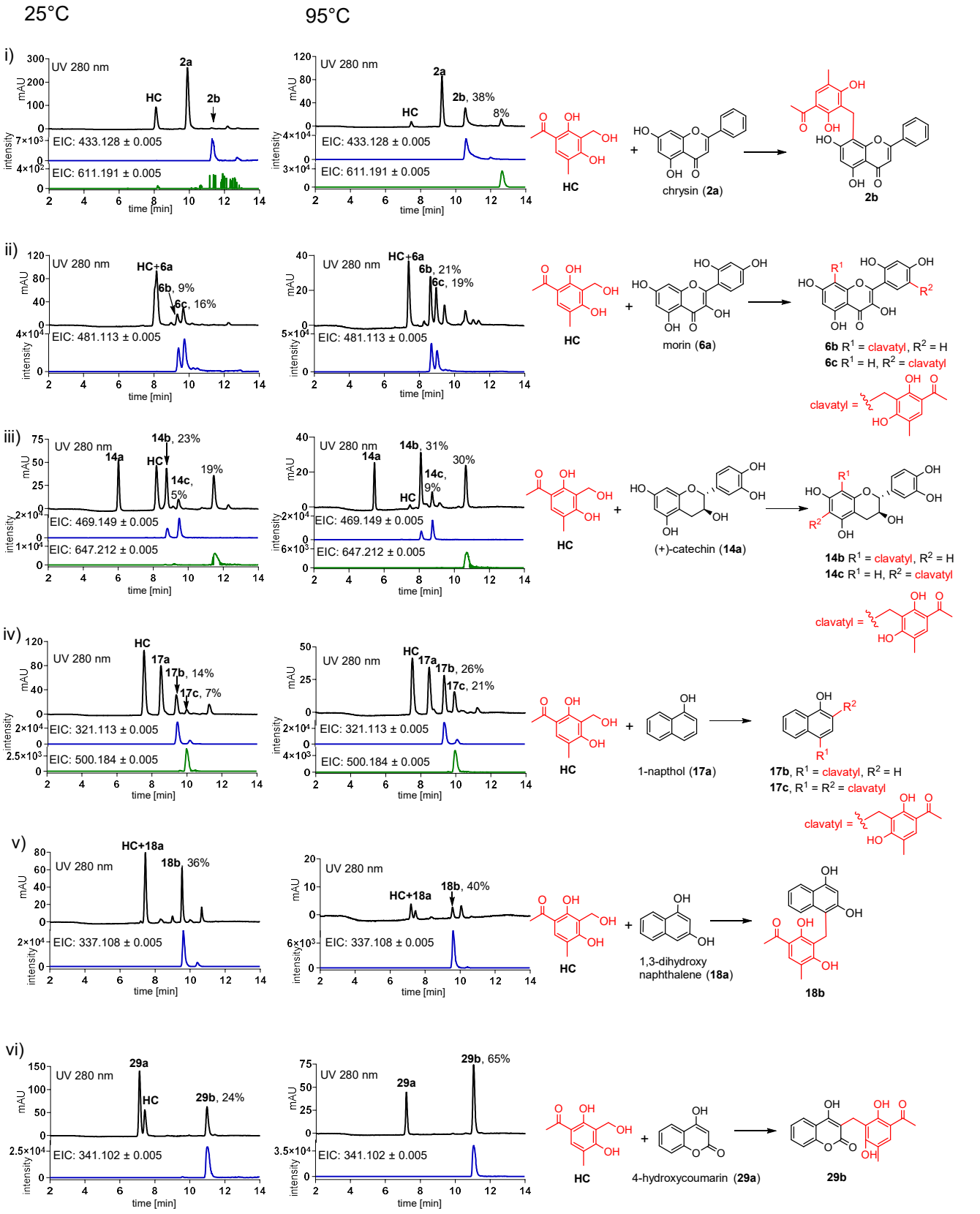

Figure S5. LC-MS analysis of reaction mixtures of hydroxyclavatol with different reactants.
HC: hydroxyclavatol, UV absorptions at 280 nm (black) are illustrated. EICs in blue or green refer $[M+H]^+$ of products with one or two clavatol moieties with a tolerance range of ± 0.005. EICs refer $[M-H]^-$ of **17b**, **17c**, and **18b**.

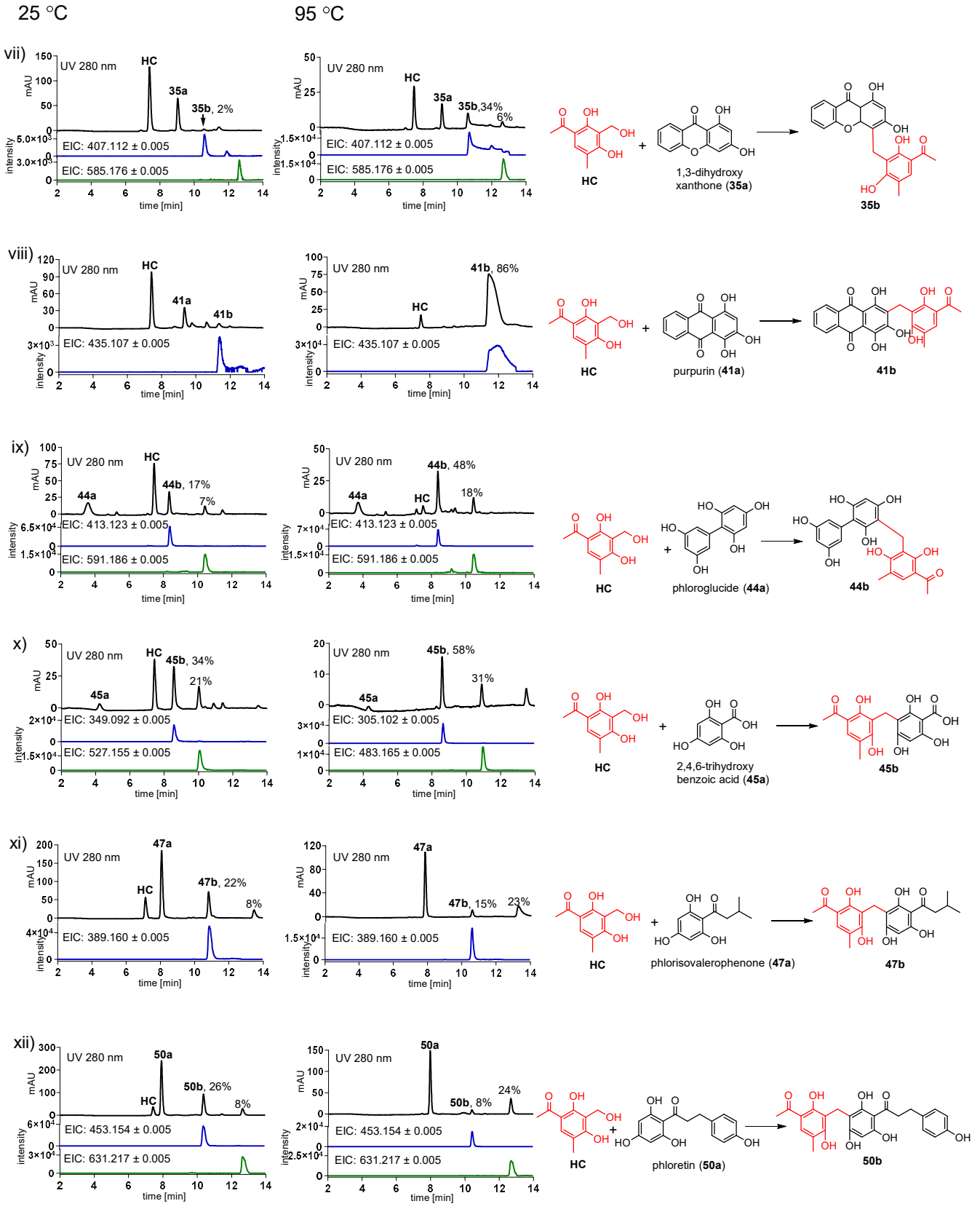

Figure S6. LC-MS analysis of reaction mixtures of hydroxyclavatol with different reactants.
HC: Hydroxyclavatol, UV absorptions at 280 nm (black) are illustrated. EICs in blue or green refer $[M+H]^+$ of products with one or two clavatol moieties with a tolerance range of ± 0.005.

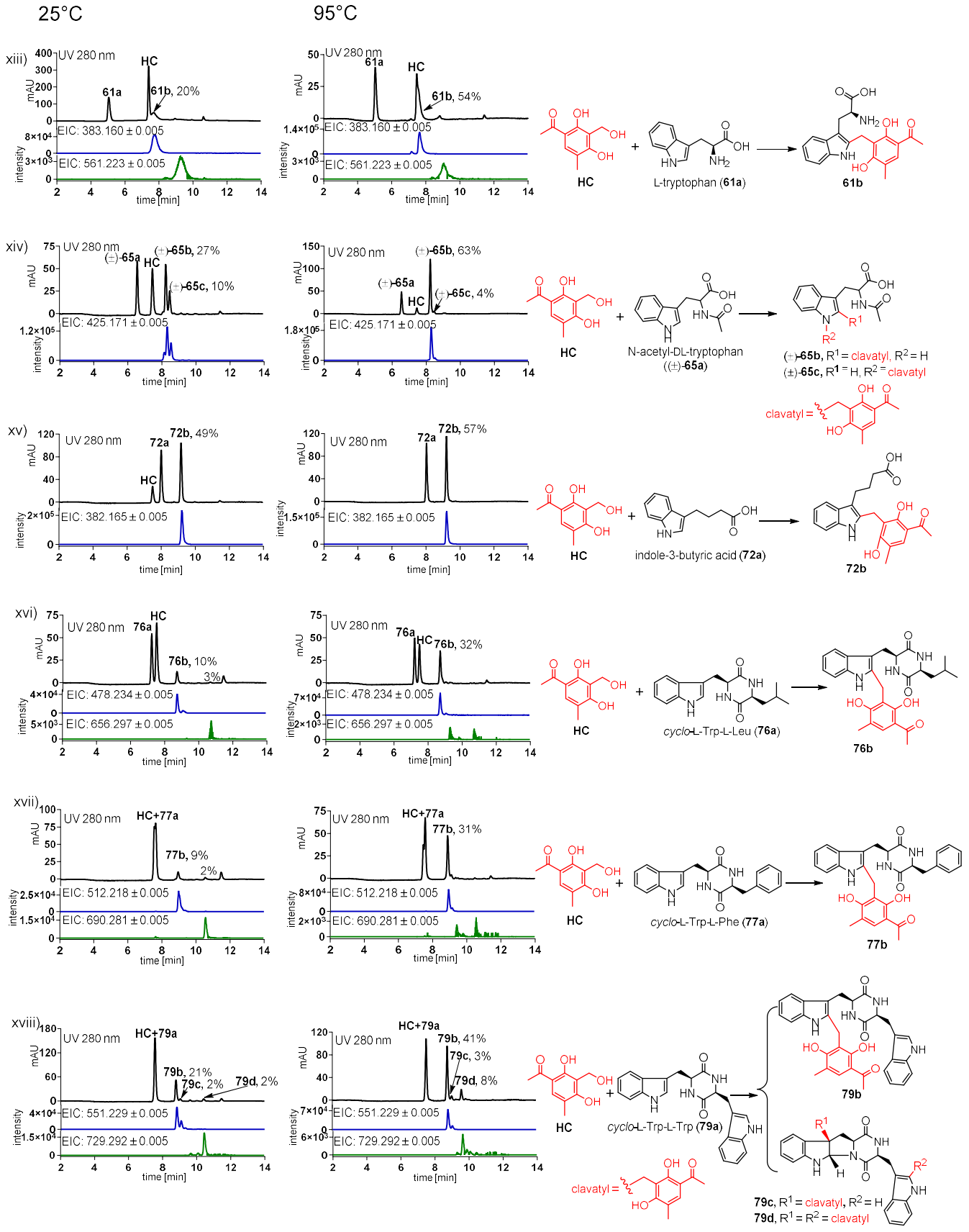

Figure S7. LC-MS analysis of reaction mixtures of hydroxyclavatol with different reactants.
HC: hydroxyclavatol, UV absorptions at 280 nm (black) are illustrated. EICs in blue or green refer $[M+H]^+$ of products with one or two clavatol moieties with a tolerance range of ± 0.005.

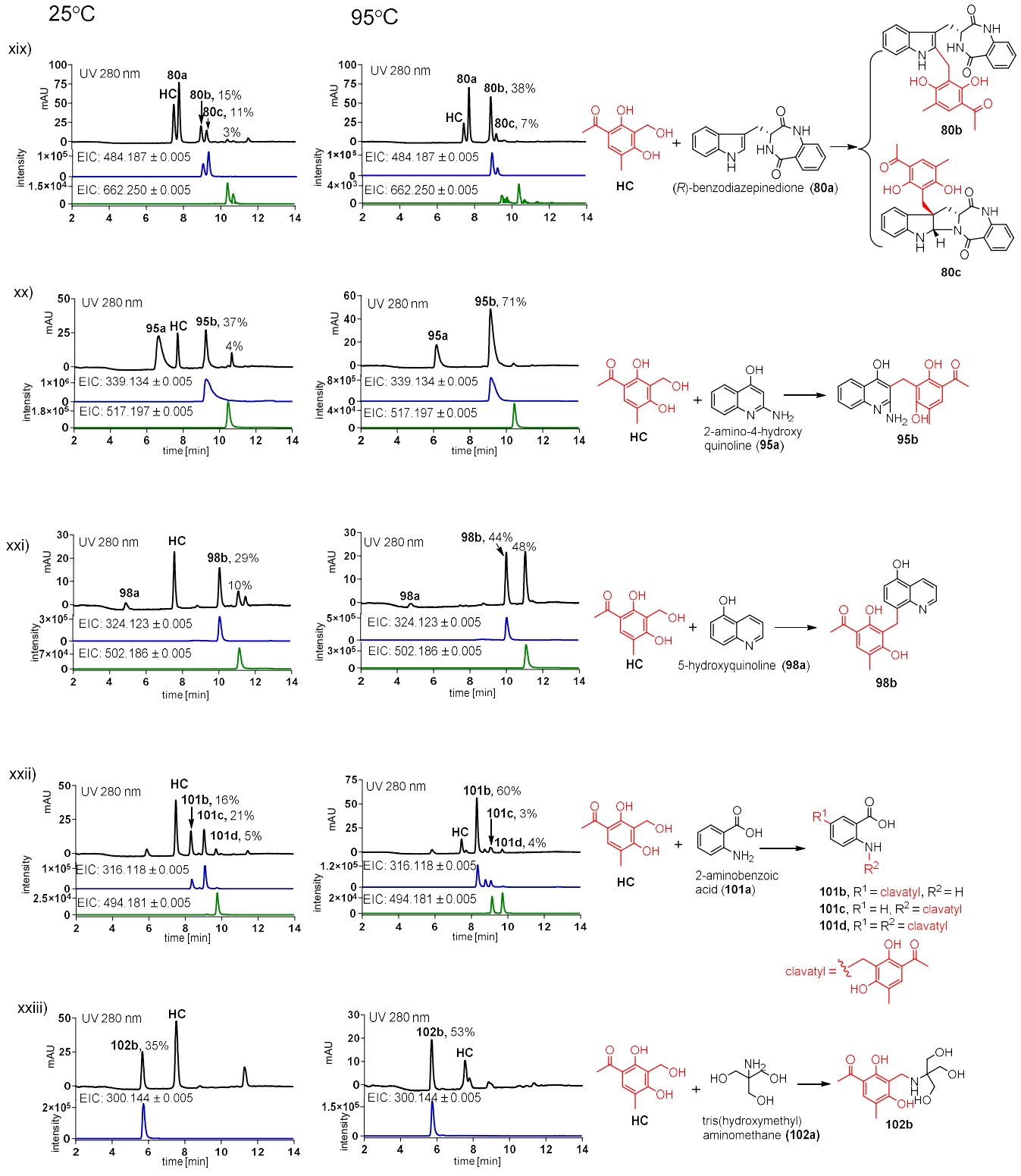

Figure S8. LC-MS analysis of reaction mixtures of hydroxyclavatol with different reactants.
HC: hydroxyclavatol, UV absorptions at 280 nm (black) are illustrated. EICs in blue or green refer $[M+H]^+$ of products with one or two clavatol moieties with a tolerance range of ± 0.005.

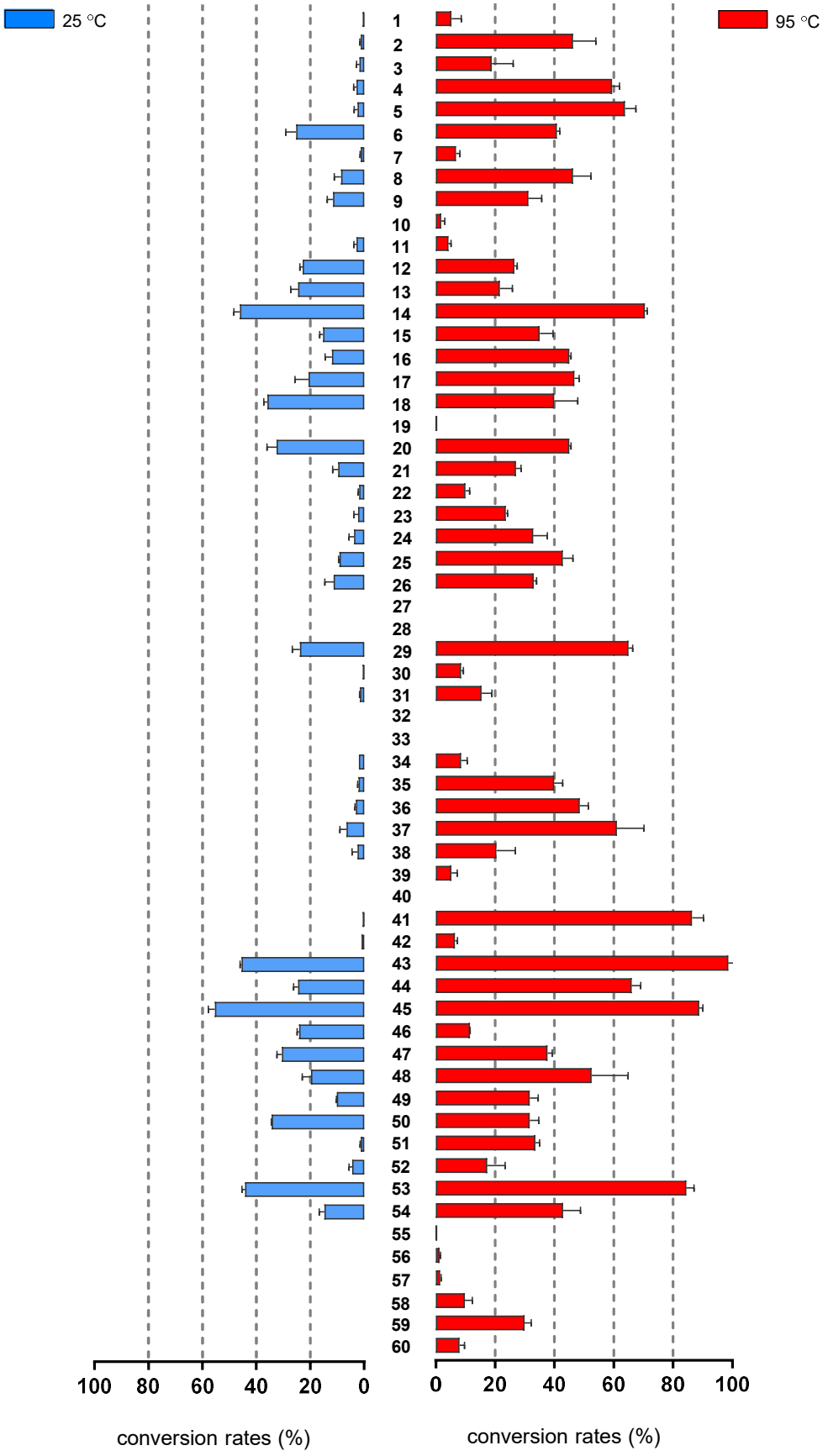

Figure S9. Conversions of hydroxyclavatol reactions with nitrogen-free reactants at 25 °C (left) or 95 °C (right).

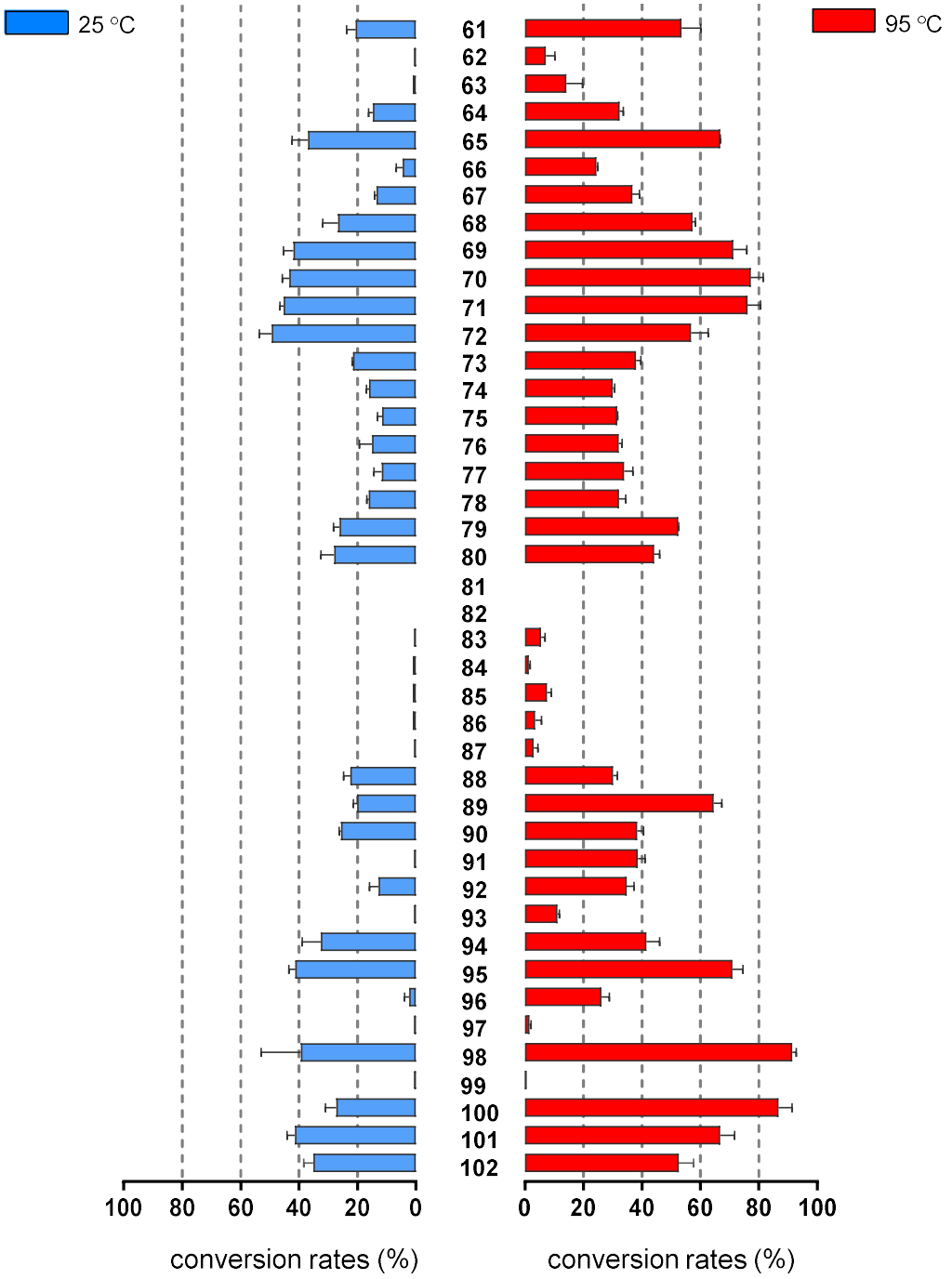

Figure S10. Conversions of hydroxyclavatol reactions with nitrogen-containing reactants at 25 °C (left) or 95 °C (right).

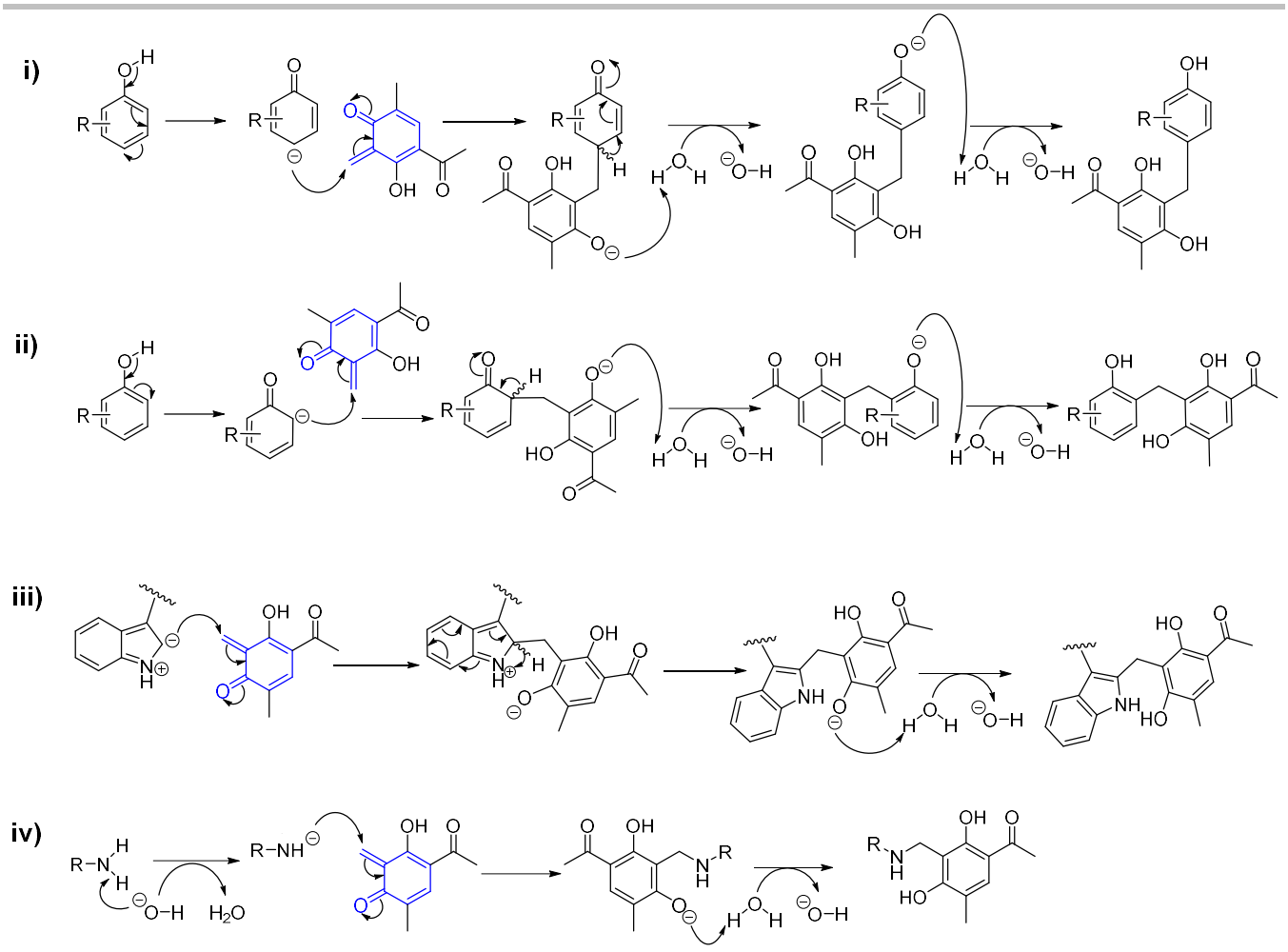

Figure S11. Reaction mechanisms of different nucleophile additions to the *ortho*-quinone methide intermediate.

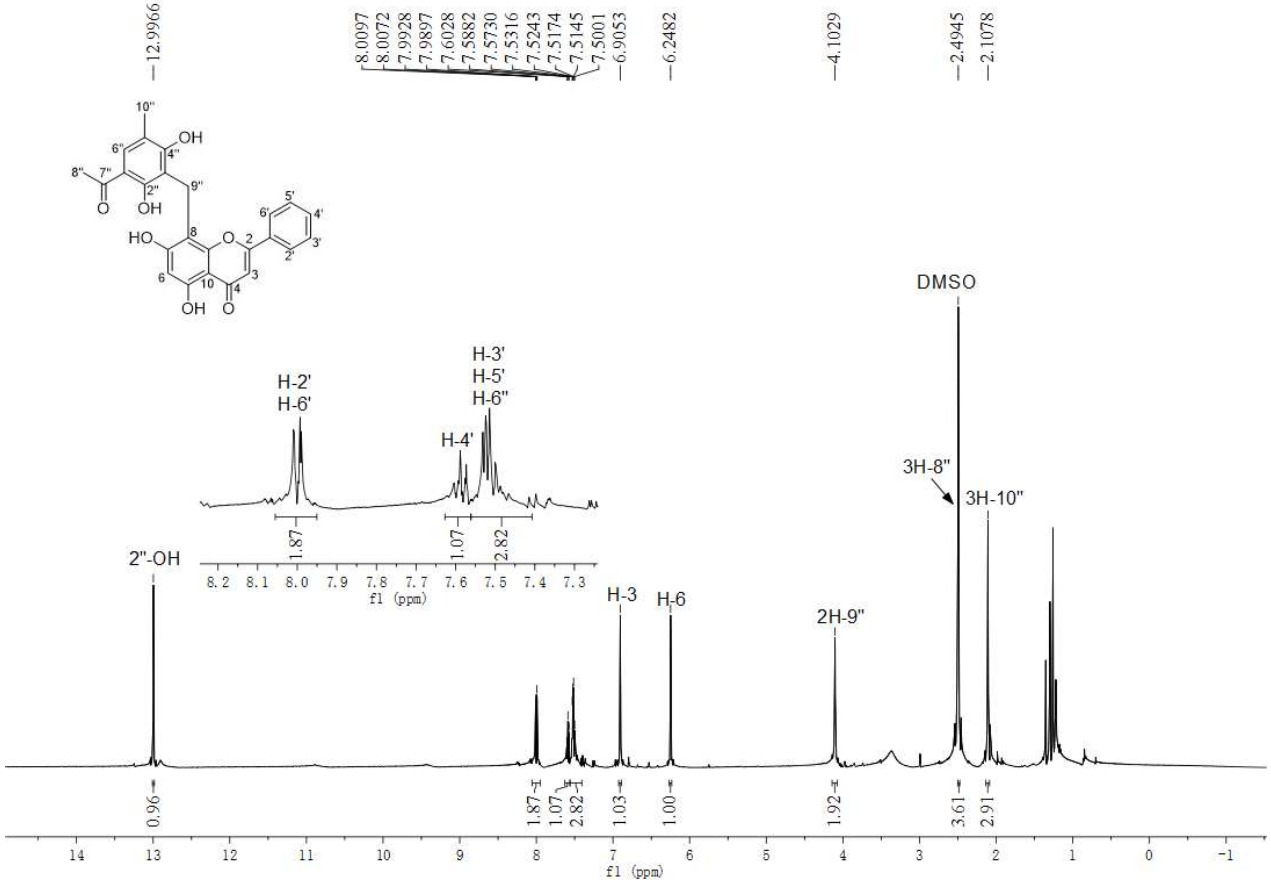

Figure S12. ^{1}H NMR spectrum of **2b** in DMSO-d_6 (500 MHz).

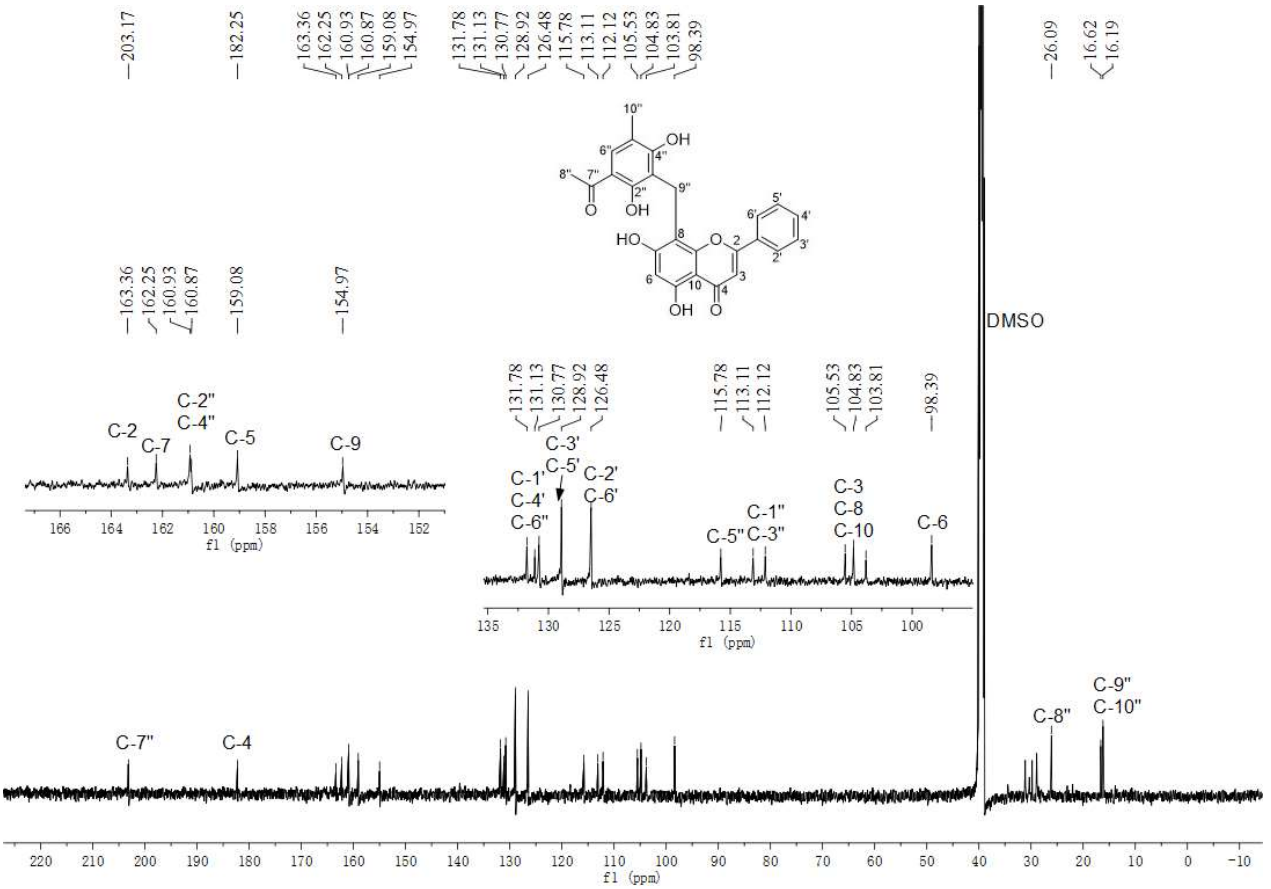

Figure S13. ^{13}C{^{1}H} NMR spectrum of **2b** in DMSO-d_6 (125 MHz).

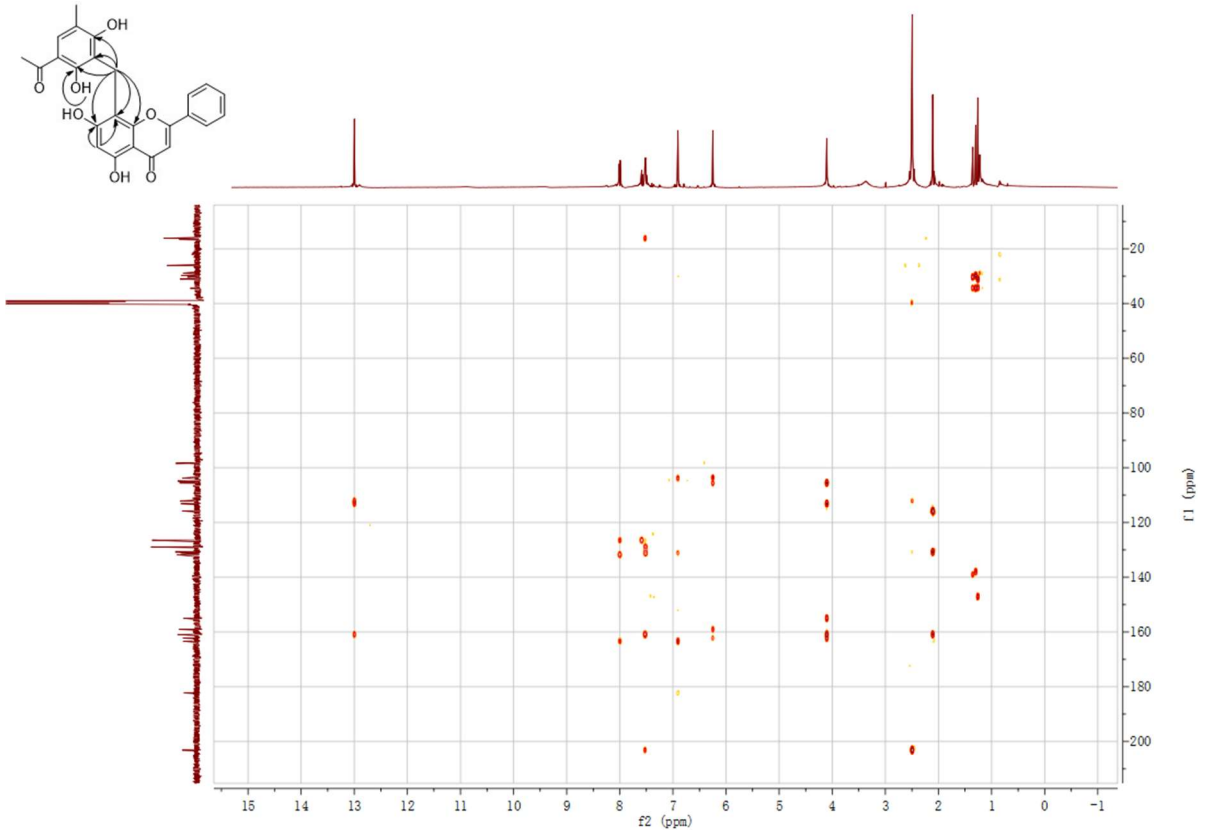

Figure S14. HMBC spectrum of **2b** in DMSO-d_6.

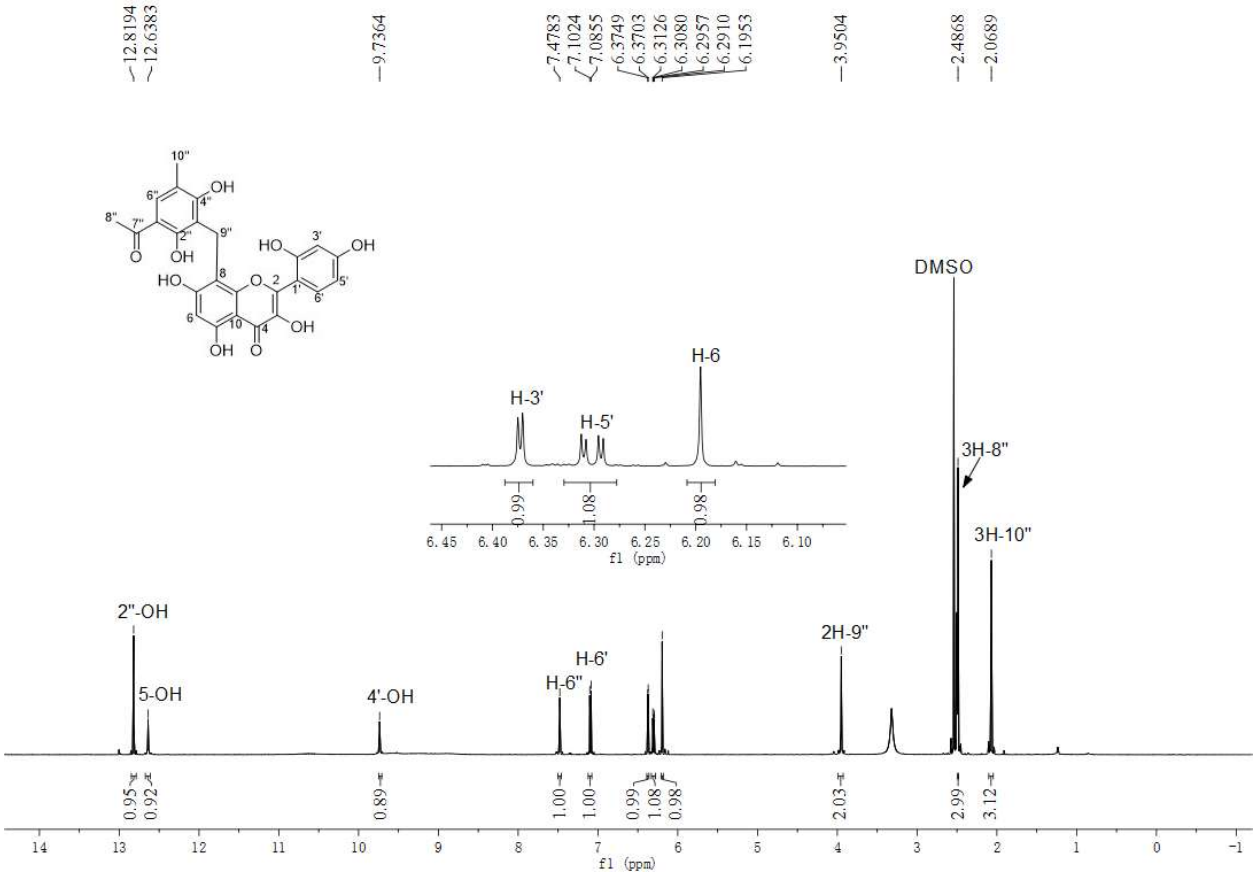

Figure S15. ^{1}H NMR spectrum of **6b** in DMSO-d_6 (500 MHz).

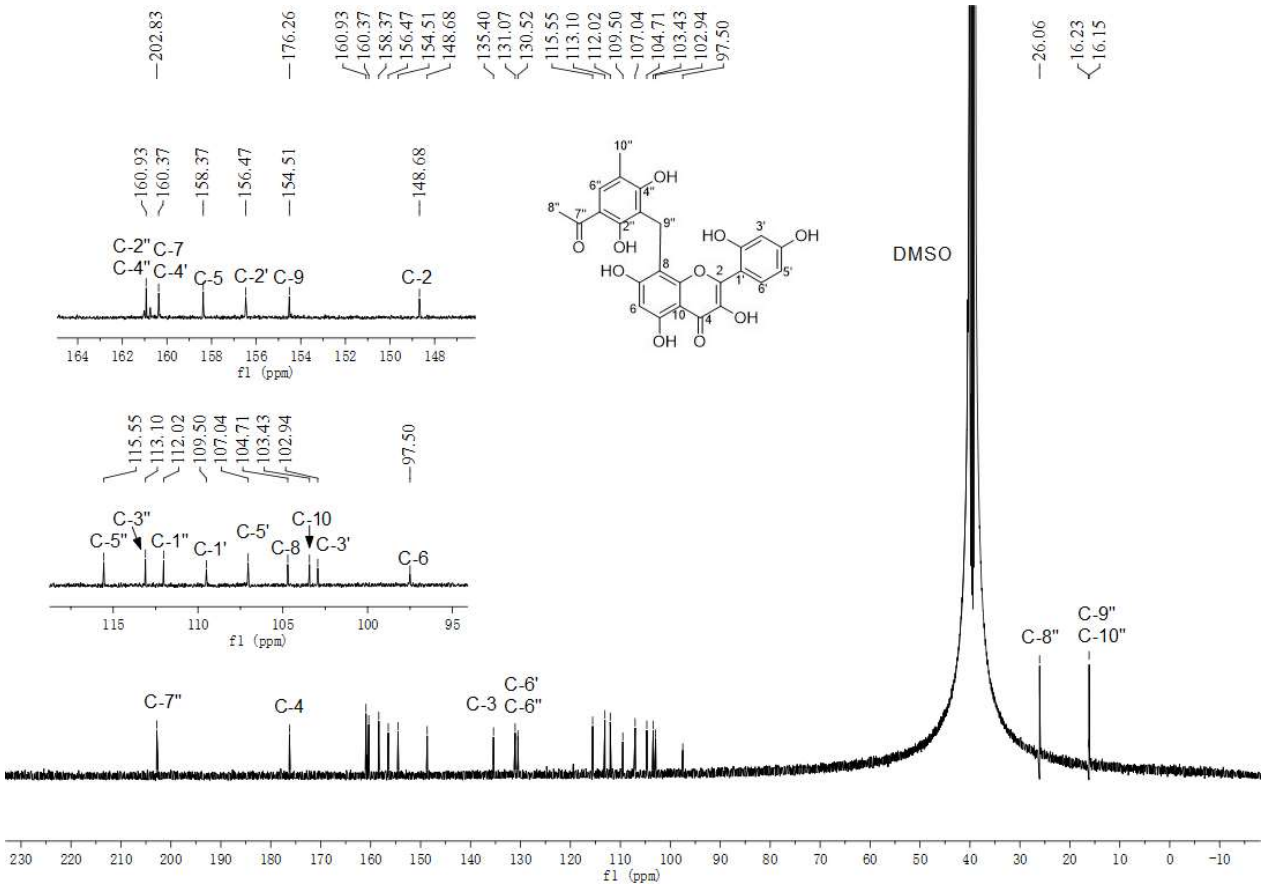

Figure S16. $^{13}C\{^{1}H\}$ NMR spectrum of **6b** in DMSO-d_6 (125 MHz).

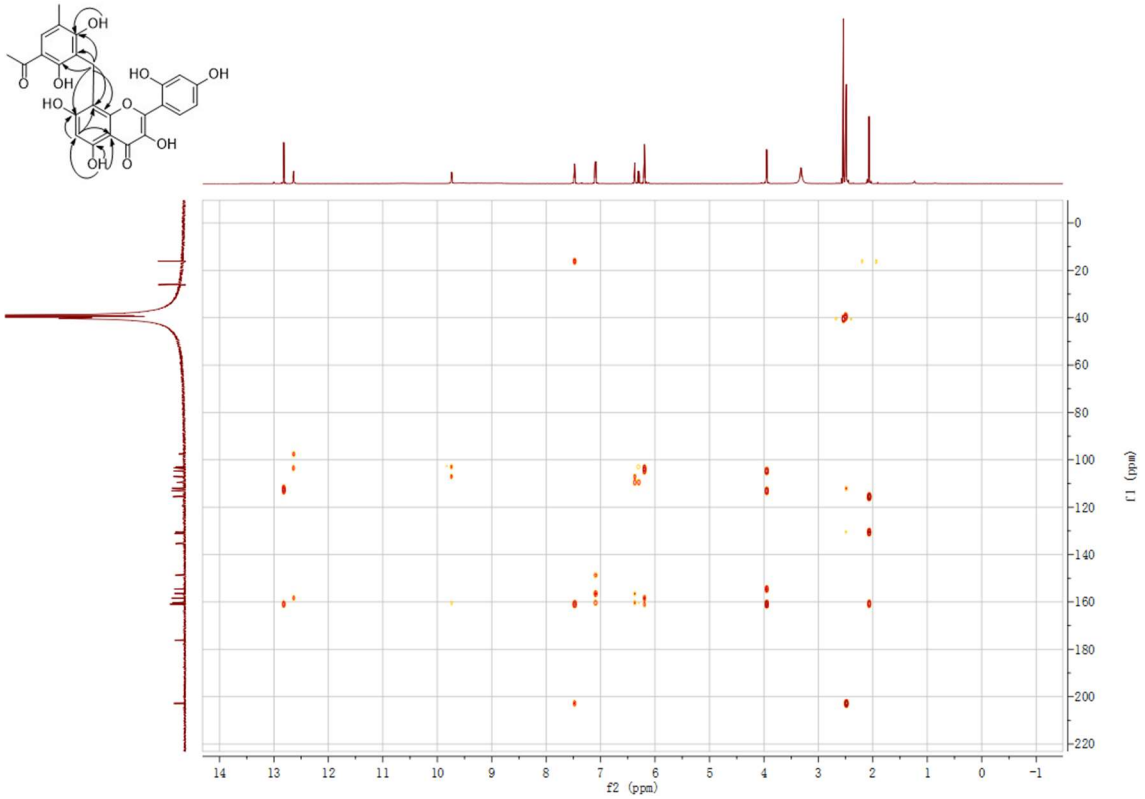

Figure S17. HMBC spectrum of **6b** in DMSO-d_6.

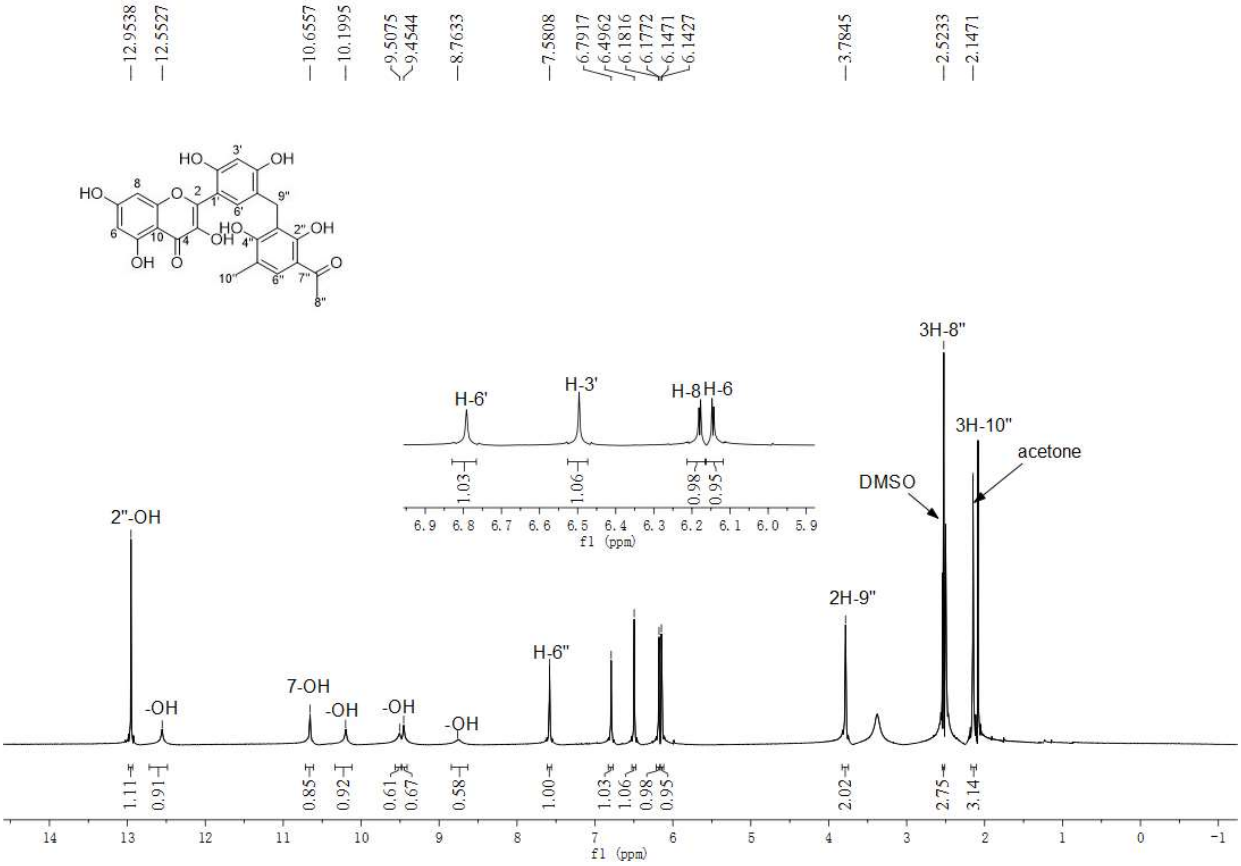

Figure S18. ^{1}H NMR spectrum of **6c** in DMSO-d_6 (500 MHz).

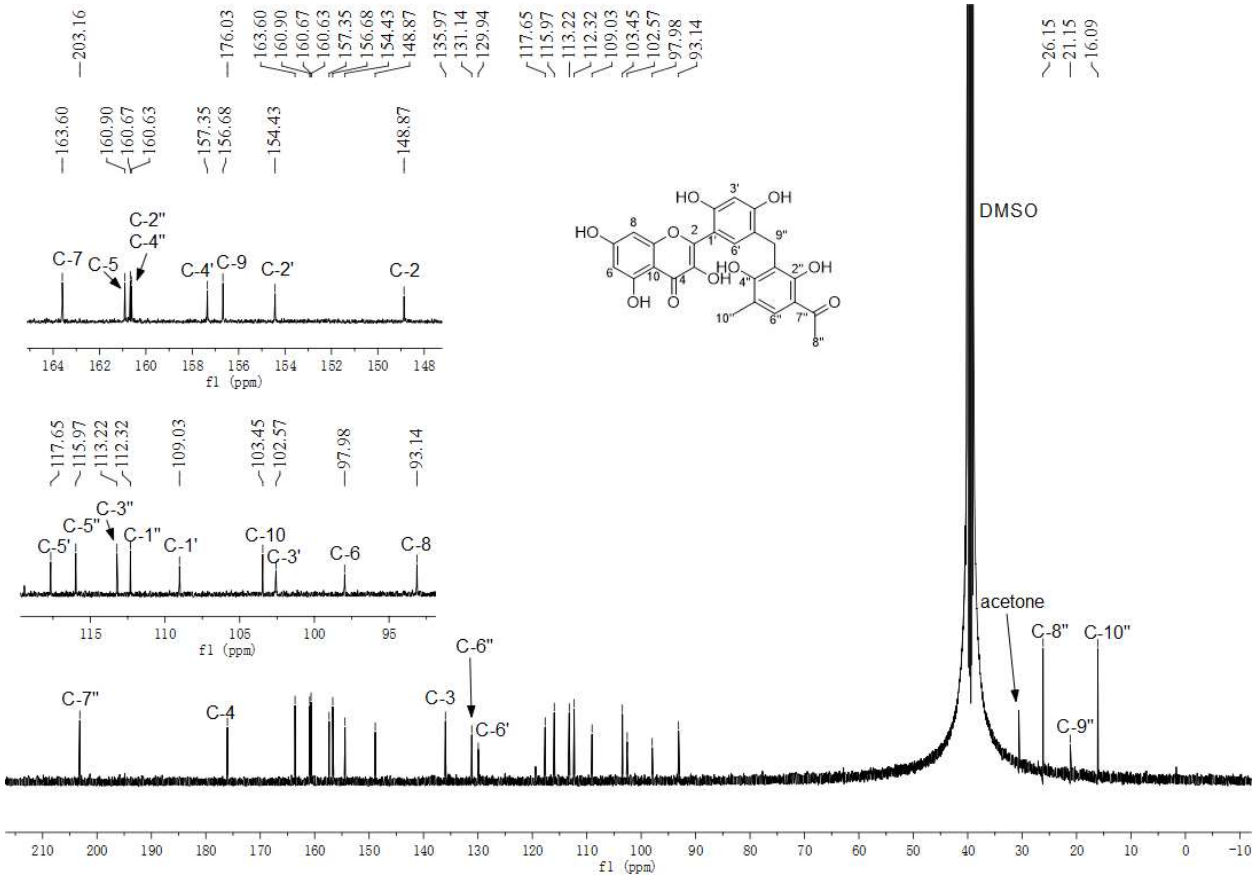

Figure S19. ^{13}C{^{1}H} NMR spectrum of **6c** in DMSO-d_6 (125 MHz).

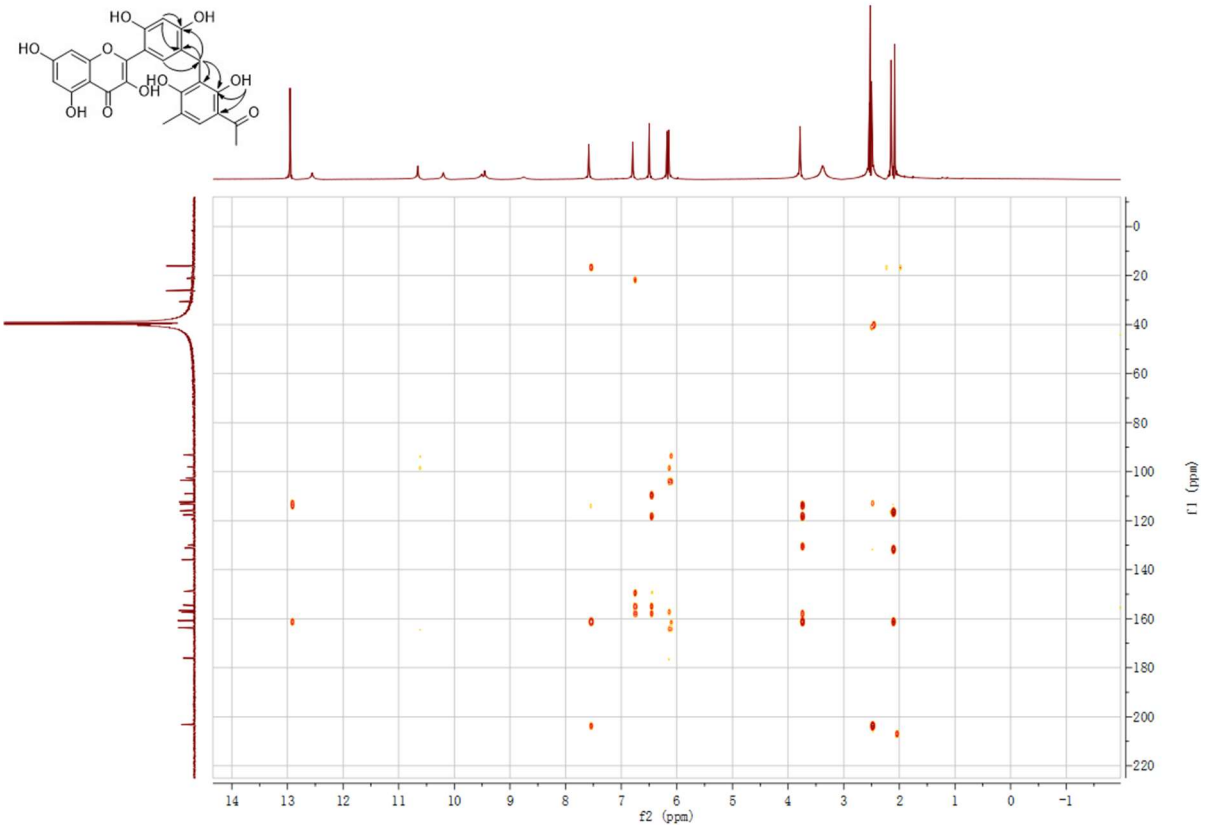

Figure S20. HMBC spectrum of **6c** in DMSO-d_6.

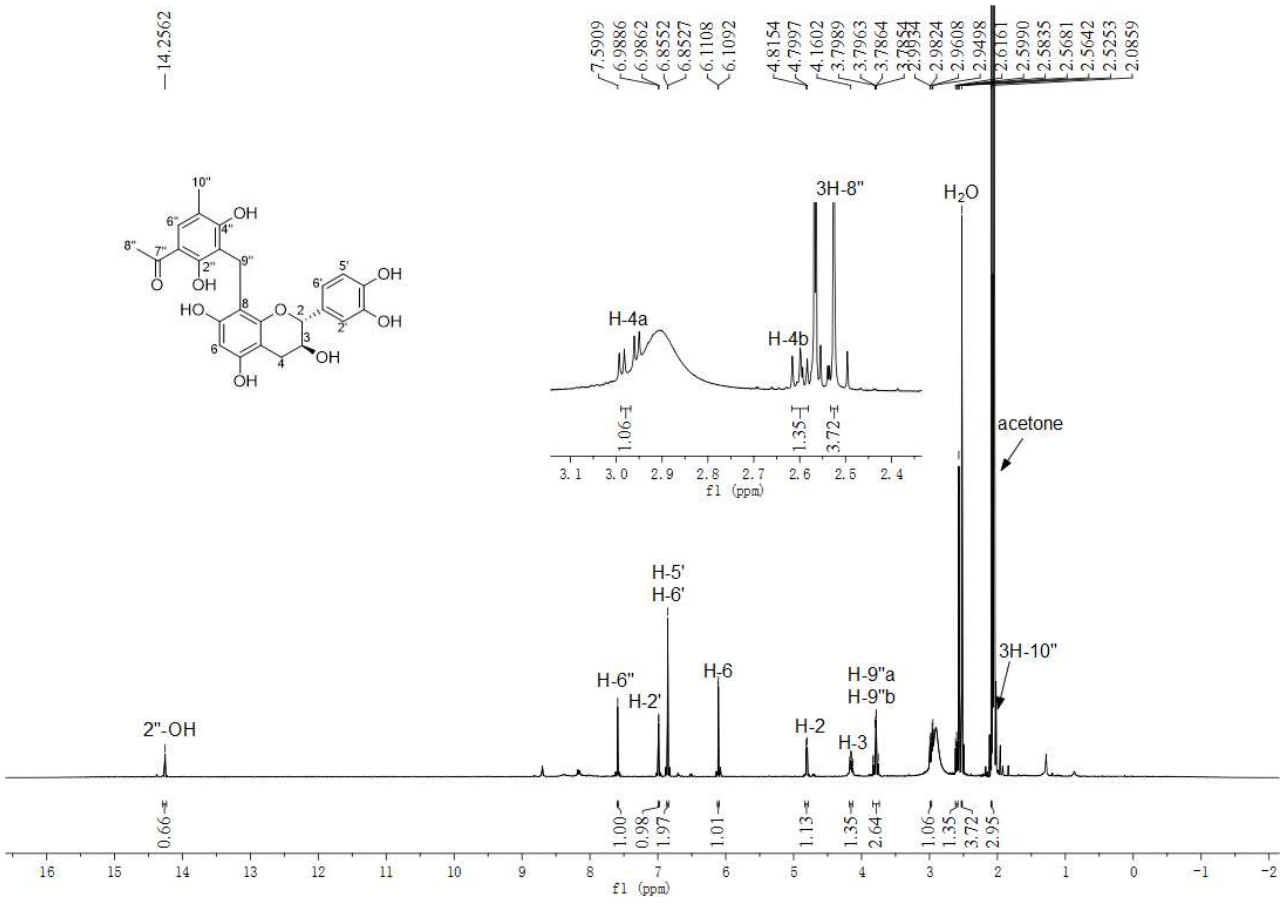

Figure S21. ^{1}H NMR spectrum of **14b** in acetone-d_6 (500 MHz).

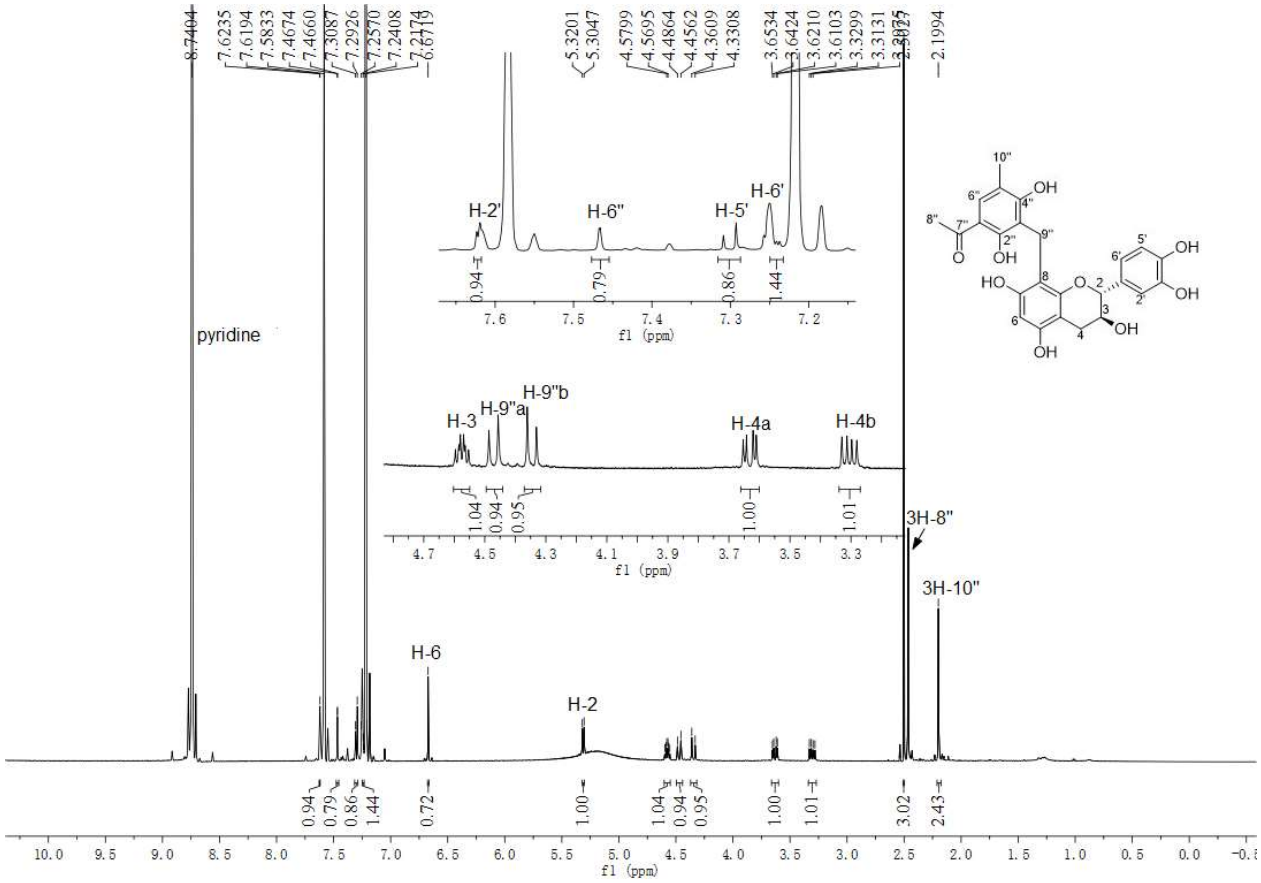

Figure S22. ^{1}H NMR spectrum of **14b** in pyridine-d_5 (500 MHz).

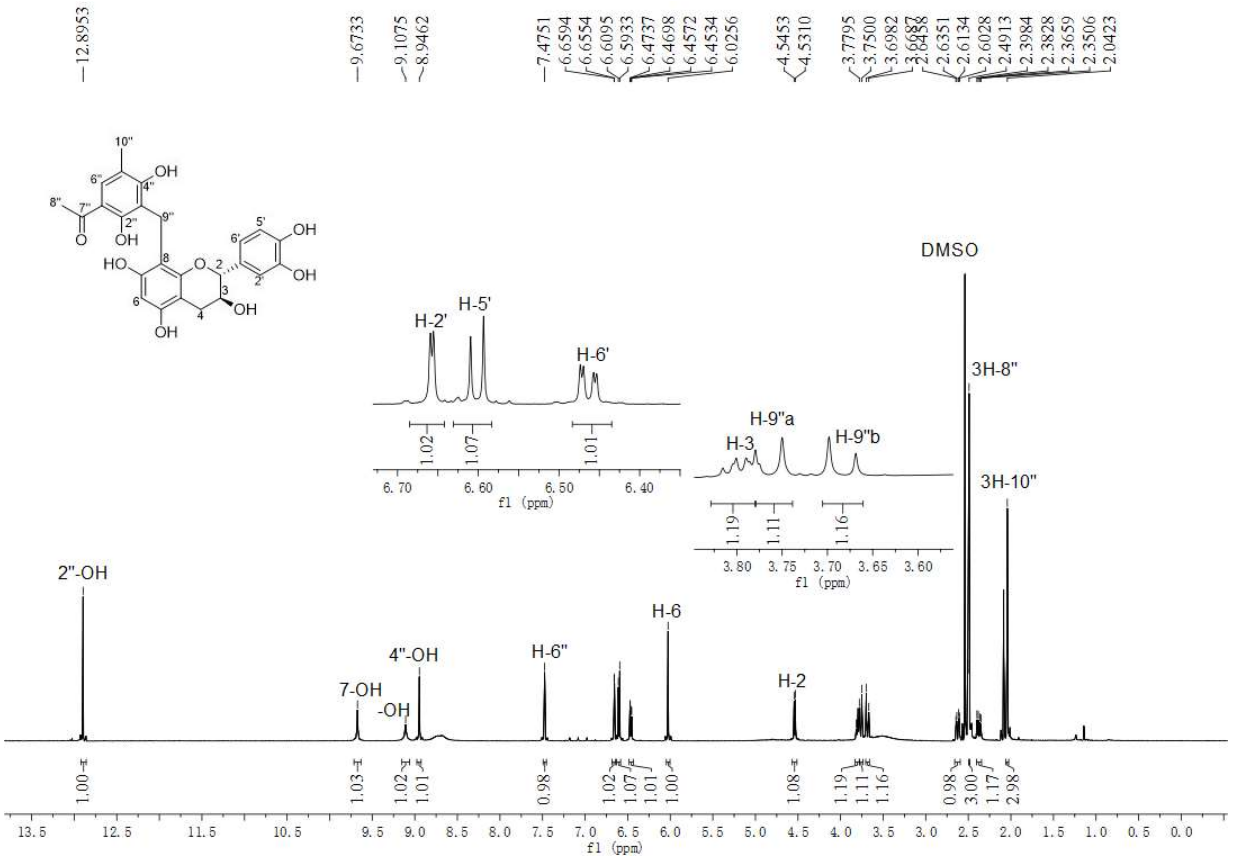

Figure S23. ^{1}H NMR spectrum of **14b** in DMSO-d_6 (500 MHz).

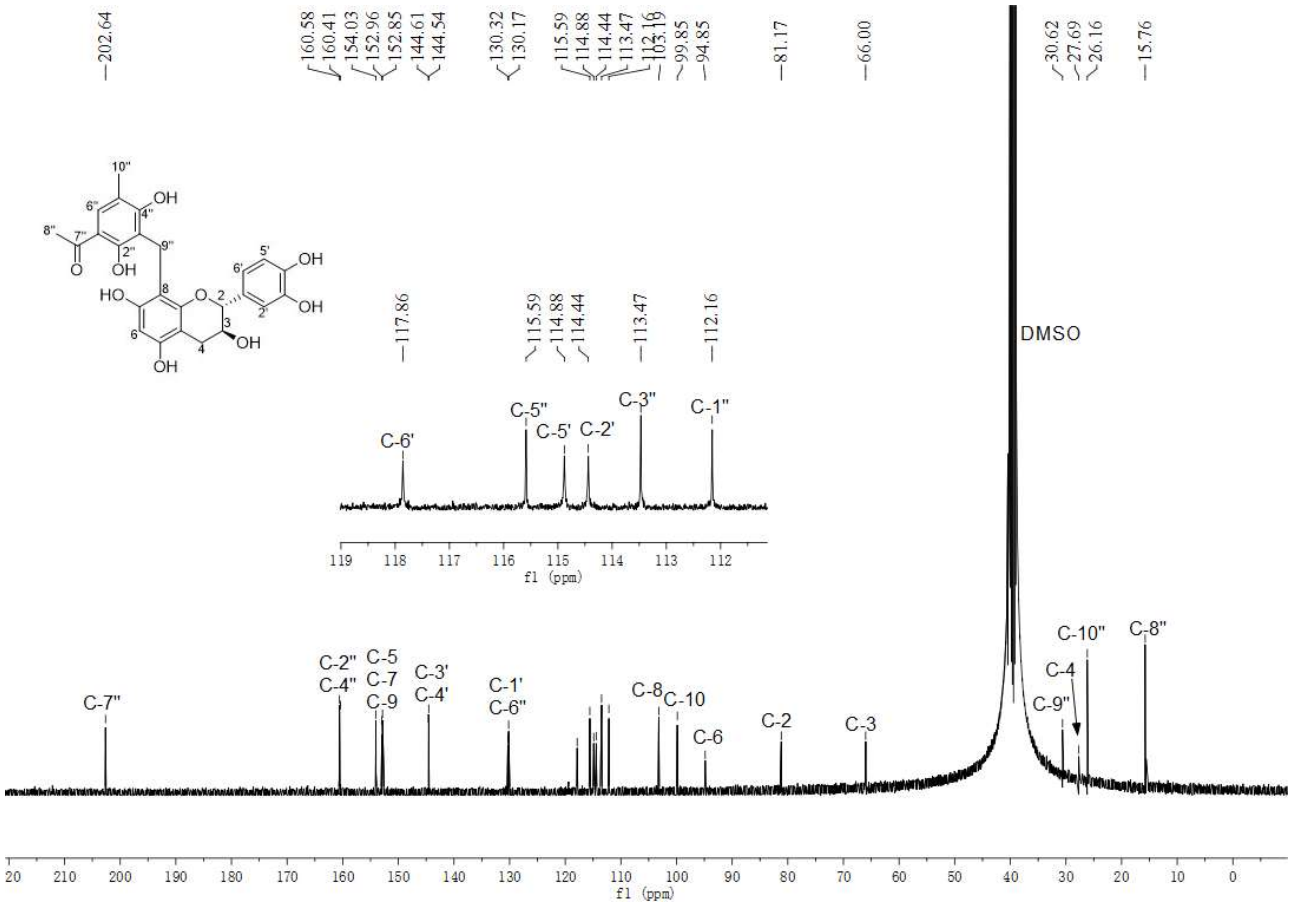

Figure S24. $^{13}C\{^{1}H\}$ NMR spectrum of **14b** in DMSO-d_6 (125 MHz).

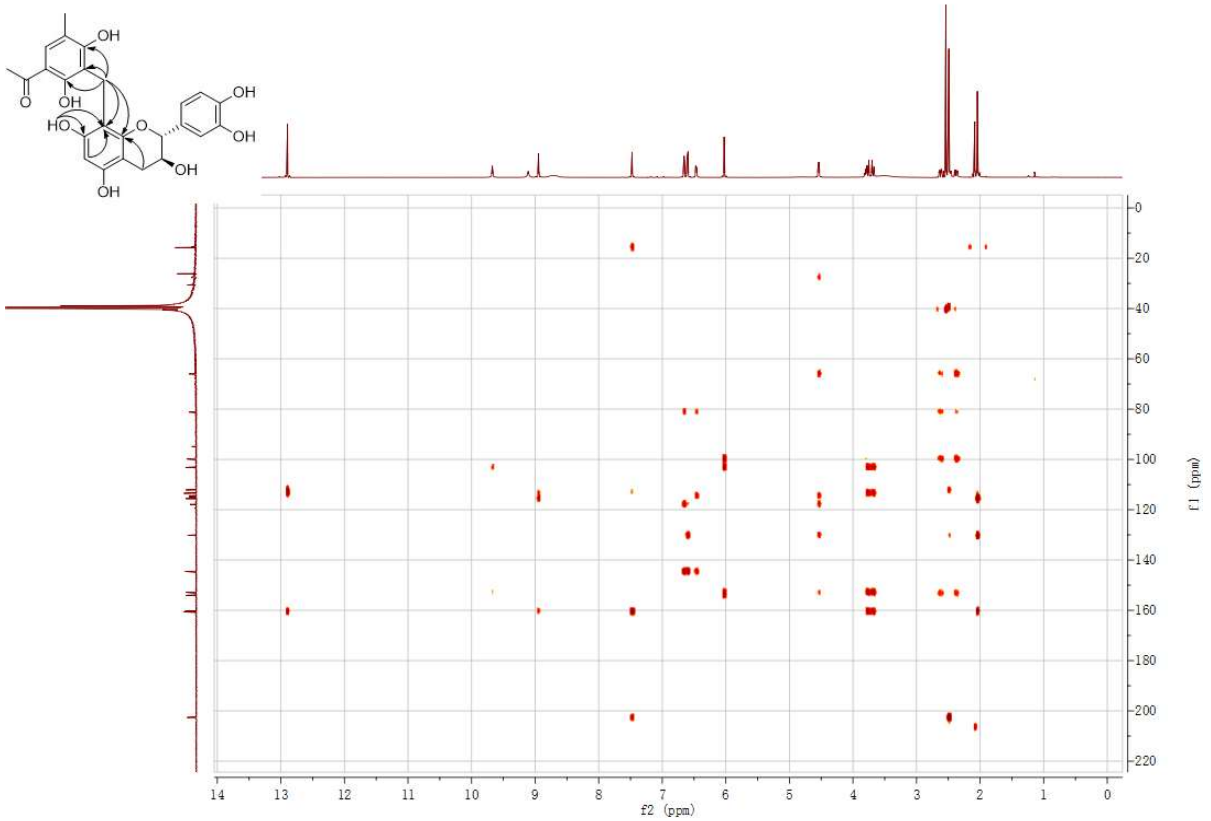

Figure S25. HMBC spectrum of **14b** in DMSO-d_6.

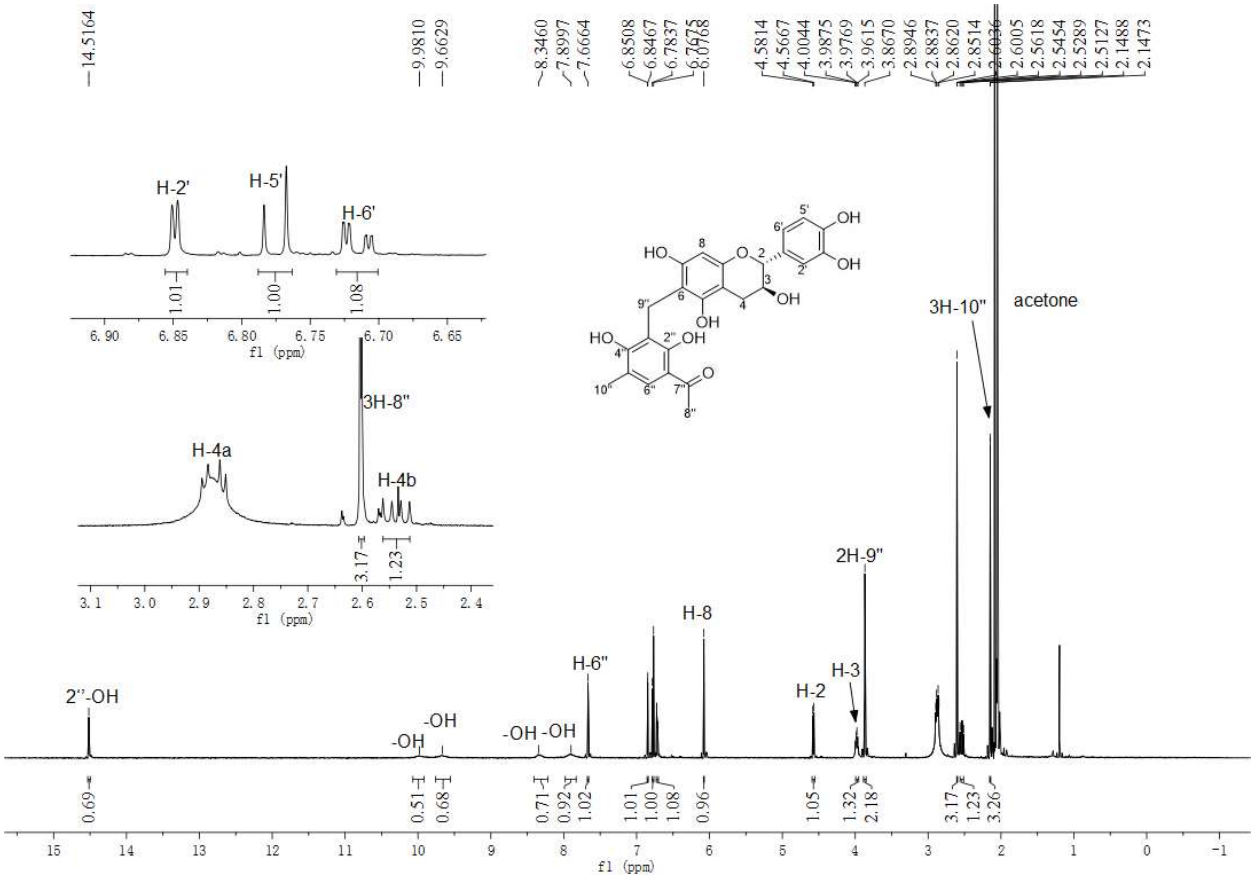

Figure S26. ^{1}H NMR spectrum of **14c** in acetone-d_6 (500 MHz).

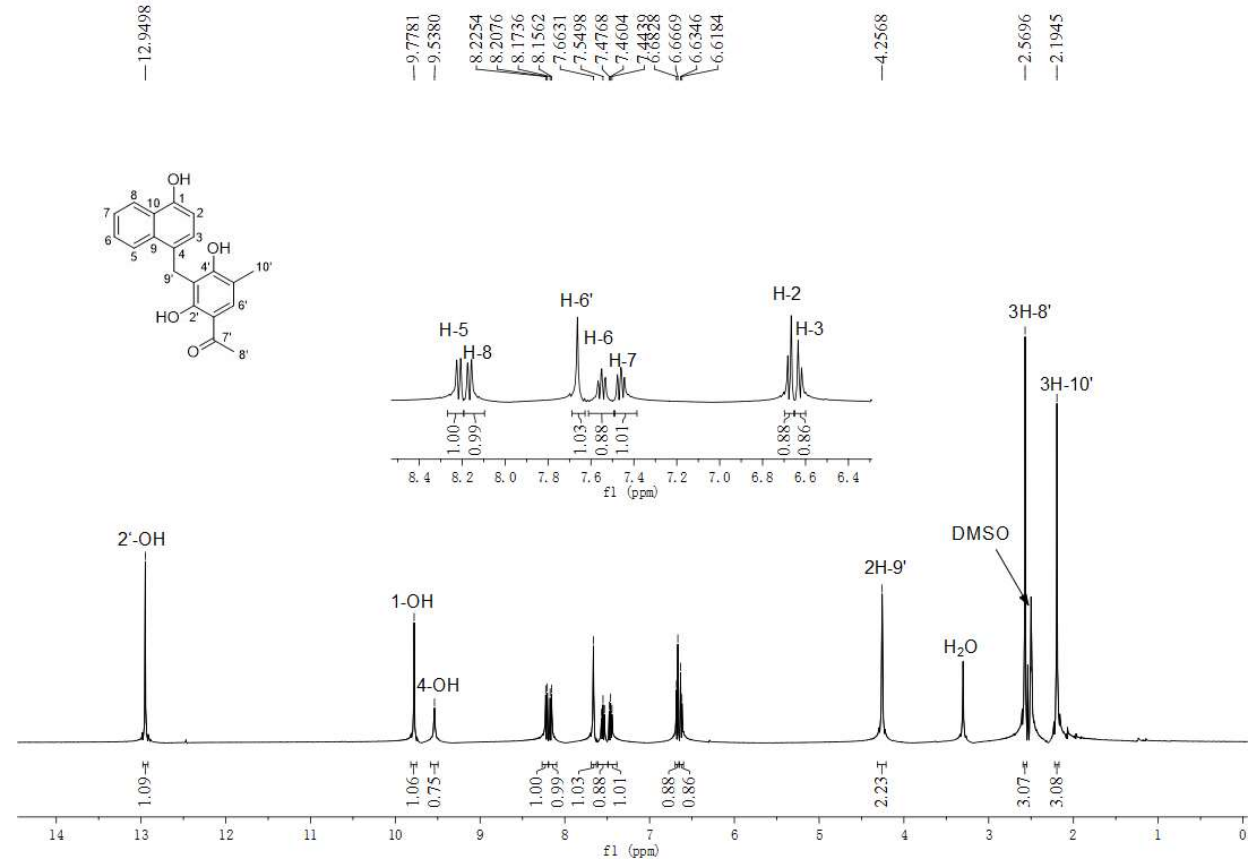

Figure S27. ^{1}H NMR spectrum of **17b** in DMSO-d_6 (500 MHz).

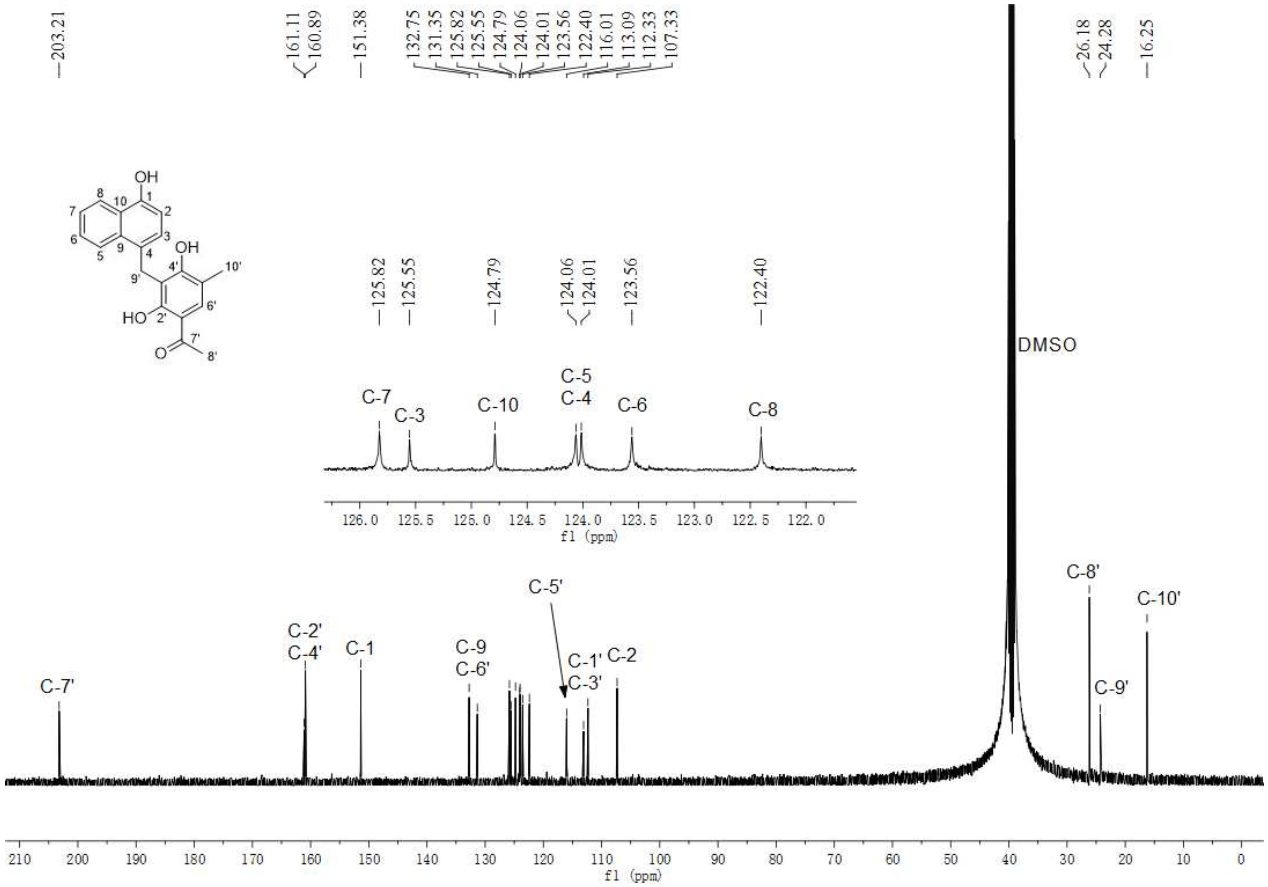

Figure S28. $^{13}C\{^{1}H\}$ NMR spectrum of **17b** in DMSO-d_6 (125 MHz).

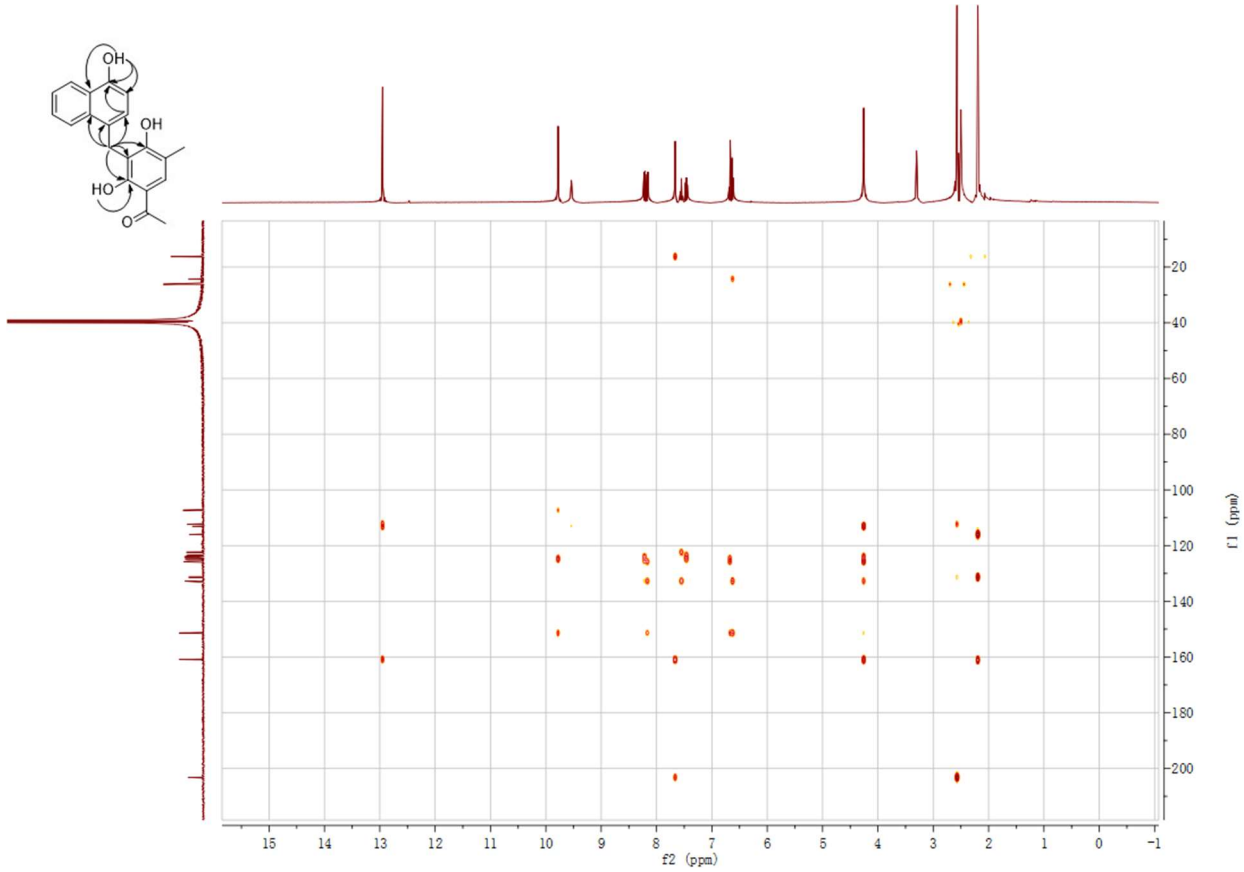

Figure S29. HMBC spectrum of **17b** in DMSO-d_6.

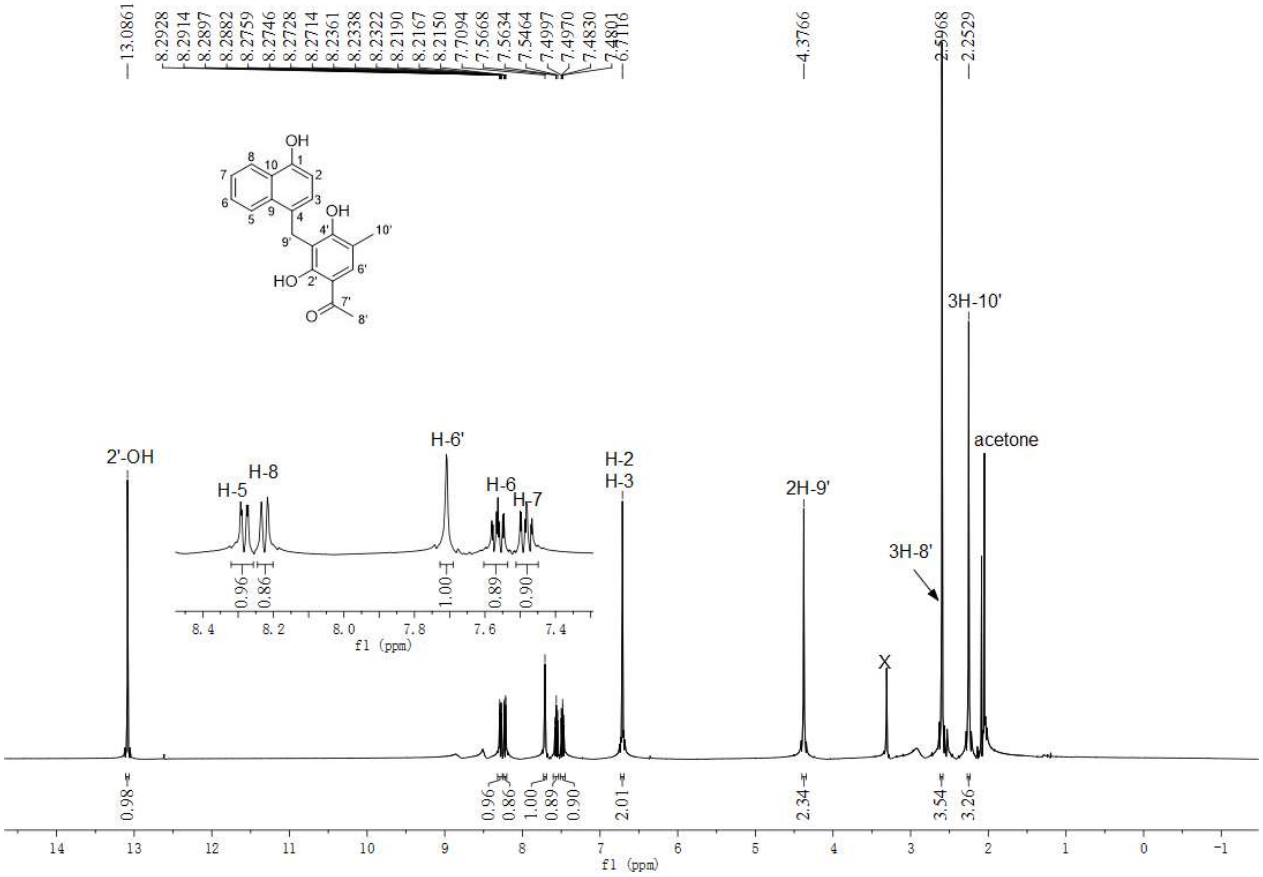

Figure S30. ^{1}H NMR spectrum of **17b** in acetone-d_6 (500 MHz).

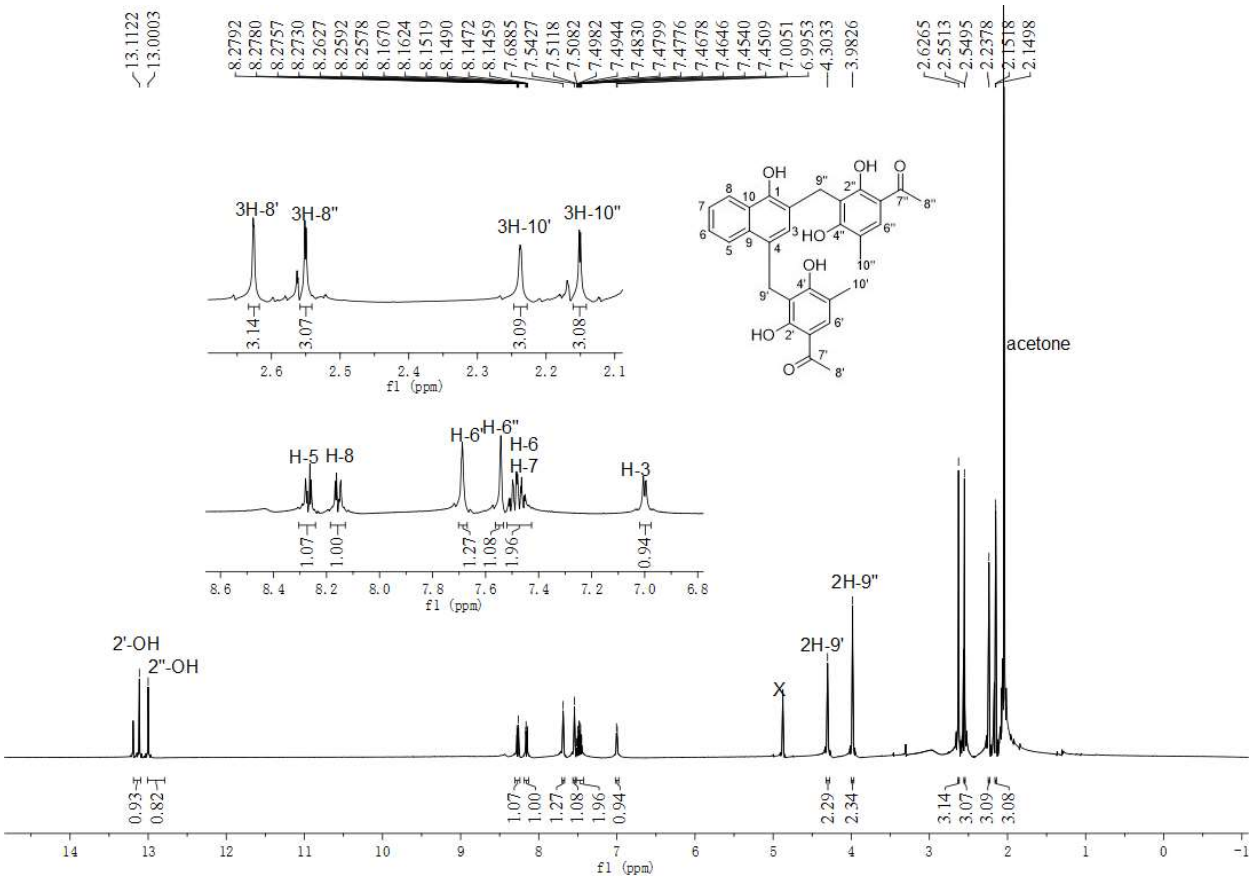

Figure S31. ^{1}H NMR spectrum of **17c** in acetone-d_6 (500 MHz).

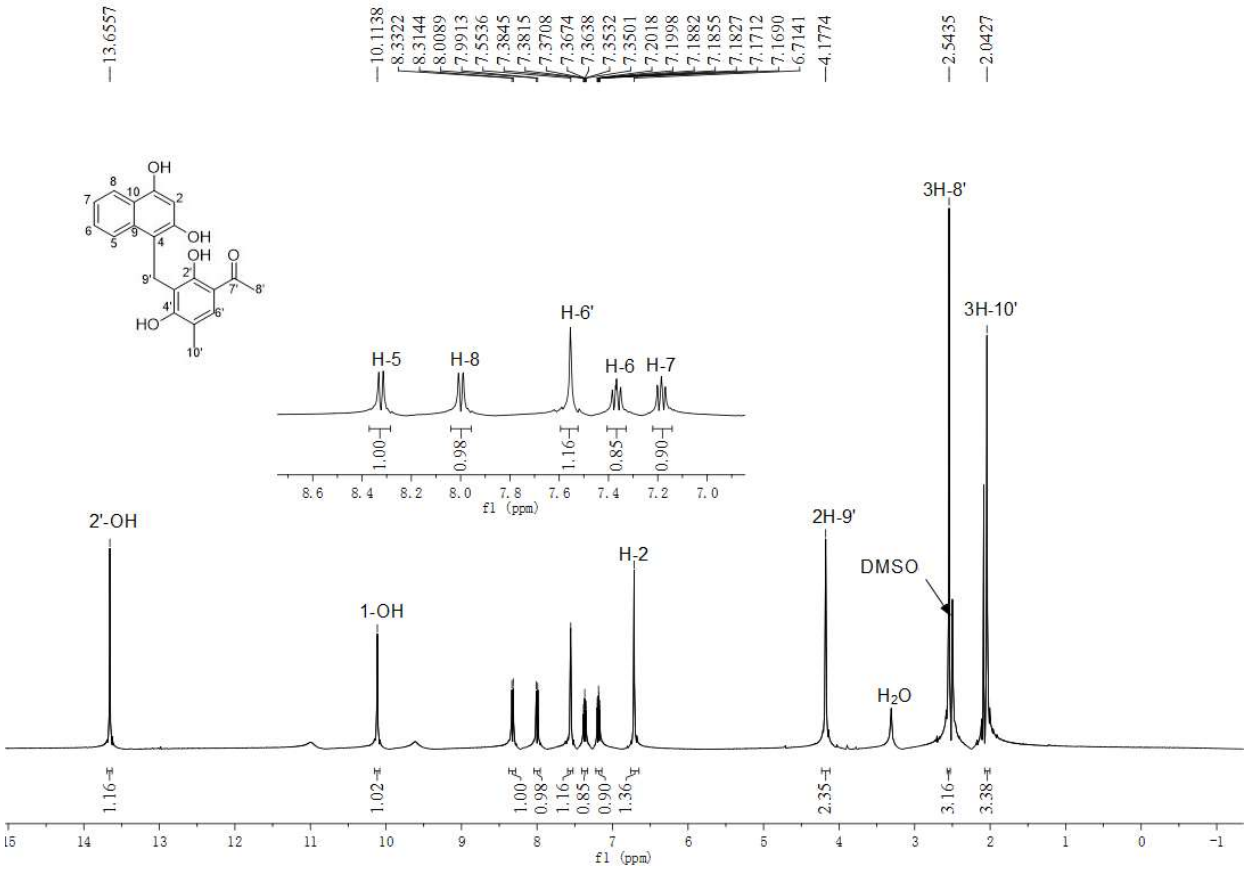

Figure S32. ^{1}H NMR spectrum of **18b** in DMSO-d_6 (500 MHz).

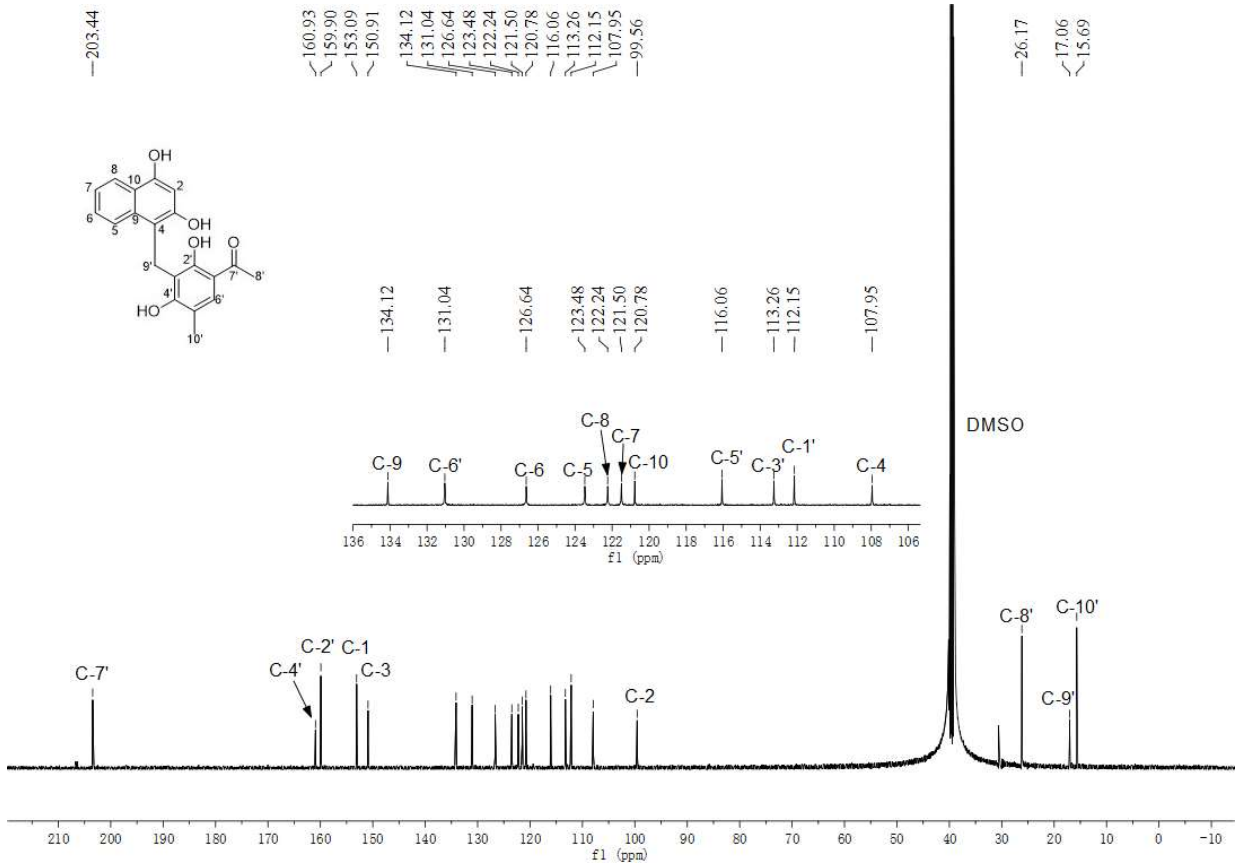

Figure S33. ^{13}C{^{1}H} NMR spectrum of **18b** in DMSO-d_6 (125 MHz).

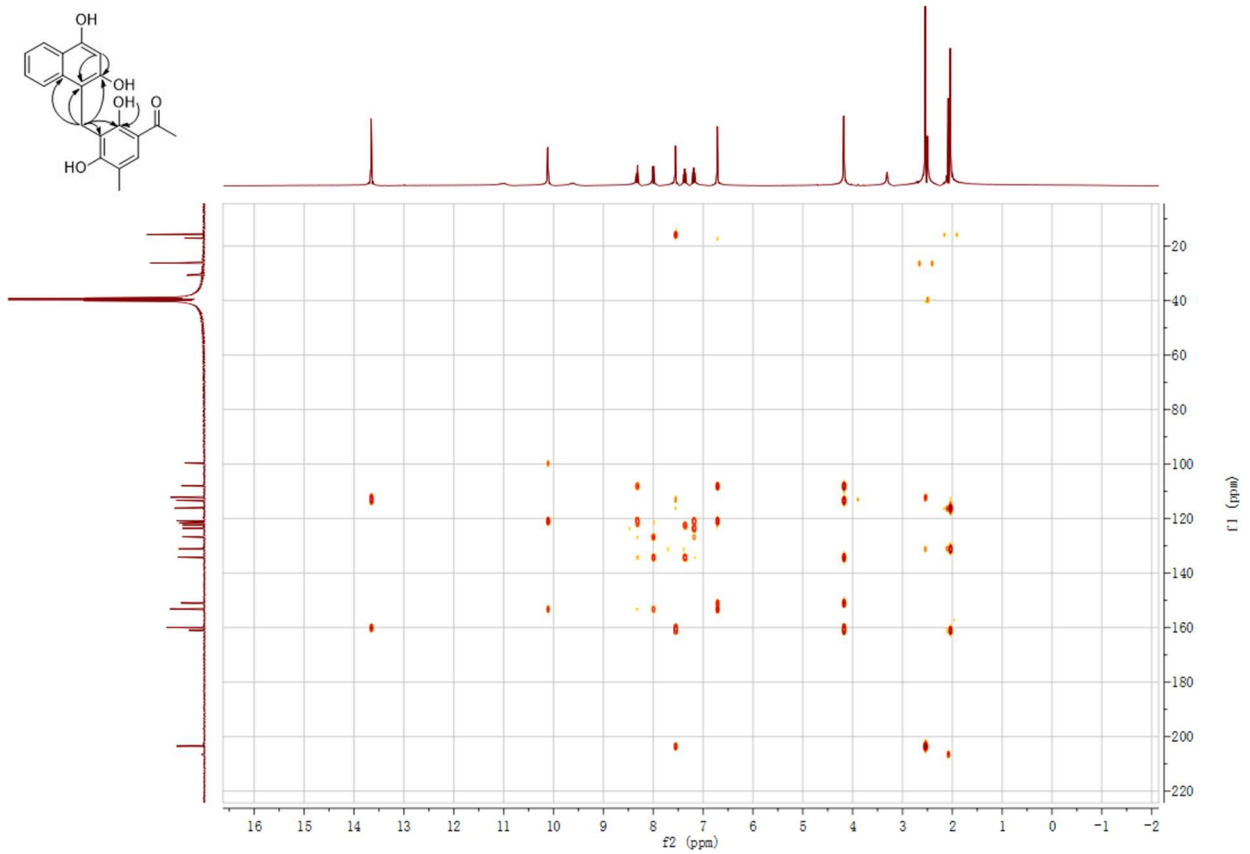

Figure S34. HMBC spectrum of **18b** in DMSO-d_6.

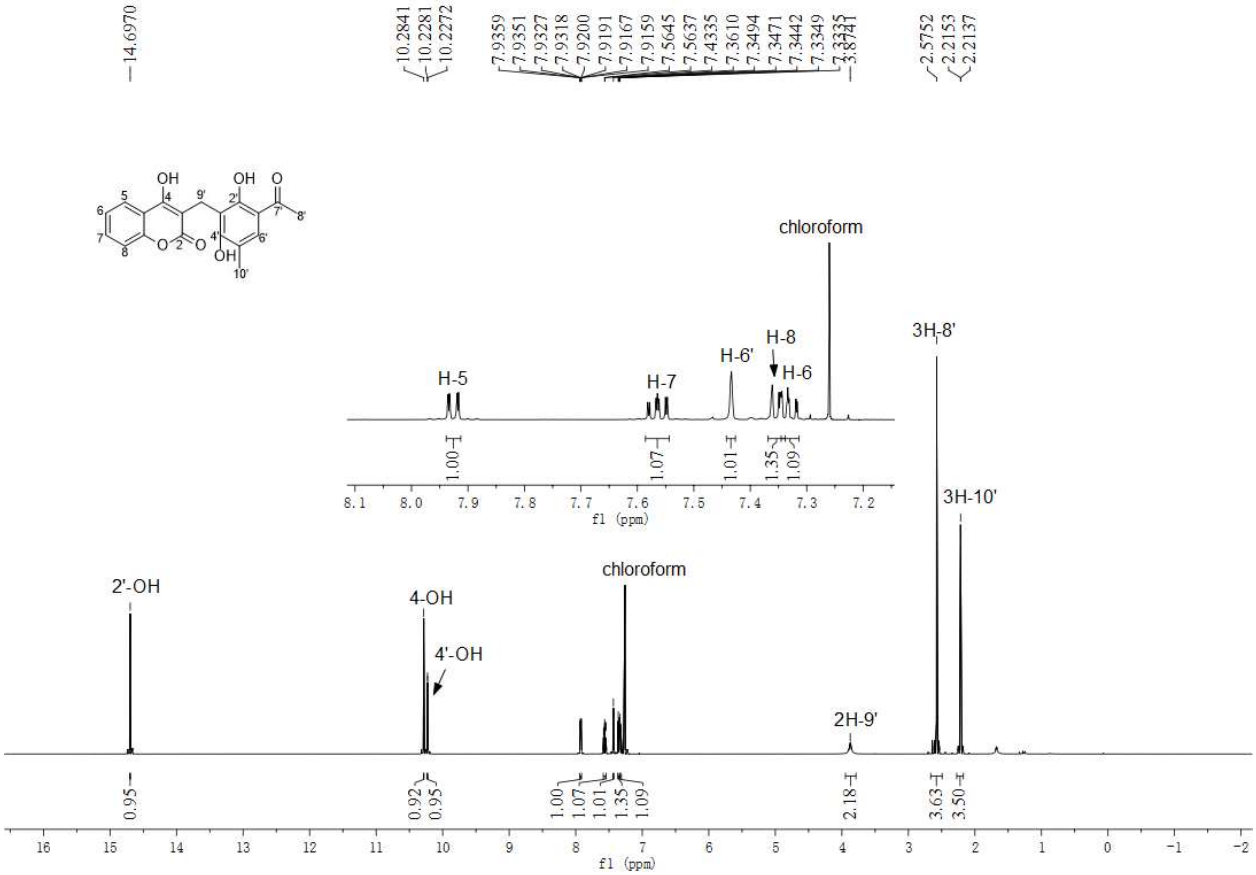

Figure S35. ^{1}H NMR spectrum of **29b** in $CDCl_3$ (500 MHz).

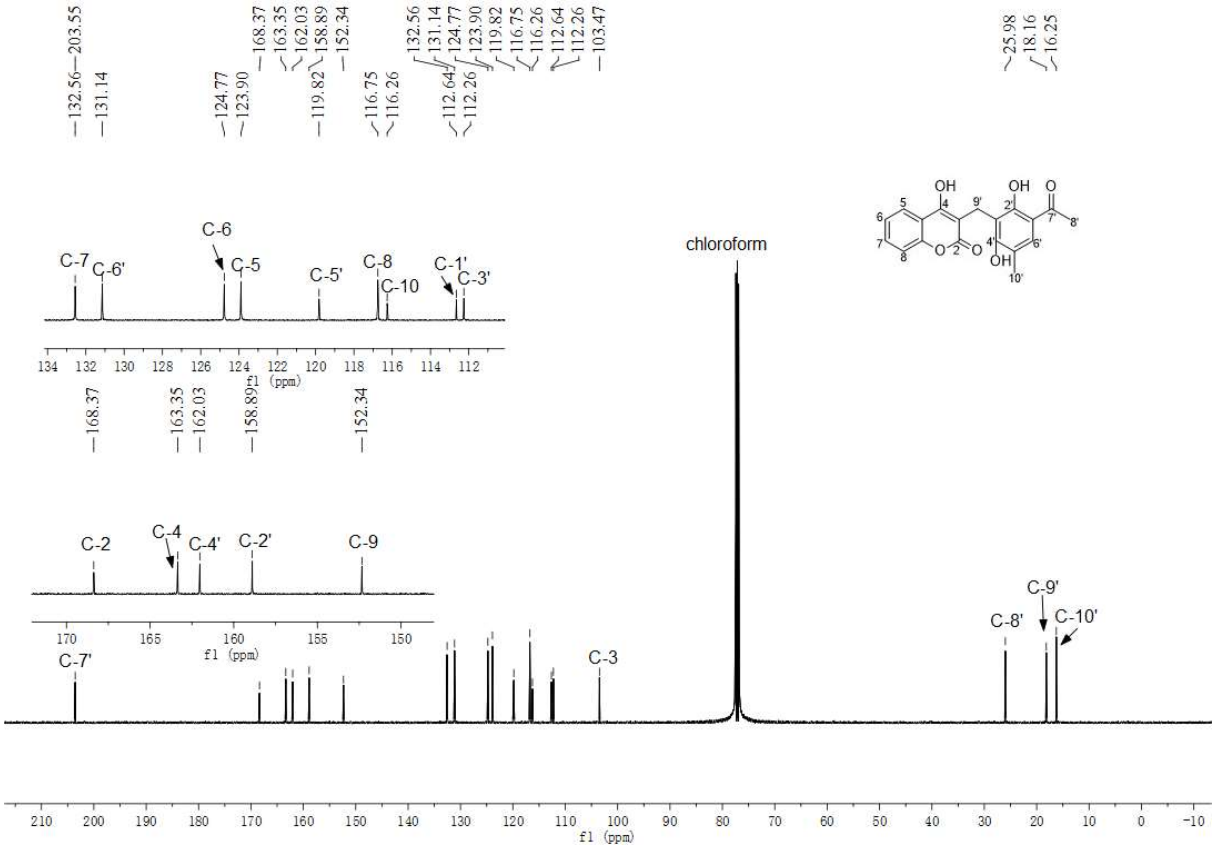

Figure S36. $^{13}C\{^{1}H\}$ NMR spectrum of **29b** in $CDCl_3$ (125 MHz).

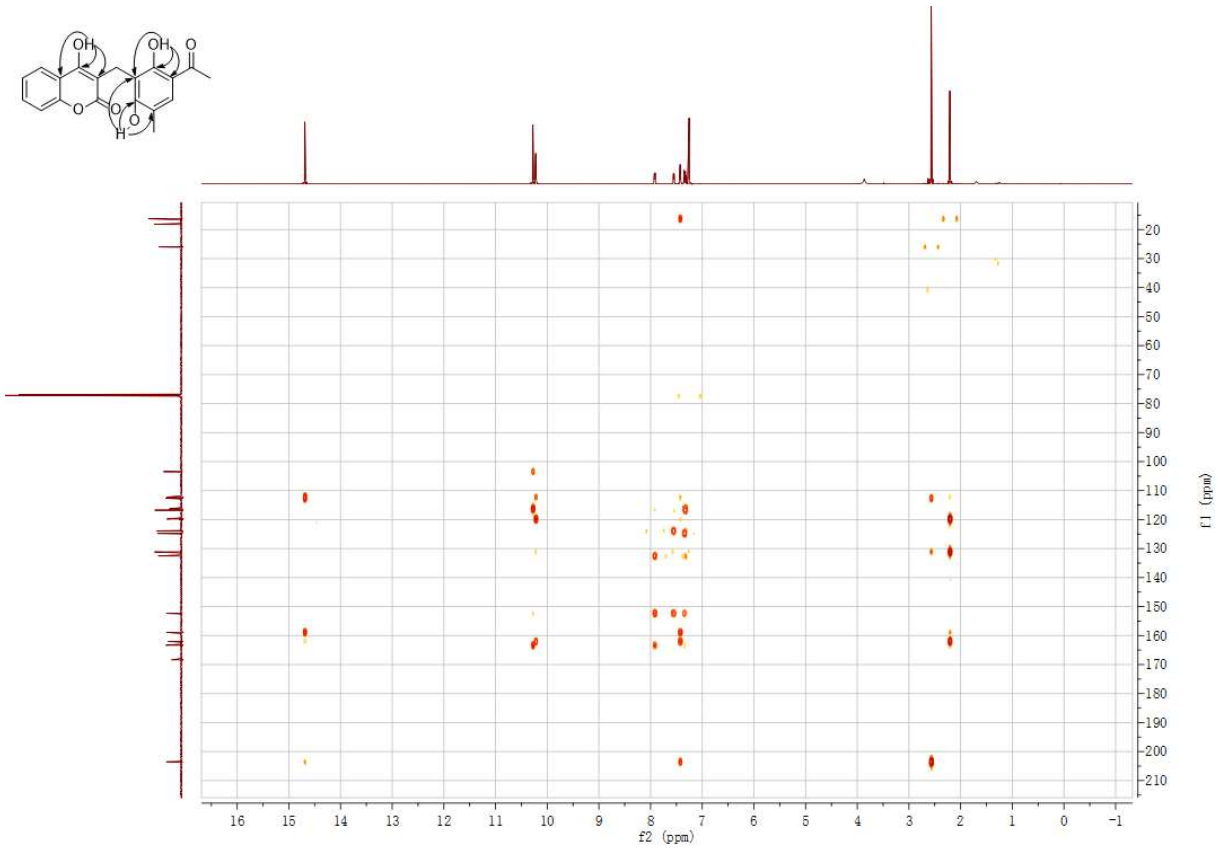

Figure S37. HMBC spectrum of **29b** in $CDCl_3$.

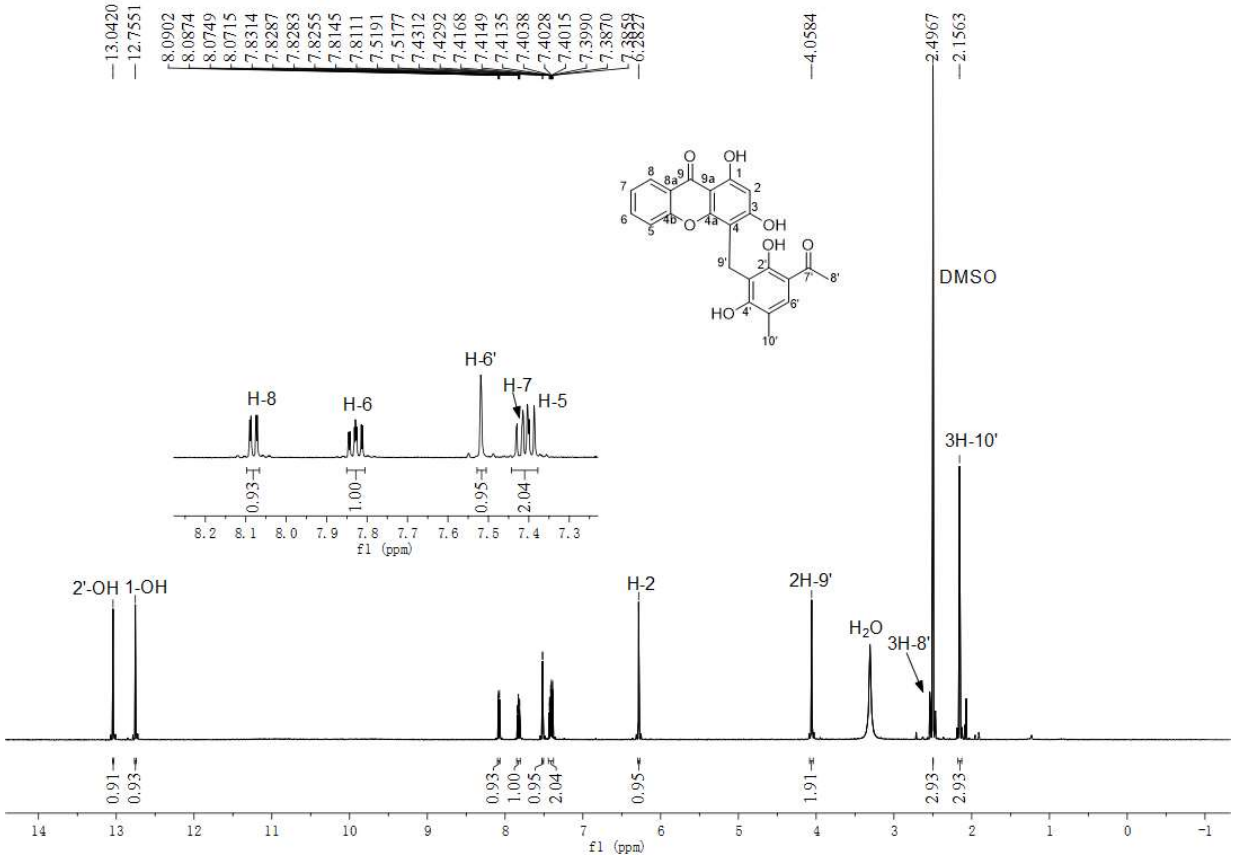

Figure S38. ^{1}H NMR spectrum of **35b** in DMSO-d_6 (500 MHz).

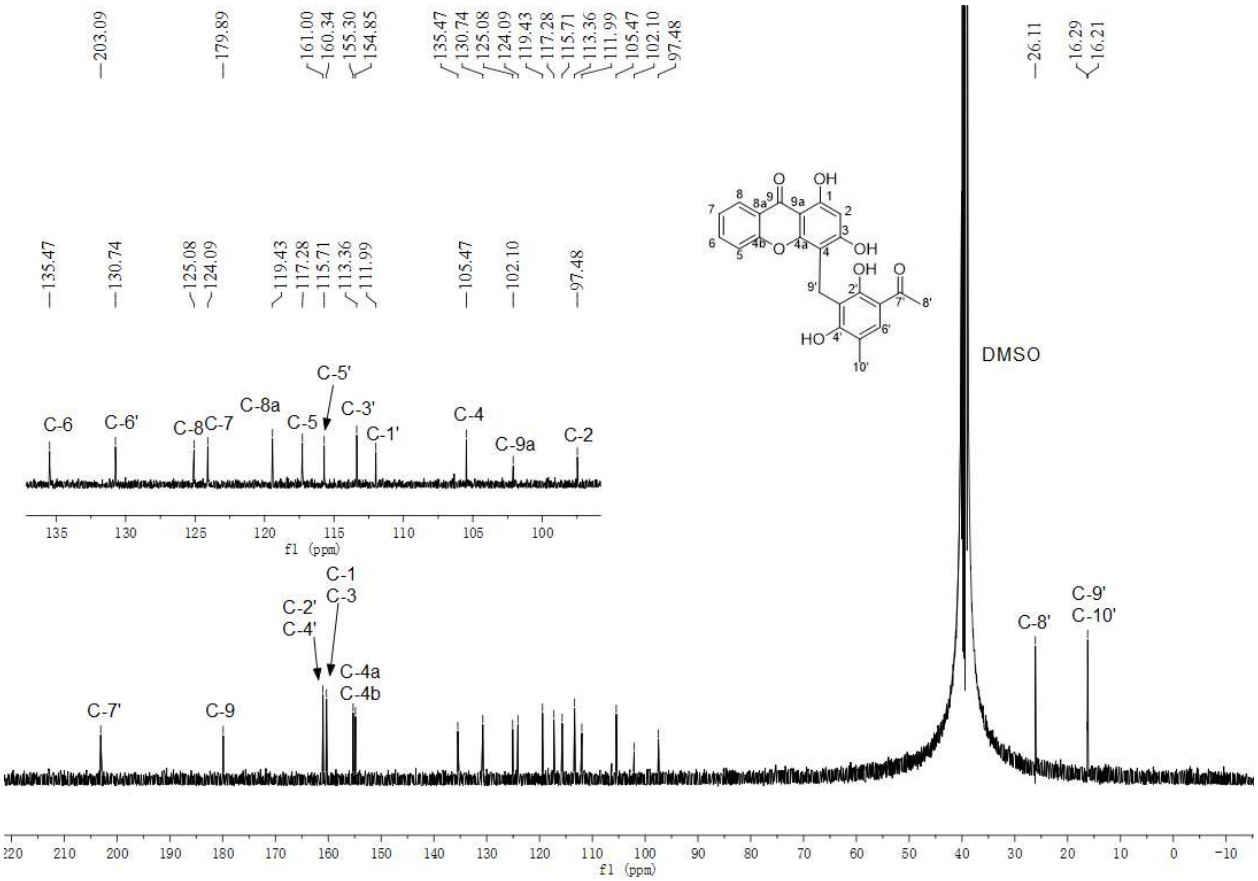

Figure S39. ^{13}C{^{1}H} NMR spectrum of **35b** in DMSO-d_6 (125 MHz).

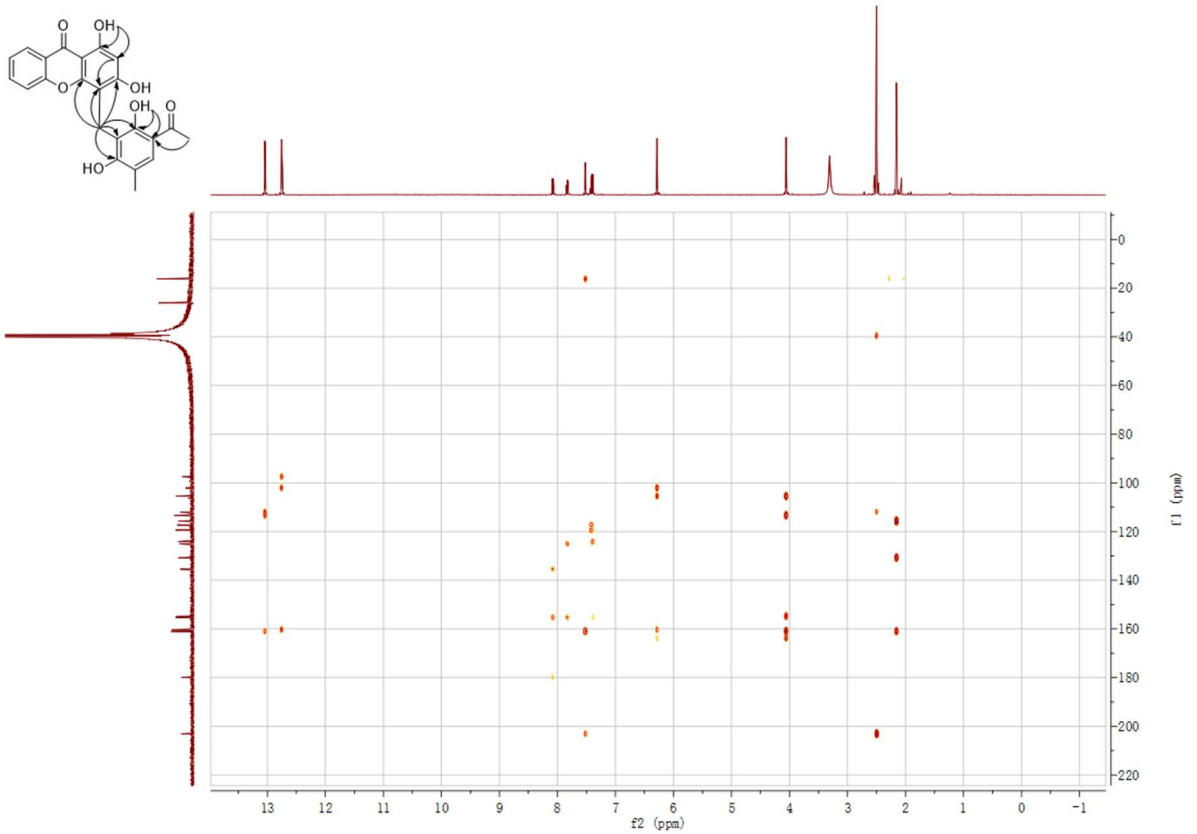

Figure S40. HMBC spectrum of **35b** in DMSO-d_6.

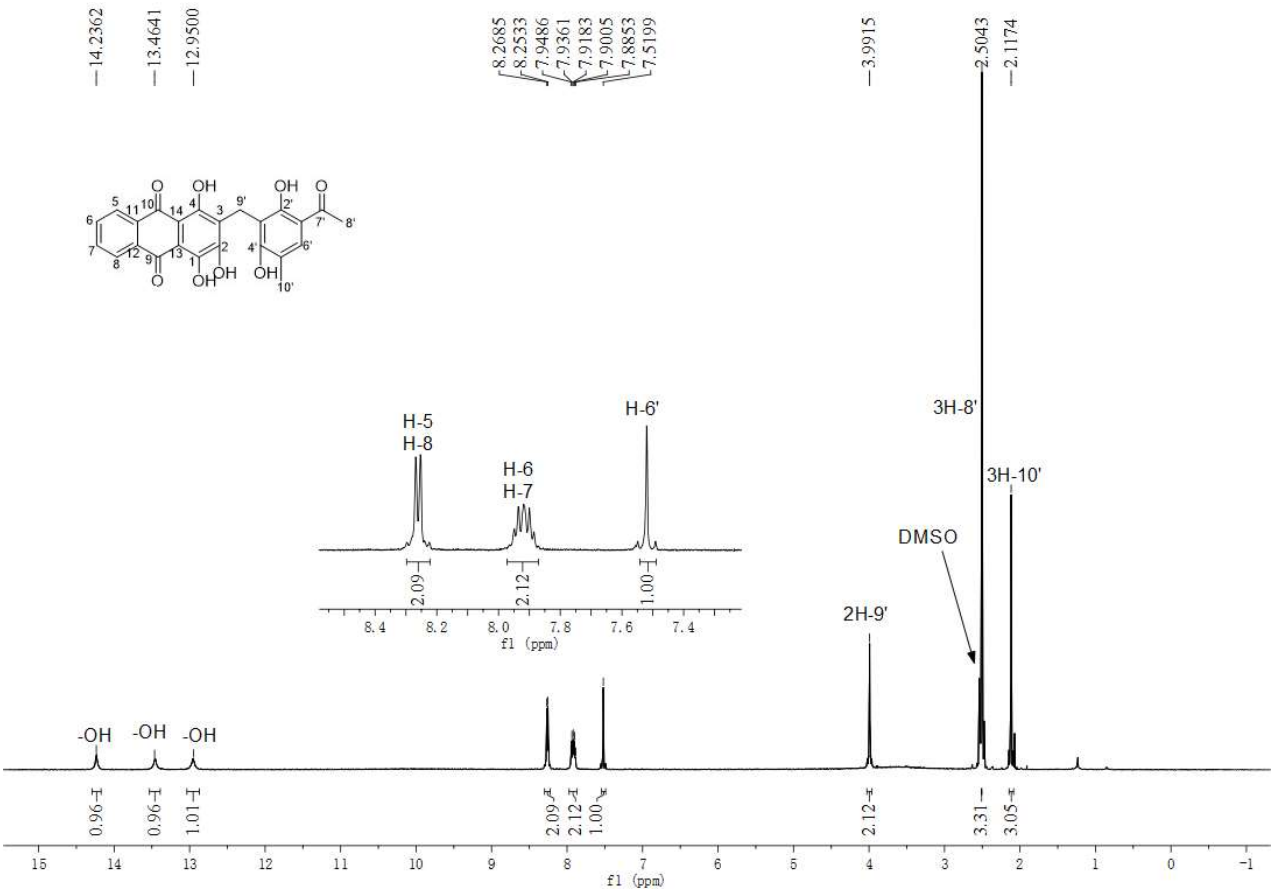

Figure S41. ^{1}H NMR spectrum of **41b** in DMSO-d_6 (500 MHz).

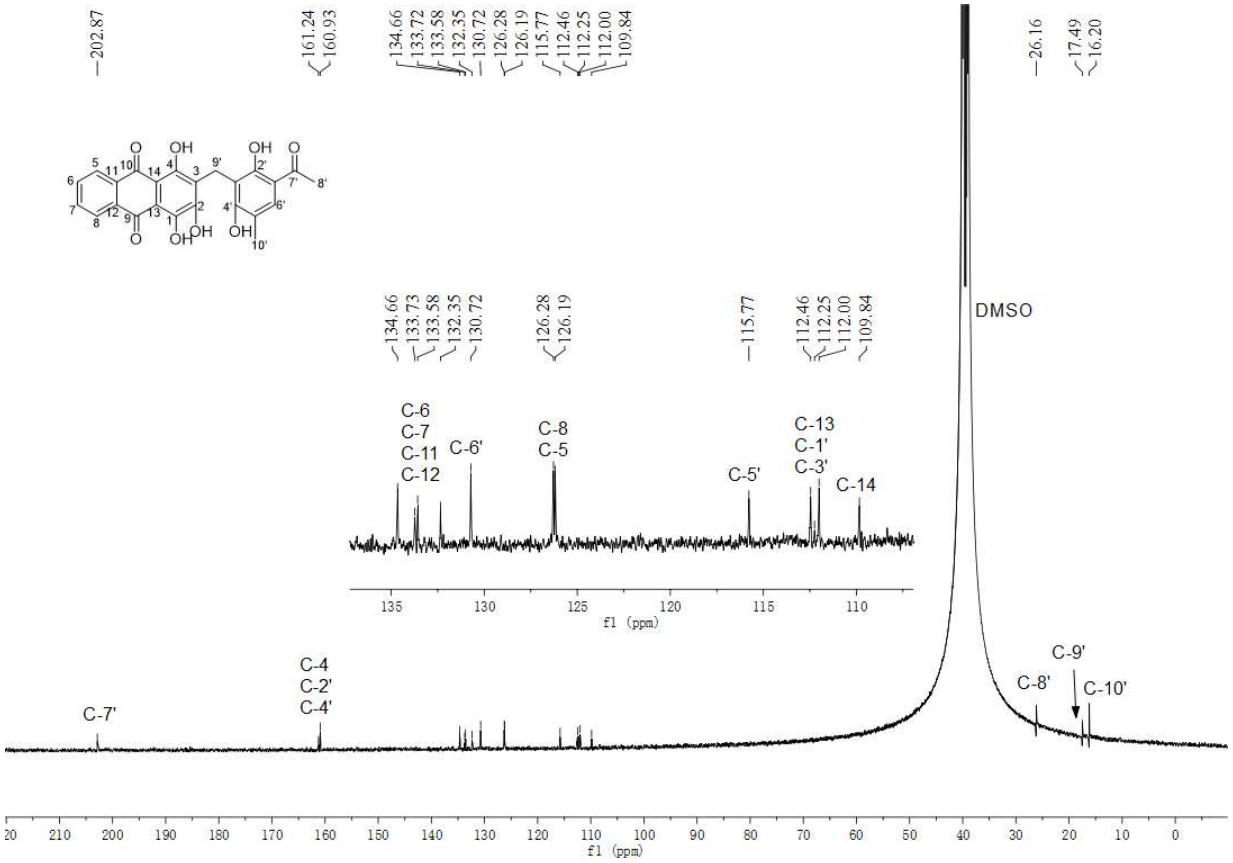

Figure S42. $^{13}C\{^{1}H\}$ NMR spectrum of **41b** in DMSO-d_6 (125 MHz).

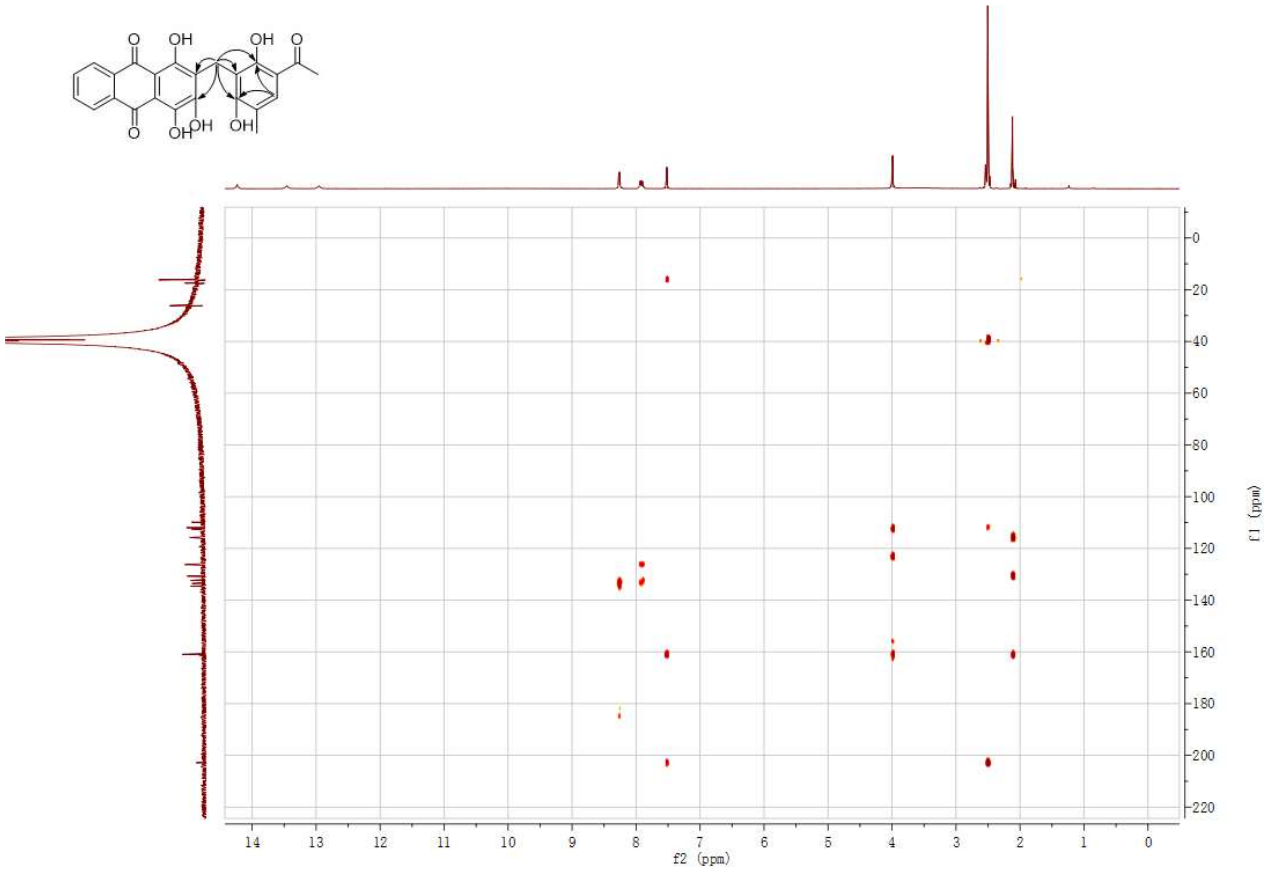

Figure S43. HMBC spectrum of **41b** in DMSO-d_6.

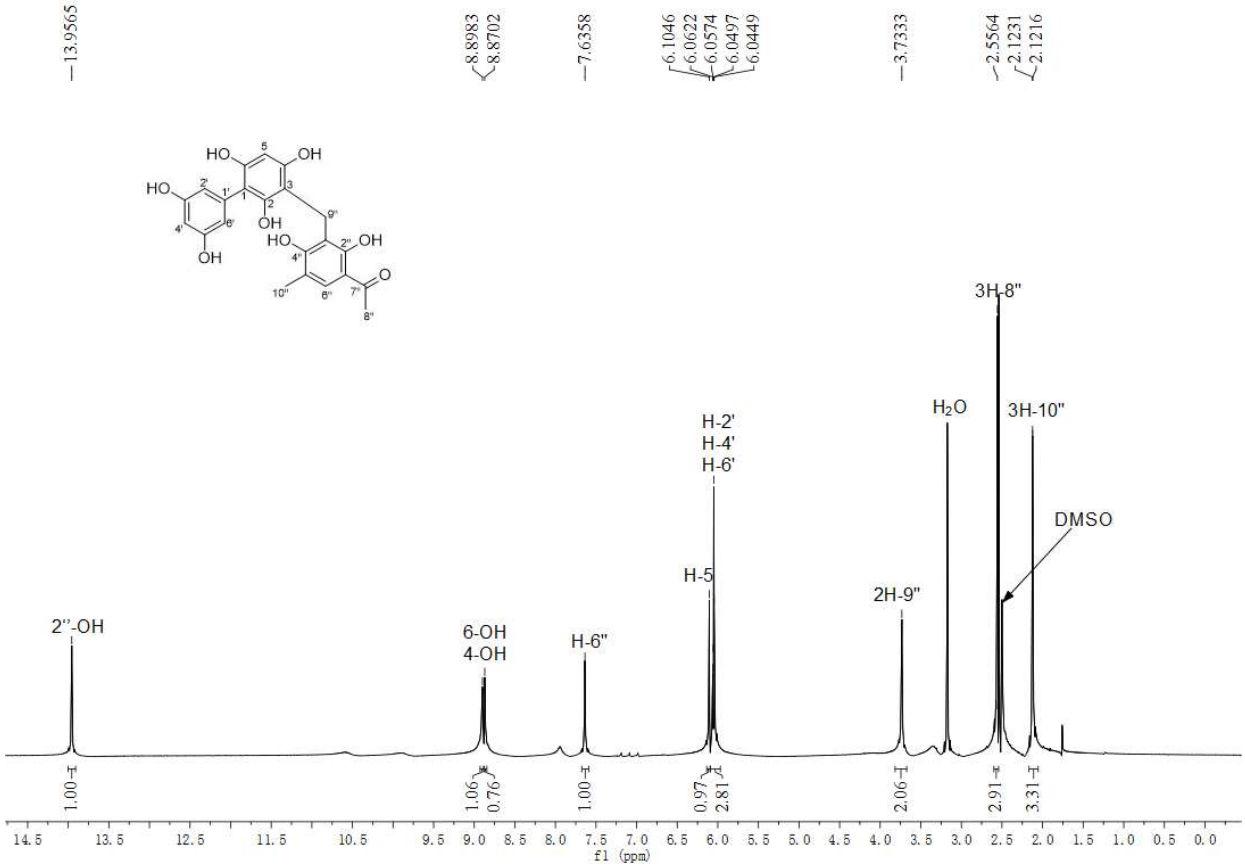

Figure S44. ^{1}H NMR spectrum of **44b** in DMSO-d_6 (500 MHz).

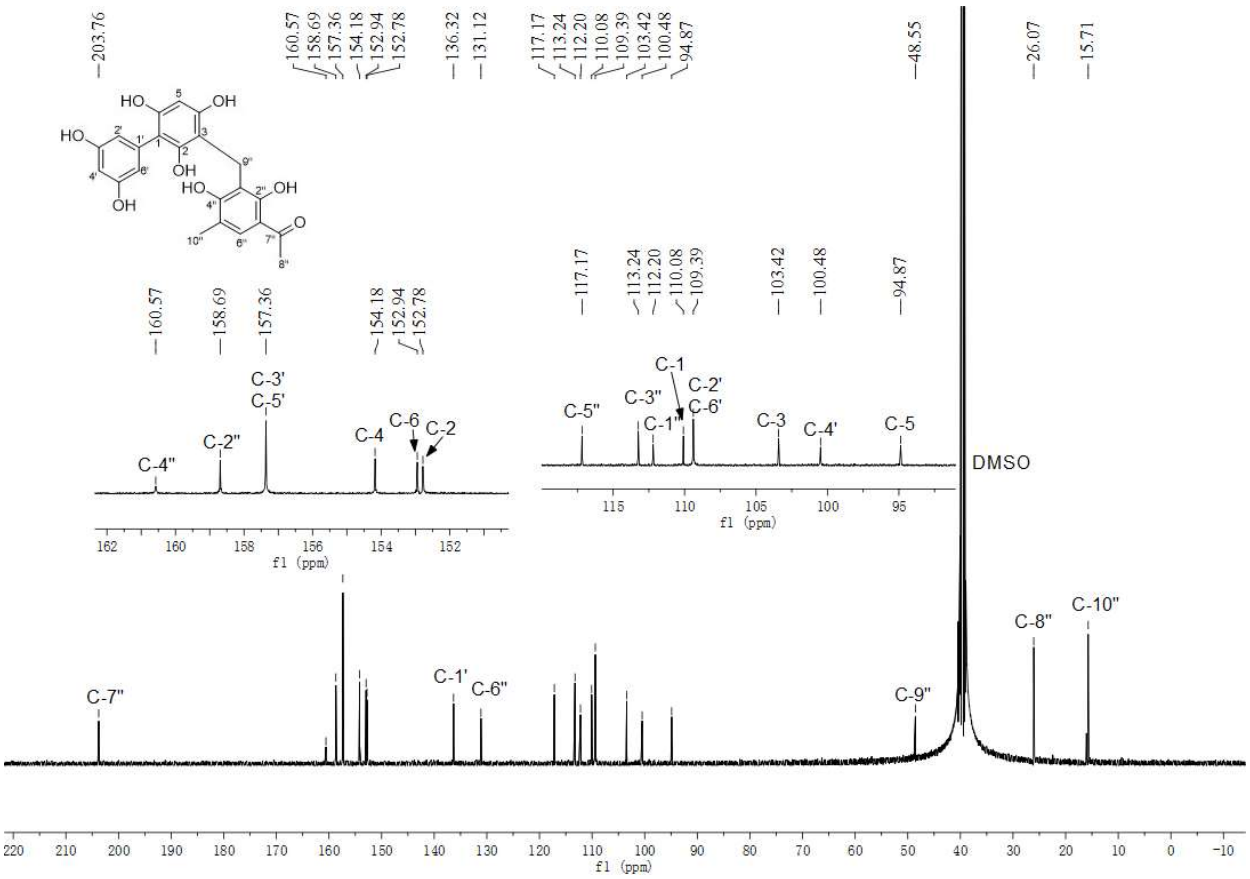

Figure S45. ^{13}C{^{1}H} NMR spectrum of **44b** in DMSO-d_6 (125 MHz).

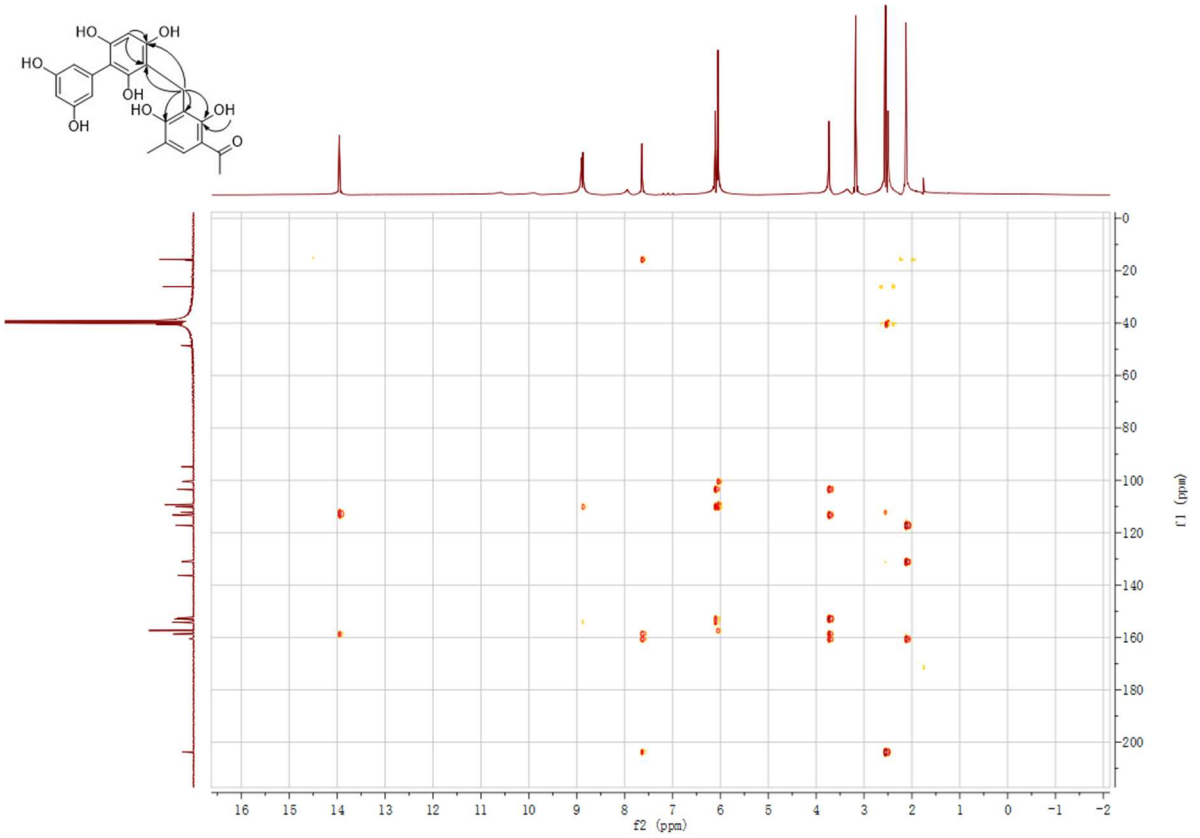

Figure S46. HMBC spectrum of **44b** in DMSO-d_6.

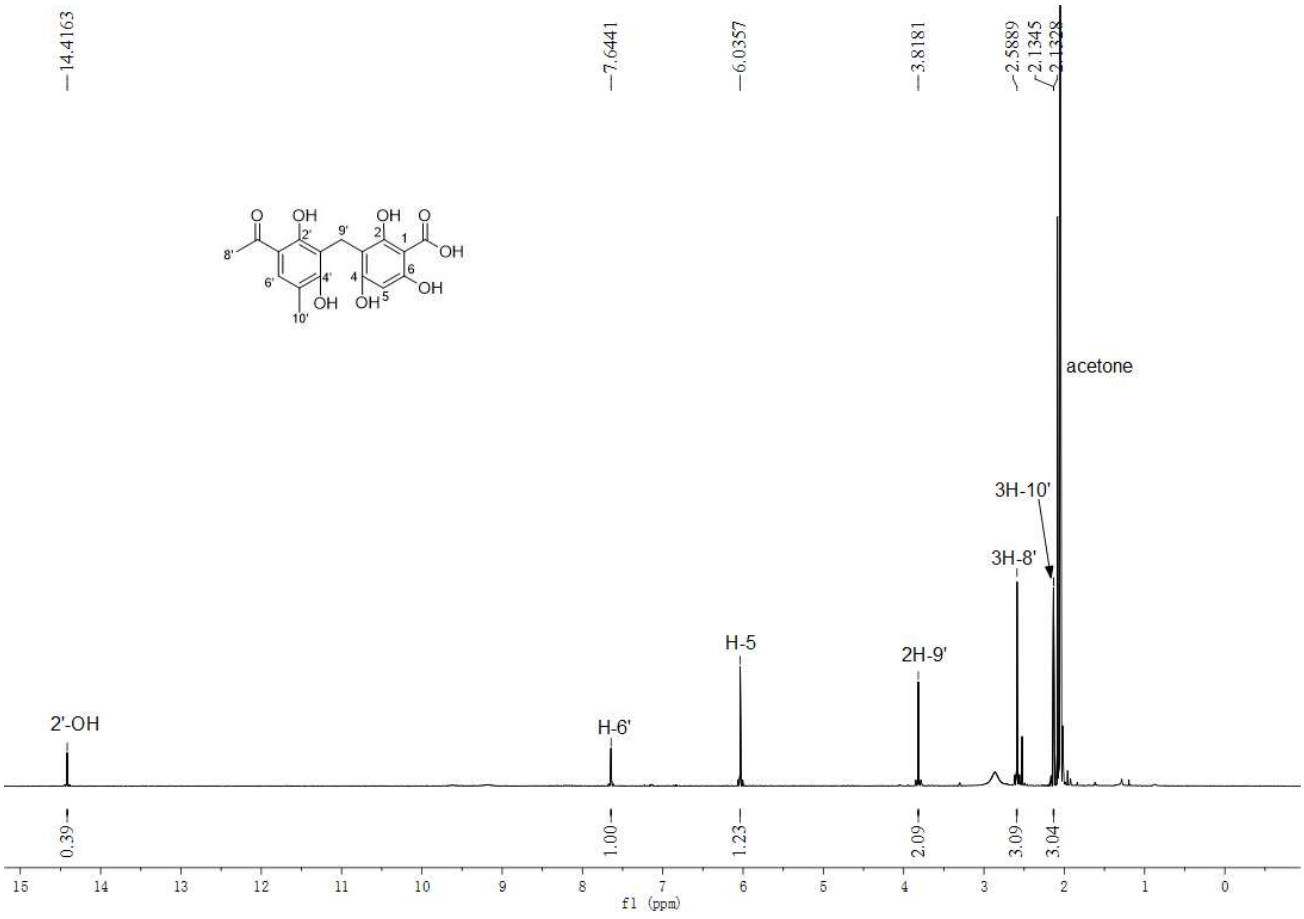

Figure S47. ^{1}H NMR spectrum of **45b** in acetone-d_6 (500 MHz).

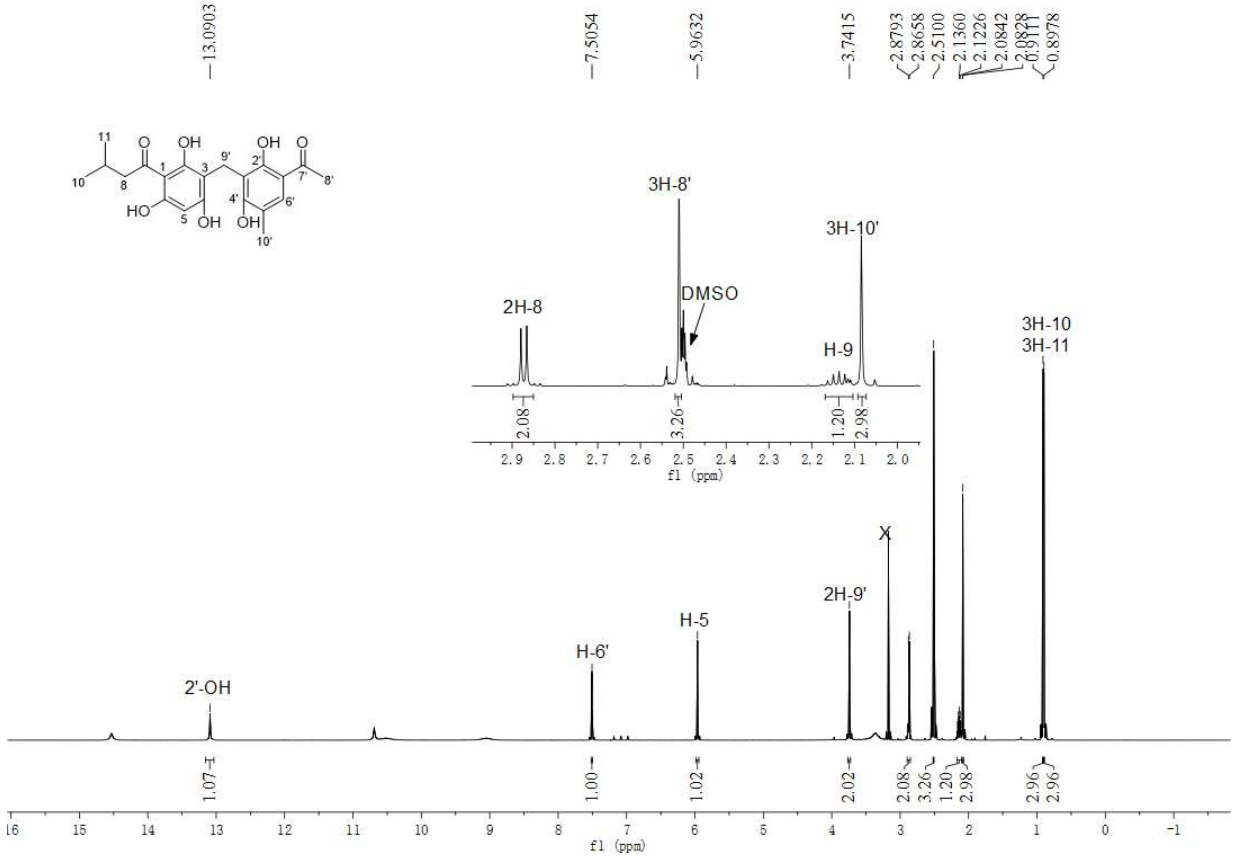

Figure S48. ^{1}H NMR spectrum of **47b** in DMSO-d_6 (500 MHz).

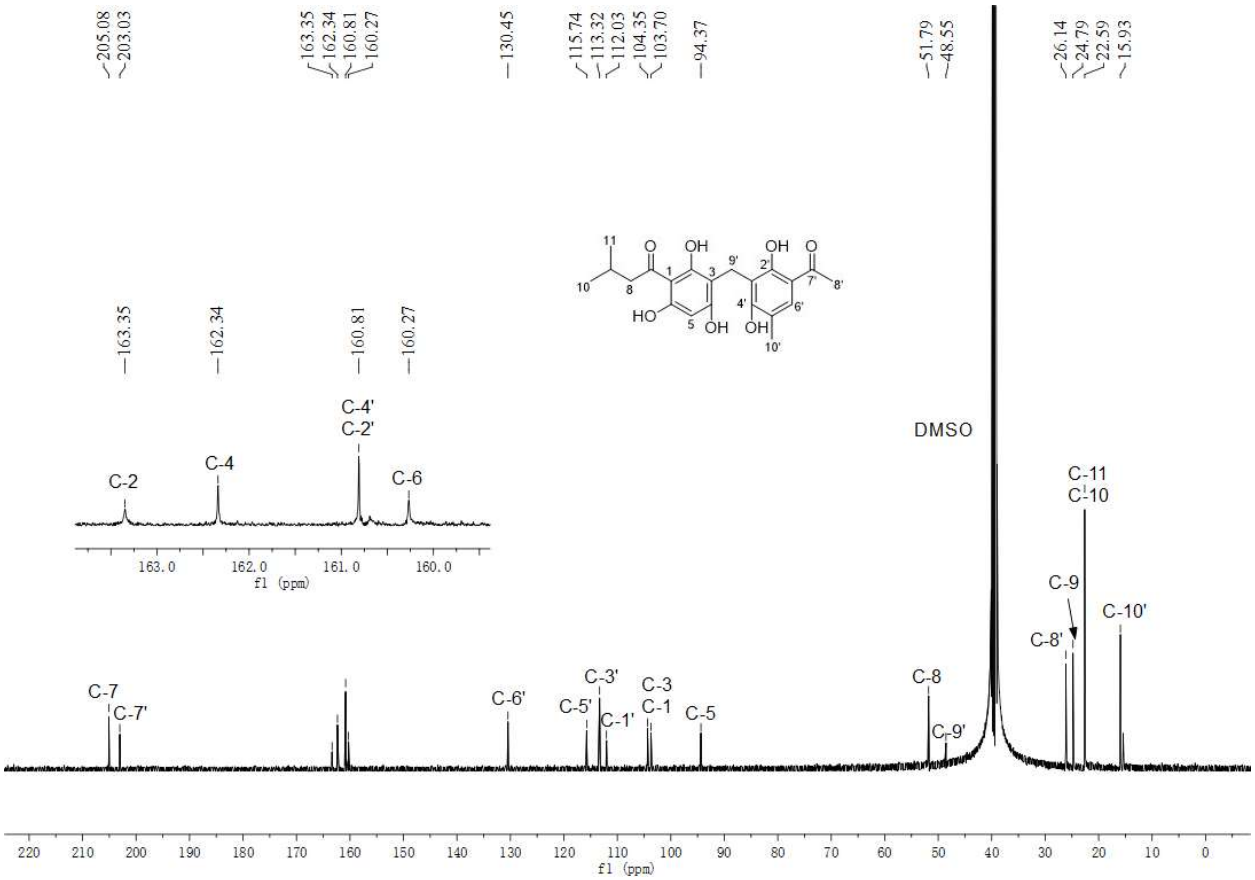

Figure S49. ^{13}C{^{1}H} NMR spectrum of **47b** in DMSO-d_6 (125 MHz).

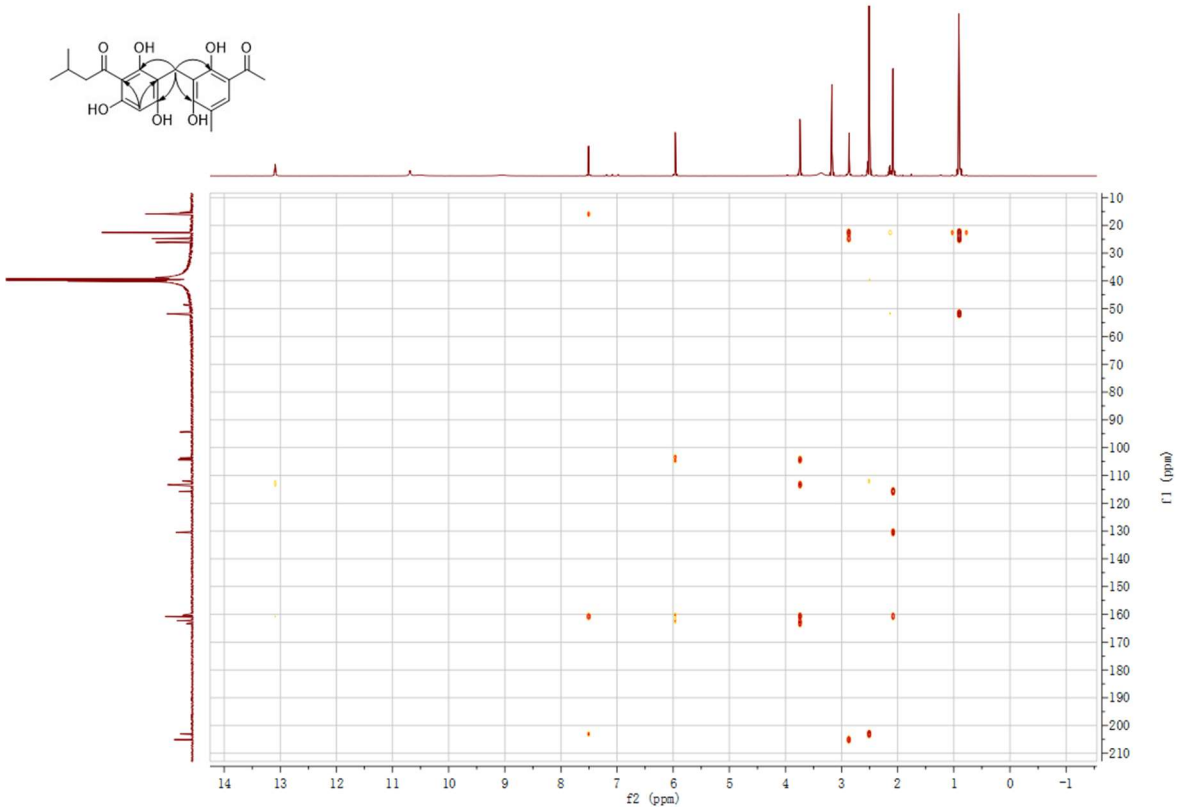

Figure S50. HMBC spectrum of **47b** in DMSO-d_6.

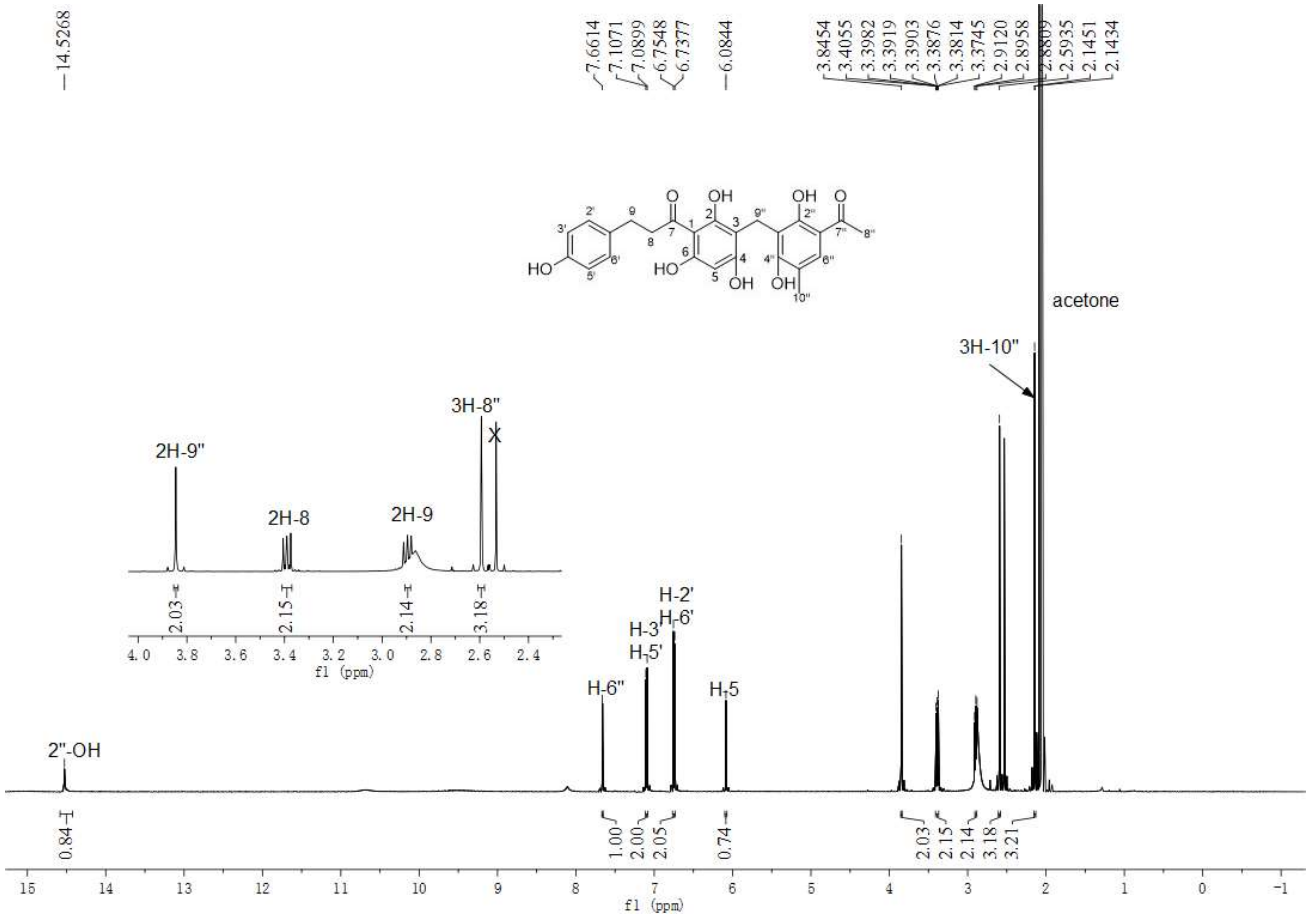

Figure S51. ^{1}H NMR spectrum of **50b** in acetone-d_6 (500 MHz).

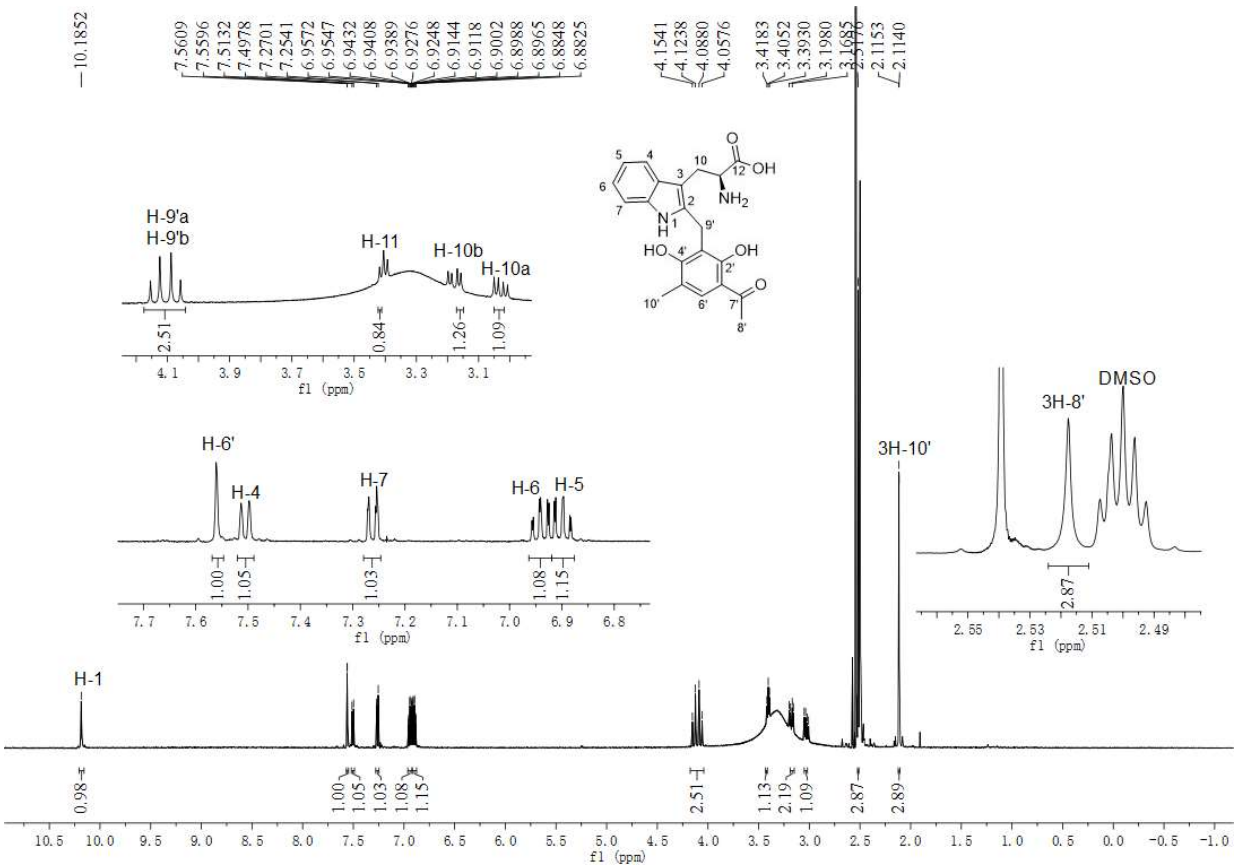

Figure S52. ^{1}H NMR spectrum of **61b** in DMSO-d_6 (500 MHz).

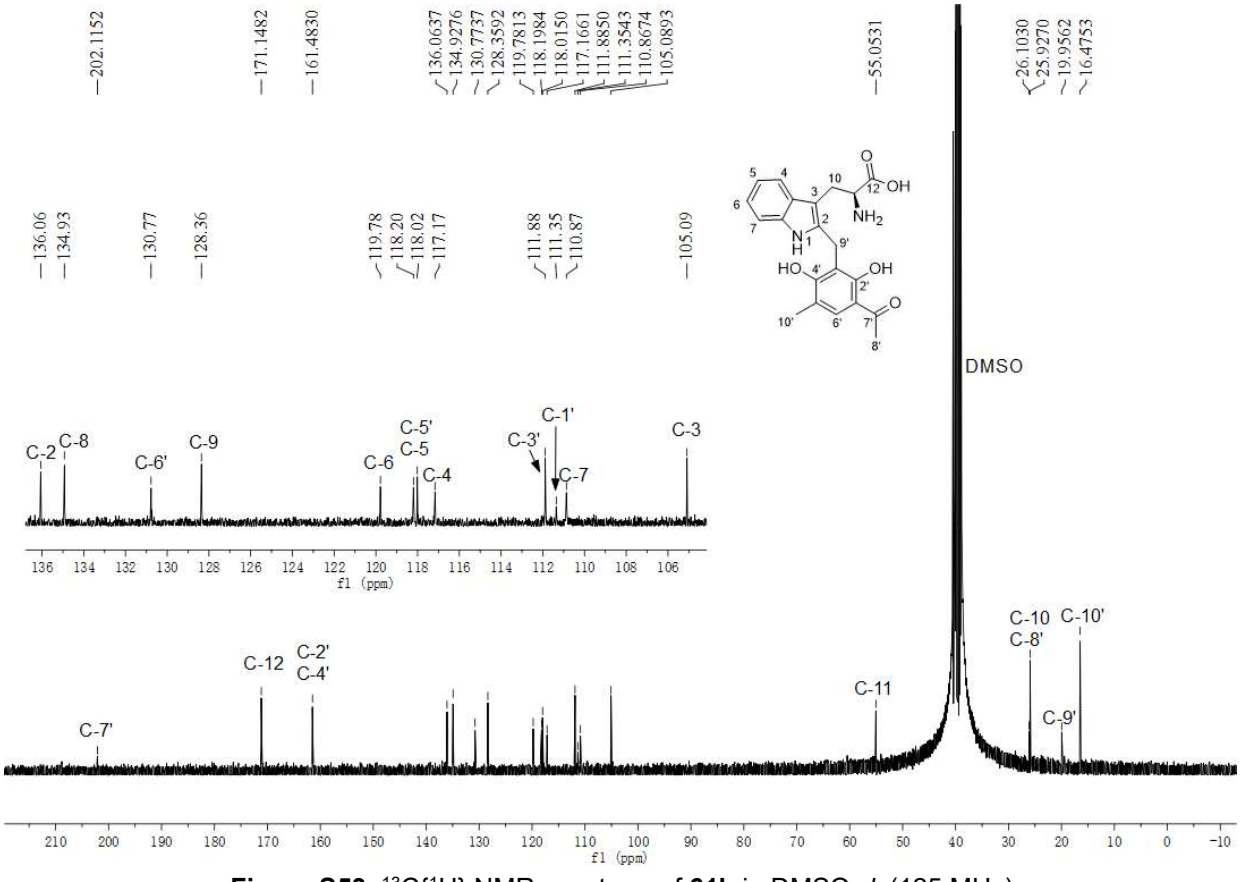

Figure S53. ^{13}C{^{1}H} NMR spectrum of **61b** in DMSO-d_6 (125 MHz).

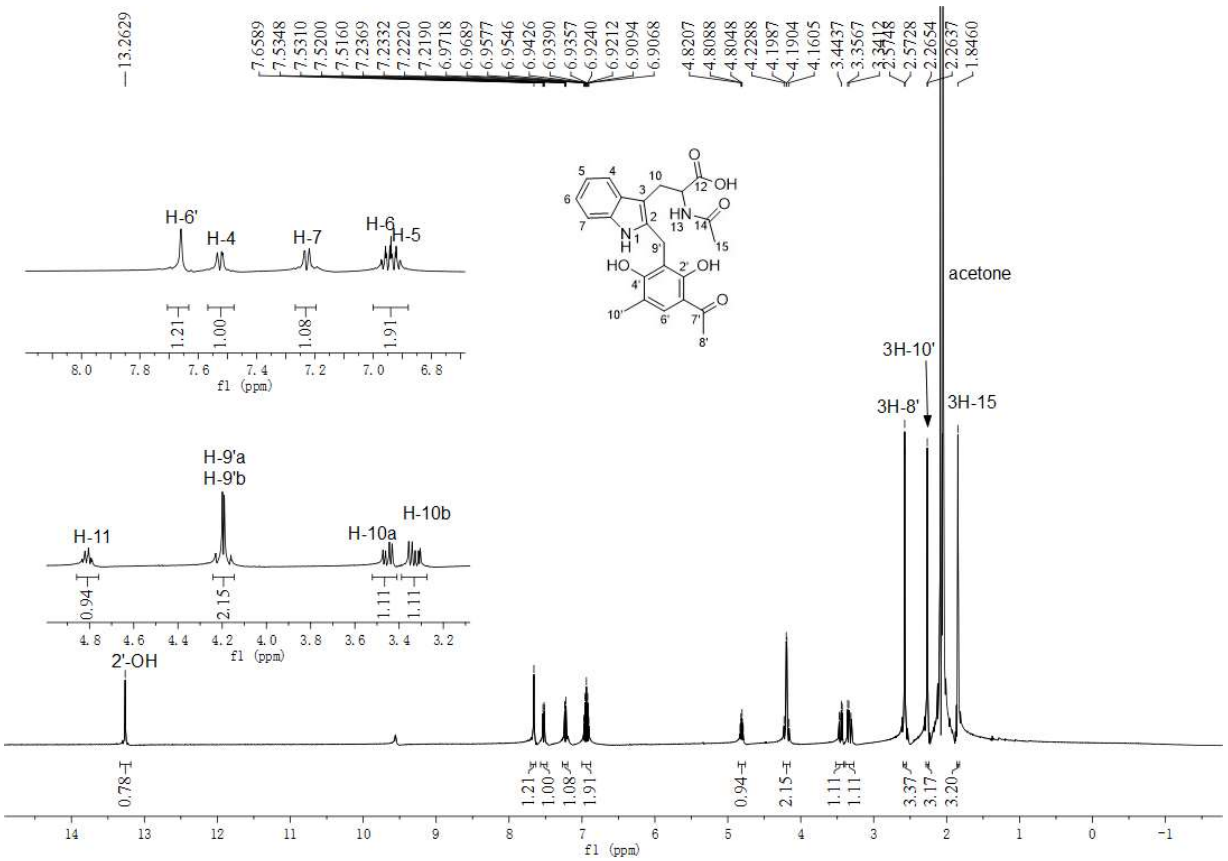

Figure S54. ^{1}H NMR spectrum of (±)-**65b** in acetone-d_6 (500 MHz).

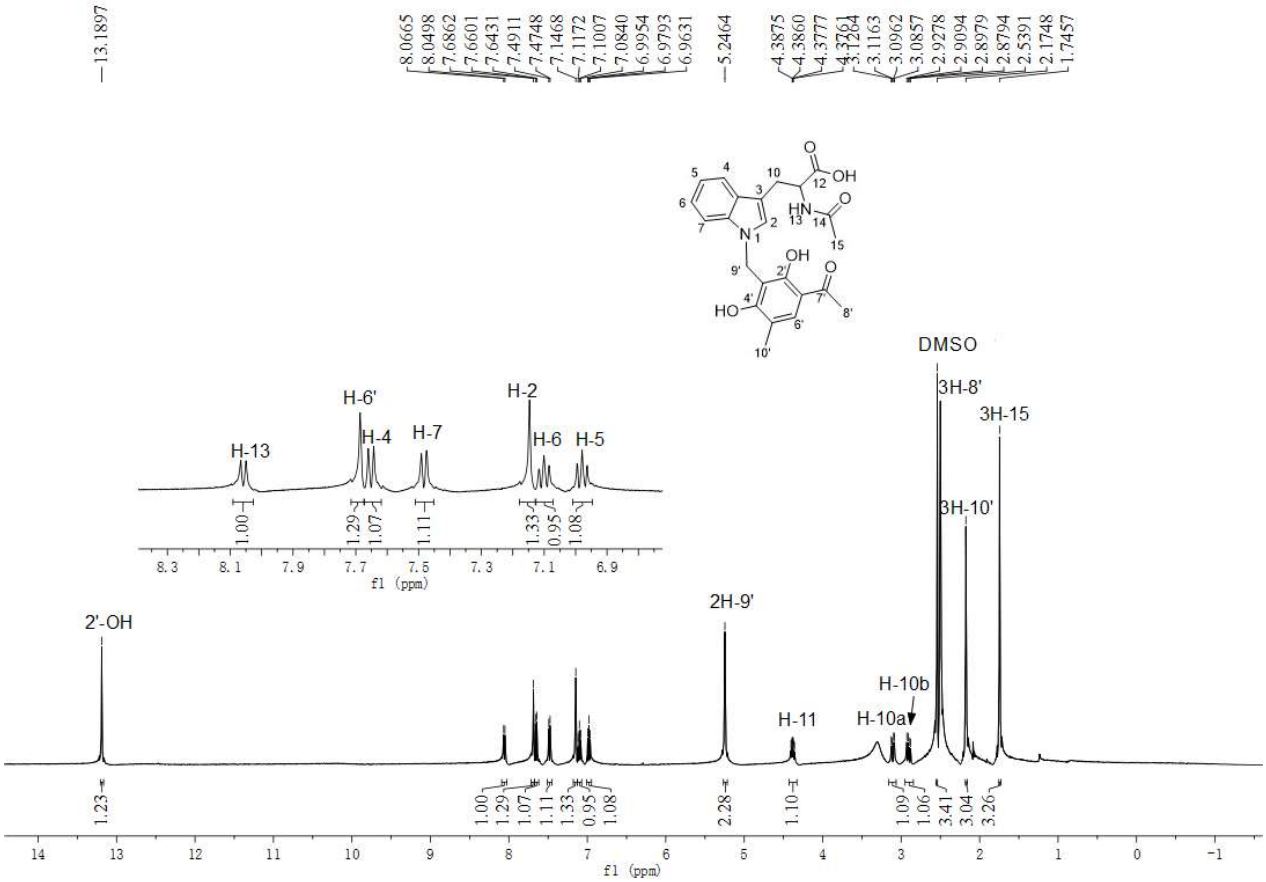

Figure S55. ^{1}H NMR spectrum of (±)-**65c** in DMSO-d_6 (500 MHz).

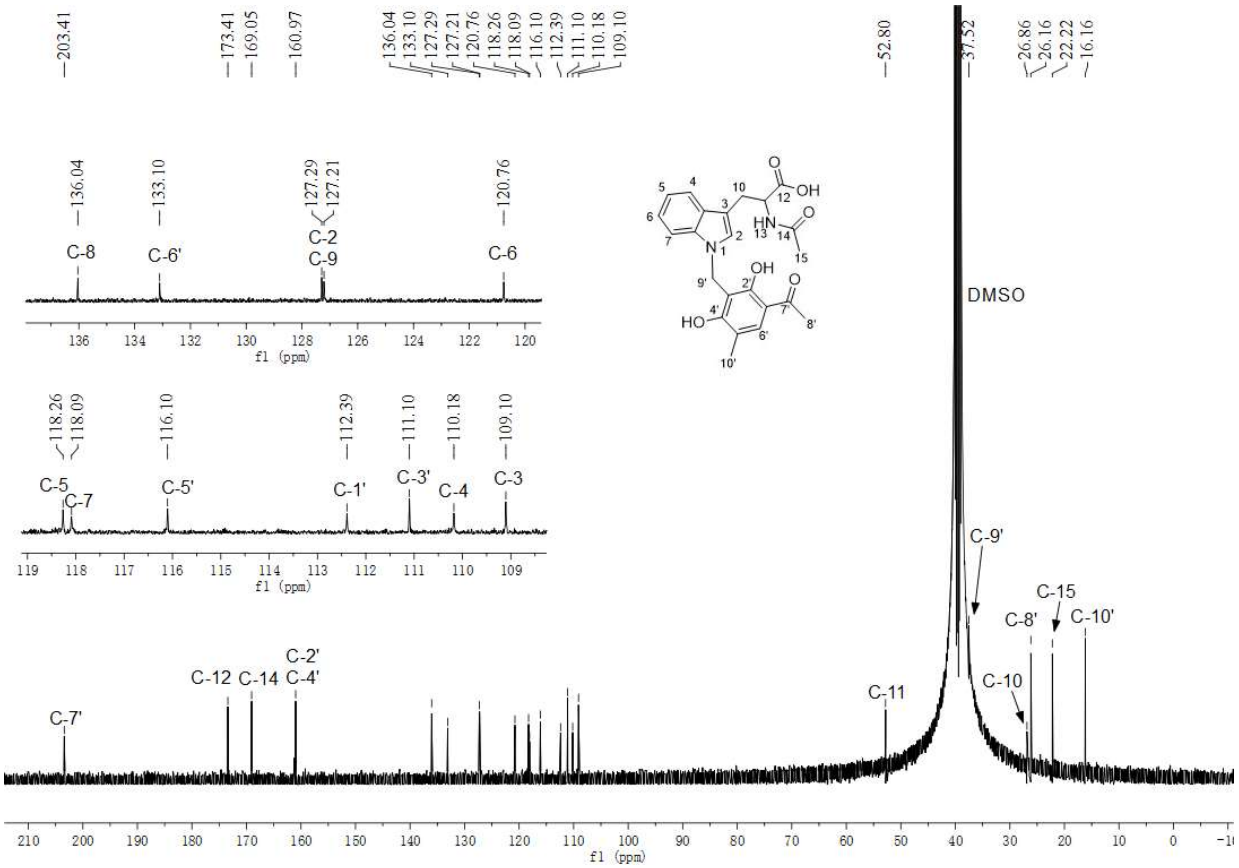

Figure S56. $^{13}C\{^{1}H\}$ NMR spectrum of (±)-**65c** in DMSO-d_6 (125 MHz).

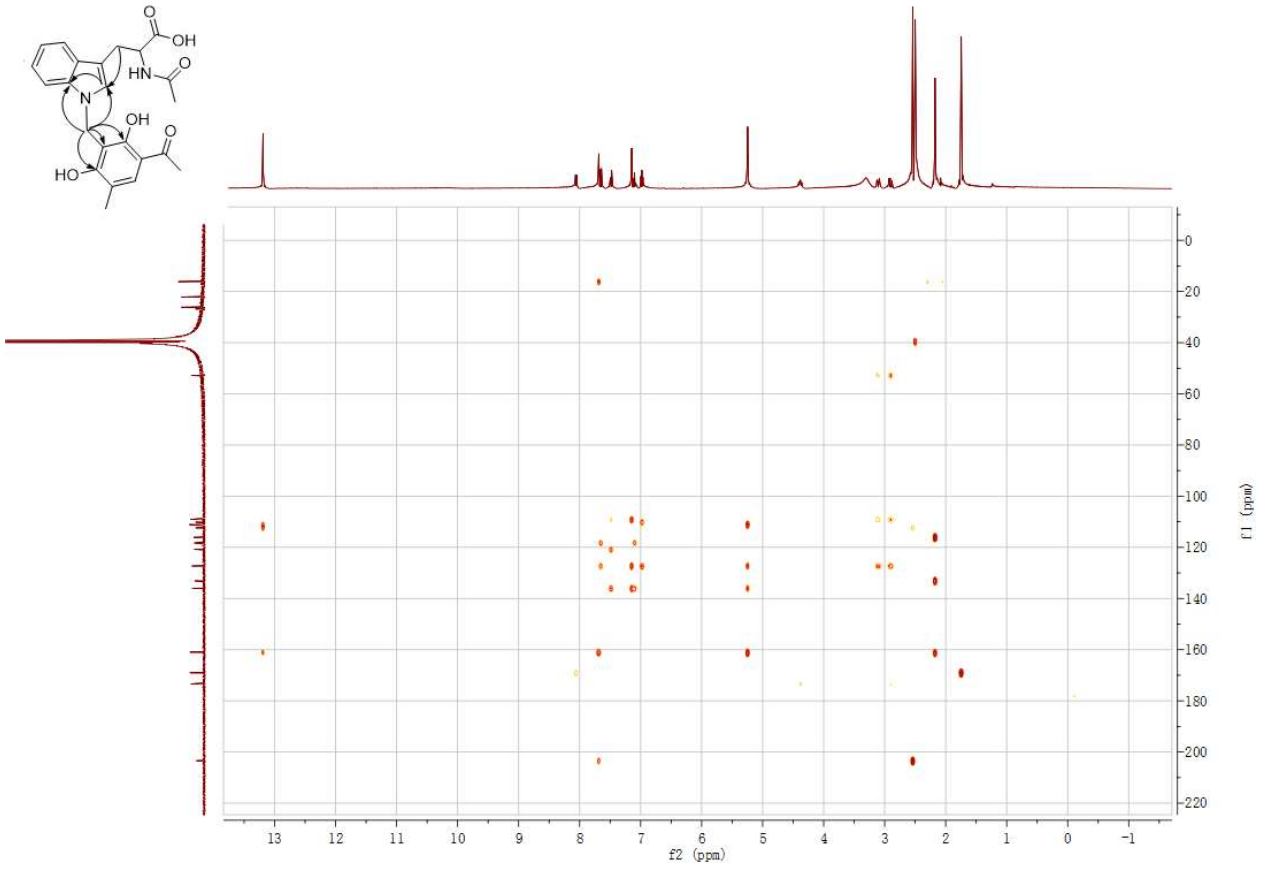

Figure S57. HMBC spectrum of (±)-**65c** in DMSO-d_6.

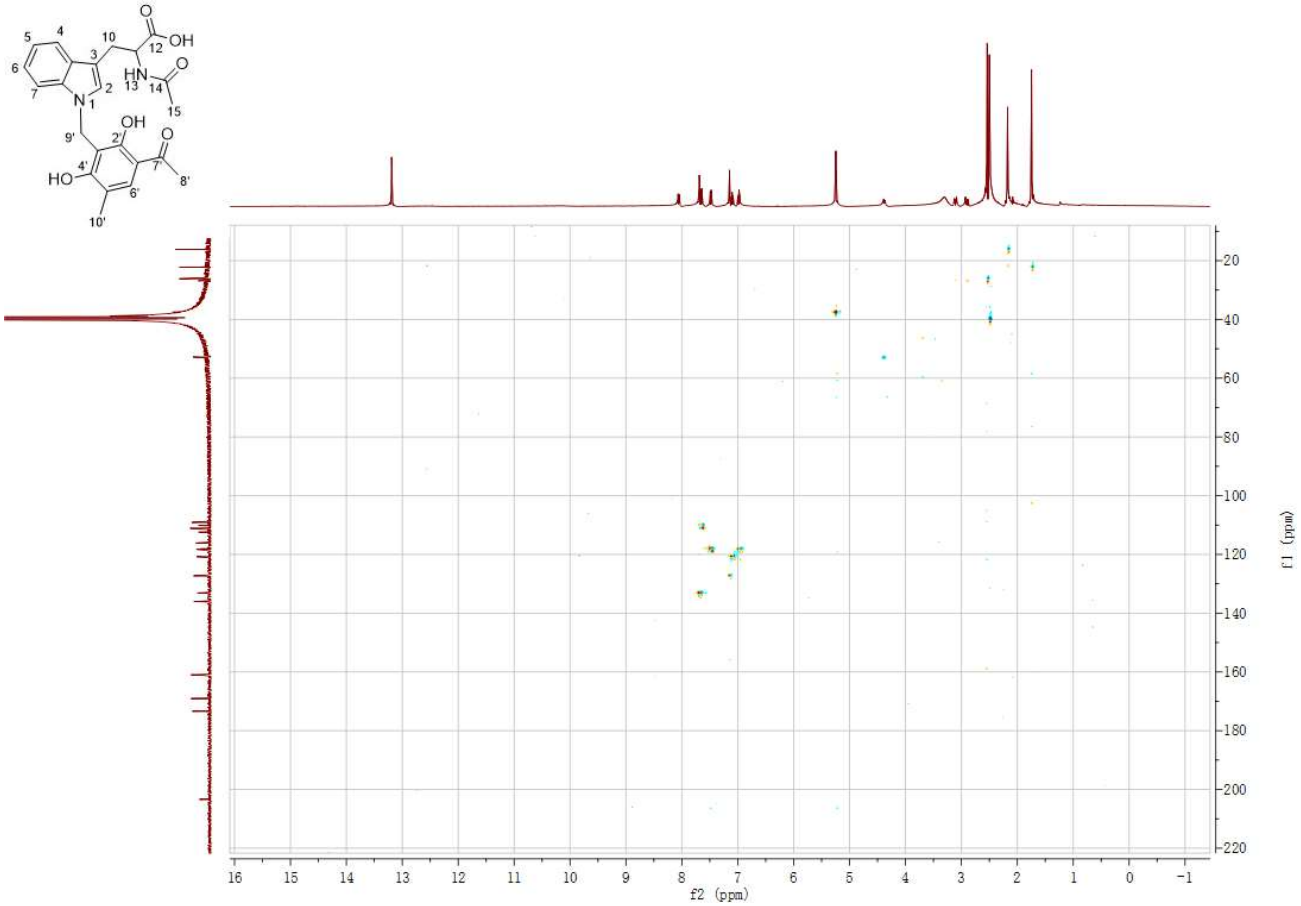

Figure S58. HSQC spectrum of (±)-**65c** in DMSO-d_6.

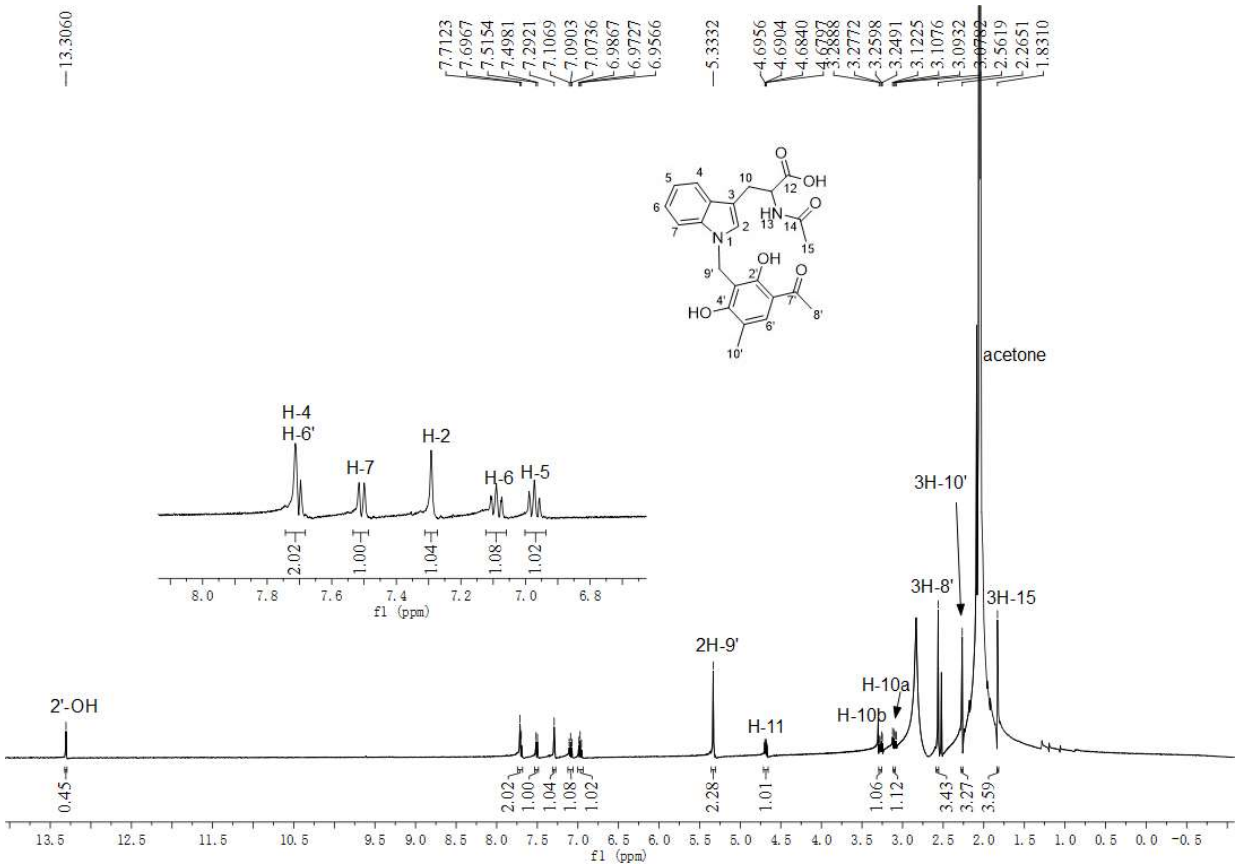

Figure S59. ^{1}H NMR spectrum of (±)-**65c** in acetone-d_6 (500 MHz).

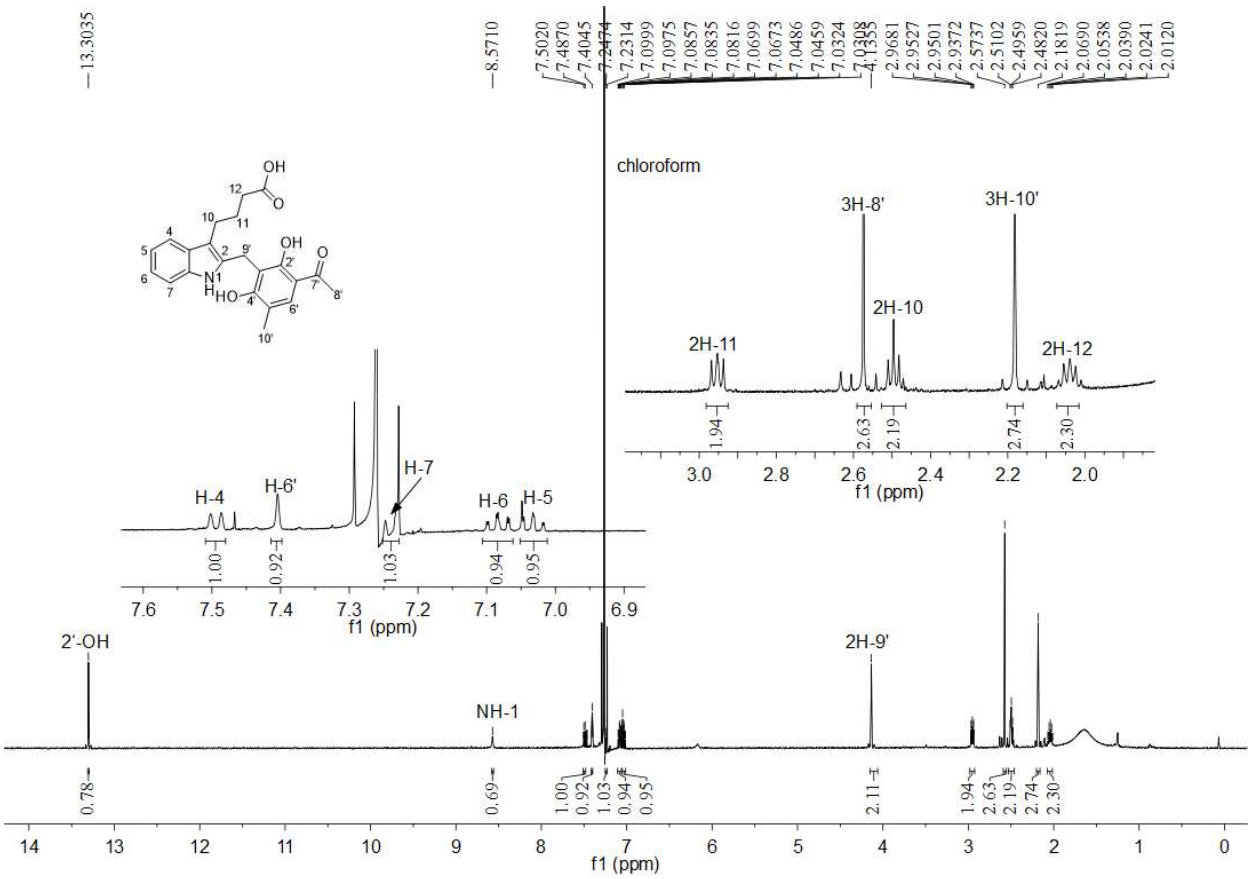

Figure S60. ^{1}H NMR spectrum of **72b** in $CDCl_3$ (500 MHz).

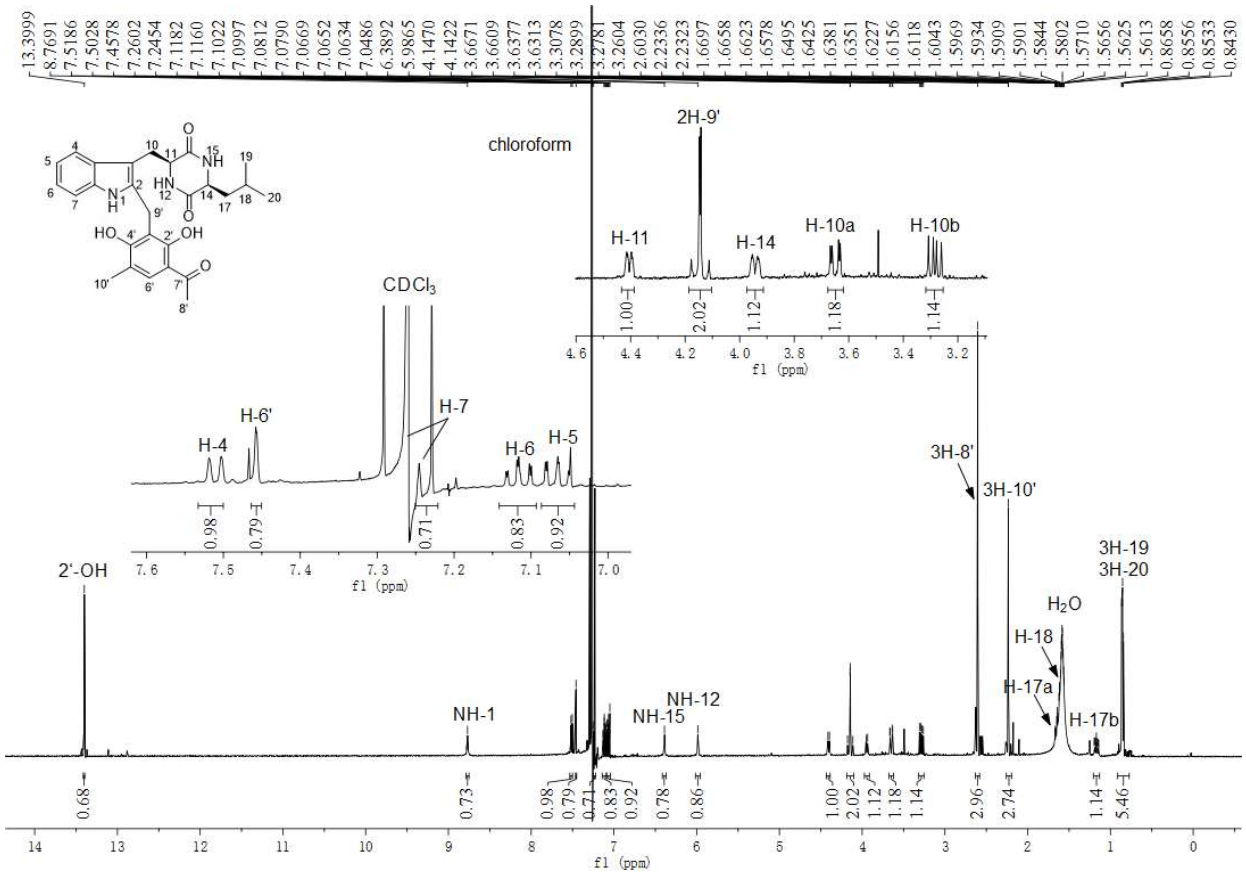

Figure S61. ^{1}H NMR spectrum of **76b** in $CDCl_3$ (500 MHz).

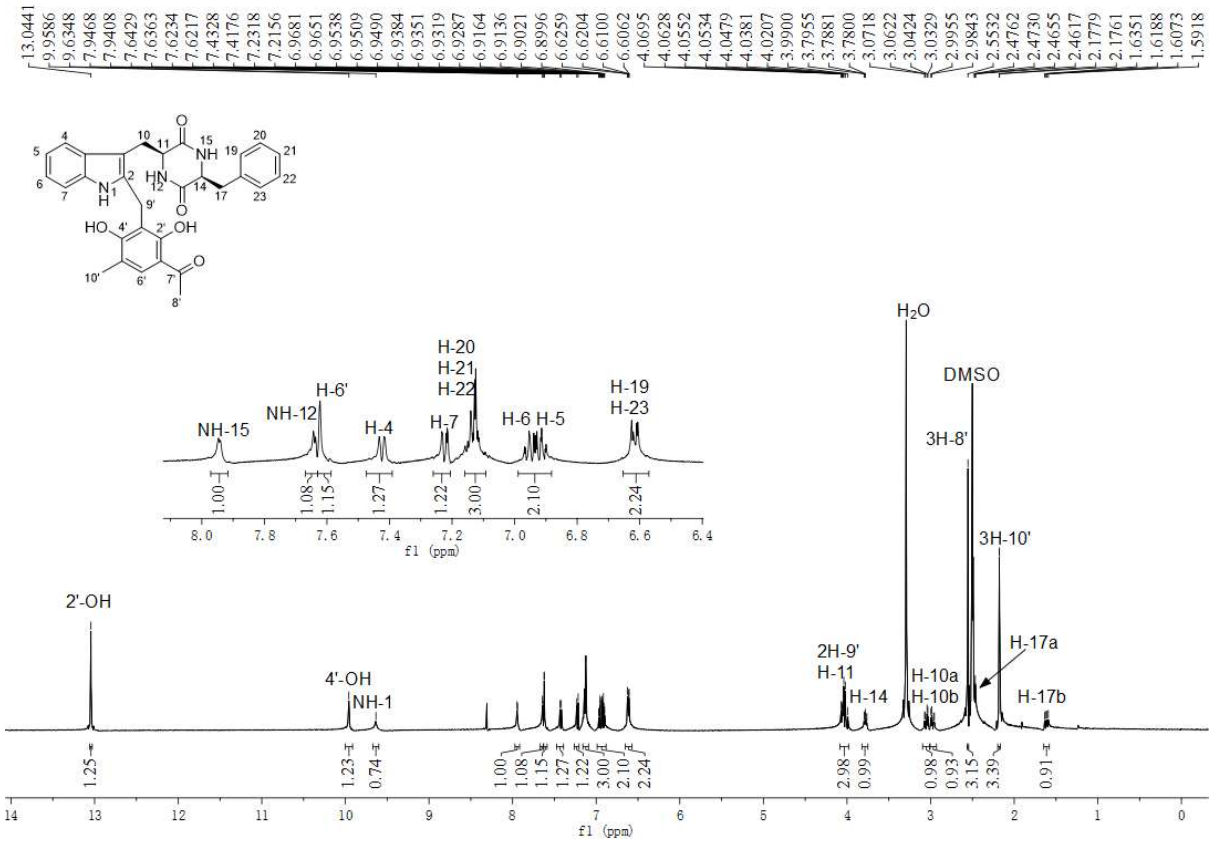

Figure S62. ^{1}H NMR spectrum of **77b** in DMSO-d_6 (500 MHz).

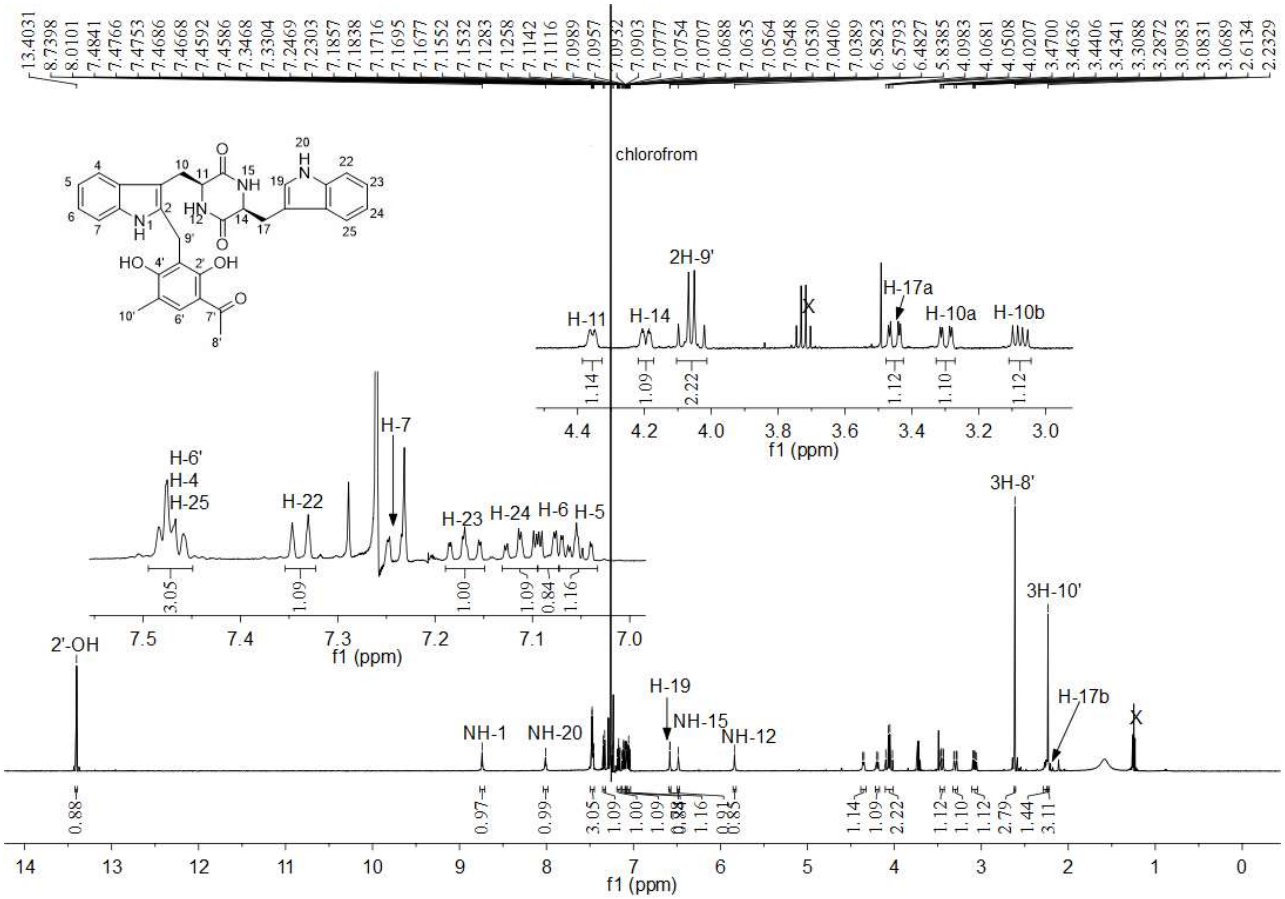

Figure S63. ^{1}H NMR spectrum of **79b** in $CDCl_3$ (500 MHz).

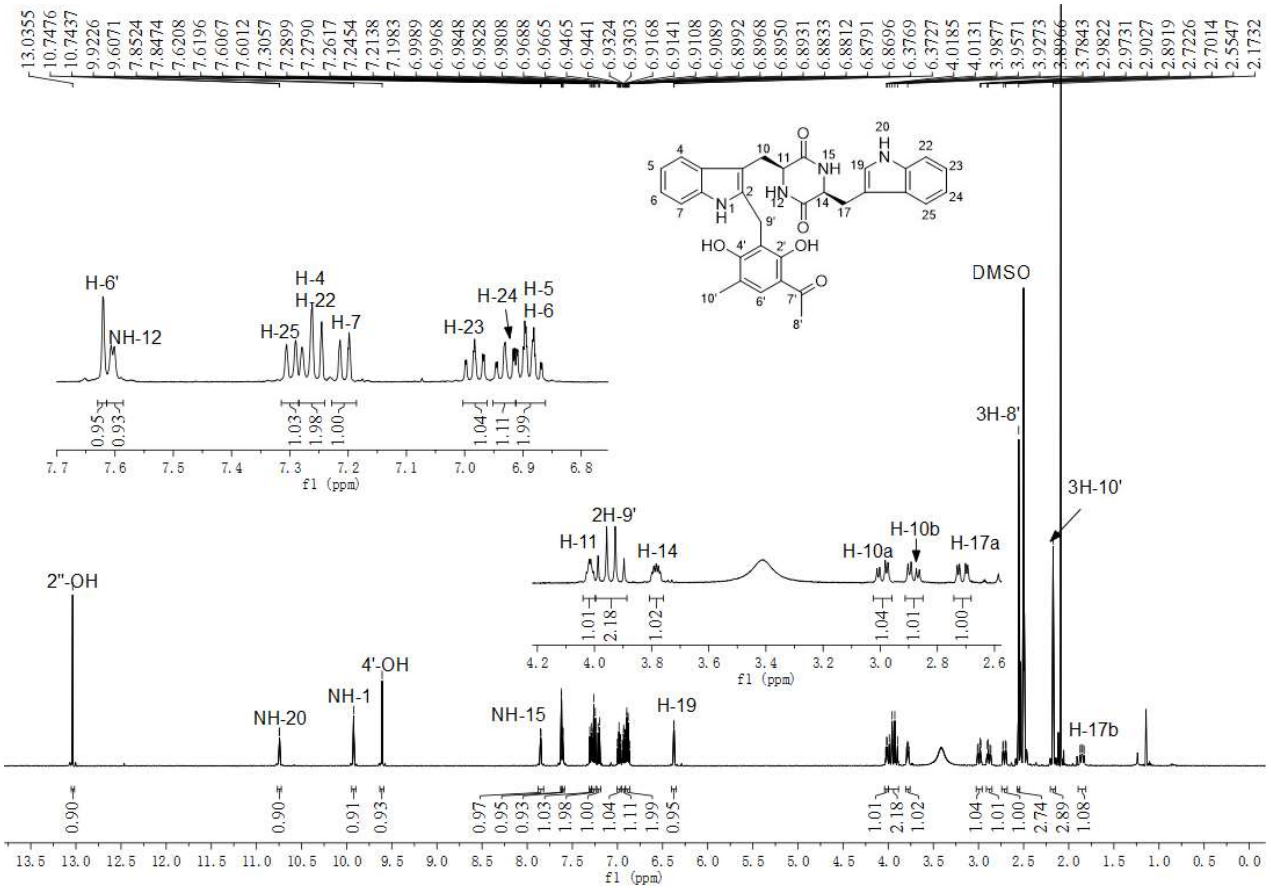

Figure S64. ^{1}H NMR spectrum of **79b** in DMSO-d_6 (500 MHz).

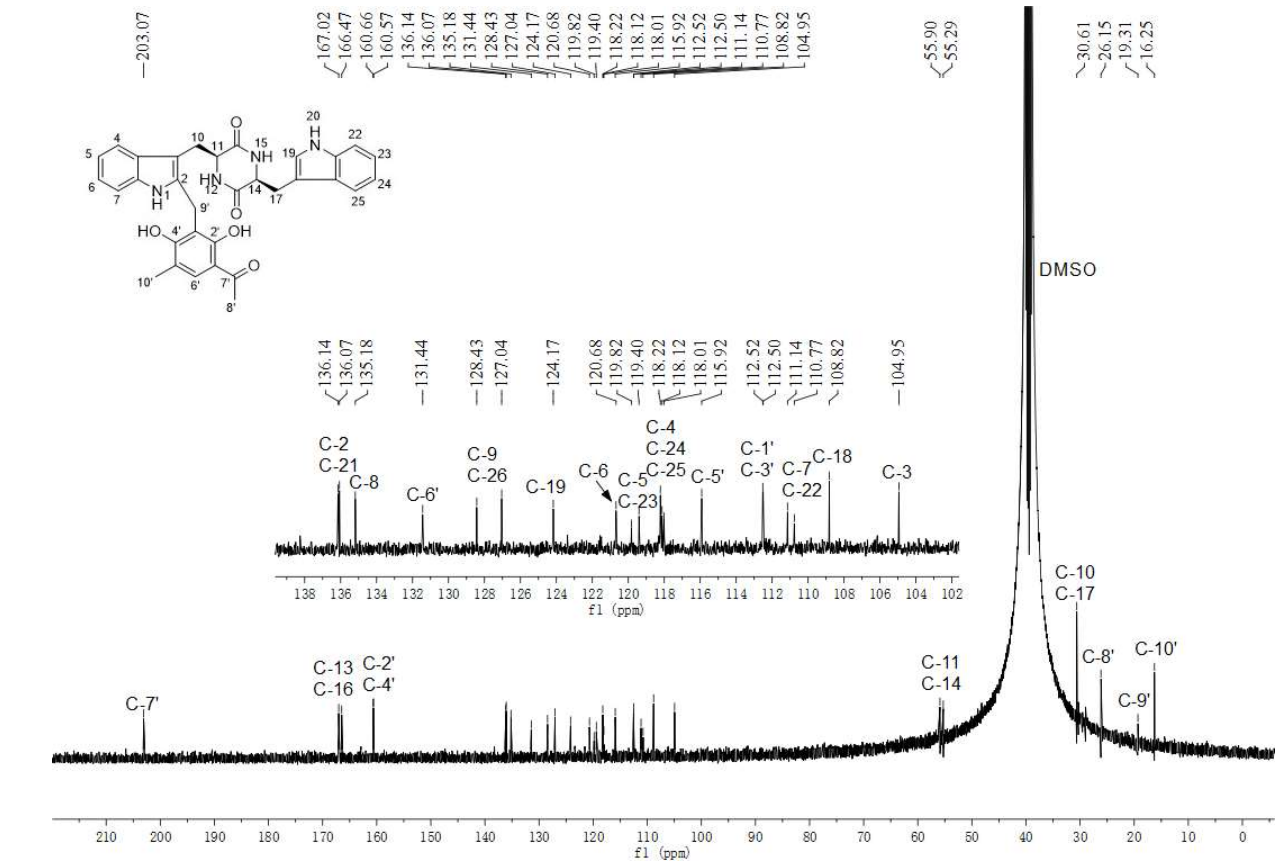

Figure S65. ^{13}C{^{1}H} NMR spectrum of **79b** in DMSO-d_6 (125 MHz).

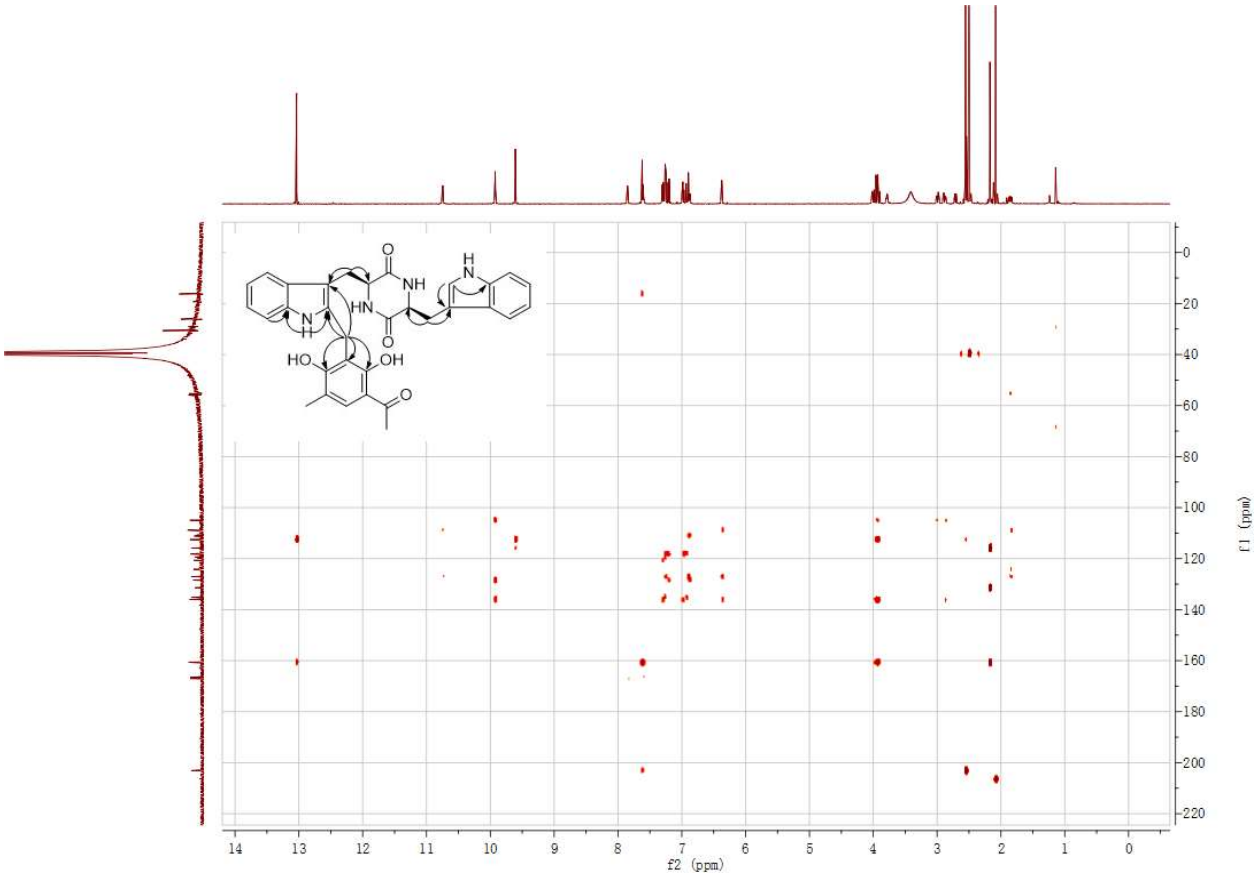

Figure S66. HMBC spectrum of **79b** in DMSO-d_6.

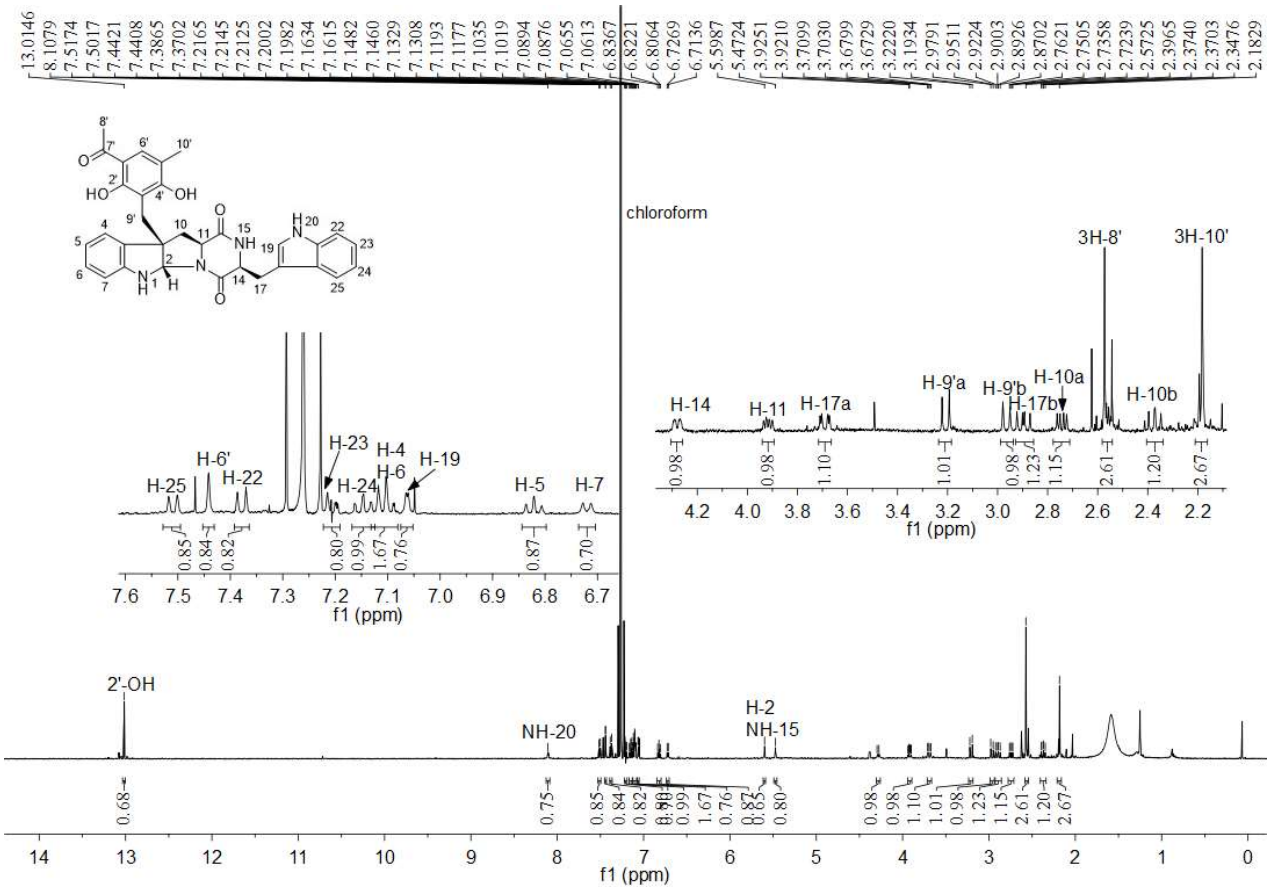

Figure S67. ^{1}H NMR spectrum of **79c** in $CDCl_3$ (500 MHz).

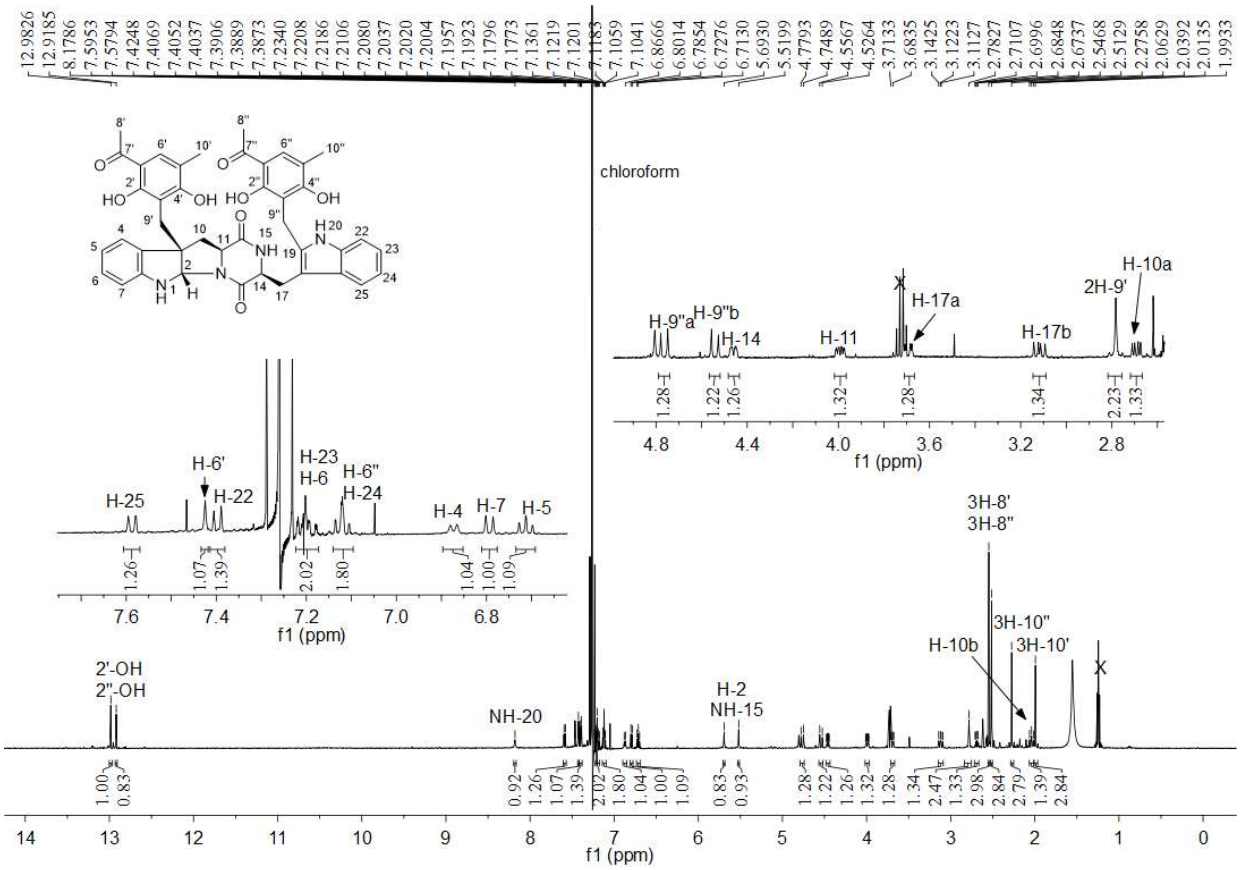

Figure S68. ^{1}H NMR spectrum of **79d** in $CDCl_3$ (500 MHz).

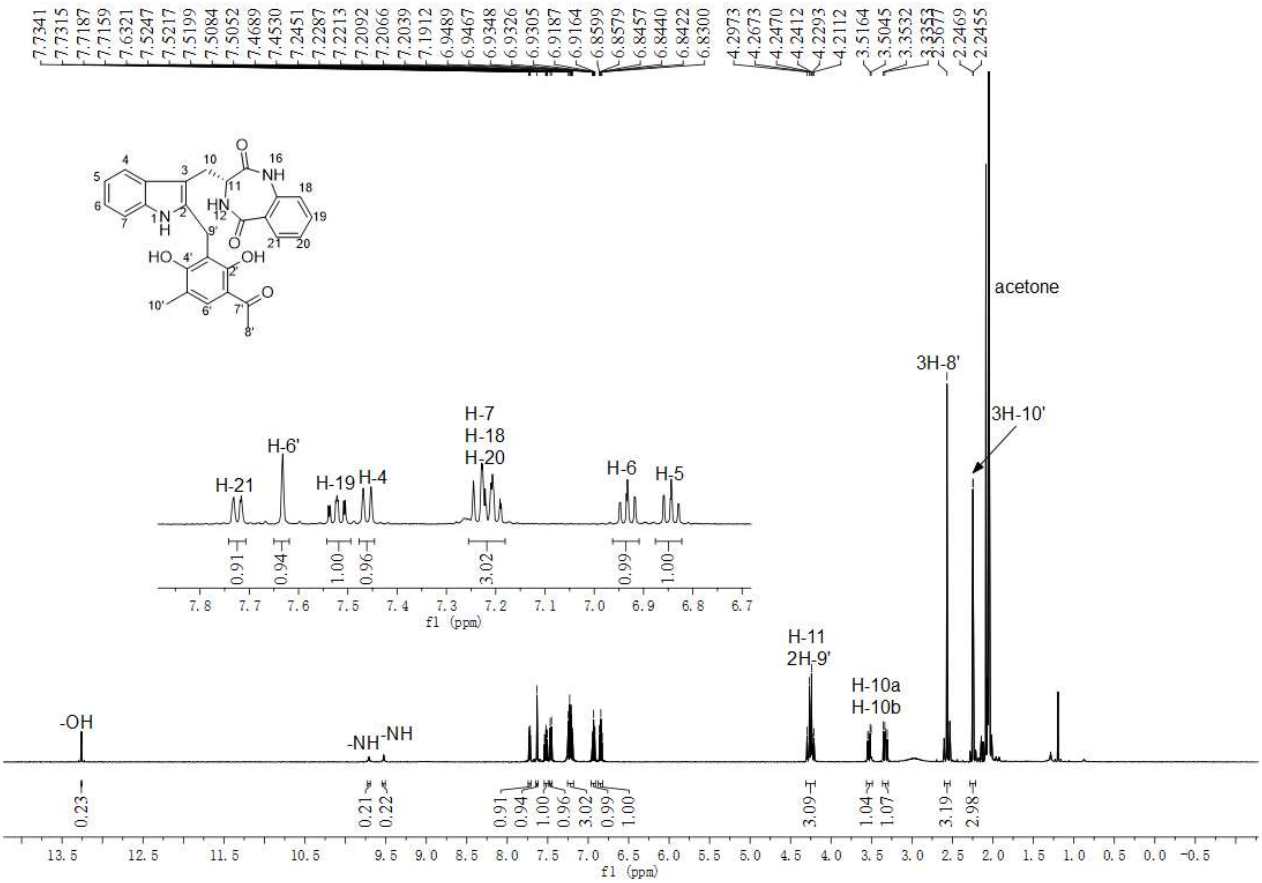

Figure S69. ^{1}H NMR spectrum of **80b** in acetone-d_6 (500 MHz).

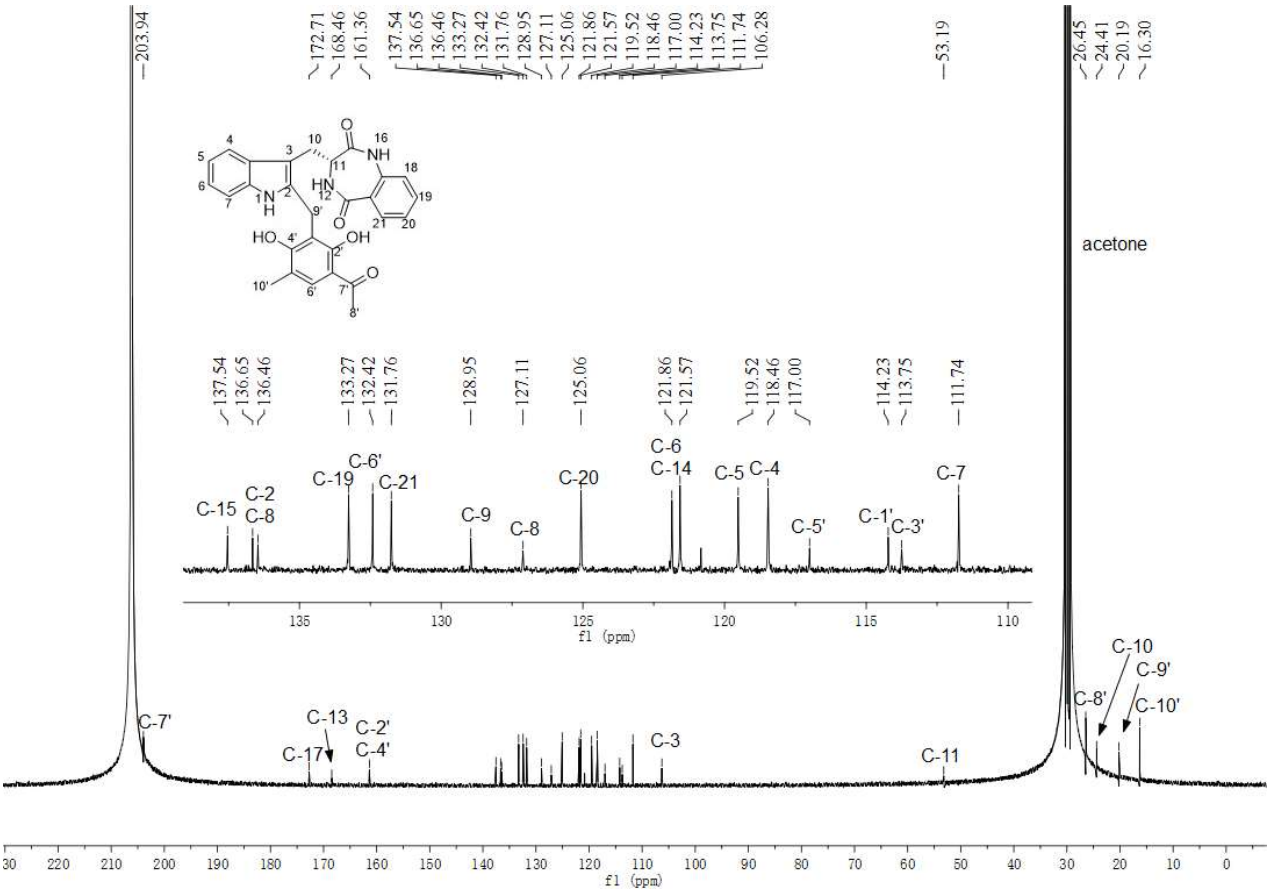

Figure S70. $^{13}C\{^{1}H\}$ NMR spectrum of **80b** in acetone-d_6 (125 MHz).

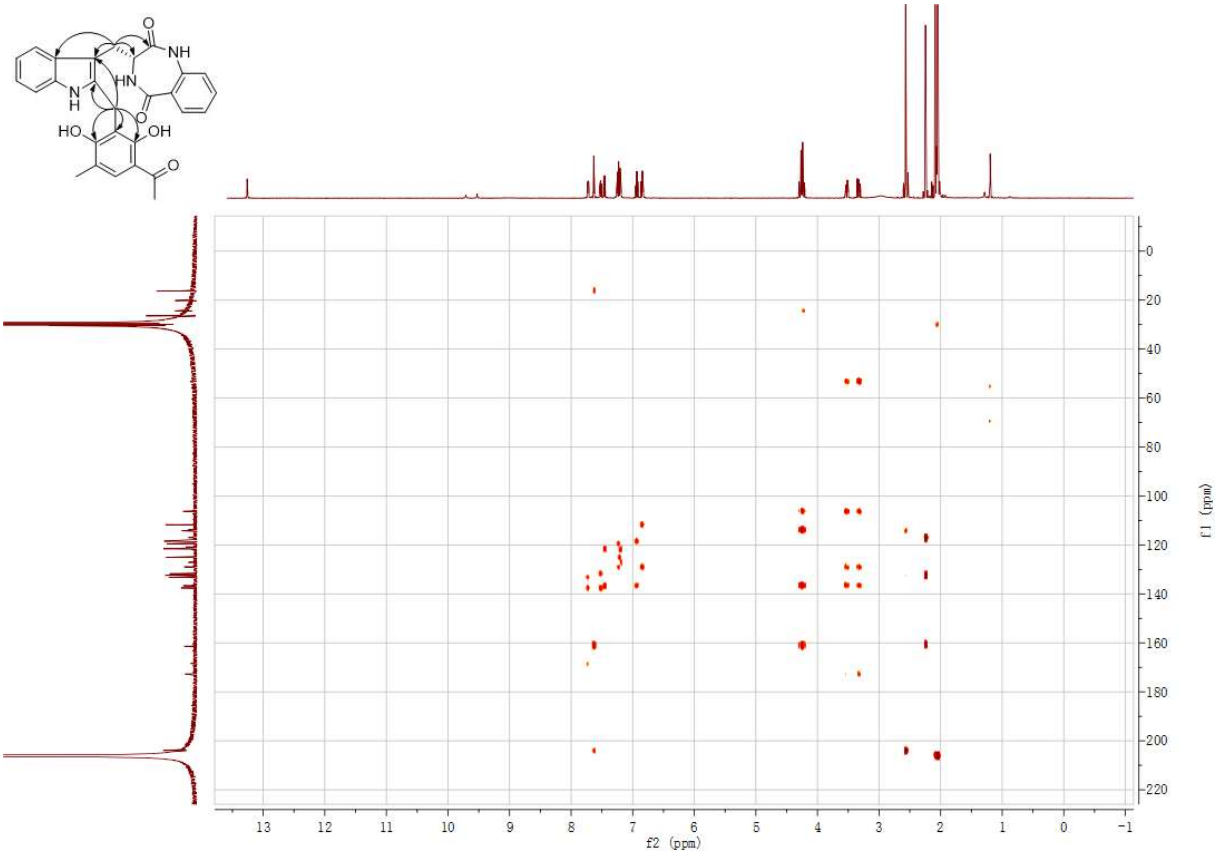

Figure S71. HMBC spectrum of **80b** in acetone-d_6.

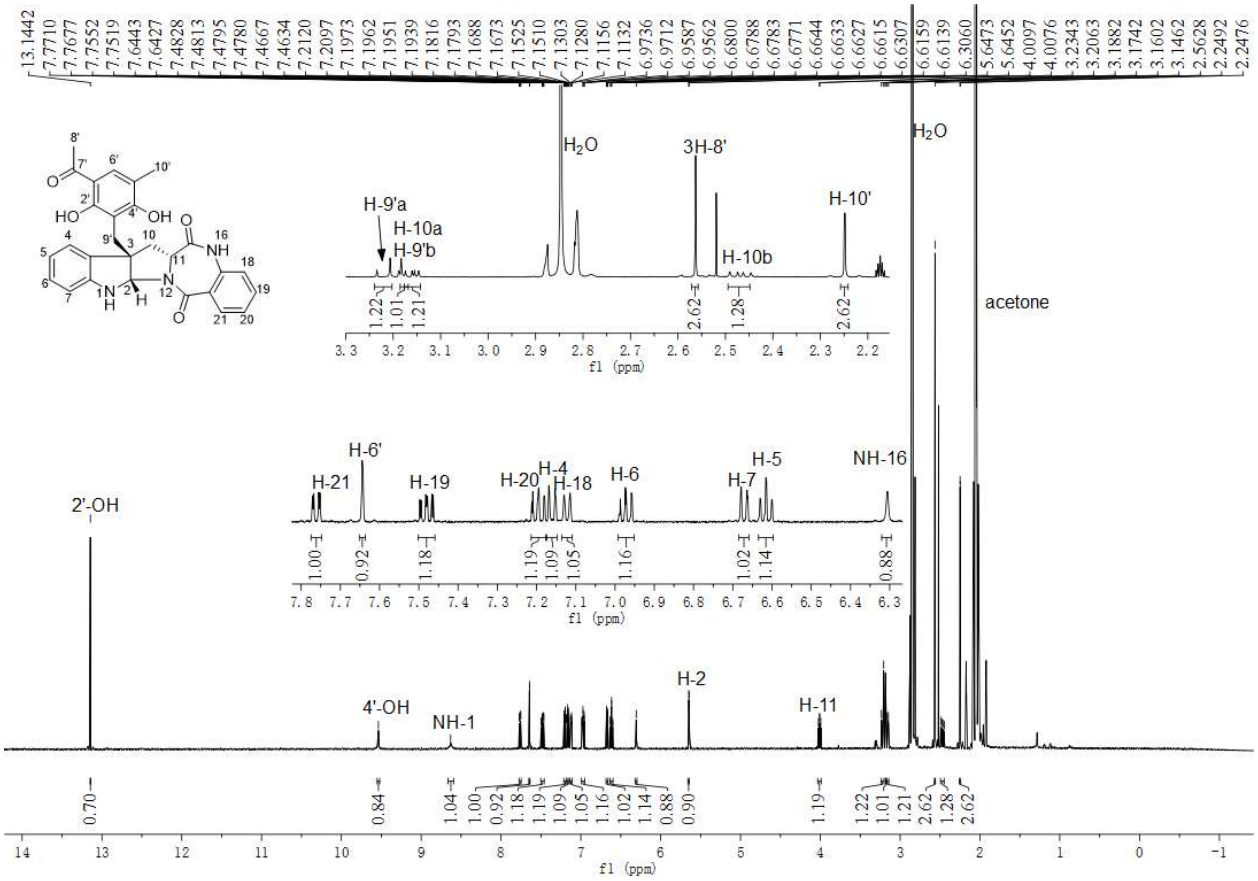

Figure S72. ^{1}H NMR spectrum of **80c** in acetone-d_6 (500 MHz).

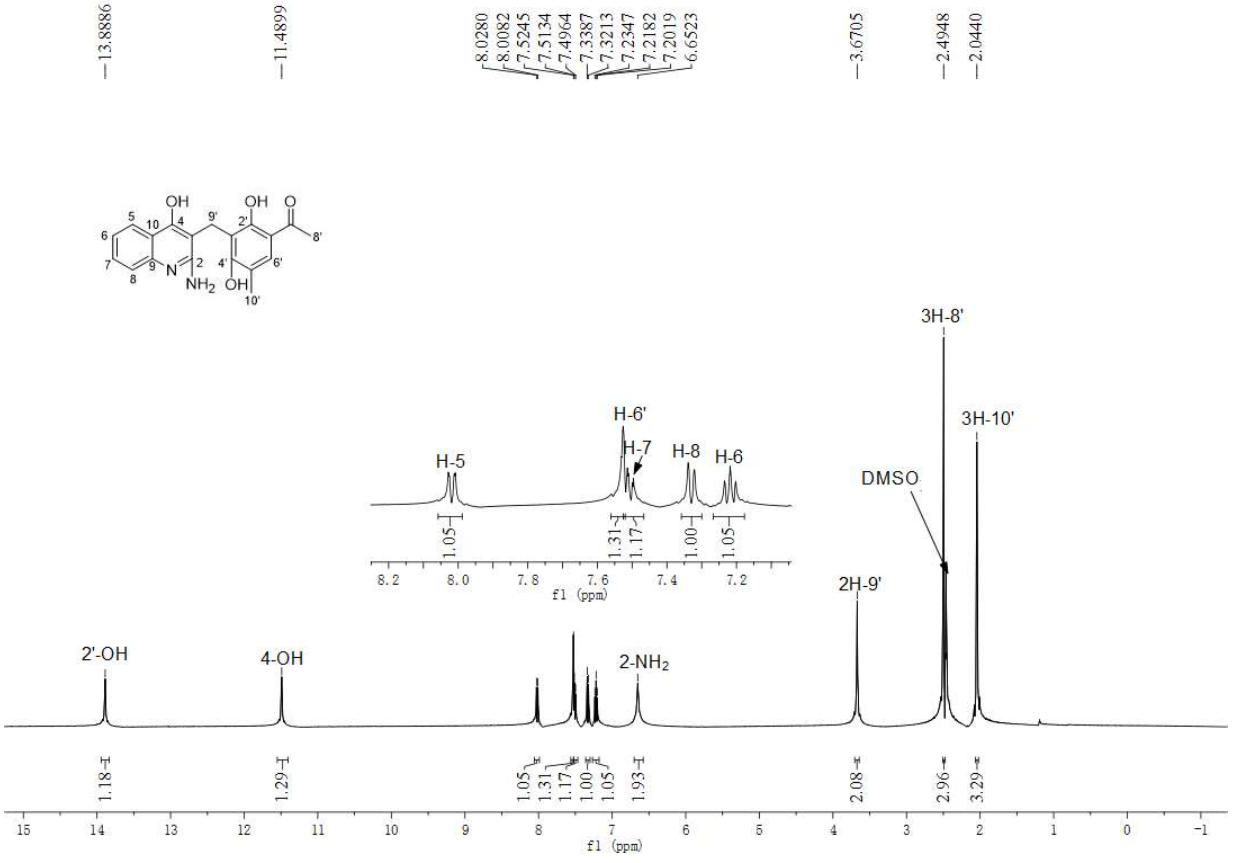

Figure S73. ^{1}H NMR spectrum of **95b** in DMSO-d_6 (500 MHz).

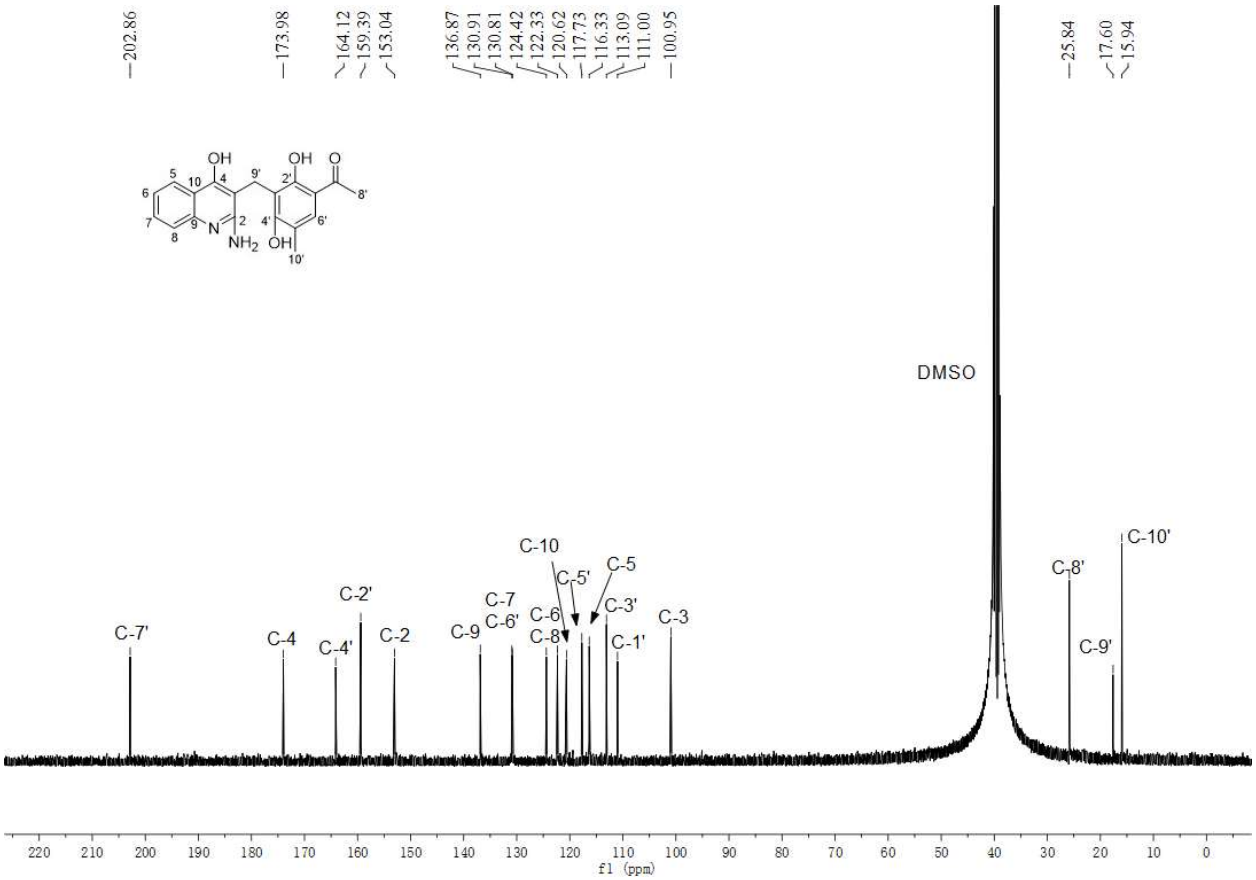

Figure S74. $^{13}C\{^{1}H\}$ NMR spectrum of **95b** in DMSO-d_6 (125 MHz).

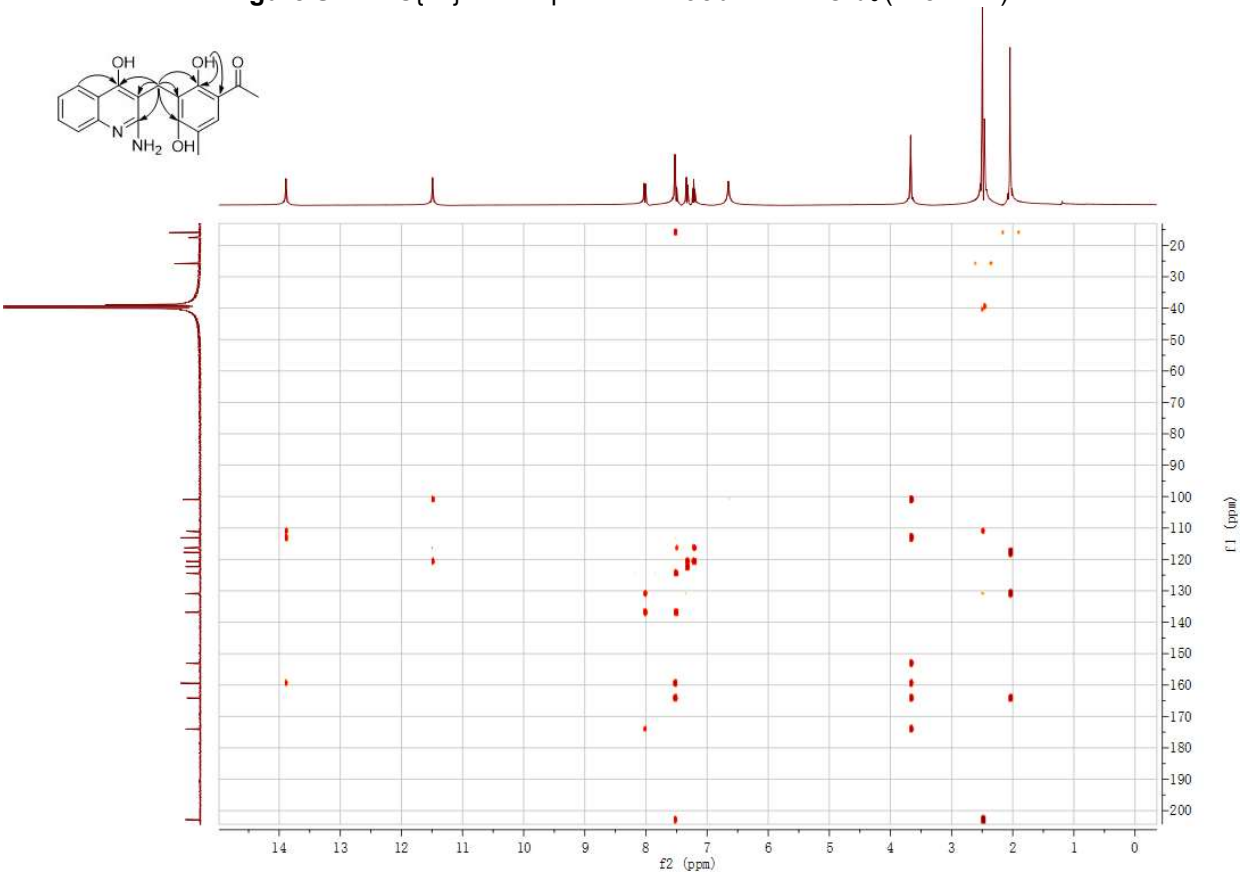

Figure S75. HMBC spectrum of **95b** in DMSO-d_6.

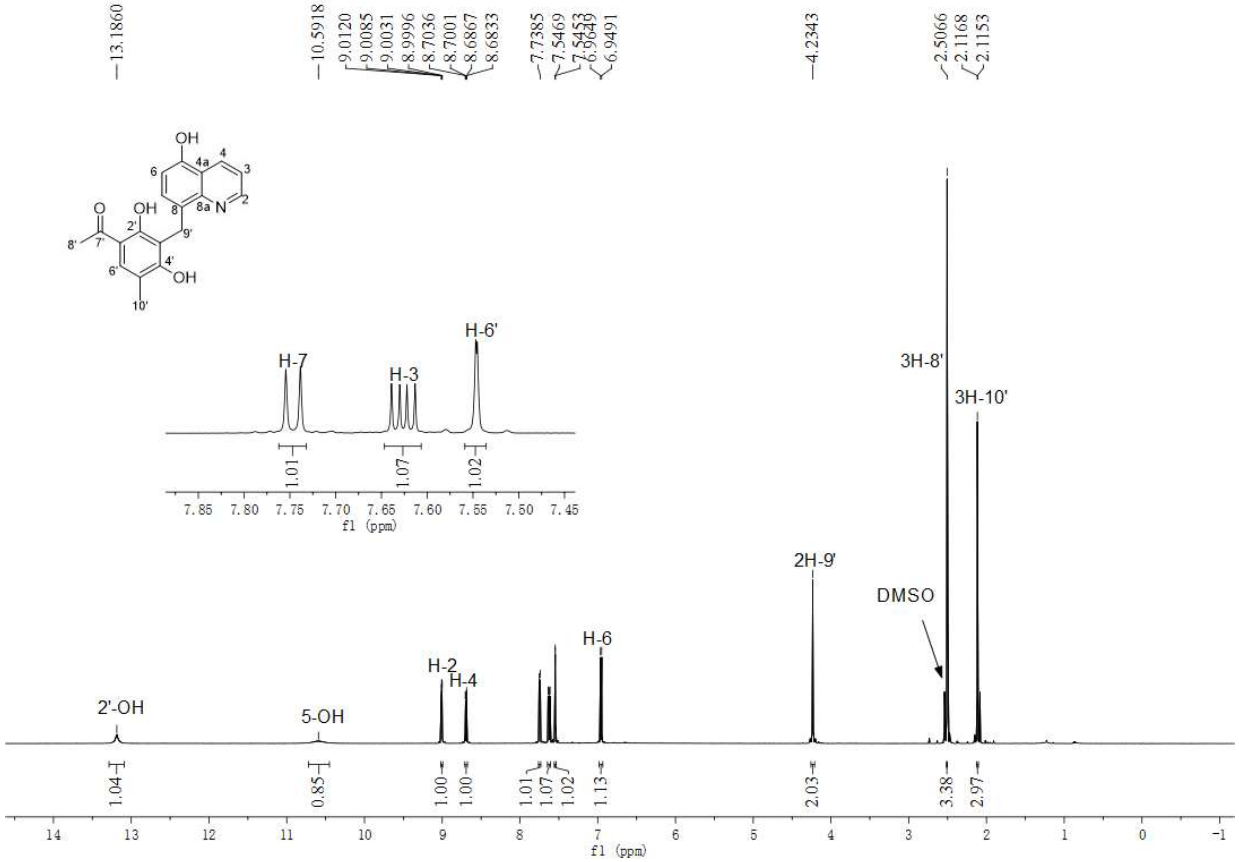

Figure S76. ^{1}H NMR spectrum of **98b** in DMSO-d_6 (500 MHz).

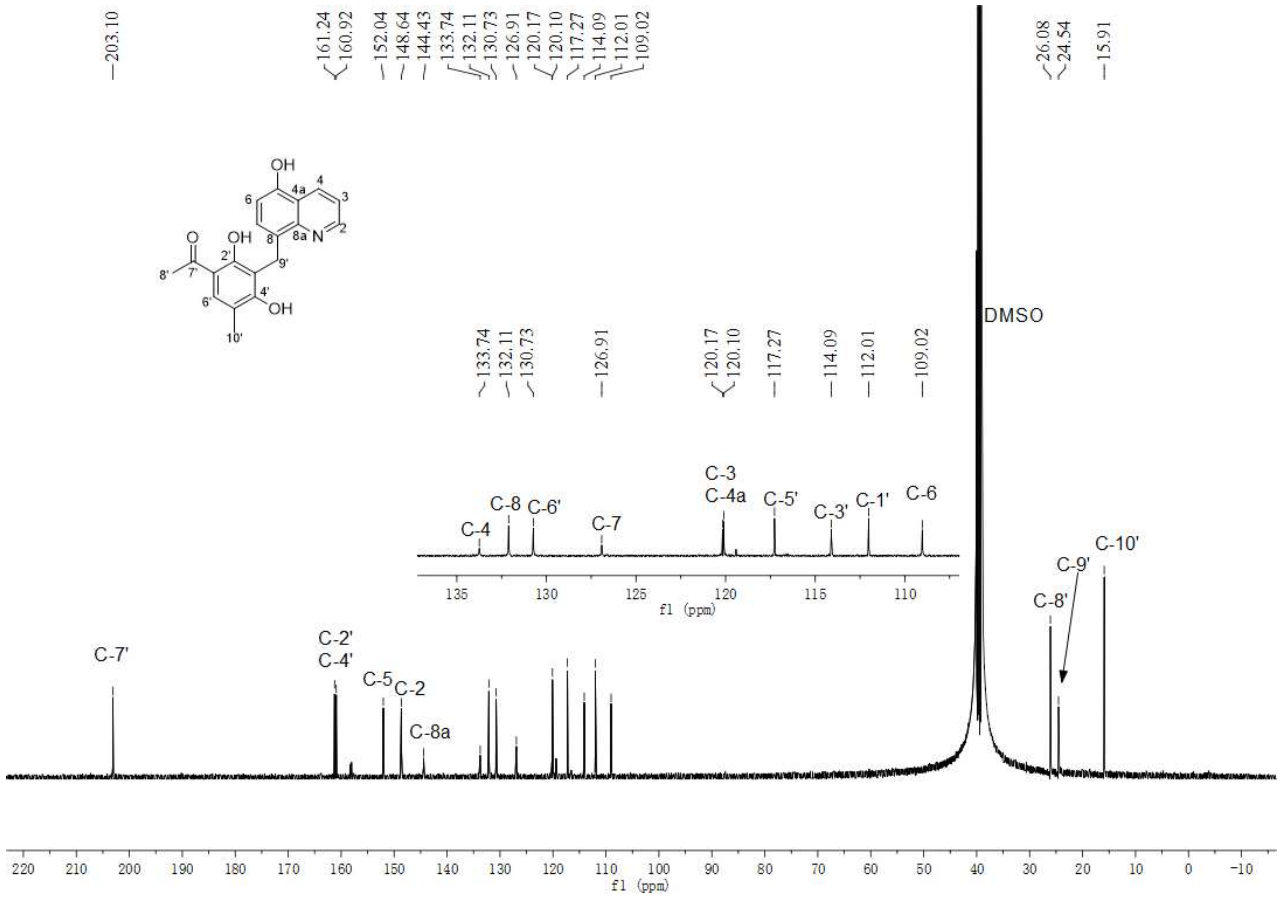

Figure S77. ^{13}C{^{1}H} NMR spectrum of **98b** in DMSO-d_6 (125 MHz).

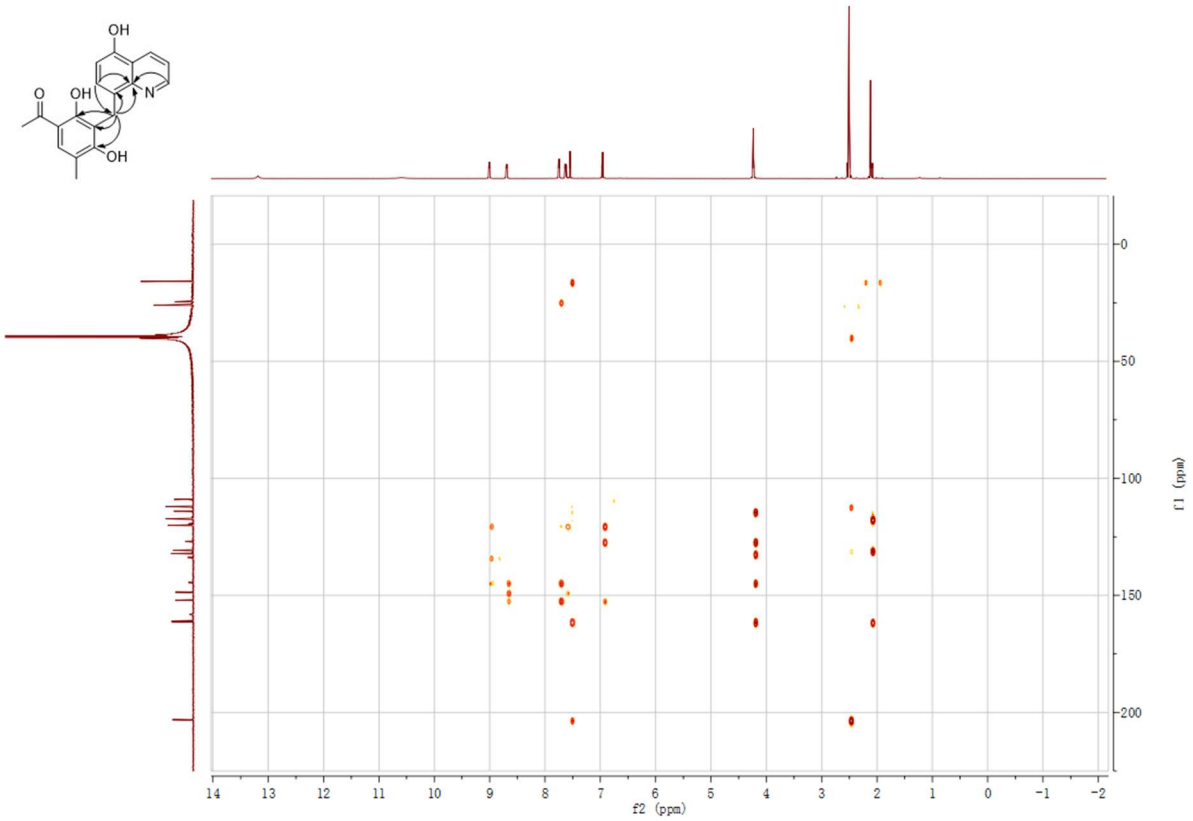

Figure S78. HMBC spectrum of **98b** in DMSO-d_6.

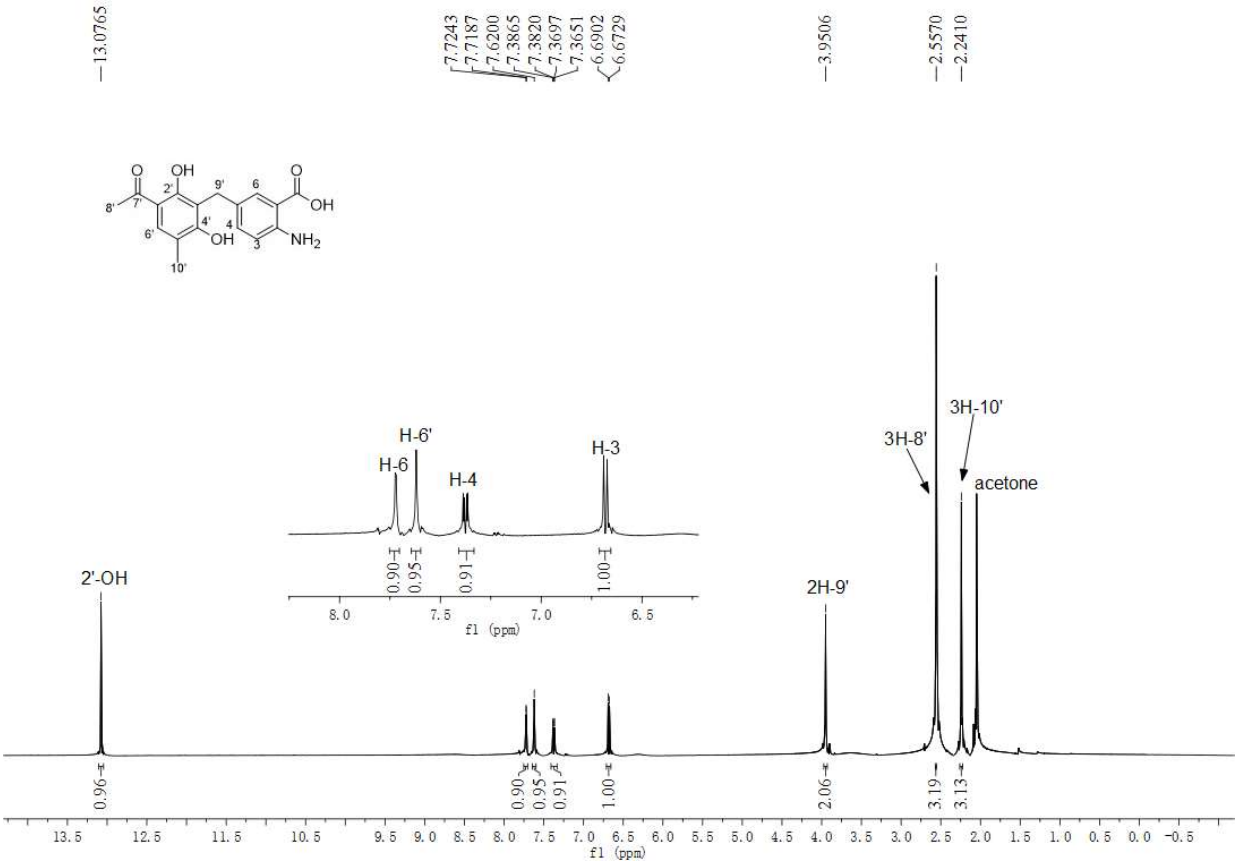

Figure S79. ^{1}H NMR spectrum of **101b** in acetone-d_6 (500 MHz).

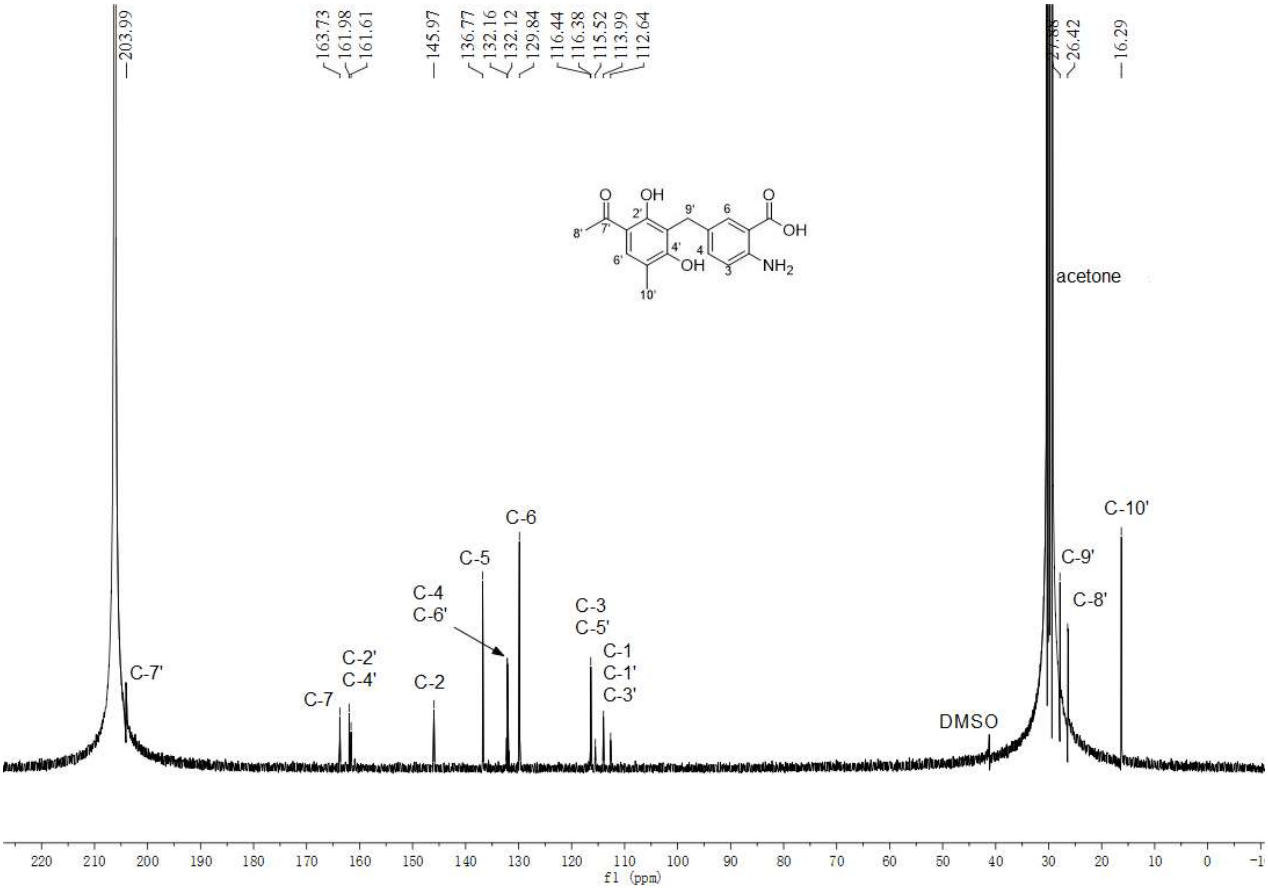

Figure S80. $^{13}C\{^{1}H\}$ NMR spectrum of **101b** in acetone-d_6 (125 MHz).

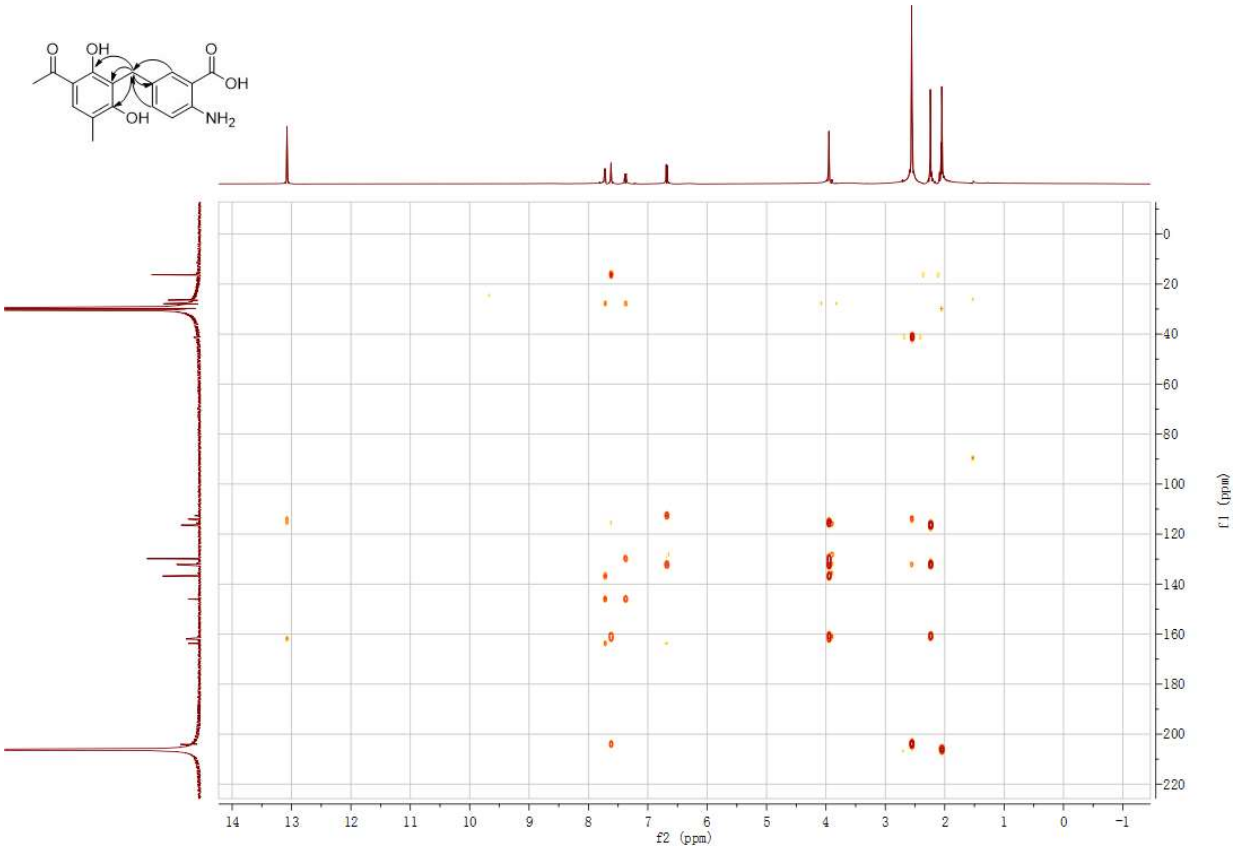

Figure S81. HMBC spectrum of **101b** in acetone-d_6.

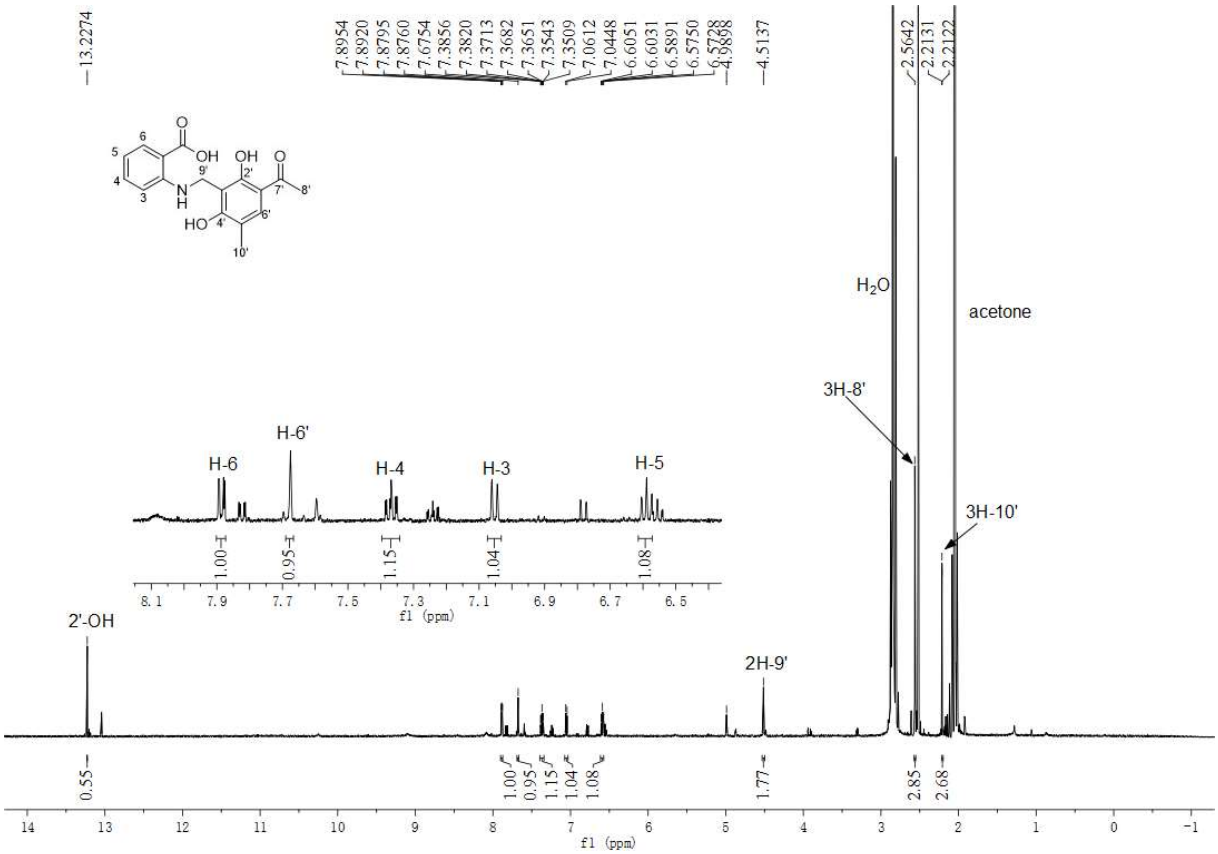

Figure S82. ^{1}H NMR spectrum of **101c** in acetone-d_6 (500 MHz).

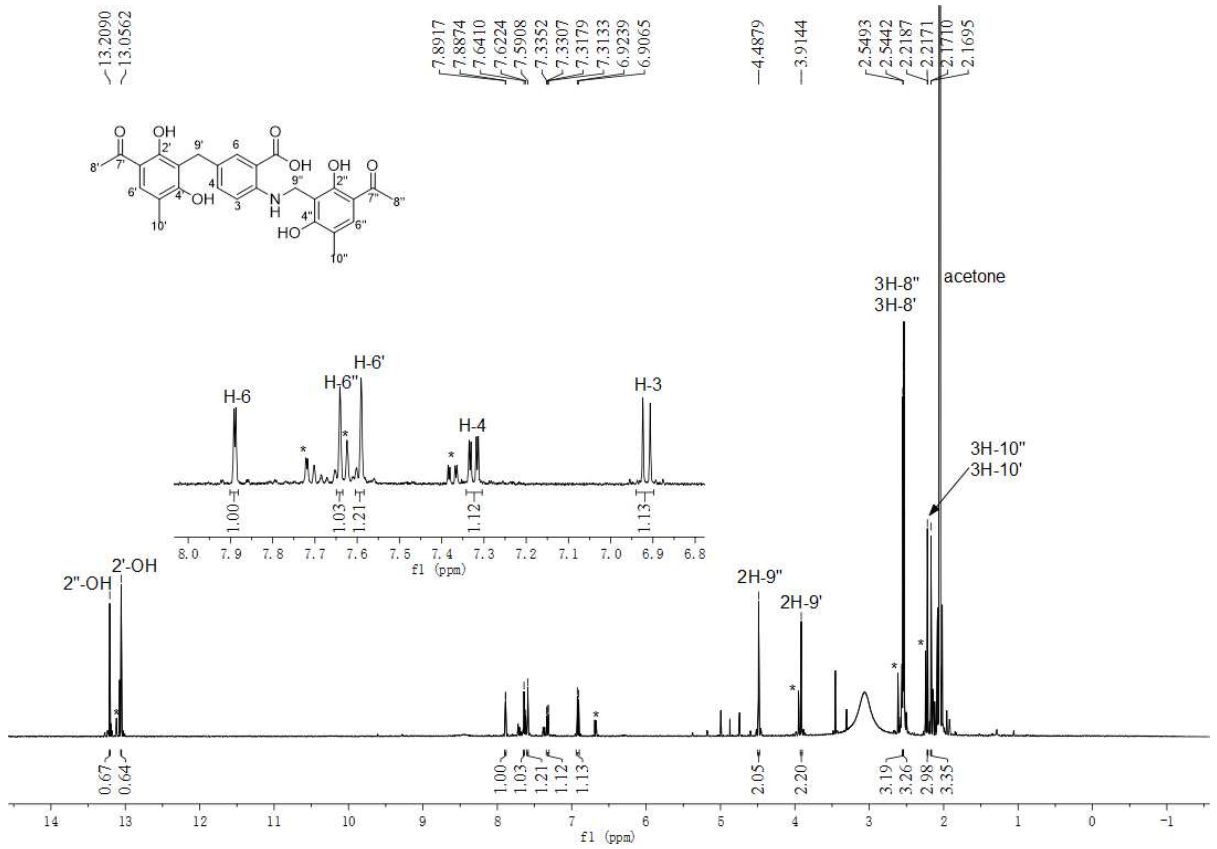

Figure S83. ^{1}H NMR spectrum of **101d** in acetone-d_6 (500 MHz).
Peaks labelled with * are signals belong to **101b**.

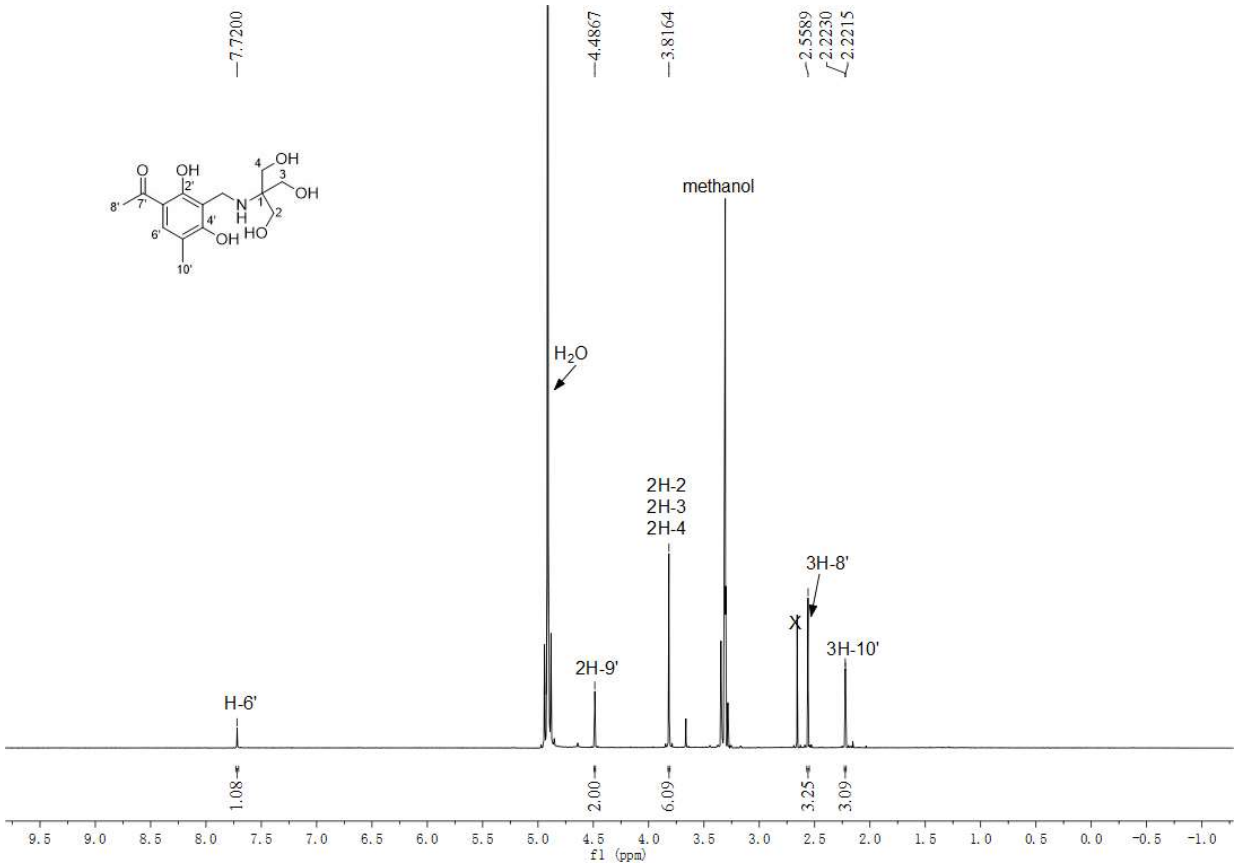

Figure S84. ^{1}H NMR spectrum of **102b** in CD_3OD (500 MHz).

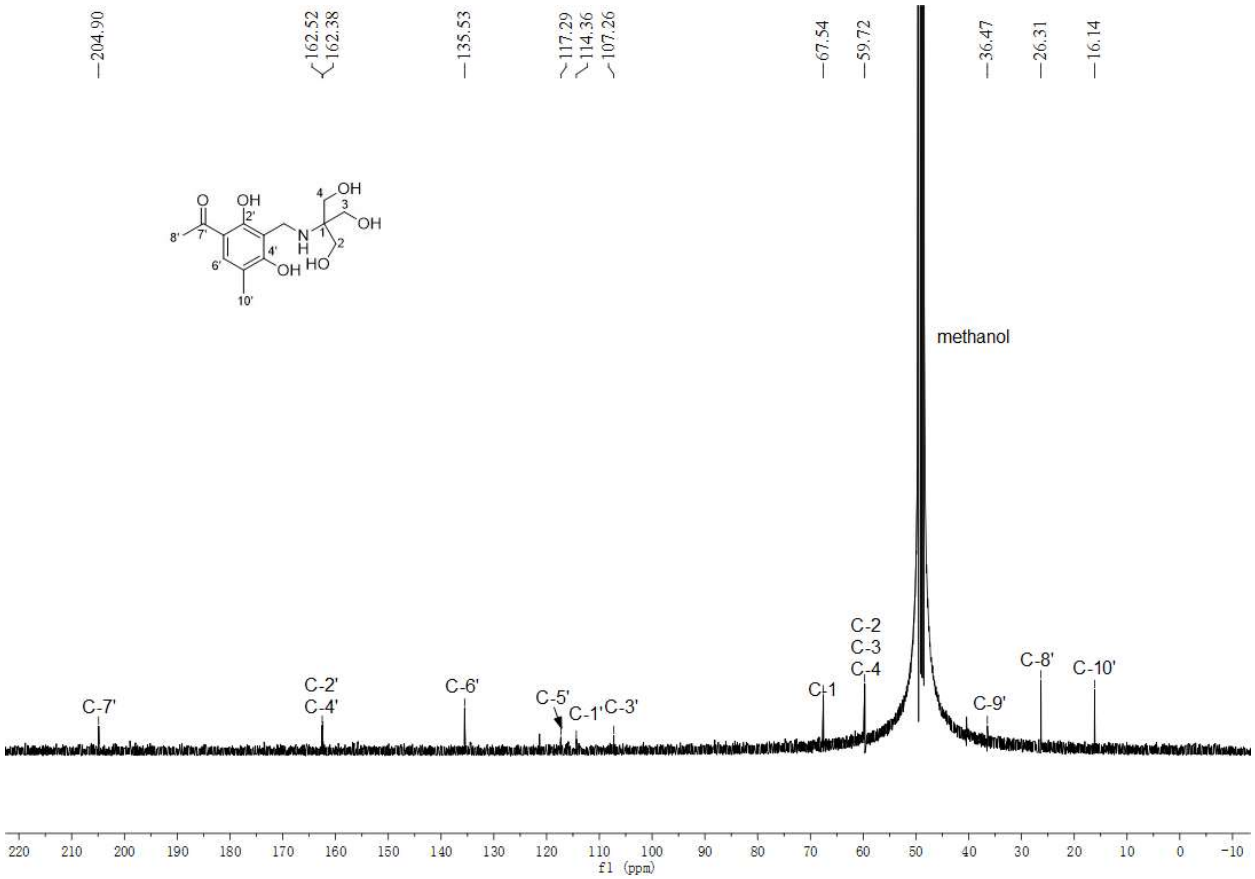

Figure S85. $^{13}C\{^{1}H\}$ NMR spectrum of **102b** in CD_3OD (125 MHz).

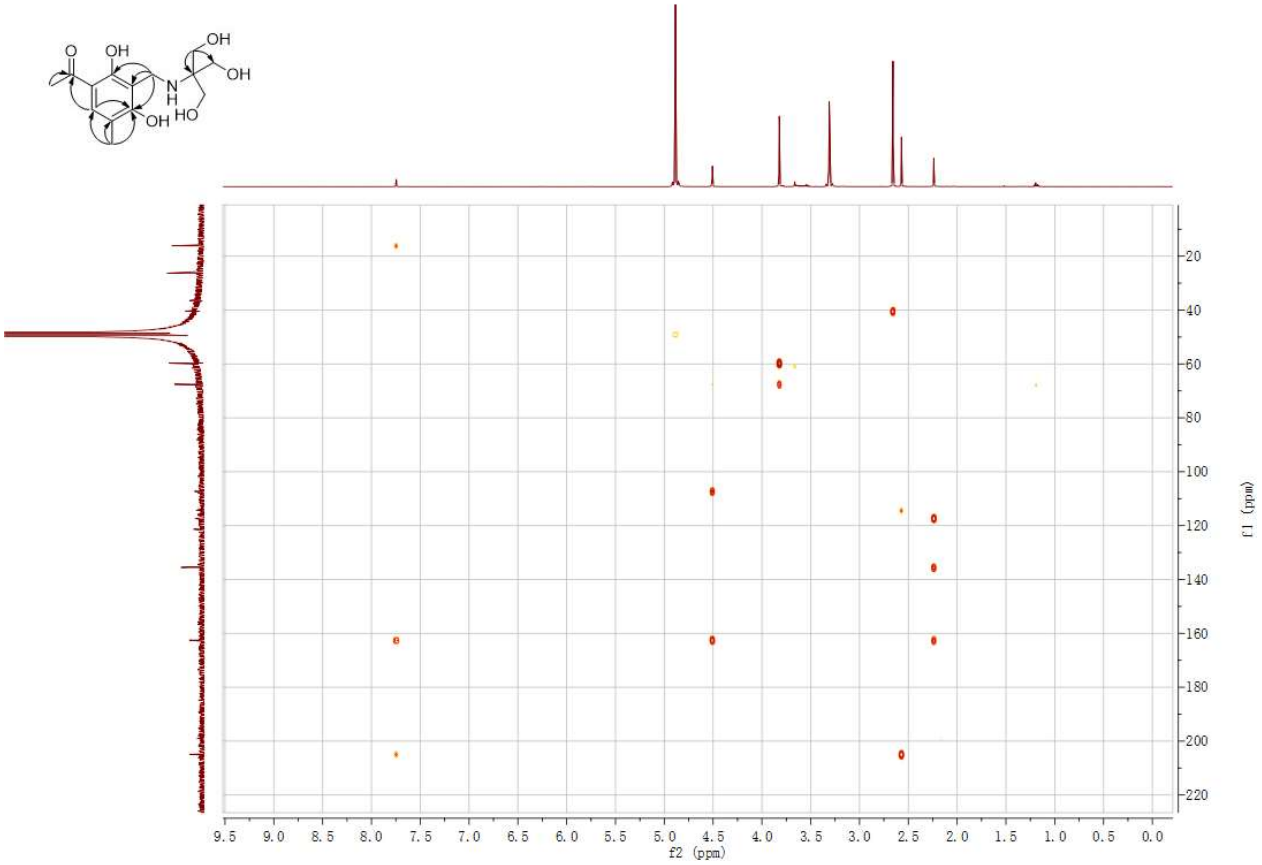

Figure S86. HMBC spectrum of **102b** in CD_3OD.

References

1. Spence, J. T.; George, J. H. Biomimetic total synthesis of *ent*-penilactone A and penilactone B. *Org. Lett.* **2013,** *15* (15), 3891-3893.
2. Davies, M. W.; Maskell, L.; Shipman, M.; Slawin, A. M.; Vidot, S. M.; Whatmore, J. L. Studies toward the synthesis of luminacin D: assembly of simplified analogues devoid of the epoxide displaying antiangiogenic activity. *Org. Lett.* **2004,** *6* (22), 3909-3912.
3. Wu, G.; Ma, H.; Zhu, T.; Li, J.; Gu, Q.; Li, D. Penilactones A and B, two novel polyketides from Antarctic deep-sea derived fungus *Penicillium crustosum* PRB-2. *Tetrahedron* **2012,** *68*, 9745-9749.
4. Wang, J.; Liu, P.; Wang, Y.; Wang, H.; Li, J.; Zhuang, Y.; Zhu, W. Antimicrobial aromatic polyketides from Gorgonian-associated fungus, *Penicillium commune* 518. *Chin. J. Chem.* **2012,** *30*, 1236-1242.
5. Li, H.; Jiang, J.; Liu, Z.; Lin, S.; Xia, G.; Xia, X.; Ding, B.; He, L.; Lu, Y.; She, Z. Peniphenones A-D from the mangrove fungus *Penicillium dipodomyicola* HN4-3A as inhibitors of *Mycobacterium tuberculosis* phosphatase MptpB. *J. Nat. Prod.* **2014,** *77* (4), 800-806.
6. Sun, W.; Chen, X.; Tong, Q.; Zhu, H.; He, Y.; Lei, L.; Xue, Y.; Yao, G.; Luo, Z.; Wang, J.; Li, H.; Zhang, Y. Novel small molecule 11beta-HSD1 inhibitor from the endophytic fungus *Penicillium commune*. *Sci. Rep.* **2016,** *6*, 26418.
7. Yu, G.; Sun, Z.; Peng, J.; Zhu, M.; Che, Q.; Zhang, G.; Zhu, T.; Gu, Q.; Li, D. Secondary metabolites produced by combined culture of *Penicillium crustosum* and a *Xylaria* sp. *J. Nat. Prod.* **2019,** *82* (7), 2013-2017.
8. Tomoda, H.; Tabata, N.; Masuma, R.; Si, S. Y.; Omura, S. Erabulenols, inhibitors of cholesteryl ester transfer protein produced by *Penicillium* sp. FO-5637. I. Production, isolation and biological properties. *J. Antibiot. (Tokyo)* **1998,** *51* (7), 618-623.
9. da Silva, B. F.; Rodrigues-Fo, E. Production of a benzylated flavonoid from 5,7,3',4',5'-pentamethoxyflavanone by *Penicillium griseoroseum*. J. *Mol. Catal. B - Enzyme* **2010,** *67* (3-4), 184-188.

5 Conclusions and future prospects

In this thesis, the structural diversification of natural products was achieved by using either enzymes or reactive intermediates from the nature's biosynthetic machinery. Enzymes involved in the biosynthesis of natural products catalyze an expansive array of chemical transformations for the construction or modification of secondary metabolites. Recent advances in chemoenzymatic synthesis proved it as a promising tool to access various chemical entities. In addition, reactive intermediates from the biosynthetic pathway of secondary metabolites often exhibit multipotent behavior and can be used as starting points in diversity-oriented semi-synthesis. Therefore, usage of biosynthetic intermediates can be considered as an alternative strategy to expand the structural diversity of natural products.

An attempt of manipulating five DMAPP-specific PTs was achieved by large-to-small mutation of the gatekeeping residues for prenyl donor selectivity. The generated mutants, *i.e.* FtmPT1_M364G, BrePT_I337G, CdpC2PT_T351G, CdpNPT_M349G, and CdpC3PT_F335G showed an increased activity towards GPP compared to their corresponding wild-types. As a result, the generated mutants catalyzed the conversion of 15 tested CDPs to their geranylated derivatives with different geranylation patterns. In total, 42 geranylated derivatives were obtained from one-step chemoenzymatic reactions. Particularly, nine products carrying geranyl moieties at all seven possible positions of the indole ring were obtained from the incubation mixtures of *cyclo*-L-Trp-L-Trp with the mutants in the presence of GPP. This study has proven structure-based protein engineering as an efficient and effective way to enrich the structural library of geranylated CDPs.

Over the course of searching reactive intermediates from biosynthetic pathway of natural products, we focused on an *ortho*-QM intermediate involved in the biosynthesis of peniphenone and penilactones in *Penicillium crustosum* PRB-2. The *ortho*-QM is formed by spontaneous water elimination of hydroxyclavatol, which was the oxidative product of clavatol by the nonheme Fe^{II}/2-oxoglutarate dependent oxygenase ClaD. The reactivity of the *ortho*-QM was confirmed by proving the nonenzymatic 1,4-Michael addition between the *ortho*-QM and the γ-butyrolactones in aqueous system, which led to the formation of peniphenone D and penilactone A or penilactones D and B. In addition to peniphenone and penilactones, the frequent occurrence of clavatol-containing natural products in fungi also implied the involvement of the *ortho*-QM intermediate in their formation. Therefore, subsequent efforts were made for the application of the *ortho*-QM in facile synthesis of clavatol-containing compounds. The reactivity of the *ortho*-QM derived from hydroxyclavatol was tested with 102 natural products or natural product-like compounds ranging from different phenolic compounds to indole derivatives. Totally, 32 clavatol-containing products were obtained in this study by incorporation of one or two clavatol units onto the *ortho*- or *para*-positions of the phenolic hydroxyl groups at the benzene ring, as well as by connection between the methylene group of the clavatol unit and the C-2 position of indole skeletons. We thus succeeded in the generation of diverse clavatol-

containing products by exploiting the reactivity of the *ortho*-QM intermediate derived from hydroxyclavatol.

For future prospects, the following works can be performed:

- In the project of protein engineering of PTs, the constructed mutants exhibited increased GPP acceptance but reduced regioselectivity. Therefore, further mutagenesis experiments are required to increase the desired regio- and stereoselectivity, which will facilitate the product isolation from one-step incubations.
- Since the structural information of more and more PTs will be available in the future, it is possible to mutate additional available PTs at the corresponding positions. The structural spectrum of geranylated and farnesylated products can be further expanded by using more mutants and testing more aromatic substrates.
- One of the prerequisites for the generation of the *ortho*-QM is the employment of the nonheme Fe^{II}/2-oxoglutarate dependent oxygenase ClaD for oxidation of clavatol to hydroxyclavatol. Incubating ClaD with more clavatol-like substrates may lead to the formation of more hydroxyclavatol-like benzylic alcohol products, which may also undergo spontaneous dehydration to yield various *ortho*-QM intermediates. By doing so, it is possible that not only clavatol-containing products but also other coupling products of clavatol-like molecules can be easily created.

6 References

1. Walsh, C. T.; Tang, Y., *Natural Product Biosynthesis*. Royal Society of Chemistry: 2017.

2. Yin, W.; Keller, N. P., Transcriptional regulatory elements in fungal secondary metabolism. *Journal of Microbiology* **2011,** *49* (3), 329-339.

3. Wiemann, P.; Keller, N. P., Strategies for mining fungal natural products. *Journal of Industrial Microbiology and Biotechnology* **2014,** *41* (2), 301-313.

4. Dufour, N.; Rao, R. P., Secondary metabolites and other small molecules as intercellular pathogenic signals. *FEMS Microbiology Letters* **2011,** *314* (1), 10-17.

5. Yim, G.; Wang, H. H.; Davies Frs, J., Antibiotics as signalling molecules. *Philosophical Transactions of the Royal Society B: Biological Sciences* **2007,** *362* (1483), 1195-1200.

6. Brakhage, A. A., Regulation of fungal secondary metabolism. *Nature Reviews Microbiology* **2013,** *11* (1), 21-32.

7. Fox, E. M.; Howlett, B. J., Secondary metabolism: regulation and role in fungal biology. *Current Opinion in Microbiology* **2008,** *11* (6), 481-487.

8. Rohlfs, M.; Churchill, A. C. L., Fungal secondary metabolites as modulators of interactions with insects and other arthropods. *Fungal Genetics and Biology* **2011,** *48* (1), 23-34.

9. Rodrigues, A. P. D.; Carvalho, A. S. C.; Santos, A. S.; Alves, C. N.; do Nascimento, J. L. M.; Silva, E. O., Kojic acid, a secondary metabolite from *Aspergillus* sp., acts as an inducer of macrophage activation. *Cell Biology International* **2011,** *35* (4), 335-343.

10. Bérdy, J., Thoughts and facts about antibiotics: where we are now and where we are heading. *The Journal of Antibiotics* **2012,** *65* (8), 385-395

11. Bérdy, J., Bioactive microbial metabolites. *The Journal of Antibiotics* **2005,** *58* (1), 1-26

12. Azmir, J.; Zaidul, I. S. M.; Rahman, M. M.; Sharif, K. M.; Mohamed, A.; Sahena, F.; Jahurul, M. H. A.; Ghafoor, K.; Norulaini, N. A. N.; Omar, A. K. M., Techniques for extraction of bioactive compounds from plant materials: A review. *Journal of Food Engineering* **2013,** *117* (4), 426-436.

13. Fischer, R.; Zekert, N.; Takeshita, N., Polarized growth in fungi–interplay between the cytoskeleton, positional markers and membrane domains. *Molecular Microbiology* **2008,** *68* (4), 813-826.

14. Bennett, R. J.; Turgeon, B. G., Fungal sex: the Ascomycota. *Microbiology Spectrum* **2016,** *4* (5), 115-145.

15. Webster, J.; Weber, R., *Introduction to fungi*. Cambridge University Press: 2007.

16. Hoffmeister, D.; Keller, N. P., Natural products of filamentous fungi: enzymes, genes, and their regulation. *Natural Product Reports* **2007,** *24* (2), 393-416.

17. Chavez, R.; Fierro, F.; Garcia-Rico, R. O.; Vaca, I., Filamentous fungi from extreme environments as a promising source of novel bioactive secondary metabolites. *Frontiers in Microbiology* **2015,** *6*, 903-909.

18. Demain, A. L.; Sanchez, S., Microbial drug discovery: 80 years of progress. *The Journal of Antibiotics* **2009,** *62* (1), 5-16.

19. Dictionary of Natural Products http://dnp.chemnetbase.com.

20. Chen, Y.; de Bruyn Kops, C.; Kirchmair, J., Data resources for the computer-guided discovery of bioactive natural products. *Journal of Chemical Information and Modeling* **2017,** *57* (9), 2099-2111.

21. Lyu, H. N.; Liu, H. W.; Keller, N. P.; Yin, W. B., Harnessing diverse transcriptional regulators for natural product discovery in fungi. *Natural Product Reports* **2020,** *37* (1), 6-16.

22. Brakhage, A. A.; Schroeckh, V., Fungal secondary metabolites–strategies to activate silent gene clusters. *Fungal Genetics and Biology* **2011,** *48* (1), 15-22.

23. Fan, A.; Mi, W.; Liu, Z.; Zeng, G.; Zhang, P.; Hu, Y.; Fang, W.; Yin, W. B., Deletion of a histone acetyltransferase leads to the pleiotropic activation of natural products in *Metarhizium robertsii*. *Organic Letters* **2017,** *19* (7), 1686-1689

24. Szewczyk, E.; Chiang, Y. M.; Oakley, C. E.; Davidson, A. D.; Wang, C. C. C.; Oakley, B. R., Identification and characterization of the asperthecin gene cluster of *Aspergillus nidulans*. *Applied and Environmental Microbiology* **2008,** *74* (24), 7607-7612

25. Cichewicz, R. H., Epigenome manipulation as a pathway to new natural product scaffolds and their congeners. *Natural Product Reports* **2010,** *27* (1), 11-22.

26. Yin, W. B.; Baccile, J. A.; Bok, J. W.; Chen, Y.; Keller, N. P.; Schroeder, F. C., A nonribosomal peptide synthetase-derived iron(III) complex from the pathogenic fungus *Aspergillus fumigatus*. *Journal of the American Chemical Society* **2013,** *135* (6), 2064-2067.

27. Lim, F. Y.; Hou, Y.; Chen, Y.; Oh, J. H.; Lee, I.; Bugni, T. S.; Keller, N. P., Genome-based cluster deletion reveals an endocrocin biosynthetic pathway in *Aspergillus fumigatus*. *Applied and Environmental Microbiology* **2012,** *78* (12), 4117-4125.

28. Bouhired, S.; Weber, M.; Kempf-Sontag, A.; Keller, N. P.; Hoffmeister, D., Accurate prediction of the *Aspergillus nidulans* terrequinone gene cluster boundaries using the transcriptional regulator LaeA. *Fungal Genetics and Biology* **2007,** *44* (11), 1134-1145.

29. Baba, S.; Kinoshita, H.; Nihira, T., Identification and characterization of *Penicillium citrinum* VeA and LaeA as global regulators for ML-236B production. *Current Genetics* **2012,** *58* (1), 1-11.

30. Yang, X. L.; Awakawa, T.; Wakimoto, T.; Abe, I., Three acyltetronic acid derivatives: noncanonical cryptic polyketides from *Aspergillus niger* identified by genome mining. *Chembiochem* **2014,** *15* (11), 1578-1583.

31. Sørensen, J. L.; Hansen, F. T.; Sondergaard, T. E.; Staerk, D.; Lee, T. V.; Wimmer, R.; Klitgaard, L. G.; Purup, S.; Giese, H.; Frandsen, R. J. N., Production of novel fusarielins by ectopic activation of the polyketide synthase 9 cluster in *Fusarium graminearum*. *Environmental Microbiology* **2012,** *14* (5), 1159-1170.

32. König, C. C.; Scherlach, K.; Schroeckh, V.; Horn, F.; Nietzsche, S.; Brakhage, A. A.; Hertweck, C., Bacterium induces cryptic meroterpenoid pathway in the pathogenic fungus *Aspergillus fumigatus*. *Chembiochem* **2013,** *14* (8), 938-942.

33. Chooi, Y. H.; Fang, J.; Liu, H.; Filler, S. G.; Wang, P.; Tang, Y., Genome mining of a prenylated and immunosuppressive polyketide from pathogenic fungi. *Organic Letters* **2013,** *15* (4), 780-783.

34. Chiang, Y. M.; Oakley, C. E.; Ahuja, M.; Entwistle, R.; Schultz, A.; Chang, S. L.; Sung, C. T.; Wang, C. C.; Oakley, B. R., An efficient system for heterologous expression of secondary metabolite genes in *Aspergillus nidulans*. *Journal of the American Chemical Society* **2013,** *135* (20), 7720-7731.

35. Sakai, K.; Kinoshita, H.; Shimizu, T.; Nihira, T., Construction of a citrinin gene cluster expression system in heterologous *Aspergillus oryzae*. *Journal of Bioscience and Bioengineering* **2008,** *106* (5), 466-472

36. Bai, T.; Quan, Z.; Zhai, R.; Awakawa, T.; Matsuda, Y.; Abe, I., Elucidation and heterologous reconstitution of chrodrimanin B biosynthesis. *Organic Letters* **2018,** *20* (23), 7504-7508.

37. Harvey, C. J. B.; Tang, M.; Schlecht, U.; Horecka, J.; Fischer, C. R.; Lin, H. C.; Li, J.; Naughton, B.; Cherry, J.; Miranda, M., HEx: A heterologous expression platform for the discovery of fungal natural products. *Science Advances* **2018,** *4* (4), 2375-2548.

38. Lim, F. Y.; Keller, N. P., Spatial and temporal control of fungal natural product synthesis. *Natural Product Reports* **2014,** *31* (10), 1277-1286.

39. Hill, A. M., The biosynthesis, molecular genetics and enzymology of the polyketide-derived metabolites. *Natural Product Reports* **2006,** *23* (2), 256-320.

40. Priest, J. W.; Light, R. J., Patulin biosynthesis: epoxidation of toluquinol and gentisyl alcohol by particulate preparations from *Penicillium patulum*. *Biochemistry* **1989,** *28* (23), 9192-9200

41. Puel, O.; Galtier, P.; Oswald, I. P., Biosynthesis and toxicological effects of patulin. *Toxins* **2010,** *2* (4), 613-631.

42. Forrester, P. I.; Gaucher, G. M., Conversion of 6-methylsalicylic acid into patulin by *Penicillium urticae*. *Biochemistry* **1972,** *11* (6), 1102-1107

43. Sanchez, J. F.; Chiang, Y. M.; Szewczyk, E.; Davidson, A. D.; Ahuja, M.; Elizabeth, O. C.; Woo, B. J.; Keller, N.; Oakley, B. R.; Wang, C. C. C., Molecular genetic analysis of the orsellinic acid/F9775 gene cluster of *Aspergillus nidulans*. *Molecular Biosystems* **2010,** *6* (3), 587-593.

44. Hesseltine, C. W.; Shotwell, O. L.; Ellis, J. J.; Stubblefield, R. D., Aflatoxin formation by *Aspergillus flavus*. *Bacteriological reviews* **1966,** *30* (4), 795-805.

45. Yu, J.; Chang, P. K.; Ehrlich, K. C.; Cary, J. W.; Bhatnagar, D.; Cleveland, T. E.; Payne, G. A.; Linz, J. E.; Woloshuk, C. P.; Bennett, J. W., Clustered pathway genes in aflatoxin biosynthesis. *Applied and Environmental Microbiology* **2004,** *70* (3), 1253-1262

46. Yabe, K.; Nakajima, H., Enzyme reactions and genes in aflatoxin biosynthesis. *Applied Microbiology and Biotechnology* **2004,** *64* (6), 745-755.

47. Brown, J. P.; Cartwright, N. J.; Robertson, A.; Whalley, W. B., Structure of citrinin. *Nature* **1948,** *162* (4106), 72-73.

48. He, Y.; Cox, R. J., The molecular steps of citrinin biosynthesis in fungi. *Chemical Science* **2016,** *7* (3), 2119-2127.

49. Davison, J.; al Fahad, A.; Cai, M.; Song, Z.; Yehia, S. Y.; Lazarus, C. M.; Bailey, A. M.; Simpson, T. J.; Cox, R. J., Genetic, molecular, and biochemical basis of fungal tropolone biosynthesis. *Proceedings of the National Academy of Sciences* **2012,** *109* (20), 7642-7647.

50. Tobert, J. A., Lovastatin and beyond: the history of the HMG-CoA reductase inhibitors. *Nature reviews Drug discovery* **2003,** *2* (7), 517-526

51. Havel, R. J.; Hunninghake, D. B.; Illingworth, D. R.; Lees, R. S.; Stein, E. A.; Tobert, J. A.; Bacon, S. R.; Bolognese, J. A.; Frost, P. H.; Lamkin, G. E., Lovastatin (mevinolin) in the treatment of heterozygous familial hypercholesterolemia: a multicenter study. *Annals of Internal Medicine* **1987,** *107* (5), 609-615.

52. Campbell, C. D.; Vederas, J. C., Biosynthesis of lovastatin and related metabolites formed by fungal iterative PKS enzymes. *Biopolymers* **2010,** *93* (9), 755-763.

53. Walsh, C. T., Insights into the chemical logic and enzymatic machinery of NRPS assembly lines. *Natural Product Reports* **2016,** *33* (2), 127-135.

54. Wainwright, M., *Miracle cure: The story of penicillin and the golden age of antibiotics*. Blackwell publishing: 1990.

55. Kardos, N.; Demain, A. L., Penicillin: the medicine with the greatest impact on therapeutic outcomes. *Applied Microbiology and Biotechnology* **2011,** *92* (4), 677-687.

56. Abraham, E. P.; Newton, G. G. F., The structure of cephalosporin C. *Biochemical Journal* **1961,** *79* (2), 377-393.

57. Scharf, D. H.; Heinekamp, T.; Remme, N.; Hortschansky, P.; Brakhage, A. A.; Hertweck, C., Biosynthesis and function of gliotoxin in *Aspergillus fumigatus*. *Applied Microbiology and Biotechnology* **2012,** *93* (2), 467-472.

58. Waring, P.; Beaver, J., Gliotoxin and related epipolythiodioxopiperazines. *General Pharmacology: The Vascular System* **1996,** *27* (8), 1311-1316.

59. Elliott, C. E.; Gardiner, D. M.; Thomas, G.; Cozijnsen, A.; Van de Wouw, A.; Howlett, B. J., Production of the toxin sirodesmin PL by *Leptosphaeria maculans* during infection of *Brassica napus*. *Molecular Plant Pathology* **2007,** *8* (6), 791-802.

60. Denning, D. W., Echinocandins and pneumocandins–a new antifungal class with a novel mode of action. *The Journal of Antimicrobial Chemotherapy* **1997,** *40* (5), 611-614

61. Matsuda, S.; Koyasu, S., Mechanisms of action of cyclosporine. *Immunopharmacology* **2000,** *47* (2-3), 119-125

62. Miziorko, H. M., Enzymes of the mevalonate pathway of isoprenoid biosynthesis. *Archives of Biochemistry and Biophysics* **2011,** *505* (2), 131-143

63. Caruthers, J. M.; Kang, I.; Rynkiewicz, M. J.; Cane, D. E.; Christianson, D. W., Crystal structure determination of aristolochene synthase from the blue cheese mold, *Penicillium roqueforti*. *Journal of Biological Chemistry* **2000,** *275* (33), 25533-25539

64. Tanaka, S.; Wada, K.; Katayama, M.; Marumo, S., Isolation of sporogen-AO1, a sporogenic substance, from *Aspergillus oryzae*. *Agricultural and Biological Chemistry* **1984,** *48* (12), 3189-3191.

65. Wei, R. D.; Schnoes, H. K.; Hart, P. A.; Strong, F. M., The structure of PR toxin, a mycotoxin from *Penicillium roqueforti*. *Tetrahedron* **1975,** *31* (2), 109-114

66. Capasso, R.; Iacobellis, N. S.; Bottalico, A.; Randazzo, G., Structure-toxicity relationships of the eremophilane phomenone and PR-toxin. *Phytochemistry* **1984,** *23* (12), 2781-2784.

67. Avalos, J.; Cerdá-Olmedo, E.; Reyes, F.; Barrero, A. F., Gibberellins and other metabolites of *Fusarium fujikuroi* and related fungi. *Current Organic Chemistry* **2007,** *11* (8), 721-737

68. Kong, F. D.; Huang, X. L.; Ma, Q. Y.; Xie, Q. Y.; Wang, P.; Chen, P. W.; Zhou, L. M.; Yuan, J. Z.; Dai, H. F.; Luo, D. Q., Helvolic acid derivatives with antibacterial activities against *Streptococcus agalactiae* from the marine-derived fungus *Aspergillus fumigatus* HNMF0047. *Journal of Natural Products* **2018,** *81* (8), 1869-1876.

69. Lv, J. M.; Hu, D.; Gao, H.; Kushiro, T.; Awakawa, T.; Chen, G. D.; Wang, C. X.; Abe, I.; Yao, X. S., Biosynthesis of helvolic acid and identification of an unusual C-4-demethylation process distinct from sterol biosynthesis. *Nature Communications* **2017,** *8* (1), 1644-1654.

70. Xu, W.; Gavia, D. J.; Tang, Y., Biosynthesis of fungal indole alkaloids. *Natural Product Reports* **2014,** *31* (10), 1474-1487.

71. Borthwick, A. D., 2,5-Diketopiperazines: synthesis, reactions, medicinal chemistry, and bioactive natural products. *Chemical Reviews* **2012,** *112* (7), 3641-3716.

72. Maiya, S.; Grundmann, A.; Li, S. M.; Turner, G., The fumitremorgin gene cluster of *Aspergillus fumigatus*: identification of a gene encoding brevianamide F synthetase. *Chembiochem* **2006,** *7* (7), 1062-1069.

73. Li, S. M., Genome mining and biosynthesis of fumitremorgin-type alkaloids in ascomycetes. *The Journal of Antibiotics* **2011,** *64* (1), 45-49.

74. Balibar, C. J.; Howard-Jones, A. R.; Walsh, C. T., Terrequinone A biosynthesis through L-tryptophan oxidation, dimerization and bisprenylation. *Nature Chemical Biology* **2007,** *3* (9), 584-592.

75. Haynes, S. W.; Gao, X.; Tang, Y.; Walsh, C. T., Complexity generation in fungal peptidyl alkaloid biosynthesis: A two-enzyme pathway to the hexacyclic MDR export pump inhibitor ardeemin. *ACS Chemical Biology* **2013,** *8*, 741-748.

76. Wallwey, C.; Li, S. M., Ergot alkaloids: structure diversity, biosynthetic gene clusters and functional proof of biosynthetic genes. *Natural Product Reports* **2011,** *28* (3), 496-510.

77. Liu, H.; Jia, Y., Ergot alkaloids: synthetic approaches to lysergic acid and clavine alkaloids. *Natural Product Reports* **2017,** *34* (4), 411-432.

78. Cole, R. J.; Kirksey, J. W.; Dorner, J. W.; Wilson, D. M.; Johnson Jr, J. C.; Johnson, A. N.; Bedell, D. M.; Springer, J. P.; Chexal, K. K., Mycotoxins produced by *Aspergillus fumigatus* species isolated from molded silage. *Journal of Agricultural and Food Chemistry* **1977,** *25* (4), 826-830

79. Haarmann, T.; Lorenz, N.; Tudzynski, P., Use of a nonhomologous end joining deficient strain (Δku70) of the ergot fungus *Claviceps purpurea* for identification of a nonribosomal peptide synthetase gene involved in ergotamine biosynthesis. *Fungal Genetics and Biology* **2008,** *45* (1), 35-44.

80. Liu, X.; Walsh, C. T., Cyclopiazonic acid biosynthesis in *Aspergillus* sp.: Characterization of a reductase-like R* domain in cyclopiazonate synthetase that forms and releases *cyclo*-acetoacetyl-L-tryptophan. *Biochemistry* **2009,** *48* (36), 8746-8757.

81. Young, C.; McMillan, L.; Telfer, E.; Scott, B., Molecular cloning and genetic analysis of an indole-diterpene gene cluster from *Penicillium paxilli*. *Molecular Microbiology* **2001,** *39* (3), 754-764

82. Eley, K. L.; Halo, L. M.; Song, Z.; Powles, H.; Cox, R. J.; Bailey, A. M.; Lazarus, C. M.; Simpson, T. J., Biosynthesis of the 2-pyridone tenellin in the insect pathogenic fungus *Beauveria bassiana*. *Chembiochem* **2007,** *8* (3), 289-297.

83. Sims, J. W.; Fillmore, J. P.; Warner, D. D.; Schmidt, E. W., Equisetin biosynthesis in *Fusarium heterosporum*. *Chemical Communications* **2005,** (2), 186-188.

84. Hu, J.; Okawa, H.; Yamamoto, K.; Oyama, K.; Mitomi, M.; Anzai, H., Characterization of two cytochrome P450 monooxygenase genes of the pyripyropene biosynthetic gene cluster from *Penicillium coprobium*. *The Journal of Antibiotics* **2011,** *64* (3), 221-227.

85. Omura, S.; Tomoda, H.; Kim, Y. K.; Nishida, H., Pyripyropenes, highly potent inhibitors of acyl-CoA: cholesterol acyltransferase produced by *Aspergillus fumigatus*. *The Journal of Antibiotics* **1993,** *46* (7), 1168-1169.

86. Lin, H. C.; Chooi, Y. H.; Dhingra, S.; Xu, W.; Calvo, A. M.; Tang, Y., The fumagillin biosynthetic gene cluster in *Aspergillus fumigatus* encodes a cryptic terpene cyclase involved in the formation of β-*trans*-bergamotene. *Journal of the American Chemical Society* **2013,** *135* (12), 4616-4619.

87. Keller, N. P.; Hohn, T. M., Metabolic pathway gene clusters in filamentous fungi. *Fungal Genetics and Biology* **1997,** *21* (1), 17-29.

88. Walton, J. D., Horizontal gene transfer and the evolution of secondary metabolite gene clusters in fungi: an hypothesis. *Fungal Genetics and Biology* **2000,** *30* (3), 167-171.

89. Moore, B. S.; Hertweck, C., Biosynthesis and attachment of novel bacterial polyketide synthase starter units. *Natural Product Reports* **2002,** *19* (1), 70-99.

90. Keatinge-Clay, A. T., The structures of type I polyketide synthases. *Natural Product Reports* **2012,** *29* (10), 1050-1073.

91. Shen, B., Polyketide biosynthesis beyond the type I, II and III polyketide synthase paradigms. *Current Opinion in Chemical Biology* **2003,** *7* (2), 285-295.

92. Hertweck, C.; Luzhetskyy, A.; Rebets, Y.; Bechthold, A., Type II polyketide synthases: gaining a deeper insight into enzymatic teamwork. *Natural Product Reports* **2007,** *24* (1), 162-190.

93. Austin, M. B.; Noel, J. P., The chalcone synthase superfamily of type III polyketide synthases. *Natural Product Reports* **2003,** *20* (1), 79-110.

94. Hashimoto, M.; Nonaka, T.; Fujii, I., Fungal type III polyketide synthases. *Natural Product Reports* **2014,** *31* (10), 1306-1317.

95. Chan, Y. A.; Podevels, A. M.; Kevany, B. M.; Thomas, M. G., Biosynthesis of polyketide synthase extender units. *Natural Product Reports* **2009,** *26* (1), 90-114.

96. Miyanaga, A., Structure and function of polyketide biosynthetic enzymes: various strategies for production of structurally diverse polyketides. *Bioscience, Biotechnology, and Biochemistry* **2017,** *81* (12), 2227-2236.

97. Cox, R. J., Polyketides, proteins and genes in fungi: programmed nano-machines begin to reveal their secrets. *Organic & biomolecular chemistry* **2007,** *5* (13), 2010-2026.

98. Zhou, H.; Li, Y.; Tang, Y., Cyclization of aromatic polyketides from bacteria and fungi. *Natural Product Reports* **2010,** *27* (6), 839-868.

99. Klaus, M.; Grininger, M., Engineering strategies for rational polyketide synthase design. *Natural Product Reports* **2018,** *35* (10), 1070-1081.

100. Liu, T.; Chiang, Y. M.; Somoza, A. D.; Oakley, B. R.; Wang, C. C. C., Engineering of an “unnatural” natural product by swapping polyketide synthase domains in *Aspergillus nidulans*. *Journal of the American Chemical Society* **2011,** *133* (34), 13314-13316.

101. Petkovic, H.; Lill, R. E.; Sheridan, R. M.; Wilkinson, B.; McCormick, E. L.; McArthur, H. A.; Staunton, J.; Leadlay, P. F.; Kendrew, S. G., A novel erythromycin, 6-desmethyl erythromycin D, made by substituting an acyltransferase domain of the erythromycin polyketide synthase. *The Journal of Antibiotics* **2003,** *56* (6), 543-551.

102. Hur, G. H.; Vickery, C. R.; Burkart, M. D., Explorations of catalytic domains in non-ribosomal peptide synthetase enzymology. *Natural Product Reports* **2012,** *29* (10), 1074-1098.

103. Jin, J. M.; Lee, S.; Lee, J.; Baek, S. R.; Kim, J. C.; Yun, S. H.; Park, S. Y.; Kang, S.; Lee, Y. W., Functional characterization and manipulation of the apicidin biosynthetic pathway in *Fusarium semitectum*. *Molecular Microbiology* **2010,** *76* (2), 456-466.

104. Xu, Y.; Orozco, R.; Wijeratne, E. M. K.; Gunatilaka, A. A. L.; Stock, S. P.; Molnár, I., Biosynthesis of the cyclooligomer depsipeptide beauvericin, a virulence factor of the entomopathogenic fungus *Beauveria bassiana*. *Chemistry & Biology* **2008,** *15* (9), 898-907.

105. Marshall, C. G.; Hillson, N. J.; Walsh, C. T., Catalytic mapping of the vibriobactin biosynthetic enzyme VibF. *Biochemistry* **2002,** *41* (1), 244-250.

106. Challis, G. L.; Ravel, J.; Townsend, C. A., Predictive, structure-based model of amino acid recognition bynonribosomal peptide synthetase adenylation domains. *Chemistry & Biology* **2000,** *7* (3), 211-224.

107. Belshaw, P. J.; Walsh, C. T.; Stachelhaus, T., Aminoacyl-CoAs as probes of condensation domain selectivity in nonribosomal peptide synthesis. *Science* **1999,** *284* (5413), 486-489.

108. Kittilä, T.; Mollo, A.; Charkoudian, L. K.; Cryle, M. J., New structural data reveal the motion of carrier proteins in nonribosomal peptide synthesis. *Angewandte Chemie International Edition* **2016,** *55* (34), 9834-9840.

109. Süssmuth, R. D.; Mainz, A., Nonribosomal peptide synthesis–Principles and prospects. *Angewandte Chemie International Edition* **2017,** *56* (14), 3770-3821.

110. Gao, X.; Haynes, S. W.; Ames, B. D.; Wang, P.; Vien, L. P.; Walsh, C. T.; Tang, Y., Cyclization of fungal nonribosomal peptides by a terminal condensation-like domain. *Nature Chemical Biology* **2012,** *8* (10), 823-830.

111. Walsh, C. T.; O'Brien, R. V.; Khosla, C., Nonproteinogenic amino acid building blocks for nonribosomal peptide and hybrid polyketide scaffolds. *Angewandte Chemie International Edition* **2013,** *52* (28), 7098-124.

112. Nguyen, K. T.; Ritz, D.; Gu, J. Q.; Alexander, D.; Chu, M.; Miao, V.; Brian, P.; Baltz, R. H., Combinatorial biosynthesis of novel antibiotics related to daptomycin. *Proceedings of the National Academy of Sciences* **2006,** *103* (46), 17462-17467

113. Miyanaga, A.; Kudo, F.; Eguchi, T., Protein-protein interactions in polyketide synthase-nonribosomal peptide synthetase hybrid assembly lines. *Natural Product Reports* **2018,** *35* (11), 1185-1209.

114. Bergmann, S.; Schümann, J.; Scherlach, K.; Lange, C.; Brakhage, A. A.; Hertweck, C., Genomics-driven discovery of PKS-NRPS hybrid metabolites from *Aspergillus nidulans*. *Nature Chemical Biology* **2007,** *3* (4), 213-217.

115. Tokuoka, M.; Seshime, Y.; Fujii, I.; Kitamoto, K.; Takahashi, T.; Koyama, Y., Identification of a novel polyketide synthase-nonribosomal peptide synthetase (PKS-NRPS) gene required for the biosynthesis of cyclopiazonic acid in *Aspergillus oryzae*. *Fungal Genetics and Biology* **2008,** *45* (12), 1608-1615.

116. Schümann, J.; Hertweck, C., Molecular basis of cytochalasan biosynthesis in fungi: gene cluster analysis and evidence for the involvement of a PKS-NRPS hybrid synthase by RNA silencing. *Journal of the American Chemical Society* **2007,** *129* (31), 9564-9565.

117. Qiao, K.; Chooi, Y. H.; Tang, Y., Identification and engineering of the cytochalasin gene cluster from *Aspergillus clavatus* NRRL 1. *Metabolic Engineering* **2011,** *13* (6), 723-732.

118. Song, Z.; Cox, R. J.; Lazarus, C. M.; Simpson Tj, T. J., Fusarin C biosynthesis in *Fusarium moniliforme* and *Fusarium venenatum*. *Chembiochem* **2004,** *5* (9), 1196-1203.

119. Halo, L. M.; Marshall, J. W.; Yakasai, A. A.; Song, Z.; Butts, C. P.; Crump, M. P.; Heneghan, M.; Bailey, A. M.; Simpson, T. J.; Lazarus, C. M.; Cox, R. J., Authentic heterologous expression of the tenellin Iterative polyketide synthase nonribosomal peptide synthetase requires coexpression with an enoyl reductase. *Chembiochem* **2008,** *9* (4), 585-594.

120. Maiya, S.; Grundmann, A.; Li, X.; Li, S. M.; Turner, G., Identification of a hybrid PKS/NRPS required for pseurotin A biosynthesis in the human pathogen *Aspergillus fumigatus*. *Chembiochem* **2007,** *8* (14), 1736-1743.

121. Phonghanpot, S.; Punya, J.; Tachaleat, A.; Laoteng, K.; Bhavakul, V.; Tanticharoen, M.; Cheevadhanarak, S., Biosynthesis of Xyrrolin, a new cytotoxic hybrid polyketide/non−ribosomal peptide pyrroline with anticancer potential, in *Xylaria* sp. BCC 1067. *Chembiochem* **2012,** *13* (6), 895-903.

122. Heneghan, M. N.; Yakasai, A. A.; Williams, K.; Kadir, K. A.; Wasil, Z.; Bakeer, W.; Fisch, K. M.; Bailey, A. M.; Simpson, T. J.; Cox, R. J.; Lazarus, C. M., The programming role of trans-acting enoyl reductases during the biosynthesis of highly reduced fungal polyketides. *Chemical Science* **2011,** *2* (5), 972-979.

123. Conti, E.; Stachelhaus, T.; Marahiel, M. A.; Brick, P., Structural basis for the activation of phenylalanine in the non-ribosomal biosynthesis of gramicidin S. *The EMBO Journal* **1997,** *16* (14), 4174-4183.

124. Yun, C. S.; Motoyama, T.; Osada, H., Biosynthesis of the mycotoxin tenuazonic acid by a fungal NRPS-PKS hybrid enzyme. *Nature Communications* **2015,** *6* (1), 1-9.

125. Hai, Y.; Huang, A.; Tang, Y., Biosynthesis of amino acid derived α-pyrones by an NRPS–NRPKS hybrid megasynthetase in Fungi. *Journal of Natural Products* **2020,** *83* (3), 593-600.

126. Xu, W.; Cai, X.; Jung, M. E.; Tang, Y., Analysis of intact and dissected fungal polyketide synthase-nonribosomal peptide synthetase in vitro and in *Saccharomyces cerevisiae*. *Journal of the American Chemical Society* **2010,** *132* (39), 13604-13607.

127. Alhassan, A. M.; Abdullahi, M. I.; Uba, A.; Umar, A., Prenylation of aromatic secondary metabolites: a new frontier for development of novel drugs. *Tropical Journal of Pharmaceutical Research* **2014,** *13* (2), 307-314.

128. Heide, L., Prenyl transfer to aromatic substrates: genetics and enzymology. *Current Opinion in Chemical Biology* **2009,** *13* (2), 171-179.

129. Mori, T., Enzymatic studies on aromatic prenyltransferases. *Journal of Natural Medicines* **2020,** *74* (3), 501-512.

130. Li, W., Bringing bioactive compounds into membranes: The UbiA superfamily of intramembrane aromatic prenyltransferases. *Trends in Biochemical Sciences* **2016,** *41* (4), 356-370.

131. Young, I. G.; Leppik, R. A.; Hamilton, J. A.; Gibson, F., Biochemical and genetic studies on ubiquinone biosynthesis in *Escherichia coli* K-12: 4-hydroxybenzoate octaprenyltransferase. *Journal of Bacteriology* **1972,** *110* (1), 18-25.

132. Guo, R. T.; Kuo, C. J.; Chou, C. C.; Ko, T. P.; Shr, H. L.; Liang, P. H.; Wang, A. H., Crystal structure of octaprenyl pyrophosphate synthase from hyperthermophilic *Thermotoga maritima* and mechanism of product chain length determination. *The Journal of Biological Chemistry* **2004,** *279* (6), 4903-4912.

133. Guo, R. T.; Ko, T. P.; Chen, A. P.; Kuo, C. J.; Wang, A. H.; Liang, P. H., Crystal structures of undecaprenyl pyrophosphate synthase in complex with magnesium, isopentenyl pyrophosphate, and farnesyl thiopyrophosphate: roles of the metal ion and conserved residues in catalysis. *The Journal of Biological Chemistry* **2005,** *280* (21), 20762-20774.

134. Winkelblech, J.; Fan, A.; Li, S. M., Prenyltransferases as key enzymes in primary and secondary metabolism. *Applied Microbiology and Biotechnology* **2015,** *99* (18), 7379-7397.

135. Pojer, F.; Wemakor, E.; Kammerer, B.; Chen, H.; Walsh, C. T.; Li, S. M.; Heide, L., CloQ, a prenyltransferase involved in clorobiocin biosynthesis. *Proceedings of the National Academy of Sciences* **2003,** *100* (5), 2316-2321.

136. Kuzuyama, T.; Noel, J. P.; Richard, S. B., Structural basis for the promiscuous biosynthetic prenylation of aromatic natural products. *Nature* **2005,** *435* (7044), 983-987.

137. Li, S. M., Prenylated indole derivatives from fungi: structure diversity, biological activities, biosynthesis and chemoenzymatic synthesis. *Natural Product Reports* **2010,** *27* (1), 57-78.

138. Fan, A.; Winkelblech, J.; Li, S. M., Impacts and perspectives of prenyltransferases of the DMATS superfamily for use in biotechnology. *Applied Microbiology and Biotechnology* **2015,** *99* (18), 7399-7415.

139. Tsai, H. F.; Wang, H.; Gebler, J. C.; Poulter, C. D.; Schardl, C. L., The *Claviceps purpurea* gene encoding dimethylallyltryptophan synthase, the committed step for ergot alkaloid biosynthesis. *Biochemical and Biophysical Research Communications* **1995,** *216* (1), 119-125.

140. Unsöld, I. A.; Li, S. M., Overproduction, purification and characterization of FgaPT2, a dimethylallyltryptophan synthase from *Aspergillus fumigatus*. *Microbiology* **2005,** *151* (5), 1499-1505.

141. Metzger, U.; Schall, C.; Zocher, G.; Unsöld, I.; Stec, E.; Li, S. M.; Heide, L.; Stehle, T., The structure of dimethylallyl tryptophan synthase reveals a common architecture of aromatic prenyltransferases in fungi and bacteria. *Proceedings of the National Academy of Sciences* **2009,** *106* (34), 14309-14314.

142. Markert, A.; Steffan, N.; Ploss, K.; Hellwig, S.; Steiner, U.; Drewke, C.; Li, S. M.; Boland, W.; Leistner, E., Biosynthesis and accumulation of ergoline alkaloids in a mutualistic association between *Ipomoea asarifolia* (Convolvulaceae) and a clavicipitalean fungus. *Plant Physiology* **2008,** *147* (1), 296-305.

143. Ding, Y.; Williams, R. M.; Sherman, D. H., Molecular analysis of a 4-dimethylallyltryptophan synthase from *Malbranchea aurantiaca*. *The Journal of Biological Chemistry* **2008,** *283* (23), 16068-16076.

144. Yu, X.; Liu, Y.; Xie, X.; Zheng, X. D.; Li, S. M., Biochemical characterization of indole prenyltransferases: Filling the last gap of prenylation positions by a 5-dimethylallyltryptophan synthase from *Aspergillus clavatus*. *The Journal of Biological Chemistry* **2012,** *287* (2), 1371-1380.

145. Winkelblech, J.; Xie, X.; Li, S. M., Characterisation of 6-DMATS$_{Mo}$ from *Micromonospora olivasterospora* leading to identification of the divergence in enantioselectivity, regioselectivity and multiple prenylation of tryptophan prenyltransferases. *Organic & Biomolecular Chemistry* **2016,** *14* (41), 9883-9895.

146. Kremer, A.; Westrich, L.; Li, S. M., A 7-dimethylallyltryptophan synthase from *Aspergillus fumigatus*: overproduction, purification and biochemical characterization. *Microbiology* **2007,** *153* (10), 3409-3416.

147. Miyamoto, K.; Ishikawa, F.; Nakamura, S.; Hayashi, Y.; Nakanishi, I.; Kakeya, H., A 7-dimethylallyl tryptophan synthase from a fungal *Neosartorya* sp.: Biochemical characterization and structural insight into the regioselective prenylation. *Bioorganic & Medicinal Chemistry* **2014,** *22* (8), 2517-2528.

148. Kremer, A.; Li, S. M., A tyrosine *O*-prenyltransferase catalyses the first pathway-specific step in the biosynthesis of sirodesmin PL. *Microbiology* **2010,** *156* (1), 278-286.

149. Fan, A.; Chen, H.; Wu, R.; Xu, H.; Li, S. M., A new member of the DMATS superfamily from *Aspergillus niger* catalyzes prenylations of both tyrosine and tryptophan derivatives. *Applied Microbiology and Biotechnology* **2014,** *98* (24), 10119-10129.

150. Grundmann, A.; Li, S. M., Overproduction, purification and characterization of FtmPT1, a brevianamide F prenyltransferase from *Aspergillus fumigatus*. *Microbiology* **2005,** *151* (7), 2199-2207.

151. Ding, Y.; Wet, J. R.; Cavalcoli, J.; Li, S.; Greshock, T. J.; Miller, K. A.; Finefield, J. M.; Sunderhaus, J. D.; McAfoos, T. J.; Tsukamoto, S.; Williams, R. M.; Sherman, D. H., Genome-based characterization of two prenylation steps in the assembly of the stephacidin and notoamide anticancer agents in a marine-derived *Aspergillus* sp. *Journal of the American Chemical Society* **2010,** *132* (36), 12733-12740.

152. Yin, S.; Yu, X.; Wang, Q.; Liu, X. Q.; Li, S. M., Identification of a brevianamide F reverse prenyltransferase BrePT from *Aspergillus versicolor* with a broad substrate specificity towards tryptophan-containing cyclic dipeptides. *Applied Microbiology and Biotechnology* **2013,** *97* (4), 1649-1660.

153. Mundt, K.; Li, S. M., CdpC2PT, a reverse prenyltransferase from *Neosartorya fischeri* with distinct substrate preference from known C2-prenyltransferases. *Microbiology* **2013,** *159* (10), 2169-2179.

154. Schuller, J. M.; Zocher, G.; Liebhold, M.; Xie, X.; Stahl, M.; Li, S. M.; Stehle, T., Structure and catalytic mechanism of a cyclic dipeptide prenyltransferase with broad substrate promiscuity. *Journal of Molecular Biology* **2012,** *422* (1), 87-99.

155. Yin, W. B.; Grundmann, A.; Cheng, J.; Li, S. M., Acetylaszonalenin biosynthesis in *Neosartorya fischeri*: Identification of the biosynthetic gene cluster by genomic mining and functional proof of the genes by biochemical investigation. *The Journal of Biological Chemistry* **2009,** *284* (1), 100-109.

156. Yin, W. B.; Yu, X.; Xie, X. L.; Li, S. M., Preparation of pyrrolo[2,3-b]indoles carrying a β-configured reverse C3-dimethylallyl moiety by using a recombinant prenyltransferase CdpC3PT. *Organic & Biomolecular Chemistry* **2010,** *8* (10), 2430-2438.

157. Wunsch, C.; Zou, H. X.; Linne, U.; Li, S. M., *C7*-prenylation of tryptophanyl and *O*-prenylation of tyrosyl residues in dipeptides by an *Aspergillus terreus* prenyltransferase. *Applied Microbiology and Biotechnology* **2015,** *99* (4), 1719-1730.

158. Zou, H. X.; Xie, X. L.; Linne, U.; Zheng, X. D.; Li, S. M., Simultaneous C7-and N1-prenylation of cyclo-L-Trp-L-Trp catalyzed by a prenyltransferase from *Aspergillus oryzae*. *Organic & Biomolecular Chemistry* **2010,** *8* (13), 3037-3044.

159. Schneider, P.; Weber, M.; Hoffmeister, D., The *Aspergillus nidulans* enzyme TdiB catalyzes prenyltransfer to the precursor of bioactive asterriquinones. *Fungal Genetics and Biology* **2008,** *45* (3), 302-309.

160. Liu, C.; Noike, M.; Minami, A.; Oikawa, H.; Dairi, T., Functional analysis of a prenyltransferase gene (paxD) in the paxilline biosynthetic gene cluster. *Applied Microbiology and Biotechnology* **2014,** *98* (1), 199-206.

161. Pockrandt, D.; Ludwig, L.; Fan, A.; König, G. M.; Li, S. M., New insights into the biosynthesis of prenylated xanthones: XptB from *Aspergillus nidulans* catalyses an *O*-prenylation of xanthones. *Chembiochem* **2012,** *13* (18), 2764-2771.

162. Steiner, U.; Leibner, S.; Schardl, C. L.; Leuchtmann, A.; Leistner, E., *Periglandula*, a new fungal genus within the *Clavicipitaceae* and its association with *Convolvulaceae*. *Mycologia* **2011,** *103* (5), 1133-1145.

163. Luk, L. Y.; Qian, Q.; Tanner, M. E., A cope rearrangement in the reaction catalyzed by dimethylallyltryptophan synthase? *Journal of the American Chemical Society* **2011,** *133* (32), 12342-12345.

164. Fan, A.; Li, S. M., Saturation mutagenesis on Arg244 of the tryptophan C4-prenyltransferase FgaPT2 leads to enhanced catalytic ability and different preferences for tryptophan-containing cyclic dipeptides. *Applied Microbiology and Biotechnology* **2016,** *100* (12), 5389-5399.

165. Zheng, L.; Mai, P.; Fan, A.; Li, S. M., Switching a regular tryptophan *C4*-prenyltransferase to a reverse tryptophan-containing cyclic dipeptide *C3*-prenyltransferase by sequential site-directed mutagenesis. *Organic & Biomolecular Chemistry* **2018,** *16* (36), 6688-6694.

166. Mai, P.; Zocher, G.; Stehle, T.; Li, S. M., Structure-based protein engineering enables prenyl donor switching of a fungal aromatic prenyltransferase. *Organic & Biomolecular Chemistry* **2018,** *16* (40), 7461-7469.

167. Herr, C. Q.; Hausinger, R. P., Amazing diversity in biochemical roles of Fe(II)/2-oxoglutarate oxygenases. *Trends in Biochemical Sciences* **2018,** *43* (7), 517-532.

168. Islam, M. S.; Leissing, T. M.; Chowdhury, R.; Hopkinson, R. J.; Schofield, C. J., 2-Oxoglutarate-dependent oxygenases. *Annual Review of Biochemistry* **2018,** *87* (1), 585-620.

169. Hegg, E. L.; Jr, L. Q., The 2-His-1-carboxylate facial triad–an emerging structural motif in mononuclear non-heme iron (II) enzymes. *European Journal of Biochemistry* **1997,** *250* (3), 625-629

170. Martinez, S.; Hausinger, R. P., Catalytic Mechanisms of Fe(II)- and 2-oxoglutarate-dependent oxygenases. *The Journal of Biological Chemistry* **2015,** *290* (34), 20702-20711.

171. Wang, X. C.; Liu, J.; Zhao, J.; Ni, X. M.; Zheng, P.; Guo, X.; Sun, C. M.; Sun, J. B.; Ma, Y. H., Efficient production of *trans*-4-hydroxy-L-proline from glucose using a new trans-proline 4-hydroxylase in *Escherichia coli*. *Journal of Bioscience and Bioengineering* **2018,** *126* (4), 470-477

172. Hillwig, M. L.; Zhu, Q.; Ittiamornkul, K.; Liu, X., Discovery of a promiscuous non-heme iron halogenase in ambiguine alkaloid biogenesis: Implication for an evolvable enzyme family for late-stage halogenation of aliphatic carbons in small molecules. *Angewandte Chemie International Edition* **2016,** *55* (19), 5780-5784.

173. Crawford, J. M.; Portmann, C.; Zhang, X.; Roeffaers, M. B. J.; Clardy, J., Small molecule perimeter defense in entomopathogenic bacteria. *Proceedings of the National Academy of Sciences* **2012,** *109* (27), 10821-10826.

174. Matsuda, Y.; Iwabuchi, T.; Fujimoto, T.; Awakawa, T.; Nakashima, Y.; Mori, T.; Zhang, H.; Hayashi, F.; Abe, I., Discovery of key dioxygenases that diverged the paraherquonin and acetoxydehydroaustin pathways in *Penicillium brasilianum*. *Journal of the American Chemical Society* **2016,** *138* (38), 12671-12677.

175. Nakashima, Y.; Mori, T.; Nakamura, H.; Awakawa, T.; Hoshino, S.; Senda, M.; Senda, T.; Abe, I., Structure function and engineering of multifunctional non-heme iron dependent oxygenases in fungal meroterpenoid biosynthesis. *Nature Communications* **2018,** *9* (1), 1-10.

176. Stapon, A.; Li, R.; Townsend, C. A., Carbapenem biosynthesis: confirmation of stereochemical assignments and the role of CarC in the ring stereoinversion process from L-proline. *Journal of the American Chemical Society* **2003,** *125* (28), 8486-8493.

177. Chang, W. C.; Guo, Y.; Wang, C.; Butch, S. E.; Rosenzweig, A. C.; Boal, A. K.; Krebs, C.; Bollinger, J. M., Mechanism of the C5 stereoinversion reaction in the biosynthesis of carbapenem antibiotics. *Science* **2014,** *343* (6175), 1140-1144.

178. Ishikawa, N.; Tanaka, H.; Koyama, F.; Noguchi, H.; Wang, C. C. C.; Hotta, K.; Watanabe, K., Non-heme dioxygenase catalyzes atypical oxidations of 6,7-bicyclic systems to form the 6,6-quinolone core of viridicatin-type fungal alkaloids. *Angewandte Chemie International Edition* **2014,** *53* (47), 12880-12884.

179. Hamed, R. B.; Gomez-Castellanos, J. R.; Henry, L.; Ducho, C.; McDonough, M. A.; Schofield, C. J., The enzymes of β-lactam biosynthesis. *Natural Product Reports* **2013,** *30* (1), 21-107.

180. Roach, P. L.; Clifton, I. J.; Fülöp, V.; Harlos, K.; Barton, G. J.; Hajdu, J.; Andersson, I.; Schofield, C. J.; Baldwin, J. E., Crystal structure of isopenicillin N synthase is the first from a new structural family of enzymes. *Nature* **1995,** *375* (6533), 700-704

181. Rabe, P.; Kamps, J.; Schofield, C. J.; Lohans, C. T., Roles of 2-oxoglutarate oxygenases and isopenicillin N synthase in β-lactam biosynthesis. *Natural Product Reports* **2018,** *35* (8), 735-756.

182. Tamanaha, E.; Zhang, B.; Guo, Y.; Chang, W. C.; Barr, E. W.; Xing, G.; St Clair, J.; Ye, S.; Neese, F.; Bollinger, J. M., Jr.; Krebs, C., Spectroscopic Evidence for the Two C-H-Cleaving Intermediates of *Aspergillus nidulans* Isopenicillin N Synthase. *Journal of the American Chemical Society* **2016,** *138* (28), 8862-8874.

183. Steffan, N.; Grundmann, A.; Afiyatullov, A.; Ruan, H.; Li, S. M., FtmOx1, a non heme Fe(II) and alpha-ketoglutarate-dependent dioxygenase, catalyses the endoperoxide formation of verruculogen in *Aspergillus fumigatus*. *Organic & Biomolecular Chemistry* **2009,** *7* (19), 4082-4087.

184. Yan, W.; Song, H.; Song, F.; Guo, Y.; Wu, C. H.; Sae, H. A.; Pu, Y.; Wang, S.; Naowarojna, N.; Weitz, A.; Hendrich, M. P.; Costello, C. E.; Zhang, L.; Liu, P.; Zhang, Y. J., Endoperoxide formation by an α-ketoglutarate-dependent mononuclear non-haem iron enzyme. *Nature* **2015,** *527* (7579), 539-543.

185. Dunham, N. P.; Del Rio Pantoja, J. M.; Zhang, B.; Rajakovich, L. J.; Allen, B. D.; Krebs, C.; Boal, A. K.; Bollinger, J. M., Jr., Hydrogen Donation but not Abstraction by a Tyrosine (Y68) during Endoperoxide Installation by Verruculogen Synthase (FtmOx1). *Journal of the American Chemical Society* **2019,** *141* (25), 9964-9979.

186. Zwick, C. R.; Renata, H., Harnessing the biocatalytic potential of iron- and α-ketoglutarate-dependent dioxygenases in natural product total synthesis. *Natural Product Reports* **2020**, doi: 10.1039/C9NP00075E.

187. Dockrey, S. A. B.; Lukowski, A. L.; Becker, M. R.; Narayan, A. R. H., Biocatalytic site- and enantioselective oxidative dearomatization of phenols. *Nature Chemistry* **2018,** *10* (2), 119-125.

188. Ueberbacher, B. T.; Hall, M.; Faber, K., Electrophilic and nucleophilic enzymatic cascade reactions in biosynthesis. *Natural Product Reports* **2012,** *29* (3), 337-350.

189. Lin, C. I.; McCarty, R. M.; Liu, H. W., The enzymology of organic transformations: a survey of name reactions in biological systems. *Angewandte Chemie International Edition* **2017,** *56* (13), 3446-3489.

190. Huang, C.; Yang, C.; Zhang, W.; Zhang, L.; De, B. C.; Zhu, Y.; Jiang, X.; Fang, C.; Zhang, Q.; Yuan, C. S.; Liu, H. W.; Zhang, C., Molecular basis of dimer formation during the biosynthesis of benzofluorene-containing atypical angucyclines. *Nature Communications* **2018,** *9* (1), 2088-2098.

191. Chen, G. D.; Hu, D.; Huang, M. J.; Tang, J.; Wang, X. X.; Zou, J.; Xie, J.; Zhang, W. G.; Guo, L. D.; Yao, X. S.; Abe, I.; Gao, H., Sporormielones A–E, bioactive novel C–C coupled orsellinic acid derivative dimers, and their biosynthetic origin. *Chemical Communications* **2020,** *56* (33), 4607-4610.

192. Dehn, R.; Katsuyama, Y.; Weber, A.; Gerth, K.; Jansen, R.; Steinmetz, H.; Höfle, G.; Müller, R.; Kirschning, A., Molecular basis of elansolid biosynthesis: evidence for an unprecedented quinone methide initiated intramolecular Diels-Alder cycloaddition/macrolactonization. *Angewandte Chemie International Edition* **2011,** *50* (17), 3882-3887.

193. Ohashi, M.; Liu, F.; Hai, Y.; Chen, M.; Tang, M. C.; Yang, Z.; Sato, M.; Watanabe, K.; Houk, K. N.; Tang, Y., SAM-dependent enzyme-catalysed pericyclic reactions in natural product biosynthesis. *Nature* **2017,** *549* (7673), 502-506.

194. Ramakrishnan, K.; Fisher, J., 7-Deoxydaunomycinone quinone methide reactivity with thiol nucleophiles. *Journal of Medicinal Chemistry* **1986,** *29* (7), 1215-1221.

195. Yan, Y.; Yang, J.; Yu, Z.; Yu, M.; Ma, Y. T.; Wang, L.; Su, C.; Luo, J.; Horsman, G. P.; Huang, S. X., Non-enzymatic pyridine ring formation in the biosynthesis of the rubrolone tropolone alkaloids. *Nature Communications* **2016,** *7* (1), 13083-13093.

196. Colosimo, D. A.; MacMillan, J. B., Detailed mechanistic study of the non-enzymatic formation of the discoipyrrole family of natural products. *Journal of the American Chemical Society* **2016,** *138* (7), 2383-2388.

197. Rix, U.; Zheng, J.; Remsing Rix, L. L.; Greenwell, L.; Yang, K.; Rohr, J., The dynamic structure of jadomycin B and the amino acid incorporation step of its biosynthesis. *Journal of the American Chemical Society* **2004,** *126* (14), 4496-4497

198. Robertson, A. W.; Martinez-Farina, C. F.; Smithen, D. A.; Yin, H.; Monro, S.; Thompson, A.; McFarland, S. A.; Syvitski, R. T.; Jakeman, D. L., Eight-membered ring-containing jadomycins: implications for non-enzymatic natural products biosynthesis. *Journal of the American Chemical Society* **2015,** *137* (9), 3271-3275.

199. Fu, P.; Legako, A.; La, S.; MacMillan, J. B., Discovery, characterization, and analogue synthesis of bohemamine dimers generated by non-enzymatic biosynthesis. *Chemistry-A European Journal* **2016,** *22* (10), 3491-3495.

200. Rohr, J., Biosynthetic formation of the S-methyl group of the angucycline antibiotic urdamycin E. *Journal of the Chemical Society, Chemical Communications* **1989,** *8* (8), 492-493.

201. Rohr, J., A novel type of non-enzymatic reaction during the late steps in the biosynthesis of the angucycline antibiotics urdamycins C and D. *Journal of the Chemical Society, Chemical Communications* **1990,** *2* (2), 113-114.

202. Van De Water, R. W.; Pettus, T. R. R., *o*-Quinone methides: intermediates underdeveloped and underutilized in organic synthesis. *Tetrahedron* **2002,** *58* (27), 5367-5406.

203. Willis, N. J.; Bray, C. D., *ortho*-Quinone methides in natural product synthesis. *Chemistry-A European Journal* **2012,** *18* (30), 9160-9173.

204. Steinmetz, H.; Zander, W.; Shushni, M. A. M.; Jansen, R.; Gerth, K.; Dehn, R.; Dräger, G.; Kirschning, A.; Müller, R., Precursor-directed syntheses and biological evaluation of new elansolid derivatives. *Chembiochem* **2012,** *13* (12), 1813-1817.

205. Asai, T.; Tsukada, K.; Ise, S.; Shirata, N.; Hashimoto, M.; Fujii, I.; Gomi, K.; Nakagawara, K.; Kodama, E. N.; Oshima, Y., Use of a biosynthetic intermediate to explore the chemical diversity of pseudo-natural fungal polyketides. *Nature Chemistry* **2015,** *7* (9), 737-743.

206. Capon, R. J., Extracting value: mechanistic insights into the formation of natural product artifacts-case studies in marine natural products. *Natural Product Reports* **2019,** *37* (1), 55-79.

207. Hemphill, C. F. P.; Daletos, G.; Liu, Z.; Lin, W.; Proksch, P., Polyketides from the Mangrove-derived fungal endophyte *Pestalotiopsis clavispora*. *Tetrahedron Letters* **2016,** *57* (19), 2078-2083.

208. Pockrandt, D.; Li, S. M., Geranylation of cyclic dipeptides by the dimethylallyl transferase AnaPT resulting in a shift of prenylation position on the indole ring. *Chembiochem* **2013,** *14* (15), 2023-2028.

209. Chen, R.; Gao, B.; Liu, X.; Ruan, F.; Zhang, Y.; Lou, J.; Feng, K.; Wunsch, C.; Li, S. M.; Dai, J.; Sun, F., Molecular insights into the enzyme promiscuity of an aromatic prenyltransferase. *Nature Chemical Biology* **2017,** *13* (2), 226-234.

210. Mori, T.; Zhang, L.; Awakawa, T.; Hoshino, S.; Okada, M.; Morita, H.; Abe, I., Manipulation of prenylation reactions by structure-based engineering of bacterial indolactam prenyltransferases. *Nature Communications* **2016,** *7* (1), 10849-10860.

211. Chooi, Y. H.; Wang, P.; Fang, J.; Li, Y.; Wu, K.; Wang, P.; Tang, Y., Discovery and characterization of a group of fungal polycyclic polyketide prenyltransferases. *Journal of the American Chemical Society* **2012,** *134* (22), 9428-9437.

212. Liu, X.; Hillwig, M. L.; Koharudin, L. M.; Gronenborn, A. M., Unified biogenesis of ambiguine, fischerindole, hapalindole and welwitindolinone: identification of a monogeranylated indolenine as a cryptic common biosynthetic intermediate by an unusual magnesium-dependent aromatic prenyltransferase. *Chemical Communications* **2016,** *52* (8), 1737-1740.

213. Wu, G.; Ma, H.; Zhu, T.; Li, J.; Gu, Q.; Li, D., Penilactones A and B, two novel polyketides from Antarctic deep-sea derived fungus *Penicillium crustosum* PRB-2. *Tetrahedron* **2012,** *68* (47), 9745-9749.

214. Wu, G., Studies on secondary metabolites of three different marine environment-derived fungi: structures and bioactivities. *Dissertation, Ocean University of China* **2014**.

215. Spence, J. T.; George, J. H., Biomimetic total synthesis of *ent*-penilactone A and penilactone B. *Organic Letters* **2013,** *15* (15), 3891-3893.

216. Nukina, M., Terrestric acid as a phytotoxic metabolite from *Pyricularia oryzae* Cavara. *Agricultural and Biological Chemistry* **1988,** *52* (9), 2357-2358.

217. Clutterbuck, P. W.; Haworth, W. N.; Raistrick, H.; Smith, G.; Stacey, M., Studies in the biochemistry of micro-organisms: The metabolic products of *Penicillium charlesii* G. Smith. *Biochemical Journal* **1934,** *28* (1), 94-110.

218. Weber, T.; Blin, K.; Duddela, S.; Krug, D.; Kim, H. U.; Bruccoleri, R.; Lee, S. Y.; Fischbach, M. A.; Müller, R.; Wohlleben, W.; Breitling, R.; Takano, E.; Medema, M. H., antiSMASH 3.0 - a comprehensive

resource for the genome mining of biosynthetic gene clusters. *Nucleic Acids Research* **2015,** *43* (W1), W237-W243.

219. Chiang, Y. M.; Ahuja, M.; Oakley, C. E.; Entwistle, R.; Asokan, A.; Zutz, C.; Wang, C. C. C.; Oakley, B. R., Development of genetic dereplication strains in *Aspergillus nidulans* results in the discovery of aspercryptin. *Angewandte Chemie International Edition* **2016,** *55* (5), 1662-1665.

220. Bentley, R.; Bhate, D. S.; Keil, J. G., Tetronic acid biosynthesis in molds I. Formation of carlosic and carolic acids in *Penicillium charlesii*. *Journal of Biological Chemistry* **1962,** *237* (3), 859-866.

221. Pathak, T. P.; Sigman, M. S., Applications of *ortho*-quinone methide intermediates in catalysis and asymmetric synthesis. *The Journal of Organic Chemistry* **2011,** *76* (22), 9210-9215.

222. Fan, J.; Liao, G.; Kindinger, F.; Ludwig-Radtke, L.; Yin, W. B.; Li, S. M., Peniphenone and penilactone formation in *Penicillium crustosum* via 1,4-Michael additions of *ortho*-quinone methide from hydroxyclavatol to γ-butyrolactones from crustosic acid. *Journal of the American Chemical Society* **2019,** *141* (10), 4225-4229.

223. Tomoda, H.; Tabata, N.; Masuma, R.; Si, S. Y.; Omura, S., Erabulenols, inhibitors of cholesteryl ester transfer protein produced by *Penicillium* sp. FO-5637. I. Production, isolation and biological properties. *The Journal of Antibiotics* **1998,** *51* (7), 618-623.

224. Li, H.; Jiang, J.; Liu, Z.; Lin, S.; Xia, G.; Xia, X.; Ding, B.; He, L.; Lu, Y.; She, Z., Peniphenones A-D from the mangrove fungus *Penicillium dipodomyicola* HN4-3A as inhibitors of *Mycobacterium tuberculosis* phosphatase MptpB. *Journal of Natural Products* **2014,** *77* (4), 800-806.

225. Wang, J.; Liu, P.; Wang, Y.; Wang, H.; Li, J.; Zhuang, Y.; Zhu, W., Antimicrobial aromatic polyketides from Gorgonian-associated fungus, *Penicillium commune* 518. *Chinese Journal of Chemistry* **2012,** *30* (6), 1236-1242.

226. Sun, W.; Chen, X.; Tong, Q.; Zhu, H.; He, Y.; Lei, L.; Xue, Y.; Yao, G.; Luo, Z.; Wang, J.; Li, H.; Zhang, Y., Novel small molecule 11β-HSD1 inhibitor from the endophytic fungus *Penicillium commune*. *Scientific Reports* **2016,** *6* (1), 26418-26428.

Statutory Declaration

Ich, Ge Liao, versichere, dass ich meine Dissertation

„Increasing structural diversity of natural products by enzymatic or nonenzymatic reactions“

selbständig ohne unerlaubte Hilfe angefertigt und mich dabei keiner anderen als der von mir ausdrücklich bezeichneten Quellen bedient habe. Alle vollständig oder sinngemäß übernommenen Zitate sind als solche gekennzeichnet.

Die Dissertation wurde in der jetzigen oder einer ähnlichen Form noch bei keiner anderen Hochschule eingereicht und hat noch keinen sonstigen Prüfungszwecken gedient.

Marburg, den.....

.....

Ge Liao

Acknowledgements

Firstly, I would like to take this opportunity to express my sincere gratitude to Prof. Dr. Shu-Ming Li for giving me the chance to study as a PhD student in University of Marburg. I'm very grateful for his supervision and guidance during my PhD study. It is of great value for his advices on the projects, his endeavors on the manuscripts, and his help in my daily life. All I have learned and trained in the research group of Prof. Li will benefit me greatly in my future life.

I'm very grateful to Prof. Dr. Michael Keusgen for his agreement to be my second supervisor and examiner. I would like to thank Dr. Jie Fan as the best partner when we worked together. Many thanks to Dr. Peter Mai for his idea and his help in the cooperation of the first project. I would also like to thank Lena Ludwig-Radtke for the chemical synthesis, Rixa Kraut for measuring LC-MS samples, Dr. Regina Ortmann and Stefan Newel for recording NMR spectra, Prof. Dr. Andreas Heine for X-ray crystal analysis, Prof. Dr. Ulrich Mühlenhoff for his assistant with CD measurement, and Dr. Katija Backhaus for her help in cytotoxicity tests. I'm also really appreciate the efforts made by Bastian Kemmerich for translating the summary part and together with Dr. Jie Fan for proof reading the dissertation.

Special thanks must go to Huomiao Ran who accompanied with me to experience the whole stay in Germany. I also want to thank Jing Liu as a very nice roommate to get along with. Also great thanks to Dr. Huili Yu, Pan Xiang, Lindsay Coby, Zhengxi Zhang, Johanna Schäfer, and Lena Mikulski for the wonderful time we have spent together. Without you I wouldn't have so much fun during the past four years.

I also want to express my sincere gratitude to all my current and former colleagues, Wei Li, Liujuan Zheng, Jonas Nies, Florian Kindinger, Lauritz Harken, Kristin Öqvist, Elisabeth Hühner, Kirsten Brockmeyer, Linus Naumann, Alexander Frehse, Viola Wohlgemuth, Haowen Wang, Wen Li, Jenny Zhou, Sina Stierle, Yiling Yang, Yu Dai, Marlies Peter, Danniel Jonathan Janzen, Andreas Martin, Dr. Kang Zhou, Dr. Nina Gerhards, and Dr. Dieter Kreusch.

I wish to thank the constant encouragement from my friends outside of the laboratory.

I would like to acknowledge the China Scholarship Council (CSC) for financial supports.

Finally, I must extend my heartfelt thanks to my family. Deeply thanks to my parents for giving me love and supports as always.

Curriculum Vitae

Personal Information

Name: Ge Liao

Date of Birth: 28.08.1991

Place of Birth: Changsha, Hunan Province, P. R. China

Nationality: Chinese

Address: Robert-Koch-Str. 4, 35032, Marburg

Email: liaog@staff.uni-marburg.de

Education & Research

PhD candidate: 10.2016 ─ now

Philipps-University Marburg, Germany

Institute for Pharmaceutical Biology and Biotechnology

Thesis title: “Increasing structural diversity of natural products by enzymatic or nonenzymatic reactions”

Supervisor: Prof. Dr. Shu-Ming Li

Master of Science: 09.2013 ─ 06.2016

Hainan University, China

College of Horticulture and Landscape

Thesis title: “Isolation, identification and dynamic regularity of 2-(2-phenylethyl)chromone derivatives in artificial agarwood”

Supervisor: Prof. Dr. Xiqiang Song and Prof. Dr. Haofu Dai

Bachelor of Science: 09.2009 ─ 06.2013

Hunan Agricultural University, China

College of Horticulture and Landscape

Thesis title: “Isolation and purification of gallic acid in *Galla chinensis* by chromatography”

Supervisor: Prof. Dr. Wenjun Xiao

High School: 09.2006 ─ 06.2009

Changsha County No.10 Middle School, China